USGS
science for a changing world

Prepared in cooperation with the
U.S. Department of Energy, Nevada Operations Office (Interagency Agreement DE–AI08–97NV12033)

Quaternary Paleoseismology and Stratigraphy of the Yucca Mountain Area, Nevada

Professional Paper 1689

125 years of science for America ★ ★ ★ ★ ★ 1879–2004

U.S. Department of the Interior
U.S. Geological Survey

Cover photograph: Exposure of the Paintbrush Canyon Fault zone on west side of Busted Butte. South end of Yucca Mountain is visible in middle distance to left, and Lathrop Wells basaltic cone is on horizon to right. View southward; photograph courtesy of J.A. Coe, U.S. Geological Survey.

Quaternary Paleoseismology and Stratigraphy of the Yucca Mountain Area, Nevada

William R. Keefer, John W. Whitney, and Emily M. Taylor, Editors

Prepared in cooperation with the
U.S. Department of Energy, Nevada Operations Office
(Interagency Agreement DE–AI08–97NV12033)

Professional Paper 1689

U.S. Department of the Interior
U.S. Geological Survey

U.S. Department of the Interior
Gale A. Norton, Secretary

U.S. Geological Survey
Charles G. Groat, Director

U.S. Geological Survey, Reston, Virginia: 2004

For sale by U.S. Geological Survey Information Services
Box 25286, Denver Federal Center
Denver, CO 80225

This report and any updates to it are available online at:
http://pubs.usgs.gov/pp/2004/1689/

For additional information write to:
Chief, Yucca Mountain Project Branch
U.S. Geological Survey
Box 25046, Mail Stop 421, Denver Federal Center
Denver, CO 80225-0046

Additional USGS publications can be found at:
http://geology.usgs.gov/products.html

For more information about the USGS and its products:
Telephone: 1–888–ASK–USGS (1–888–275–8747)
World Wide Web: http://www.usgs.gov/

Cataloging-in-publication data are on file with the Library of Congress (URL http://www.loc.gov/).

Produced in the Western Region, Menlo Park, California
Manuscript approved for publication, December 23, 2003
Text edited by George A. Havach
Layout and design by Sara Boore and Susan Mayfield

Foreword

The U.S. Geological Survey has conducted a comprehensive series of fault studies to determine the history and extent of Quaternary deformation in the Yucca Mountain area of southwestern Nevada as part of a broad, multidisciplinary site-characterization program to evaluate the suitability of the mountain to host a geologic repository for the safe and permanent storage of high-level radioactive wastes. The results of the detailed studies reported here provide basic data that are fundamental to assessing the risks posed by potential future earthquakes and fault displacements with respect to the design and long-term performance of the proposed facilities. The scope and objectives of fault investigations were largely guided by regulations established by the U.S. Nuclear Regulatory Commission and the U.S. Department of Energy for the siting of geologic repositories for the storage of high-level radioactive wastes.

This report focuses primarily on eight faults within and near Yucca Mountain that are known to have been active during Quaternary time, as well as on two other conspicuous fault systems in nearby areas that also demonstrate neotectonic activity. The overall objective was to obtain, for each individual fault or fault system, definitive information on the number, magnitude, and estimated dates of surface-rupturing paleoearthquakes. Compiling such information involved extensive field investigations, excavation and logging of trenches, detailed descriptions of surficial deposits and soils, and selected sampling and analyses for numerical age determinations, all of which were performed in accordance with a rigorous set of technical procedures and guidelines that were formulated to comply with quality-assurance standards—an essential requirement for activities related to the siting of nuclear facilities.

Beyond the specific purpose of providing a basis for the seismic-risk analysis of Yucca Mountain, the accumulated data and resulting interpretations constitute a valuable contribution to our knowledge and understanding of the neotectonics in this part of the Basin and Range Province. Faults in few other parts of the region have been studied as thoroughly and comprehensively, and so the pattern of Quaternary deformation within this limited area may serve as an example of the structural relations and the locations and magnitudes of potential future earthquakes elsewhere in the Great Basin.

Contents

[Numbers designate chapters]

Foreword iii

1. Introduction to Quaternary Paleoseismology and Stratigraphy of the Yucca Mountain Area.....1
   By John W. Whitney, Emily M. Taylor, and Christopher M. Menges
2. Quaternary Stratigraphy and Mapping in the Yucca Mountain Area 11
   By John W. Whitney, Emily M. Taylor, and John R. Wesling
3. Distribution of Quaternary Faults at Yucca Mountain 23
   By Christopher M. Menges and John W. Whitney
4. Summary of Studies in Midway Valley..... 33
   By John R. Wesling, John W. Whitney, Frank H. Swan, and Michael M. Angell
5. Summary of Quaternary Faulting on the Paintbrush Canyon, Bow Ridge, and Stagecoach Road Faults 41
   By Christopher M. Menges, Emily M. Taylor, John R. Wesling, Frank H. Swan, Jeffrey A. Coe, Daniel J. Ponti, and John W. Whitney
6. Results of Paleoseismic Investigations on the Ghost Dance Fault..... 71
   By Emily M. Taylor, Christopher M. Menges, and David C. Buesch
7. Quaternary Faulting on the Solitario Canyon Fault 89
   By Alan R. Ramelli, John A. Oswald, Giovanni Vadurro, Christopher M. Menges, and James B. Paces
8. Quaternary Faulting on the Fatigue Wash Fault 111
   By Jeffrey A. Coe, John Oswald, Giovanni Vadurro, and Scott C. Lundstrom
9. Quaternary Faulting on the Windy Wash Fault..... 125
   By John W. Whitney, F. William Simonds, Ralph R. Shroba, and Michele Murray
10. Quaternary Faulting on the Southern Crater Flat Fault 135
    By Emily M. Taylor
11. Quaternary Faulting on the Northern Crater Flat Fault..... 145
    By Jeffrey A. Coe
12. Quaternary Faulting on the Bare Mountain Fault..... 155
    By Larry W. Anderson and Ralph E. Klinger
13. Paleoseismic Investigations on the Rock Valley Fault System..... 175
    By Jeffrey A. Coe, James C. Yount, Dennis W. O'Leary, and Emily M. Taylor
14. Summary of the Temporal and Spatial Relations of Quaternary Faulting During the Past 100 k.y. at Yucca Mountain: Evidence for Distributive Surface Ruptures on Multiple Faults..... 197
    By William R. Keefer and Christopher M. Menges

References Cited 201

Plates

1–26. Logs of:
1. South wall of trench MWV–T7
2. Trench A1
3. Trench T14
4. Trench WBR
5. South wall of trench T4
6. South wall of trench T4A
7. South wall of trench T2
8. South wall of trench SCF–T1
9. South wall of trench SCF–T4
10. South wall of trench SCF–T2
11. Trenches CF1 and CF1A
12. North wall of trench CF2
13. South wall of trench CF2
14. North wall of trench CF2.5
15. North wall of trench CF3
16. South wall of trench CF3
17. North wall of trench CFF–T1A
18. North wall of trench CFF–T1
19. South wall of trench CFF–T2A
20. Trench BMT–1
21. Trench BMT–2
22. Trench BMT–3
23. Trenches RV3, RV3CT, and RV3A
24. Trenches RV4 and RV4A
25. Trench RV5
26. West wall of the trench in Frenchman Flat

Figures

1. Map of southwestern Nevada, showing location of Yucca Mountain area, geographic features, general distribution of major rock types, and locations of trenches outside site area 2
2. Index map of Yucca Mountain area, showing locations of major faults and trench sites 3
3. Schematic stratigraphic column showing age distribution of mapped Quaternary deposits in Midway Valley and Fortymile Wash 17
4. Map showing faults in the Yucca Mountain area 24
5. Schematic cross section showing stratigraphic relations among bedrock, alluvium, and colluvium in western Midway Valley, southwestern Nevada 34
6. Maps of test pits shown in figure 8 35
7. Cross section showing structure across Exile Hill and western Midway Valley 36

8. Map of Exile Hill area, southwestern Nevada, showing general geology and locations of faults, trenches, test pits, and boreholes 37
9–10. Simplified logs of natural exposures across the Paintbrush Canyon Fault at:
9. Busted Butte wall 4 44
10. Busted Butte wall 1 48
11–12. Topographic profile of:
11. Sand-ramp geomorphic surface on interfluve across the Paintbrush Canyon Fault on west side of Busted Butte 50
12. Colluvial footslope south of trench MWV–T4 55
13. Simplified log of north wall of trench MWV–T4, which exposes western splay of the Paintbrush Canyon Fault 56
14–15. Topographic profile of colluvial footslope:
14. At north edge of trench A1 57
15. Across the Bow Ridge Fault south of trench T14D 59
16–17. Logs of south wall of:
16. Northern section of trench T14D across the Bow Ridge Fault 60
17. Southern section of trench T14D across the Bow Ridge Fault 62
18. Topographic profiles of geomorphic surfaces across the Stagecoach Road Fault 63
19–20. Simplified logs of central part of:
19. Trench SCR–T1 across the Stagecoach Road Fault 64
20. Trench SCR–T3 across the Stagecoach Road Fault 66
21. Aerial photograph of east slope of Yucca Mountain, showing locations of topographic features, Ghost Dance and Sundance Fault traces, and trenches 72
22. Photographs showing the Ghost Dance and Northern Solitario Canyon Faults along slopes of Yucca Mountain 73
23. Aerial photograph of Whale Back and Antler Ridges in Split Wash along slopes of Yucca Mountain, showing locations of topographic profiles across the Ghost Dance Fault 74
24. Topographic profiles across the Ghost Dance Fault on Whale Back and Antler Ridges in Split Wash along slopes of Yucca Mountain, showing locations of bedrock samples collected for determinations of whole-rock cosmogenic ^{10}Be estimated ages 75
25. Photographs showing exposures of the Ghost Dance Fault 76
26–29. Diagrams showing:
26. Simplified lithostratigraphy and structural features in trench WBR across the Ghost Dance Fault 77
27. Generalized stratigraphic column of crystal-rich member of the Tiva Canyon Tuff 78
28. Ti contents in samples of Tiva Canyon Tuff 80
29. Zr contents in samples of Tiva Canyon Tuff 80
30. Surficial geologic map of area of trench T8 across the Solitario Canyon Fault 91
31–32. Logs of:
31. South wall of trench T8 across the Solitario Canyon Fault 92
32. North wall of trench T8 across the Solitario Canyon Fault 94
33. Diagram showing simple model for estimating fault displacement 97
34. Log of south wall of trench SCF–T3 across the Solitario Canyon Fault 100
35. Aerial photograph showing distribution of surficial deposits in the vicinity of trenches CF1 and CF–1 across the Fatigue Wash Fault 113

36. Schematic diagram illustrating parameters measured for topographic profiles 114
37. Diagrams showing topographic profiles SP1 through SP7 across west-facing scarp of the Fatigue Wash Fault 115
38–40. Photographs showing:
38. Stratigraphy and faulting-event horizons exposed on south wall of trench CF1A across the Fatigue Wash Fault 120
39. Stratigraphy and faulting-event horizons exposed on south wall of trench CF1 across the Fatigue Wash Fault 123
40. Photograph of surface rupture from a late Holocene coseismic event on the Windy Wash Fault 127
41–42. Aerial photographs showing:
41. Offset of 3.7-Ma basalt along the Windy Wash Fault 133
42. Distribution of surficial deposits along the Southern Crater Flat Fault and locations of trenches CFF–T1 and CFF–T1A 136
43. Schematic diagrams showing sequential development of structures on north wall of trench CFF–T1A across the Southern Crater Flat Fault 143
44–45. Photographs of part of south wall of trench CFF–T2A across the Northern Crater Flat Fault zone, showing:
44. Main fault zone, mapped surficial deposits, and event horizons marking Quaternary faulting events 150
45. Stratigraphic relations bearing on event X on upthrown block 152
46. Aerial photograph of the Bare Mountain Fault along east side of Bare Mountain 156
47–49. Geologic maps of Bare Mountain Fault area along east side of Bare Mountain, showing:
47. Tarantula Canyon trench site 158
48. Wildcat Peak trench site 162
49. Stirling trench site 163
50. Plot of scarp height versus maximum scarp-slope angles for topographic profiles of Stirling and Tarantula Canyon scarps along the Bare Mountain Fault along east side of Bare Mountain, in comparison with scarps of known age in the Basin and Range Province 165
51–52. Maps showing:
51. Location of the Rock Valley Fault system in Rock Valley 176
52. Surficial geology of area surrounding trenches RV–1 and RV–2 across medial fault of the Rock Valley Fault system 178
53–54. Aerial photographs showing surficial geology of area surrounding:
53. Trenches RV3, RV3CT, and RV3A across the northern fault of the Rock Valley Fault system 181
54. Trenches RV4, RV4A, and RV5 on northern and southern strands of the southern fault of the Rock Valley Fault system 182
55–58. Photographs showing geologic features exposed on:
55. West wall of trench RV3 across northern fault of the Rock Valley Fault system 187
56. East wall of trench RV3A across northern fault of the Rock Valley Fault system 188
57. West wall of trench RV4A across northern fault of the Rock Valley Fault system 189
58. East and west walls of trench RV5 across northern fault of the Rock Valley Fault system 191
59. Plot showing ranges in estimated dates of Quaternary faulting events identified in trenches excavated in the Yucca Mountain area 198

Tables

1. Trench excavations across faults in the Yucca Mountain area, southwestern Nevada 4
2. Comparison of surficial deposits in the Yucca Mountain area, southwestern Nevada, with local and regional surficial stratigraphic sequences 12
3. Summary of diagnostic surface and soil properties of Quaternary map units in the Yucca Mountain area, southwestern Nevada 13
4. Numerical ages of samples collected from Quaternary deposits in Midway Valley and Fortymile Wash in the Yucca Mountain area, southwestern Nevada 16
5. Summary of characteristics of major faults in the Yucca Mountain area, southwestern Nevada 26
6. Estimated dates and numbers of surface-rupturing paleoearthquakes on the Paintbrush Canyon, Bow Ridge, and Stagecoach Road Faults in the Yucca Mountain area, southwestern Nevada 50
7. Summary of measured displacements on the Paintbrush Canyon, Bow Ridge, and Stagecoach Road Faults in the Yucca Mountain area, southwestern Nevada 50
8. Dip-slip and net displacements for individual faulting events on the Paintbrush Canyon, Bow Ridge, and Stagecoach Road Faults in the Yucca Mountain area, southwestern Nevada 51
9. Numerical ages of Quaternary deposits in trenches MWV–T4, A1, T14, and T14D and at Busted Butte in the Yucca Mountain area, southwestern Nevada 52
10. Estimated dates of selected faulting events on the Paintbrush Canyon, Bow Ridge, and Stagecoach Road Faults in the Yucca Mountain area, southwestern Nevada 53
11. Recurrence intervals and slip rates calculated for the Paintbrush Canyon, Bow Ridge, and Stagecoach Road Faults in the Yucca Mountain area, southwestern Nevada 54
12. Fault-slip rates calculated for selected dated reference horizons in trenches across the Paintbrush Canyon, Bow Ridge, and Stagecoach Road Faults in the Yucca Mountain area, southwestern Nevada 55
13. Lithostratigraphic features in bedrock units of the Tiva Canyon Tuff exposed in trench WBR across the Ghost Dance Fault in the Yucca Mountain area, southwestern Nevada 79
14. Quaternary stratigraphy exposed in trench WBR across the Ghost Dance Fault in the Yucca Mountain area, southwestern Nevada 82
15. Numerical ages of deposits in trenches T2, T4A, and WBR across the Ghost Dance Fault in the Yucca Mountain area, southwestern Nevada 82
16. Quaternary stratigraphy exposed in trench T4 across the Ghost Dance Fault in Split Wash in the Yucca Mountain area, southwestern Nevada 84
17. Particle-size distribution, carbonate content, and pH in soils exposed in trenches T2, T4, and T4A across the Ghost Dance Fault in the Yucca Mountain area, southwestern Nevada 86
18. Quaternary stratigraphy exposed in trench T4A across the Ghost Dance Fault in Split Wash in the Yucca Mountain area, southwestern Nevada 87
19. Quaternary stratigraphy exposed in trench T2 across the Ghost Dance Fault in Drill Hole Wash in the Yucca Mountain area, southwestern Nevada 88
20. Summary of stratigraphic relations and correlations in trenches across the Solitario Canyon Fault in the Yucca Mountain area, southwestern Nevada 90
21. Numerical ages of deposits exposed in trenches T8, T8A, and SCF–T3 across the Solitario Canyon Fault in the Yucca Mountain area, southwestern Nevada 90

22. Estimated displacements associated with mid-Quaternary to late Quaternary faulting events along the Solitario Canyon Fault in the Yucca Mountain area, southwestern Nevada 97
23. Numerical ages of deposits exposed in trenches CF1 and CF1A across the Fatigue Wash Fault in the Yucca Mountain area, southwestern Nevada 114
24. Data on topograpahic profiles across the west-facing scarp of the Fatigue Wash Fault near trench CF1 in the Yucca Mountain area, southwestern Nevada 114
25A. Summary of characteristics of lithologic units exposed in trench CF1 across the Fatigue Wash Fault in the Yucca Mountain area, southwestern Nevada 116
25B. Descriptions of topographic profiles across the west-facing scarp of the Fatigue Wash Fault near trench CF1 in the Yucca Mountain area, southwestern Nevada 117
26. Estimated vertical displacements on the Fatigue Wash Fault in trenches CF1 and CF1A in the Yucca Mountain area, southwestern Nevada 121
27. Numerical ages of deposits exposed in trenches CF2, CF2.5, and CF3 across the Windy Wash Fault in the Yucca Mountain area, southwestern Nevada 126
28. Soil and stratigraphic units exposed on the north wall of trench CFF–T1A across the Southern Crater Flat Fault in the Yucca Mountain area, southwestern Nevada 137
29. Soil and stratigraphic units exposed on the north wall of trench CFF–T1 across the Southern Crater Flat Fault in the Yucca Mountain area, southwestern Nevada 140
30. Numerical ages of deposits exposed in trench CFF–T1A across the Southern Crater Flat Fault in the Yucca Mountain area, southwestern Nevada 141
31. Numerical ages of deposits exposed in trench CFF–T2A across the Northern Crater Flat Fault in the Yucca Mountain area, southwestern Nevada 146
32. Descriptions of stratigraphic units exposed on the south wall of trench CFF–T2A across the Northern Crater Flat Fault in the Yucca Mountain area, southwestern Nevada 147
33. Descriptions of soil profiles in trench CFF–T2A across the Northern Crater Flat Fault in the Yucca Mountain area, southwestern Nevada 151
34. Summary of faulting events on the Northern Crater Flat Fault in the Yucca Mountain area, southwestern Nevada 153
35. Surface characteristics used to subdivide surficial deposits and geomorphic surfaces along the Bare Mountain Fault in southwestern Nevada 159
36. Correlation chart for Quaternary alluvial deposits in the vicinity of the Bare Mountain Fault, southwestern Nevada 159
37. Data from topographic profiles on fault scarps along the Bare Mountain Fault, southwestern Nevada 165
38. Numerical ages of surficial deposits exposed in trenches BMT–1 and BMT–2 across the Bare Mountain Fault, southwestern Nevada 167
39. Numerical ages of surficial deposits exposed in trenches RV2, RV3, RV3A, RV4, and RV5 and in the trench in Frenchman Flat across the Rock Valley Fault system in the Yucca Mountain area, southwestern Nevada 183
40. Summary of the characteristics of lithologic units exposed in trenches across the Rock Valley Fault system in the Yucca Mountain area, southwestern Nevada 184
41. Descriptions of soil profiles in trenches across the Rock Valley Fault system in the Yucca Mountain area, southwestern Nevada 186
42. Summary of faulting events on the Rock Valley Fault system in the Yucca Mountain area, southwestern Nevada 192
43. Estimated dates of faulting events during the past 100 k.y. in the Yucca Mountain area, southwestern Nevada 199

Conversion Factors and Abbreviations

Multiply	By	To obtain
kilometers (km)	0.6214	miles
meters (m)	3.2808	feet
centimeters (cm)	0.3937	inches
millimeters (mm)	0.0394	inches

yr	years
k.y.	thousand years
ka	thousands of years before present
m.y.	million years
Ma	millions of years before present

Chapter 1

Introduction to Quaternary Paleoseismology and Stratigraphy of the Yucca Mountain Area

By John W. Whitney, Emily M. Taylor, and Christopher M. Menges

Contents

Abstract....1
Purpose and Scope of Paleoseismic Studies....1
Trenching Activities....6
Methods....6
Trenches with No Quaternary Deformation....8
Paintbrush Canyon Fault....8
Bow Ridge Fault....8
Exile Hill Fault....8
Ghost Dance Fault....9
Abandoned Wash Fault....9
Drill Hole Wash, Pagany Wash, and Sever Wash Faults....9
Stagecoach Road Fault....9
Solitario Canyon Fault....9
Northern Crater Flat Fault....9

Abstract

Eight faults with demonstrable Quaternary activity have been identified in and adjacent to the proposed repository site for the storage of high-level radioactive wastes at Yucca Mountain in southwestern Nevada. Data regarding fault geometry and displacements, ages and characteristics of closely associated Quaternary deposits, paleoearthquake-recurrence intervals, and fault-slip rates were collected principally from trenches excavated across faults or from cleaned-off natural exposures. Specific results of the large-scale geologic mapping of fresh exposures and the numerical dating of soils and other surficial deposits involved in Quaternary fault activity are discussed in succeeding chapters of this report.

Three measurements of fault displacement—individual, cumulative, and net cumulative—were used in recording faulting events. Surficial deposits were dated by two basic dating techniques: (1) U-Th-disequilibrium-series (U series) analyses of pedogenic carbonate-silica laminae and clast rinds, matrix soil carbonate, and rhizoliths; and (2) thermoluminescence analyses of fine-grained polymineralic material. Recurrence intervals between successive surface-rupturing paleoearthquakes were computed for each trench site on the basis of available numerical ages for the affected Quaternary deposits. Fault-slip rates were calculated by dividing the cumulative net slip (sum of all individual displacements) by the age of a specific faulted marker horizon.

Purpose and Scope of Paleoseismic Studies

Since the late 1970s, Yucca Mountain in southwestern Nevada (fig. 1) has been investigated by the U.S. Department of Energy as a geologic repository for the storage of high-level radioactive wastes. As part of an interdisciplinary site-characterization program (U.S. Department of Energy, 1988), a series of specific studies bearing on the location, extent, timing, and magnitude of Quaternary faulting within and adjacent to Yucca Mountain were conducted for the purposes of seismic-hazard assessment, seismic design of surface and subsurface facilities, and repository-performance evaluations and to satisfy regulatory licensing requirements. The history of Quaternary faulting and seismic activity within the proposed repository-site area provides essential information for the integrated safety analysis as required by the U.S. Nuclear Regulatory Commission (10CFR Part 60), which calls for the identification of potential geologic hazards and characterization of future faulting events. Relative to this requirement, paleoseismic data are especially critical to both deterministic and probabilistic seismic-hazard analyses, wherein faults, on the basis of their past history of surface ruptures and seismicity, are evaluated as to their potential for generating future earthquakes of a given magnitude and within a given time period.

During the 1980s, two sets of studies were conducted to identify faults with evidence of Quaternary surface ruptures. Preliminary mapping of Quaternary deposits around Yucca Mountain was completed at 1:48,000 scale (Swadley, 1983;

Swadley and Carr, 1987; Swadley and Parrish, 1988) and later refined by more detailed mapping at 1:12,000 scale (Swadley and Hoover, 1989a, b; Swadley and Huckins, 1989, 1990). During that period, Swadley and Hoover (1983) and Swadley and others (1984) also made a preliminary identification of faults with probable Quaternary activity. Subsequently, detailed examinations of the exposures of all faults in the Yucca Mountain area (fig. 1) were compiled by Simonds and others (1995), whose map then served as a basis for selecting those faults that either demonstrated evidence of Quaternary surface ruptures or were suspected of Quaternary activity and therefore required additional study with regard to paleoseismicity.

A detailed discussion of stratigraphic studies and the mapping of Quaternary deposits is presented in chapter 2, and fault descriptions are summarized in chapter 3. The results of paleoseismic studies for eight identified Quaternary faults—the Paintbrush Canyon, Bow Ridge, Stagecoach Road, Solitario Canyon (including Iron Ridge), Fatigue Wash, Windy Wash, and Southern and Northern Crater Flat Faults (fig. 2)—and for several other faults suspected of Quaternary activity in the immediate vicinity of Yucca Mountain are presented in chapters 4 through 11. Chapters 12 and 13 describe similar studies that were conducted on the Bare Mountain and Rock Valley Fault systems that lie 14 km west and 25 km southeast, respectively, of the proposed repository site (fig. 1). The combined paleoseismic event data as presented in the individual fault studies are used in chapter 14 to summarize the evidence for distributive surface ruptures on multiple faults during the past 100 k.y., which is an important consideration in evaluating future seismicity at Yucca Mountain.

Plates, figures, and tables are numbered consecutively throughout this report for convenience in cross-referencing, and a combined reference list is provided at the end.

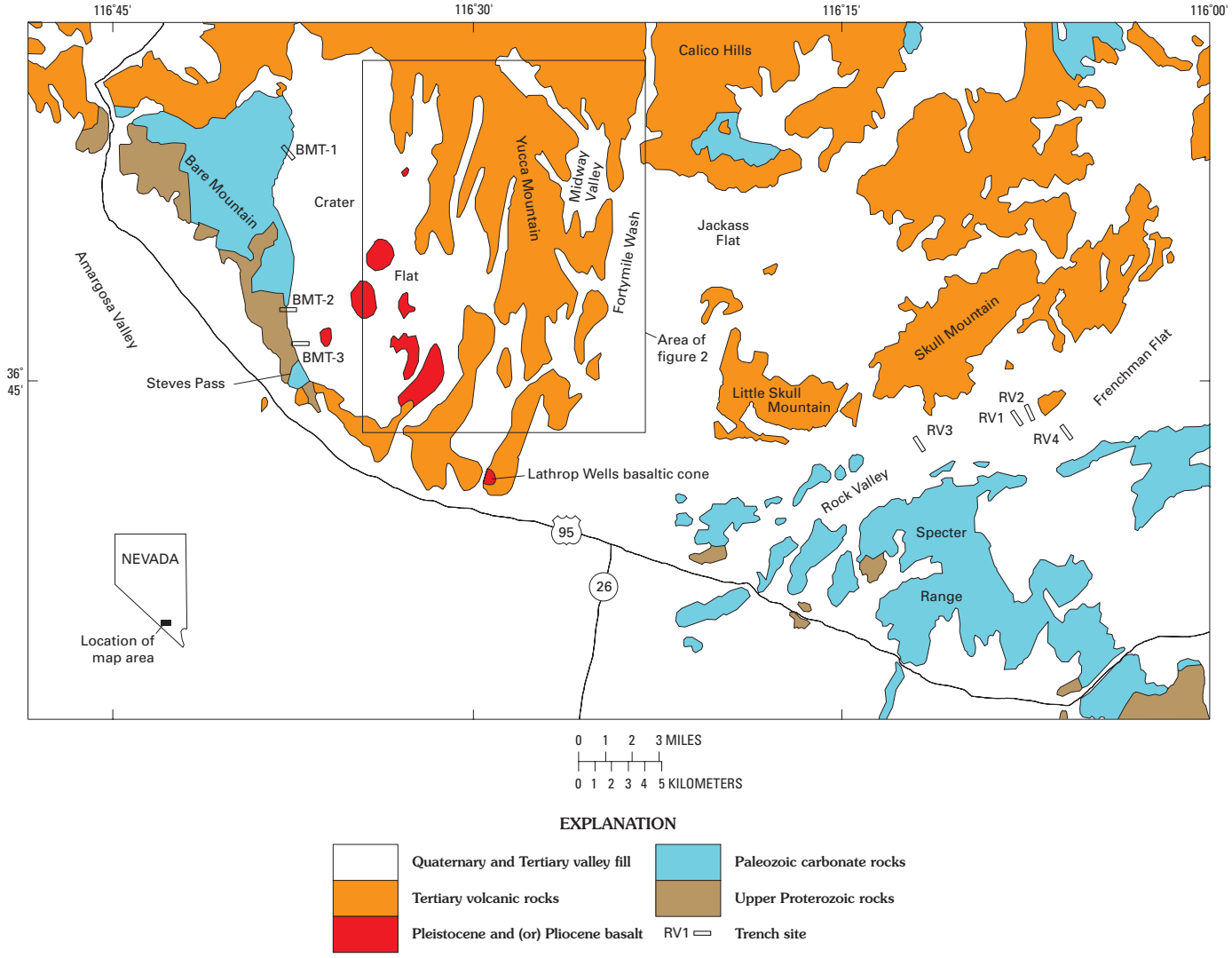

Figure 1. Southwestern Nevada, showing location of Yucca Mountain area, geographic features, general distribution of major rock types, and locations of trenches and other sites outside area of figure 2.

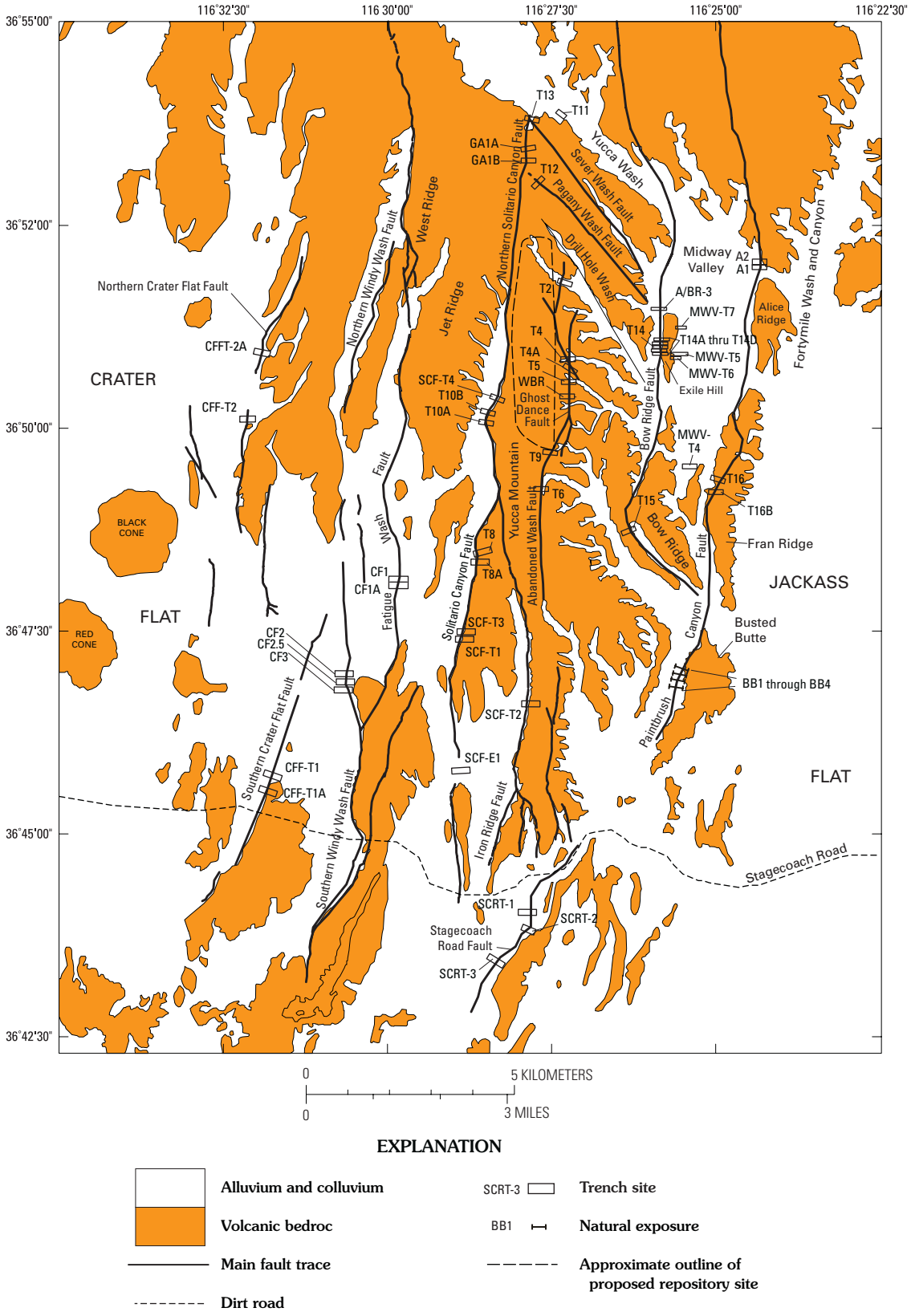

Figure 2. Index map of Yucca Mountain area, southwestern Nevada, showing locations of major faults and trench sites. All faults (solid lines) include segments that either cut or are interpreted to extend beneath Quaternary deposits. Adapted from Simonds and others (1995) and Day and others (1998a). Dashed outline, area of proposed repository site for storage of high-level radioactive wastes.

Table 1. Trench excavations across faults in the Yucca Mountain area, southwestern Nevada.

[See figures 1 and 2 for locations. References: Rpt, this report; SHR, Swadley and others (1984); T, Taylor and Huckins (1995); W, Whitney and others (1986). Modified?, statement whether original excavation was significantly modified: N, no; Y, yes. Logged?, statement whether trench walls were logged or mapped: N, no; Y, yes. Method, technique used to log excavation: MG, manual gridding; na, not applicable; Ph, photogrammetry; S, sketch log; Th, theodolite. Sampled geochrologically?, statement whether trench site was sampled for geochronologic analyses as part of present study. Fault exposed?, statement whether a fault is present in bedrock and (or) Quaternary deposits in trench: N, no; Y, yes. Fault exposed?, statement whether evidence was observed for Quaternary faulting or deformation: F, surface displacement on fault; Fr, fractures in Quaternary deposits that may or may not be associated with surface rupture on fault; I, indeterminate faulting, generally of unknown age only in bedrock; N, none. Report?, statement whether trench is described in this report: N, no; Y, yes]

Trench	Reference	Modified?	Logged?	Method	Sampled geochronologically?	Fault exposed?	Quaternary deformation?	Report?
Paintbrush Canyon Fault								
A1	SHR, rpt	Y	Y	S, Th	Y	Y	F	Y
A2	SHR	N	N	S	N	N	N	N
MWV–T3	rpt	N	N	na	N	N	N	N
MWV–T4	SHR, rpt	Y	Y	S, MG	Y	Y	F	Y
T16	SHR	N	Y	S	N	N	N	N
T16B	SHR	N	Y	S	N	N	Fr	N
BB–1	rpt	N	Y	Ph	Y	Y	F	Y
BB–2	rpt	N	Y	Ph	N	Y	F	N
BB–3	rpt	N	N	na	N	Y	F	N
BB–4	rpt	N	Y	Ph	Y	Y	F	Y
Bow Ridge Fault								
A–BR/3	rpt	N	Y	MG	N	N	N	N
T14	SHR, T	Y	Y	S, Ph	N	Y	F	Y
T14A	T	N	N	na	N	Y	I	N
T14B	T	N	N	na	N	Y	I	N
T14C	T, rpt	N	Y	MG	Y	Y	F	N
T14D	T, rpt	Y	Y	S, MG, Th	Y	Y	F	Y
T15	SHR	N	N	na	N	Y	I	N
Exile Hill Fault								
MWV–T5	rpt	N	Y	MG	Y	Y	Fr	N
MWV–T6	rpt	N	Y	MG	N	Y	Fr	N
MWV–T7	rpt	N	Y	MG, Ph	Y	Y	N	Y
Ghost Dance Fault								
T2	SHR, rpt	Y	Y	S, Th	Y	N	N	Y
T4	SHR, rpt	Y	Y	S, Th	N	N	N	Y
T4A	rpt	N	Y	Th	Y	N	N	Y
T5 (Antler Pavement)	rpt	N	Y	Th	N	Y	N	N
WBR	rpt	N	Y	Th	Y	Y	Fr	Y
Abandoned Wash Fault								
T9	SHR	N	Y	S	N	N	N	N
T6	SHR	N	Y	S	N	N	N	N
Pagany Wash Fault								
T12	SHR, rpt	N	Y	S	N	Y	N	N

Table 1. Trench excavations across faults in the Yucca Mountain area, southwestern Nevada—Continued

Trench	Reference	Modified?	Logged?	Method	Sampled geochronologically?	Fault exposed?	Quaternary deformation?	Report?
Sever Wash Fault								
T11	SHR	N	Y	S	N	N	N	N
Stagecoach Road Fault								
SCR–T1	rpt	N	Y	Ph, MG	Y	Y	F	Y
SCR–T2	rpt	N	N	na	N	N	N	N
SCR–T3	rpt	N	Y	Ph, MG	Y	Y	F	Y
Solitario Canyon Fault								
T13	SHR	N	Y	S	N	N	N	N
GA1A	SHR, rpt	N	Y	S	N	Y	F?	N
GA1B	SHR, rpt	N	Y	S	N	Y	F?	N
Ammo Ridge	rpt	N	N	na	N	Y	F?	N
SCF–T4	rpt	N	Y	Th	N	Y	F	Y
T10A	SHR	N	Y	S	N	N	N	N
T10B	SHR	N	Y	S	N	Y	I	N
T8	SHR, rpt	Y	Y	S, Th	Y	Y	F	Y
SCF–T3	rpt	N	Y	Th	Y	Y	F	Y
SCF–T1	rpt	N	Y	Th	Y	Y	F	Y
SCF–E1	rpt	N	N	na	N	Y	F	N
Iron Ridge Fault								
SCF–T2	rpt	N	Y	Th	N	Y	F	Y
Fatigue Wash Fault								
CF1	SHR, rpt	Y	Y	S, Ph	Y	Y	F	Y
CF1A	rpt	N	Y	S	Y	Y	F	Y
Windy Wash Fault								
CF2	SHR, W, rpt	Y	Y	S, MG	Y	Y	F	Y
CF2.5	W, rpt	N	Y	MG	N	Y	F	Y
CF3	SHR, W, rpt	Y	Y	S, MG	Y	Y	F	Y
Southern Crater Flat Fault								
CFF–T1	rpt	N	Y	Th	Y	Y	F	Y
CFF–T1A	rpt	N	Y	Th	Y	Y	F	Y
Northern Crater Flat Fault								
CFF–T2	rpt	N	N	na	N	N	N	N
CFF–T2A	rpt	N	Y	Ph	Y	Y	F	Y

Trenching Activities

Typically, the Quaternary faults in the Yucca Mountain area (fig. 1) show little evidence of historical activity, and so they require a systematic collection of data on (1) fault geometry; (2) characteristics and ages of surficial deposits closely associated with each fault; (3) number, amounts, and ages of individual surface displacements; (4) paleoearthquake-recurrence intervals; and (5) fault-slip rates (Allen, 1986; Schwartz, 1988; dePolo and Slemmons, 1990; Reiter, 1990; Coppersmith, 1991). Such data were collected principally from trenches that were excavated across faults to provide fresh exposures of Quaternary deposits and their stratigraphic and structural relations (see Hatheway and Leighton, 1979).

Some 50 exploratory trenches have been excavated, or natural exposures cleaned, since the early 1980s in the vicinity of Yucca Mountain (fig. 2; table 1). In all, 41 of these trenches and natural exposures are associated with the eight proximal faults with demonstrable Quaternary activity. Most excavations are located on the surface traces of those faults, although a few are located across the projections of a fault through undisturbed alluvium or a geomorphic surface. The rest of the trenches were located across mostly bedrock faults in the central Yucca Mountain area (fig. 1), such as the Ghost Dance, Abandoned Wash, and Pagany Wash Faults, that exhibit no surface evidence for Quaternary activity, as indicated by the mapping of Simonds and others (1995). These trenches were designed to provide additional information on possible Quaternary activity by excavating fault traces where they project beneath Quaternary deposits and surfaces.

A total of 25 trenches contain clear evidence for Quaternary activity on their respective faults in the form of surficial deposits that are displaced or deformed across the fault trace (table 1). The other trenches lack such evidence; either undisturbed deposits bury the fault zone, or, in some places, no fault is exposed in Quaternary deposits that overlie the fault zone as projected from nearby outcrops of bedrock, indicating no discernible Quaternary activity. These relations provide minimum constraints on the presence and (or) recency of displacements within such deposits on a particular fault.

The trenching operations were conducted in three phases that are tied to different elements of the Yucca Mountain site-characterization studies. During the first phase, a group of trenches were excavated in the early 1980s as part of reconnaissance studies of known faults. Most trenches were excavated by bulldozer, and generalized sketch logs were prepared and preliminary results reported by Swadley and others (1984). During the second phase, additional localized work was conducted in the middle to late 1980s at several sites, including trenches T14, CF2, and CF3 (fig. 2; Whitney and others, 1986; Taylor and Huckins, 1995). Existing trenches were modified, and some additional trenches were excavated by backhoe (table 1). Complete logs were compiled for selected trenches by using photogrammetric and standard-grid techniques. During the third phase, trenching investigations were resumed in 1992 when many existing trenches were modified, backhoes were used to excavate new trenches, and several natural exposures of faults were enhanced by extensive cleaning. Most of the trenches with demonstrable Quaternary faulting were subsequently logged by various techniques, including standard manual grid, theodolite, and photogrammetric. Most of the paleoseismic data and interpretations presented in this report were collected and developed during the third phase of trenching operations.

Trenches (fig. 2) were located on the basis of several criteria. Many trench sites were identified initially by a combination of ground reconnaissance and photointerpretative mapping on aerial photography. Where possible, a trench was located along a fault scarp or other geomorphic expression of a fault zone where evidence of Quaternary activity had been observed—generally where the fault trace crosses surficial deposits associated with such geomorphic surfaces as alluvial fans, fluvial terraces, sand ramps, or hillslope colluvial aprons. Commonly, a trench was located on a younger geomorphic surface so as to better record the most recent activity on a given fault. Trenches were located on older geomorphic surfaces to provide a record of earlier faulting for the purposes of long-term paleoseismic analyses, such as recurrence-interval calculations.

Some trenches were located across various types of lineament as mapped on aerial photographs where a fault crosses or projects beneath a Quaternary surface. Many such lineaments are subtle features defined by tonal contrasts or vegetation alignments. The purpose of these excavations was to determine whether mappable surface lineaments are related to tectonic features in the subsurface.

The dimensions and configurations of trenches range from 3 to 300 m in length, from 1.5 to 10 m in width, and from 2 to 10 m in depth. Most are 10 to 50 m long, 2 to 4 m wide, and 2.5 to 3 m deep. Orientations are mainly east-west, approximately perpendicular to the predominantly north-south strike of most faults. Bulldozer trenches generally have two vertical walls, whereas backhoe trenches commonly have one vertical wall on the south side opposite a benched wall on the north. The different configurations were determined by Occupational Safety and Health Administration regulations pertaining to trenches of a particular width. A benched configuration, for example, was used in 3-m-deep backhoe trenches because it removed the need for emplacement of shoring, which makes detailed logging more difficult. Generally, only vertical walls were logged because they are most amenable to accurate mapping and best preserve the geometric relations of stratigraphy and structure.

Methods

Logging of trenches and exposures after 1984 followed the same basic procedures. The walls were first cleaned to allow identification and mapping of fault deformation and the stratigraphy and soil relations of surficial deposits. Structures, stratigraphic contacts, and soil horizon boundaries were

identified and flagged, and the relative positions of flagged features were measured and plotted on trench logs, using one of the three techniques outlined below. Deformational features, stratigraphic units, and soils were mapped and described; and where possible, critical stratigraphic units and soils related to faulting events were sampled for geochronologic dating (see chap. 2).

Detailed logs were assembled from the mapped trench exposures according to one of three techniques:

1. The standard manual gridding technique uses a grid with a level line that is constructed on the trench wall (Hatheway and Leighton, 1979). Flagged features are measured relative to this reference grid and plotted to scale on graph paper.
2. The theodolite technique uses a theodolite to precisely survey the position of each flagged point on the trench wall. The surveyed points are plotted to scale, and then lines are drawn between the points to define the mapped structural, stratigraphic, and soil features.
3. The close-range photogrammetric technique uses a series of photographs of the trench walls that are taken with a prescribed amount of stereographic overlap (Fairer and others, 1989; Coe and others, 1991). The mapped features are drawn on these photographs in the field. The surveyed positions of control points in the photographs are then used to construct a rectified stereomodel, and an accurately scaled log is drawn with a stereoplotter.

The resulting logs and field data from trenches along a given fault were integrated to derive paleoseismic interpretations. Foremost among such interpretations are the stratigraphic positions, displacements, and ages of surface ruptures associated with paleoearthquakes on the fault zone (Schwartz, 1988; Nelson, 1992). Individual surface ruptures were identified in trench-wall exposures by using several criteria, including (1) abrupt increases in the amount of offset or backtilting of marker horizons or stratigraphic units across the fault; (2) recognition of buried deposits or features, such as scarp-derived colluvial wedges or debris-filled fissures, that commonly are associated with surface ruptures (Nelson, 1992); and (3) upward termination of fractures, fissures, or shears at the base of a stratigraphic unit. Commonly, uncertainties arise in identifying at least a few of the surface ruptures at a given trench site because of ambiguities and complexities in structural and stratigraphic interpretations.

Three measurements of fault displacements (individual, cumulative, and net cumulative) were used in the recording of faulting events. Where possible, individual dip-slip displacements associated with each faulting event were determined directly by measuring the displacement of marker horizons across the fault and then subtracting the offset related to any later events identified higher in the stratigraphic section. This procedure could not be used, however, if the same marker horizons are not present on opposite sides of the fault. At some trench sites, for example, upper Quaternary deposits on the hanging-wall block are faulted against older deposits or bedrock on the footwall block from which younger deposits have been stripped off by erosion. Several different methods were used in those situations. At some trench sites, single-event offsets were based on the thickness of fault-related colluvial wedges, resulting in minimum estimates that are commonly 50 to 80 percent of the actual surface displacement (Swan and others, 1980; Machette and others, 1992; Nelson, 1992). An alternative method involved measurement of the vertical separation between a displaced event horizon in the hanging-wall block and the stratigraphically highest, but older, faulted unit on the footwall block to determine the total offset. Displacements per event were then calculated by subtracting from this measurement the offsets related to individual faulting events that are identifiable at stratigraphically higher event horizons in the hanging-wall blocks. A similar technique used the stratigraphic thickness of deposits between successive event horizons on the hanging-wall block as a maximum estimate for the displacement associated with the stratigraphically lower event. The uncertainties inherent in all of these methods are accounted for in the range of reported displacements.

Cumulative dip-slip displacements were determined analogously either by measuring the total offset along the fault of a given marker horizon or stratigraphic unit or, where correlative units are absent across the fault, by summing the thicknesses of all fault-related colluvial wedges at and above the reference unit. Cumulative dip-slip displacements were adjusted in two ways to determine cumulative net-slip displacements: (1) normal-oblique slip was calculated for any trench site that contains possible slip indicators, such as slickenlines on bedrock shears that are related to Quaternary deformation, or, less reliably, striations on carbonate coatings within fault zones; and (2) at some trench sites, displacement of units that were deformed near the main fault zone, either by backtilting toward the fault surface and (or) by development of antithetic grabens, was measured and evaluated. The effects of this secondary deformation were removed by projecting displaced units into the fault zone from undeformed sections of the hanging wall and footwall before measuring displacements on the main fault zone. All measurement uncertainties are propagated through the derivations of both cumulative and net displacements.

Recurrence intervals—the time periods between successive surface-rupturing paleoearthquakes—were computed for each trench site by using all available dated deposits that could be related to faulting events. Individual recurrence intervals were determined where adequate age control exists to isolate the relative timing of pairs of successive faulting events. This procedure is most precise where the dated units are colluvial wedges or fissures that can be associated closely with faulting events, although such conditions are rare. More commonly, dated deposits were formed at some unknown time between successive faulting events and so simply bracket two or more events. For such events, average recurrence intervals were calculated by dividing the time between the age constraints by the number of possible intervals between events. Uncertainties in both the dating of stratigraphic units (reported as $\pm 2\sigma$ analytical-error limits) and the number of possible faulting events are incorporated into the reported ranges of recurrence intervals.

Fault-slip rates were calculated by dividing the cumulative net slip by the age of a specific faulted deposit or event horizon. Most slip rates are averages derived from the oldest faulted units with adequate age control, which typically are displaced by two or, commonly, three or more faulting events. The range of slip rates accounts for uncertainties in both age control and displacement.

Age controls for both faulted and unfaulted stratigraphic units and soils were provided by several techniques, as discussed in chapter 2. A general chronologic framework was provided by the composite Quaternary chronosequence of surficial deposits in the Yucca Mountain area from previous studies (Taylor, 1986; Hoover, 1989; Wesling and others, 1992; Lundstrom and others, 1993). Samples were collected from mapped lithologic units at all trench sites to provide direct geochronologic control for paleoseismic investigations at Yucca Mountain (Paces and others, 1994; J.B. Paces, written commun., 1995). The studies employ two basic dating techniques (1) U-Th-disequilibrium-series (U series) analyses of pedogenic carbonate-silica laminae and clast rinds, matrix soil carbonate, and rhizoliths (carbonate-replaced root casts); and (2) thermoluminescence analyses of fine-grained polymineralic material.

Trenches with No Quaternary Deformation

As noted previously, some trenches did not reveal evidence of Quaternary faulting (table 1). Typically, undisturbed stratigraphic units in those trenches overlie the fault trace in bedrock, or no fault is present in Quaternary deposits that are situated above the projection of the fault from adjacent outcrops. The absence of such evidence, however, still provides important information that helps delimit the extent and timing of Quaternary faulting activity. At some trench sites, for example, the presence of undeformed deposits constrains the lateral (along strike) extent of surface ruptures related to Quaternary activity elsewhere on a particular fault. The absence of evidence for faulting may also provide information on the presence and degree of activity on subsidiary strands of potentially wide and complex fault zones. Commonly, the trenches furnish minimum age constraints on the most recent fault displacements, as determined by the ages of the oldest undisturbed Quaternary deposits. A few trenches lack evidence of Quaternary deformation because they are not properly located on the fault trace. Some of the more important individual trenches that did not intersect Quaternary faults are summarized below.

Paintbrush Canyon Fault

Two trenches at the north end of Alice Ridge near Yucca Wash (fig. 2) expose no fault zone or show no evidence of Quaternary deformation in fluvial-terrace deposits. A Quaternary surface rupture on a distinct shear zone of the Paintbrush Canyon Fault is present only in trench A1 at this site. One of the trenches without faults, A2, was excavated across upper Pleistocene terrace gravel (unit Qa3; see chap. 2; fig. 3; tables 2, 3) on the southward projection of the fault trace from a bedrock outcrop to the north (Swadley and others, 1984). This relation indicates either that the fault does not cut material of that age or that the fault trace lies farther east and was not intersected by the trench. Surface rupture possibly did not extend northward from the nearby trench A1 to the south. The other trench, MWV–T3 (not shown in fig. 2), was excavated on a vegetation lineament formed in middle Pleistocene terrace deposits (unit Qa1) west of the main trace of the fault exposed in trench A1. The absence of a fault in trench MWV–T3 indicates that the zone of Quaternary surface rupture is narrow and that the fault is exposed to the east only in trench A1 at the base of Alice Ridge.

Faulting is also absent in two trenches excavated in middle to upper Pleistocene sand-ramp deposits in a saddle at the base of Fran Ridge (fig. 2; Swadley and others, 1984). The north end of the southern section of the Paintbrush Canyon Fault zone was mapped through this area (Simonds and others, 1995). No fault was intersected in trench T16, probably because the trench is located west of the main fault trace. Trench T16B, which contains only carbonate-coated fractures, may not have been excavated deep enough to expose the main fault trace. Alternatively, the zone of Quaternary surface rupture may not have continued this far northward on the southern section of the fault.

Bow Ridge Fault

Trench A/BR–3 (figs. 2, 8) was located on a vegetation lineament in the upper Pleistocene alluvial fan that lies on the northward projection of the Bow Ridge Fault from the complex of trenches (T14, T14A–T14D) on the west side of Exile Hill. The absence of faulting or Quaternary deformation is present in the fan gravel exposed in the trench indicates that either the subsurface fault trace lies west of the trench or surface rupture on the fault probably did not continue northward of Exile Hill.

The Bow Ridge Fault is exposed only in bedrock in two shallow trenches (trenches T14A, T14B, fig. 2) north of trench T14 at the base of Exile Hill. Another trench (trench T15; see Swadley and others, 1984) at the base of Bow Ridge on the southern section of the fault zone and online with a nearly 2-m-high bedrock scarp likewise did not expose Quaternary deposits.

Exile Hill Fault

The Exile Hill Fault displaces buried bedrock at the base of the eastern margin of Exile Hill at the west edge of Midway Valley (figs. 1, 2; see chap. 4). Trenches MWV–T5, MWV–T6, and MWV–T7 (fig. 2) reveal that an overlying thin veneer

of mostly upper Pleistocene colluvium (units Qa3, Qa4; see chap. 2) is fractured locally but not displaced along the fault. Those relations, which were established during highly detailed logging of the trenches, resulted in placing a minimum age constraint for the most recent surface rupture on the Exile Hill Fault. Determining a minimum date for this faulting event is important for the placement and design of surface facilities at the proposed repository site.

Ghost Dance Fault

The Ghost Dance Fault is a down-to-the-west bedrock normal fault that trends north along the east side of the proposed repository block for about 7 km (figs. 2, 4; Day and others, 1998a). Thus, this fault has been the subject of extensive investigations to determine whether any Quaternary surface displacements occurred along its trace. As described in chapter 6, the fault is well exposed in Tertiary volcanic rocks, but no Quaternary activity is indicated in the intersecting trenches.

Abandoned Wash Fault

The Abandoned Wash Fault (fig. 2) is a north-striking fault that may represent a southwestern splay of the Ghost Dance Fault (Day and others, 1998b). For much of its length, the Abandoned Wash Fault occupies a narrow valley floored with uppermost Pleistocene to Holocene alluvium. These deposits are tectonically undisturbed in trench T6 (Swadley and others, 1984), which lies along the projection of the fault across the valley floor. Similar undisturbed alluvial and colluvial deposits are exposed in trench T9, which is located in a small valley north of the canyon containing trench T6 (Swadley and others, 1984); however, trench T9 may not be properly located to intersect the fault (Simonds and others, 1995).

Drill Hole Wash, Pagany Wash, and Sever Wash Faults

The Drill Hole Wash, Pagany Wash, and Sever Wash Faults (fig. 2) strike northwest at the northeast corner of Yucca Mountain (fig. 1) and for much of their lengths occupy similarly trending valleys (Day and others, 1998a). The Drill Hole Wash Fault is almost entirely concealed by alluvial deposits, although strands are exposed for short distances in bedrock. Trench T2 is located in the southern arm of the wash but was sited to intersect a north-trending splay of the Ghost Dance Fault rather than the Drill Hole Wash Fault farther north. The Pagany Wash Fault is well exposed in bedrock in trench T12, which is located where the fault transects a broad ridgecrest (Swadley and others, 1984). Thin colluvial deposits with argillic and calcic soil horizons indicative of at least a late Pleistocene age overlie the fault trace with no displacement. Thus, evidence for late Quaternary activity on the Pagany Wash Fault was not observed. Trench T11 was excavated in upper Pleistocene to Holocene alluvium and colluvium on a strand of the Sever Wash Fault as projected southeastward from bedrock outcrops into the alluvium-floored valley bottom of Yucca Wash (Swadley and others, 1984). No fault or evidence of any Quaternary deformation was observed in the trench, although it may not be located accurately above the poorly constrained surface projection of the fault.

Stagecoach Road Fault

Trench SCR–T2 (fig. 2) was excavated across a subtle topographic break and tonal photolineament located a short distance east of the Stagecoach Road Fault trace. No Quaternary faults are evident in the lower to middle Pleistocene surficial deposits exposed in the trench; thus, the features observed at the surface before trenching are nontectonic. This absence of fault deformation in trench SCR–T2 indicates that Quaternary activity on the Stagecoach Road Fault was restricted to the main fault zone, which was intersected in trench SCR–T1 to the west (see chap. 5).

Solitario Canyon Fault

Trench T13 (fig. 2) is located toward the north end of the Solitario Canyon Fault along a northward projection of the fault trace in bedrock beneath the alluvium of Yucca Wash (Swadley and others, 1984). No fault or evidence of any Quaternary deformation was observed in the upper Pleistocene and Holocene deposits exposed in the trench. Either the trench missed the fault trace, or the late Quaternary surface rupture that is evident along the Solitario Canyon Fault farther south (see chap. 7) probably did not continue so far northward.

Trenches T10A and T10B (fig. 2) were excavated across an eastern splay of the fault within Solitario Canyon (Swadley and others, 1984). No fault is evident in the lower to middle Pleistocene alluvium and colluvium exposed in trench T10A. Either the trench may not have been properly located with respect to the fault zone, or no Quaternary deformation has occurred on that splay of the fault. Improper location seems the more likely explanation because similar deposits are displaced by a fault zone in trench T10B, which is located on the same splay. Upper Pleistocene and Holocene deposits are not tectonically disturbed in either trench, indicating that no late Quaternary activity has occurred on the eastern strand of the fault. Late Pleistocene surface ruptures, however, are observed in trench SCF–T4 (fig. 2), which is located on another fault strand to the east.

Northern Crater Flat Fault

Trench CFF–T2 (fig. 2) was excavated across a weakly defined photolineament on a middle Pleistocene to upper Pleistocene alluvial fan that extends across the projected trace

of the Northern Crater Flat Fault between bedrock outcrops to the south and north. The lineament is the only apparent expression of the fault zone on the alluvial-fan surface. No fault or evidence of Quaternary deformation was observed in the upper Pleistocene alluvium exposed in the trench, although a fault with late Quaternary displacements is evident in older Pleistocene alluvium in trench CFF–T2A several kilometers to the north (see chap. 11). Absence of faulting in trench CFF–T2 indicates either that (1) a gap exists in surface displacements in the vicinity of the fan, (2) surface rupture terminates between the two trenches, or (3) no faulting event has occurred since the accumulation of Quaternary deposits at the trench site.

Chapter 2

Quaternary Stratigraphy and Mapping in the Yucca Mountain Area

By John W. Whitney, Emily M. Taylor, and John R. Wesling[1]

Contents

Abstract....11
Introduction....11
Quaternary Deposits, Soils, and Geomorphic Surfaces....14
Alluvial Deposits and Geomorphic Surfaces....14
Unit QT0....16
Unit Qa1....17
Unit Qa2....18
Unit Qa3....18
Unit Qa4....18
Unit Qa5....19
Unit Qa6....19
Unit Qa7....19
Colluvial Deposits....19
Middle Pleistocene to Holocene Undifferentiated Colluvium (Unit Qu)....20
Eolian Deposits....20
Middle Pleistocene to Holocene Eolian-Colluvial Deposits (Unit Qea)....20
Eolian Accumulations on Geomorphic Surfaces....20
Summary....21

Abstract

Stratigraphic studies and mapping of near-surface deposits, soils, and geomorphic surfaces provide essential data for determining the history of Quaternary faulting at Yucca Mountain. Eight surficial units, ranging in age from Pliocene(?) to Holocene, have been differentiated largely on the basis of relative stratigraphic and geomorphic position, lithology, soil-profile development, degree of desert-pavement development, amount and degree of desert-varnish accumulation, and degree of preservation of original bar-and-swale topography. Some deposits were dated by U-series analysis of pedogenic material and by thermoluminescence analysis of silt-size fractions of eolian and fluvial deposits. The presence of basaltic ash in fissure fills associated with fault zones aided in establishing the probable age of one of the major Quaternary surface-rupturing events; the ash is correlated with the eruption of the nearby Lathrop Wells volcanic center at 77±6 ka.

Deposits associated with geomorphic surfaces, including mostly alluvium and colluvium containing minor amounts of eolian and debris-flow deposits, make up the bulk of the surficial materials in the Yucca Mountain area. Descriptions of soil profiles and other distinguishing characteristics of the eight Quaternary map units were defined partly on the basis of natural exposures and partly on the basis of sequences exposed in trenches that were excavated to intersect and expose several of the major faults. The integration of stratigraphic, geomorphic, and numerical age data serves as a primary means for dating Quaternary fault activity at Yucca Mountain.

Introduction

Detailed studies and mapping of Quaternary stratigraphic sequences in the Yucca Mountain area (fig. 1) were conducted to determine the characteristics, relative ages, and distribution of the near-surface deposits, soils, and geomorphic surfaces that can be used to assess the history of Quaternary faulting in and near the proposed repository site for the storage of high-level radioactive wastes. An alluvial geomorphic surface (see Bull and Ku, 1975; Bull, 1991) is analogous to the top of an allostratigraphic unit, which is a mappable stratiform body defined and delineated on the basis of its bounding discontinuities (North American Commission on Stratigraphic Nomenclature, 1983). Primary characteristics used to date the map units include relative stratigraphic and geomorphic position, lithology, soil-profile development, degree of desert-pavement development, amount and degree of desert-varnish accumulation, and preservation of original bar-and-swale topography.

Surficial mapping of Quaternary deposits in the Yucca Mountain area has been progressively refined over the years (table 2). Early work in and near the Nevada Test Site (Yucca Mountain is at the west edge of the site) differentiated three

[1]Geomatrix Consultants, Inc., Oakland, Calif.

Table 2. Comparison of surficial deposits in the Yucca Mountain area, southwestern Nevada, with local and regional surficial stratigraphic sequences.

[Numbers in parentheses, ages in thousands of years]

Yucca Mountain (this report)	Yucca Wash, Nev. (Swadley and others, 1984; Taylor, 1986)	Crater Flat, Nev. (Peterson and others, 1995)	Kyle Canyon fan, Nev. (Reheis and others, 1992)	Fish Lake Valley, Nev.-Calif. (Harden and others, 1991; Slate, 1991)	East-central Mojave Desert, Calif. (Reheis and others, 1989; Wells and others, 1990)	Lower Colorado River, Calif.-Ariz. (Bull and Ku, 1975; Bull, 1991)
Qa7 (historical)	Q1b (0–15)	Modern (0)	Q4 (0)	Modern	Modern (0)	Q4b (0)
Qa6 (middle to late Holocene)	Q1b (0–15)	Crater Flat (<0.3–>1.3)	– – –	Late Marble Creek (0.1–1)	Q3b3 (0.5–2.5)	Q4a (0.1–2)
– – –	– – –	– – –	– – –	Middle Marble Creek (1–6)	Q3b2 (2.0–4.5)	Q3c (2–4)
– – –	– – –	– – –	– – –	Early Marble Creek (2–5.8)	– – –	Q3b (4–8)
Qa5 (latest Pleistocene to early Holocene)	Q1c (7–30)	Little Cones (>6–>11)	Q3 (15, 4–80)	Leidy Creek (6–11)	Q3b1 (6–11)	Q3a (8–12)
Qa4 (late Pleistocene)	Q2b (145–290)	Late Black Cone (>17–>30)	Q3 (15, 4–80)	Late Indian Creek (>50–<700)	Q3a (13–50)	Q2c (12–70)
Qa3 (middle? to late Pleistocene)	Q2c (270–440)	Early Black Cone (>159–>201)	Q2 (130, 18–750)	Early Indian Creek (>50–<700)	Q2b (110–130)	Q2b (70–200)
					Q2a (140–190)	– – –
Qa2 (middle Pleistocene)	QTa (900–2,000)	Yucca (>375)	– – –	Late Trail Canyon(?) (<700 [middle Pleistocene])	Q1b (>400–>650)	Q2a (400–730)
Qa1 (early to middle Pleistocene)	QTa (900–2,000)	Solitario (>433–>659 but <730)	Q1 (800, 750–800)	Early Trail Canyon (<700 [early Pleistocene])	Q1b (>400–>650)	Q2a (400–730)
QT0 (Pliocene? to early Pleistocene?)	– – –	– – –	– – –	– – –	Q1 (>650–>800)	Q1 (>1,200)

major upper Cenozoic stratigraphic units by using "correlation characteristics" (Hoover and Morrison, 1980; Hoover and others, 1981; Swadley and others, 1984; Hoover, 1989). The concept of correlation characteristics utilizes physical and morphologic features of landscape elements, including landforms, drainage network, soils (presence or absence of Av horizon), topographic position, desert pavement, desert varnish, depositional environment, and lithology. According to Swadley and others (1984), the oldest surficial deposits (unit QTa) in the Yucca Mountain area (fig. 1) are early Pleistocene and Pliocene(?), on the basis of an underlying deposit dated at about 2 Ma and an overlying deposit containing ash correlated with the Bishop ash, which was then dated at 740 ka but more recently at 760 ka (Sarna-Wojcicki, 1993). Units Q2 and Q1 of Swadley and others (1984) represent middle to upper Pleistocene and Holocene deposits, respectively (table 2). Each of the major geologic units of Hoover and others (1981) is divided into several subunits. A total of 10 subunits of units Q1 and Q2 and, possibly, 3 additional subunits of uncertain age that may belong to unit Q2 (Hoover and others, 1981) have been mapped in and near the Nevada Test Site. Swadley and others (1984) mapped the major upper Cenozoic stratigraphic units in Midway Valley, which adjoins Yucca Mountain to the east (fig. 2), but no detailed surficial geologic mapping that subdivided those units had been published for the Midway Valley area until Taylor (1986) mapped the fluvial-terrace sequence along Yucca and Fortymile Washes, as well as in a small area in northernmost Midway Valley.

Table 3. Summary of diagnostic surface and soil characteristics of Quaternary map units in the Yucca Mountain area, southwestern Nevada.

[See Wesling and others (1992) for definitions of surface characteristics. Desert pavement, relative degree of interlocking of surface clasts, based on a qualitative estimate. Desert varnish: first number, average varnish cover (in percent, ±1σ); second number, abundance of varnished clasts (in percent) (Wesling and others, 1992). Rubification, abundance of rubified clasts (in percent) (Wesling and others, 1992). Depositional-bar relief, relative height of depositional bars from top of bar to trough of adjacent swale. Horizon sequence, sequence of soil horizons that is representative of each map unit: A, surface soil horizon characterized by accumulation of organic matter, typically as a zone of illuviation of clay, sesquioxides, silica, gypsum, carbonate, and (or) salts; B, subsurface soil horizon characterized by reddening, stronger development, and (or) accumulation of secondary illuvial materials (clay, sesquioxides, silica, gypsum, and salts); C, subsurface soil horizon that may appear similar or dissimilar to parent material and that includes unaltered material and material in various stages of weathering; K, subsurface soil horizon engulfed with carbonate to the extent that its morphology is determined by the carbonate. Master-horizon modifiers: j, used in conjunction with other modifiers to denote incipient development of that particular soil characteristic; k, carbonate accumulation; m, strong cementation; q, silica accumulation; t, clay accumulation; u, undifferentiated; v, vesicularity; w, color or structural B soil horizon. Structure: 1, weak; 2, moderate; 3, strong; f, fine grained; m, medium grained; pl, platy; sbk, subangular blocky; sg, single grained; vf, very fine grained. Clay films: 1, few; 2, common; 3, many; co, colloidal stains; mk, moderately thick; n, thin; pf, ped face. Maximum reddening, hue determined with Munsell Soil Color Charts (Munsell Color Co., Inc., 1988). $CaCO_3$ stage morphology from Gile and others (1966) and Birkeland (1984). Do., ditto; n.p., not present]

Unit (table 2)	Surface characteristics				Soil characteristics				
	Desert pavement	Desert varnish	Rubification	Depositional-bar relief	Horizon sequence	Structure	Clay films	Maximum reddening	Maximum $CaCO_3$ stage morphology
Qa7	None	1±2 12	4	High, unaltered---	Cu	sg	n.p..	10YR	n.p.
Qa6	None	0±0 0	0	do----------	A-Ck	sg	n.p.	10YR	n.p.
Qa5	Weak to moderate--	1±1 28	33	Moderately high, slightly altered.	A-Bwk/ Btjk-Bk-Ck	1 vf-f sbk	n.p.-1 n co	10YR	I
Qa4	Moderate to strong--	62±27 97	87	Low----------	Av-Btkq-Bkq-Ck	2–3 f-m sbk	3 n-mk pf	7.5YR	I–II
Qa3	Strong----------	43±28 94	54	do----------	Av-BA-Btkq-Kq/ Bkq-Ck	3 m sbk	3 n-mk pf	7.5YR	II+–III
Qa2	Strong----------	80 (est.) 100 (est.)	100 (est.)	do----------	Av-Btq-Btkq-Kq-Bkq-Ck	3 m sbk	3 mk pf	7.5–5YR	IV
Qa1	Locally strong-------	20±21 84	80	None----------	Av-BA-Btkq-Kqm-Bkq-Ck	m-3 m pl	2 n pf	10–7.5YR	IV
QT0	Degraded----------	Eroded----------							

Taylor (1986) mapped six surficial deposits along Yucca and Fortymile Washes (fig. 2). Geologic units were differentiated and pedogenic soil profiles described to assess the influence of time and climate on soil development and to quantify the variation in past Quaternary climates on the basis of the degree of calcic-horizon development. Map units were assigned on the basis of an inferred correlation with the stratigraphic and numerical ages of Hoover and others (1981), Szabo and others (1981), and Swadley and Hoover (1983). Taylor demonstrated that the soil morphology and the progressive accumulation of secondary carbonate, clay, and silica correlate with age. Ca carbonate, Ca-Mg carbonate, and other carbonate species in soils were not distinguished. In this report, the term "carbonate" is used to refer to all pedogenic carbonate species, and the term "silica" to all pedogenic silica species, which Taylor (1986) showed to be predominately opal-CT. Taylor's work clearly demonstrated the usefulness of soils for stratigraphic correlation and for estimating the relative ages of surficial deposits in the Yucca Mountain area.

Wesling and others (1992) mapped the surficial geology of Midway Valley at a scale of 1:6,000, and S.C. Lundstrom (written commun., 1995) mapped the surficial geology of the eastern and southern Yucca Mountain area at a scale of 1:12,000. Those studies delineated eight informal alluvial geomorphic surfaces (QT0 through Qa7, table 2), as well as colluvial and eolian deposits, that represent the general Quaternary stratigraphic sequence now recognized in the Yucca Mountain area (col. 1, table 2).

Six major allostratigraphic units were delineated by Faulds and others (1994) and Peterson and others (1995) in Crater Flat, west of Yucca Mountain (figs. 1, 2). The stratigraphic framework thus established (col. 3, table 2) was applied for correlative purposes in studies of the surficial deposits and trench exposures along the Bare Mountain Fault on the west side of Crater Flat (see chap. 12).

Quaternary Deposits, Soils, and Geomorphic Surfaces

Quaternary deposits in the Yucca Mountain area include (1) alluvium that underlies alluvial-fan and fluvial-terrace surfaces and was deposited along active washes, (2) colluvial and debris-flow deposits present along the base and lower parts of the hillslopes bounding the valleys, (3) areas of mixed bedrock and thin colluvium in midslope and hilltop areas, and (4) eolian deposits. The informal allostratigraphic units exhibit surface properties that reflect variations among soil development, eolian deposition, clast weathering, desert-varnish accumulation, biologic activity, and progressive erosional instability that largely reflect their relative ages (table 3). The younger deposits (units Qa5–Qa7, table 2) exhibit relatively unaltered original-surface characteristics, including incipient to weak soil development, little to no desert-varnish accumulation or desert-pavement development, relatively unaltered bar-and-swale relief, and minimal eolian accumulations in the upper horizons of soil profiles. The older deposits (units Qa2–Qa4) have more strongly developed desert pavement, more continuously and darkly varnished clasts, greatly reduced bar-and-swale relief, strongly developed soils, and relatively thick accumulations of silt and fine sand in the upper parts of soil profiles. The oldest deposits (units QT0, Qa1) have degraded surface characteristics and soil profiles, reflecting erosional modification of geomorphic surfaces.

Soil profiles provide important supplementary information for reconstructing Quaternary history because the individual soil layers (or "horizons," the term used by soil specialists for both the soil layer and its component parts) represent time periods when the land surface was subjected to such soil-forming processes as physical weathering, infiltration and precipitation of secondary carbonate, and accumulation of eolian materials. Such factors as the composition of the parent material, climate, plant life, topographic relief, and time all affect soil development; the time factor is of principal interest with respect to the fault studies presented in this report. Given enough time, soils in the Yucca Mountain area developed with characteristics distinctive enough to locally form "marker" beds or horizons that can be mapped in trench exposures and have been used to help determine the timing and magnitude of Quaternary fault displacements. The chief value of well-developed soil horizons is that their secondary accumulation of mineral components can provide age data and be used as criteria for the relative dating of the host deposits. Although numerical age data are sparse, a well developed soil in the Yucca Mountain area is considered to represent a period of tens of thousands of years—evidence that, if that soil is subsequently displaced, can be used to date a faulting event.

The mapping of soil horizons is independent of the mapping of lithostratigraphic units in the same trench exposure. Soils form not only on undisturbed deposits, but also on erosional surfaces that may crosscut such deposits; thus, soils may be conformable or nonconformable horizons within a trench section. Furthermore, soils are formed within (or "on," as expressed by soil specialists) the host depositional sequence as physical and chemical processes alter the primary characteristics of that sequence. Subsequent accumulations of alluvial, colluvial, and eolian deposits can erode into or bury older soils and sedimentary sequences. Thus, soil profiles are typically described separately from stratigraphic sequences, as noted on many of the trench logs and tables presented in various chapters of this report.

Alluvial Deposits and Geomorphic Surfaces

Alluvial geomorphic surfaces are the dominant Quaternary landforms in the Yucca Mountain area (fig. 1). The materials associated with those surfaces include alluvium and minor eolian and debris-flow deposits. Sedimentologic properties of the various alluvial deposits are similar. In general, the fluvial deposits consist predominately of sandy gravel, with interbedded gravelly sand and sand. The fluvial facies include relatively coarse grained channel bars and intervening finer grained swales. The texture of materials in the bars and swales depends on their position within the landscape (proximal- or distal-fan region) and on sediment source. In the proximal-fan region, grain size is greater where coarser sediment is available for transport and where streamflow is concentrated; in the distal-fan region, grain size is smaller, although coarser grained facies are present locally. Gravel size ranges from pebble to boulder, and clasts generally are subangular to subrounded.

In test-pit and streamcut exposures of units Qa5 through Qa7 (table 2), the cross-sectional bar-and-swale characteristics are so well preserved that the facies changes between the bars and swales are readily distinguishable. The materials associated with bars include non-indurated, cobble-boulder gravel and finer grained sand and gravel; the materials associated with swales include a finer grained, silt-rich, sandy gravel and gravelly sand. The boulder-gravel deposits associated with the bars typically are about 0.5 m thick. Unweathered deposits are light gray (10YR 7/2 d; Munsell Color Co. Inc., 1992), poorly to moderately well sorted, well bedded to massive, and clast to matrix supported. Rodent burrows are ubiquitous in units Qa5 and Qa6, likely reflecting the ease of excavation. Unit Qa5 and younger deposits are relatively loose and do not hold a well-formed free face when excavated. In test-pit and streamcut exposures, buried soils are commonly observed

in intervals less than 2 to 3 m thick. The buried soils may be older stratigraphic units, or they may represent a hiatus in the aggradational sequence of a single depositional unit. Where they represent a hiatus, the surface-soil characteristics reflect variations in the length of exposure.

Debris-flow deposits, observed locally in outcrops, test pits, and trenches, are matrix supported and range in textures from silt to cobbles; the gravel fraction composes approximately 15 to 30 volume percent of the deposit. The debris-flow deposits are massive and relatively hard.

Although the relative ages of the deposits, soils, and geomorphic surfaces around Yucca Mountain are well established on the basis of distinctive surface properties and soil-profile characteristics, as discussed above, only limited direct numerical-age control is available. Establishing a reliable temporal framework is difficult because of the uncertainties involved in dating complex geomorphic and pedogenic systems in an arid environment. The difficulties are further compounded by a general lack of suitable materials for dating and by variation in the ages of individual deposits not only from top to bottom but also laterally, owing to their time-transgressive nature. The two primary dating techniques used in the paleoseismic studies presented in the various chapters of this report are (1) U-Th-disequilibrium series (U series) analysis of carbonate- and silica-rich materials in soils and (2) thermoluminescence analysis of the silt-size fraction of eolian and fluvial deposits. These two techniques, which have been widely applied in recent years, are considered to provide the most reliable ages for investigating the Quaternary stratigraphy and structure of the Yucca Mountain area.

Earlier studies of surficial deposits (for example, Swadley and others, 1984; Rosholt and others, 1985) depended on dating by U-trend analysis, the results of which have since been considered to be highly unreliable (J.B. Paces, written commun., 1995). For the stratigraphic and fault studies presented in various chapters of this report, the only U-trend dates cited are those from trench T14 on the Bow Ridge Fault (fig. 2; see chap. 5; table 9) and from trench CF3 on the Windy Wash Fault (see chap. 9, table 27). In neither trench have such ages been used to date paleoearthquakes, but they are merely cited as previously published information.

We emphasize that most of the samples collected and analyzed for age determinations were obtained from trenches that were located mainly to expose fault relations, rather than specifically for optimum study of surficial sequences and depositional processes, thus hindering to some degree a more systematic approach to establishing a complete, age-constrained stratigraphic framework.

For the present study, the numerical ages of the various surficial deposits (units QT0 through Qa7, table 2) that compose the Quaternary sequence at Yucca Mountain are based primarily on samples collected from units Qa2 through Qa5 as defined and mapped in the Midway Valley and Fortymile Wash areas (fig. 2; Wesling and others, 1992; S.C. Lundstrom, written commun., 1995). The ages of units Qa2 through Qa5 as determined by U-series and thermoluminescence analyses are listed in table 4, and the data are plotted in figure 3, which shows probability-density functions (PDFs) for the ages of these mapped surficial deposits as determined by S.K. Pezzopane (written commun., 2000). Each PDF is constructed from the sum of normal-distribution functions (not shown) that represent the sample age and laboratory errors, normalized by the number of ages (N, above each PDF) from each stratigraphic unit (Qa2–Qa5 beneath each PDF). The normal-distribution function for each age is based on the mean and a 3σ error, which is spread about the mean out to ± 3 times the 2σ (95-percent confidence) errors, as reported by J.B. Paces and S.A. Mahan (written commun., 1995). The relative scale for each PDF is expressed as relative probability (in percent) per thousand years. The median age (number beside bar) and the $\pm 2\sigma$ (numbers at limits of shaded areas) age ranges for the units are derived from the cumulative distribution functions (not shown) summed from each PDF. A few obvious outlier data were eliminated, such that each shaded area represents the principal age distribution based on a subset number (n) of dates. The data show that for units Qa2, Qa4, and Qa5, a distinct clustering of dates is noticeable within relatively narrow segments of the age ranges (shaded areas on each PDF, fig. 3), which are interpreted to best represent the main periods of deposition and (or) soil development for those units. Ages outside these ranges (unshaded areas) could be caused by miscorrelation of the sampled deposits, or they may, in fact, represent valid extensions of the age boundaries, thus indicating that absolute temporal boundaries cannot be established between successive units. For unit Qa3, for example, at least two depositional episodes may be included within the whole unit.

On the basis of the data discussed above, the preferred ages of the dated surficial deposits are as follows: unit Qa2, 380+350/−110 ka (middle Pleistocene); unit Qa3, 86+40/−16 ka (older subunit) and 51+12/−17 ka (younger subunit) (middle? to late Pleistocene); unit Qa4, 27±10 ka (late Pleistocene); and unit Qa5, 7+10/−5 ka (latest Pleistocene to early Holocene). Evidence indicates that unit Qa1 is associated with a period of deposition as early as the Bishop ash (760 ka; Sarna-Wojcicki and others, 1993), and so the unit is dated at possibly early to middle Pleistocene. The underlying unit QT0 is assumed to be older than 760 ka, possibly as old as Pliocene. Units Qa6 and Qa7 are presumed to be younger than 7 ka; unit Qa6 is dated at middle to late Holocene, and unit Qa7 is the deposit presently accumulating along modern streamcourses.

Numerous samples were collected from the surficial deposits exposed in trenches for numerical-age determinations that can be used to estimate the timing of Quaternary depositional and deformational events along or near the 11 major faults (or fault systems) discussed in the various chapters of this report. Such numerical-age determinations are listed in the tables in each chapter. In some fault studies, the presence of basaltic ash in fault zones that correlate with an eruption of the nearby Lathrop Wells volcanic center (fig. 1), which is dated at 77±6 ka (Heizler and others, 1999), aided in reconstructing the timing of Quaternary deformation.

Table 4. Numerical ages of samples collected from Quaternary deposits (units Qa2–Qa5, table 2) in Midway Valley and Fortymile Wash in the Yucca Mountain area, southwestern Nevada.

[See figures 1 and 2 for locations. Samples: TL– (error limits, ±2σ), thermoluminescence analyses by S.A. Mahan; HD (error limits, ±2σ), U-series analyses by J.B. Paces]

Unit (table 2)	Sample	Material sampled	Age (ka)
Qa5	TL–08	Sand and silt	12±2
	TL–13, TL–14	Eolian sand	7±1, 8±1
	TL–41	Sandy lens	4±0.4
	TL–42	Gravelly alluvium	7±1
	TL–50	Bt soil horizon	26±2
	TL–51	do	4±3, 5±1
	TL–52	do	4±1
	TL–76	do	13±2
	TL–79	Silt and sand	7±1
	TL–80	do	6±0.5
	HD 2138	Clast rind	7±6, 9±1, 9±1
	HD 1637	Gravelly alluvium	7±5, 7±6
Qa4	TL–01	Av soil horizon	27±5
	TL–50	Bt soil horizon	26±2
	HD 2123	Clast rind in K soil horizon	21±3, 23±2, 25±6, 36±1
	HD 2124	do	27±2, 30±2, 31±3
Qa3	TL–48	Bt soil horizon	27±3
	TL–78	Silt and sand	55±7
	HD 972	Colluvium, platy K soil horizon	41±8
	HD 1375	Clast rind in K soil horizon	45±2, 49±3, 51±7, 53±2
	HD 1916	Ck soil horizon	27±3, 30±8, 74±3
	HD 2136	Clast rind in K soil horizon	49±3, 53±2, 60±3
	HD 2137	K soil horizon	75±1, 78±1, 85±5
	TL–47	Sand below K soil horizon	103±17
	HD 1740	2Btb soil horizon	90±7, 93±4, 101±21, 108±8
	HD 1741	K soil horizon	152±8, 169±5, 170±3
Qa2	TL–77	Silt and sand	104±44
	HD 2134	K soil horizon	411±63
	HD 2135	do	305±21, 347±16, 449±53, 567±147

General descriptions of the eight identified surficial deposits and associated soil profiles, as well as additional discussions of their assigned ages, are given below, in ascending order.

Unit QT0

Unit QT0 (table 2) consists of a single terrace remnant on the upthrown block of the Paintbrush Canyon Fault at the north end of Alice Ridge (fig. 2). The surface forms a pronounced topographic bench (elev 1,168 m) that is 25 m higher than unit Qa1 and 46 m above the active channel of Yucca Wash. Deposits associated with unit QT0 consist of lag gravel on a bedrock surface eroded into the 12.7-Ma Tiva Canyon Tuff (Sawyer and others, 1994). Clast types that include the rhyolites of Fortymile Wash are sufficiently abundant and distinct to indicate that the clasts are exotic to Alice Ridge. Because of its limited areal extent and the extensive postdepositional erosion of surficial materials, no detailed soil data were collected from the unit QT0 surface (table 3). An unusual characteristic of the deposit is that the cemented matrix commonly is more resistant to erosion than the clasts. The thickness of the unit is unknown but is probably only a few meters. The possibly Tertiary to early Quaternary age of unit QT0 is based not only on its stratigraphic position relative to unit Qa1 but also on its highly dissected and eroded surface and its rounded landform morphology.

Unit Qa1

Unit Qa1 (table 2) is preserved at the surface on the Yucca Wash alluvial fan north of Sever Wash in Midway Valley (fig. 2); the fan surface has been dissected by younger drainages and is preserved as slightly rounded interfluves. Unit Qa1 also is mapped on the west flank of Yucca Mountain and in northeastern Crater Flat. Locally, the desert pavement associated with the unit Qa1 surface is well developed, but in most areas it has been extensively degraded (table 3). Several characteristics, including freshly exposed rock surfaces on clasts, fragments of secondary carbonate and silica platelets, and surface or near-surface calcic horizons, collectively impart a light tonal quality to the unit as viewed in the field or on aerial photographs. Although darkly varnished clasts are present in some areas, surface clasts typically are not darkly varnished. No original depositional bar-and-swale morphology is preserved on the unit Qa1 surface, and larger clasts appear to be distributed randomly rather than concentrated in areas that define depositional bars. Angular unvarnished rock fragments are common on the surface, where larger varnished clasts have spalled, exposing fresh rock surfaces. Many clasts are fractured and strongly weathered. A buried soil was observed beneath unit Qa1 at 2.5-m-depth in one test pit, but no buried soils were exposed more than 3.3 m deep in other test pits.

The strongly developed Qa1 soil is more than 1.5 to 2.0 m thick and has a laminar petrocalcic horizon (Kqm) with $CaCO_3$ stage IV morphology at or near the surface (table 3). The petrocalcic horizon locally is overlain by as much as 30 cm of fine-grained eolian sand and silt. Soil development on the eolian deposits is characterized by brown to red (10–7.5YR) Bkq and Btkq horizons with a strong, medium-subangular blocky structure and continuous, moderately thick clay films. The soil developed in the overlying eolian sand and silt

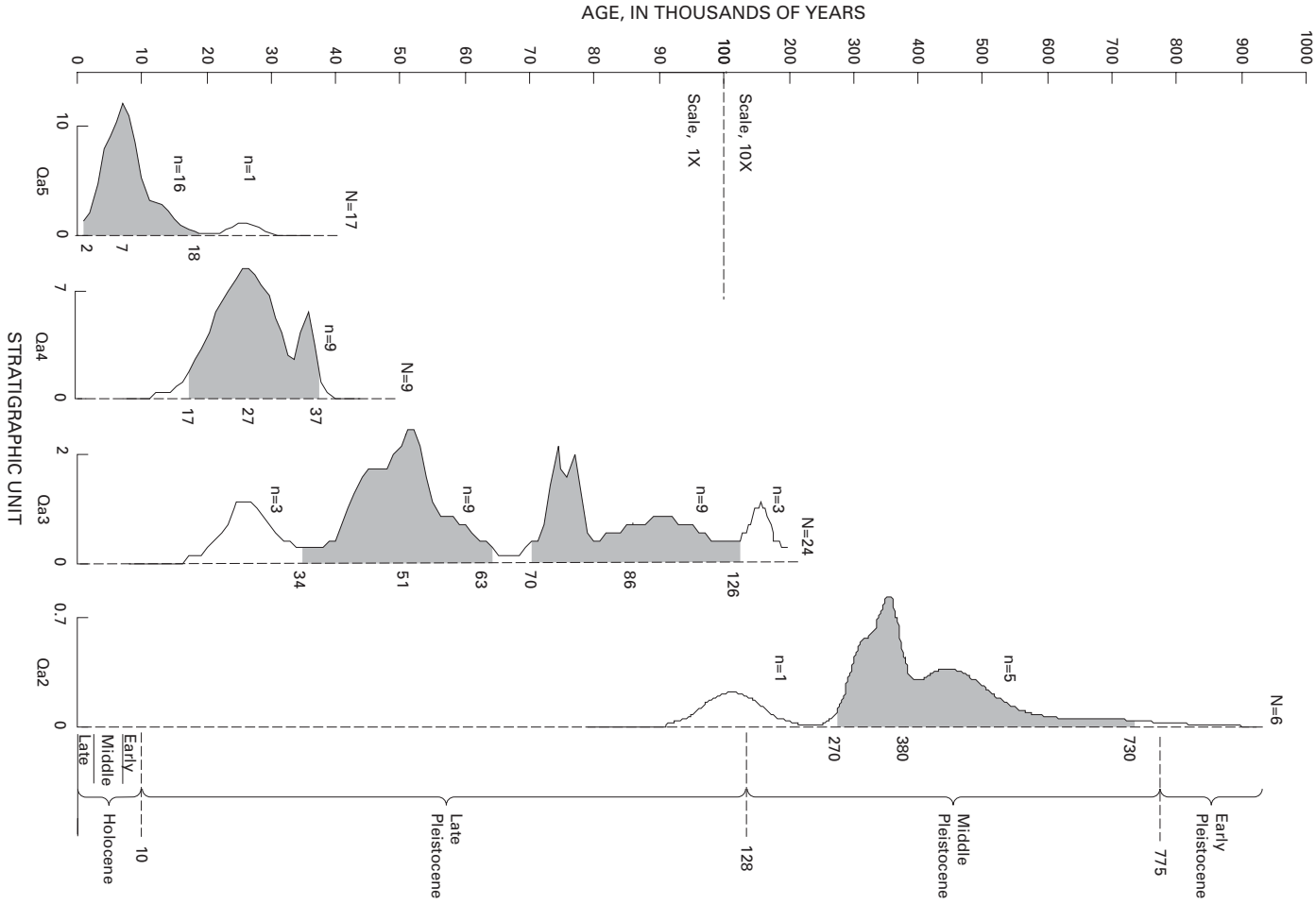

Figure 3. Schematic stratigraphic column showing age distribution (in percent) of mapped Quaternary deposits (units Qa2–Qa5) in Midway Valley and Fortymile Wash in the Yucca Mountain area, southwestern Nevada (figs. 1, 2). Marker dates: 775 ka, age of Matuyama-Brunhes chronozone boundary (Morrison, 1991); 128 ka, astronomical age of marine O-isotopic-substage 5e boundary (Imbrie and others, 1984); 10 ka, arbitrary age suggested for Pleistocene-Holocene boundary (Hopkins, 1975).

appears to be much younger than the underlying petrocalcic horizon formed in alluvial deposits.

Unit Qa1, of possibly early to middle Pleistocene age, which is correlated with unit QTa of Swadley and others (table 2) in Midway Valley, was considered by them to be overlain by alluvial deposits containing Bishop tephra (~760 ka; Sarna-Wojcicki and others, 1993). M.C. Reheis (oral commun., 1993) and Peterson and others (1995), however, reported Bishop tephra within alluvial deposits mapped earlier as unit QTa by Swadley and others (1984) in northeastern Crater Flat. Peterson and others (1995) correlated unit QTa with their Solitario geomorphic surface, which they dated at 430–730 ka on the basis of varnish cation-ratio ages and the age of the Bishop ash (760 ka in the present study). According to S.C. Lundstrom (written commun., 2001), ash deposits interpreted to be representative of the Bishop ash are also present in unit Qa1 deposits along Yucca Wash (fig. 2). Furthermore, the slightly rounded, eroded morphology of unit Qa1 surfaces, as well as the strongly developed soils, are similar features of deposits dated at early to middle Pleistocene elsewhere in Nevada and in California (Wells and others, 1990; Harden and others, 1991a, b; Slate, 1991; Reheis and others, 1992; McDonald and McFadden, 1994).

Unit Qa2

Unit Qa2 (table 2) is recognized at the surface primarily as thin elongate patches of alluvium in Midway Valley, where it is inset into unit Qa1. On color aerial photographs, unit Qa2 surfaces have a darker, redder hue than those of other units. The unit also has a well-developed desert pavement that contains darkly varnished clasts (table 3). Some clasts are split and fractured, and varnish has developed on some fractured surfaces of clasts. The original bar-and-swale morphology has been reduced to the height of the larger clasts above the surface. The upper part of the unit typically has a cap of eolian silt and fine sand, 30 to 50 cm thick. As observed in test pits, unit Qa2 ranges from 2.5 to more than 3.5 m in thickness.

The strongly developed Qa2 soil has a 40- to 70-cm-thick, reddened (7.5–5YR) argillic Btkq horizon and a zone of secondary carbonate and silica accumulation exhibiting $CaCO_3$ stage II–III+ morphology (table 3). The upper column (Av and Bkq horizons) of the Qa2 soil is formed in the eolian deposits that accumulated on the surface (table 3). The upper part of the Bkq soil horizon lacks significant carbonate but contains a laminar silica-cemented zone that is reddish brown to yellowish red (5YR 5/4–6 d). Therefore, the morphology of the upper part of the soil is controlled by silica accumulation, whereas the morphology of the lower part of the soil is controlled by both secondary carbonate and silica accumulation, giving the Qa2 soil an overall appearance of $CaCO_3$ stage IV morphology.

The few dated samples from unit Qa2 (fig. 3) indicate a middle Pleistocene age, which is supported by its stratigraphic position, as well as by the degree of soil development within it.

Unit Qa3

Unit Qa3 (table 2), which is represented by large remnant alluvial-fan surfaces and fluvial terraces, is one of the dominant lithologic units in the Yucca Mountain area, where it underlies the main Fortymile Wash terrace. A well-developed desert pavement containing darkly varnished clasts characterizes the unit Qa3 surface, which has a dark-brown or black tone on color aerial photographs (table 3). Larger clasts, some more than 30 cm in diameter, are distributed on the surface in diffuse, poorly defined bars. The original depositional bar-and-swale morphology has been reduced to the height of individual clasts above the surface. Unit Qa3 averages 2 to 2.5 m in thickness and locally is more than 3.3 m thick in test pits and along the Fortymile Wash terraces.

The strongly developed Qa3 soil has a 20- to 75-cm-thick argillic (Bt and Bkq) horizon overlying a 100- to 130-cm-thick zone of secondary carbonate and silica accumulation (table 3). Clay films, reddening (7.5YR), and strong blocky structure are characteristic of the argillic horizon, which also commonly contains secondary carbonate and silica accumulations. A Bkq or weakly developed Kq soil horizon with $CaCO_3$ stage II–III morphology typically underlies the Bkq soil horizon.

Unit Qa3 is dated at middle(?) to late Pleistocene on the basis of numerical-age determinations (fig. 3), as well as on stratigraphic relations and lithologic and soil characteristics. As discussed above, the unit may be represented by more than one depositional episode.

Unit Qa4

Unit Qa4 (table 2) consists of small, inset fluvial-terrace and alluvial-fan remnants on the east side of Yucca Mountain and of thin alluvial deposits overlying older basin deposits in Crater Flat. The desert pavement of the unit Qa4 surface ranges in appearance from loosely to tightly interlocking and is noticeably less well developed than pavements formed on the older fluvial surfaces. Although desert varnish is discernible on surface clasts of the unit Qa4 pavement, varnish is much less common than on surface clasts of older units (table 3). Indistinct depositional bars are preserved as diffuse accumulations of larger clasts; bar-and-swale relief on unit Qa4 mostly has been reduced to clast height above the surface. Unit thickness averages about 1 m and does not exceed 2 m where observed in test-pit and trench exposures.

The strongly developed Qa4 soil is characterized by a reddened (7.5YR) argillic horizon and by secondary carbonate and silica accumulations (table 3). The upper part of the soil exhibits silica accumulation, $CaCO_3$ stage I–II morphology, and a strongly developed Bkq horizon with a sandy or silty clay-loam texture. Continuous, thin to moderately thick clay films coat ped faces of the Bkq soil horizon, which is overlain by an Av soil horizon.

Unit Qa4 is dated at late Pleistocene on the basis of U-series and thermoluminescence analyses (fig. 3; table 4), supported by similarities in soil-morphologic characteristics

with chronosequences in other areas that were deposited about 80–15 ka (table 2).

Unit Qa5

Unit Qa5 (table 2) covers large areas of alluvial fans and occurs as inset terraces along drainages. The desert pavement of the unit Qa5 surface is loosely packed and poorly formed, and surface clasts have minor accumulations of rock varnish (table 3). Unit Qa5 surfaces display well-developed bar-and-swale morphology. The amount of bar-and-swale relief is related to landscape position and sediment source. The coarsest grained bars lie in proximal-fan region, whereas smaller, lower, partly buried bars lie in the distal-fan region, where the intervening swales are partly filled by fine-grained eolian silt and sand. Surface clasts are relatively unweathered. Unit Qa5 averages 1 m in thickness, and is as much as 2.5 m thick in test-pit and trench exposures.

Weakly developed soils are formed on unit Qa5 (table 3). Soil development is stronger in the swales, where a silt-rich zone occurs in the upper 30 to 40 cm of the unit; soils are more weakly developed on bars. The unit Qa5 soil typically has a Bwk or incipient Btjk horizon with 10YR hues, weak subangular blocky structure, and colloidal stains on grains. Carbonate is disseminated in the matrix, and below about 30-cm depth in the Bk soil horizon the bottoms of clasts have powdery coats of carbonate with $CaCO_3$ stage I morphology. Where unit Qa5 is sufficiently thick, the carbonate content decreases below the Bk soil horizon to form a transitional horizon (BC or CB) or a Ck soil horizon (see table 3 for explanation). Where the unit Qa5 surface is relatively thin and underlain by a buried soil, the Bk horizon persists to the base of the unit.

Unit Qa5 is dated at latest Pleistocene to early Holocene on the basis of numerical-age determinations on samples from the Yucca Mountain area (fig. 3) and correlations to regional soil profiles (table 2). In Crater Flat, for example, Peterson and others (1995) reported that radiocarbon dating of rock varnish yielded a minimum age of 6–11 ka for the Little Cones unit, which has a soil profile similar to that of unit Qa5. The characteristically weak soil development exhibited by correlative units was interpreted by Dohrenwend and others (1991) as indicative of a Holocene age.

Unit Qa6

Unit Qa6 (table 2) is present along the active washes as low flood plains less than 1 m above the active channels, and as vegetated bars. No desert pavement has developed (table 3), and surface clasts are unvarnished and unweathered. Relief on the unit Qa6 surface is primarily the result of preservation of original bar-and-swale morphology. Locally, an eolian cap, as much as 5 to 10 cm thick, buries all but the largest surface clasts. Natural outcrops and manmade exposures indicate that the total thickness of unit Qa6 does not exceed 2 m.

Unit Qa6 soils lack the prominent eolian cap common to the older surfaces (Av horizon), and soil development is limited to minimal oxidation of the deposit and sparse secondary carbonate accumulation (table 3). Carbonate is more concentrated toward the uppermost 10 cm of the deposit but typically is widely disseminated in the matrix. Clasts in the upper 30 cm contain little visible carbonate yet effervesce when HCl is applied. Carbonate content ranges from isolated patches on the undersides of clasts to relatively continuous, thin coatings. Evidence that many of the clasts within unit Qa6 have been reworked from older deposits includes randomly oriented carbonate coatings on clasts and percussion marks where the coatings have been chipped from the clasts.

Unit Qa6 is assigned a middle to late Holocene age because of its very weak to weak soil development and its inset relation to unit Qa5. No color or structural B soil horizon is evident, and morphology ranges from incipient to $CaCO_3$ stage I. As listed in table 2, several middle to upper Holocene alluvial deposits are recognized in the region (Wells and others, 1990; Bull, 1991; Harden and others, 1991a; Slate, 1991).

Unit Qa7

Unit Qa7 (table 2) consists of deposits along active channels and the adjacent flood plains. No desert pavement has formed on its surface (table 3). No desert varnish has developed on clasts, except where it is apparently inherited. Thick, dark desert varnish is present in small protected areas (small fractures and exposed voids) on some surface and subsurface clasts; however, that varnish is too well developed to be actively accreting in modern channels and apparently has been reworked from older surfaces. Clasts are unweathered, and the original depositional bar-and-swale relief is unaltered. The total exposed thickness of unit Qa7 does not exceed 2 m.

No inplace pedogenic alterations were observed for unit Qa7 deposits (table 3). The overall color is pale brown to brown (10YR 5–6/3 d). The matrix contains reworked, disseminated carbonate. Reworking of older surficial materials is indicated by numerous clasts with thick secondary carbonate accumulations; such clasts appear to be distributed randomly throughout unit Qa7. The coatings, originally formed on the bottoms of the clasts, have no preferred orientation in the reworked deposits. Although carbonate is generally not apparent on the undersides of clasts, noticeable effervescence occurs when HCl is applied. This unit includes modern deposits in channels (unit Qa7) and on hillslopes (unit Qc7).

Colluvial Deposits

Colluvial deposits are undifferentiated as surficial map units because of their limited areal extent and the limited exposure of all but the youngest materials. However, colluvial sequences are exposed in fault trenches around Yucca Mountain and in test pits at the prospective site of surface facilities on the east side of Exile Hill (such as units Qc2, Qc3; see chap. 4; fig. 5). The colluvial stratigraphy of Midway Valley, as described below, is based primarily on test-pit and trench exposures.

Middle Pleistocene to Holocene Undifferentiated Colluvium (Unit Qu)

Unit Qu is mapped as colluvial and debris-flow deposits mantling hillslopes and locally includes areas mantled by eolian and reworked eolian deposits; patches of darkly varnished colluvial boulders are commonly on upper hillslopes (Whitney and Harrington, 1993). The colluvial deposits generally consist of gravelly-silty sand and silty fine to medium gravel with pebble to small cobble clasts. Colors are very pale brown (10YR 7/4 d) to reddish yellow (7.5YR 6/6), with white (10YR 8/1 d) for the older carbonate-cemented units. The colluvial and debris-flow deposits are poorly sorted and very crudely bedded to massive; they are predominantly matrix and locally clast supported and consist of as much as 90 percent gravel composed of angular to subangular pebbles with lesser cobbles, as much as 20 cm in diameter, and small boulders, as much as 30 cm in diameter. Individual colluvial deposits are generally less than 2 to 3 m thick, on the basis of test-pit and trench exposures.

The younger colluvial deposits, possibly equivalent to unit Qa5 (table 2), have thin, weakly developed soils, with an AB horizon over a weakly developed Bwk horizon. Colluvial deposits of probable unit Qa4 age display well-developed Bkq textural B soil horizons, 40 to 50 cm thick. Deposits possibly equivalent to units Qa2 and Qa3 have multiple superimposed soils consisting of Bkq and Btjkq horizons with $CaCO_3$ stage II morphology. The oldest exposed colluvial deposits have strongly developed Kqm soil horizons. The colluvial boulder deposits are dated at mid-Quaternary to late Quaternary (Whitney and Harrington, 1993).

Most of the hillslope areas mapped as undifferentiated colluvium have the same surface characteristics as units Qa5 and Qa6. Colluvial deposits with surface characteristics similar to those of unit Qa4 are common near the toe of the hillslope.

Eolian Deposits

Two types of eolian deposits were observed in the Yucca Mountain area: (1) reworked eolian materials within sand ramps surrounding Busted Butte and along the southeastern margin of Midway Valley, and (2) thin accumulations of silt and fine sand in the A and B horizons of most surface soils and relict accumulations within some buried soils.

Middle Pleistocene to Holocene Eolian-Colluvial Deposits (Unit Qeu)

Sand ramps at Busted Butte and in southeastern Midway Valley (fig. 2) consist of a stacked eolian-colluvial sequence composed of pebbly, silty, fine- to medium-grained sand interbedded with sandy pebble to cobble gravel. Minor sandy-pebble-gravel alluvial deposits are present locally. The sand-ramp deposits range in color from very pale brown to light gray (10YR 7/2–4 d), are poorly to moderately well sorted, and are moderately well bedded to massive. Unit Qeu is predominantly matrix supported, although the alluvial gravel and parts of some colluvial deposits locally are clast supported. Gravel clasts are angular to subangular and commonly less than 5 cm in diameter, some as much as 50 cm in diameter. The sand-ramp deposits do not exceed 15 m in thickness.

A weakly to moderately interlocking desert pavement covers most of the unit Qeu surface. Soil development in the near-surface deposits consists of a well-developed reddish-yellow (7.5YR 6/6 d) Bkq horizon with a sandy clay loam texture that appears to be similar to the unit Qa4 soil. Typically, one or more buried soils are within the sand-ramp deposits in Midway Valley. The buried soil observed within trench MWV–T4 (fig. 2) has a Kq horizon with $CaCO_3$ stage IV morphology. Additionally, multiple buried soils have been observed within the Busted Butte sand-ramp deposits south of Midway Valley (figs. 1, 2; Whitney and others, 1985; Whitney and Muhs, 1991; Menges and others, 1994).

The presence of Bishop tephra in the lower sand-ramp deposits at Busted Butte (Whitney and others, 1985; Menges and others, 1994) and in other localities near Yucca Mountain (Hoover, 1989) indicates that those landforms began forming before about 760 ka. At Busted Butte, some of the buried soils have been (U series) dated at middle to late Pleistocene (Menges and others, 1994). Multiple buried soils above the Bishop tephra indicate that accumulation of the sand ramps is episodic and punctuated by periods of surface stabilization and soil formation. Thermoluminescence ages of 73±9 and 38±6 ka on two successive units in the uppermost 3 m of the deposits exposed in trench MWV–T4 (fig. 2) in southern Midway Valley (samples TL–03, TL–04, table 9; see chap. 5) may date two of the more recent depositional episodes, and another thermoluminescence age of 6±1 ka (sample TL–05, table 9) on the A soil horizon indicates continuing eolian deposition during the Holocene.

Eolian Accumulations on Geomorphic Surfaces

A few to several tens of centimeters of eolian silt and fine sand have accumulated on most alluvial geomorphic surfaces and been incorporated into the soil profiles formed on those surfaces. These eolian deposits are not mapped separately because of their broad areal distribution and relative thinness. Models of desert pavement and soil formation recognize the importance of eolian materials as a source for the fine-earth fraction, carbonate, and soluble salts that occur within otherwise-clean sandy-gravel deposits in arid regions (Birkeland, 1984; McFadden and Weldon, 1987; McFadden and others, 1987; McDonald and McFadden, 1994).

Over time, surface weathering, soil formation, and eolian deposition result in incremental modifications to geomorphic surfaces, including reduction of the original surface topographic (bar and swale) relief, formation of Av soil horizons, desert-pavement development, desert-varnish accumulations on surface clasts, and weathering of surface clasts. In Midway Valley, these modifications have produced a distinctive surface morphology for a given unit that has been used as a

basis for mapping alluvial geomorphic surfaces, whereby older surfaces generally have a more subdued surface topography, stronger desert-pavement development, darker and thicker desert varnish on surface clasts, stronger soil development, and thicker eolian deposits. Eolian additions to units Qa6 and Qa7 (table 2) are minimal, whereas eolian materials plug the upper part of unit Qa5 deposits and partly fill paleoswales to form a muted bar-and-swale topography. Unit Qa2 through Qa4 surfaces are plugged with eolian deposits that form a continuous surface sheet and result in a nearly smooth topography. The original eolian mantle on unit Qa1 has been stripped and replaced by a younger eolian mantle.

Summary

The differentiation and characterization of surficial deposits provide a stratigraphic framework that can be used as a common reference for interpreting Quaternary deformation across the Yucca Mountain area. The relative- and numerical-age relations among the various deposits and their correlative units in trench exposures are especially important for determining the timing and magnitude of past surface-rupturing paleoearthquakes, fault-slip rates, and recurrence intervals—data that are essential for evaluating the potential seismic hazards at Yucca Mountain.

Chapter 3

Distribution of Quaternary Faults at Yucca Mountain

By Christopher M. Menges and John W. Whitney

Contents

Abstract....23
Introduction....23
Major Faults....25
- Paintbrush Canyon Fault....26
- Midway Valley Fault....27
- Bow Ridge Fault....27
- Stagecoach Road Fault....27
- Ghost Dance and Sundance Faults....27
- Solitario Canyon Fault....28
- Fatigue Wash Fault....29
- Windy Wash Fault....29
- Northern and Southern Crater Flat Faults....29
- Northwest-Trending Faults....30
- Bare Mountain Fault....30
- Rock Valley Fault....31

Abstract

Information on the extent, characteristics, and timing of Quaternary faulting is essential to evaluations of earthquake-recurrence intervals, event magnitudes, and potential seismic hazards, as well as to the development of tectonic models, for the proposed repository site for the storage of high-level radioactive wastes at Yucca Mountain. As a part of the site-characterization program, all major faults that cut through the area were mapped in detail and extensively studied in trench excavations to determine whether, and to what degree, associated Quaternary surficial units were involved in the faulting. The investigations resulted in the recognition that displaced or disturbed alluvial and colluvial deposits record late Quaternary faulting along eight faults, including (from east to west) the Paintbrush Canyon, Bow Ridge, Stagecoach Road, Solitario Canyon (including Iron Ridge), Fatigue Wash, Windy Wash, and Northern and Southern Crater Flat Faults. Nearly all of these features are north-trending normal faults with steep westward dips and down-to-the-west displacements. Neither the Ghost Dance and Sundance normal faults that are closest to the planned repository block, nor the northwest-trending strike-slip faults in Drill Hole, Pagany, and Sever Washes, show evidence of Quaternary activity.

Most of the Quaternary faults within the proposed repository-site area are major block-bounding features that form the structural boundaries of large east-dipping fault blocks with several hundred meters of bedrock displacement. Cumulative Quaternary fault movements along these faults range from less than 1 to as much as 8 m, and multiple surface ruptures are recorded on several of them. Bedrock scarps, subtle scarps and lineaments in alluvium, and short but abrupt bedrock-alluvium contacts commonly provide evidence of Quaternary fault activity and also serve as a basis for siting trench excavations that display fresh exposures of Quaternary stratigraphic sequences and fault relations.

In addition to faults within the immediate repository-site area, two other faults displaying Quaternary activity—the Bare Mountain and Rock Valley Faults, 14 km to the west and 25 km to the southeast, respectively—were studied as a part of paleoseismic investigations in the vicinity of Yucca Mountain.

Introduction

Information on the extent, characteristics, and timing of Quaternary faulting is essential to evaluations of earthquake-recurrence intervals, event magnitudes, and potential seismic hazards, as well to the development of tectonic models, for the proposed repository site for the storage of high-level radioactive wastes at Yucca Mountain (fig. 1).

Principal sources of the geologic mapping used in this report include the maps by Scott and Bonk (1984), Simonds and others (1995), and Day and others (1998a, b). The 1:12,000-scale mapping by Scott and Bonk (1984), which showed the complex fault patterns in the Yucca Mountain area in considerably greater detail than did earlier mapping (for example, Christiansen and Lipman, 1965; Lipman and McKay, 1965), served as a valuable guide for the planning of subsequent site investigations. The 1:24,000-scale map

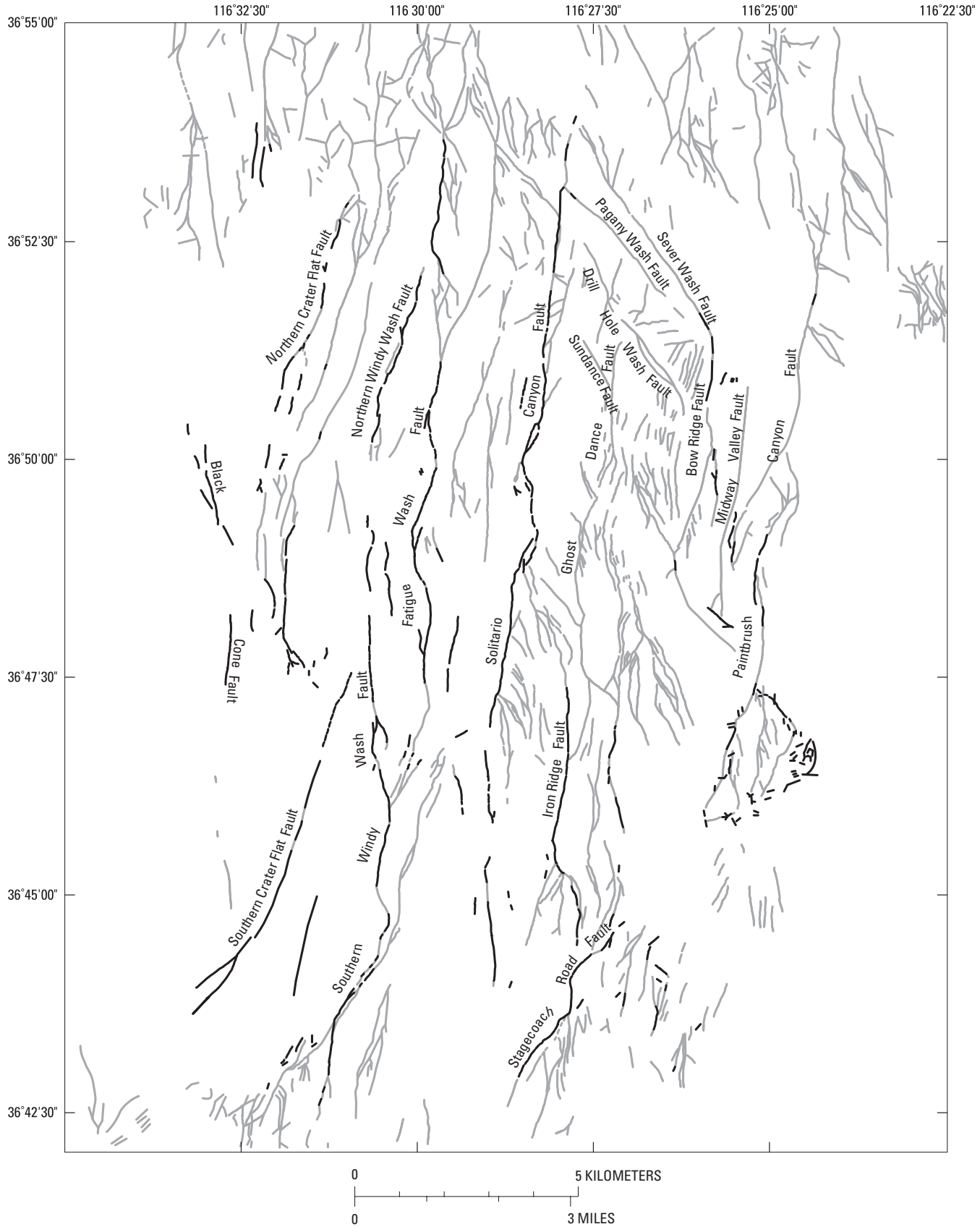

Figure 4. Faults in the Yucca Mountain area, southwestern Nevada (figs. 1, 2), simplified from map by Simonds and others (1995). Dark lines, faults with Quaternary or suspected Quaternary activity.

by Simonds and others (1995)—a compilation of all available data on Quaternary fault activity that had been collected through 1993—resulted in the recognition that displaced or disturbed alluvial and colluvial deposits record late Quaternary faulting along at least seven to nine major faults at Yucca Mountain. Such findings assisted in the selection of new trench sites and the location of key natural exposures for additional paleoseismic investigations. A more recent geologic-mapping program, begun in 1995, resulted in publication of two detailed geologic maps: (1) a 1:24,000-scale map of the Yucca Mountain area (Day and others, 1998a); and (2) a 1:6,000-scale map of the central-block area, centered over the proposed repository block itself (Day and others, 1998b). These two mapping efforts focused primarily on the distribution of the thick Miocene volcanic sequence, as defined and subdivided according to the presently accepted stratigraphic framework for the area (for example, Buesch and others, 1996), and on the geologic structures within bedrock units, resulting in further refinement of the fault patterns at Yucca Mountain and providing new data, especially on possible extensions and interconnections of major individual faults as their traces are projected beneath alluvial cover.

A simplified fault map of the Yucca Mountain area, based primarily on data from the 1:24,000-scale map of Simonds and others (1995), is shown in figure 4. Simonds and others' map is especially useful for showing the general extent of known or suspected Quaternary activity along individual faults or fault systems and includes notations describing the evidence for such activity as observed during field investigations or interpreted from aerial photographs along the mapped or projected fault traces.

The geologic maps by Day and others (1998a, b) do not extend far enough to show the location and extent of the Bare Mountain and Rock Valley Faults. The Bare Mountain Fault zone was mapped in detail at a scale of 1:24,000 by Monsen and others (1992), and the Rock Valley Fault system is shown on the 1:100,000-scale geologic-map compilation by Frizzell and Shulters (1990).

For the purposes of this report, faults with known late Quaternary displacement are categorized as traceable faults or fractures and scarps in alluvial material. Fractured or disturbed soil horizons and carbonate-cemented fault breccias that show fracturing or shearing in surficial materials are considered to be evidence for Quaternary fault activity. Places where late Quaternary displacement is suspected but unequivocal proof is absent include (1) traceable faults, suspected fault contacts, or fault traces along the projection of a fault that in some places has known or suspected Quaternary displacement; (2) possible fault-controlled lineaments, such as linear stream channels, aligned vegetation or burrows, stonelines, and photolineaments in Quaternary deposits; and (3) faultline scarps along bedrock-alluvium contacts where differential erosion has produced prominent linear scarps on the bedrock footwall. Faultline scarps are suspected to be of Quaternary age because local evidence typically exists for displacement of hanging-wall alluvial and colluvial deposits.

Major Faults

The drainage pattern at Yucca Mountain is controlled largely by faults, and so most of the main faults are named for the drainages in which they are mapped; other faults are named for nearby geographic features (figs. 2, 4). The major faults form the boundaries of large east-dipping structural fault blocks (Day and others, 1998 a, b), and most of them also define the bedrock-alluvium contact at the base of west-facing scarps in bedrock for at least part of their lengths.

The following sections provide general descriptions of the surface characteristics of the major faults, the locations of and evidence for Quaternary activity, the amounts and sense of displacement of both bedrock and Quaternary deposits, fault lengths, and, where applicable, evidence for geometric segmentation of a fault. The term "geometric segmentation" refers to subdivision of a fault into segments based on variations in its geometry or structure. Criteria used to define geometric-segment boundaries include abrupt changes in fault pattern marked by (1) zones of overlap between two strands of the fault zone, (2) bifurcation into large fault splays, (3) large gaps in the fault trace, (4) sharp deflections in the strike of the fault, and (or) (5) reversals in dip direction or sense of displacement along the fault. Fault characteristics are summarized in table 5. Results of the detailed mapping of trenches excavated across faults, which are sites where the geologic relations along faults and evidence for Quaternary activity are best exposed, as well as information on the timing, slip rates, and recurrence intervals of faulting events, are discussed in other chapters of this report.

Paintbrush Canyon Fault

The Paintbrush Canyon Fault (figs. 2, 4) is a major block-bounding fault on the east side of Midway Valley (fig. 1; Day and others, 1998a). The fault is exposed for a distance of 5 km in bedrock forming the highlands north of Yucca Wash, where it is shown as a west-dipping (56°–76°) normal fault with down-to-the-west displacement of 210 m (Dickerson and Drake, 1998). Along that section of the fault, the trace is marked by a discontinuous, west-dipping fault scarp, 0.3 to 4.0 m high. To the south, the fault extends beneath alluvial cover for 5 km before strands are exposed for about 1 km in bedrock along the west side of Fran Ridge (Day and others, 1998a); it may then continue southward for another 8 km to a possible intersection with the southwest-striking Stagecoach Road Fault.

Estimates of the amount of bedrock displacement on the Paintbrush Canyon Fault range from 210 m in the northern segment to as much as 500 m along other segments (Scott and Bonk, 1984; Day and others, 1998a). Evidence for Quaternary fault activity is observed in trenches and in natural exposures in sand ramps along the west side of Busted Butte, as discussed in chapter 5. Maximum observed displacements of surficial deposits range from 5.5 to 8.0 m.

Table 5. Summary of characteristics of major faults in the Yucca Mountain area, southwestern Nevada.

[See figures 1 and 2 for locations]

Fault (fig. 4)	Surface characteristics	Evidence of Quaternary activity	Average dip of fault	Sense of displacement	Amount of displacement (bedrock)	Amount of displacement (Quaternary)	Fault length
Crater Flat Fault zone (Northern and Southern).	Bedrock faults, bedrock scarps, subtle scarps and lineaments in alluvium, and bedrock-alluvium fault contacts.	Lineaments in alluvium; subtle scarps and fractures in alluvium.	70° W.	Oblique, left lateral	Unknown, down to the west.	1.2 m, late Quaternary	Min 1 km, max 20 km
Windy Wash Fault.	Prominent faultline scarp, east-facing scarps in alluvium, and bedrock- alluvium fault contacts. Merges with the Fatigue Wash Fault.	Three trenches show multiple events, fractures and scarps in alluvium, and basaltic ash in fault plane.	63° W.	Dip slip	Increases southward to ~500 m down to the west	3.7 m, late Quaternary	Min <3 km, max 25 km
Fatigue Wash Fault.	Bedrock fault, faultline scarp, scarps and lineament in alluvium, and bedrock scarps. Merges with the Windy Wash Fault.	One trench shows multiple events, fractures and scarps in alluvium, and basaltic ash in fault plane.	70° W.	Oblique, left lateral	100–400 m down to the west	1.3–2.8 m, late Quaternary	Min 9 km, max 17 km
Solitario Canyon Fault.	Prominent faultline scarp, discontinuous traces, and subtle scarps in alluvium. Iron Ridge Fault splay forms prominent faultline scarp. Merges (?) with the Stagecoach Road Fault.	12 trenches, 9 of which show multiple events, fractures in alluvium, and basaltic ash in fault plane.	72° W. (main trace), 68° W. (Iron Ridge Fault)	Oblique, left lateral	Increases southward from 50 m down to the east to 500 m down to the west	1.7–2.5 m, late Quaternary	Min 12.5 km, max >21 km
Stagecoach Road Fault.	Prominent scarp and traceable faults in alluvium. Merges with the Solitario Canyon and (or) Paintbrush Canyon Fault.	3 trenches, 2 of which show multiple events, fractures and scarps in alluvium, and basaltic ash in faulted alluvium.	73° W.	Dip slip	400–600 m, down to the west	1.0–3.1 m, late Quaternary	Min 4 km, max 7 km
Ghost Dance Fault.	Bedrock fault in a zone of subparallel minor faults and breccia zones.	None----------	Near vertical	Dip slip	Increases southward from 0 to 27 m down to the west	None	Min 2.5 km, max 7 km
Bow Ridge Fault.	Faultline scarp along bedrock-alluvium contact, subtle lineaments. May merge with the Paintbrush Canyon Fault.	6 trenches, 5 of which show multiple events, fractures in alluvium, and basaltic ash in fault plane.	75°–80° W.	Oblique, left lateral	125 m down to the west	0.5–1.22 m, late Quaternary	Min 4 km, max 11.5 km
Midway Valley Fault.	Bedrock faults at north and south ends; detected by geophysical surveys in covered areas.	None----------	Unknown; west(?)	Unknown, dip slip(?)	Several tens of meters down to the west	None	Min 1 km, max 13 km
Paintbrush Canyon Fault.	Bedrock faults, bedrock scarps, lineaments, bedrock-alluvium fault contacts, and faults in alluvium. May merge with the Stagecoach Road Fault.	4 trenches and natural exposures at Busted Butte show multiple events, fractures in alluvium, and basaltic ash in fault plane (locally).	71° W.	Dip slip to oblique, left lateral	210–500 m down to the west	5.5–8.0 m at Busted Butte, late Quaternary	Min 11 km, max 19 km
Northwest-trending faults.	Bedrock faults with local small bedrock scarps; some faults located on the basis of geophysical or drillhole evidence.	None, except for 1 trench located on the Pagany Wash Fault that shows possible Quaternary activity.	>70° S. to vertical	Strike slip, right lateral	5–10 m vertical, ~40 m right lateral	None	4 km
Bare Mountain Fault.	Faultline marked in places by bedrock-alluvium contact; offset of pre-Tertiary rocks evidenced by seismic-reflection data.	Surficial deposits displaced; scarps formed in alluvial fans.	50°–70° E.	Dip slip to oblique slip	3.5 km down to the east	Max 4–5 m	20 km
Rock Valley Fault.	Composed of multiple east-northeast-striking faults that form distinct scarps and lineaments in surficial deposits; bedrock offsets indicated by seismic data.	Scarps and lineaments in surficial deposits.	Varying to near vertical	Strike slip (left lateral) to oblique slip	≤4 km, left lateral	Min 5 cm, max 17 m	Min 19 km, max 65 km

Midway Valley Fault

The Midway Valley Fault (figs. 2, 4) is shown by Day and others (1998a) to extend northward from a 1-km-long exposure in bedrock (Tiva Canyon Tuff) at the southeast end of Bow Ridge for a distance of about 9 km beneath the surficial deposits flooring Midway Valley, and then to continue northward for at least another 3 km as a west-dipping normal fault that displaces bedrock about 120 m down to the west in the upper part of the Paintbrush Group (Dickerson and Drake, 1998). Displacements of buried bedrock within the valley are interpreted from gravity and magnetic surveys to be 40 to 60 m (Ponce and Langenheim, 1994), and the cross sections by Scott and Bonk (1984) show about 70 m of down-to-the-west displacement on a fault that dips 70° W. The Midway Valley Fault does not displace Quaternary alluvial deposits, as discussed in chapter 4.

Bow Ridge Fault

The Bow Ridge Fault (figs. 2, 4) has been studied in detail on the west side of Exile Hill, where it is well exposed in a 200-m-long segment marked by a low faultline bedrock escarpment. Trenches T14 and T14A through T14D (figs. 2, 8), which were excavated across projections of the fault beneath surficial deposits, revealed small-displacement Pleistocene faulting events (see chap. 5). Trench A/BR–3, excavated across a northward projection of the fault marked by a vegetation-change lineament, however, revealed no disturbance of the exposed surficial deposits.

Bedrock is displaced about 125 m down to the west along the Bow Ridge Fault on the west side of Exile Hill (Scott and Bonk, 1984). The fault dips 75°–80° W. (Simonds and others, 1995), and net displacement is left oblique. Upper Quaternary colluvial deposits are vertically displaced 0.5 m, but left-lateral striations on carbonate laminae in the fault plane indicate that cumulative net slip may be as much as 1.22 m (table 5).

Although the northward extent of the Bow Ridge Fault is uncertain, Day and others (1998a) showed it to extend beneath surficial deposits north of Exile Hill to the north side of Yucca Wash, a distance of about 4.5 km, and Dickerson and Drake (1998) mapped it cutting bedrock in the upper part of the Paintbrush Group for another 1 to 2 km to the north. From a point opposite the mouth of Yucca Wash, the fault is shown to have down-to-the-east displacement. About 4 km south of Exile Hill, at the south end of Midway Valley, displaced bedrock marks the fault trace along the west side of Bow Ridge. The fault is then shown to bend to the southeast beneath alluvium for a distance of another 2.5 km, where it may connect with the Paintbrush Canyon Fault (Day and others, 1998a). The total length of the Bow Ridge Fault may be as much as 11.5 km.

Stagecoach Road Fault

The Stagecoach Road Fault (figs. 2, 4), a northeast-trending structure south of Stagecoach Road, is traceable for 4 to 5 km as northeast-striking fractures and truncated alluvial surfaces in Quaternary alluvium (Simonds and others, 1995). A distinct west-facing topographic fault scarp, as much as 1.0 m high, is present along most of the fault trace, particularly where the fault exposes resistant well-developed carbonate soil in the footwall. The scarp is at the west edge of a 0.5-km-wide alluvium-mantled bedrock pediment formed to the west of a low bedrock ridge.

Upper Quaternary alluvial deposits are displaced along the entire trace of the Stagecoach Road Fault. Trenches SCR–T1 and SCR–T3 (fig. 2), which were excavated across the fault, contain evidence of multiple faulting events (see chap. 5). Trench SCR–T2 was excavated across a photolineament east of the Stagecoach Road Fault but did not expose a fault.

The amount of bedrock displacement on the fault is estimated at 400 to 600 m down to the west (Scott, 1990). Upper Quaternary alluvium is displaced 1.0 to 3.1 m. The fault has an average dip of 73° W.; slickenside measurements indicate that Quaternary movement is predominantly dip slip.

The Stagecoach Road Fault is traceable as a topographic fault scarp for nearly 4 km before disappearing under uppermost Quaternary materials. Continuation of surface rupture along the fault to the southwest or northeast of the main fault trace, if present, could consist only of minor fracturing or small displacements that have not persisted as fault scarps because of erosion or burial. Northeast-striking fractures at the north end of the Stagecoach Road Fault indicate a possible connection with the Paintbrush Canyon Fault south of Busted Butte, and northeastward structural continuation of the fault is supported by anomalies in shallow geophysical (aeromagnetic) surveys as well (V.E. Langenheim, written commun., 1995). However, no fault scarps or other surface expressions of faulting in alluvial fans were observed between the two faults. Its simple trace and the short length of the main fault zone indicate that the fault consists of only a single geometric segment.

Ghost Dance and Sundance Faults

The Ghost Dance Fault (figs. 2, 4) is the main structural feature in a diffuse zone of minor bedrock faults and fractures east of the crest of Yucca Mountain (Day and others, 1998b). Though not one of the major block-bounding faults at Yucca Mountain (it is classed as an “intrablock” fault), the fault is important because it extends across the proposed repository-site area (Day and others, 1998b). The Sundance Fault is a nearby subsidiary feature that also traverses the proposed repository site area.

The Ghost Dance Fault trends generally north to north-northeast, with subvertical to steep (>65°) westward dips; the main fault zone extends from Wren Wash near the southern margin of Drill Hole Wash southward to Broken Limb Ridge, a distance of about 2.5 km (Day and others, 1998b). Farther south, the fault zone bifurcates, striking southwest into the Abandoned Wash Fault of Scott and Bonk (1984) and southeast toward, but not into, the Dune Wash Fault.

As mapped and described in detail by Day and others (1998b), the Ghost Dance Fault zone can be divided into three sections on the basis of the amount of offset and brecciation within units of the Miocene Tiva Canyon Tuff:

1. The northern section, which lies north of Split Wash, is represented by a relatively narrow (2–4 m wide) damaged-rock zone with as much as 6 m of down-to-the-west displacement (see fig. 21 for location)
2. The central section, which extends from Split Wash to Broken Limb Ridge, displays 13 to 27 m of cumulative down-to-the-west displacement across two or more splays, distributed over a 55- to 150-m-wide zone.
3. The southern section, south of Broken Limb Ridge to where it merges with the Abandoned Ridge Fault, is represented by numerous splays that parallel the main north-striking zone. Here, the displacement (3–17 m) and width of brecciation (2–15 m) are considerably less than in the central section.

The Ghost Dance Fault is difficult to trace continuously across hillslopes either by surface mapping or by interpretation of aerial photographs, because only small segments are associated with linear gullies or with topographic steps or scarps that would give rise to noticeable lineaments marking the fault trace. The absence of strong geomorphic expression, in combination with the apparent absence of deformation of surficial deposits observed in several trenches excavated across the Ghost Dance Fault (see chap. 6), indicates that faulting events did not occur as late as Quaternary time.

The Sundance Fault is mapped as a 750-m-long zone extending from Dead Yucca Ridge southeastward to Live Yucca Ridge and is shown to have a maximum cumulative down-to-the-northeast displacement in bedrock of 6 to 11 m (Day and others, 1998b; Potter and others, 1999). In places, as many as four splays within a 70-m-wide brecciated fault zone are distinguishable. The Sundance Fault zone, as mapped by Potter and others (1999), terminates west of the Ghost Dance Fault, contrary to an earlier interpretation by Spengler and others (1994); the Ghost Dance Fault is shown to extend across Split Wash beneath surficial deposits, with no apparent offset by a younger fault (Day and others, 1998b). Like the Ghost Dance Fault, the Sundance Fault shows no evidence of Quaternary activity.

Solitario Canyon Fault

The longest continuously exposed fault trace at Yucca Mountain is associated with the Solitario Canyon Fault, the main trace of which extends from northernmost Yucca Mountain at the south margin of Yucca Wash to Stagecoach Road (including the section labeled “Iron Ridge Fault” in figs. 2 and 4; Day and others, 1998a). The fault is well expressed along the east side of Solitario Canyon, where, for much of its length, it forms a prominent faultline scarp along the bedrock-alluvium contact at the base of a large topographic bedrock escarpment. Scarp height ranges from 0.3 m (east facing) at the north end of the fault to as much as 5.0 m (west facing) at the south end. The fault bifurcates into several splays at its south end. The central splay consists of discontinuous fault traces and subtle scarps in alluvium that continue as far southward as Stagecoach Road. A discontinuous series of bedrock scarps has formed along the western splay, which trends south-southwest and may merge with the Southern Windy Wash Fault. Bedrock fault splays split off the central section of the main Solitario Canyon Fault trace and connect with a prominent west-facing faultline scarp, as much as 15 m high, at the base of a prominent bedrock escarpment. This eastern section of the Solitario Canyon Fault was called the Iron Ridge Fault by Scott (1992), a usage retained here even though it is now considered to be a splay of the Solitario Canyon Fault. To the south, the Iron Ridge Fault also strikes toward, and may connect with, the Stagecoach Road Fault (Simonds and others, 1995).

Naturally exposed evidence of Quaternary displacement is limited to sheared carbonate-cemented fault breccia at the bases of faultline scarps and to a few fractures in alluvium in the hanging wall of the Solitario Canyon Fault. A total of 11 trenches and 1 natural cleared exposure have been excavated across or near the Solitario Canyon and Iron Ridge Faults (fig. 2). Three of the older trenches—T13, T10A, and T10B—did not cross the main trace of the fault, and the others—GA1A, GA1B, Ammo Ridge, SCF–T4, SCF–T8, SCF–T3, SCF–T1, SCF–T2, and SCF–E1—contain evidence of multiple mid-Quaternary to late Quaternary faulting events (see chap. 7). Bedrock displacements on the Solitario Canyon Fault range from about 50 m down to the east at the north end to as much as 500 m down to the west near the mouth of Solitario Canyon to the south (Day and others, 1998a). Thus, the fault zone displays a scissors geometry that contains a null point with essentially no displacement where movement is reversed. Dips on the Solitario Canyon Fault range from 60° to 80° W. south of the null point; slickenside measurements indicate that the net slip is left oblique. The Iron Ridge Fault dips an average of 68° W. and displays left-oblique slip. Preliminary examination of four trenches on the Solitario Canyon Fault indicates that Quaternary deposits are displaced 1.7 to 2.5 m down to the west (table 5).

The Solitario Canyon Fault is exposed continuously for a distance of 12.5 km. If the fault extends as far southward as Stagecoach Road, its overall length is at least 18 km. If the fault is connected with the Iron Ridge Fault and also with the Stagecoach Road Fault, the total length may exceed 21 km. No evidence was observed for geometric segmentation of the central and southern sections of the fault where its trace is continuous. The part of the northern section with east-side-down displacement may represent a separate geometric segment, although the reversal in offset may reflect continuous scissoring movement of the hanging-wall or footwall blocks, with no relation to fault-rupture segmentation. The Iron Ridge Fault is a large splay that is considered to be a distinct geometric fault segment; the small central and western splays at the south end of the Solitario Canyon Fault may also represent distinct short fault segments.

Fatigue Wash Fault

The Fatigue Wash Fault (figs. 2, 4) is a poorly exposed bedrock fault in Fatigue Wash, about 2.25 km west of the Solitario Canyon Fault. From a point where it merges with bedrock splays from the Northern Windy Wash Fault (fig. 4) that cross the south end of West Ridge, the Fatigue Wash Fault forms a nearly continuous, 9-km-long sinuous trace toward the south. The fault trace consists of a faultline scarp at the base of a bedrock escarpment near the mouth of Fatigue Wash, and of traceable faults, piedmont fault scarps, and lineaments in alluvial and colluvial deposits near the mouth of Solitario Canyon. The south end of the Fatigue Wash Fault consists of bedrock faults and bedrock scarps that appear to merge with the Southern Windy Wash Fault, indicating that the two faults are interconnected (Simonds and others, 1995).

Quaternary alluvial-fan and colluvial deposits are displaced where the fault cuts across the mouth of Solitario Canyon. Trench CF–1 (fig. 2), which was excavated across a scarp in Quaternary alluvium, shows evidence of several Quaternary faulting events (see chap. 8). Several scarps in Quaternary alluvium lie between the Fatigue Wash and Windy Wash Faults to the west; the east-facing scarps may be antithetic to the Fatigue Wash Fault.

The down-to-the-west displacement of bedrock along the northern section of the Fatigue Wash Fault is about 100 m, but south of the mouth of Fatigue Wash, displacement is nearly 400 m (Day and others, 1998a). The average dip of the fault plane is about 70° W.; slickenside lineations on the fault plane have a moderate component of left slip that indicates net left-oblique displacement. The Quaternary displacement is about 2.2 m (table 5).

Although the Fatigue Wash Fault is well exposed for a distance of 9 km, the overall length of the fault may be as much as 17 km if its poorly exposed north end extends to Yucca Wash. However, little evidence was observed for Quaternary displacements on the fault north of its intersection with the northern section of the Windy Wash Fault at West Ridge. Thus, the central and, possibly, southern sections of the Fatigue Wash Fault south of that intersection appear to represent a geometric segment of the fault that exhibits the best evidence for Quaternary activity.

Windy Wash Fault

The Windy Wash Fault (figs. 2, 4), named for a prominent faultline scarp on the east side of Windy Wash, is traceable nearly continuously from the south rim of Claim Canyon Caldera (one of the eruptive centers in the southwestern Nevada volcanic field; Christiansen and Lipman, 1965) to the southeast edge of Crater Flat (Swadley and Carr, 1987; Frizzell and Shulters, 1990). The fault can be subdivided into three sections on the basis of contrasts in geomorphic expression and changes in dip direction. (1) The Northern Windy Wash Fault is marked by a west-dipping faultline scarp at the base of a bedrock escarpment that is continuous for 7 km, except for a 600-m-long interval where a bedrock fault splays to the east and appears to connect with the Fatigue Wash Fault (Simonds and others, 1995; Day and others, 1998a). (2) The central section of the fault is characterized by a 4- to 5-km-long discontinuous zone of east-facing scarps in the alluvial fan at the mouth of Solitario Canyon. (3) The geomorphic expression of the 9-km-long Southern Windy Wash Fault consists of a short (1 km long) series of west-facing fault scarps at the southernmost edge of the Solitario Canyon alluvial fan that continues southward into a prominent west-dipping faultline scarp at the base of a bedrock ridge. This scarp can be traced discontinuously for 5.5 km as the bedrock-alluvium contact along the southeast edge of Crater Flat. Near Stagecoach Road, the Southern Windy Wash Fault bends to the west. That southwest-trending segment of the fault consists of two parallel strands that merge to the south to form a 75-m-wide breccia zone. The fault appears to continue southward, except for a 500-m-wide gap where the faultline scarp bends to the south.

Evidence for Quaternary displacement along the Northern and most of the Southern Windy Wash Faults is limited to subtle scarps in Quaternary alluvium and fractures in the hanging walls of faultline scarps. Limits on the age of Quaternary displacements on the Northern Windy Wash Fault are provided by (1) several undisturbed mid-Quaternary to upper Quaternary talus fans that overlie the fault trace, and (2) results of exposure dating that show the exhumed fault surface to be no younger than late Pleistocene. Quaternary activity is indicated by fault scarps in alluvium along the central section of the fault. Trenches CF–2 and CF–3 (fig. 2), which were excavated across scarps in alluvium along the north end of the Southern Windy Wash Fault, contain evidence of multiple late Quaternary surface ruptures totaling about 3.7 m of offset, including a faulted upper Holocene deposit (see chap. 9; Whitney and others, 1986).

The bedrock displacement on the Windy Wash fault is uncertain; down-to-the-west displacement is interpreted to increase southward but is probably less than 500 m (Scott, 1990). Average dip is 63° W. on the Northern and Southern Windy Wash Faults, but east-facing fault scarps indicate eastward dips along the central section of the fault (Simonds and others, 1995). Slickenside measurements indicate mostly dip-slip displacement; slight components of both right and left slip were observed in some outcrops. Quaternary displacement is small, as indicated by subtle scarps in alluvium.

Individual exposures of the fault traces generally are less than 3 km long, and alluvial scarps are 1 to 2 km long. Connecting the fault traces, including east-facing scarps in alluvium, yields a total fault length of about 25 km for the Windy Wash Fault system (Simonds and others, 1995).

Northern and Southern Crater Flat Faults

Several bedrock faults and suspected Quaternary faults lie west of Windy Wash along the northeast edge of Crater Flat; these previously unnamed faults are here referred to

collectively as the Northern Crater Flat Fault (fig. 4). The fault zone contains two subparallel, north-northeast-trending faults, 300 to 600 m apart, that are marked by small discontinuous bedrock scarps, subtle scarps and lineaments in alluvium, and short bedrock-alluvium contacts. The faults are best exposed in northeastern Crater Flat and are poorly exposed east and south of Black Cone (fig. 2). The section of the fault east of Black Cone has been referred to as the Black Cone Fault (fig. 4).

Though lacking surface expression directly south of Black Cone, the Crater Flat Fault zone originally was postulated by Simonds and others (1995) to continue southward and to connect with a suspected Quaternary fault in southeastern Crater Flat. However, abrupt changes in orientation, differences in geomorphic expression, and contrasts in paleoseismic history revealed in trenches indicate that the two faults are probably separate structures (see chaps. 10, 11). The southernmost fault, referred to as the Southern Crater Flat Fault (fig. 4), is marked by a northeast-striking linear basalt-alluvium contact, fractured carbonate-cemented alluvium, subtle scarps in alluvium, and a linear stream channel. Other down-to-the-west structures may be present in the subsurface 1 to 2 km west of the Crater Flat Fault zone, on the basis of a northerly alignment of basaltic dikes and fissure vents and north-northwest-trending, 0.3- to 0.7-m-high, east-facing scarps in alluvium near Black Cone.

Four trenches were excavated on the Northern and Southern Crater Flat Faults (fig. 2): trenches CFF–T1 and CFF–T1A across scarps north of the basalt flows along the Southern Crater Flat Fault, and trenches CFF–T2 and CFF–T2A across a lineament and a fault scarp along the Northern Crater Flat Fault. Three of these trenches expose fault zones that disrupt alluvium, thus providing clear evidence for multiple Quaternary displacements on both faults that supplements the surface expressions of Quaternary activity. No trenches were excavated across the postulated faults to the west, although topographic scarps indicate that at least some of these structures may have had Quaternary activity.

The down-to-the-west normal faults displace bedrock by an unknown amount. One slickenside measurement indicates a moderate left-lateral component of slip on a 70°-dipping fault plane. Trench exposures, in combination with subtle scarps and lineaments in alluvium, indicate that late Quaternary displacement is small—less than 1 m (table 5).

Individual exposures of the fault traces generally are less than 1 km long, but several traces are as much as 2 km. Connecting the exposed traces of the Northern Crater Flat Fault in northeastern Crater Flat yields a total length of about 10 km. The Southern Crater Flat Fault ranges from 4 to 7 km in length, depending on the extent of stream and basalt-alluvium contact lineaments included in the measurement. If the two faults are connected, the total length could be as much as 20 km. No evidence for geometric segmentation was observed in either the Northern or Southern Crater Flat Fault.

Northwest-Trending Faults

Sever, Pagany, and Drill Hole Washes are conspicuous northwest-trending drainages that appear to be controlled by northwest-striking faults, as identified on the basis of geophysical investigations, bedrock mapping, and examination of drill cores from Drill Hole Wash (Scott and others, 1984). A similar fault also was inferred to project beneath the Quaternary alluvial deposits of Yucca Wash, but more extensive geologic and geophysical investigations have been unable to confirm the existence of this structure (Langenheim and Ponce, 1994; Dickerson and Drake, 1998; Day and others, 1998a). The Sever Wash and Pagany Wash Faults are exposed in bedrock and locally are expressed as small bedrock scarps. The Drill Hole Wash Fault is largely concealed by Quaternary alluvium, but examination of drill cores from the wash confirms the presence of several separate but interconnected faults (Rousseau and others, 1999). Quaternary alluvial terraces on the floors of the washes do not appear to be displaced by the northwest-trending faults. Trench T12 (fig. 2), which was excavated across the Pagany Wash Fault, exposes faulted bedrock on the trench floor, but the overlying bedrock regolith and colluvium are not displaced.

The northwest-trending faults are believed to be strike-slip faults because they dip steeply (>70°), fault-plane surfaces locally contain slickenside lineations that are nearly horizontal, and vertical displacements generally are less than 5 to 10 m (Scott and others, 1984). The Sever Wash and Pagany Wash Faults show slickenside orientations and Riedel shears that indicate right-lateral slip. The amount of right-lateral slip on each fault was estimated at about 40 m (Scott and others, 1984). O'Neill and others (1991) concluded that the northwest-trending faults are extensional structures related to the left-oblique component of displacement along the north-trending faults.

The Sever Wash and Pagany Wash Faults are each about 4 km long. Both faults appear to terminate against the Solitario Canyon Fault to the west and, though concealed, are postulated to merge with a western strand of the Bow Ridge Fault to the east (Day and others, 1998b). The Drill Hole Wash Fault, which also is about 4 km long, appears to merge with a strand of the Bow Ridge Fault.

Bare Mountain Fault

The Bare Mountain Fault is a generally north striking, east-dipping (50°–70°), normal- to oblique-slip fault that forms the structural boundary between Bare Mountain to the west and Crater Flat Basin on the east (fig. 1; Reheis, 1988; Monson and others, 1992). The fault is approximately 20 km long and for part of its length is traceable as the bedrock-alluvium contact. Although no direct surface evidence was observed as to the amount of down-to-the-east displacement

of bedrock (Paleozoic and Precambrian sedimentary strata), seismic-reflection data have been interpreted to indicate that the total offset of pre-Tertiary rocks is about 3.5 km (Brocher and others, 1998). Quaternary deposits are displaced along the Bare Mountain Fault, and young scarps are developed in alluvial fans (see chap. 12).

Rock Valley Fault

The Rock Valley Fault system includes several east-northeast-striking left-lateral faults and numerous other complex interconnecting faults within Rock Valley (fig. 1). A transverse seismic profile across the valley indicates that the fault zone is characterized by a series of narrow blocks cut by faults that dip steeply north and do not change in dip within the upper few thousand feet of bedrock (Tertiary volcanic rocks underlain by Paleozoic strata; Hinrichs, 1968). The result is a subdued half-graben in which the Tertiary strata are horizontal or dip slightly (≤20°) north. Various lengths have been shown for the fault system. If only faults in central Rock Valley are included, a minimum length of 19 km is indicated (Yount and others, 1987). However, if these faults are continuous with those to the northeast in Frenchman Flat, the minimum length would be 32 km, and a maximum length of 65 km is possible if they also connect southwestward to faults in Amargosa Valley (see Piety, 1994). O'Leary (2000) showed a length of 50 km, not extending the fault system into Amargosa Valley.

The Rock Valley Fault zone has been episodically active since late Oligocene time, with a total left-lateral displacement of less than 4 km (O'Leary, 2000). Although no large vertical displacement has occurred during the past 10 m.y., clear evidence was observed that Holocene deposits are displaced (see chap. 13). Quaternary fault scarps are preserved in many places, particularly in the central section of the fault zone, where scarps range in height from less than 1.0 to 2.5 m. Relations exposed in western Rock Valley show the formation of a 3-km-wide graben with a scarp relief of nearly 2 m. A trench across one of the bounding graben faults reveals a faulting event with 10 to 32 cm of vertical displacement during the past 38 k.y. (Yount and others, 1987). Evidence was also observed of earlier Quaternary faulting events, as well as an event possibly later than 2.5 ka. Repeated small earthquakes within Rock Valley and vicinity indicate that faults within the zone remain active—for example, the Little Skull Mountain M=5.6 earthquake of June 29, 1992 (Harmsen, 1994) and M=3.5 earthquake of September 7, 1995 (Smith and others, 2000).

Chapter 4

Summary of Studies in Midway Valley

By John R. Wesling,[1] John W. Whitney, Frank H. Swan,[1] and Michael M. Angell[1]

Contents

Abstract 33
Introduction 33
Geologic Setting 34
    Bedrock Stratigraphy 34
    Surficial Deposits 34
    Structure 35
Trenching Activities and Results 38

Abstract

Midway Valley, a gently east sloping alluviated lowland lying east of Yucca Mountain in southwestern Nevada, has been studied extensively as the location for surface facilities associated with the proposed underground repository site for the storage of high-level radioactive wastes. Detailed geologic mapping, logging of trenches across faults, core drilling, and geophysical surveys provide data for determining the location and recency of faulting with respect to the proposed surface facilities.

The Tiva Canyon Tuff of Miocene age forms the bulk of bedrock exposed in the hills and ridges directly east, west, and south of Midway Valley, and post-Tiva Canyon rocks are exposed to the north. Surficial deposits, ranging in age from early Pleistocene to Holocene, that blanket the valley floor have been divided into eight map units for the purpose of determining the history of sedimentation and faulting during the Quaternary.

Structurally, Midway Valley is an east-dipping half-graben that is elongate north-south and bounded by two north-trending, west-dipping normal faults along the valley margins: the Bow Ridge Fault to the west and the Paintbrush Canyon Fault to the east. These two faults vertically displace bedrock as much as 125 and 500 m, respectively, and both faults display evidence of Quaternary activity. A series of inferred small-scale north-trending normal faults has been projected beneath the surficial deposits flooring the valley; one of these faults, in central Midway Valley (Midway Valley Fault) is depicted as having an estimated down-to-the-west displacement in bedrock of several tens of meters. The presence of such faulting is supported by geophysical data; however, no evidence was observed for displacement of the overlying surficial deposits within the valley.

Three trenches, excavated across faults on the east side of Exile Hill (west edge of Midway Valley), expose fractured but unfaulted Quaternary deposits overlying a bedrock fault (Exile Hill Fault). Although fracture zones were observed in alluvial deposits exposed in one of these trenches, as well as in some test pits east of Exile Hill, no bedrock was exposed in the excavations to determine the relation of the fractures to any known fault. A fourth trench was located across a projected trace of the Bow Ridge Fault north of Exile Hill, but no evidence of displacement of the exposed alluvium was observed. However, Quaternary faulting events are conspicuously displayed in trenches across the Bow Ridge Fault on the west side of Exile Hill and across the Paintbrush Canyon Fault at the south end of Midway Valley. Neither of these two faults is in areas where future surface ruptures would intersect the proposed site of surface facilities in Midway Valley.

Introduction

Midway Valley, lying between Yucca Mountain on the west and Alice and Fran Ridges on the east (figs. 1, 2), forms a gently east sloping alluviated lowland crossed by drainages heading in Drill Hole, Pagany, Sever, and Yucca Washes to the west and northwest and flowing eastward into Fortymile Wash. The valley has been considered as the location of surface facilities associated with the proposed repository site for the storage of high-level radioactive wastes beneath Yucca Mountain to the west (Neal, 1985). Accordingly, the geology of Midway Valley has been the subject of extensive study during the Yucca Mountain site-characterization program, with the general objective of acquiring surface and near-surface geologic data on the stratigraphic and structural relations of Quaternary deposits and Tertiary bedrock. Such data are required to evaluate the potential for future faulting and seismicity near the proposed site of surface facilities for the handling of high-level radioactive wastes.

[1]Geomatrix Consultants, Inc., Oakland, Calif.

This chapter briefly summarizes the results of detailed geologic mapping, logging of trenches across faults, core drilling, and geophysical profiling that have been conducted for the specific purpose of ascertaining the location and recency of faulting near the proposed surface facilities in Midway Valley; such studies were discussed in detail by Swan and others (2001). Additional sources of published data include the maps and reports by Scott and Bonk (1984), Neal (1985, 1986), Gibson and others (1992), Wesling and others (1992), Ponce (1993), Ponce and Langenheim (1994), Simonds and others (1995), and Day and others (1998a).

Geologic Setting

Bedrock Stratigraphy

The Miocene Tiva Canyon Tuff forms the bulk of bedrock exposed in the hills and ridges directly east, west, and south of Midway Valley, and post-Tiva Canyon rocks (rhyolite of Comb Peak) are exposed to the north (Scott and Bonk, 1984; Day and others, 1998a). The Tiva Canyon is one of the younger formations in the Paintbrush Group, which consists of an extensive series of welded and nonwelded silicic pyroclastic flow and fallout tephra deposits and volcanic breccia erupted from nearby calderas in the southwestern Nevada volcanic field (Sawyer and others, 1994). In addition to voluminous pyroclastic deposits, the Paintbrush Group also contains lava flows and domes, such as the rhyolites of Delirium Canyon, the rhyolite of Vent Pass, and the rhyolite of Black Glass Canyon. Other units exposed locally at the surface and (or) penetrated in shallow excavations and boreholes include the Topopah Spring and Pah Canyon Tuffs of the Paintbrush Group and the Rainier Mesa Tuff of the Timber Mountain Group. Each of these formations has been subdivided to facilitate detailed geologic mapping and the measuring of fault offsets (for example, Buesch and others, 1996). The total thickness of Tertiary volcanic rocks in the study area exceeds 1,200 m, on the basis of data from borehole UE–25p#1 at the extreme south end of Midway Valley (Muller and Kibler, 1984).

Surficial Deposits

Midway Valley is blanketed by surficial deposits composing a stratigraphic sequence that is closely similar to the eight alluvial units (such as units QT0 and Qal, tables 2, 3) described in chapter 2. Colluvial deposits of colluvium (such as units QTc and Qcl, pl. 1), which interfinger with correlative alluvial deposits near the valley margins, have also been dis-

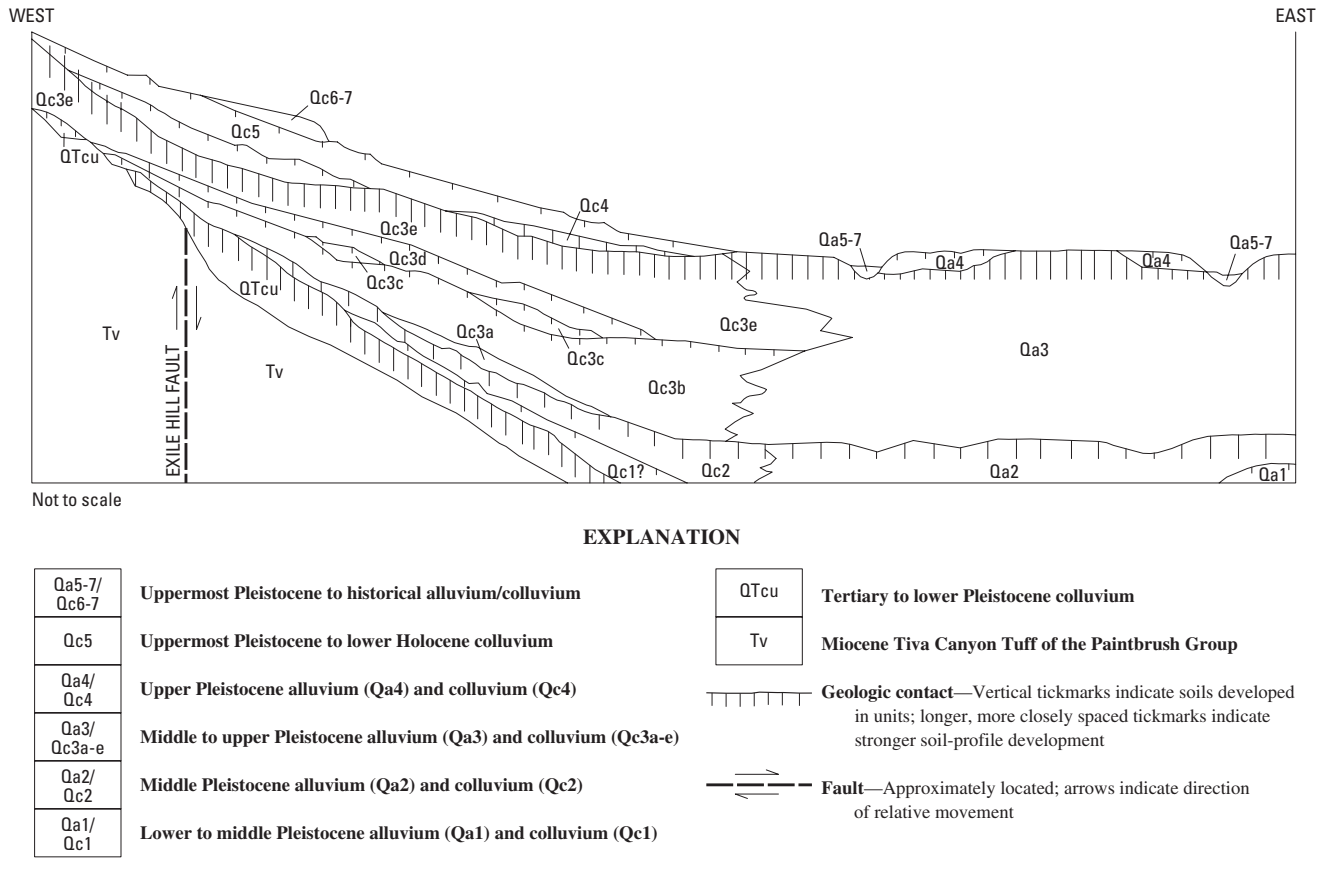

Figure 5. Schematic cross section showing stratigraphic relations among bedrock, alluvium, and colluvium in western Midway Valley, southwestern Nevada (from Swan and others, 2001).

tinguished (fig. 5). The colluvial sequences are readily observable only in test pits and trenches excavated along the east side of Exile Hill, at the west edge of the valley (pl. 1; fig. 6).

Structure

Midway Valley is a half-graben, elongate north-south, that is bounded by two north-trending, west-dipping normal faults along the valley margins: the Bow Ridge Fault to the west, on the west side of Exile Hill (fig. 7); and the Paintbrush Canyon Fault to the east (fig. 4; Scott and Bonk, 1984; Simonds and others, 1995; Day and others, 1998a). These two faults vertically displace bedrock as much as 125 and 500 m, respectively, and both faults display evidence of Quaternary activity. The Bow Ridge and Paintbrush Canyon Faults are discussed in chapters 3 and 5.

Cross sections drawn across the valley by Scott and Bonk (1984), Carr (1992), and Day and others (1998a) show a series of inferred small-scale normal faults beneath the surficial deposits; one of these faults, in central Midway Valley, is depicted as having an estimated down-to-the-west displace-

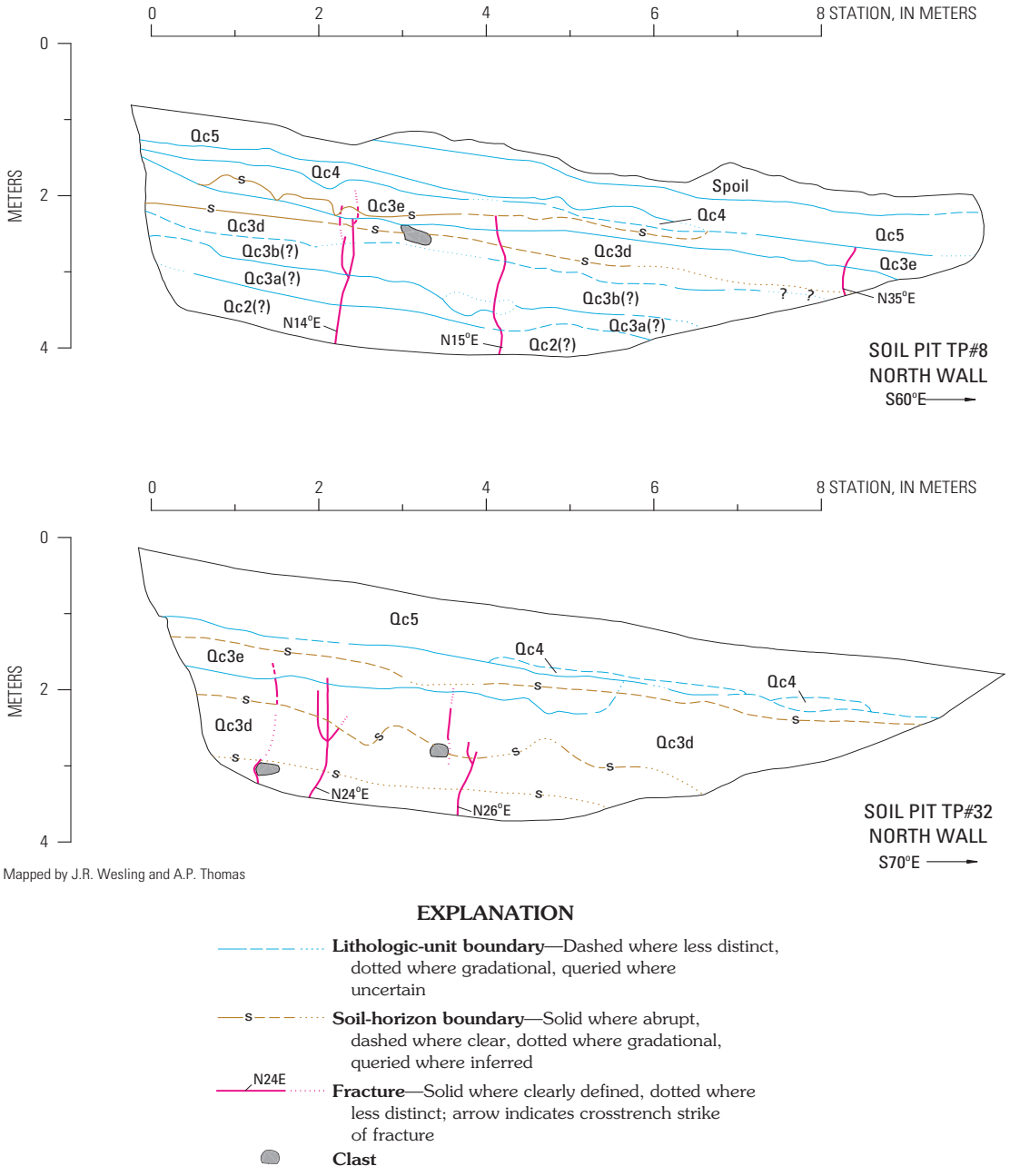

Figure 6. Cross sections of test pits shown in figure 8 (see fig. 5 for explanation of map units).

ment of several tens of meters in the underlying bedrock. This fault, considered to be the northward extension of a west-dipping normal fault mapped in the Tiva Canyon Tuff in the southern part of Bow Ridge (Scott and Bonk, 1984; Day and others, 1998a), was referred to as the Midway Valley Fault (fig. 4) by Neal (1986). Lipman and McKay (1965) and Day and others (1998a) extended the fault to the north-northeast for more than 6 km through central Midway Valley. Anomalies attributable to the presence of concealed faults have also been detected by electromagnetic-sounding data (Frischknecht and Raab, 1984), other resistivity/geoelectric surveys (Fitterman, 1982; Senterfit and others, 1982; Smith and Ross, 1982), and gravity and magnetic surveys (Ponce, 1993; Ponce and Langenheim, 1994). The combined evidence thus supports the interpretation that one or more buried faults displace the bedrock within Midway Valley (fig. 7); however, no surface displacements of surficial deposits have been observed along the projected traces of any of these faults.

The trace of a north-striking, steeply east dipping normal fault, named the Exile Hill Fault (fig. 8), was projected beneath surficial deposits along the east edge of Exile Hill by Day and others (1998a). The fault is shown to merge southward with the Midway Valley Fault. Original detection of this buried feature was based on electrical-resistivity data (Senterfit and others, 1982; U.S. Geological Survey, 1984). Subsequently, seismic reflection and refraction surveys (Neal, 1986), as well as gravity and ground magnetic data (Ponce, 1993; Ponce and Langenheim, 1994), were interpreted to indicate the presence of minor faulting along the east base of Exile Hill (see next section).

Two north-northwest-trending, near-vertical normal faults displace units of the Tiva Canyon Tuff exposed at Exile Hill (figs. 7, 8), and terminate southward against the Exile Hill Fault near the proposed site of surface facilities at the east edge of the hill (fig. 8). The East Portal Fault, which crops out along the east side of Exile Hill, is well exposed in the cutslope of the North Portal of the Exploratory Studies Facility

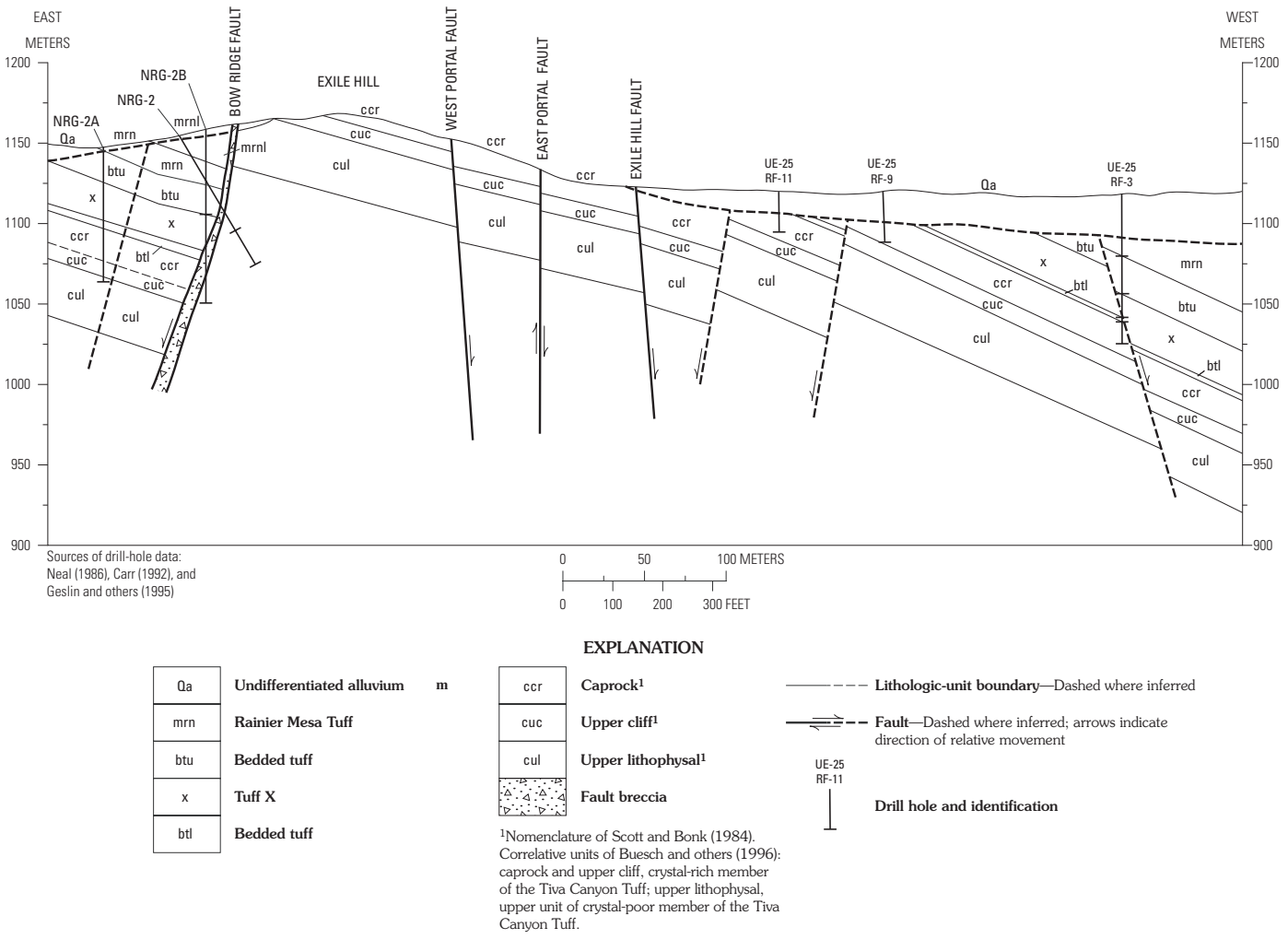

Figure 7. Cross section showing structure across Exile Hill and western Midway Valley, southwestern Nevada (from Swan and others, 2001) (see fig. 8 for locations).

(ESF) that is located near borehole UE–25 NRG#1 (fig. 8). The exposed segment of the fault strikes N. 7° W., dips steeply west to vertical, and exhibits slight right-lateral movement. Its surface trace in the Tiva Canyon Tuff has no geomorphic expression, and where buried by a thin mantle of upper Quaternary alluvium, these deposits do not appear to be displaced. At the North Portal excavation, the fault zone is 3 to 4 m wide, and the apparent down-to-the-east displacement in bedrock is 30 to 40 m. To the southeast, the East Portal Fault terminates abruptly against the Exile Hill Fault (as is readily observable in the North Portal excavation). From a point northwest of the northern peak of Exile Hill, the West Portal Fault extends

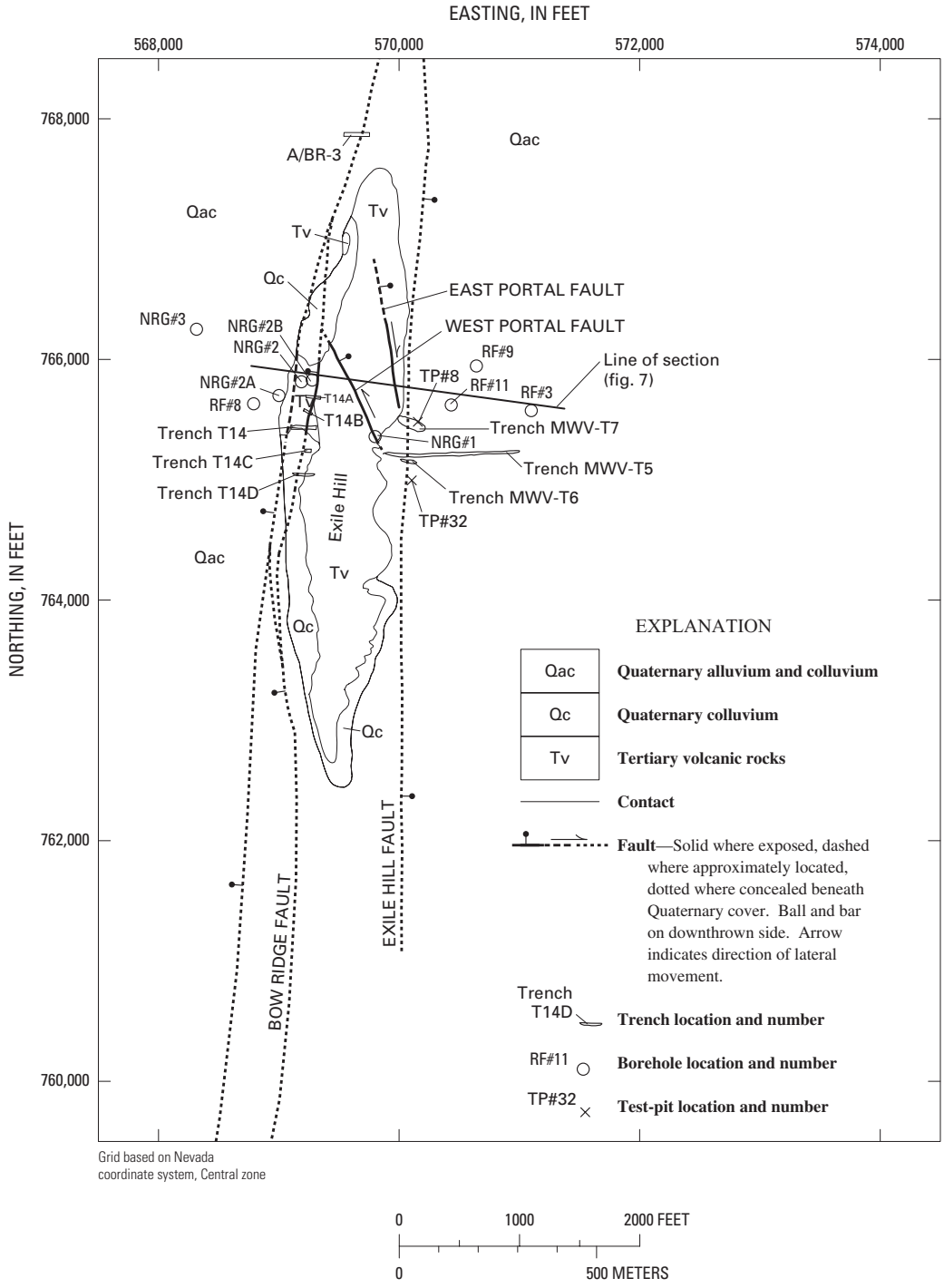

Figure 8. Exile Hill area, southwestern Nevada (fig. 2), showing general geology and locations of faults, trenches, test pits, and boreholes (labeled without prefix "UE–25"). North Portal of Exploratory Studies Facility is near borehole NRG#1. Adapted from Swan and others (2001).

southeastward to where it also terminates against the Exile Hill Fault, a distance of about 500 m (fig. 8). The fault strikes about N. 20° W., dips 88° NE., and displays down-to-the-east displacement with a minor left-lateral component. In exposures, the fault consists of a breccia zone, less than 1 m wide. At its northwest end, units of the Tiva Canyon Tuff locally are vertically offset about 10 m, and maximum displacement elsewhere along the fault is estimated at less than 15 m. Quaternary colluvium does not appear to be displaced by the West Portal Fault.

The strike-slip faults mapped along Drill Hole, Pagany, and Sever Washes project southeastward toward the west edge of Midway Valley but were shown to terminate against a strand of the Bow Ridge Fault west of Exile Hill on the map by Day and others (1998a). These faults are described in chapter 3.

Trenching Activities and Results

A principal element in the program of geologic and related studies in Midway Valley was the selection of sites for test-pit and trench excavations, the mapping of which would provide data needed to (1) identify possible Quaternary fault movements with respect to proposed surface facilities for the handling of high-level radioactive wastes, and (2) characterize the amount and timing of possible Quaternary displacements. During the course of the investigations, three trenches (MWV–T5, MWV–T6, MWV–T7, fig. 2) were excavated across faults on the east side of Exile Hill (fig. 8). Trench MWV–T7, which is located within one of the sites for proposed surface facilities (Neal, 1985), exposes stratigraphic and structural features representative of the geologic relations along the west side of Midway Valley at Exile Hill (pl. 1). A fourth trench (A/BR–3) was excavated across a projected trace of the Bow Ridge Fault north of Exile Hill (fig. 8), and a fifth trench (MWV–T4) across the trace of the Paintbrush Canyon Fault at the south end of the valley (fig. 2; see chap. 5). In addition, some 30 test pits were excavated at selected localities and described to characterize the soils and lithology of deposits associated with each of the principal surficial deposits and to facilitate the correlation of map units within the study area.

The Exile Hill Fault is exposed in bedrock in trench MWV–T7 ("crushed" zone 3, pl. 1), as well as in trenches MWV–T5 and MWV–T6, and in the North Portal excavation. Structural and stratigraphic relations among these exposures indicate a stratigraphic throw (down to the east) of as much as 15 m or less within the Tiva Canyon Tuff (fig. 7). Average dip is greater than 80° E. Steeply dipping, northeast-striking fractures that break, but do not measurably displace, upper Pleistocene and older colluvial deposits were identified in these trenches, as well as in test pits that were excavated across the fault; the fracture systems observed in trench MWV–T7 and in two of these test pits are shown in plate 1 and figure 6, respectively. The fractures in the colluvium, within a zone about 15 m wide, are traceable downward into northeast-trending bedrock faults that define the main trace of the Exile Hill Fault (for example, within "crushed" zone 3, pl. 1). Mapping and related studies of the faults and fractures clearly demonstrate the following relations:

1. Upper Pleistocene deposits (units Qa4, Qc4, pl. 1) are essentially continuous, are not displaced by surface faults, and are not fractured (fig. 6).
2. Known and inferred bedrock faults are overlain by lower to upper Pleistocene deposits (units Qc3/Qa3, Qc2/Qa2, Qcl/Qal, pl. 1) that have distinct soil and lithologic horizons which are fractured but not measurably displaced (within the limits of mapping resolution, which mostly ranges from 0 to 5 cm).
3. Locally, the contact between much older (Pliocene? to lower Pleistocene) cemented calcrete soils and bedrock appears to be offset slightly downward (≤10 cm) across minor shears in the Exile Hill Fault zone (for example, stas. 24–30, pl. 1). Carbonate- and silica-filled fractures in unit QTc are continuous with bedrock shears. The fractures either die out within unit QTc or are truncated at the QTc-Qcl? contact, and they are discontinuous with fractures in the overlying colluvium (unit Qcl and younger). Fractures that disrupt the colluvial sequence are observable east of these steps at the QTc-Tv contact.

A second fracture zone was observed in alluvial deposits near the east end of trench MWV–T5 (figs. 2, 8), as well as in test pits, approximately 155 m east of Exile Hill. No bedrock exposures were observed in these excavations, however, to determine the relation of the fracture zone to any known fault. No displacement of lithologic contacts and soil horizons within the Quaternary units could be detected.

The origin of the fractures in the Quaternary deposits is uncertain. Nontectonic causes cannot be completely ruled out, including such mechanisms as (1) fracturing caused by an ephemeral disruption during the transmission of seismic waves (for example, strong ground shaking from an earthquake on a nearby fault), and (2) release of residual stress in the Tertiary bedrock. However, despite the presence of faults and fractures widely varying in trend along the fault zone at the base of Exile Hill, fracturing does not explain why Quaternary fractures are associated with only the north- to northeast-trending faults. The episodic, though infrequent, development of tension fractures during the early Quaternary and mid-Quaternary is also difficult to explain simply by release of residual stress, as in mechanism 2. Partial release of residual stress in shallow rock during successive, widely separated episodes on a preexisting bedrock fault seems unlikely without an external triggering mechanism. Paleoseismic data indicate repeated mid-Quaternary to late Quaternary surface ruptures on the Bow Ridge and Paintbrush Canyon Faults, which bound the Midway Valley structural block (see chap. 5). Given the apparent episodic occurrence of the fractures and their consistent north-northeastward orientation, continuity along strike, and coincidence with the Exile Hill Fault and other faults in the underlying Tertiary bedrock, a more likely explanation is that the Quaternary fractures represent minor intrablock deformation of the otherwise relatively stable

Midway Valley structural block, triggered by activity on block-bounding faults, rather than from nontectonic causes.

Minor northwest-trending bedrock fractures and shears, possibly associated with the East Portal Fault, were observed in the west end of trench MWV–T7 (pl. 1; fig. 2). None of these northwest-trending fractures or shears, also observed in trench MWV–T5, extends upward into the overlying lower to middle Pleistocene colluvial deposits, and they do not cause offset of the bedrock-colluvium contact.

Trench A/BR–3 (figs. 2, 8) was excavated across two subparallel photolineaments defined by a weak alignment of vegetation. The photolineaments coincide with the projected northward trace of the Bow Ridge Fault as mapped by Scott and Bonk (1984) and Day and others (1998a). The trench was excavated in alluvial-fan deposits similar in age to those at or near the surface on the east side of Exile Hill. No evidence was observed during detailed mapping of the sedimentary contacts and soil-horizon boundaries to indicate that any of the deposits or soils are displaced or otherwise deformed by faulting, at least to the extent detectable within the limits of resolution of the mapping techniques used.

Trenches across the Bow Ridge Fault on the west side of Exile Hill (trench 14 complex, fig. 8) and along the Paint-brush Canyon Fault trace on the east side of Midway Valley (for example, trenches A1, MWV–T4, figs. 2, 8) are described in chapter 5.

Chapter 5

Summary of Quaternary Faulting on the Paintbrush Canyon, Bow Ridge, and Stagecoach Road Faults

By Christopher M. Menges, Emily M. Taylor, John R. Wesling,[1] Frank H. Swan,[1] Jeffrey A. Coe, Daniel J. Ponti, and John W. Whitney

Contents

Abstract 41
Introduction 42
Paintbrush Canyon Fault 42
    Busted Butte 42
    Trench MWV–T4 55
    Trench A1 56
Bow Ridge Fault 58
    Trench T14D 59
    Trench T14 63
Stagecoach Road Fault 63
    Trenches SCR–T1 and SCR–T3 63

Abstract

The Paintbrush Canyon, Bow Ridge, and Stagecoach Road Faults east and southeast of Yucca Mountain all show evidence of multiple Quaternary faulting events. Variations in available numerical-age control, in combination with uncertainties in both estimated age and (or) displacements, typically result in a range of such time-dependent faulting parameters as recurrence intervals and slip rates.

Gullies incised into sand ramps along the west side of Busted Butte expose the most complete record of Quaternary activity along the southern section of the Paintbrush Canyon Fault. Six to seven faulting events have been distinguished, with a cumulative dip-slip displacement of about 600 cm and preferred estimates of the net displacement per event ranging from 28 to 167 cm. Average preferred recurrence intervals range from 50 to 120 k.y., and for the three latest faulting events from 65 to 95 k.y. Preferred estimates of late Quaternary slip rates at Busted Butte range from 0.004 to 0.009 mm/yr, and long-term average slip rates for the entire post-early Pleistocene paleoseismic record in the Busted Butte exposures range from 0.008 to 0.01 mm/yr.

Trenches also reveal details of Quaternary fault activity. Trench MWV–T4, located on the central section of the Paintbrush Canyon Fault near the south end of Midway Valley, exposes a record of three or four Quaternary faulting events with an estimated cumulative dip-slip displacement of 170 to 270 cm and preferred estimates of the displacement per event of 20 to 98 cm. Average recurrence intervals range from 20 to 50 k.y., and slip rates from 0.01 to 0.03 mm/yr. Trench A1, which was excavated across the projected trace of the northern section of the Paintbrush Canyon Fault, exposes a 5-m-thick sequence of Quaternary deposits that shows evidence of at least four faulting events. Cumulative vertical displacement of Quaternary deposits is 145 to 170 cm, with calculated recurrence intervals of 80–100 k.y. and an estimated fault slip rate of 0.002 mm/yr.

The history of Quaternary activity on the Bow Ridge Fault is based largely on exposures in trench T14D, which was excavated across the northern section of the fault on the west side of Exile Hill. A well-defined sequence of alluvial, colluvial, and eolian deposits displays evidence of two or three middle to late Pleistocene faulting events, with preferred estimates of the net displacement per event ranging from 13 to 44 cm. Preferred average estimates of the recurrence interval and slip rate are 100–140 k.y. and 0.003 mm/yr, respectively. Trench T14, located about 50 m north of trench T14D, exposes a well-defined fault zone between Tertiary bedrock and Quaternary deposits that contains numerous vertical veins of secondary calcite and opaline silica whose origin is interpreted to be associated with downward percolation of meteoric water rather than with ascending spring water.

Fault relations on the Stagecoach Road Fault are well expressed in a 3- to 3.5-m-thick sequence of varied mid-Quaternary to upper Quaternary deposits that is exposed in

[1]Geomatrix Consultants, Inc., Oakland, Calif.

trenches SCR–T1 and SCR–T3. Two to four late Pleistocene to Holocene(?) faulting events are represented, with a cumulative net displacement of 1.0 to 3.1 m and preferred estimates of the net and dip-slip displacements per event of 40 to 67 cm. The most internally consistent set of geochronologic controls, which also agrees with age correlations of disseminated basaltic-ash horizons, yields preferred estimates of the average paleoearthquake-recurrence intervals and fault-slip rate of 20–50 k.y. and 0.02 to 0.03 mm/yr, respectively.

Introduction

This chapter summarizes available data on the geometry, structural style, stratigraphic displacement (including both cumulative displacement and individual displacement per faulting event), slip orientation, and chronology of Quaternary faulting events on the Paintbrush Canyon, Bow Ridge, and Stagecoach Road Faults. Because of their close proximity to Yucca Mountain and the proposed repository site for the storage of high-level radioactive wastes (figs. 1, 2), the history and extent of Quaternary surface ruptures along these faults is especially important for estimating paleoearthquake-recurrence intervals and fault-slip rates, as required for seismic-hazard analysis.

Paintbrush Canyon Fault

Paleoseismic investigations were conducted at three sites on the Paintbrush Canyon Fault (fig. 2): (1) at Busted Butte, toward the south end of the fault (Busted Butte walls 1–4); (2) in the central section of the fault (trench MWV–T4); and (3) to the north (trench A1). These exposures, discussed individually below, indicate that multiple Quaternary displacements have occurred on all three sections of the fault.

Busted Butte

The Paintbrush Canyon Fault is well exposed in two 25-m-deep gullies incised into sand ramps that are banked against the west slope of Busted Butte (Whitney and Muhs, 1991). Four of these gully walls (BB–W1 through BB–W4, hereinafter referred to as Busted Butte walls 1 through 4) were cleaned in August 1992 to enhance natural exposures of a succession of buried soils and stonelines displaced by the main fault (figs. 9, 10). Two of these exposures (Busted Butte walls 1, 4) were logged in detail because they contain the most complete stratigraphic record of faulting; the discussion below therefore focuses on the logs and interpretations from these two walls. No fault scarp or other topographic expression of the fault was observed where it crosses broad interfluves between the gullies (fig. 11).

Busted Butte wall 4 contains a west-dipping sequence of 10 unconsolidated lithologic units, including seven buried soils that represent the most complete stratigraphic succession at the Busted Butte trench site (fig. 9*A*). Bedrock is exposed locally in the footwall block at the bottom of the gully. The lower part of the sequence consists of thick massive sand layers (units 1–5), which are differentiated primarily on the basis of discontinuous stonelines at lithologic-unit boundaries. These stonelines are associated in places with two weakly developed carbonate soils (S1, S2, fig. 9*A*). The Bishop ash (760 ka; van den Bogaard and Schirnick, 1995) is preserved near the base of eolian sand-ramp deposits at the south end of Busted Butte, and similar silicic ash is intercalated with sand layers at the base of Busted Butte wall 4 (unit 1, fig. 9*A*). Thus, the sand ramps in this area chronicle approximately the past 600–700 k.y. of fault-displacement history. Lithologic units in the upper part of the wall (units 6–10, figs. 9, 10) generally are thinner and display greater lateral variations in thickness relative to the lower sand layers. The predominantly sandy deposits in the upper wall also contain coarser gravelly layers that typically mantle the slopes of two distinct buried fault scarps (see below).

Two moderately well developed buried soils (S3, S5, fig. 9) with $CaCO_3$ stage II–IV morphology (after Birkeland, 1984, and Machette, 1985) and locally abundant rhizoliths are conspicuous features in the upper part of Busted Butte wall 4. Both of these major soils are disrupted by prominent buried fault scarps. Soils continued to development after formation of the scarps, producing zones of silica-carbonate laminae (S3a, S5a) that mantle the scarp slope. At least one thin, poorly developed carbonate soil formed locally on units that bury the fault scarps as well (S4 on unit 7a and S6 on unit 9b, fig. 9*B*). On other walls, the two conspicuous buried soils are erosionally truncated at or west of the fault beneath weak pavements and thin soils developed on the erosional upper surface of the sand ramps (fig. 10). That type of erosional truncation apparently did not occur on wall 4, possibly in part because there the fault intersected the sand ramp at a site of net deposition downslope from areas of erosional stripping.

The main fault trace is well defined by a 0.2- to 5-m-wide zone of carbonate-coated shears and fractures that commonly increase in complexity upsection (figs. 9, 10). The average orientation and dip of the fault zone in these wall exposures are N. 15° E. and 70° W., respectively. Striations of probable tectonic origin on carbonate-coated shears (N. 11° E., 71° W.) in the sand-ramp fault zone exhibit left-oblique slip with a rake of 73° SW., and slickenlines with left-oblique slip with a rake of 47° were observed in nearby similarly oriented bedrock exposures of the fault (Whitney and Muhs, 1991; Simonds and others, 1995). The slickenside orientation was used to correct for net tectonic displacement because it represents the most direct and unambiguous link to Quaternary fault slip. The hanging-wall block in the upper part of most exposures is deformed by a complex network of minor synthetic and antithetic faults and fractures. Secondary hanging-wall deformation, which approaches 25 m in width in the northernmost exposure (Busted Butte wall 1), includes a small antithetic graben adjacent to the main fault near the top of the wall (fig. 10). On Busted Butte wall 4, two secondary synthetic fault

strands displace sand-ramp units in the footwall block to the east of the main fault trace (fig. 9*A*).

Structural and stratigraphic relations are summarized below for Busted Butte wall 4 because that exposure provides the most complete record of fault displacements. Successively smaller displacements of younger horizons, fault-generated colluvial wedges, and several buried scarps are interpreted to represent six or seven individual faulting events (table 6) with dip-slip surface displacements per event; factoring in measurement uncertainties, these displacements range from 0 to 246 cm, commonly from 40 to 130 cm (tables 7, 8). All of the six buried soils described above and three additional distinct stonelines are offset along the main fault trace (fig. 9).

The uppermost buried soil (S5, fig. 9) appears to have been displaced by at least two faulting events—most recent event Z and penultimate event Y—that produced colluvial slope deposits 9c and 9b, respectively (fig. 9*B*; table 8). These units drape downslope across the upper composite fault scarp formed above unit 8e. Event Z deformed and thus postdates a colluvial gravel (unit 9b) with a thin calcic soil (S6) that buried the initial fault scarp and related soil (S5a). The scarp and units associated with event Z were, in turn, buried by several undisturbed gravel or sand deposits that locally are plugged with secondary carbonate (for example, units 9c–9e, fig. 9*B*). Event Y is interpreted from a set of shears and fractures that displace the scarp and related soil (S5a) but terminate at the base of unit 9b. A possible third faulting event (X) may have produced a small initial paleoscarp (represented by the top of unit 8e) that developed after offsetting of the original buried soil (S5). This paleoscarp was reruptured subsequently by the two later faulting events (Y, Z) to form the composite upper buried scarp. Event X is queried because the composite scarp might have been formed by only events Y and Z. The cumulative vertical displacement of two to three of the latest faulting events affecting the upper buried soil is approximately 1.2 m, as measured by the total offset of unit 7a along all strands of the fault zone below the upper composite scarp (fig. 9*B*).

The next lower buried soil (S3, fig. 9), developed on unit 6, is displaced by one earlier faulting event (W) that occurred during soil development, causing a dip-slip displacement along the main fault trace of about 1.3 m that is associated with a lower buried fault scarp formed at the top of a colluvial wedge (unit 6e). An additional 25-cm displacement occurred on one of the eastern fault strands as well. The total dip-slip displacement across the main fault strand above and below the lower scarp is 2.2 to 2.5 m, including the cumulative displacement of the three or four faulting events at and above this stratigraphic horizon.

Below the two upper buried soils, two earlier faulting events (T, V) are recorded by carbonate-impregnated colluvial wedges in the midslope to lower slope of the sand ramp (units 4a, 6a, fig. 9*A*). A third earlier faulting event (U) is indicated in the lower part of the exposure by terminations of fractures beneath a small gravelly channel deposit adjacent to the fault zone (unit 5a, fig. 9*A*) and by decreasing differential displacements of units 4 and 5.

Minimum estimates of the cumulative dip-slip displacement of the buried stoneline on top of unit 3 (fig. 9*B*) are estimated to range from 4.3 to 6.7 m (preferred value, 5.1 m); net-slip adjustments increase this range to 4.5–7.0 m (preferred value, 5.3 m). These values were calculated by adding the cumulative offset of the top of unit 4, as measured on the log, to the total displacement from event T that is recorded in a stratigraphically lower colluvial wedge within unit 4 (unit 4a, fig. 9*A*). This procedure is required because the downthrown equivalent of the unit 3 stoneline is not exposed on the hanging wall. These estimates of the cumulative dip-slip displacement on Busted Butte wall 4 are somewhat larger, but within the same general range, as a dip-slip offset that was measured at the same approximate stratigraphic level on Busted Butte wall 2, where the lowermost soil, which is correlative with the soil horizon on unit 2 exposed on Busted Butte wall 4, is displaced 4 m along the main fault zone (Whitney and Muhs, 1991). This correlation is based on the morphology and relative stratigraphic positions of the soils on the two exposures. The two eastern secondary faults on Busted Butte wall 4 add another 0.9 m of cumulative dip-slip displacement at the stratigraphic levels of units 5 and 6, which, in combination with offsets observed on the main fault strand, yields a minimum estimate of 5.5 to 8.0 m (preferred value, 6.3 m) for the net cumulative displacement on units 1 and 2 at the base of the exposure.

The number and amount of the younger displacements cannot be deciphered clearly on Busted Butte walls 1 through 3 because the stratigraphic record at the fault zone is incomplete, resulting from erosional truncation of soils and units beneath the upper surface of the sand ramps. This problem is especially acute on the footwall block of these exposures. Busted Butte walls 2 and 3 were not logged in detail because of severe erosion of units at upper stratigraphic levels. On the lower part of Busted Butte wall 2, units beneath the lowermost buried soil (S1, fig. 9) are displaced by one or two faulting events (R, S) on a secondary eastern fault strand, although the soil itself is not much offset by that faulting event(s). As noted above, between this exposure and Busted Butte wall 4 the cumulative dip-slip displacement of that soil across the main fault zone is generally consistent. On Busted Butte wall 1, the latest two or three faulting events (X–Z) associated with graben deformation on the main fault zone can be correlated confidently with the faulting chronology of Busted Butte wall 4. Three earlier faulting events (U–W) have been correlated provisionally as well, but those correlations are more difficult because much of the stratigraphic section underlying the graben was stripped from the area now exposed on Busted Butte wall 2, indicating a period of erosion that predates graben formation. Erosion during and after graben development is confined primarily to the footwall block.

Age constraints on the long paleoseismic record of displacements on the Paintbrush Canyon Fault at the Busted Butte exposures are summarized below.

Earlier events T through V.—A maximum date for events T through V is provided by an approximate maximum age of 650–700 ka for the lowermost buried soil (S1, fig. 9) dis-

placed by these events. This estimate is derived from the stratigraphic position of the soil above the Bishop ash (760 ka; van den Vogaard and Schirnick, 1995) in unit 1 on Busted Butte wall 4 (fig. 9*A*). A minimum date of approximately 400 ka for this series of faulting events is derived from the estimated age of soil S3 (see below). Individual events in the series cannot be dated because no direct age control exists for units 2 through 6 in the lower and middle sections of the wall that contain events T through V.

Event W.—Event W occurred sometime between the formation of soils S3 and S5 (fig. 9). U-series analyses of pedogenic carbonate laminae collected on Busted Butte wall 4 (sample HD 961, fig. 9*A*; table 9; Paces and others, 1994) yielded poorly constrained ages of approximately 400 ka for soil unit S3, which predates event W and the formation of the lower buried scarp (unit 6, fig. 9), and of 270 to 300 ka (samples HD 962 and HD 1449, fig. 9*A*; table 9) for soil unit S5, which is disrupted across the upper fault scarp stratigraphically above this event (top of unit 8, figs. 8, 9).

Possible event X.—The latest two or three faulting events (X?, Y, Z) on the Paintbrush Canyon Fault postdate the formation of soil unit S5 and rhizolith-bearing soils on Busted Butte wall 4 and similar dated soils correlated from Busted Butte wall 1. A suite of rhizoliths in soil S5a that formed along the crest of a scarp on Busted Butte wall 1 yielded U-series ages of about 140 ka (sample HD 955A, fig. 10; table 9), somewhat younger than the cluster of rhizolith ages of 215 to 340 ka from a stratigraphically and lithologically similar unit (8b) in Busted Butte wall 4 (samples HD 962 and HD 1449, fig. 9*B*; table 9). Thus, the earliest of these faulting events (X?) may have occurred sometime between 300 ka, the approximate age of soil S5 (see above), and before at least the partial development of soil S5a, which has an estimated age of 150 to 300 ka derived from the associated rhizolith ages of units on both Busted Butte walls 1 and 4.

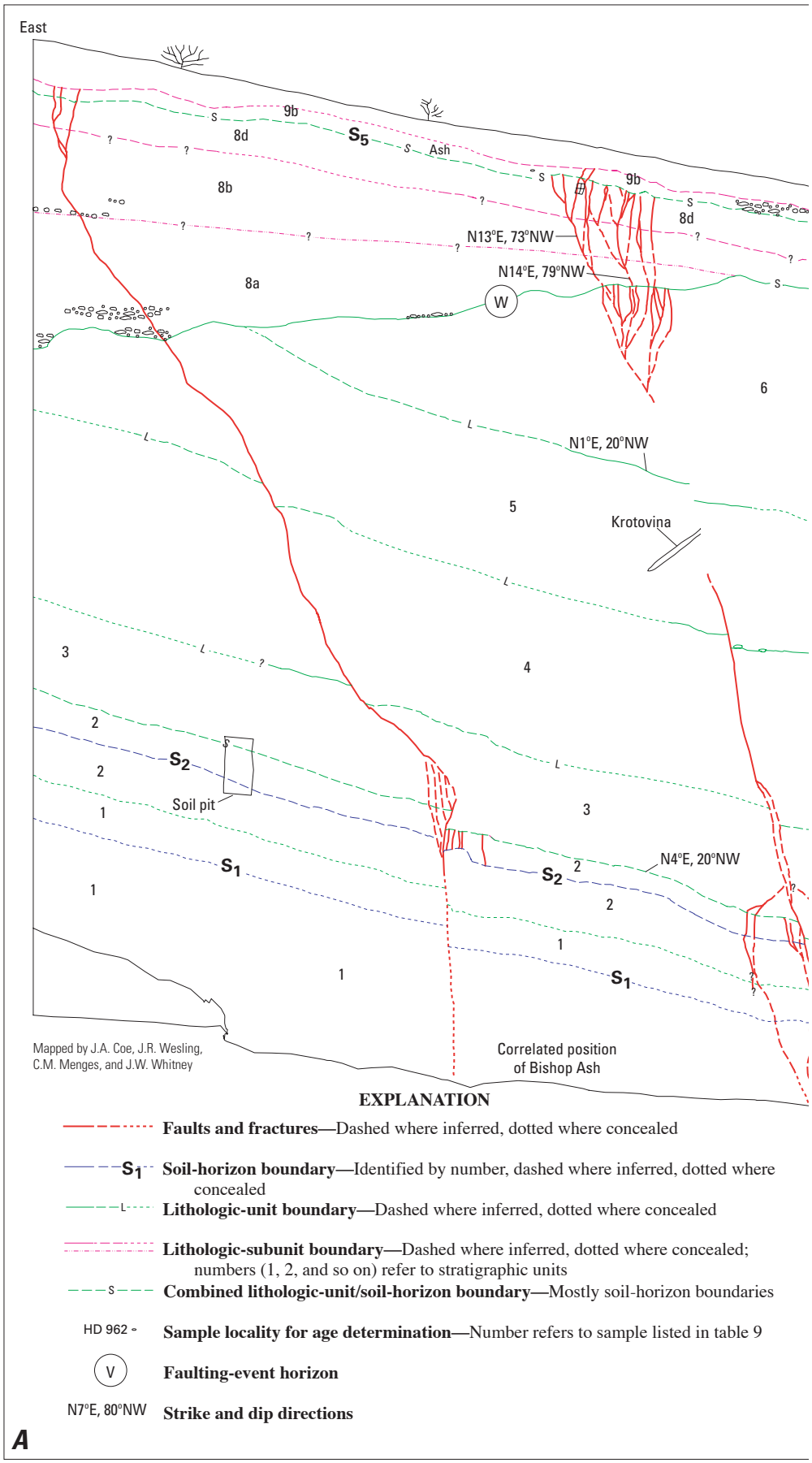

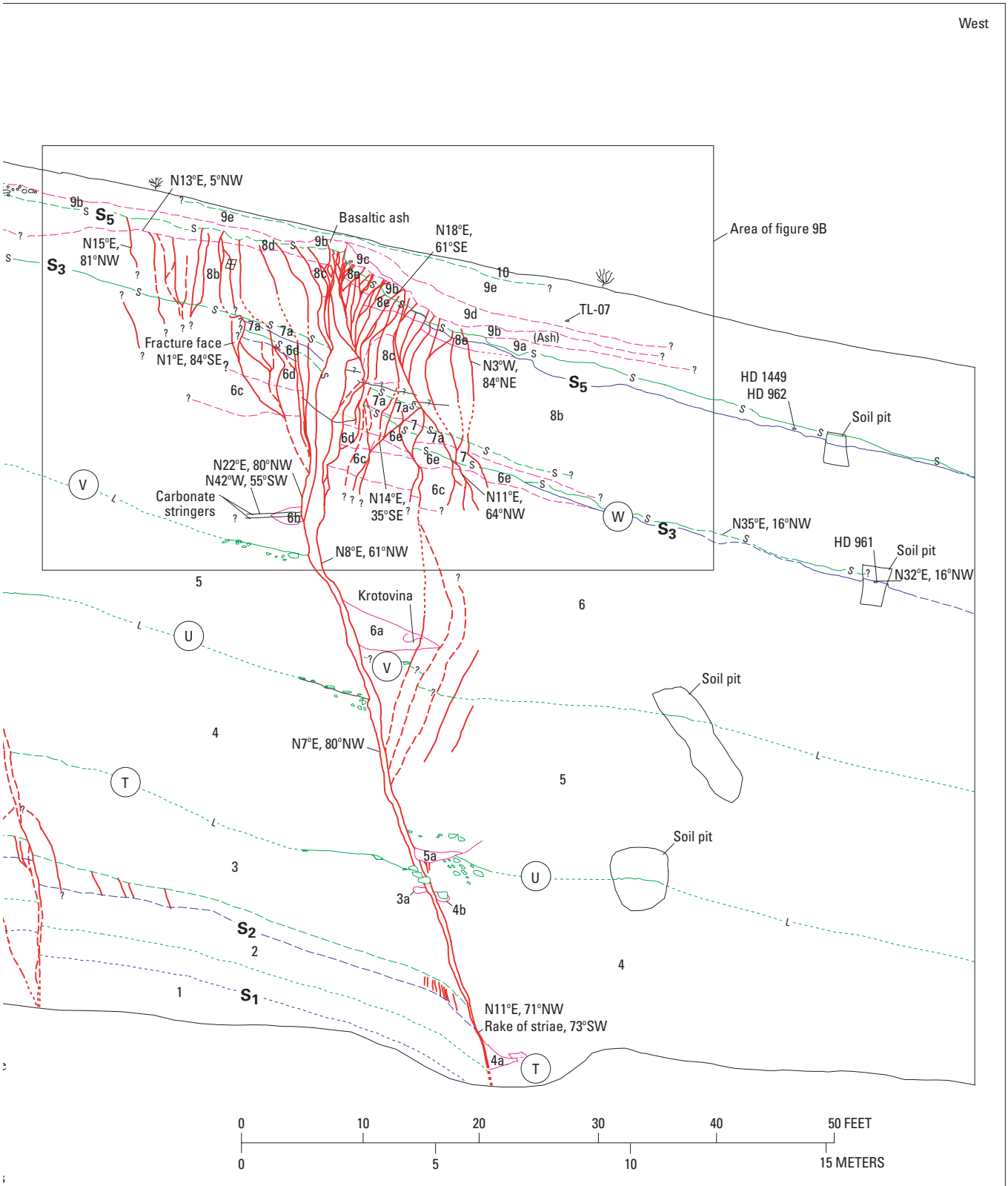

Figure 9. Simplified logs of natural exposures across the Paintbrush Canyon Fault in the Yucca Mountain area, southwestern Nevada (see fig. 1 for locations). *A*, At Busted Butte wall 4 (BB4, fig. 2). *B*, In upper part of Busted Butte wall 4.

Penultimate event Y.—The time interval between the development of soils S5a and S6 (fig. 9) brackets the penultimate faulting event (Y). Carbonate laminae with U-series ages of 70 to 80 ka along the fault zone toward the east end of Busted Butte wall 1 (sample HD 954, fig. 10; table 9) are correlated with soil unit S6, which formed on lithologic unit 9b and buried the upper scarp on Busted Butte wall 4 (fig. 9*B*). These ages, in combination with the broad estimated ages for soil 5a (see above), bracket event Y at approximately 300–80 ka, more likely 150–80 ka (table 10), allowing for uncertainties in the use of minimum ages (of rhizoliths and soils) to constrain event timing.

Most recent event Z.—Soil S6 (fig. 9) is displaced only by the most recent faulting event (Z), providing a minimum age constraint for that faulting event. A maximum age constraint is derived from a sand layer (unit 9b, fig. 9*B*) containing sparse basaltic ash that overlies both the carbonate laminae and upper fault-scarp soil (see events X, Y), and was deposited between events Y and Z. The basaltic ash is correlated provisionally with tephra from the Lathrop Wells basaltic cone south of Yucca Mountain (fig. 1), which is dated by the $^{40}Ar/^{39}Ar$ method at about 77±6 ka (Heizler and others, 1999). A minimum age constraint for event Z is provided by unfaulted sand layers, with a thermoluminescence age of 44±13 ka (sample TL–07, fig. 9*A*; table 9), that bury the fault scarp and postdate all faulting events (fig. 9*B*). These combined age relations establish a crude age bracket of 80–40 ka for the most recent faulting event (table 10). Fractures related to this event are coated extensively with carbonates, indicating that the most recent surface rupture probably occurred early within this interval (50–40 ka).

The above relations indicate average recurrence intervals ranging from 30 to 270 k.y. (preferred value, 50–120 k.y.) for the complete sequence of recognizable faulting events in the Busted Butte exposures (table 11). Individual recurrence intervals for the three latest faulting events range from 10 to 275 k.y. (preferred value, 65–95 k.y.). Average slip rates of 0.001 to 0.01 mm/yr in mid-Quaternary to late Quaternary time were computed, based on the displacements of three units at different stratigraphic levels (tables 11, 12); the preferred value for the entire sequence is 0.007 mm/yr. Long-term average slip rates computed for the lowermost soil (S1), spanning the entire exposed paleoseismic record, range from 0.008 to 0.01 mm/yr.

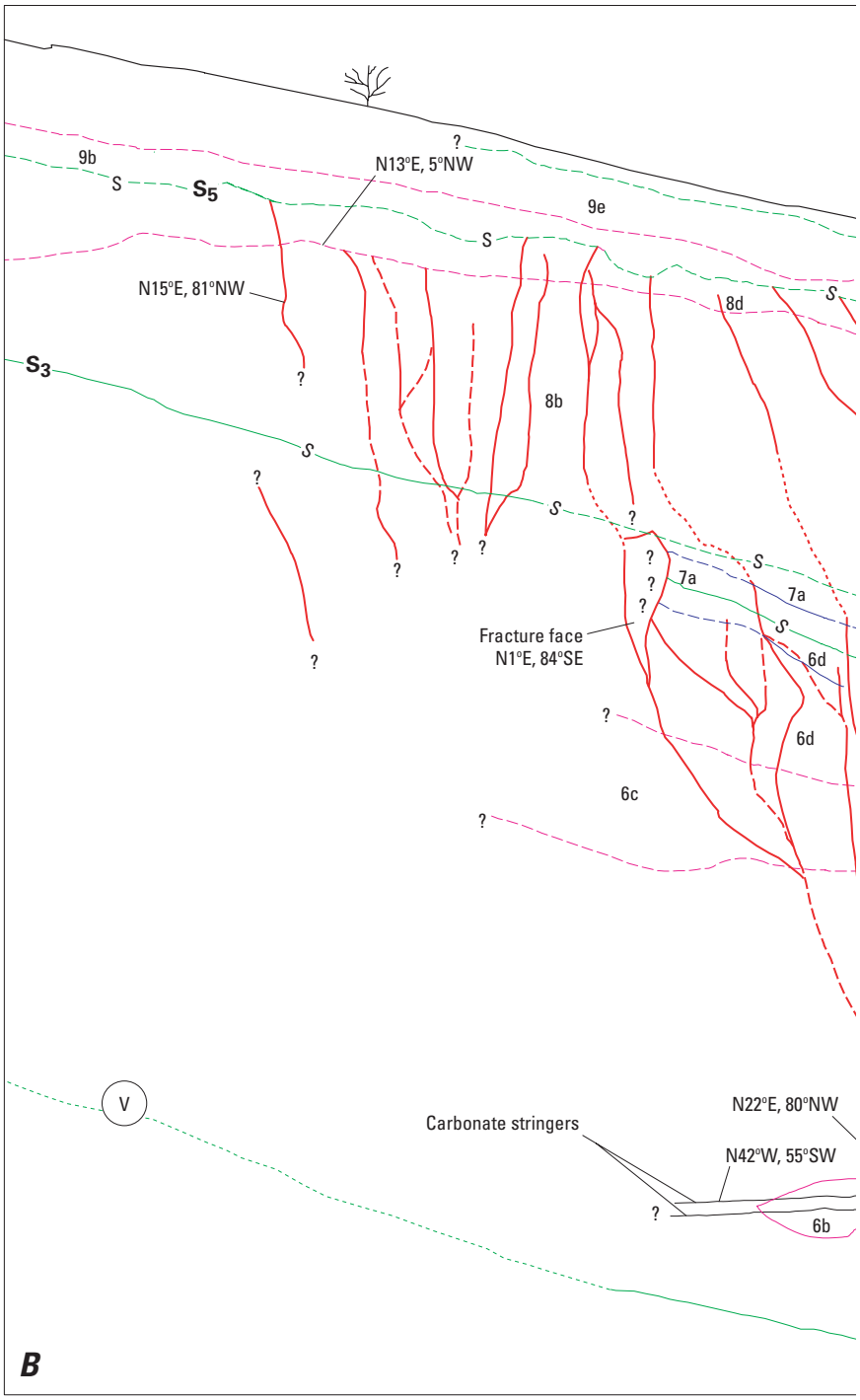

Mapped by J.A. Coe, J.R. Wesling, C.M. Menges, and J.W. Whitney.

Figure 9.—Continued

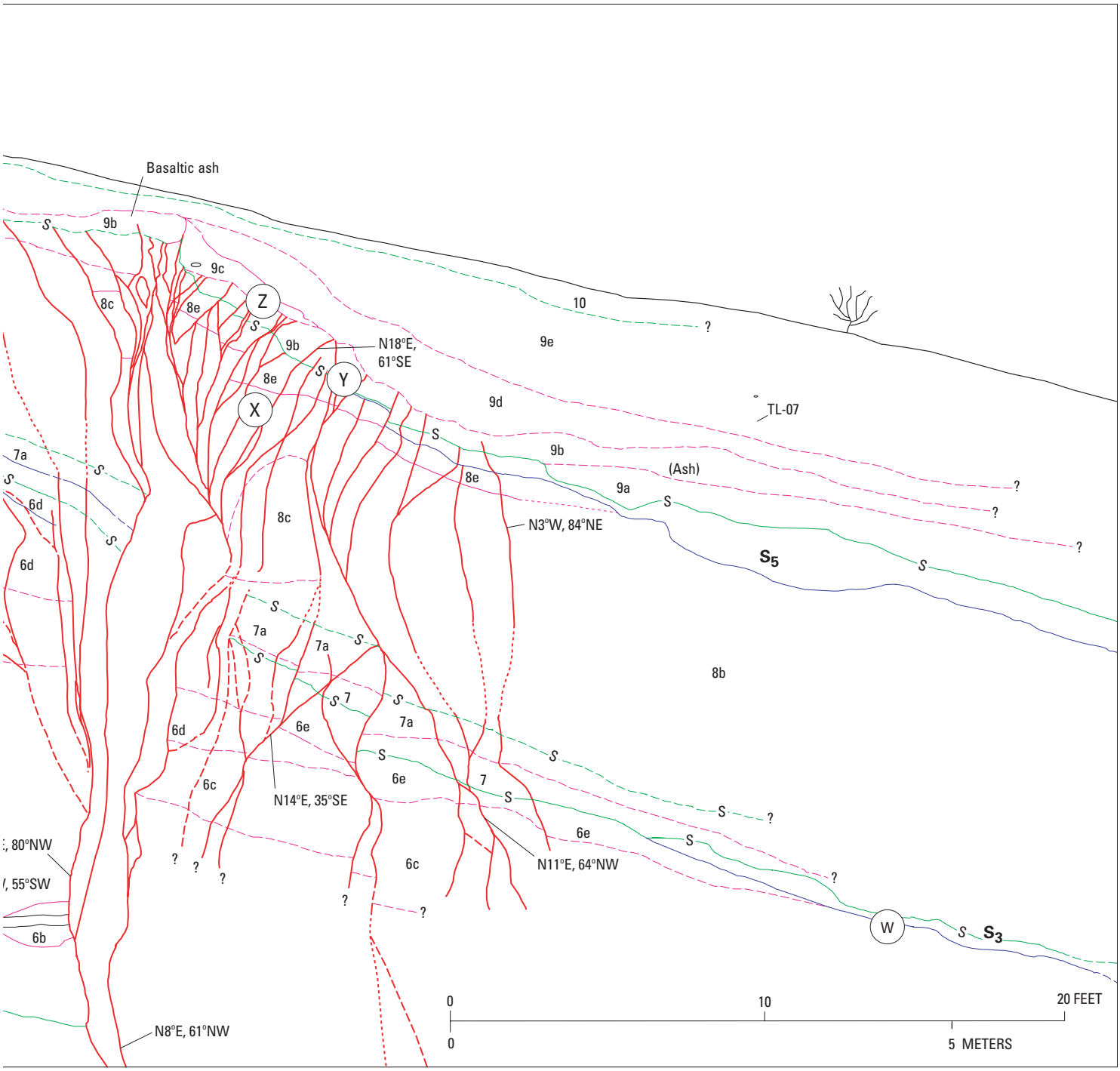

EXPLANATION

Faults and fractures—Dashed where inferred, dotted where concealed

S_3 **Soil-horizon boundary**—Identified by number, dashed where inferred, dotted where concealed

Lithologic-unit boundary—Dashed where inferred, dotted where concealed

Lithologic-subunit boundary—Dashed where inferred, dotted where concealed; labels (7a, 8c, and so on) refer to numbered subunits

S **Combined lithologic-unit/soil-horizon boundary**—Mostly soil-horizon boundaries

TL- 7 **Sample locality for dated material**—Number refers to sample listed in table 9

V **Faulting-event horizon**

N8°E, 61°NW **Strike and dip directions**

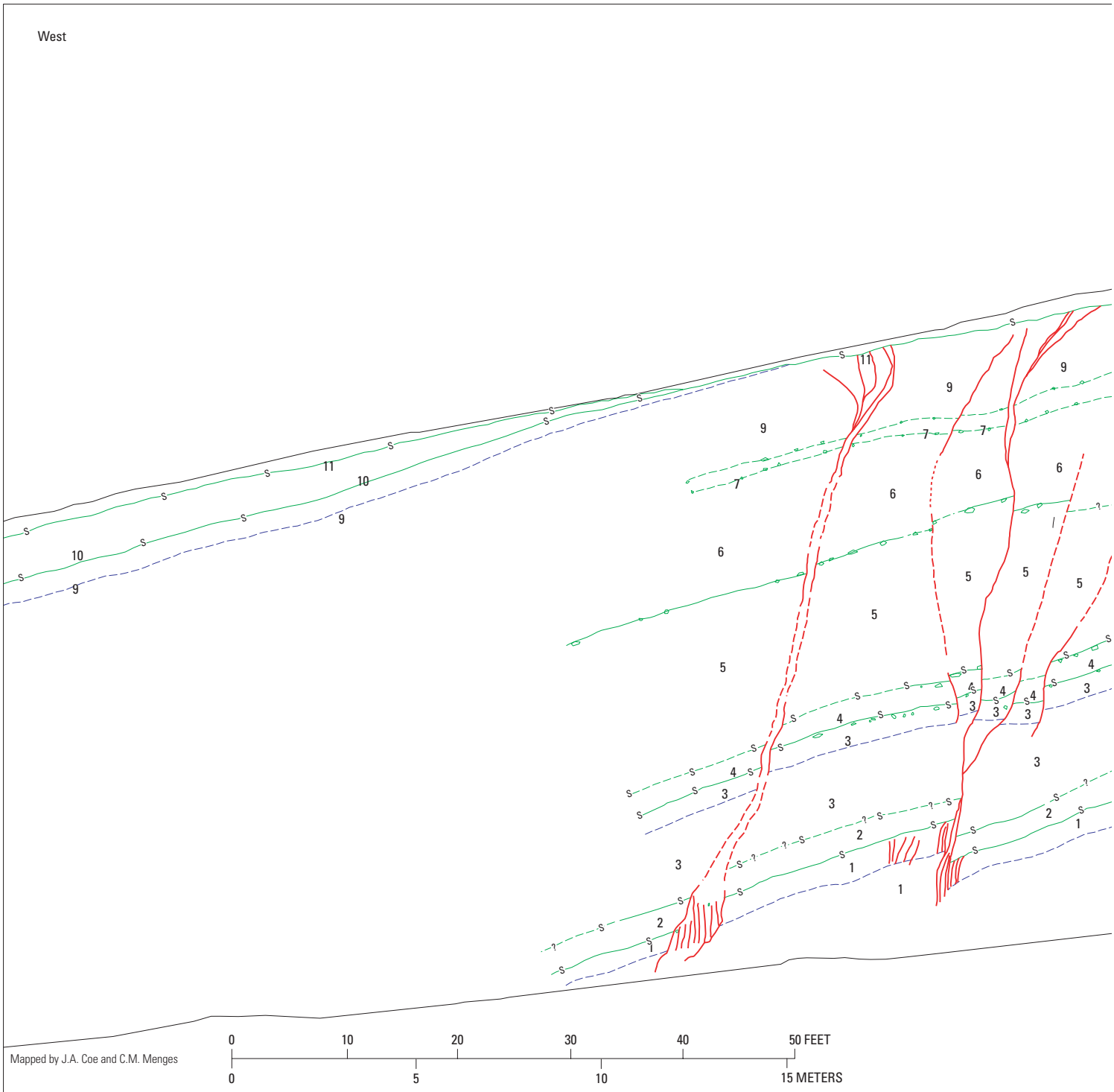

Figure 10. Simplified log of natural exposure across the Paintbrush Canyon Fault at Busted Butte wall 1 (BB1, fig. 2) in the Yucca Mountain area, southwestern Nevada (see fig. 1 for locations).

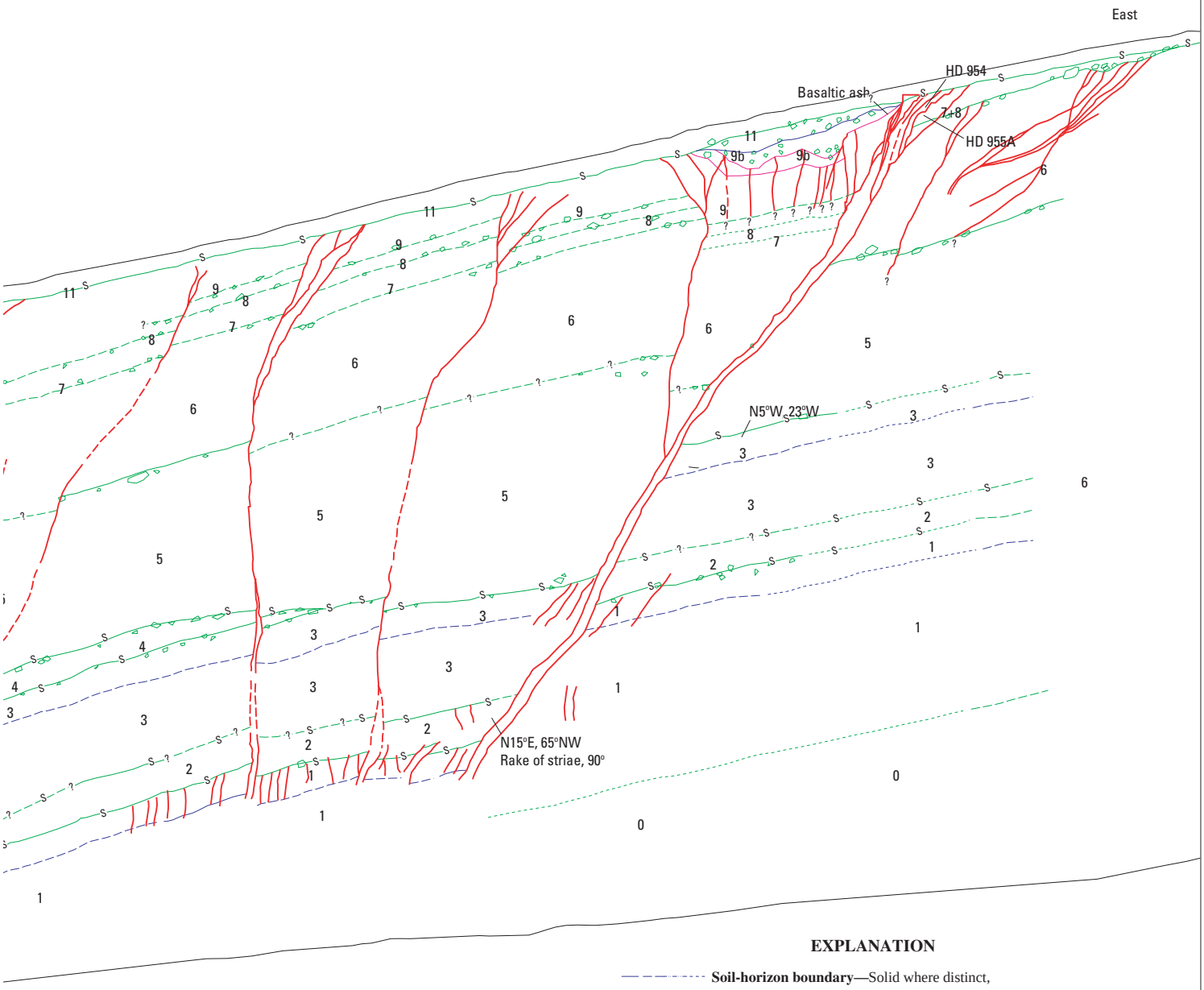

EXPLANATION

Soil-horizon boundary—Solid where distinct, dashed where inferred, dash-dotted where gradational, dotted where concealed

Lithologic-unit boundary—Solid where distinct, dashed where inferred, dotted where concealed

Lithologic-subunit boundary—Solid line where distinct, dashed where inferred, dash-dotted where gradational, dotted where concealed

Combined lithologic-unit/soil-horizon boundary—Mostly soil-horizon boundaries corresponding to lithologic-unit boundaries

Faults and fractures—Dashed where inferred, queried where uncertain

HD 954 **Sample locality for dated material**—Number refers to sample listed in table 9

N35°E, 16°NW **Strike and dip directions**

8 **Lithologic unit**

Table 6. Estimated dates and numbers of surface-rupturing paleoearthquakes on the Paintbrush Canyon, Bow Ridge, and Stagecoach Road Faults in the Yucca Mountain area, southwestern Nevada.

[See figure 2 for locations. Date is based on maximum age range of stratigraphic units exposed in hanging wall of trench: eP, early Pleistocene (1,650–775 ka); mP, middle Pleistocene (775–128 ka); lP, late Pleistocene (128–10 ka); H, Holocene (10–0 ka). Age controls: A, basaltic-ash horizon; S, soil stratigraphy; TL, thermoluminescence analysis; U, U-series analysis. Number of events, number of surface-rupturing paleoearthquakes recognized from stratigraphic and structural relations. Criteria for identifying events: D, incremental downsection increase in measurable displacement at event horizon; F, fissure filled with debris at and below event horizon; S, disruption of unit by shearing; T, incremental increase in stratal backtilting; U, upward termination of two or more fractures or shears at event horizon; W, colluvial wedge inferred to be scarp derived]

Trench	Date	Age control	Number of events	Criteria
Paintbrush Canyon Fault				
MWV–T4	H–mP	TL, U, S	3–4	W, S, U
Busted Butte	H–mP	TL, U, S, A	6–7	D, U, S, W
A1	H–m–eP	TL, U, S, A	≥4	D, U, S
Bow Ridge Fault				
T14D	H–mP	TL, U, S	2–3	D, U, S, W, F
Stagecoach Canyon Fault				
SCR–T1	H–lP	TL, U, S, A	2–4	T, U, W
SCR–T3	H–lP	TL, U, S, A	3–5	T, U, W, F

Table 7. Summary of measured displacements on the Paintbrush Canyon, Bow Ridge, and Stagecoach Road Faults in the Yucca Mountain area, southwestern Nevada.

[See figure 2 for locations. All values in centimeters. Individual displacement, dip slip, with most common range in parentheses. Cumulative displacement, dip slip on reference event horizon at base of exposure; direct age control does not exist for all reference units, and so these units do not necessarily correspond to those used for slip-rate calculations in table 12. Net cumulative displacement is adjusted for oblique slip, where possible, and (or) for tectonic rotation or local grabens at fault, where present; absence of reliable oblique-slip indicators in trenches A1 and MWV–T4 adds uncertainty to listed range]

Trench	Individual displacement	Cumulative displacement	Net cumulative displacement
Paintbrush Canyon Fault			
MWV–T4	20–140 (45–65)	170–270	– – –
Busted Butte wall 4	0–246 (40–130)	≥522–762	≥545–796
A1	0–49	– – –	>145–170
Bow Ridge Fault			
T14D	[1]1–46 (12–40)	[1]30–45, [2]45–70	[1]33–70, [2]50–122
Stagecoach Road Fault			
SCR–T1	15–105 (40–60)	117–367	99–309
SCR–T3	25–160 (70–105)	153–493	103–299

[1]Based on displacement of unit 4 in southern section of trench T14D.
[2]Based on all measurements of displacements in trench T14D complex, as reported by Menges and others (1997).

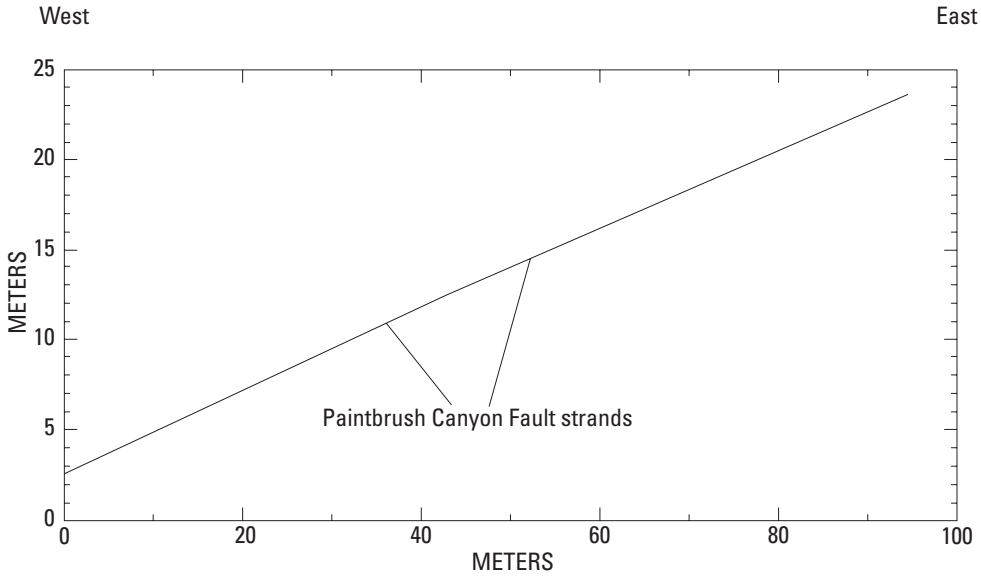

Figure 11. Topographic profile of sand-ramp geomorphic surface on interfluve across the Paintbrush Canyon Fault above Busted Butte wall 4 on west side of Busted Butte in the Yucca Mountain area, southwestern Nevada (figs. 1, 2).

Table 8. Dip-slip and net displacements for individual faulting events on the Paintbrush Canyon, Bow Ridge, and Stagecoach Road Faults in the Yucca Mountain area, southwestern Nevada.

[See figure 2 for locations. All values in centimeters. Faulting events refer to local chronology at each trench site and do not necessarily imply correlation between sites; faulting events in parentheses are less certain. Dip-slip displacement is measured along fault zone; net displacement is adjusted from dip-slip displacement by including (1) oblique slip, using possible slickenline orientations; and (2) removal of such local deformation effects as backfilling and antithetic graben formation]

Trench	Faulting event	Dip-slip displacement		Net displacement	
		Range	Preferred	Range	Preferred
Paintbrush Canyon Fault					
Busted Butte	Z	0–69	42	0–72	44
	Y	15–54	27	16–56	28
	(X)	33–66	45	35–69	47
	W	84–196	160	88–205	167
	V	0–212	136	0–222	142
	U	12–246	100	12–257	105
	T	72–192	90	75–201	94
MWV–T4	Z	20	20	– –	– –
	Y	47–77	62	– –	– –
	X	53–143	98	– –	– –
	(W)	0–140	40	– –	– –
A1	Z	– –	– –	5–10	6
	Y	– –	– –	29–49	39
	X	– –	– –	0–14	7
Bow Ridge Fault					
T14D	Z	14–46	40	15–80	44
	Y	4–40	12	4–70	13
	(X)	1–23	13	1–40	14
Stagecoach Canyon Fault					
SCR–T1	Z	40–90	40	40–50	40
	Y	34–84	50	34–70	42
	(X)	15–105	50	28–75	47
	(W)	28–88	60	34–67	51
SCR–T3	Z	60–160	105	41–45	43
	Y	25–100	75	47–79	59
	(X)	30–103	70	49–65	57
	(W)	38–130	100	44–74	67

Table 9. Numerical ages of Quaternary deposits in trenches MWV–T4, A1, T14, and T14D and at Busted Butte in the Yucca Mountain area, southwestern Nevada.

[See figure 2 for locations. Analytical methods used for age determination: Samples: HD (error limits, ±2σ), U-series analyses by J.B. Paces; TL– (error limits, ±2σ), thermoluminescence analyses by S.A. Mahan; YM, U-trend analyses]

Trench or exposure	Sample	Unit and material sampled	Estimated age (ka)
Busted Butte wall 1 (fig. 10)	HD 954	7-8, upper K soil horizon	70±28, 77±19, 79±20
	HD 955A	7-8, rhizolith, upper K soil horizon	134±23, 137±27, 142±20
Busted Butte wall 4 (fig. 9)	TL–07	9e, sand above upper K soil horizon	44±13
	HD 961	8b, lower K soil horizon	400+∞/–130, 410+∞/–150
	HD 962	8b, upper K soil horizon	300+82/–53, 340+140/–74
	HD 1449	8b, upper K soil horizon	272+35/–28
Trench MWV–T4 (fig. 13)	TL–03	VIIe, sand	73±9
	TL–04	VIIIb, Bt soil horizon	38±6
	TL–05	IX, Av soil horizon	6±1
	ND 1368	II, soil carbonate	232±15, 344±35
	HD 1370	V?, stringer of opaline silica	383±24, 423±44
	HD 1371	VI, rhizolith	44±0.5, 55±0.5, 63±1.6
	HD 1372	VI, rhizolith	119±2, 131±3
	HD 1372	VI, rhizolith	133±5, 140±5
	HD 1589	Ib, opaline silica	600+∞/–1±70
Trench A1 (pl. 2)	TL–34	5, Av soil horizon	9±1
	TL–35	4c, buried Av soil horizon	17±2
	TL–37	2b, sand	163±26
	HD 1622	3b, laminar K soil horizon	14±2, 16±4
	HD 1623, 1624	2b, rhizolith	71±2, 126±7, 195±18, 218±6, 224±21, 266±9
	HD 1625	1b, soil carbonate, opaline silica	640+∞/–180, 700+∞/–200, 900+∞/–420
	HD 1627	1b-c, rhizolith	403+64/–47, 129±3
	HD 1640	3a, string of opaline silica	127±4, 134±5
	HD 1641	31-b, rind, stringer of opaline silica	85±4, 101±4, 102±4
Trench 14 (pl. 3)	HD 1A	8S, upper K soil horizon, $CaCO_3$ stage IV morphology.	88±5
	YM 14 10–14	8S, laminar carbonate	270±90
	YM 14 15–17	7S, sand	420±50
	YM 14 18–22	5-6S, basalt gravel in sand	488±90
Trench 14D (fig. 16)	TL–06	7a, composite soil sample	48±20
	TL–09	4, sand	132±23
	HD 968	1, composite soil sample	>700
	HD 969	2, composite soil sample	340+∞/–120
	HD 970	3b, composite soil sample	234+47/–35
	HD 971	5, composite soil sample	98±15, 137±32, 139±31, 144±33
Trench SCR–T1 (fig. 19)	TL–02, –26	H1, sand and silt	9±1, 12±6
	TL–16	F2b, sand surrounding rhizolith	28±4
	TL–25	G2b, sand and silt	12±2
	TL–27	D1b, sand and silt	49±9
	HD 1067	D1b, rhizolith	24±1, 24±2, 25±4, 27±1
	HD 1068	F2b, rhizolith	13±6, 17±2, 18±2, 20±2
Trench SCR–T3 (fig. 20)	TL–18	I2-3, sand	22±5
	TL–19	G5, sand	87±18
	TL–29	G2, sand	60±16
	HD 1447	G2, carbonate-cemented sand	88±9, 94±35, 104±7, 107±9

Table 10. Estimated dates of selected faulting events on the Paintbrush Canyon, Bow Ridge, and Stagecoach Road Faults in the Yucca Mountain area, southwestern Nevada.

[See figure 2 for locations. Dates: mP, middle Pleistocene (730–128 ka); lP, late Pleistocene (128–10 ka); lsP, latest Pleistocene (40–10 ka); mH, middle Holocene (7–3 ka). MRE, most recent event; PEN, penultimate event. Ash present?, statement whether basaltic ash is present in trench, with stratigraphic position of ash indicated; all ash deposits are provisionally correlated with eruption of the Lathrop Wells volcanic center at 77±6 ka, based on major-ion and trace-element geochemistry, except ash deposit in trench A1, which differs geochemically from ash deposits in other trenches and more closely matches tephra at the Sleeping Buttes volcanic center (B.M. Crowe and F.V. Perry, oral commun., 1996)]

Trench	Date of MRE (ka)	Date of PEN (ka)	Ash present?
Paintbrush Canyon Fault			
MWV–T4	lP (6–40)	lP (70–100)	None recognized.
Busted Butte	lP (40–80)	lP–mP (80–150)	Yes; layer.
A1	lsP (10–20)	mP (130–140)	Yes; fissure, layer (different source?).
Bow Ridge Fault			
T14D	lP (>30–130; ~50)	lP (130–150)	Yes (T14 only); fracture.
Stagecoach Road Fault			
SCR–T1, SCR–T3	mH–lsP (5–15)	lsP (20–30)	Yes; layers.

Trench MWV–T4

Trench MWV–T4 was modified from a preexisting trench excavated across the north end of the western splay of the Paintbrush Canyon Fault that diverges from the main fault strand at the southeast edge of Midway Valley (fig. 2). The trench is located on a short section of the fault associated with low bedrock-controlled scarps (fig. 12). No Quaternary fault activity was reported from studies of the original trench (Swadley and others, 1984); however, the results of more recent reconnaissance work and reviews of existing trenches and geomorphic relations in southern Midway Valley indicated a need to reexamine the fault in that area. Accordingly, the original trench was deepened in June 1992, exposing a distinct fault zone that displaces Quaternary colluvial and eolian deposits (fig. 13).

The main fault trace in trench MWV–T4 (figs. 2, 13) is a 7-m-wide multistrand zone that strikes approximately N. 45° E. and dips 80° NW. Strands in the western and central parts of the fault zone dip 65°–70° SE. The southeastward dips are considered to be more likely related to local oversteepening of fault strands in the shallow subsurface than to reverse faulting. Secondary fractures and shears are formed in deposits as much as 8 m west of the main fault zone. Faulting in loose friable sand layers (for example, unit VI_1, fig. 13) is expressed as a wide zone of numerous, closely spaced shears and fractures with minimal coatings of silica or carbonate, whereas faulting in moderately to strongly cemented deposits (units II, III, fig. 13) and bedrock is manifested as a narrow zone of discrete silica- and carbonate-plated shears.

The footwall block exposed in the trench contains bedrock (Tiva Canyon Tuff of the Paintbrush Group) thinly mantled with surficial deposits. A well-developed carbonate soil with $CaCO_3$ stage II–IV morphology is developed on unit II, which overlies bedrock (fig. 13). The hanging-wall block is composed of unconsolidated colluvial and eolian deposits

Table 11. Recurrence intervals and slip rates calculated for the Paintbrush Canyon, Bow Ridge, and Stagecoach Road Faults in the Yucca Mountain area, southwestern Nevada.

[See figure 2 for locations. Average recurrence intervals span two or more faulting events bracketed by age control, with preferred values in parentheses; values for trenches SCR–T1 and SCR–T3 are based on correlation with basaltic ash. Faulting-event chronologies are combined, and so recurrence intervals are identical for trenches SCR–T1 and SCR–T3; average recurrence intervals listed for these two trenches are based on ages determined both by correlation with the Lathrop Wells basaltic ash (A) and by thermoluminescence analysis (TL), with preferred values based solely on ash correlation. Individual recurrence intervals span pairs of successive faulting events with adequate age control; numbers in parentheses, preferred values. Faulting-event pairs used to estimate individual recurrence intervals refer to local chronology at each trench site and do not necessarily imply correlation between sites. Slip rates are calculated from cumulative net slip and age of displaced stratigraphic units, with preferred value in parentheses]

Trench	Recurrence interval (k.y.)			Slip rate (mm/yr)
	Average	Individual		
		Range	Event	
Paintbrush Canyon Fault				
MWV–T4	20–50	40–90 (60)	Z–Y	0.007–0.03 (0.015)
Busted Butte	30–270 (50–120)	25–275 (95) 10–260 (65)	Z–Y Y–X	.001–0.01 (0.007)
A1	50–145 (80–100)	105–130 (115)	Z–Y	.001–0.004 (0.002
Bow Ridge Fault				
T14D	75–215 (100–140)	40–130 (90) 65–350 (210)	Z–Y Y–X	0.002–0.007 (0.003
Stagecoach Road Fault				
SCR–T1	A: 18–55 (20–50)	3–78 (10–5 0–88 (5–50	Z–Y Y–X	0.02 (0.02)
	TL: 5–50 (10–30)	3–26 (10–2 0–88 (5–50	Z–Y Y–X	.02–0.07 (0.05)
SCR–T3	A:18–55 (20–50)	3–78 (10–5 0–88 (5–50	Z–Y Y–X	.02–0.03 (0.03)
	TL:5–50 (10–30)	3–26 (10–2 0–88 (5–50	Z–Y Y–X	.006–0.04 (0.03)

resembling small sand ramps. The sequence is dominated by poorly bedded to massive sand and silt layers with local gravel accumulations indicative of alluvial channels (for example, units VI, VIIa). Hanging-wall deposits contain several weakly to moderately well developed buried soils characterized by argillic horizons and weak carbonate accumulations with $CaCO_3$ stage I–II morphology, commonly associated with rhizoliths, that are dispersed in the sandy parent material. The surface soil is thin and weakly developed, with a thin incipient B horizon and carbonate coatings with $CaCO_3$ stage I–II morphology on gravel clasts.

In the hanging-wall block, the depositional contact between unconsolidated deposits and bedrock (Rainier Mesa Tuff of the Timber Mountain Group) is at a depth of 40 m in a borehole (UE–25p#1) located 40 m north of the trench (Muller and Kibler, 1984). The apparent step in the bedrock-alluvium contact is interpreted to represent the approximate vertical displacement of the top of bedrock across the fault, although some modification of the contact by fluvial erosion cannot be excluded. Structural cross sections indicate that the apparent vertical separation in the Tiva Canyon Tuff across this fault strand is approximately 200 m (Scott and Bonk, 1984).

Table 12. Fault-slip rates calculated for selected dated reference horizons in trenches across the Paintbrush Canyon, Bow Ridge, and Stagecoach Road Faults in the Yucca Mountain area, southwestern Nevada.

[See figure 2 for locations. Number of faulting events is interpreted above reference horizon. Age of reference horizon is determined from geochronologic control. Cumulative net tectonic displacement used to calculate fault-slip rate is derived from measured vertical displacement of reference horizon, adjusted for oblique slip by using slickenlines and (or) local hanging-wall deformation. Values for two trenches (SCR–T1, SCR–T3) across the Stagecoach Road Fault are based on ages determined both by correlation with the Lathrop Wells basaltic ash (A) and by thermoluminescence analysis (TL)]

Trench	Reference horizon	Number of faulting events	Date (ka)	Cumulative net tectonic displacements (cm)		Fault slip rates (mm/yr)	
				Range	Preferred	Range	Preferred
MWV–T4	VIIe	2	73±9	67–97	82	0.007–0.015	0.01
	VII	3–4	<130	170–270	220	.01–0.02	>.015
	VI	3–4	>140	250–350	300	.02–0.03	– –
Busted Butte	8a (soil)	2–3	215–350	51–197	119	.001–0.009	.004
	6 (soil)	3–4	270–560	139–402	286	.003–0.015	.007
	3	6–7	600–700	≥525–786	≥608	≥.009–0.01	.009
A1	2b	3	160–275	35–70	45	.001–0.004	.002
T14D (N)	4	2	132±23	30–70	35	.002–0.006	.003
T14D (S)	9	1	109–155	40–80	44	.002–0.007	.003
SCR–T1	A:F2c	2	77±6	138–165	145–155	.04–0.07	.02
	TL: F2b	2	28±4	138–165	145–155	.02	.05
SCR–T3	A: H3c	2	77±6	177–240	205	.02–0.03	.025
	TL: G5a	2–3	87±18	208–255	220–240	.02–0.04	.025

Three or four individual faulting events that postdate unit VI are interpreted from observations in trench MWV–T4 (figs. 2, 13). These faulting events are identified on the basis of colluvial wedges associated with paleoscarps (fig. 13; Swan and others, 1993). The uncertainties primarily arise from the difficulty in accurately identifying this type of wedge in the poorly stratified fine-grained sandy deposits of the hanging-wall block. At least three faulting events are indicated by upward terminations of fractures and shears at three discrete stratigraphic horizons as well. One or two faulting events (W, X) occurred in the central part of the shear zone, on the basis of the presence of several colluvial wedges (units VIIb, VIIc, fig. 13). Ambiguity results from uncertainty over whether the two wedges represent individual faulting events (the preferred interpretation) or are simply parts of a single composite wedge. The two most recent surface ruptures are on the easternmost main fault shear. Unit VIIe is considered a scarp-derived colluvial wedge from the penultimate faulting event (Y), and unit IX thickened across the fault after the most recent surface rupture of unit VIIIb in event Z. Another faulting event could be interpreted on the westernmost fault strand, on the basis of the presence of a colluvial wedge (unit VIIa, fig. 13); however, the deposition of this unit is considered to be more likely in response to a faulting event on the central fault strand (event W or X), rather than related to a separate, discrete surface rupture on the western fault strand.

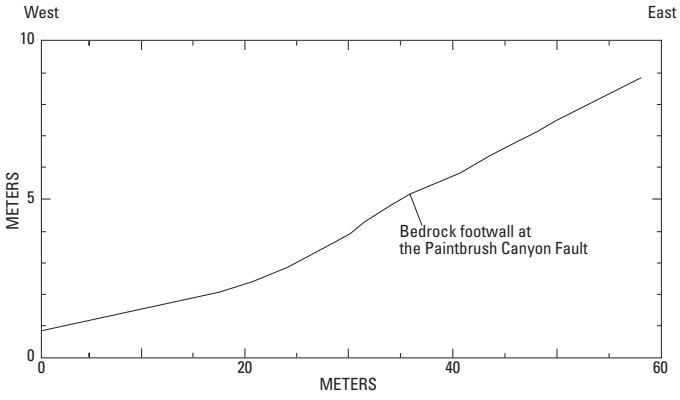

Figure 12. Topographic profile of colluvial footslope south of trench MWV–T4 in the Yucca Mountain area, southwestern Nevada (figs. 1, 2).

Minimum individual dip-slip displacements, which were estimated from the differential cumulative displacements of successive units and thickness of colluvial wedges, range from 20 to 140 cm, typically from 45 to 65 cm (table 7). The largest displacement is interpreted from the two overlying colluvial wedges (units VIIb, VIIc, fig. 13) to be associated with a single surface rupture. The most recent surface rupturing event has the smallest displacement, approximately 20 cm (tables 7, 8). Estimated cumulative dip-slip displacement of the oldest surficial deposit in the trench ranges from 170 to 270 cm (table 7); these values could not be adjusted for net slip because no slip indicators were observed in the trench.

Displaced surficial deposits are correlated with the middle to upper Pleistocene alluvial deposits mapped in Midway Valley and vicinity (Swan and others, 1993; Wesling and others, 1992; S.C. Lundstrom, written commun., 1993). The available geochronologic data for dating faulting events on the Paintbrush Canyon Fault in trench MVW–T4 (figs. 2, 13) are as follows:

1. The oldest unit is a series of highly cemented and deformed deposits in the fault zone with a U-series age of approximately 600 ka (unit I; sample HD 1589, fig. 13; table 9). The carbonate soil on unit II, which overlies bedrock on the footwall block, yielded U-series ages of 232±15 and 344±35 ka (sample HD 1368). Opaline stringers in unit V, a cemented sandy layer at the base of the trench on the hanging-wall block, yielded U-series ages of 383±24 and 423±44 ka (sample HD 1370).
2. The overlying unit (VI_1), contains numerous rhizoliths with U-series ages ranging from 44±0.5 to 140±5 ka (samples HD 1371, HD 1372, HD 1373, fig. 13; table 9). The oldest of these ages is considered an approximate minimum age for the unit, although the deposit itself could be older than any of the rhizoliths. The minimum rhizolith ages from this unit provide a lower age constraint on the main sequence of late Quaternary faulting events (W–Z) recognized on the hanging-wall block.
3. Two thermoluminescence analyses provide additional age controls for the youngest two identified surface ruptures. A colluvial wedge associated with penultimate event Y (unit VIIe, fig. 13) yielded a thermoluminescence age of 73±9 ka (sample TL–03, table 9), which represents a close minimum for the faulting event itself.
4. The most recent surface rupture (event Z) cuts a mixed eolian-colluvial unit (VIIIb, fig. 13) that yielded a thermoluminescence age of 38±6 ka (sample TL–04). A thermoluminescence age of 6±1 ka (sample TL–05) was obtained on a young surface Av soil horizon that formed on top of unit VIIIb, as well as on unit IX. Neither the soil nor unit IX is cut by event Z, which brackets the most recent faulting event at this site between approximately 40 and 6 ka.

These ages collectively indicate average recurrence intervals ranging from 20 to 50 k.y. (table 12), with individual recurrence intervals ranging from 10 to 75 k.y. The long interval is associated with events Z and Y, whereas the short intervals are estimated for events Y, X, and, possibly, W, which are separated by colluvial wedges with little or no soil development (Swan and others, 1993). The observed net displacement of 67 to 97 cm on unit VIIe with the older thermoluminescence age of 73±9 ka indicates a poorly constrained preferred slip rate of about 0.01 mm/yr (table 12). Slip rates calculated for units VII and VI, using the oldest minimum rhizolith ages, range from 0.01 to 0.03 mm/yr (preferred value, 0.015–0.025 mm/yr).

Trench A1

The Paintbrush Canyon Fault is exposed in colluvium in trench A1, which is located on the north end of Alice Ridge at the northeastern margin of Midway Valley (fig. 2). No fault scarps or other direct surface expressions of the fault were observed in that area (fig. 14). Both this trench and an adjacent trench (trench A2, fig. 2) were originally excavated in 1979. Mapping of the north wall of trench A1 at that time revealed carbonate-filled fractures, but no faults or discrete displacements were described (Swadley and others, 1984). No deformation was observed in the terrace gravels exposed in trench A2. In December 1993, new excavations were initiated to provide evidence for the northward extent of surface rupture on the Paintbrush Canyon Fault zone in the northern Midway Valley-Yucca Wash area. Trench A1 was deepened and extended to its present length of 110 m, thereby clearly exposing a complex fault zone in mid-Quaternary to upper Quaternary deposits. An additional 1.5-m-deep backhoe trench, or slot, also was cut into the floor of the main trench across the main fault trace (pl. 2). Another trench (MWV–T3, not shown in fig. 2) that was excavated at that time across a vegetation lineament to the west of trench A1 exhibited no fracturing or

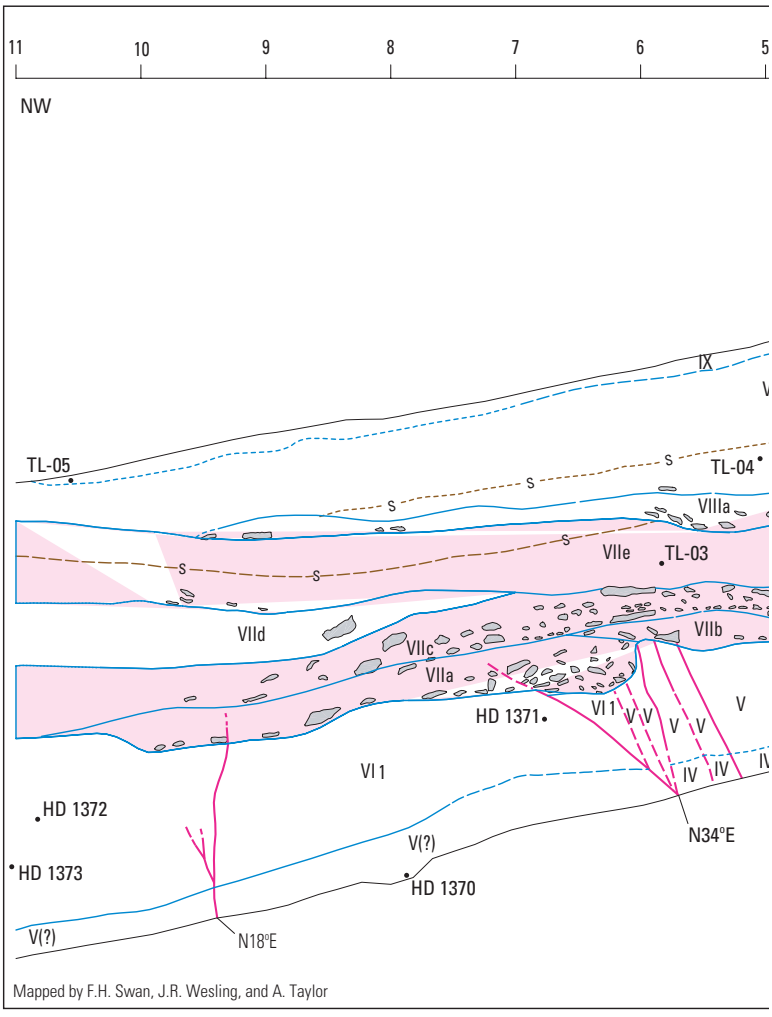

Figure 13. Simplified log of section of north wall of trench MWV–T4, which exposes western splay of the Paintbrush Canyon Fault in the Yucca Mountain area, southwestern Nevada (figs. 1, 2).

fault deformation and was not logged. The absence of deformation in that trench indicates that Quaternary surface rupture on the Paintbrush Canyon Fault is constrained to the relatively narrow fault zone visible in trench A1.

Trench A1 (fig. 2) exposes a nearly 5-m-thick section of alluvial, colluvial, and eolian deposits; 15 individual depositional layers were recognized and grouped into five soil-stratigraphic units (pl. 2). Most of units 2 through 5 in the upper and middle parts of the trench consist of sand and silt, with a varying, somewhat localized component of pebble-cobble gravel. Coarser grained pebble-boulder gravel predominates in unit 1 in the bottom of the trench. Basaltic ash is dispersed in a silt pod and a fissure fill in the fault zone within the inner slot of the trench. Ash within the fissure fill is restricted to a zone adjacent to the ash-bearing pod. This pod, which appears to be stratabound at the base of unit 2, is buried beneath more than 3 m of sediment.

Each of the principal soil-stratigraphic units contains a distinctive soil presumed to have formed during a period of surface stability. The degree of soil development ranges from weak Bw cambric soils near the surface to Btk horizons containing carbonate accumulations with $CaCO_3$ stage II–III morphology that locally reach K-horizon cementation in unit 1 (fig. 9). Throughout the entire length of the trench, individual depositional layers pinch out and change in characteristics laterally, reaching maximum thicknesses within the fault zone at the footslope position of the hillslope. Soil horizons likewise vary laterally and merge upslope and downslope from an area of maximum differentiation near the fault zone.

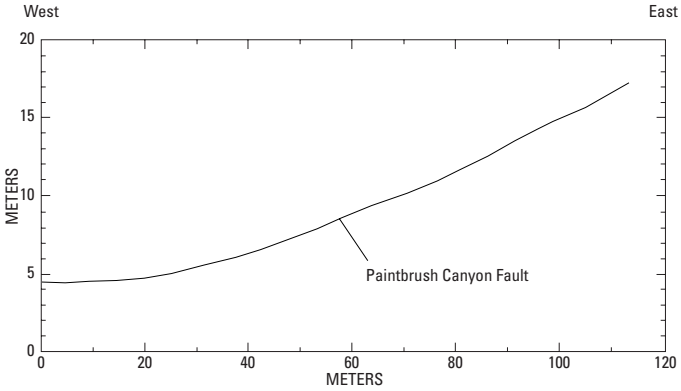

Figure 14. Topographic profile of colluvial footslope at north edge of trench A1 in the Yucca Mountain area, southwestern Nevada (figs. 1, 2).

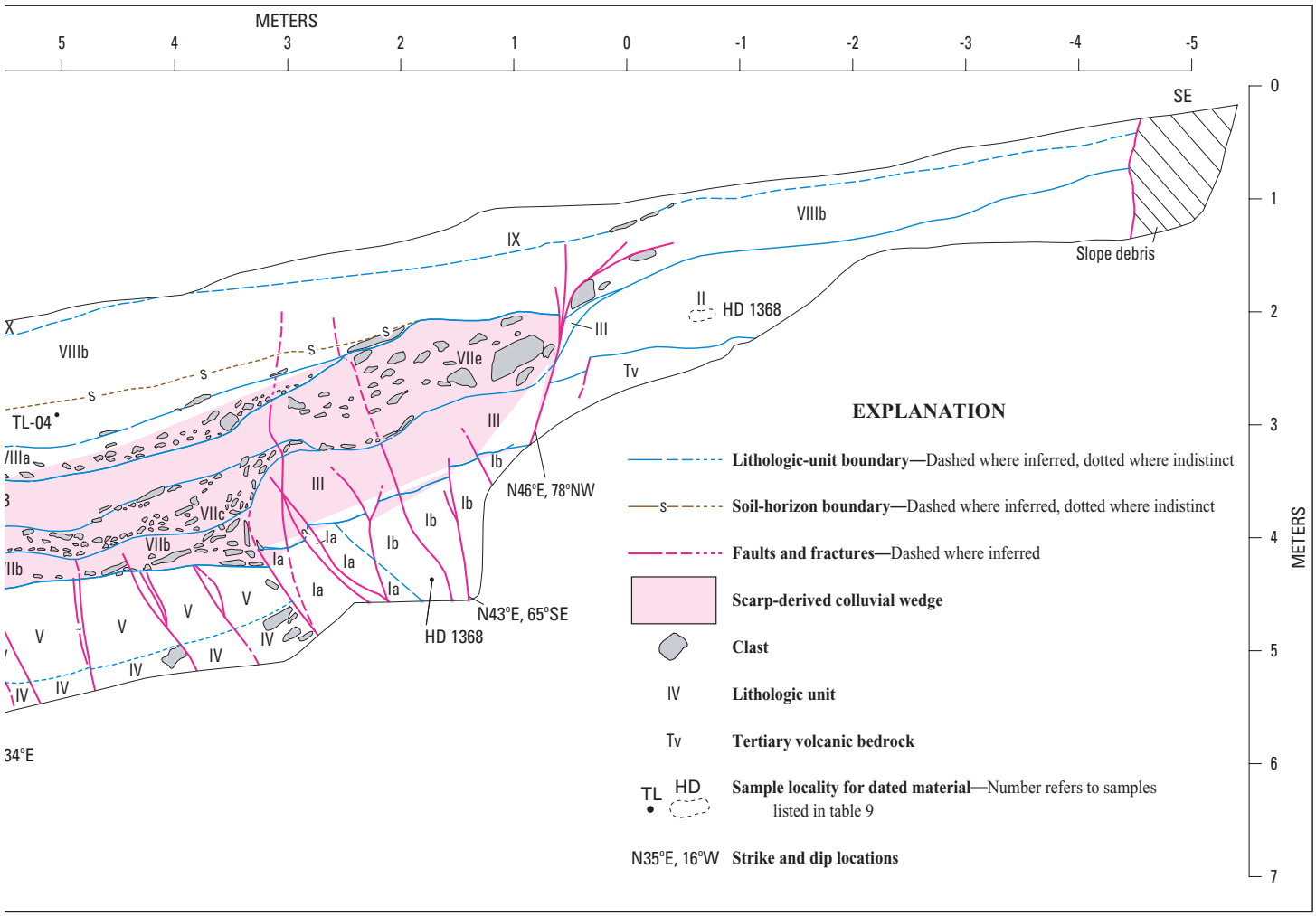

Trench A1 (fig. 2) exposes a 15-m-wide multiple-strand fault zone that records at least four Quaternary faulting events (see pl. 2). The zone contains a complex array of synthetic and antithetic high-angle normal faults, fractures showing no apparent displacement, and low-angle thrust faults; however, most of the displacement is concentrated on two fault strands (B, C/D, pl. 2), approximately 2 m apart, that compose the main fault zone. These fault strands strike N. 17°–23° E., with predominantly subvertical dips (85° E.–85° W.), although both strands develop upsection into principally east dipping low-angle splays. The lowermost exposed 3 m of the fault zone is characterized by carbonate-engulfed fractures and shears and zones of loose breccia, as much as 50 cm wide, that may represent either broad shear zones or a series of fissure fills, or both. Subsidiary fault strands and fractures that are both east and west of the main fault zone are characterized by carbonate-filled fractures and shears. Many of the fractures show no apparent displacements. Small antithetic east-side-down displacements are present on two fault strands (A, F, pl. 2). Strand C/D has several low-angle east-dipping thrust-fault splays that sole into the main fault zone near the bottom of the trench. Such geometry probably is related to accommodation of local stresses caused by shallowing of the dip on the main fault zone at depth, and (or) a component of strike-slip displacement. No striations or slickensides were observed that could establish the presence or amount of lateral slip, although changes in thickness of some units on opposite sides of the fault zone probably indicate a component of lateral slip.

At least four faulting events are interpreted on the Paintbrush Canyon Fault at trench A1 (fig. 2; table 6). The main criteria used to define these events are (1) progressively smaller vertical displacements of successively younger stratigraphic units and (2) upward terminations of fractures and fissure fills at a given stratigraphic horizon. Small scarp-derived colluvial wedges that are associated with the penultimate faulting event (Y, table 8) are interpreted from unit 1, although wedge features are difficult to recognize because of small displacements and the massive fine-grained texture of many deposits. Evidence for the earliest faulting event (W) is interpreted from unit 1 on the basis of incremental increases in the offset of the unit and possible fault-scarp colluvium. Event W probably includes multiple surface ruptures that cannot be differentiated individually, owing to poor stratigraphic control in the trench. Evidence for event X is the most equivocal, consisting mainly of a few fracture terminations at the interpreted event horizon (top of unit 2c, fig. 9), a slight increase in displacement at the horizon, and a possible fissure-fill unit. In contrast, penultimate event (Y) is well defined by widespread fracture and shear terminations at the top of unit 3c, by differential displacement that on many strands ends at the event horizon, and by a possible small colluvial wedge within unit 3c. The most recent event (Z) is less conspicuous but is clearly indicated by a small displacement of units 4a through 4c (fig. 9) and by fracture terminations.

All of the vertical displacements are small, ranging from 0 to 49 cm for the three recognizable individual faulting events (tables 7, 8). The smallest net displacements are associated with events X and Z (preferred displacements, 7 and 6 cm, respectively), whereas net displacements resulting from penultimate event (Y), which are distributed among all of the fault strands with observed offsets, are estimated to range from 29 to 49 cm (preferred value, 39 cm; table 8). The minimum net cumulative vertical separation measured at the lowest event horizon (W) in the trench is 145 to 170 cm on the two walls. Displacements per event are generally higher on the north wall and considered more representative than those on the south wall.

The deposits exposed in trench A1 range in age from early(?) through middle Pleistocene to Holocene, on the basis of a series of U-series and thermoluminescence ages (table 9) in combination with general soil-stratigraphic relations (pl. 2). Carbonate from petrocalcic soil in the stratigraphically lowest alluvial deposits (unit 1c, pl. 2) at the base of the slot trench yields poorly constrained U-series ages ranging from 640 to 900 ka (sample HD 1625, table 9); these deposits are overlain by carbonate-cemented gravel layers with silica rinds on clasts that contain excess Th and are depleted in ^{234}U. Rhizoliths from the same general interval in unit 1b in the slot trench yield minimum U-series ages of 129±3 and 403+64/–47 ka (sample HD 1627). Unit 1, which predates all of the interpreted events in the trench, has an age of at least 750 ka, based on slip-rate constraints (see below). Unit 2b (pl. 2) contains a series of rhizoliths with U-series ages ranging from 71±2 to 266±9 ka (samples HD 1623, HD 1624, pl. 2; table 9), mostly from 220 to 230 ka. One sample (TL–37) with a thermoluminescence age of 163±16 ka that was also collected from this unit is considered to represent a minimum age that is related to postdepositional translocation of silt during soil formation. The probable age of unit 2b is 220–275 ka. Event X, which is above unit 2b within the same soil-stratigraphic unit, probably does not significantly postdate the minimum estimated age for unit 2b. A minimum date for penultimate event (Y) is based on U-series ages of 127±4 to 134±5 ka (sample HD 1640) from a carbonate stringer precipitated along a fracture created by the event. Assuming that carbonate accumulates rapidly within an open fracture, these ages provide a close minimum date and, within analytical error, likely approximate the date of event Y. Laminae and clast rinds from the overlying upper calcic horizon in unit 3b yielded U-series ages ranging from 14±2 to 102±4 ka (samples HD 1622 and HD 1641, respectively, pl. 2; table 9), illustrating that calcic soils commonly provide only crude minimum age constraints. The most recent event (Z) is closely bracketed between unfaulted unit 5, with a thermoluminescence age of 9±1 ka (sample TL–34), and the underlying displaced unit 4c, with a thermoluminescence age of 17±1 ka (sample TL–35).

The age and source of the basaltic ash in the slot trench are potentially problematic. The ash-bearing units, including the fissure fill, appear to be stratabound beneath unit 2b (with a minimum age of 220–275 ka); however, the ash might extend higher upsection in a fissure outside the plane of the trench walls. Given these relations, the eruption of the nearby Lathrop Wells volcanic center at 77±6 ka (Heizler and others, 1999) does not appear to be a likely source for the ash. A pos-

sible alternative source vent consistent with the age constraints in trench A1 is the Sleeping Buttes volcanic center, approximately 40 km to the northwest, which has yielded K-Ar ages of 350 ka (Crowe and others, 1995). Preliminary geochemical analyses of the ash in trench A1 support this correlation with the Sleeping Butte tephra and are not consistent with a source from the Lathrop Wells volcanic center.

Recurrence intervals calculated from these age data range from 50 to 145 k.y. (preferred value, 80–100 k.y.; table 11). The individual recurrence interval between events Y and Z is relatively long, about 105–130 k.y. Fault-slip rates computed from 35 and 70 cm of cumulative dip-slip displacement of unit 2b, with an age of 160–275 ka, range from 0.001 to 0.004 mm/yr (preferred value, 0.002 mm/yr; tables 10, 11). These low rates primarily reflect the small displacements observed at the trench site.

Bow Ridge Fault

The two trenches (T14, T14D, figs. 2, 8) discussed in this chapter are part of a series of five trenches excavated across the surface trace of the Bow Ridge Fault at the west base of Exile Hill, about midway along the mapped north-south length of the fault (see Day and others, 1998a). Trench T14 was excavated in 1982, and preliminary mapping was completed by Swadley and others (1984). Though exposing a well-defined fault zone, the trench provided sparse and poorly resolved data on the amount and timing of late Quaternary fault movements. The excavation, however, yielded valuable information on the composition and origin of the secondary carbonate and silica veins in the fault zone, as described below.

Trench T14 was deepened, and four new trenches (T14A–T14D, fig. 2) were excavated, in 1985 to better define the Quaternary displacement history of the Bow Ridge Fault. The fault zone exposed in trenches T14A and T14B is entirely within bedrock (Tiva Canyon Tuff), and so neither trench was logged. Trench T14C was logged, but paleoseismic relations are obscure because of poorly defined Quaternary stratigraphy, overprinting by pedogenic carbonate, and the absence of discrete vertical displacements on the fault that can be tied to specific marker horizons (Menges and others, 1997).

In 1992, trench T14D was extended 40 m eastward, for a total length of 50 m, to investigate whether another Quaternary strand of the Bow Ridge Fault exists in bedrock at the west base of Exile Hill. A box network of auxiliary trenches, 7 m on a side, also was excavated around the main fault zone north of the west end of trench T14D in an attempt to gain three-dimensional exposures of displaced Quaternary deposits. Results of the mapping of this complex of trenches are summarized below.

Trench T14D

Trench T14D (fig. 2) contains a vertical succession of lower Pleistocene to Holocene deposits along the western margin of Exile Hill; no fault scarp or other topographic expression was observed along this part of the Bow Ridge Fault (fig. 15). Bedrock of the Miocene Tiva Canyon Tuff is exposed only in the eastern section of the trench, 15 m east of the main fault zone. The tuff is overlain by carbonate-engulfed colluvial fragments that are buried, in turn, by 1.5 to 2 m of surficial deposits representing a westward-thickening sequence of mixed alluvial, colluvial, and eolian origin that has been subdivided into 8 to 16 lithologic units (figs. 16, 17). Most of the units consist of fine- to medium-grained silty sand to sandy silt, with varying proportions of pebble-cobble gravel and local gravelly debris-flow and alluvial-channel deposits. These deposits generally are unconsolidated to moderately cemented, very poorly sorted, and poorly bedded to massive.

Deposits in the west end of trench T14D contain a complex sequence of weakly to moderately well developed soils, including a vertically stacked to partly overlapping series of two to five buried paleosols below a thin surface soil. The buried soils are moderately well to well developed and consist of carbonate and silica accumulations (Bkq to Kq horizons containing carbonate with $CaCO_3$ stage II–IV morphology) or argillic (Bt or Btk) horizons. The surface soil is relatively thin and weakly developed, consisting mostly of a Bw or weak Bt horizon above a Bk horizon containing carbonate coatings with $CaCO_3$ stage I morphology on clasts.

The main Bow Ridge Fault trace in trench T14D is characterized on the lower part of the trench walls by a distinct, but irregular, 20- to 40-cm-wide shear zone (figs. 16, 17) that strikes N. 5°–15° E. and dips 80°–85° SE., indicative of slight oversteepening of the fault in the direction of the downdropped block. This oversteepening is probably a near-surface phenomenon, inasmuch as subsurface data indicate steep northwestward dips at depth, as noted above. Multiple veins and laminae of secondary carbonate and silica coat the walls of the shear zone. Several sets of striations on carbonate laminae in the main fault zone, if tectonic in origin, indicate left-oblique slip plunging 35°–65° SE. Three sets of fissures have formed along the main fault trace in the northern section of trench T14D (for example, units F1–F3, fig. 16). The fissures are filled with sand, silt, and

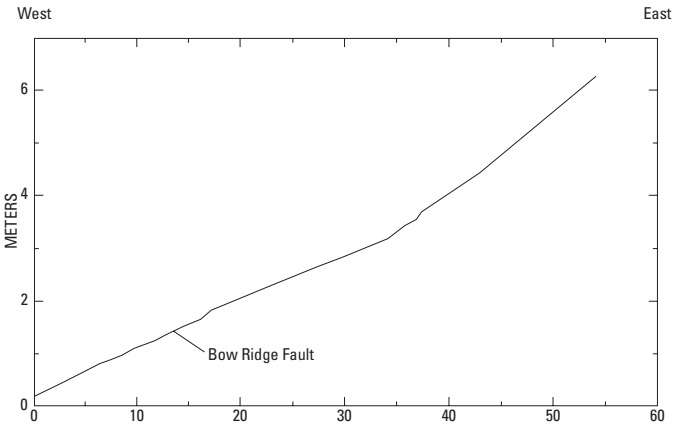

Figure 15. Topographic profile of colluvial footslope across the Bow Ridge Fault south of trench T14D in the Yucca Mountain area, southwestern Nevada (figs. 1, 2).

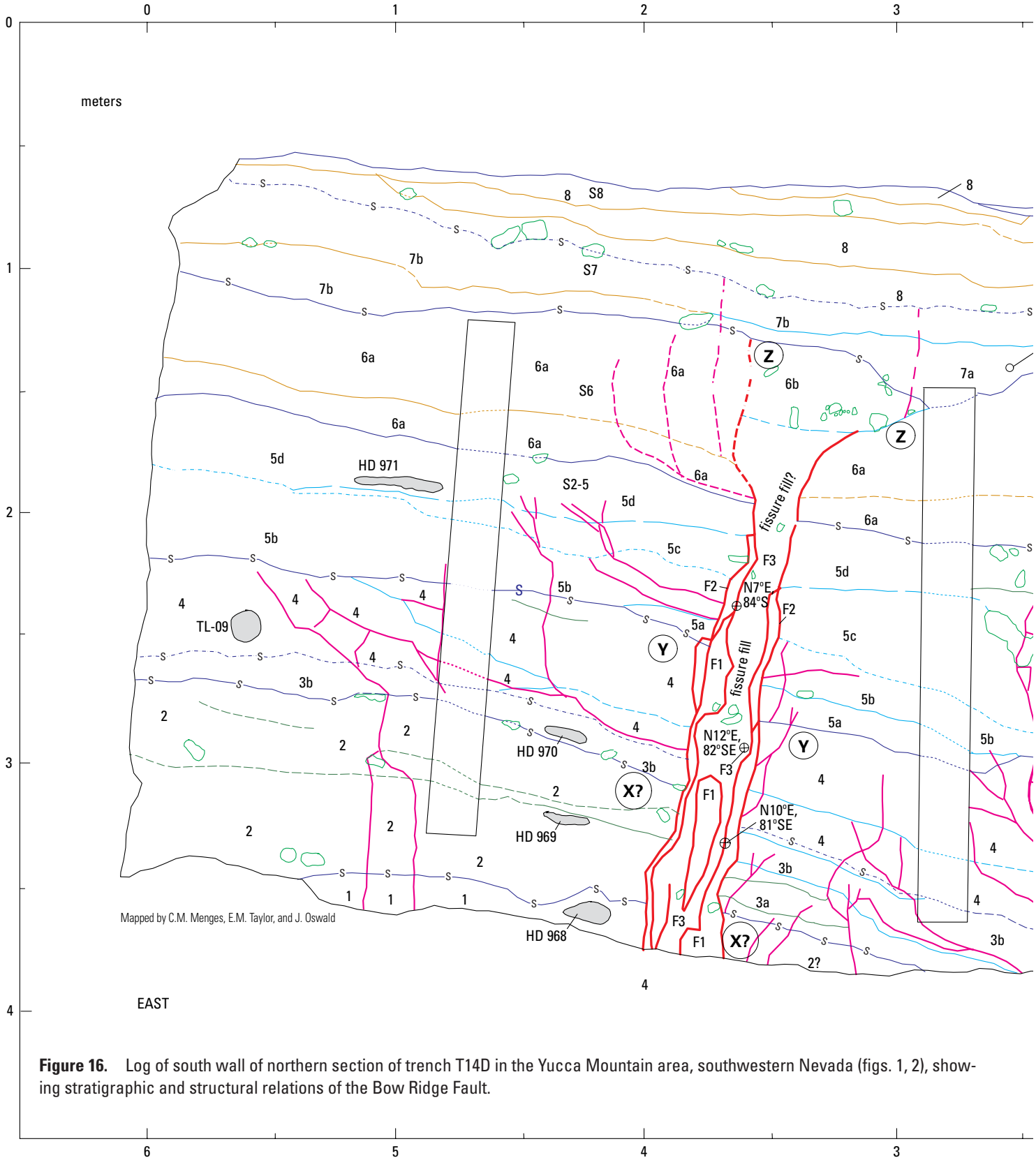

Figure 16. Log of south wall of northern section of trench T14D in the Yucca Mountain area, southwestern Nevada (figs. 1, 2), showing stratigraphic and structural relations of the Bow Ridge Fault.

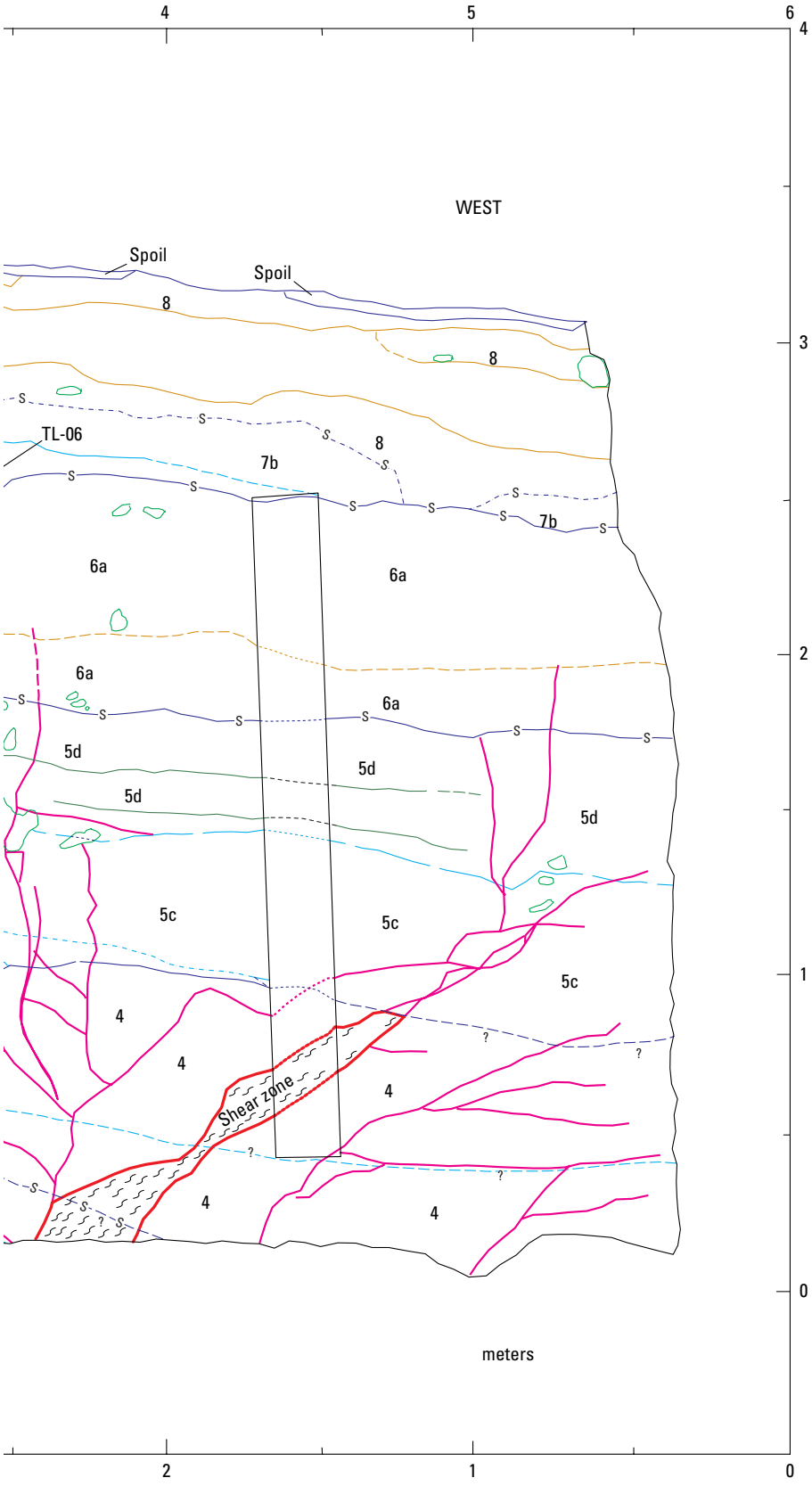

EXPLANATION

Lithologic-unit boundary—Dashed where approximate, dotted where concealed, queried where uncertain

Fault boundary—Dashed where approximate, dotted where concealed, queried where uncertain

Fractures and shears—Dotted where concealed, queried where uncertain

Free-face boundary

Lithologic-subunit boundary—Dashed where approximate, dotted where concealed, queried where uncertain

Combined lithologic-unit/soil-horizon boundary—Dashed where approximate,dotted where concealed, queried where uncertain

Soil-horizon boundary—Dashed where approximate, dotted where concealed, queried where uncertain

Carbonate laminae—Dashed where approximate, dotted where concealed

Paleosurface corresponding to a buried fault scarp

Single clasts or clustered gravel clasts

TL-09 **Sample locality for dated material**—Number refers to sample listed in table 9

7b **Lithologic unit**

Y **Faulting-event horizon**

Shoring

N7°E, 84°S **Strike and dip directions**

Orientation: N. 75° W.

gravel that appear to be more cemented by carbonate and silica with increasing age of faulting. Numerous aligned clasts were observed in both walls of the trench that reflect fissure infilling or buildup of colluvial wedges against scarp-free faces. The fault trace is terminated abruptly by undisturbed colluvial deposits exposed in the uppermost 1 m of the trench (units 7, 8, fig. 16; units 14, 15, fig. 17). The lowermost unfaulted units (unit 7, fig. 16; unit 14, pl. 3) are locally fractured, but not displaced, above the fault. Numerous small secondary fault strands and fractures with little to no offset are within 2 to 3 m of the main fault trace.

Two to three middle to late Pleistocene faulting events are evident in trench T14D (figs. 2, 16, 17; table 6). A possible early faulting event (X, table 8) near the bottom of the trench (northern section, fig. 16) is identified by an apparent increase in stratigraphic offset of unit 2 and by a possible colluvial wedge (unit 3a, fig. 9), although that event is difficult to identify with certainty because of poor stratigraphic definition and pedogenic overprinting. Two later events (Y, Z) are more clearly defined and are recognized on the basis of multiple criteria, including (1) incremental upsection decrease in the offsets of successive marker horizons, (2) differential development of fissure fills and carbonate coatings that terminate at specific horizons, (3) local upward terminations of fractures at a given horizon, and (4) small colluvial wedges (units 5a, 7a, fig. 9) possibly related to scarp degradation after surface rupture. In the southern section of the trench (fig. 17), event Z is especially well defined by a conspicuous gravelly colluvial wedge, but evidence for penultimate event Y is more ambiguous in this exposure.

Dip-slip displacements per event range from 1 to 46 cm (preferred value, 12–40 cm; tables 7, 8). Cumulative displacements of unit 4 (fig. 9) in the northern section of the trench are small (30–45 cm); vector addition of the oblique-slip component increases the net cumulative displacement of this horizon to 33–70 cm. Similar adjustments also indicate net oblique-slip displacements per event ranging from 1 to 15 cm for smaller faulting events and from 46 to 80 cm for larger faulting events (preferred value, 13–44 cm). Fractures with no displacement were formed in unit 7 (northern section of trench, fig. 16) and unit 14 (southern section of trench, fig. 17) above the main fault

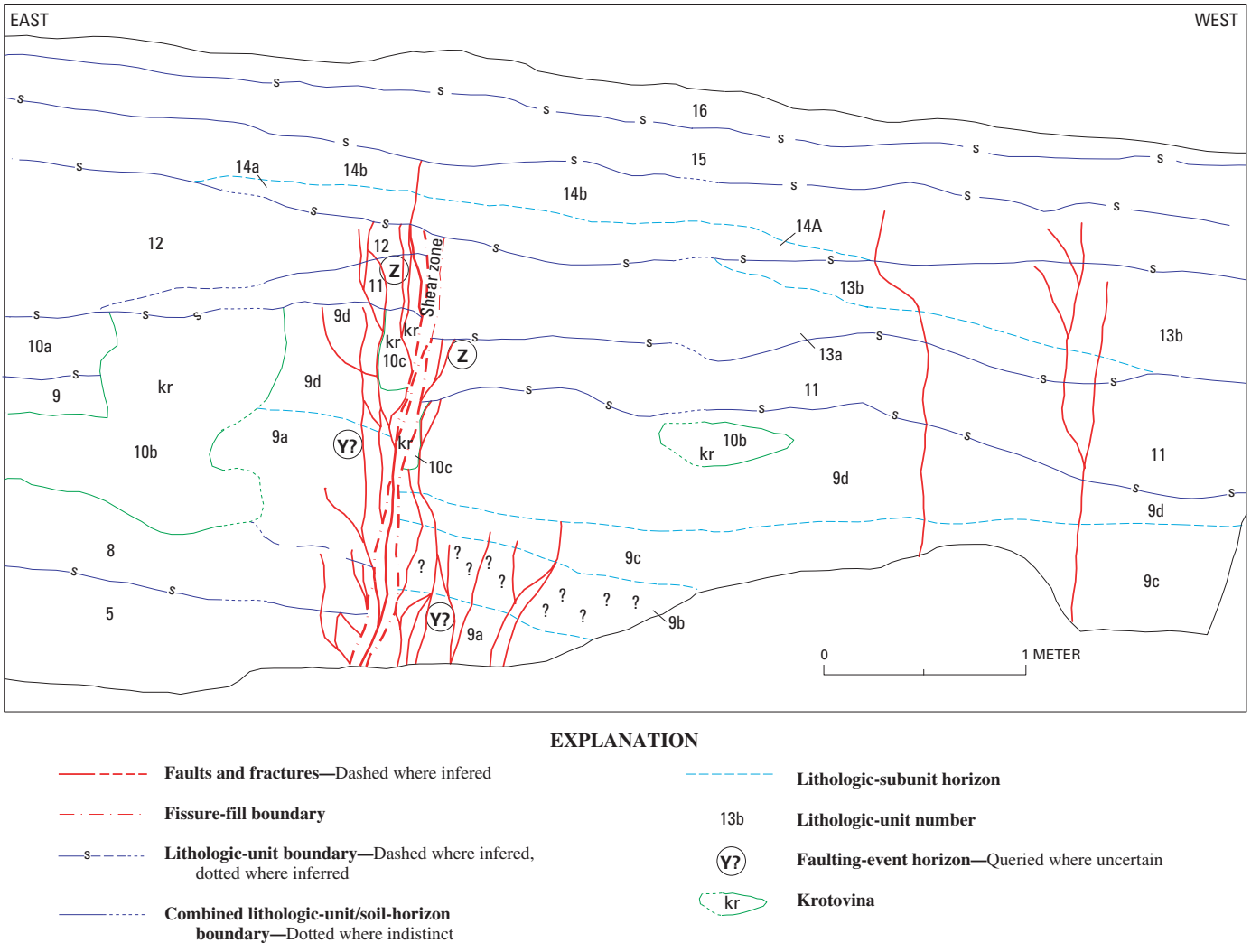

EXPLANATION

Faults and fractures—Dashed where infered

Fissure-fill boundary

Lithologic-unit boundary—Dashed where infered, dotted where inferred

Combined lithologic-unit/soil-horizon boundary—Dotted where indistinct

Lithologic-subunit horizon

13b **Lithologic-unit number**

Y? **Faulting-event horizon**—Queried where uncertain

kr **Krotovina**

Figure 17. Log of south wall of southern section of trench T14D in the Yucca Mountain area, southwestern Nevada (figs. 1, 2), showing stratigraphic and structural relations of the main Bow Ridge Fault zone.

trace, although these features may be nontectonic in origin or related to ground motion on another fault. The size of individual and cumulative late Quaternary displacements at a given stratigraphic level decreases northward along the fault zone from trench T14D to trenches T14C and T14 (fig. 2).

The timing of faulting events was estimated by correlating trench units with the surficial deposits mapped in Midway Valley (tables 2, 4; Wesling and others, 1992), and numerically by U-series and thermoluminescence analyses of selected deposits in the northern section of trench T14D (figs. 2, 8, 16). The oldest faulted colluvial unit in the footwall block (unit 1, fig. 16) is early Pleistocene, on the basis of a U-series age of 700 ka on pedogenic carbonate (sample HD 968, fig. 16; table 9), although its downfaulted equivalent is not exposed on the hanging-wall block. Above this unit is a package of mixed middle to upper Pleistocene colluvial and eolian deposits. Poorly constrained U-series ages of 340+∞/–120 and 234+47/–35 ka (samples HD 969 and HD 970, respectively, table 9) were obtained on two samples collected from laminae in a calcic soil developed on units 2 and 3 (fig. 16) that postdates the possible earliest faulting event (X) in the trench. A thermoluminescence age of 132±23ka (sample TL–09) was obtained from a mixed eolian-colluvial deposit (unit 4, fig. 16), the top of which forms the event horizon for the penultimate faulting event (Y). Carbonate laminae from a calcic soil developed in the overlying unit 5 that is cut by the most recent faulting event yielded a U-series age of 98–144 ka (sample HD 971). A close minimum date for the most recent surface-rupturing event is established by a thermoluminescence age of 48±20 ka (sample TL–06) from unit 7a (fig. 16), which is interpreted as the fine-grained facies of the colluvial wedge deposited after the event. These timing constraints indicate general ranges of 130–30 and 150–130 ka for the dates of events Z and Y, respectively (table 10).

The available age control on faulting events indicates average recurrence intervals ranging from 75 to 215 k.y. (preferred value, 100–140 k.y.; table 11) and individual recurrence intervals ranging from 40 to 350 k.y. (preferred value, 90–210 k.y.). Fault-slip rates computed on unit 4 in the northern section of the trench and on unit 9d in the southern section range from 0.002 to 0.007 mm/yr (preferred value, 0.003 mm/yr; tables 11, 12). We note, however, that these slip rates are necessarily based on only two faulting events, with one intervening interval, and that the slip rates include the effect of the time elapsed since the most recent event, which somewhat limits their significance although no other paleoseismic data are presently available. Long recurrence intervals are supported by such features in the trench as petrocalcic soils developed on units deposited between faulting events and several buried, degraded fault scarps formed above colluvial wedges associated with event horizons.

Trench T14

As mentioned earlier, trench T14 (pl. 3; figs. 2, 8) provides little information for interpreting the history of Quaternary activity on the Bow Ridge Fault but does yield valuable data on the nature and origin of secondary carbonate and silica veins that intersect both Quaternary deposits and Tertiary bedrock within the main fault zone. Bedrock is exposed at the east end of the trench, and Quaternary deposits at the west end; in between is a well-defined, 2.5- to 4-m-wide vertical fissure-filled fault zone (pl. 3).

During the course of trench-wall mapping, Taylor and Huckins (1995) distinguished 12 colluvial units within the Quaternary stratigraphic sequence on the north wall of trench 14 and 10 units on the south wall (pl. 3). Except for two units absent on the south wall, these deposits can be correlated across the trench. The colluvial units consist of poorly sorted, poorly bedded soft sand to silty sand and pebble-cobble gravel that becomes indurated where cemented by carbonate and opaline silica. The gravel content ranges from about 5 to as much as 80 volume percent with increasing trench depth. The dip of the colluvial depositional packages, defined by bedding and subparallel stringers and laminae of carbonate and opaline silica, flattens from 30°–60° SW. in the basal unit to 8°–10° SW. in the upper unit (pl. 3).

Although surficial deposits are in fault contact with brecciated volcanic tuff (pl. 3), no measurable displacements were observed within the Quaternary sequence from which to determine the magnitude and date of individual faulting events. The trench T14 exposure provides evidence, however, that before the depositional period represented by units 5S through 8S (south wall, pl. 3), two colluvial wedges that probably reflect two faulting events were deposited against fault scarps which were later beveled by erosion. Units 5S through 8S were reported by Taylor and Huckins (1995) to range in age from 270±90 to 488±90 ka, on the basis of U-trend dates (samples YM 14 10–14, YM 14 15–17, YM14 18–22, table 9). Sometime later, but before deposition of the upper K soil horizon that caps unit 8S (88±5 ka; sample HD 1–A, table 9), two or more other fracturing or faulting events occurred. Subsequently, other fractures formed and were filled with black ash, whose source is considered to be from an eruption of the nearby Lathrop Wells volcanic center at 77±6 ka (Heizler and others, 1999).

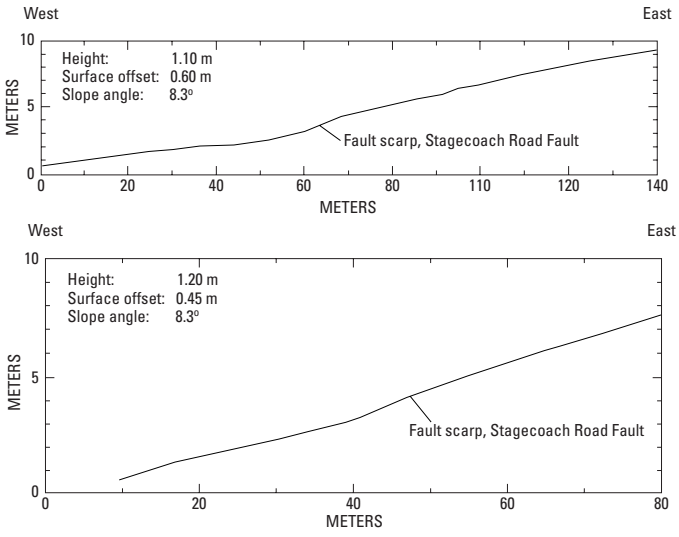

Figure 18. Topographic profiles of geomorphic surfaces across the Stagecoach Road Fault in the Yucca Mountain area, southwestern Nevada (figs. 1, 2).

The fissure-filled Bow Ridge Fault zone in the central part of trench T14 (pl. 3) is characterized by vertical veins containing fine-grained sediment, secondary carbonate and opaline silica, and black ash (Taylor and Huckins, 1995), with a minor component (<5 volume percent) of local volcanic-rock fragments. The ash loosely fills some fractures, which generally are near the center of vertically oriented veins; locally, however, the ash-filled fractures are adjacent to the surrounding bedrock. Laminae of secondary carbonate and silica range in thickness from 0.2 to 10 cm but are not continuous for more than 20 to 30 cm.

The origin of the secondary carbonate- and silica-filled veins—whether by ascending or descending water—has been a matter of considerable controversy. Physical, chemical, mineralogic, biologic, petrographic, and isotopic data collected in trench T14 indicate that the vein fillings are characteristic of an environment with descending meteoric water—that is, a pedogenic environment. Supporting evidence, such as (1) lateral persistence of the colluvial deposits, (2) decrease in the concentration of secondary carbonate below a zone of maximum concentration, (3) presence of discrete soil horizons, and (4) isotopic ratios consistent with those of meteoric water, was discussed in detail by Taylor and Huckins (1995). In summary, the interpretation is that episodes of faulting temporarily created open fractures that formed conduits for percolating water and for the accumulation of fine-grained materials.

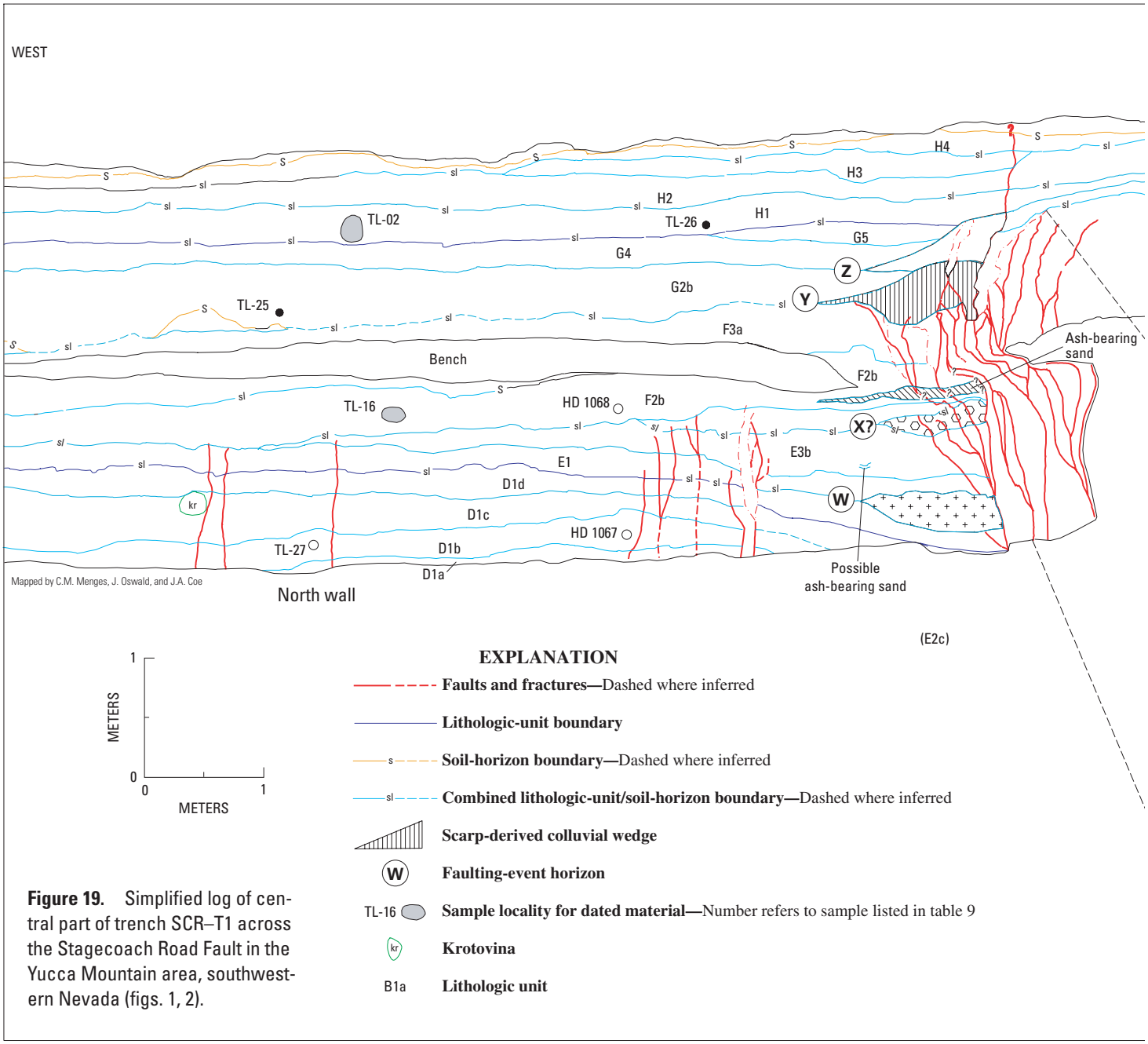

Figure 19. Simplified log of central part of trench SCR–T1 across the Stagecoach Road Fault in the Yucca Mountain area, southwestern Nevada (figs. 1, 2).

Movement of water within the fractures was enhanced after the deposits were cemented by carbonate and opaline silica and subsequently fractured. Surface runoff percolated through the near-vertical fractures and precipitated carbonate laminae.

Stagecoach Road Fault

Trenches SCR–T1 and SCR–T3

The Stagecoach Road fault (figs. 2, 4), though recognized as a potentially important Quaternary fault (O'Neill and others, 1991), was not evaluated by paleoseismic studies until three trenches, SCR–T1 through SCR–T3 (fig. 2), were excavated across it in September 1992. The main fault trace is defined by a distinct scarp. At two trench sites, the scarp is 1.1 to 1.3 m high and has a maximum slope of 8° (fig. 18). Two of these trenches (SCR–T1, SCR–T3), which are located within 2 km of each other on the main fault trace (fig. 2), exhibit fundamentally similar structural and stratigraphic relations; these trenches are discussed together herein, and both were described in greater detail in Menges and others (1998). A third trench (SCR–T2) was excavated across the projection of a bedrock fault south of trench SCR–T1 but was not logged (and is not discussed further here) because no Quaternary deformation was observed at the site.

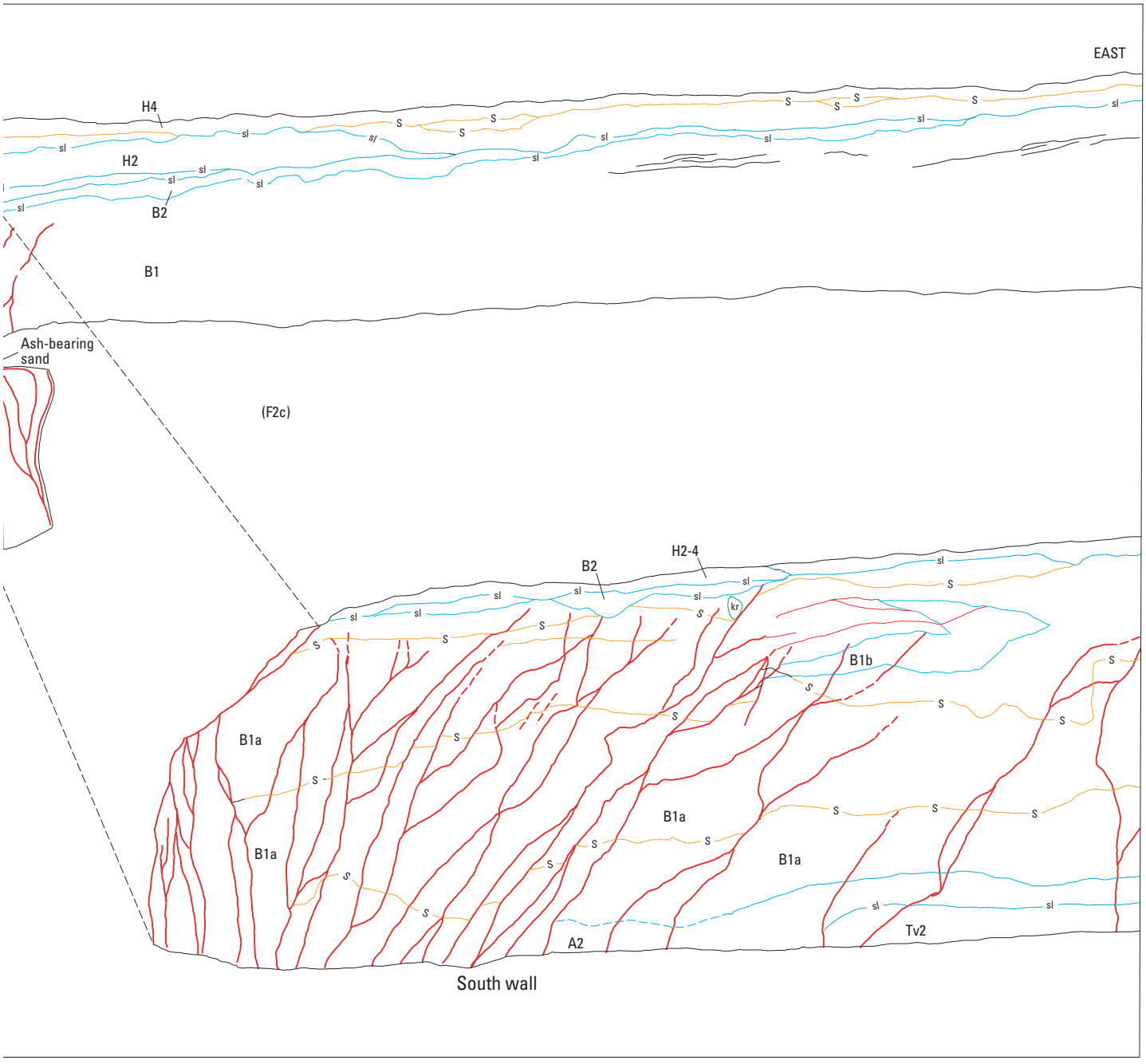

Trenching studies were augmented by drilling three shallow boreholes in August 1994 near trench SCR–T1. Two adjacent boreholes (SR–1, SR–2) with offset, but partly overlapping, depth ranges were drilled 50 m west of the fault zone that is exposed in the trench; a third borehole (SR–3) is located 75 m west of the fault. The drill holes were designed to sample units at depth within the hanging-wall block. Specific objectives included determination of depth to bedrock and a search for carbonate soils in the hanging-wall block comparable in strength of development to the petrocalcic soils in the footwall block (see below).

The fault as exposed in trenches SCR–T1 and SCR–T3 juxtaposes markedly different stratigraphic and soil sequences of mixed alluvium, colluvium, and eolian material on the hanging-wall and footwall blocks (figs. 19, 20). The footwall blocks contain a 2- to 3-m-thick sand-and-gravel layer deposited across the west-sloping erosional surface cut across Tertiary volcanic bedrock. A distinctive reworked volcanic tuff is exposed at the base of surficial deposits in the footwall block of trench SCR–T1 (unit Tv2, fig. 19). The hanging-wall blocks lack deposits correlative with footwall-block units and instead contain younger sequences of locally gravelly alluvium, mostly unconsolidated

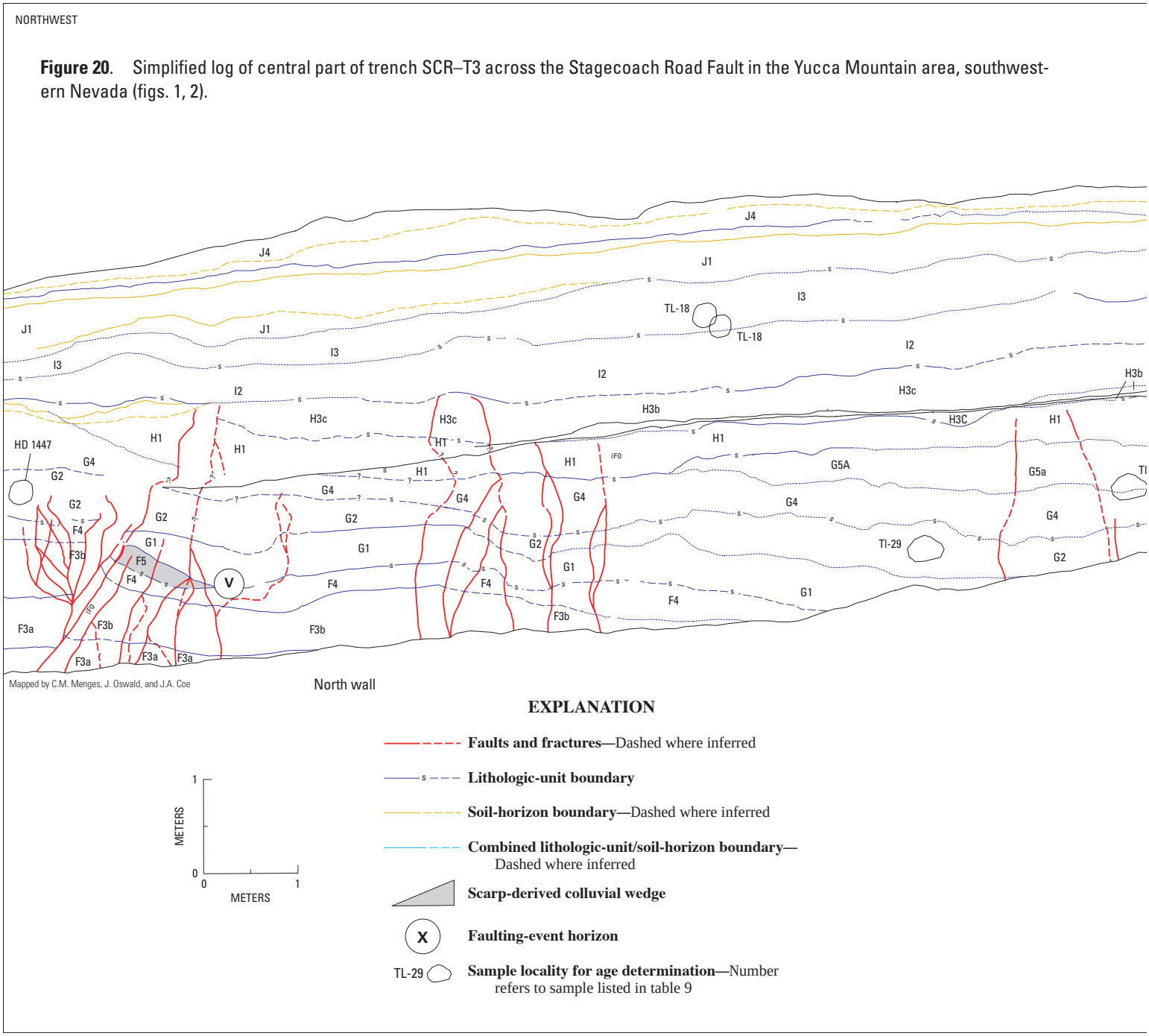

Figure 20. Simplified log of central part of trench SCR–T3 across the Stagecoach Road Fault in the Yucca Mountain area, southwestern Nevada (figs. 1, 2).

sandy colluvium and eolian material (sequences D–H, fig. 19; sequences G–J, fig. 20). These deposits typically consist of fine-grained sand and silt that are poorly bedded to massive and thus lack sharp stratigraphic definition. One or two thin undeformed sand and silt layers (units H1–H2, fig. 19; unit J4, fig. 20) continue along the entire length of the trenches and bury the fault zone. A strong contrast in the degree of soil development was observed across the fault as well. Well-developed carbonate-cemented ($CaCO_3$ stage III–V morphology) petrocalcic soils have formed at the upper surface of the footwall blocks in both trenches, whereas soils on the hanging-wall blocks typically are weakly to only moderately well developed. The maximum carbonate development observed in any of the soils exposed in the middle and upper parts of trench walls generally does not exceed $CaCO_3$ stage I–II+ morphology and cambric B horizon.

The boreholes west of trench SCR–T1 penetrated 82 to 101 m of unconsolidated to poorly consolidated fine-grained deposits, consisting mostly of sand and silt with local gravel layers that were deposited above weathered bedrock. These deposits contain numerous zones of dispersed carbonate but lack thick well-developed petrocalcic soils. A tuffaceous sand layer at 99-m depth that overlies a welded tuff in borehole

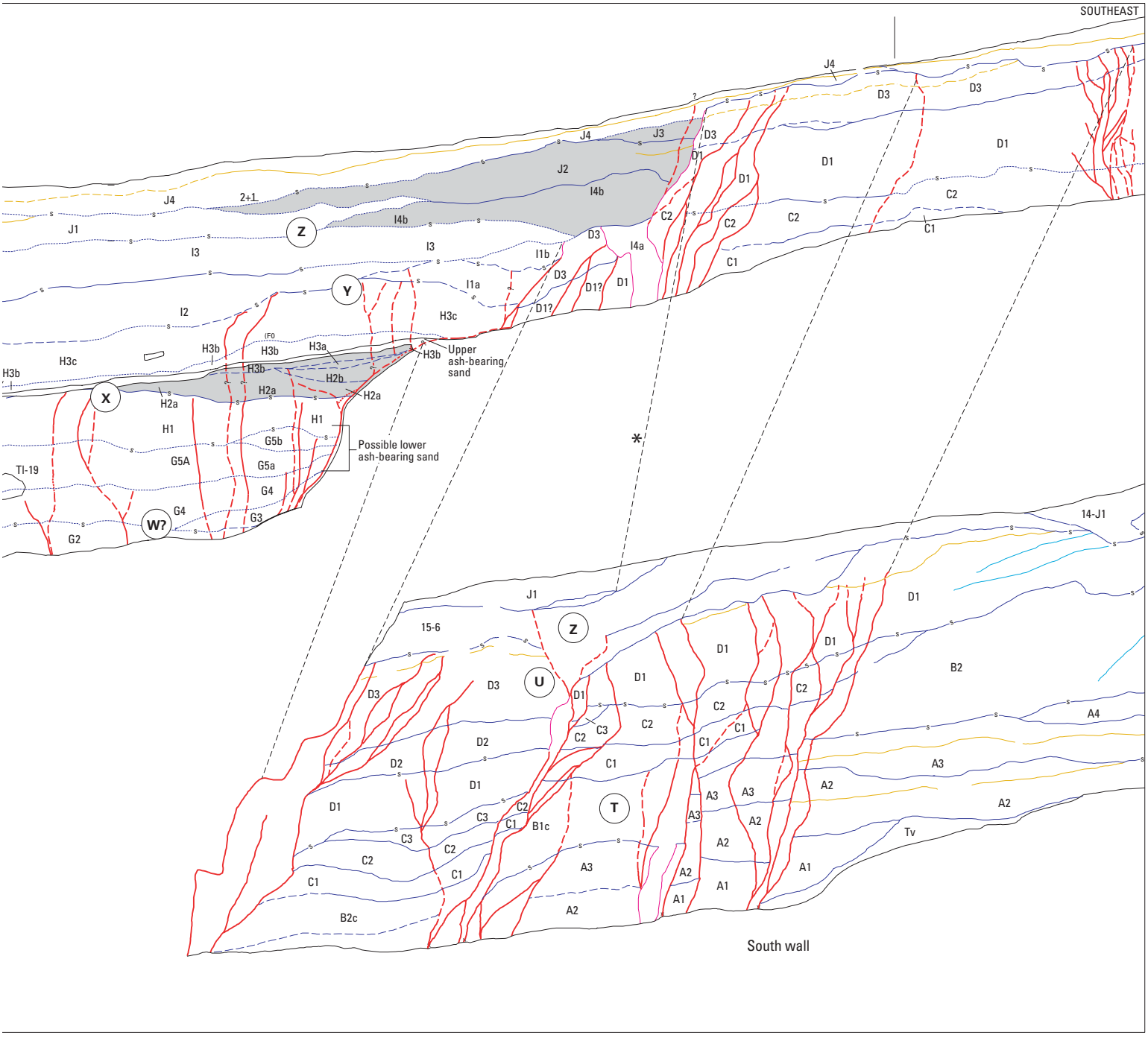

SR–3 is correlated with a similar pumiceous tuff (unit Tv2, fig. 19) in the footwall block of trench SCR–T1.

The Stagecoach Road Fault is well expressed in both trenches as multiple-strand zones containing numerous carbonate-coated shears and fractures (figs. 19, 20). The fault zone in trench SCR–T3 consists of four discrete, closely spaced strands, and another fault strand is present 20 m to the east of the main fault zone in the footwall block of trench SCR–T1 (located beyond section of trench shown in fig. 19). The dominant strike and dip of the fault zone is N. 0°–10° W., 85° W., in trench SCR–T1, where the fault trace deflects to the north, and N. 20°–30° E., 55°–65° W., in trench SCR–T3. The petrocalcic soil in the footwall block is extensively fractured adjacent to the main fault zone in trench SCR–T1 (fig. 19). The eastern fault strand is capped by this soil, and so deformation on that strand predates petrocalcic-soil development. The footwall block in trench SCR–T3 is undeformed east of the complex main fault zone (fig. 20). The hanging wall in both trenches is complexly deformed by secondary synthetic and antithetic fractures and shears that commonly are associated with eastward backtilting of strata toward the fault and by asymmetric graben formation adjacent to the main fault zone (figs. 19, 20). Previous surface mapping found evidence for significant amounts of left-oblique slip on the Stagecoach Road Fault (O'Neill and others, 1992); however, essentially dip slip slickenlines were observed on a bedrock fault strand that displaces overlying Quaternary deposits in the bottom of trench SCR–T3.

At least two, possibly as many as four, late Pleistocene to Holocene(?) faulting events were interpreted from deposits and structural relations observed on the hanging-wall block adjacent to the main fault zone in trench SCR–T1 (table 6), on the basis of such criteria as incremental downsection increases in stratal backtilting against the fault, upward termination of fractures and shears at discrete horizons, and the presence of colluvial wedges and fissures on the hanging-wall block. The wedges commonly are indistinct and lack stratigraphic definition.

The two latest faulting events (Y, Z, table 8) are represented by the best-defined surface ruptures in both trenches. The most recent event (Z) is interpreted from relations observed in the upper sedimentary sequence (unit G, fig. 19; unit I, fig. 20), such as fault truncations, displaced wedges from the penultimate event, and scarp-derived colluvial wedges. The penultimate event (Y), which is recognized at the top of the uppermost calcic soil (in unit F3a, fig. 19, and unit H3c, fig. 20), is associated with several fracture terminations, colluvial wedges, and fissures. A single fracture with no detectable offset was formed in otherwise undisturbed deposits (units H1–H4, fig. 19; unit J4, fig. 20) that bury the fault trace in each trench. These fractures may be either nontectonic in origin or related to ground shaking from a nearby paleoearthquake; thus, they are not necessarily associated with a surface-rupturing paleoearthquake on the Stagecoach Road Fault.

Faulting events are more difficult to identify in the poorly stratified and structurally overprinted deposits in the lower parts of the trench walls, although the presence of progressively backtilted units downfaulted against footwall sequences requires additional faulting events within that interval. One faulting event (X) is inferred at the top of unit E3b in trench SCR–T1 (fig. 19) and above unit H1 in trench SCR–T3 (fig. 20), on the basis of upward fracture truncations, stratal backtilting, and indistinct colluvial wedges. Similar criteria were used to define a possible fourth faulting event (W) near the base of the exposures in the hanging-wall blocks in both trenches.

The three latest faulting events (X–Z) can easily be correlated between trenches. An earlier event (W) that also is correlated, on the basis of similarities in stratigraphic relations between the trenches, might be a discrete event in each trench. In trench SCR–T3, an earlier faulting event (V) is identified on the antithetic bounding fault of the hanging-wall graben, although the affected tilted deposits project eastward beneath the trench bottom before reaching the main fault trace. Two additional earlier faulting events (T, U) are present only on eastern strands of the fault on the footwall block in trench SCR–T3.

Displacements are difficult to estimate because of the absence of most hanging-wall units on the footwall block. Apparent dip slip was estimated from the thicknesses of colluvial wedges, which are considered minimums, and from the total stratigraphic thicknesses between event horizons, which represent maximums. Displacements per event range from 15 to 160 cm, commonly from 40 to 100 cm (tables 7, 8). Cumulative displacements near the bottoms of trenches range from 117 to 493 cm; corrections for local backtilting of units and graben formation reduce the amount of net slip to 28–79 cm for individual events and to 99–309 cm for net cumulative offsets.

No direct age determinations are available for units in the footwall block in either trench. Footwall deposits are approximately dated at middle Pleistocene in trench SCR–T3, on the basis of soil development. The thick, well-developed petrocalcic soil in trench SCR–T1 indicates an age of at least early Pleistocene, possibly Pliocene, for surficial units above bedrock in the footwall block.

Various geochronologic data—including both U-series and thermoluminescence analyses and the correlated age of basaltic ash disseminated within sandy layers—establishes a late Pleistocene through Holocene age for the hanging-wall deposits in both trenches (figs. 19, 20; tables 6, 7, 9). Some of the U-series and thermoluminescence ages summarized herein differ slightly from those of Menges and others (1998), and the age assignment and significance of the ash-bearing strata have also been adjusted from their report. Rhizolith-rich sandy layers containing evidence for one or two poorly defined faulting events (W, X) are exposed in the lower half of trench SCR–T1 (fig. 19). These rhizoliths yielded U-series ages ranging from 13±6 to 27±1 ka (samples HD 1068 and HD 1067, respectively, table 9) that are considered minimum ages because the dated carbonate in rhizoliths replaces plant roots that postdate deposition of the unit by an unknown, but

potentially significant, time interval. Older depositional ages for this stratigraphic interval are indicated by thermoluminescence ages of 28±4 and 49±9 ka (samples TL–16, TL–27) from units F2b and D1b, respectively, in trench SCR–T1 (fig. 19); however, a lithologically similar stratigraphic interval in the lower part of trench SCR–T3 (fig. 20) may be even older, on the basis of a thermoluminescence age of 87±18 ka (sample TL–19) from unit G5 and U-series ages from an underlying carbonate soil in unit G2 of about 80–115 ka (sample HD 1447)—significantly older than a thermoluminescence age of 60±16 ka (sample TL–29), also from unit G2. Thus, similar stratigraphic intervals in the lower parts of both trenches have two sets of only slightly overlapping U-series or thermoluminescence estimated ages: one set approximately 30–60 ka and the other set closer to 80–110 ka. The older ages are preferred for the lower section containing events W(?) and X in both trenches because (1) they provide the best concordance between both geochronologic methods in trench SCR–T3 and (2) the older ages agree better with the stratigraphic positions and correlated ages of basaltic ash observed in both trenches, as described below. The older age is also more consistent with the degree of soil development associated with unit G2 in trench SCR–T3.

Disseminated but distinctive basaltic ash is present in a sandy layer at approximately the same stratigraphic position in both trenches (units F2c and H3c in trenches SCR–T1 and SCR–T3, respectively, figs. 19, 20). Preliminary geochemical analysis of the ash from trench SCR–T1 indicates a source from the nearby Lathrop Wells volcanic center (F.V. Perry, written commun., 1996), which erupted at 77±6 ka (Heizler and others, 1999). That age is consistent with the position of the ash-bearing layer relative to the older U-series and thermoluminescence ages (80–115 ka) determined for the lower part of trench SCR–T3 described above, but it mostly lies outside the 30–60-ka interval indicated by the oldest thermoluminescence age in that trench and both of the older thermoluminescence ages in trench SCR–T1.

A second ash-bearing horizon was identified in each trench below the primary upper ash layer, but the stratigraphic context of these lower ash horizons is more problematic. The lower ash in trench SCR–T1 (figs. 2, 19) is concentrated in a small pocket within a sandy layer and so may represent an ash-filled krotovina (animal burrow) related to the overlying upper ash layer, whereas basaltic ash is extremely diffuse and dispersed in a poorly defined lower horizon in trench SCR–T3 (figs. 2, 20). The two ash horizons were originally considered by Menges and others (1998) to reflect multiple eruptions at Lathrop Wells—the prevailing interpretation during early stages of the paleoseismic investigations at Yucca Mountain (Crowe and others, 1995; Menges and others, 1998). On the basis of the single eruption (77±6 ka) reported by Heizler and others (1999), however, the present interpretation is that the upper ash-bearing horizon, which is well defined in both trenches, correlates with that eruption.

The slightly oxidized sand layer in the upper part of the hanging-wall block that overlies the penultimate-event Y horizon in trench SCR–T1 (unit G2b, fig. 19) yielded a thermoluminescence age of 12±1 ka (sample TL–25, table 9); the thermoluminescence age of a lithologically similar unit in trench SCR–T3 with a similar stratigraphic relation to event Y is 22±5 ka (units I2, I3, fig. 20; sample TL–18, table 9). Evidence for the most recent event (Z) in trench SCR–T1 is above faulted unit G2b, but is buried by an undeformed unit (unit H1, fig. 19) with two thermoluminescence ages of 12±6 and 9±1 ka (samples TL–02 and TL–26, respectively, table 9) that are consistent with the morphology of the soil developed on the colluvium, which is weakly developed with minimal secondary carbonate, similar to soils on uppermost Pleistocene to middle Holocene deposits in the Yucca Mountain area (figs. 1, 2).

Estimated recurrence intervals and slip rates vary, depending on which set of discordant ages is assigned to the stratigraphic units in the middle and lower sections of the trenches. The age assignment of 70–100 ka for that interval, based primarily on the ash correlations in both trenches and the older set of U-series and thermoluminescence ages in trench SCR–T3 (fig. 20), yields preferred average recurrence intervals of 20–50 k.y. and preferred individual recurrence intervals of 5–50 k.y. (table 11). A preferred slip rate of 0.02 to 0.03 mm/yr is consistently calculated in both trenches from several different datums, using both ash correlations and directly dated layers as independent age control (tables 11, 12). Preferred estimated average and individual recurrence intervals are shorter (10–30 and 5–30 k.y., respectively) and slip rates are higher (0.03–0.05 mm/yr) if the younger set of thermoluminescence ages in trench SCR–T1 are used to assign an age range of 30–60 ka for the middle to lower stratigraphic interval in the trench. As noted above, we prefer the older age assignment and resulting recurrence intervals and slip rates because of the better internal concordance among various geochronologic methods, including ash correlations. We consider the younger set of thermoluminescence ages in the lower part of the trenches to be unreliable, possibly contaminated by postdepositional infiltration and accumulation of younger eolian fines in these highly unconsolidated deposits.

Chapter 6

Results of Paleoseismic Investigations on the Ghost Dance Fault

By Emily M. Taylor, Christopher M. Menges, and David C. Buesch

Contents

Abstract....71
Introduction....71
Characteristics of the Ghost Dance Fault....72
Geomorphic Expression....73
Outcrop Characteristics....76
Fault Characteristics in Trench Exposures....77
Trench on Whale Back Ridge....77
Trench T4....83
Trench T4A....83
Trench T2....85

Abstract

The Ghost Dance Fault is a north-striking, steeply west dipping normal fault that lies close to and partly intersects the proposed repository site for the storage of high-level radioactive wastes at Yucca Mountain. The fault, which is as much as 7 km long, is expressed as a complex zone of subparallel and branching strands that narrows and decreases in cumulative offset northward. Topographic profiles across bedrock traces of the fault have none of the pronounced steps or scarps typical of Quaternary surface ruptures elsewhere in the Yucca Mountain area.

Six trenches were excavated in Quaternary deposits that overlie bedrock projections of the Ghost Dance Fault—one on Whale Back Ridge, one at the base of Antler Ridge, three in Split Wash, and one in Drill Hole Wash. Three of these trenches exposed fractured bedrock, which in places is draped and (or) infilled by secondary carbonate and opaline silica ranging in age from 10±0.1 to 392±29 ka (U-series analysis). The origin of a single fracture in the dense carbonate and opaline silica deposit in the trench on Whale Back Ridge is problematic. With the possible exception of this fracture, no evidence of Quaternary movement was observed on the Ghost Dance Fault.

Introduction

This chapter summarizes the results of investigations of possible seismic hazards associated with the Ghost Dance Fault, a north-striking fault that lies close to, and partly intersects, the proposed repository site for the storage of high-level radioactive wastes at Yucca Mountain (figs. 1, 2; Day and others, 1998b). We emphasize the geologic relations exposed in trenches excavated in Quaternary deposits that overlie projections of the fault (figs. 2, 21). One or both walls of these trenches were mapped in detail to define the physical stratigraphy and the soils developed on the Quaternary deposits and to determine whether these deposits were faulted. For the purposes of this report, we describe the trenches on Whale Back Ridge (trench WBR), in Split Wash (trenches T4, T4A), and in Drill Hole Wash (trench T2).

Detailed logs of mapped trench walls were prepared by using a total-station theodolite. Stratigraphic units were described, and samples were collected for laboratory analysis of particle-size distribution, secondary-carbonate content, and pH. The soil nomenclature used to describe the soils and surficial deposits conforms to that of Birkeland (1984). Color names for bedrock and lithologic units are those on the Munsell Soil Color Chart (Munsell Color Co., Inc., 1992). Samples were also collected for U-series analysis of opaline silica and of pedogenic carbonate where material was available for study.

Other methods used to assess Quaternary activity on the Ghost Dance Fault include (1) a comparative analysis of the geomorphic expression of the fault, relative to the northern section of the Solitario Canyon Fault (fig. 2; see chap. 7); (2) exposure dating of the faultline escarpment formed along the fault; (3) descriptive analysis of fault characteristics in outcrop; and (4) analog studies of total bedrock displacements relative to other faults at Yucca Mountain. Though less direct than trenching investigations, these techniques provide useful information regarding possible Quaternary displacements.

The Sundance Fault, a small auxiliary fault that trends northwest across the northern part of the proposed repository site from near the Ghost Dance Fault trace (Potter and others,

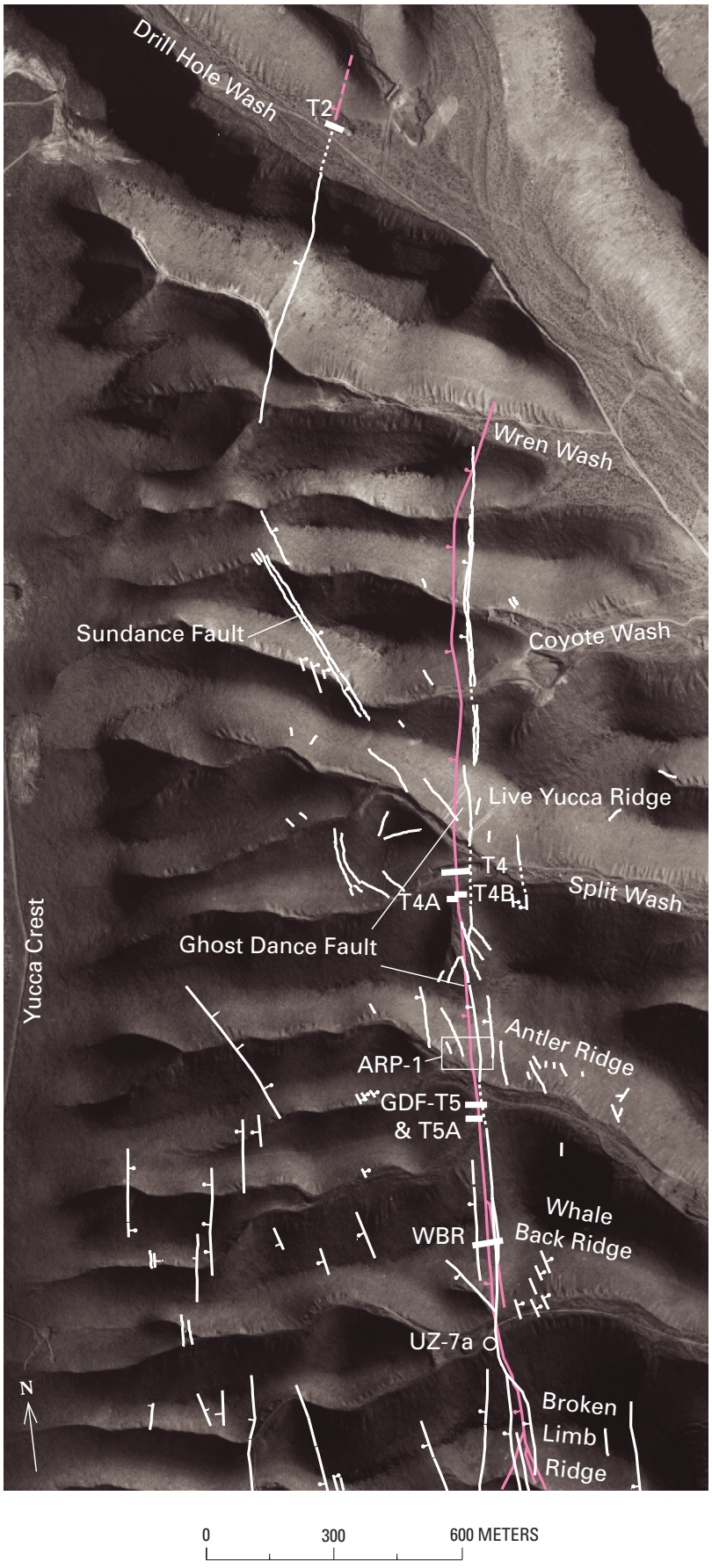

EXPLANATION

Faults—Dashed where approximate, dotted where concealed, bar and ball on down-thrown side; white, Day, and others (1998b); red, Scott and Bonk (1984)

Drill hole

Trench

Figure 21. East slope of Yucca Mountain, southwestern Nevada (figs. 1, 2), showing locations of topographic features, Ghost Dance and Sundance Fault traces, and trenches. Fault traces modified from maps of Scott and Bonk (1984) and Day and others (1998b).

1999), was not trenched. The Sundance Fault, which is exposed in bedrock for about 750 m, was examined at the surface in conjunction with a detailed study of the Ghost Dance Fault, but no evidence was observed to indicate Quaternary activity. The Sundance Fault is briefly discussed in chapter 3.

Characteristics of the Ghost Dance Fault

Geomorphic Expression

The Ghost Dance Fault zone cuts transversely across a series of bedrock ridges (fig. 21) created by incision of central Yucca Mountain by the eastward-draining tributaries of Fortymile Wash (fig. 2). The fault zone traverses bedrock across narrow to broadly rounded ridgecrests and side slopes thinly mantled with colluvium (fig. 22) but is buried beneath colluvial and alluvial fill in the narrow floors of the intervening washes.

Little geomorphic expression of the Ghost Dance Fault zone is evident. Both the main fault trace and ancillary faults are exposed discontinuously on hillslopes in subdued bedrock outcrops interspersed among rubbly colluvial talus and scree. Only small segments of the fault zone are expressed as linear gullies, topographic steps or scarps, or saddles or other topographic depressions that would produce recognizable lineaments on aerial photographs. No scarps or other geomorphic expressions of the fault were observed in the valley floors. For these reasons,

the Ghost Dance Fault must be located by careful geologic mapping of displaced lithologic contacts or aligned outcrops of brecciated rock cemented by white secondary carbonate.

On ridgecrests, the Ghost Dance Fault generally is near the base of west-sloping 5- to 15-m-high bedrock scarps that commonly reflect displacements of resistant bedrock units within the Miocene Tiva Canyon Tuff across the fault zone. Although such features superficially resemble large composite fault scarps, careful examination indicated that they are more likely faultline scarps formed primarily by differential erosion of bedrock units with varying degrees of resistance to weathering which are juxtaposed along the fault. Topographic profiles across the escarpments indicate broadly concave to linear forms with no pronounced steps or scarps that would reflect late Quaternary displacement.

Four slope profiles were measured across the Ghost Dance Fault—two on Whale Back Ridge, one on Antler Ridge, and one across the buried fault trace exposed at trench

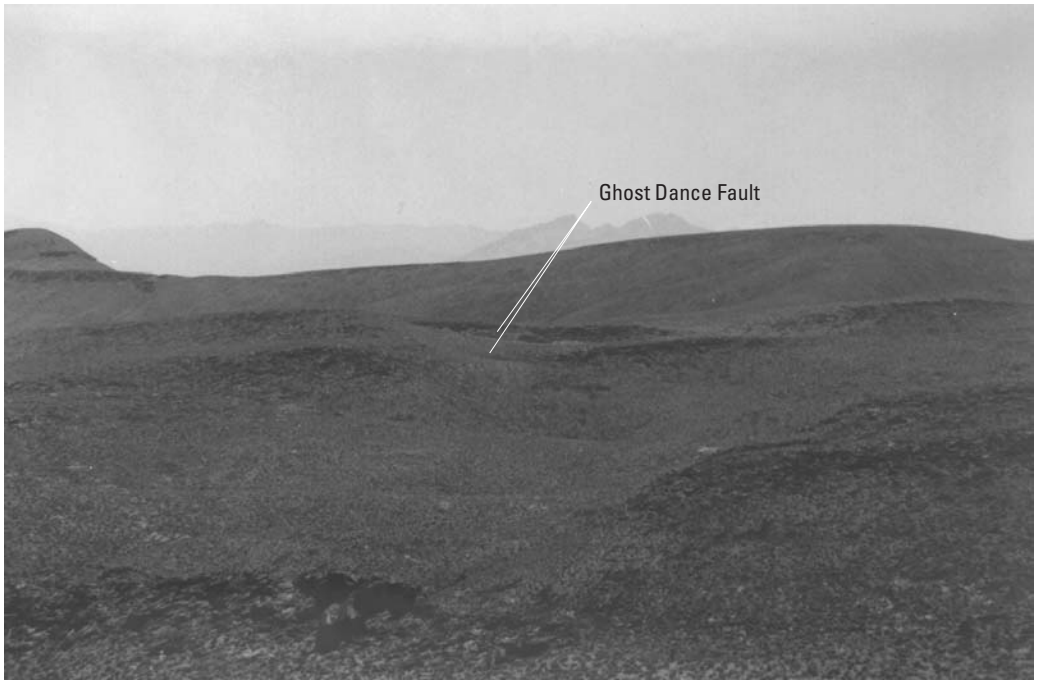

A

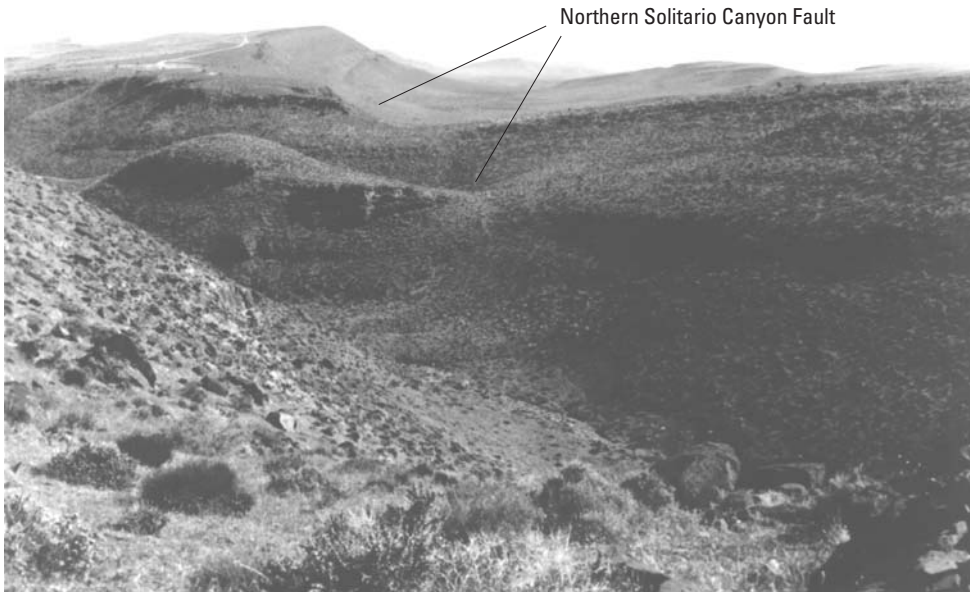

B

Figure 22. Ghost Dance and Northern Solitario Canyon Faults along slopes of Yucca Mountain, southwestern Nevada (figs. 1, 2, 21). *A*, Ghost Dance Fault exposed in Whale Back and Antler Ridges (in middle distance). Note poor physiographic expression of fault on sideslopes and gently sloping, west-facing faultline escarpments on ridgecrests. *B*, Northern Solitario Canyon Fault at northwest corner of Yucca Mountain. Fault is marked by conspicuous notches in saddles on ridgecrests and by lineaments or gullies on canyon walls.

T4 in Split Wash (figs. 21, 23, 24). Bedrock units were sampled along the Whale Back and Antler Ridge profiles for analyses of the cosmogenic radionuclides ^{10}Be and ^{26}Al that could be used to infer surface-erosion rates, and to estimate the minimum duration of burial by fault-scarp colluvium (fig. 24). Preliminary analytical data provided by C.D. Harrington (oral commun., 1995) indicate that erosion has been minimal and that the surface has been stable for at least 700–1,100 k.y. The whole-rock cosmogenic-^{10}Be estimated ages of samples collected at various localities along the Whale Back Ridge and Antler Ridge profiles are noted in figure 24. These estimated ages are uncorrected for erosion and so are only

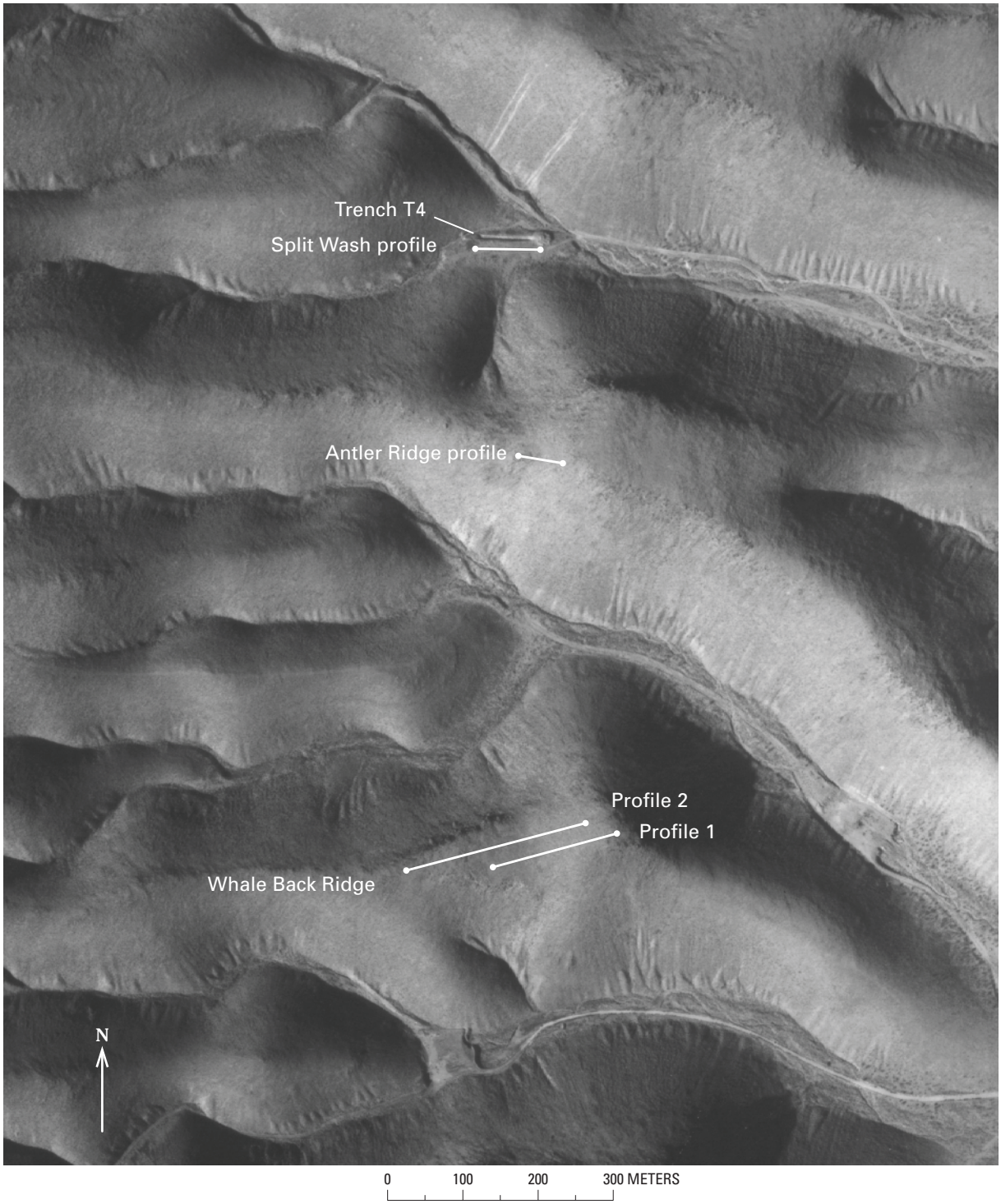

Figure 23. Whale Back and Antler Ridges in Split Wash along slopes of Yucca Mountain, southwestern Nevada (figs. 1, 2, 21), showing locations of topographic profiles across the Ghost Dance Fault.

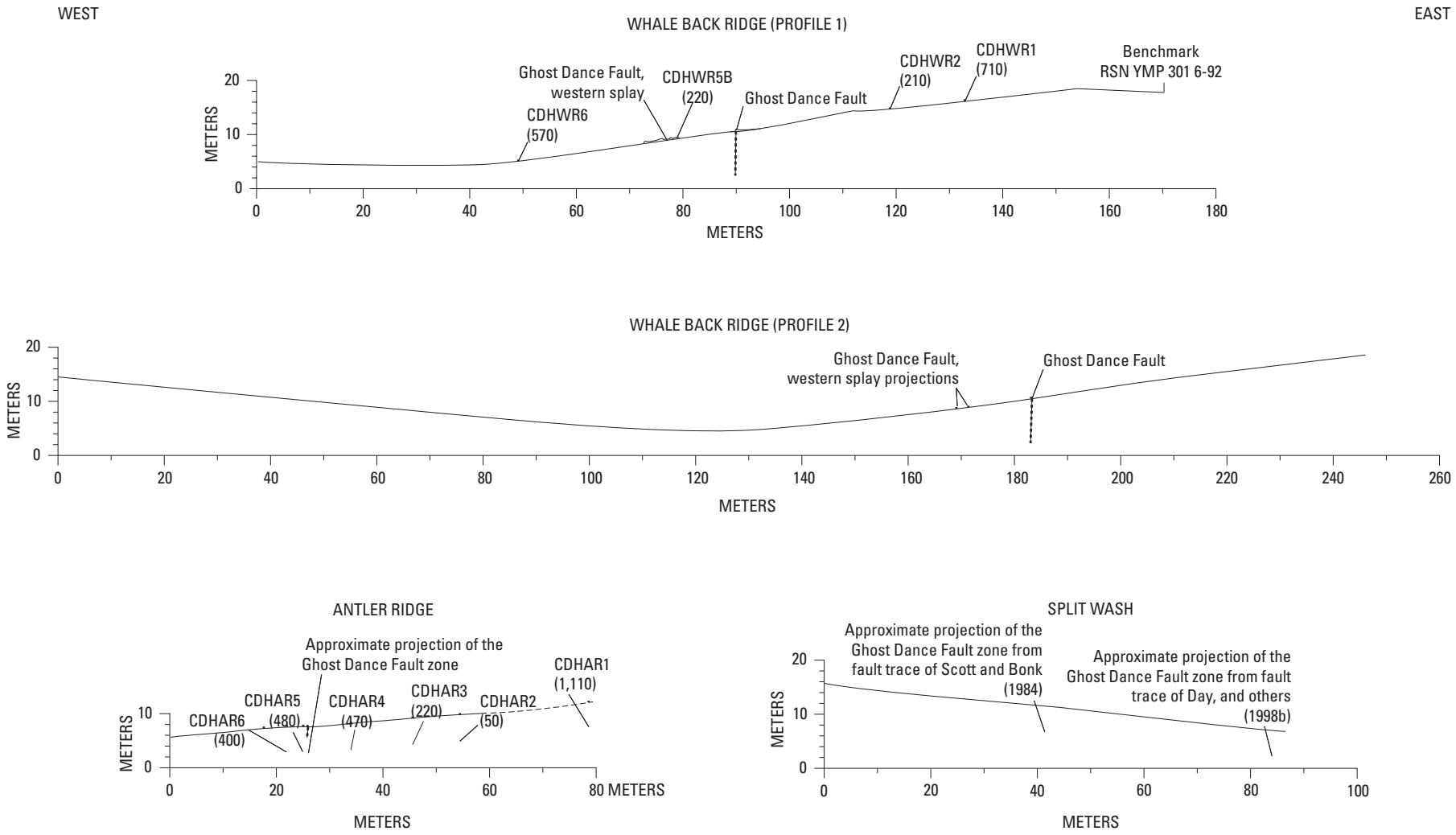

Figure 24. Topographic profiles (see fig. 23) across the Ghost Dance Fault on Whale Back and Antler Ridges and in Split Wash along slopes of Yucca Mountain, southwestern Nevada (figs. 1, 2, 21), showing locations of bedrock samples (arrows) collected for determination of whole-rock cosmogenic ^{10}Be estimated ages (numbers in parentheses, in thousands of years).

minimum limiting ages. The production rate (of ^{10}Be atoms in the rock) used in the analyses, normalized for sea level and high latitude, is 5.8 atoms/g per year, with an uncertainty of ±25 percent.

The Ghost Dance Fault varies in its position with respect to the top or bottom of the scarp faces. On Whaleback Ridge, for example, the fault is in about the middle of the scarp face, whereas on Antler Ridge it is near the base, indicating that appreciable erosion of the scarp has taken place since middle Miocene time. Also, the lowest elevations on ridgecrests generally do not correspond to the Ghost Dance Fault zone but, instead, are in saddles to the west of the fault zone where erosion has breached resistant bedrock units capping ridgecrests on the downthrown block. This relation likewise indicates erosional modification of an old fault-generated dissected landscape dating from middle Miocene time.

The slight geomorphic expression of the Ghost Dance fault as described above contrasts sharply with that of other faults in the Yucca Mountain area (for example, the nearby Solitario Canyon Fault; see chap. 7) that have undergone repeated late Quaternary displacements indicating little, if any, Quaternary activity on the Ghost Dance Fault. As discussed below, the fault also displays no evidence of displacement of any of the Quaternary deposits exposed above the fault zone in trench excavations.

A

B

Figure 25. Exposures of the Ghost Dance Fault in the Yucca Mountain area, southwestern Nevada (figs. 1, 2, 21). *A*, Ghost Dance Fault zone in a cleared bedrock exposure at Antler Ridge; main fault zone is defined by carbonate-cemented breccia below hammer. *B*, Main strand of the Ghost Dance Fault exposed in south wall of drillhole UZ–7a pad; east (left) side of fault zone is carbonate cemented, in contrast to loose breccia zone on west (right) side below gully.

Outcrop Characteristics

The Ghost Dance Fault is well exposed in an artificially cleared hillslope exposure of bedrock at the base of Antler Ridge (fig. 23), where the fault is characterized by a 0.5- to 2-m-wide zone of carbonate-cemented rock breccia cut by a dense network of north- to northwest-trending fractures (fig. 25*A*). Some of the rock fragments appear to be colluvial in origin, but at least some brecciation probably is related to fault deformation. This breccia zone is tightly cemented by carbonate, and some of the rock fragments are supported by a carbonate matrix. The breccia lacks a strong planar-shear fabric and commonly displays no strong preferential orientation subparallel to the fault. Only a few thin (<5 cm wide) planar laminae of carbonate or opaline silica are along the main fault traces. Similar types of oriented cemented breccia are also observed in most natural exposures of the Ghost Dance Fault.

The southern section of the Ghost Dance Fault is well exposed in a 60-m-wide zone in the artificially cleared southern wall of the drill-hole UZ–7a pad, which is located in the valley between Whale Back and Broken Limb Ridges (fig. 25*B*). The fault zone there contains a primary subvertical fault at the eastern margin of the zone and a secondary steeply east dipping fault 42 m to the west. Highly fractured and broken rocks in the hanging wall have been subdivided into four zones on the basis of the pattern and density of fractures (S. Williams-Stroud, written commun., 1995). The main fault zone contains a 2- to 4-m-wide zone of brecciated rock in a fine-grained matrix. The western part of this brecciated zone, near the footwall, is cemented by accumulations of secondary carbonate and silica that thin and weaken downsection through the exposure (fig. 25*B*). Unoriented fault breccia is loose and uncemented in a narrow zone at the east margin of the main fault zone; the absence of cementation there may reflect the position of a gully above the fault,

which may direct infiltration and cause carbonate to be flushed through this part of the zone. Coarse carbonate laminae impart a local subvertical-planar fabric in the cemented part of the fault zone.

Fault Characteristics in Trench Exposures

Trench on Whale Back Ridge

The trench on Whale Back Ridge (WBR, figs. 2, 21), which was excavated across the main Ghost Dance Fault trace, exposes Quaternary slopewash colluvium and fine-grained eolian deposits overlying the Tiva Canyon Tuff (pl. 4). The exposed section of the main fault (sta. 13 m, fig. 26) displays some of the largest offsets of bedrock units; the strike and dip of the fault are N. 10° W. and 83° SW., respectively. The moderately welded nonlithophysal subzone of the crystal-rich member of the Tiva Canyon Tuff is locally brecciated (stas. 13.5–27 m). Clasts in this breccia, some as much as 1 m in diameter, are rotated to dips of 10°–30° E. The matrix consists of comminuted rock fragments from the moderately welded, nonlithophysal subzone. Although minor mixing of clasts from different bedrock units occurs within this subzone, the breccia is essentially monolithologic. Adjacent to the Ghost Dance Fault is a narrow (<1 m wide) brecciated zone that contains blocks from the upper part of the nonlithophysal crystal-transition subzone or the lower part of the mixed-pumice subzone. The breccia probably represents clasts stranded along adjacent fault slices.

Two faults (stas. 25, 27 m, fig. 26) form the west boundary of the main brecciated zone associated with the main Ghost Dance Fault zone (fig. 26). The first fault (sta. 25 m), which strikes N. 3° E. and dips 85° SE., separates a relatively unbroken, but largely covered, block of tuff of the moderately welded, nonlithophysal subzone of the crystal-rich member of the Tiva Canyon Tuff on the east from brecciated rocks of the same subzone on the west. The second fault (sta. 27 m), which strikes N. 18° W. and dips steeply west, locally has associated fractures that dip about 65° NW. This fault separates brecciated rocks of the moderately welded, nonlithophysal subzone on the east from partially fractured rocks of the vitric, densely welded subzone on the west.

Most of the trench floor (stas. 30–70 m, fig. 26) is covered by excavated spoil material, but numerous fractures, many filled with secondary carbonate, are exposed. Although no well-developed fracture pattern is evident in this part of the trench, many fractures strike from N. 5° E. to N. 25° W. Some fractures (sta. 68 m) were tentatively identified by Day and others (1998b) as representing one of the western strands of the Ghost Dance Fault zone.

Lithostratigraphic relations within the Tiva Canyon Tuff (pl. 4) are well established by detailed stratigraphic studies

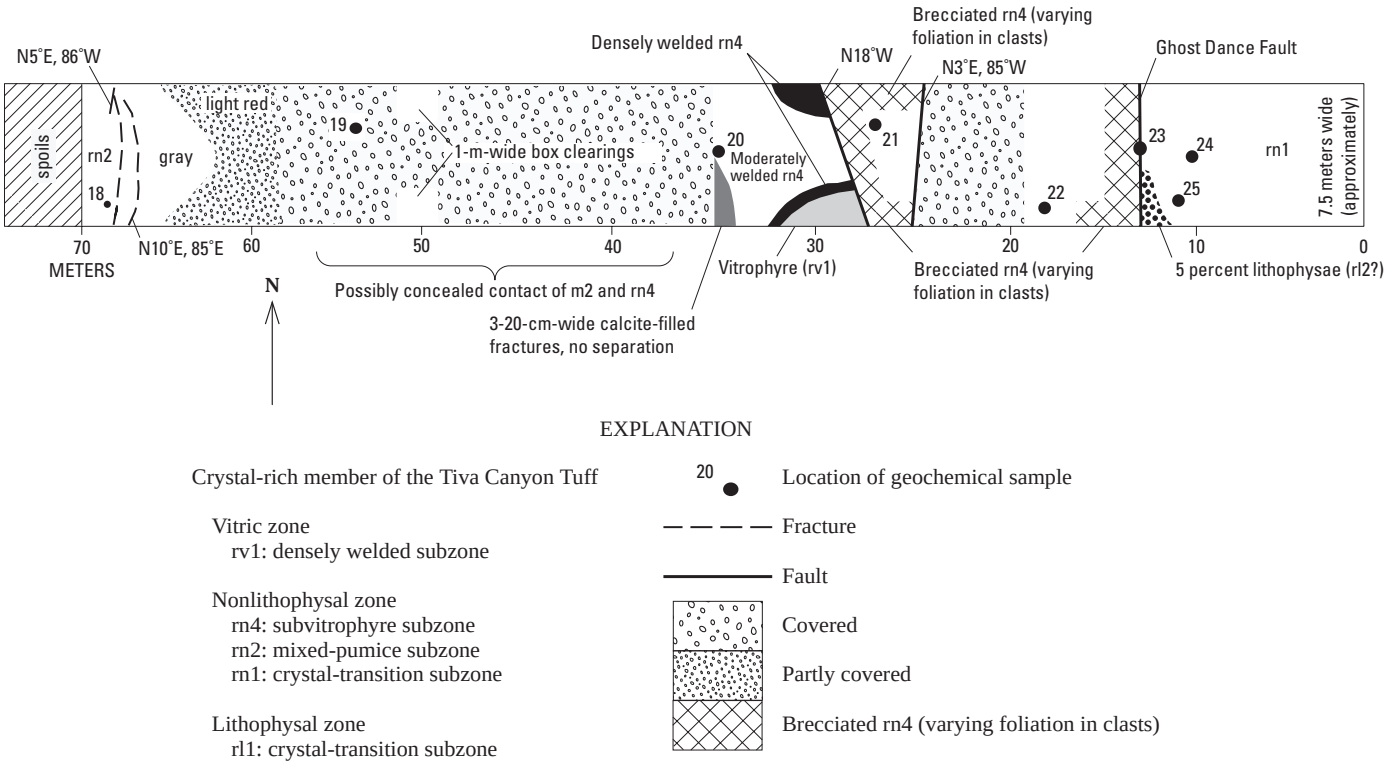

Figure 26. Simplified cross section showing lithostratigraphy and structural features in trench WBR across the Ghost Dance Fault in the Yucca Mountain area, southwestern Nevada (figs. 1, 2, 21).

(for example, Buesch and others, 1996), geologic mapping (for example, Day and others, 1998 a, b), and petrographic and geochemical studies (Peterman and Futa, 1996). Strata of the upper crystal-rich member of the formation, represented by parts of the vitric, nonlithophysal, and lithophysal zones (some of which are faulted out) that are exposed in the trench (see figs. 26, 27; table 13), dip 8°–11° E. The Ghost Dance Fault juxtaposes slightly broken rocks of the nonlithophysal and lithophysal crystal-transition subzones (units rn1 and rl1, respectively, fig. 27) with brecciated rocks of the moderately welded, nonlithophysal subzone (rn4), but the stratigraphic separation is difficult to measure directly because rocks in the hanging wall do not correlate with those in the footwall. However, one means for closely estimating the fault offset is by chemical analyses of the bedrock units involved, based on comparisons with analytical data from a measured surface sec-

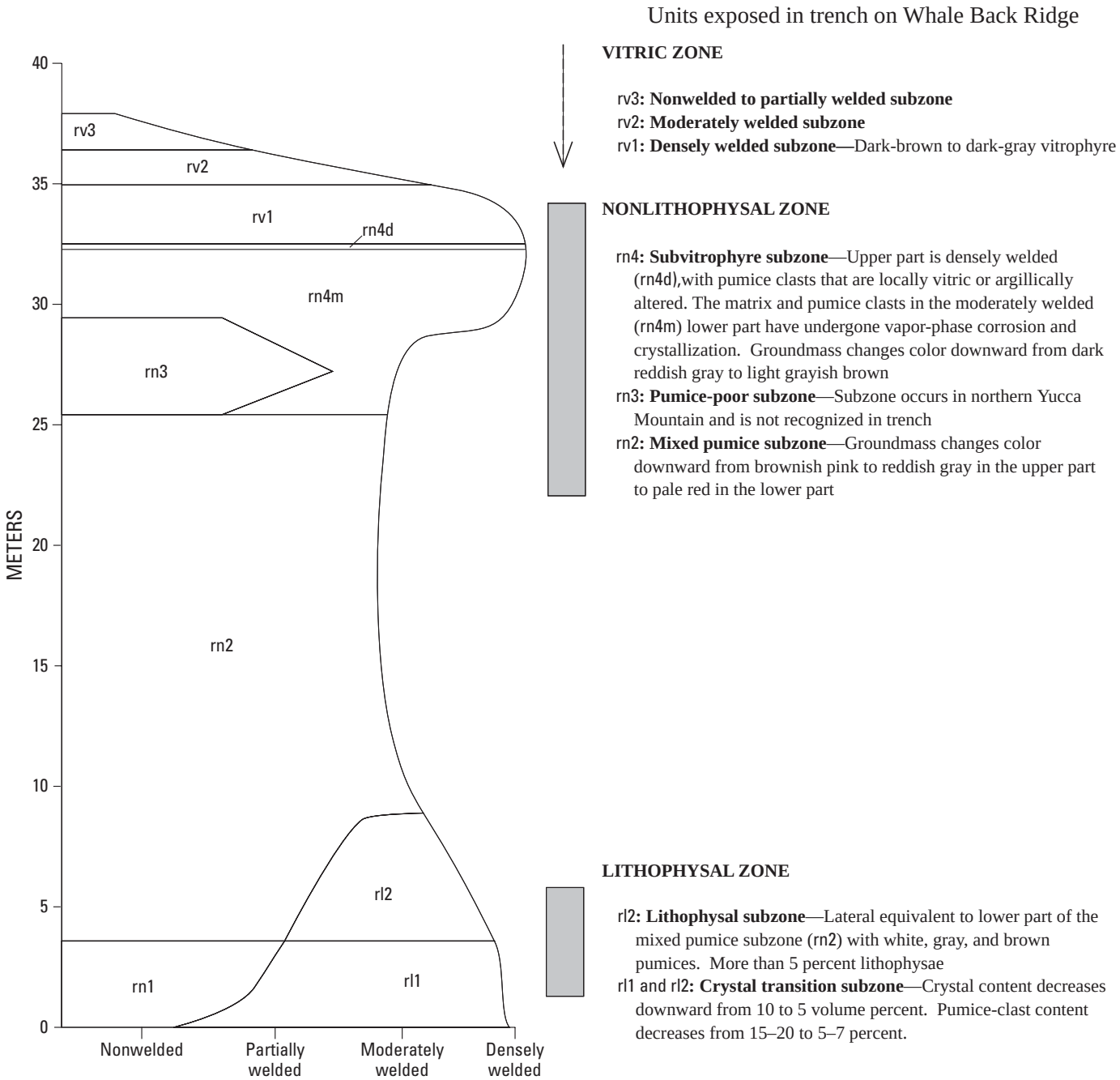

Figure 27. Generalized stratigraphic column of crystal-rich member of the Tiva Canyon Tuff in the Yucca Mountain area, southwestern Nevada (figs. 1, 2).

tion 200 m east of trench WBR (figs. 2, 21) and from borehole NRG#3 (approx 2.5 km northeast of the trench, fig. 8) that show systematic changes in cation concentrations with stratigraphic position, especially within the crystal-rich member of the Tiva Canyon Tuff (Peterman and Futa, 1996).

For the present study, several bedrock units were sampled from both the footwall and hanging-wall blocks of the Ghost Dance Fault in trench WBR (fig. 26), and analyzed for Ti and Zr contents (two of several elements useful for the purpose of correlation). The data from all three sources (measured surface section, borehole NRG#3, and trench WBR) were then plotted for comparison (figs. 28, 29). Analytical data used for determining the stratigraphic positions of the faulted units in trench WBR were from (1) sample 20 (fig. 26), located in the hanging-wall block about 1 m below the vitrophyre in the densely welded subzone (unit rv1, figs. 26, 27); and (2) sample 25,

Table 13. Lithostratigraphic features in bedrock units of the Tiva Canyon Tuff exposed in trench WBR across the Ghost Dance Fault in the Yucca Mountain area, southwestern Nevada.

[See figures 1 and 2 for locations. Nomenclature of Buesch and others (1996); colors from Munsell Soil Color Charts (Munsell Color Co., Inc., 1992). Units: rn1/rl1, crystal-transition zone of nonlithophysal zone; rn2, mixed-pumice subzone of nonlithophysal zone; rn4m, moderately welded lower part of subvitrophyre subzone of nonlithophysal zone; rn4d, densely welded upper part of subvitrophyre subzone of nonlithophysal zone; rv1, densely welded subzone of vitric zone. Central, feature observed in central part of trench (2N, 2S, pl. 4); east, feature observed in eastern part of trench (3N, 3S, pl. 4). n.o., none observed]

Feature	Unit of the Tiva Canyon Tuff				
	rn1/rl1	rn2	rn4m	rn4d	rv1
Phenocryst content (vol pct):					
Feldspar	5–7	8–12	10–12	12–15	12–15
Biotite	<1	<<1	<1–2	1	0
Pyroxene	n.o.	n.o.	Trace	Rare	Trace
Matrix/groundmass:					
Vitric/devitrified	Devitrified	Devitrified	Devitrified (incipiently devitrified below uppermost 1 m).	Devitrified	Vitric.
Color	5R 6/2	5R 6/1.5	7.5R 6/2 (upper part), 5YR 7/3 (lower part)	5R 5/1	N3
Zone of welding	Dense	Moderate	Moderate	Dense	Dense.
Macroscopic whole-rock porosity (pct).	<5	5	15–25	5	0
Lithophysae	Rare in rn1, 5 vol pct in rl1	0	0	0	0
Pumice clasts:					
Content (vol pct)	10–20	15–20	10–20	3–5	3–5
Vitric/devitrified	Devitrified	Devitrified	Devitrified	Vitric/ devitrified.	Vitric.
Color	N7	6–8% 5YR 5/3, 6–8% N7, 3–4% N3	N7–5YR 7/1, N3–5YR 3/1, 10YR 7/4–4/3, 10R 4/3	N7	N6
Maximum size (width× height) (cm).	15.5×3.0	11.2×3.0	29.5×8.5 (central), 2.8×1.0 (east)	3.5×2.6	6.7×2.9
Average maximum diameter (cm).[1]	8.8	7.3	12.1 (central), 2.6 (east)	3.0	4.4
Aspect ratio[2]	3.6–5.4	2.4–3.7	1.6–5.0 (central), 2.8–6.5 (east)	1.3–4.2	2.0–3.7
Vapor-phase corrosion	Partly	Partly	Partly	Partly	n.o.
Spherulite development	n.o.	n.o.	Trace of spherulitic intergrowths.	n.o.	Rare.
Lithic clasts:					
Content (vol pct)	None in rn1, rare in rl1	Trace	1–2	Rare	2–3
Vitric/devitrified	Devitrified	Devitrified	Devitrified	Devitrified	Devitrified.
Color	5YR 6/3	N5	N5	N7	10YR 4/2
Size (cm)	<4	<5	<5	<2	<1

[1]Average length of five largest pumice clasts. (Locally, fewer than five clasts were measured.)
[2]Ratio of longest axis to shortest axis of largest pumice clast.

located in the footwall block in the crystal-transition subzone (rn1). With respect to Ti content and comparisons with the measured surface section, sample 20 is projected to station 122.5 m and sample 25 to station 92.5 m, indicating a separation of 30 m (fig. 28). Comparison of Zr contents between the trench samples and the measured surface section show a separation of 26 m (118.5 m for sample 20 and 92.5 m for sample 25, fig. 29). The apparent difference in separation (30 versus 26 m) probably relates to uncertainties in extrapolation of the data. If the analytical results are projected to the curves for borehole NRG#3, the stratigraphic separations indicated by the Ti and Zr contents are 33 and 34 m, respectively (figs. 28,

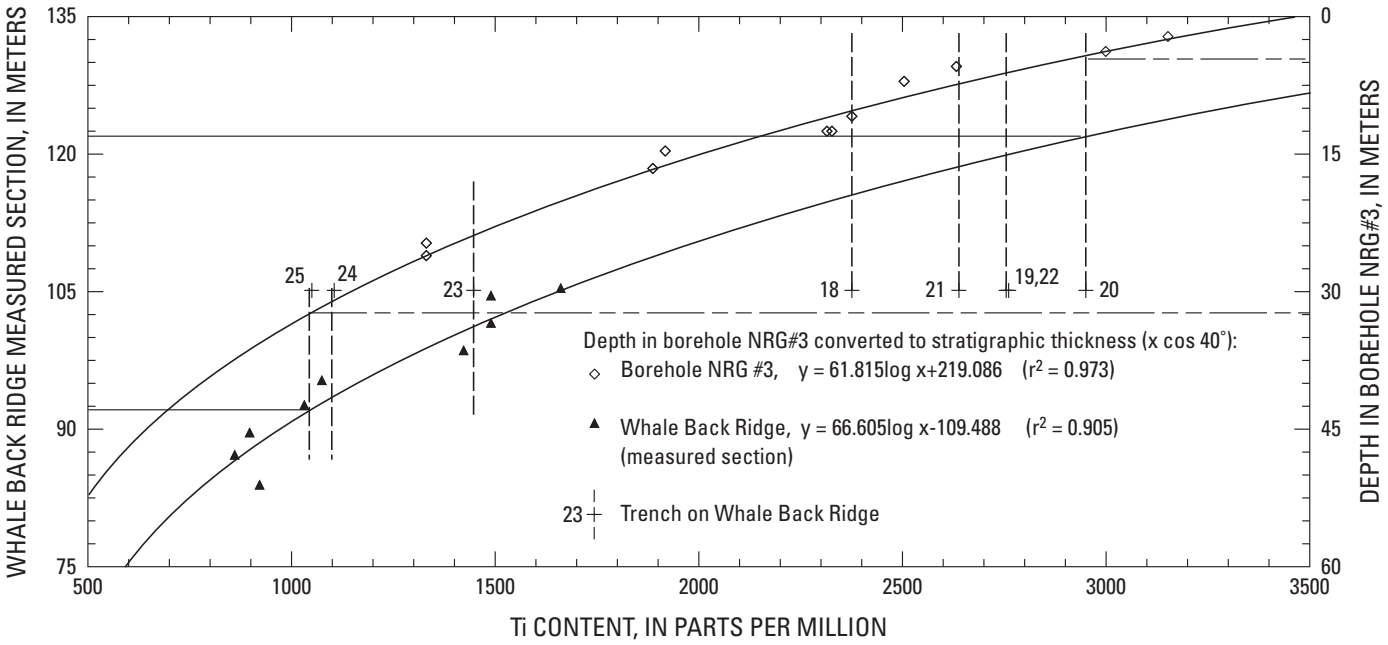

Figure 28. Ti contents in samples of Tiva Canyon Tuff collected from outcrops on Whale Back Ridge, core from borehole NRG#1, and exposures in trench WBR across the Ghost Dance Fault in the Yucca Mountain area, southwestern Nevada (figs. 1, 2, 21).

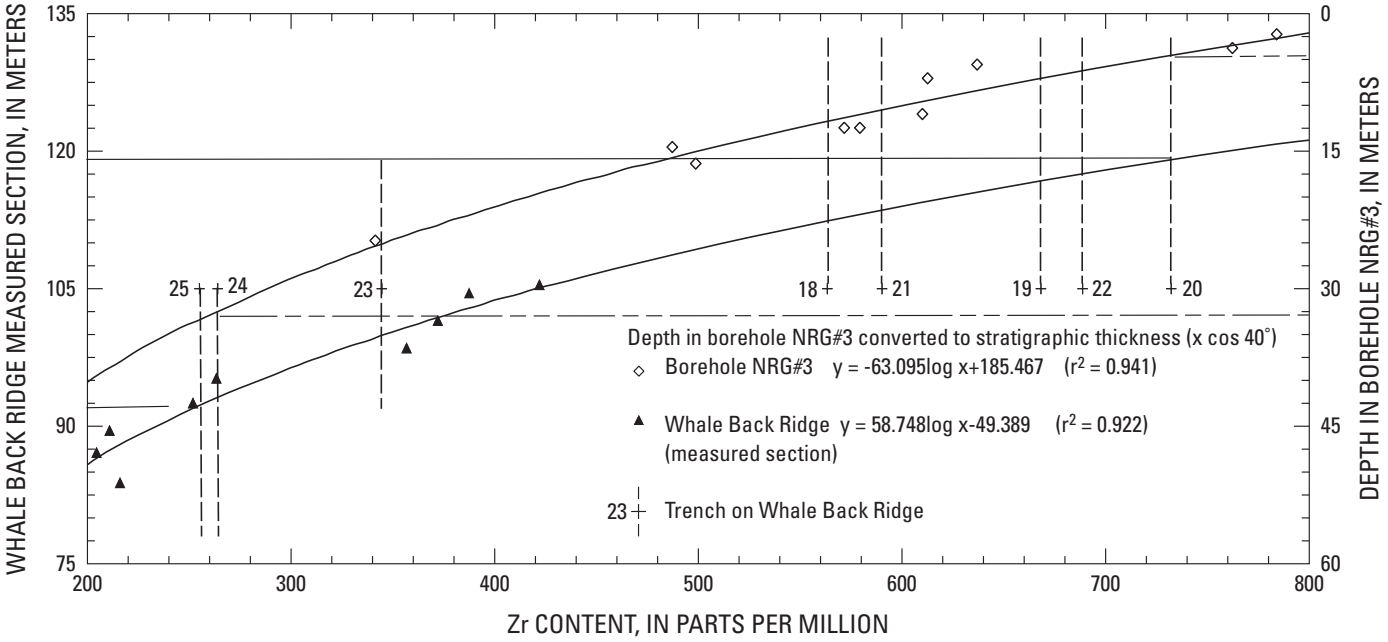

Figure 29. Zr contents in samples of Tiva Canyon Tuff collected from outcrops on Whale Back Ridge, core from borehole NRG#1, and exposures in trench WBR across the Ghost Dance Fault in the Yucca Mountain area, southwestern Nevada (figs. 1, 2, 21).

29). On the basis of surface geologic mapping, Day and others (1998b) showed 27 m of down-to-the-west displacement on the Ghost Dance Fault at this site.

In trench WBR, uppermost Pleistocene to lower Holocene slopewash colluvium and fine-grained eolian deposits (unit 1, Av+Bw, pl. 4) overlie faulted and fractured bedrock of the Tiva Canyon Tuff (table 14). In some places, the bedrock is draped with secondary carbonate and opaline silica (unit 2, 2Kqm); in other places (exposure segments 2N, 2S, pl. 4), the colluvium is separated from the dense carbonate and opaline silica that drapes the bedrock by a laminar carbonate (unit 2, 2K) of pedogenic origin. No offset of either the slopewash colluvium

Key to unit and soil descriptions for tables 14, 16, 18, and 19.

[See table 3 for soil-horizon terminology; prefixed numbers refer to differentiated soil horizons with increasing depth, and numbers within or following these designations refer to further differentiation of properties within an individual soil horizon]

Soil-horizon boundary

Distinctness	
va	very abrupt
a	abrupt
c	clear
g	gradual
d	diffuse

Topography	
s	smooth
w	wavy
i	irregular
b	broken

Soil texture

co	coarse
f	fine
vf	very fine

S	sand
LS	loamy sand
SL	sandy loam
L	loam
SiL	silt loam
Si	silt

SCL	sandy clay loam
CL	clay loam
SiCL	silty clay loam
SC	sandy clay
C	clay
SiC	silty clay

Soil structure

Grade	
m	massive
sg	single grained
1	weak
2	moderate
3	strong

Size	
vf	very fine (very thin)
f	fine (thin)
m	medium
co	coarse (thick)
vco	very coarse (very thick)

Type	
gr	granular
pl	platy
pr	prismatic
cpr	columnar
abk	angular blocky
sbk	subangular blocky

Note: If two structures, listed as primary (1°) and secondary (2°).

Soil consistence

Dry	
lo	loose
so	soft
sh	slightly hard
h	hard
vh	very hard
eh	extremely hard

Moist	
lo	loose
vfr	very friable
fr	friable
fi	firm
vfi	very firm
efi	extremely firm

Wet	
so, po	nonsticky or nonplastic
ss, ps	slightly sticky or slightly plastic
s, p	sticky or plastic
vs, vp	very sticky or very plastic

Clay films

Frequency	
vf	very few
1	few
2	common
3	many

Thickness	
n	thin
mk	moderately thick
k	thick

Morphology	
pf	ped-face coating
br	bridging grains
po	pore linings
gr	gravel coats

$CaCO_3$ effervescence on matrix

0	none in matrix
diss	disseminated
e	slightly; bubbles are readily observed
es	strongly; bubbles form a low foam
ev	violently; thick foam “jumps” up

Grain size

bd	boulders (>26 cm)
cb	cobbles (6–26 cm)
pb	pebbles (4–60 mm)
gr	gravel (2–4 mm)

Table 14. Quaternary stratigraphy exposed in trench WBR across the Ghost Dance Fault in the Yucca Mountain area, southwestern Nevada.

[See figures 1 and 2 for locations]

Lithologic unit, soil horizon, boundary (sample)	Depth or thickness (cm)	Dry color (<2 mm and/or ped face)	Moist color (<2 mm and/or ped face)	Texture	Structure	Soil consistence (dry, moist, wet)	Clay films	Secondary carbonate (gravel and disseminated)	Gravel content (volume percent)	Parent material and lithology	Miscellaneous (roots, pores, SiO_2, oxidation, concretions, salts)
1, Av+Bw; g, w	10–50	10YR 7/3	10YR 4/3	SCL	2 f-m sbk	sh; s, p	0	e0	10–15 bd cb gr, few pb, bd ≤51 cm	Eolian fines, slopewash, nonsorted, angular clasts, nonbedded, nonimbricated, matrix supported.	Dominated by eolian fines; reworked clasts with carbonate rinds present.
2, 2K; a, w	20–55	10YR 8/O	10YR 8/2	?	vco pl, 2° m	eh; so, po	0	IV, ev	5–10 cb pb gr	Nonsorted, angular clasts, nonbedded, nonimbricated, matrix supported.	Erosional unconformity; horizon is weathered from horizon below.
2, 2Kqm; c, s; (U-series samples 110494 GDF1–1 through GDF1–3)	15–40	10YR 8/2	10YR 7/3	?	m	eh; so, po	0	e	5–7 bd cb pb gr, bd ≤54 cm	Slopewash colluvium, angular clasts, nonimbricated, matrix supported.	Ubiquitous dense secondary carbonate and opaline silica precipitated on bedrock near surface.
(U-series sample 110494–4)	– –	– –	– –	– –	– –	– –	– –	– –	– –	Secondary carbonate with interspersed opaline silica, rind on clast in fault breccia.	Infiltrated fines and secondary carbonate in breccia.
(U-series sample 110494–5)	– –	– –	– –	– –	– –	– –	– –	– –	– –	Disseminated carbonate matrix within fault zone.	– – –

Table 15. Numerical ages of deposits in trenches T2, T4A, and WBR across the Ghost Dance Fault in the Yucca Mountain area, southwestern Nevada.

[See figures 1 and 2 for locations. All samples, U-series analyses by J.B. Paces; error limits, ±2σ. Do., ditto]

Trench	Sample	Unit and material sampled	Estimated age (ka)
T2 (pl. 7)	HD 1717	2, clast rind	88±12, 95±12
	HD 1718	2, rhizolith	67±2, 68±1
	HD 1719	2, opaline silica laminae	20±2, 25±1
T4A (pl. 6)	HD 1829	3, densely cemented fluvial gravel	45±0.5, 50±1
	HD 1830	Opaline silica in bedrock	132±7, 253±13, 265±12
WBR (pl. 4)	HD 1831	Opaline silica in fractured bedrock	22±1, 23±1, 37±2
	HD 1721	Kqm soil horizon draping bedrock	43±1, 53±0.5, 81±2, 83±2
	HD 1722	do	10±0.1, 17±6

(unit 1, Av+Bw) or the laminar carbonate cap (unit 2, 2K) was observed across the main Ghost Dance Fault trace (pl. 4). One discontinuous fracture, however, was noted in the lower densely cemented unit (unit 2, 2Kqm), but the fracture does not extend upward into the weathered laminar K soil horizon (see exposure segment 2S, pl. 4). This well-cemented unit draping the bedrock, which was sampled above the main Ghost Dance Fault trace, yielded estimated U-series ages of 10±0.1 to 83±2 ka (exposure segment 3S, pl. 4; samples HD 1722, HD 1721, table 15). If the rocks (unit 2, 2Kqm) dated above the fault (exposure segment 3S) are correlative in time to the fractured rocks west of the sample locality (exposure segment 2S), then the event that fractured the dense laminar horizon must have occurred at least 82 ka. The fracture may have resulted from a seismic event on one or more other faults in adjacent areas, but not from movement on the Ghost Dance Fault.

Trench T4

Trench T4 (pl. 5; figs. 2, 21) was excavated in surficial deposits in Split Wash to intersect the bedrock projection of the Ghost Dance Fault trace, although current mapping does not extend the Sundance Fault southward of Split Wash (fig. 21; Day and others, 1998b). Trench T4 was originally excavated in the early 1980s as part of the preliminary fault studies by Swadley and others (1984); it was then deepened in 1994 in an attempt to expose the bedrock fault, but no bedrock was reached (see pl. 5).

Trench T4 exposes alluvium deposited in the main drainage of Split Wash (tables 16, 17). The sequence is composed of 2-m-thick layers of poorly to well sorted, nonimbricated to weakly imbricated gravel separated by erosional unconformities. Bedding is poor to well formed in places, and the gravel is typically clast to matrix supported. The proportion of gravel was visually estimated to range from 40 volume percent at the surface to as much as 80 volume percent at depth (table 16). The gravel content is uniform through the entire depth of the profile, averaging about 70 weight percent; the remaining 30 weight percent is dominated by fine sand to coarse silt—fractions that are characteristic of eolian additions. Fine-grained eolian material is commonly concentrated at the top of the layers.

Soils are young and minimally developed in the deposits exposed in trench T4; minor accumulations of secondary carbonate (2–3 weight percent) are near the ground surface, and no evidence of clay translocation was observed. Soil horizons were identified primarily on the basis of color and structure. The physical and chemical characteristics of the soils in trench T4 are typical of the upper Pleistocene to lower Holocene soils (possibly correlative with unit Qa5; see chap. 2) that are present throughout the Yucca Mountain area (figs. 1, 2), but no numerical ages were determined.

Bedding in the alluvial deposits extends without offset across projections of the Ghost Dance and Sundance Faults. No fractures or other evidence of displacement was observed. Layers are continuous—no vertical fractures, rotated clasts, offset bedding, vertical laminae, or any other features indicative of Quaternary fault activity were observed in trench T4 (pl. 5).

Trench T4A

Trench T4A (pl. 6; figs. 2, 21), located 50 m south of trench T4 on the projection of the main Ghost Dance Fault trace (fig. 21), was excavated to expose Quaternary deposits above faulted or fractured bedrock. Fractured bedrock of the Tiva Canyon Tuff is exposed in the bottom and lower walls toward the west end of the trench (see pl. 6); these fractures are probably within the hanging wall west of the main fault trace. Secondary carbonate, derived from eolian additions and inplace processes, has infilled the fractured bedrock. In some places the carbonate appears to line vertical fractures, and in other places it appears to form a continuous layer over vertical fractures. No evidence of fracturing was observed in the Quaternary deposits that bury bedrock.

Three lithologic units, separated by erosional unconformities, are exposed in trench T4A (pl. 6; table 18). The youngest unit (1), exposed in the west end of the trench, is a mixture of slopewash colluvium and fine-grained eolian material that includes two soil horizons (A+Bk, Bk). The uppermost soil horizon (A+Bk), exposed at the surface, has an anomalous clay content of 10 volume percent with no evidence of translocation, which probably indicates reworking from older soils that had formed farther upslope.

Unit 2, the thickest of the three lithologic units (pl. 6), consists of moderately well sorted, angular to subangular, nonbedded, poorly imbricated, clast- to matrix-supported gravel; the proportion of gravel clasts generally increases with depth in the deposit, which includes five soil horizons (table 18), defined on the basis of color and texture. No numerical ages were determined on samples from either unit 1 or 2 in trench T4A; both units exhibit characteristics that are interpreted to be correlative with surficial unit Qa5 (see chap. 2).

Unit 3 (pl. 6), which drapes the fractured bedrock, is composed of nonbedded slopewash deposits containing 15 to 20 volume percent of unsorted to moderately well sorted, angular to subangular clasts that increase in size downward. The unit is characterized by a well-developed soil (Bt) horizon that contains abundant translocated or alluvial clay (max 50 volume percent) above a second soil (K) horizon that contains abundant secondary carbonate (max 20 volume percent); both components indicate a soil that is considerably older than the soils in units 1 and 2. Two U-series ages, on samples of dense opaline silica laminae in the 3K soil horizon that was developed on and near bedrock, of 45±0.5 and 50±1 ka (sample HD 1829, table 15), provide a minimum estimated age for the deposit and indicate a probable correlation with surficial unit Qa3 of the standard Yucca Mountain Quaternary sequence (see chap. 2; fig. 3).

Horizontal and vertical laminae within fractured bedrock of the Tiva Canyon Tuff (R+K soil horizon, table 18) were also sampled for U-series analysis. U-series estimated ages on three horizontally oriented samples of opaline silica are 22±1,

Table 16. Quaternary stratigraphy exposed in trench T4 across the Ghost Dance Fault in Split Wash in the Yucca Mountain area, southwestern Nevada.

[See figures 1 and 2 for locations, and table 17 for additional lithologic data. Colors from Munsell Soil Color Charts (Munsell Color Co., Inc., 1992). Do., ditto]

Lithologic unit, soil horizon, boundary (*sample)	Depth or thickness (cm)	Dry color (<2 mm and/or ped face)	Moist color (<2 mm and/or ped face)	Texture	Structure (primary and secondary)	Consistence (dry, moist, wet)	Clay films	Secondary carbonate (gravel and disseminated)	Gravel content (volume percent)	Parent material and lithology	Miscellaneous (roots, pores, SiO_2, oxidation, concretions, salts)
1T, A+Bw; c, s (*unit 1 A+Bw)	– –	10YR 6/3	10YR 4/3	LS	f-co sbk, 2° sg	so-sh; so, po	0	0	40–50 pb gr	Moderately well sorted, nonbedded, nonimbricated, matrix supported.	Coarsens and thickens upslope. Unit is characterized by infiltrated eolian fines. Boulder train intersected in center of trench. Stratigraphic unit Qa5.
2T, 2Bk1; c, s (*unit 2–1 2Bk)	– –	10YR 6/3	10YR 3.5/3	LL	sg, 2° 1f sbk	so; vss, po	0	I+ diss, ev	50 cb pb gr	Poorly sorted, nonbedded, nonimbricated, matrix supported.	Decreasing carbonate and silt contents with depth, unit thins upslope.
2T, 2Bk2; g, s (*unit 2–2 2Bk2)	– –	10YR 6.5/3	10YR 4/3	SL	sg	lo; so, po	0	I– patchy coats, diss, ev	70 clasts ≤15 cm, very few ≤30 cm, cb pb gr	Nonbedded, weakly imbricated, matrix supported.	SiO_2 stage 1. In center of trench, this horizon is in contact with unit 3.
2T, 2Bk3; a, s (erosional contact) (*unit 2–3 2Bk3)	– –	10YR 6/3	10YR 4/3	SL	sg	lo; so, po	0	I– patchy coats, diss, ev	75 pb gr, clasts ≤15 cm	Moderately well to well sorted, lenses of well sorted pb, gr at base, weakly bedded, well imbricated toward base where clast supported, matrix to clast supported.	– – –
3T, 3Btkwb; c, s (*unit 3–1 3Btkwb)	– –	10YR 6/3	10YR 4/3	SL	1–2 vf-f sbk	h; so, po	0	I patchy coats, diss, ev	80 clasts ≤7 cm, pb gr	Poorly to moderately well sorted, nonbedded, nonimbricated, matrix supported.	Unit Qa4. Horizon pinches in and out and is present only in places.
3T, 3Bkw1b; a, s (*unit 3–2 3Ckn)	– –	10YR 6.5/3	10YR 4/3	SL	sg	lo; vss, po	0	I– patchy scaly carbonate and SiO_2, diss, e	80 clasts ≤32 cm, pb cb gr, few bd	Poorly to well sorted, well bedded in places, well imbricated in places, matrix supported, clast supported in coarser beds.	Characterized by distinct and well-preserved stratigraphic layering by moderately well sorted coarse- and fine-grained lenses. Unit 3 pinches out just west of middle of trench.
3T, 3Bkw2b; a, s (not sampled)	– –	10YR 6.5/3	10YR 4/3	SL	sg	lo; so, po	0	I– patchy	80 clasts ≤15 cm, pb cb gr	Poorly to well sorted, well bedded, well imbricated, matrix supported.	– – –
4T, 4Bkwlb; c, s (*unit 4–1 4Bkwlb)	– –	10YR 6.5/4	10YR 4/3	SL	sg	lo; so, po	0	I– patchy and powdery, diss, e	60 clasts ≤15 cm, few ≤22 cm pb cb gr	Poorly sorted, nonbedded, nonimbricated, matrix supported, clast supported in coarser layers.	– – –
4T, 4Bkw2b; a, s (*unit 4–2 4Bkw2b)	– –	10YR 6.5/4	10YR 4/3	SL	sg	lo; vss, po	0	I– scaly and patchy, diss, e. $CaCO_3$ stage I on clast where unit is <1 m below surface at west end.	80 pb cb gr, few bd clasts ≤33 cm	Moderately well bedded, imbricated in lenses, moderately well sorted.	Unit characterized by stratigraphic layering of coarse- and fine-grained beds.
5T, 5Bkwb (*unit 5)	– –	10YR 7/3	10YR 4/3	SL	1 vf-f sbk, 2° sg	lo; so, po	0	diss, e	70 pb gr, clasts ≤13 cm	Moderately well sorted, nonbedded, nonimbricated, matrix supported.	– – –

Table 16. Quaternary stratigraphy exposed in trench T4 across the Ghost Dance Fault in Split Wash in the Yucca Mountain area, southwestern Nevada—Continued

Lithologic unit, soil horizon, boundary (*sample)	Depth or thickness (cm)	Dry color (<2 mm and/or ped face)	Moist color (<2 mm and/ or ped face)	Texture	Structure (primary and secondary)	Consistence (dry, moist, wet)	Clay films	Secondary carbonate (gravel and disseminated)	Gravel content (volume percent)	Parent material and lithology	Miscellaneous (roots, pores, SiO_2, oxidation, concretions, salts)
Trench deepened and widened—units tentatively correlated											
4B (top of bottom) 4Bkw1b; c, s (*unit 1B–1)	– –	10YR 6.5/4	10YR 3/4	SL	sg	lo; ss, ps	0	I– patchy diss, e	70 cb pb gr	Moderately well sorted, poorly bedded, nonimbricated, matrix-clast supported.	– – –
4B, 4Bkw2b; g, s (unit 1b–2)	– –	10YR 7/4	10YR 3/3	SL	sg	lo; so, po	0	I+ diss, ev 1° reworked carbonate on clasts	60 cb pb gr, few bd	do ----------	– – –
4B, 4Bkw3b; g, s (unit 1B–3)	– –	10YR 7/4	10YR 3.5/4	SL	sg	lo; so, vps	0	I, diss, e 1° reworked carbonate on clasts	60 cb pb gr	do ----------	– – –
4B, 4Bkw4b; a, s (unit 1B–4)	– –	10YR 7/4	10YR 4/3	SL	sg	lo; so, po	0	I– patchy diss, e	75 pb cb gr	do ----------	– – –
5B, 5Cn; a, s (erosional contact) (*unit 2B)	– –	10YR 5/4	10YR 3.5/3	SL	sg	lo; vss, po	0	0	80 pb cb gr	Well sorted, moderately well bedded, moderately imbricated, matrix-clast supported.	Fining-upward sequence repeated in layers within unit 5B.
6B, 6Cn; (*unit 3B)	Bottom of trench	10YR 6/4	10YR 4/3	SL–L	sg	lo; ss, ps	0	0	60 pb cb gr, few bd	Moderately well bedded, moderately well sorted, nonimbricated.	– – –

23±1, and 37±2 ka (sample HD 1831, table 15), and on three vertically oriented samples are 132±7, 253±13, and 265±12 ka (sample HD 1830). The vertically oriented laminae could represent the timing of opening of a fracture in the bedrock, and the early onset of filling of the fracture with fine material and the precipitation of secondary carbonate and opaline silica. Although the origin of the fractures cannot be determined, clearly no offset of the Quaternary material that overlies the fractured bedrock is evident. An alternative explanation for the estimated ages of the fracture fill would involve exhumation of the bedrock and deposition of the soil currently at the bedrock interface. The cycle of stripping and deposition of alluvium is a common phenomena in the Yucca Mountain area. Here, carbonate infilling of preexisting fractures occurs where the bedrock was for some unknown period of time out of the zone of carbonate accumulation, and so the fractures could considerably antedate carbonate deposition. The range in the estimated ages (20–200 ka) of morphologically similar laminae supports an interpretation that the youngest material may be a replacement product and not primary to the deposit; however, these questions remain unresolved.

Trench T2

Trench T2 (pl. 7; figs. 2, 21), located in Drill Hole Wash on the projection of a parallel left-stepping fault west of the Ghost Dance Fault (fig. 21), is entirely in Quaternary gravelly alluvium derived from the main drainage and so is not deep enough to expose bedrock. The gravel is moderately well sorted, nonbedded, and imbricated in silt-free lenses. Two lithologic units separated by an erosional unconformity are represented in the trench walls (table 19). Unit 1 includes two soil horizons: a surface (A+Bw) horizon that is dominated by fine-grained eolian material, grading downward into a gravel matrix (Bk) horizon. Features characteristic of soil maturity are absent, and less than 1 weight percent of secondary carbonate is present. In their physical and chemical characteristics, these soils resemble the upper Pleistocene to lower Holocene soils (unit Qa5, tables 2–4; see chap. 2) that are present throughout the Yucca Mountain area (figs. 1, 2), although they could also be as young as middle to late Holocene (unit Qa6). Unit 2 preserves well-developed soils characterized by secondary accumulations of clay and carbonate. U-series estimated ages are 20±2 and 25±1 ka (sample HD 1719, table 15) on opaline silica laminae in the 2Kb soil horizon and 88±12 to 95±12 ka (sample HD 1717) on rinds from the underside of a clast. An analysis of a rhizolith from this soil horizon resulted in U-series estimated ages of 67±2 and 68±1 ka (sample HD 1718).

As in other trenches excavated across projections of the Ghost Dance and associated faults, no evidence of faulting or fracturing of the Quaternary deposits was observed in trench T2.

Table 17. Particle-size distribution, carbonate content, and pH in soils exposed in trenches T2, T4, and T4A across the Ghost Dance Fault in the Yucca Mountain area, southwestern Nevada.

[See figures 1 and 2 for locations. Gravel, sand, silt, clay, and $CaCO_3$ contents in weight percent. See table 3 for soil-horizon terminology; prefixed numbers refer to differentiated soil horizons with increasing depth, and numbers within or following these designations refer to further differentiation of properties within an individual soil horizon]

Sample	Gravel	Sand					Silt			Clay		Total			$CaCO_3$	pH
		vco	co	m	f	vf	co	m+f	vf	co+m	f	Sand	Silt	Clay		
Trench T2																
tr2 A+Bw	56.43	4.85	4.53	4.81	30.91	21.61	15.16	8.14	2.34	4.07	4.32	65.99	25.64	8.38	0.25	9.00
tr2 Bk	68.13	15.10	8.55	7.61	31.47	19.87	7.90	3.42	2.54	1.56	1.95	82.60	13.86	3.51	.69	8.70
tr2 2Btkb	59.69	13.29	6.59	4.58	17.21	10.01	5.75	11.34	9.86	15.20	6.16	51.68	26.95	21.36	1.84	8.20
tr2 2Kb	80.96	12.16	11.62	11.80	31.70	15.51	7.49	1.80	2.78	1.80	3.33	82.79	12.07	5.13	27.07	8.40
tr2 2Bkb	71.82	22.21	14.38	10.26	29.26	15.13	4.38	1.53	.99	.55	1.31	91.24	6.89	1.86	7.33	8.35
Trench T4B (top)																
tr4–T A+Bw	52.50	6.36	4.11	4.67	35.02	25.37	10.14	4.98	2.62	3.23	3.50	75.53	17.74	6.73	0.53	9.00
tr4–T 2Bkl	65.53	7.97	5.76	6.19	36.47	19.96	11.93	4.42	1.88	1.88	3.53	76.35	18.23	5.41	2.58	8.50
tr4–T 2Bk2	71.83	14.21	7.87	7.32	32.69	17.33	10.09	4.91	1.99	.93	2.66	79.42	17.00	3.59	3.01	8.05
tr4–T 2Bk3	78.94	16.95	9.98	8.71	33.52	14.36	7.65	3.16	1.98	.79	2.90	83.52	12.79	3.69	2.00	7.85
tr4–T 3Btkwb	73.69	11.97	7.59	8.08	30.13	17.38	11.99	7.85	1.96	.55	2.51	75.15	21.80	3.05	2.61	8.00
tr4–T 3Bkwlb	65.33	19.52	12.00	9.06	27.01	11.47	8.02	6.27	2.77	1.75	2.12	79.06	17.06	3.87	.93	8.00
tr4–T 4Bkwlb	66.57	14.56	11.10	10.42	32.93	12.22	8.43	5.06	1.26	1.48	2.53	81.23	14.75	4.00	1.07	8.20
tr4–T 4Bkw2b	68.36	5.85	5.14	7.75	43.69	20.20	5.32	5.67	1.97	1.04	3.36	82.63	12.96	4.40	.83	8.50
tr4–T 5Bkwb	66.97	5.89	5.89	8.58	37.83	17.67	10.82	4.23	3.11	2.12	3.86	75.86	18.16	5.97	.58	7.90
Trench T4B (bottom)																
tr4–B 4Bkwlb	66.96	8.14	6.85	7.38	29.45	16.69	11.75	1.17	3.06	3.41	6.11	68.51	15.97	9.52	0.78	7.95
tr4–B 4Bkw2b	70.69	11.36	7.61	7.27	36.71	13.52	9.88	5.29	2.35	1.76	4.23	76.47	17.52	6.00	1.71	7.95
tr4–B 4Bkw3b	63.52	9.69	6.19	6.19	29.91	17.64	12.51	6.69	2.41	3.51	5.27	69.62	21.62	8.78	.81	8.05
tr4–B 4Bkw4b	75.18	13.65	7.57	7.10	32.04	13.73	9.13	5.96	3.29	1.95	5.60	74.09	18.38	7.55	.50	8.10
tr4–B 5Cn	75.58	4.31	2.84	3.48	28.97	15.83	15.15	11.70	5.13	5.68	6.95	55.43	31.98	12.59	.37	8.10
tr4–B 6Cn	67.71	8.20	5.80	5.71	23.78	14.78	13.07	11.47	4.80	5.87	6.83	58.27	29.34	12.70	.43	8.10
Trench T4A																
tr4a A+Bk	52.77	1.54	1.35	2.39	26.03	17.38	13.88	10.65	2.26	9.96	14.85	48.69	26.79	24.54	0.15	8.25
tr4a Bk	42.04	3.35	1.85	2.28	20.18	15.48	12.23	9.26	6.61	10.25	18.51	43.14	28.10	28.76	1.12	7.98
tr4a A+Bkw	36.68	5.66	2.44	3.02	31.13	23.43	10.68	5.83	4.21	4.21	9.94	65.68	20.72	14.15	.33	7.80
tr4a Bkl	40.97	5.53	3.90	4.55	36.98	21.16	8.26	6.54	3.10	2.07	7.91	72.12	17.89	9.98	1.70	8.06
tr4a Bk2	19.65	4.12	4.69	5.88	34.30	21.71	10.69	7.93	3.10	1.38	6.21	70.70	21.72	7.59	2.09	7.92
tr4a Bk3	36.72	8.42	5.76	7.11	36.34	15.98	7.50	2.28	5.87	2.28	8.48	73.59	15.65	10.76	2.23	7.89
tr4a Bk4	18.73	13.12	8.62	7.90	32.04	13.98	6.58	3.95	3.62	3.29	6.90	75.66	14.14	10.19	.38	8.35
tr4a 3Bt	31.89	3.43	1.92	1.83	15.26	11.23	6.26	6.63	3.96	3.32	46.43	33.67	16.58	49.75	18.08	8.48
tr4a 3K	25.63	8.43	6.30	6.15	25.73	14.61	6.46	6.82	5.03	6.46	14.00	61.22	18.31	20.46	7.57	8.14
tr4a R+3K	35.46	5.65	4.40	4.95	26.23	18.03	9.14	9.52	7.23	5.33	9.52	59.26	25.88	14.85	33.64	8.30

Table 18. Quaternary stratigraphy exposed in trench T4A across the Ghost Dance Fault in Split Wash in the Yucca Mountain area, southwestern Nevada.

[See figures 1 and 2 for locations, and table 17 for additional lithologic data. Colors from Munsell Soil Color Charts (Munsell Color Co., Inc., 1992). Do., ditto]

Lithologic unit, soil horizon, boundary (*sample)	Depth or thickness range (cm)	Dry color (<2 mm and/or ped face)	Moist color (<2 mm and/or ped face)	Texture	Structure (primary and secondary)	Consistence (dry, moist, wet)	Clay films	Secondary carbonate (gravel and disseminated)	Gravel content (volume percent)	Parent material and lithology	Miscellaneous (roots, pores, SiO_2, oxidation, concretions, salts)
1, A+Bk; c,s (*1.1)	30–60	10YR 6/4	10YR 4/3	LS to SiL	1 f abk, 2° 1 f sbk	so; vss, po	0	I–, patchy, e0	35 pb gr, few cb ≤8 cm	Slopewash, nonsorted, angular clasts, nonbedded, nonimbricated, matrix supported.	Exposed only at west end of trench, incised into unit 2, stratigraphic unit Qa5.
1, Bk; c,s grades into unit 2 (*1.2)	5–25	7.5YR 7/4	7.5YR 4/4	SiL to L	2 m sbk , 2° 2f sbk	h; ss, po	0	I–, patchy, es	40 pb gr, few cb ≤8 cm	do ----------	Very close in age to surface horizon of unit 2; same unit(?) coarsens downslope.
2, A+Bkw; c,s (*2.1)	20–55	10YR 6/3	10YR 3/4	SiL	1 m sbk, 2° sg	so; vss, ps	0	Patchy filaments on underside of clasts	30 pb gr, few clasts ≤6 cm	Slopewash/eolian deposits, nonsorted, angular clasts, nonbedded, nonimbricated, matrix supported.	– –
2, Bk1; g,s (*2.2)	50–60	10YR 5.5/3	10YR 4/3	SL	sg	lo; so po	0	II, ev	50 cb pb gr, ≤23 cm	Alluvium, moderately well sorted, subangular, nonbedded, poorly imbricated, matrix supported.	Dominated by eolian fines.
2, Bk2; g,s (*2.3)	40–80	10YR 6/3	10YR 3/4	LS	sg	lo; so po	0	I, ev	50 cb pb gr, few ≤20 cm	do ----------	Dominated by infiltrated fines (eolian).
2, Bk3; g,s (*2.4)	30–75	10YR 6.5/3	10YR 4/3	SL	sg	lo; so po	0	I, ev	70 pb gr, few cb and bd ≤38 cm	Alluvium, moderately well sorted, subangular, nonbedded, poorly imbricated, matrix and clast supported.	– –
2, Bk4; a,s (*2.5)	40–50	10YR 7/3	10YR 3/4	SL	sg	lo, so, po	0	I–, ev	80 pb gr, few cb bd ≤38 cm, coarser lenses toward base	do ----------	– –
3, 3Bt; c,s (3Bt+R also) (*3.1)	40–50	7.5YR 6/4	7.5YR 4.5/4	SiL	2–3 m-co sbk, 2° 3 f abk	vh; ss, ps-p	0	filaments on pf, I–, ev	15 pb gr, ≤5 cm	Slopewash, moderately well sorted, subangular clasts, nonbedded, nonimbricated, matrix supported.	Mn stains on pf.
3, 3K or 3K+R; a,s (*4–1) (U-series sample 1829	30–40	10YR 8/3	10YR 5/4	SL	m, 2° 1 co abk	eh; so, po	0	III continuous stringers, lenses of ooids ≤1 cm	20 pb gr, few clasts ≤10 cm	Slopewash, nonsorted, angular clasts, nonbedded, nonimbricated, matrix supported.	Unit grades into R.
R and R+K (*4–2) (U-series samples HD 1830, HD 1831	– –	– –	– –	– –	– –	– –	– –	– –	– –	Fractured bedrock of the Tiva Canyon Tuff.	– –

Table 19. Quaternary stratigraphy exposed in trench T2 across the Ghost Dance Fault in Drill Hole Wash in the Yucca Mountain area, southwestern Nevada.

[See figures 1 and 2 for locations, and table 17 for additional lithologic data. Colors from Munsell Soil Color Charts (Munsell Color Co., Inc., 1992)]

Lithologic unit, soil horizon, boundary (*sample)	Depth or thickness (cm)	Dry color (<2 mm and/or ped face)	Moist color (<2 mm and/or ped face)	Texture	Structure (primary and secondary)	Consistence (dry, moist, wet)	Clay films	Secondary carbonate (gravel and disseminated)	Gravel content (volume percent)	Parent material and lithology	Miscellaneous (roots, pores, SiO_2, oxidation, concretions, salts)
1, A+Bw (*unit 1 A+Bw)	– –	10YR 7/4	10YR 3/3	L	1f-m sbk	so; so, po	0	0	50 pb cb	Moderately well sorted, nonbedded, imbricated in silt-free lenses.	Characterized by infiltrated eolian silt; unit Q5 or Q6(?).
1, Bk; a, s (erosional contact) (*unit 1 Bk)	– –	10YR 7/3	10YR 4/4	SL	1f-m sbk, 2° sg	so; so, po	0	I, diss, ew	90 pb cb	do----------	Unit Q5 or Q6(?).
2, 2Btkb (*unit 2, Btk)	– –	7.5YR 6/4.5	7.5YR 5/4	LL	2–3 f-co sbk	h; s, ps	2 mk po	I– on 10–20% of clasts, diss, ev	30 pb cb	Moderately well sorted, nonbedded to moderately well bedded toward base of exposure.	Unit Q3
2, 2Kb (*unit 2, K) (U-series samples 110494–GDF2–1 through 110494–GDF2–3)	– –	7.5YR 8/0	7.5YR 8/0	SL?	3 f-co abk, plates preserved in places	eh	0	III–IV, diss, ev, lenses of ooids	~50 pb cb	do ----------	Unit Q3.
2, 2Bkb (2Btkb in places) (*unit 2, B1) (U-series sample 110494–GDF2–4)	– –	10YR 8/2	10YR 5/3	LS	sg	lo; so, po	0	II, lenses of III controlled by changes in gravel texture diss, ev	90 pb cb, very few bd	Clast-supported gravel.	Silica- and carbonate-cemented layers separated by matrix-supported gravel, some tonguing, unit Q3.

Chapter 7

Quaternary Faulting on the Solitario Canyon Fault

By Alan R. Ramelli,[1] John A. Oswald, Giovanni Vadurro, Christopher M. Menges, and James B. Paces

Contents

Abstract....89
Introduction....89
Trench Investigations....91
Trench T8....93
Test Pit T8A....98
Trench SCF–T1....98
Trench SCF–T3....101
Trench SCF–T4....103
Trench SCF–T2....104
Summary of Mid-Quaternary to Late Quaternary Activity on the Solitario Canyon Fault....105
Sequence of Faulting Events....106
Fracturing Events....106
Event Z....106
Event Y....106
Event X....106
Event W....106
Early Quaternary to Mid-Quaternary Hiatus in Seismicity....107
Earlier Faulting....108
Recurrence Intervals and Slip Rates....108
Possible Volcanically Related Fault Activity....108
Discussion....109

Abstract

Quaternary activity along the Solitario Canyon Fault, one of the principal north-striking, block-bounding normal faults close to the proposed repository site for the storage of high-level radioactive wastes at Yucca Mountain, was studied in 11 trenches and one natural exposure that span the fault in various places. Detailed mapping of the geologic relations exposed at these sites shows a sequence of surficial deposits, ranging in age from early Pleistocene to Holocene, that can be correlated with the general Quaternary stratigraphic framework established for the area, and which have been involved to varying degrees in surface-rupturing paleoearthquakes on the Solitario Canyon Fault.

In chronological order from youngest to oldest, interpreted faulting (and fracturing) events on the Solitario Canyon Fault include (1) two episodes of fracturing that postdate the youngest recognizable faulting event but did not involve discernible structural displacement; (2) the most recent faulting event (Z), dated at 40–20 ka, with offsets of 10 to 20 cm; (3) a penultimate faulting event (Y), the largest and best documented Quaternary faulting event along the Solitario Canyon Fault, which is characterized by fault fissures as much as 70 cm wide filled with basaltic ash correlated with the eruption of the nearby Lathrop Wells volcanic center at 77±6 ka and with cumulative dip-slip displacements of as much as 1.3 m; and (4) two older mid-Quaternary to late Quaternary faulting events (W, X), bracketed between 250–150 and 118±6 ka, which are evidenced by silt- and gravel-filled fault fissures that indicate dip-slip offsets of 20 to 60 cm.

Stratigraphic and structural relations within the exposed surficial deposits indicate little, if any, activity along the Solitario Canyon Fault for a period of several hundred thousand years before event W, although evidence was observed of one or more surface-rupturing paleoearthquakes before this hiatus, likely during early Quaternary time.

The occurrence of as many as four faulting events within a time period of about 200 k.y. indicates an average recurrence interval of about 50 k.y. during mid-Quaternary to late Quaternary time. A recurrence interval of about 35 k.y. is considered to be a minimum for the most recent and penultimate faulting events. The average slip rate for mid-Quaternary to late Quaternary fault activity appears to range from 0.01 to 0.02 mm/yr, on the basis of an average of 2.0 m of slip over 200 k.y. and 1.2 m of slip over 75 k.y.

Introduction

The Solitario Canyon Fault (fig. 2), which extends along the steep west flank of Yucca Mountain (fig. 1), is a major block-bounding fault that forms the west boundary of the

[1]Nevada Bureau of Mines and Geology, Reno.

Table 20. Summary of stratigraphic relations and correlations in trenches across the Solitario Canyon Fault in the Yucca Mountain area, southwestern Nevada.

[See figures 1 and 2 for locations. See table 3 for soil-horizon terminology. Units on east side of Yucca Mountain after Wesling and others (1992); units in Crater Flat from Peterson and others (1995). Do., ditto]

Stratigraphic unit	Trench	Unit	Soil	Correlative unit	
				East side of Yucca Mountain	Crater Flat
Eolian silt/ colluvium.	SCF–T3 SCF–T4 SCF–T2	11–12 9–10 10–11	Av	Qa5	Little Cones.
Eolian silt/ gravel.	T8 SCF–T1	14 20–22	$CaCO_3$ stage I+	Qa5	Do.
Gravelly silt------	T8 SCF–T4 SCF–T2	14 8 8–9	Bw/Bt	Qa4	Late Black Cone.
Gravel ----------	SCF–T1	12–19	Bt/Btk	Qa4	Do.
Stratified gravel.	T8	5–9	Bqkm	Qa3	Early to late Black Cone.
Silty gravel--------	T8	2–4	Bq	Qa3?	Early Black Cone(?).
Gravel ----------	T8 SCF–T1 SCF–T3 SCF–T4 SCF–T2	1 1–8 1–9 1–6 1–7	K	Qa1	Solitario.

Table 21. Numerical ages of deposits exposed in trenches T8, T8A, and SCF–T3 across the Solitario Canyon Fault in the Yucca Mountain area, southwestern Nevada.

[See figures 1 and 2 for locations. Samples: TL– (error limits, ±2σ), thermoluminescence analyses by S.A. Mahan; HD (error limits, ±2σ), U-series analyses by J.B. Paces]

Trench	Sample	Unit and material sampled	Estimated age (ka)
8 (fig. 31)	TL–30	11a, fissure fill----------	36±3
	HD 1070	10, rhizolith in fissure fill----------	27±1, 37±2, 39±1, 40±3, 48±5, 56±3
	HD 1071	11a, carbonate in vein----------	15±4, 15±7, 16±3, 16±3
	HD 1072	Carbonate stringer in fracture----------	114±5, 117±5, 119±6, 124±6
	HD 1465	12, composite soil sample----------	47±9, 66±23
8A	TL–10	Upper part of Av soil horizon----------	11±2
	TL–11	Lower part of Av soil horizon----------	14±2
SCF–T3 (fig. 34)	HD 1726	7, opaline silica in clast rind----------	144±4, 324±7, 880±160, 950±140
	HD 1730	8, opaline silica in Kqm soil horizon---	25±0.1, 28±0.2
	HD 1731	8, opaline silica in clast rind, upper part of Kqm soil horizon----------	170±3, 590±110, 870±150, 900±140, 970±450
	HD 1732	8, opaline silica in Kqm soil horizon---	199±10, 233±4, 245±4, 320±7, 394±69

proposed repository site for the storage of high-level radioactive wastes. Quaternary activity along this fault is well documented and, given its proximity to the repository site, is particularly important for assessing seismic hazards.

Characteristics of the Solitario Canyon Fault were shown on the detailed geologic maps of Day and others (1998a, b). As described in chapter 3, the fault can be traced for distances of at least 18 km (fig. 2). A prominent fault scarp, in places forming the bedrock-alluvium contact at the base of the west slope of Yucca Mountain, marks the fault trace for much of its length.

Quaternary deposits identified during the mapping of trench excavations for this study follow the stratigraphic schemes presented for the Yucca Mountain area in table 2 (see chap. 2); lithologic-unit designations and their correlations are summarized in table 20. Ages assigned to subdivisions of the Quaternary period are shown in figure 3 (chap. 2), and estimated ages of specific samples collected and analyzed during the present study are listed in table 21.

Trench Investigations

A total of 13 exploratory trenches or test pits and one natural-wash exposure have been excavated and (or) cleaned across or near the Solitario Canyon Fault (fig. 2). Seven trenches excavated in 1979–80 included three (T8, T10A, T10B) along the central section of the fault and four (GA1A, GA1B, T13, and an unnamed trench at the head of Solitario Canyon [not shown in fig. 2]) along the northern section. Excavations were also conducted at seven sites (trenches SCF–T1 through SCF–T4, SCF–E1, T8A, and a deepening of trench T8) during the present study. Descriptions and logs of five of these trenches (T8, SCF–T1 through SCF–T4) are included in this chapter, as well as a description of test pit T8A.

Interpretations of stratigraphy and fault relations are complicated by extensive silica and carbonate overprinting of the deposits. Along the Solitario Canyon Fault, as elsewhere in the Yucca Mountain area (figs. 1, 2), carbonate accumulation

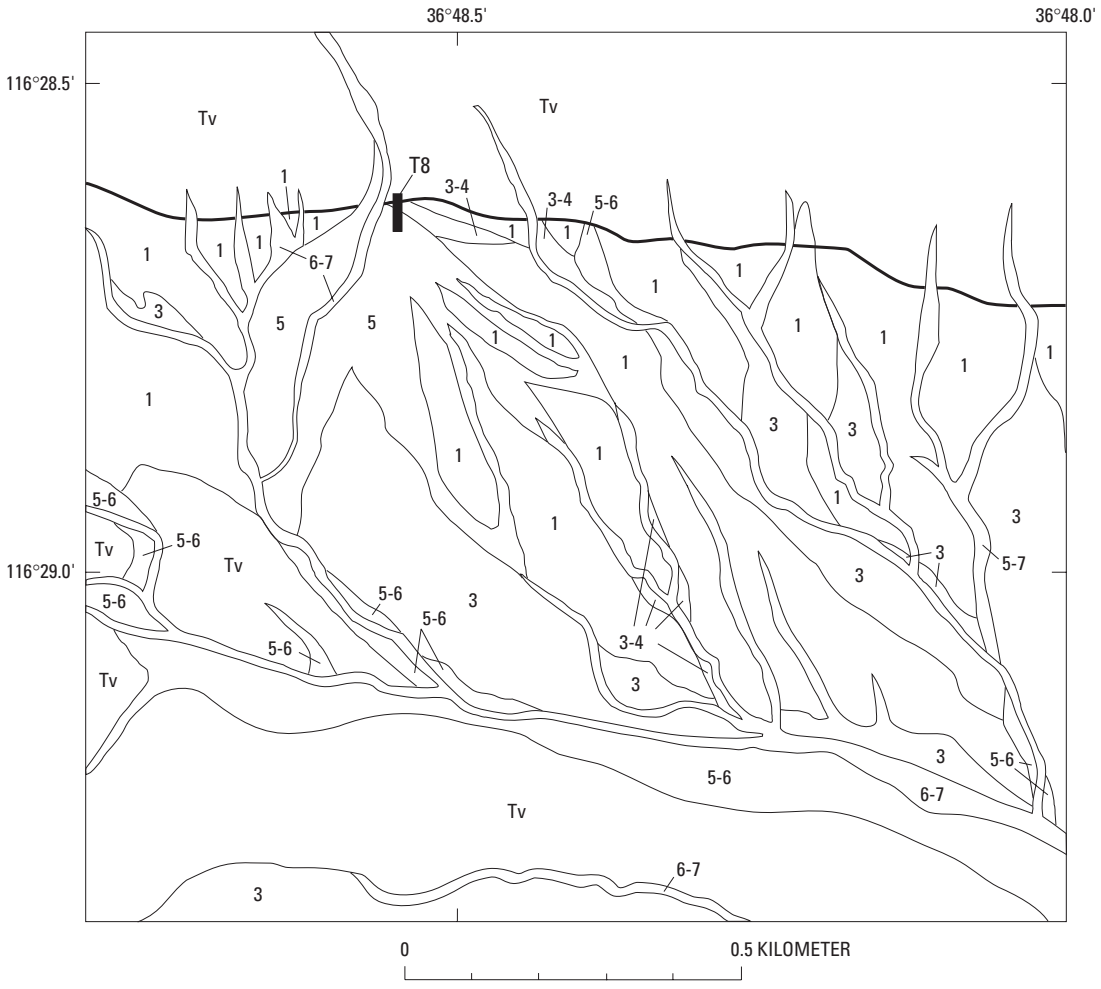

Figure 30. Surficial geologic map of area of trench T8 across the Solitario Canyon Fault in the Yucca Mountain area, southwestern Nevada (figs. 1, 2).

is greatest at and immediately downslope from faults bounding bedrock hillslopes, probably for three reasons: (1) enhanced runoff from the bedrock hillslopes, (2) a pronounced permeability contrast where alluvium is juxtaposed against bedrock, and (3) fractures that allow relatively deep moisture penetration. Morphologic stages of pedogenic carbonate used in this report are based on those of Gile and others (1966), and stages of pedogenic silica on those of Taylor (1986). Soil-horizon nomenclature follows that of Birkeland (1984) and the U.S. Soil Conservation Service. Estimated ages of Quaternary deposits

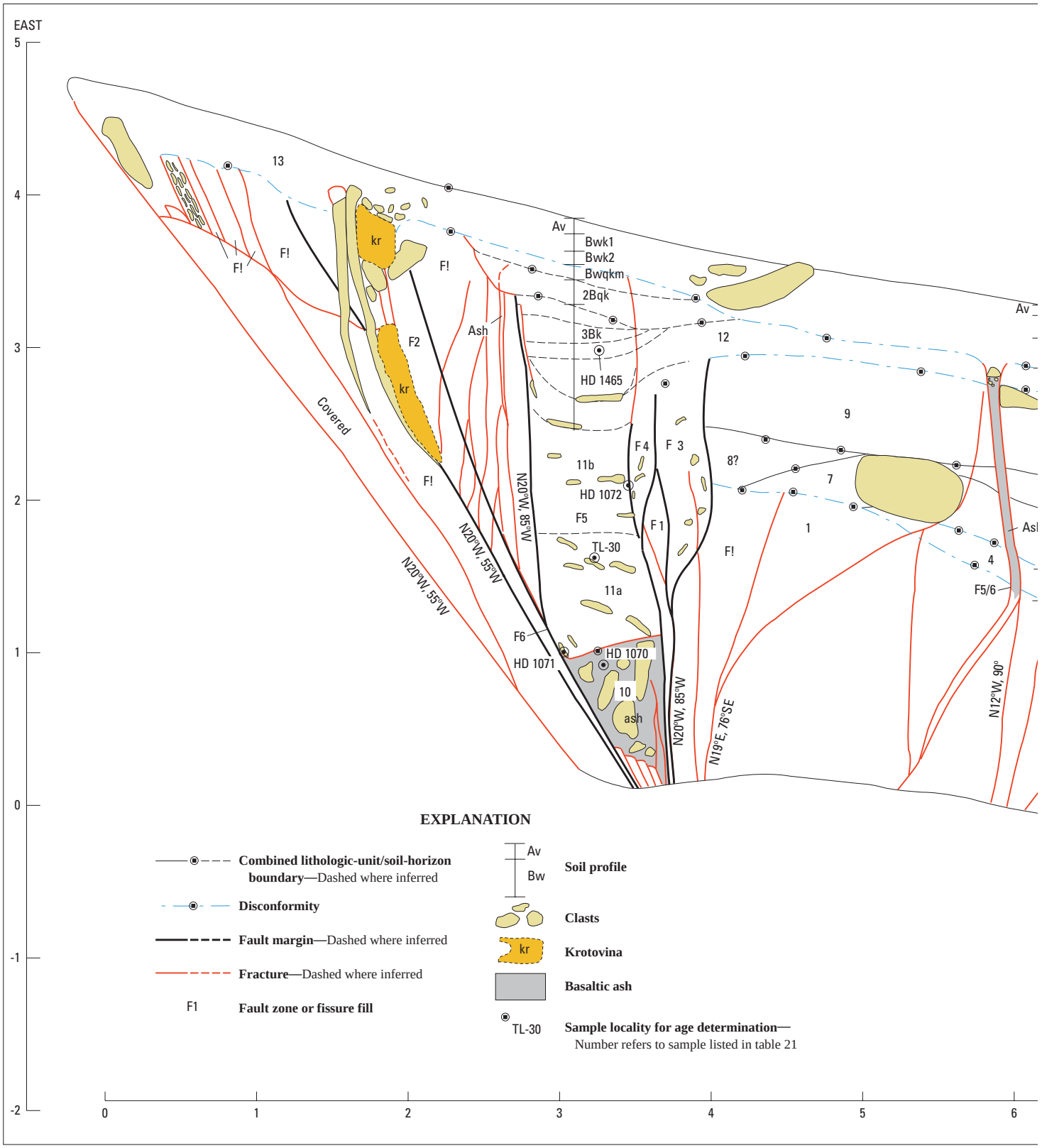

exposed in exploratory trenches and elsewhere are based on U-series and thermoluminescence analyses (table 21), and on comparisons with Quaternary stratigraphic sequences identified in the surrounding region (for example, Wesling and others, 1992; Peterson and others, 1995; see chap. 2; table 2).

Trench T8

Trench T8 (fig. 2), located at the head of an alluvial fan represented by unit Qa5 (fig. 30; table 20), is one of several original trenches excavated for the Yucca Mountain site-char-

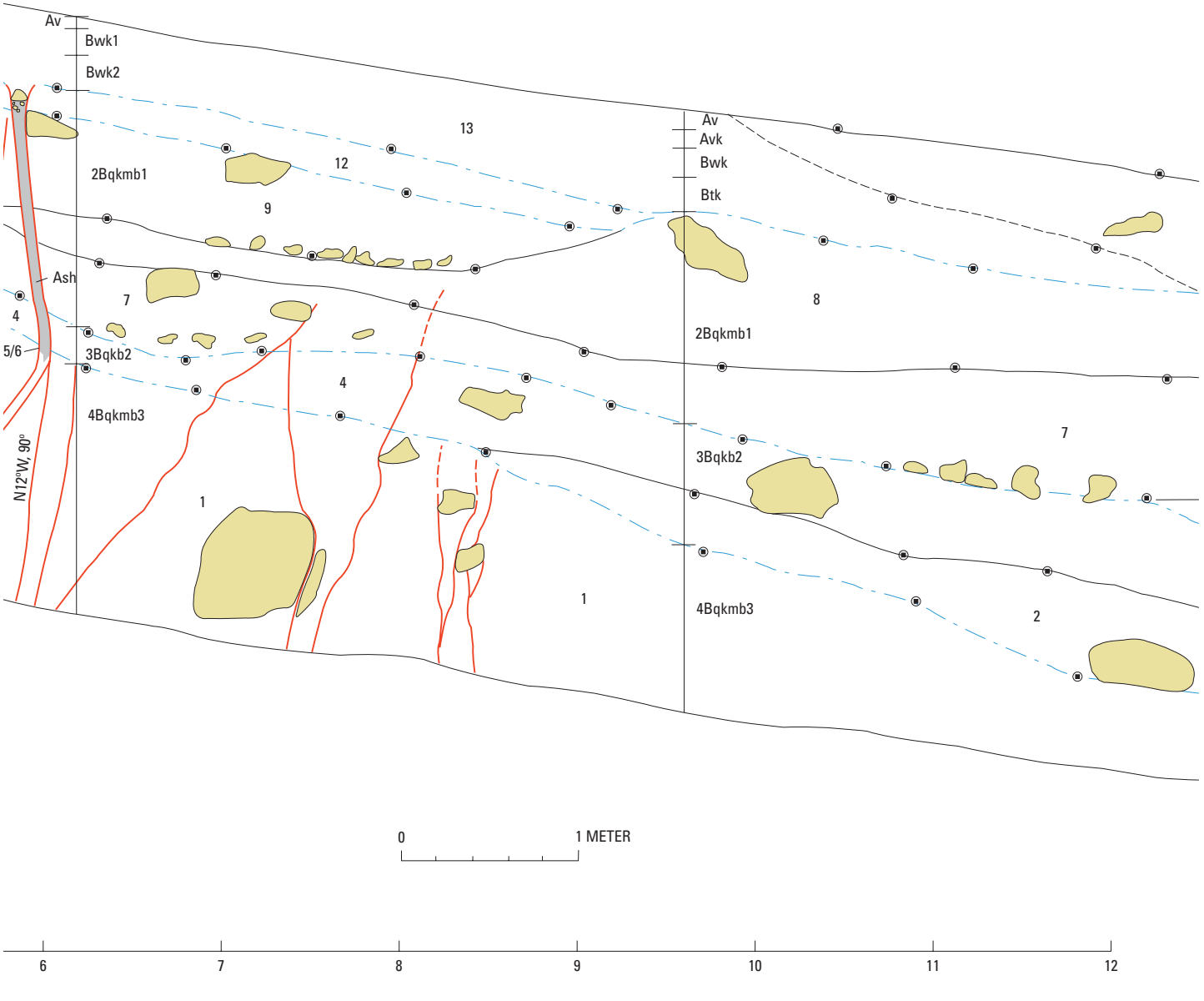

Figure 31. Log of south wall of trench T8 across the Solitario Canyon Fault in the Yucca Mountain area, southwestern Nevada (figs. 1, 2). See table 20 for correlation of map units. See table 3 for explanation of soil horizons; prefixed numbers refer to differentiated soil horizons with increasing depth, and suffixed numbers to further differentiation of properties within an individual soil horizon.

acterization project. The trench was deepened in mid-1993 to provide a better exposure of older faulted deposits, and an adjacent test pit (T8A) was excavated at that time to further assess the recency of faulting. Trench T8 exposes fanglomerate gravel deposits downthrown against welded Miocene tuff (nonlithophysal zone of the crystal-rich member of the Topopah Spring Tuff; Day and others, 1998a). The Quaternary deposits, which are exposed only on the hanging wall, are divided into five distinct age groups, each with distinguishing soil development. Most, if not all, of these age groups are represented in the fairly complex surficial geology of the alluvial fan at this site (figs. 30–32). The tuff lies basically at the ground surface on the footwall and is covered locally by a thin deposit of relatively young eolian silt and colluvium. A small strath terrace is apparently cut into the tuff on the upthrown side of the fault.

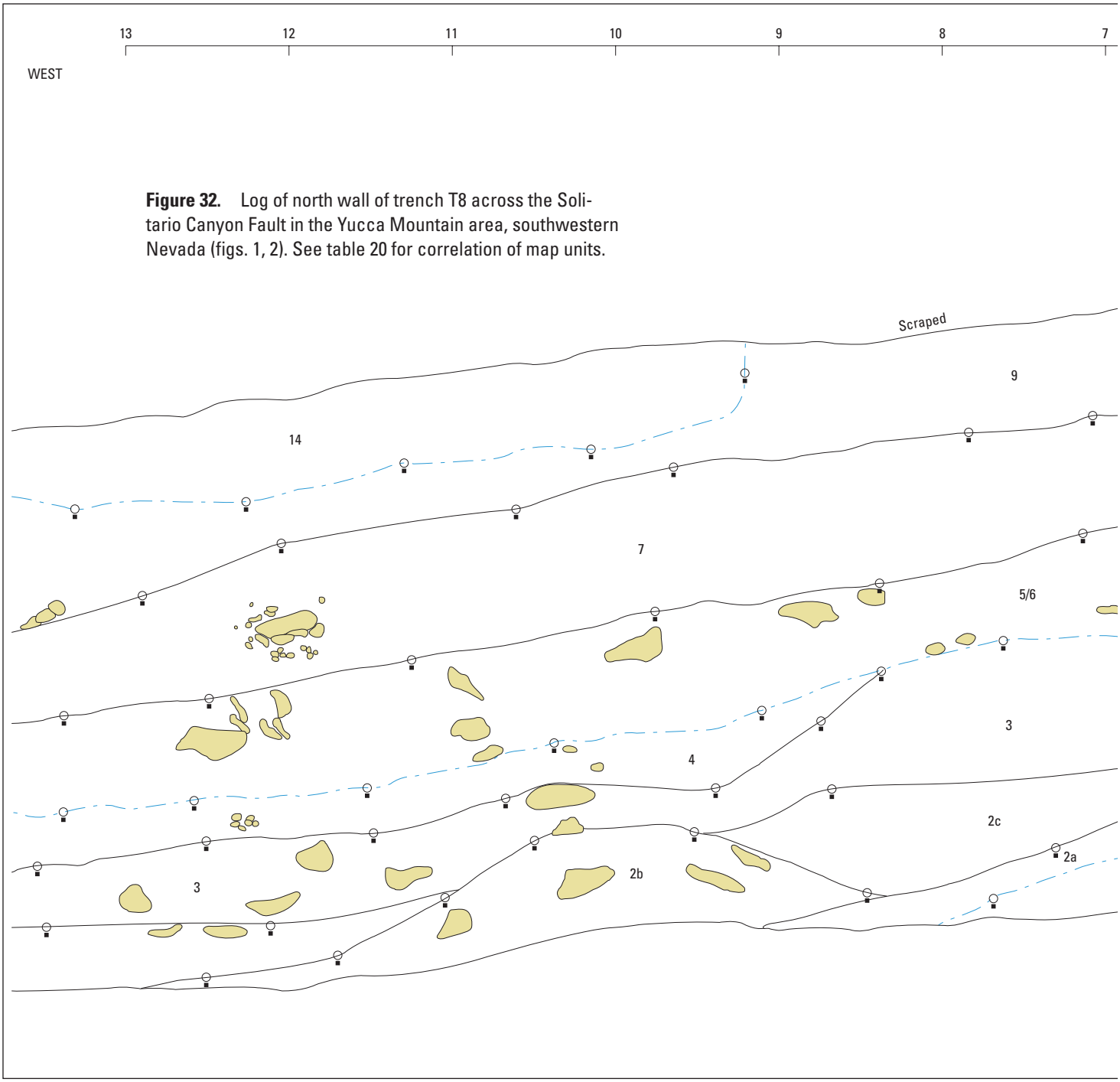

Figure 32. Log of north wall of trench T8 across the Solitario Canyon Fault in the Yucca Mountain area, southwestern Nevada (figs. 1, 2). See table 20 for correlation of map units.

Stratigraphy

The lowermost gravel deposits (unit 1, fig. 30) exposed in trench T8 (fig. 2) consist of bouldery gravel entirely engulfed in silica and carbonate ($CaCO_3$ stage III–V morphology) that have obliterated most of the original sedimentary fabric and contacts. The upper soil horizons associated with this massive petrocalcic horizon have been erosionally stripped. These gravel deposits are best exposed in the south wall of the trench (fig. 31) but are also exposed near the bottom in the north wall (fig. 32). The deposits are widely exposed across the southern and eastern parts of the alluvial fan in which trench T8 is excavated (fig. 30). On the basis of extensive silica and carbonate accumulation and stratigraphic position, unit 1 is dated at middle Pleistocene, possibly early Pleistocene (probably >500 ka) and is correlated with the oldest Quaternary deposits (unit Qa1, table 20) generally present in the Yucca Mountain area (figs. 1, 2).

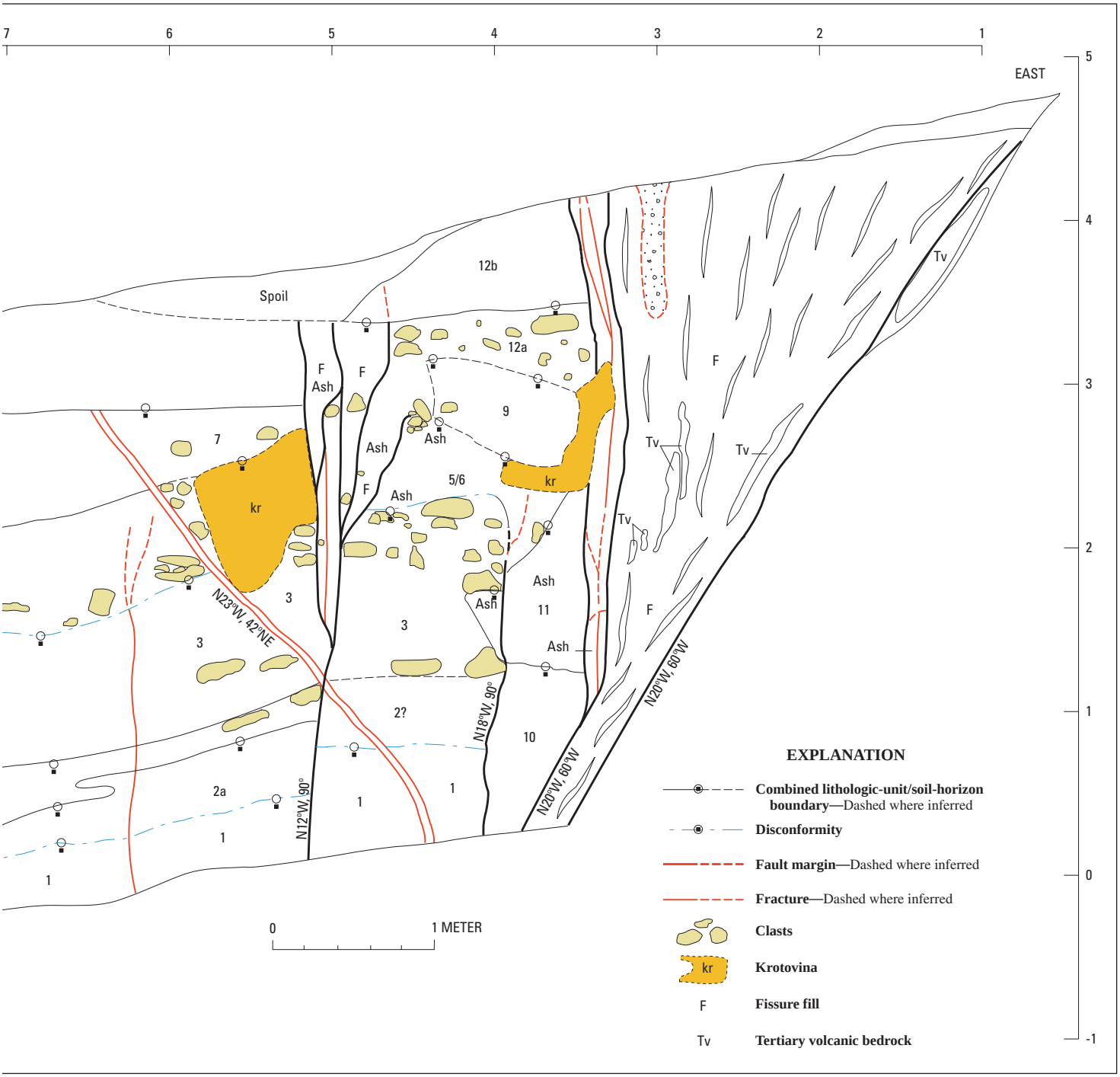

Unit 1 is overlain by gravel deposits (units 2–4, fig. 30) with a distinctive brown noncalcareous silt matrix that is moderately to strongly cemented by silica. The material was deposited in a channel just north of trench T8 (fig. 2), in the vicinity of the current active wash, and the deposits are much thicker in the north wall (fig. 32) than in the south wall (fig. 31). The only constraint on the age of units 2 through 4 is their stratigraphic position; they are likely closer in age to the overlying deposits (believed to be of unit Qa3 age; see chap. 2; fig. 3) and so are probably middle Pleistocene.

A group of moderately well stratified alluvial pebble-and-cobble gravel deposits (units 5–9, fig. 30) represents an episode of alluviation not evident at the other trench sites along the Solitario Canyon Fault. These deposits contain a well-developed petrocalcic horizon ($CaCO_3$ stage III–IV morphology), but silica and carbonate accumulations do not obliterate the sedimentary fabric. The upper soil horizons associated with this petrocalcic horizon were erosionally stripped before younger material was deposited. On the basis of stratigraphic position, carbonate accumulation, and a U-series age on material from an adjacent fracture fill (stas. 3.5–4 m, fig. 31; sample HD 1072; table 21; average age, 118±6 ka) that crosscuts and therefore postdates the deposits, units 5 through 9 are dated at middle to late Pleistocene (150–250 ka) and are tentatively correlated, at least in part, with unit Qa3 (table 20).

Units 10 and 11 were deposited in a 60- to 70-cm-wide subvertical fissure formed during the largest late Quaternary surface-rupturing paleoearthquake. In the south wall of the trench (fig. 31), unit 10 consists of nearly pure basaltic ash and mixed volcanic and carbonate clasts that fill the bottom 1 m of the fissure. The extreme angularity of the ash grains, indicating minimal transport, along with a scarcity of other detrital material (for example, eolian silt), indicates that the ash accumulated in this fissure relatively soon after faulting. In the north wall (fig. 32), unit 10 consists of ash-free pebbly silt apparently deposited just before the ash.

Unit 11, which fills the upper part of this fissure, consists predominantly of silt and fine sand, with minor gravel clasts and reworked basaltic ash; the ash content decreases gradually upward. In the south wall (fig. 31), the lower part of unit 11 (11a) has an inclined sedimentary fabric, likely because this material spilled into the fissure from upslope. The upper part of unit 11 (11b) has a more subhorizontal fabric, probably resulting from a more gradual filling of the fissure from both sides, including material backwasted from the downhill side.

Unit 12 does not have a distinct contact with unit 11 but is distinguished on the basis of position and geometry (it forms a downslope-tapering wedge of material deposited after the fissure was filled). Units 11b and 12 contain carbonate with $CaCO_3$ stage II+ morphology, indicating an age of at least a few tens of thousands of years. A maximum age for units 10 through 12 is provided by the above-mentioned U-series age of 118±6 ka on older fissure carbonate (sample HD 1072, table 21). Minimum limiting ages include (1) U-series ages of 27±1 and 56±3 ka on rhizoliths from within unit 10 (sample HD 1070), (2) a thermoluminescence age of 36±3 ka on material from the middle part of unit 11 (sample TL–30), (3) U-series ages of 47±9 and 66±23 ka on secondary carbonate from within the lower part of unit 12 (sample HD 1465), and (4) an average U-series age of 15.5±4.3 ka on vein carbonate crosscutting the basaltic ash (sample HD 1071). A sample of secondary carbonate from the upper part of unit 12 was dated at 101±4 ka, but this age was discounted because of poor sample quality and inconsistency with other results.

On the basis of geochronologic data, carbonate accumulation, and stratigraphic position, units 10 through 12 are dated at late Pleistocene (40–100 ka). Correlation with the largest eruption at the nearby Lathrop Wells volcanic center (fig. 1) indicates an age of 77±6 ka (Heizler and others, 1999) for unit 10.

A gravelly-silt deposit (unit 13, fig. 31), composed of colluvium, eolian silt, and possibly minor amounts of alluvial gravel, extends across the Solitario Canyon Fault, overlying unit 12, the fault zone, and welded tuff in the footwall. The deposit contains a weak argillic (Bt) horizon, and exhibits soil catena characteristics, wherein soil development increases downslope. Owing to the ongoing input of eolian material, the deposit is time transgressive, as evidenced by the soils and by its interfingering relation with the overlying unit 14. Thermoluminescence ages of 11±2 and 14±2 ka (samples TL–10 and TL–11, respectively, table 21) were obtained for this deposit in test pit T8A (fig. 2), a small excavation across the fault 5 m south of the main trench T8. Unit 13 is dated at late Pleistocene to Holocene and is correlated with units Qa4 and (or) Qa5 (table 20).

The uppermost deposit (unit 14, fig. 32) consists of silty alluvial gravel, about 1 m thick, that is present only downslope from the fault, and so it appears to have no direct relation to faulting. Soil development within this deposit is minimal, consisting of a fairly thin vesicular A (Av) horizon, cambic (Bw) horizon, and $CaCO_3$ stage I–I+ morphology. Unit 14 is dated at latest Pleistocene or Holocene and is correlated with unit Qa5 (table 20).

Structure

Trench T8 (fig. 2) exposes a west-dipping bedrock fault expressed as a 3- to 5-m-wide, flaring-upward zone that separates welded tuff in the footwall from alluvial gravel in the hanging wall. The fault zone is composed largely of laminar or massive silica and carbonate, carbonate-cemented gravel, slivers of tuff, and fissures filled with silt, gravel, and basaltic ash. Of all the trenches on the Solitario Canyon Fault, trench T8 exposes the largest displacements and provides the most complete record of mid-Quaternary to late Quaternary activity. The following discussion outlines evidence of apparent faulting events from youngest to oldest, including two possible fracturing events.

Uncemented, silt-filled fractures are present in the south wall of trench T8 (fig. 31) but not in the north wall (fig. 32). Although the absence of cementation of these fractures indicates a minor Holocene fracturing event, several other origins for such silt-filled openings are possible, including (1) bioturbation, (2) carbonate dissolution, (3) root wedging, (4) downslope mass

Table 22. Estimated displacements associated with middle to late Quaternary faulting events along the Solitario Canyon Fault in the Yucca Mountain area, southwestern Nevada.

[See figures 1 and 2 for locations. n.p., not present]

Event	Date (ka)	Trench (displacement in centimeters)				Comments
		SCF–T4	T8	SCF–T3	SCF–T1	
?	15–5	n.p.	0?	0?	n.p.	Silt-filled openings.
?	25–15	n.p.?	0	n.p.?	n.p.?	Cemented fracture.
Z	30–20	0–10?	10–20	0–10?	?	Minor fissure; fracturs in event Y fissure fill; dragged event Y ash.
Y	80–70	20–40	110–130	60–120	50–120	Largest event; fissures contain basaltic ash.
X	200–120	n.p.?	20–40	?	?	15-cm-wide fissure in trench T8.
W	250–150	15–30	30–60	20–40	?	Second-largest faulting event.

movement, (5) compaction, and (6) shrink/swelling. A 20-cm-wide, silt-filled opening in trench T8 (sta. 2 m, fig. 31) that appears to be an animal burrow does not noticeably displace an older gravel-filled fissure. Animal burrowing concentrated along faults is common in the Yucca Mountain area (figs. 1, 2).

A single silica- and carbonate-cemented fracture in the south wall of trench T8 (sta. 3.5 m, fig. 31) cuts all cemented deposits. This cemented fracture is distinctly older than the silt-filled fractures, yet it cuts deposits capping the more definitive displacements discussed below. The narrow, even width of the fracture indicates a slight extensional opening.

The most recent faulting event (Z, table 22) is indicated by (1) carbonate-filled fractures that cut the ash-filled fissure discussed below, (2) basaltic ash dragged along the fault, and (3) a narrow (10–15 cm wide) silt- and ash-filled fissure exposed in the north wall of the trench. These features indicate vertical displacement of about 10 to 20 cm. A U-series age of 15±4 ka on vein carbonate (sample HD 1071, table 21) from the south wall of the trench (fig. 31) provides a possible minimum date for this event.

The penultimate and, by far, largest faulting event (Y, table 22) is evidenced by a silt- and ash-filled fissure exposed in both walls of trench T8 (figs. 31, 32) and in a bench in the middle of the trench. In the south wall, the bottom 1 m of this fissure (unit 10) is filled with jumbled tuff and carbonate clasts in a matrix of loose, nearly pure basaltic ash. The absence of other detrital material indicates that the ash was emplaced soon after the fissure opened and that faulting and basaltic volcanism were essentially contemporaneous. In the north wall, this fissure is less obvious and lacks the nearly pure ash; the bottom is filled with ash-free pebbly silt similar to material (unit 5/6?) that underlies a tilted block of calcrete (unit 9); these materials apparently collapsed into the fissure before the ash was deposited, probably during the paleoearthquake. The upper fissure fill in the north wall is a mixture of silt, ash, and gravel similar to that in the south wall. The fault slip indicated by this fissure can be estimated from the fault dip (58°) and the extensional opening (consistently 60–70 cm) that splays subvertically from the dipping bedrock fault plane at about 4-m depth. The geometry (fig. 33) indicates dip slip of 1.1 to 1.3 m (0.9–1.1 m of vertical displacement). The moderately well developed soil in the upper part of the fissure fill contains thin silica and carbonate laminae in the uppermost 1 m.

Minimum dates for event Y are provided by U-series ages of 47±9 and 66±23 ka on secondary carbonate from unit 12 (sample HD 1465, table 21), and by a thermoluminescence age of 36±3 ka on material from unit 11 (sample TL–30). An average U-series age of 118±6 ka on fissure carbonate predating the faulting event (sample HD 1072) provides a maximum date. The age (77±6 ka) of the basaltic ash erupted from the nearby Lathrop Wells volcanic center (fig. 1), which is a conspicuous component of the fissure fill that is closely associated with event Y, falls within the range of maximum and minimum dates stated above. Accordingly, event Y is interpreted to have been nearly contemporaneous with that eruption.

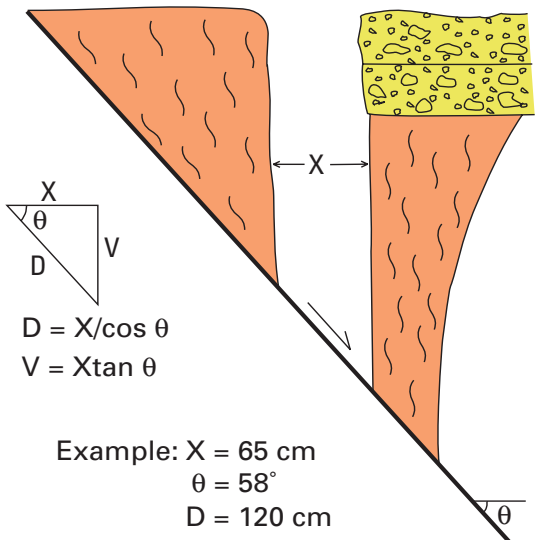

Figure 33. Simple model for estimating fault displacement (D) from genetic constraints imposed by fissure width (X) and fault dip (θ).

Two gravel-filled fissures in the south wall of trench T8 (stas. 3.5–4 m, fig. 31) appears to bound the west side of the ash-filled fissure; both gravel-filled fissures are more highly cemented than, and thus predate, the ash-filled fissure. Furthermore, crosscutting relations and carbonate accumulation indicate that both gravel-filled fissures predate the ash-filled fissure and postdate unit Qa3(?) gravel (units 7–9, fig. 31). The younger and smaller (15 cm wide) gravel-filled fissure represents event X (table 22), whereas the older and larger one (25 cm wide) represents event W (table 20), extending downward into older, massively carbonate cemented fault-zone material. The smaller fissure contains a 2-cm-wide carbonate seam that yielded an average U-series age of 118±6 ka (sample HD 1072, table 21), providing an apparent minimum date for event X. The estimated age (150–250 ka) of the faulted gravel provides an approximate maximum date for event W.

The carbonate-dominated fault zone indicates a faulting event that may predate event W, but defining discrete events within this zone is difficult, owing to carbonate overprinting. A gravel-filled fissure (easternmost fissure at sta. approx 2 m, fig. 31) that reflects one event within this fault zone is highly fractured and crosscut by 1- to 2-cm-thick silica veins but is not obviously displaced by the crosscutting fractures. The secondary silica and carbonate within the fissure indicates a fairly old age; this fissure is the only feature within the older part of the fault zone that retains recognizable sedimentary fabric, and so it may reflect the earliest faulting event preserved in the fault zone.

Test Pit T8A

A small test pit (T8A, fig. 2) was excavated a few meters south of trench T8 to further evaluate Quaternary activity on the Solitario Canyon Fault. The observed stratigraphic and structural relations (not illustrated in this report) are similar to those in the equivalent (upper) part of the south wall of trench T8. Test pit T8A exposes cemented gravel and fault-zone carbonate downthrown against welded tuff. The downthrown units and tuff are overlain by younger mixed colluvium and eolian silt, which is nearly the same deposit as unit 13 in trench T8 but contains a cambic rather than a weak argillic soil. As mentioned previously, thermoluminescence ages of 11±2 and 14±2 ka were determined on two samples (TL–10 and TL–11, respectively, table 21) from this unit in the pit. An irregular, silt-filled opening and multiple narrow silt-filled fractures observed in test pit T8A may indicate Quaternary faulting. Alternatively, these features can also be explained by bioturbation and soil creep.

Trench SCF–T1

Trench SCF–T1 (pl. 8; fig. 2) is located on an active alluvial fan whose surface is dominated by thin (≤1 m thick) gravel deposits of latest Pleistocene or early Holocene age. The trench was excavated across a weak tonal or vegetative lineament apparent on large-scale, low-sun-angle aerial photographs. This lineament and topographic features previously interpreted as small scarps (10–20 cm high) are located on line with the main Quaternary fault scarp along the fault, indicating possible minor Holocene faulting. Trench SCF–T1 was excavated to evaluate this possible faulting and to define the most recent surface rupture on the Solitario Canyon Fault. A smaller test pit was excavated nearby to provide an additional exposure of the uppermost deposits.

Stratigraphy

Trench SCF–T1 (pl. 8) exposes Quaternary fanglomerate gravel that is downthrown against and overlies nonwelded tuff of the lower part of the Tiva Canyon Tuff. The lowermost gravel layers (units 1–4, pl. 8) are present only on the hanging wall of the Solitario Canyon Fault. At the west end of the trench (pl. 8), these deposits are entirely engulfed in silica and carbonate ($CaCO_3$ stage III–V morphology), and much of the original sedimentary fabric is obliterated. On the basis of extensive silica and carbonate accumulation, units 1 through 4 are dated at middle Pleistocene or older (probably >500 ka) and are correlated with the oldest Quaternary deposits (unit Qa1, table 20) generally present in the Yucca Mountain area (figs. 1, 2).

Units 5 through 8 (pl. 8) also are entirely engulfed in carbonate ($CaCO_3$ stage III–IV morphology). These alluvial deposits are distinguished from older lithologic units by an angular unconformity, by differing carbonate accumulation within the vicinity of the fault zone, and by lesser fault deformation. Units 5 through 8 are dated at middle Pleistocene or older (probably >500 ka) and are also correlated with the oldest Quaternary deposits (unit Qa1, table 20) generally present in the Yucca Mountain area (figs. 1, 2).

Units 9 and 10 (figs. 31, 32) are thin, well-cemented ($CaCO_3$ stage III morphology) deposits, possibly scarp colluvium, present on the downthrown side of a minor fault (stas. 22–23.5 m, pl. 8) that cuts units 1 through 8. On the basis of carbonate accumulation and stratigraphic position, units 9 and 10 are loosely correlated with deposits dated at middle to late Pleistocene (probably 50–200 ka).

Moderately well cemented to well-cemented ($CaCO_3$ stage II–III morphology) gravel deposits (units 12–16, pl. 8) overlie bedrock on the upthrown side of the fault. The deposits are present only upslope from the fault (a thin layer of unit 14 is shown toward the east end of pl. 8) but trend obliquely through the trench site and cross the main fault zone that is exposed in the adjacent test pit. Within the pit, the upper part of the deposits (unit 16?) contains a minor amount of reworked basaltic ash. Cementation of units 12 through 16 is markedly less than that of the older deposits. On the basis of stratigraphic position, carbonate accumulation, and the presence of basaltic ash, which is assumed to have been erupted from the Lathrop Wells volcanic center, units 12 through 16 are dated at late Pleistocene and are tentatively correlated with unit Qa4 (table 20).

A minor pebble-gravel deposit (unit 17, pl. 8) along the main fault zone (stas. 10–11 m) may be a small colluvial wedge related to a faulting event of unknown date. The deposit has a $CaCO_3$ stage II morphology, with a single carbonate lamina on top. On the basis of stratigraphic position and carbonate accumulation, unit 17 is tentatively dated at late Pleistocene.

Units 18 and 19 consist of thin, discontinuous silt deposits overlying unit 17 that contain a weakly to moderately cemented argillic (Bt to Btk) soil horizon. This argillic soil must partly be associated with the carbonate accumulation in the underlying gravel deposit, but the silt layers extend with uniform thickness across cemented deposits of varying ages and have an abrupt basal boundary, indicating that they are distinct deposits and not entirely soil horizons. On the basis of soil development and stratigraphic position, units 18 and 19 are dated at late Pleistocene and are tentatively correlated with unit Qa4 (table 20).

The uppermost deposits in trench SCF–T1 and the adjacent test pit (units 20–22, pl. 8) are composed of silty alluvial gravel, as much as 1 m thick. An alluvial origin for unit 20 is evidenced by imbricated gravel clasts. Soil development within these deposits consists of a thin vesicular A (Av) horizon, a minimal cambic (Bw) horizon, and $CaCO_3$ stage I–I+ morphology. Units 20 through 22 are dated at latest Pleistocene or early Holocene and are correlated with unit Qa5 (table 20).

Structure

The south wall of trench SCF–T1 (pl. 8) exposes a fault zone, almost 20 m wide, consisting, from east to west, of minor displacements within the tuff and basal gravel (stas. 4.5–6 m), a main bedrock-alluvium fault zone (stas. 9–13), a zone of subvertical fractures and fissures (stas. 15.5–20 m), and irregular antithetic faults (stas. 19.5–24 m). The entire fault zone may not be exposed; minor ruptures may exist farther downslope to the west, but additional large offsets are unlikely. Only one faulting event (ash-related event Y, tables 8, 22) is clearly evident at this site; other events are primarily slip events along the main fault zone. Because erosion apparently has removed some deposits, particularly on the footwall, preserved relations are insufficient to confidently determine a sequence of faulting events.

The main bedrock-alluvium fault contact is a 1- to 2-m-wide, west-dipping zone of laminar carbonate and cemented gravel (stas. 9–13 m, pl. 8) that is downfaulted along a planar bedrock fault striking N. 11° E. and dipping 50° NW. This main fault zone flares upward slightly and likely narrows at shallow depth. The uppermost deposits (units 19–22), the oldest of which (unit 19) contains argillic soil, extend undisturbed across the main fault zone. In trench SCF–T1, an animal burrow disrupts unit 19 near the fault zone, but this unit is clearly unfaulted where exposed in the adjacent test pit.

Slight topographic irregularities on the surface above the main fault zone were originally interpreted as small scarps resulting from offset of surficial deposits, although the small amount of offset is near the limit of resolution of such features. Three topographic profiles of the fan surface all show surface irregularities at the fault zone, but only the profile surveyed on an adjacent, older surface shows down-to-the-west surface offset. Two profiles surveyed adjacent to trench SCF–T1 on the unit Qa5 (table 20) surface indicate that drainage across the cemented gravel deposits was deflected by contrasts in competence at the fault zone, but do not show any vertical separation of the unit Qa5 surface.

Although fault/stratigraphic relations across the main fault zone are poorly preserved, owing to erosion, crosscutting relations place some constraints on fault history. The most recent displacement (on the basis of the thickness of a small wedge of largely unconsolidated gravel, silt, and colluvial material within the main fault zone where all the other fill deposits are strongly cemented) is considered to have been at least 30 cm and to have occurred in late Quaternary time but before the development of the unfaulted argillic soil in unit 19 (pl. 8). Correlation of this displacement with the faulting events discussed above for trench T8 is uncertain; however, the most recent event (min 15±4 ka) interpreted for trench T8 (sample HD 1071, table 21) probably postdates unit 19 in trench SCF–T1.

The alluvial-gravel deposits (units 5–8, pl. 8) that contain the upper petrocalcic horizon with $CaCO_3$ stage IV morphology are progressively downthrown against the main fault; the surface of unconformity overlain by unit 5 is displaced about 1.5 m. This offset may be a minimum, owing to an unknown amount of erosional stripping of the footwall, but conversely, displacement may be exaggerated by backtilting. The offset of units 5 through 8 apparently occurred during mid-Quaternary to late Quaternary time, because cementation indicates these deposits to be no older (approx 900 ka; see below) than the deposits exposed in trench SCF–T3 (fig. 34). If this displacement occurred during the mid-Quaternary to late Quaternary, as is believed to be likely, then the small wedge of unconsolidated material within the fault zone that was mentioned above was deposited later. The offset across the main fault zone occurred in addition to that associated with the basaltic-ash-filled fissures (see below), which are downslope to the west (stas. 16.5–19.5 m, pl. 8). Units 5 through 8 unconformably overlie the lowermost exposed deposits (units 1–4), which are backtilted and displaced along a fault plane that is truncated by unit 5, indicating an even older displacement (of unknown age) across the main fault zone.

Trench SCF–T1 (pl. 8) also exposes a broad zone of hanging-wall deformation. A 4-m-wide zone of subvertical faults, fractures, and fissures (stas. 15.5–19.5 m, pl. 8) is largely engulfed in carbonate but also includes two conspicuous basaltic-ash-filled fissures. The eastern fissure (stas. 16.5–17 m) has a slight westward dip (85° NW.) and strikes nearly parallel to the main fault zone (N. 15° E.), whereas the western feature (sta. 19 m, pl. 8) strikes about 15° oblique to the main fault zone (N. 30° E.) and is nearly vertical. These two fissures cut the same deposits (units 1–8) and contain similar amounts of secondary carbonate; therefore, they are

assumed to represent the same faulting event. The western fissure contains reworked B-horizon peds, indicating that soil horizons, which may have been present at the time of faulting, were subsequently stripped. No direct measurements of surface offset related to these fissures are possible, owing to subsequent surface erosion, but the total width of the fissure opening (30–60 cm) indicates dip slip of 50 to 90 cm. If the small wedge of unconsolidated fill deposits within the main fault zone possibly relates to the same faulting event (Y, table 22), displacement caused by this single event may have ranged from 80 to 120 cm.

Cumulative displacement across the entire fault zone exposed in trench SCF–T1 (pl. 8) is uncertain. However, considering the displacement associated with the ash-filled fissures discussed above, the offsets on the main fault zone, the minor offset in the footwall, and possible backtilting, the cumulative mid-Quaternary to late Quaternary dip slip is estimated at 1.6 to 2.4 m.

West of the zone of subvertical fractures and fissures are several minor offsets and openings along antithetic (east dipping) faults with varying but shallow-dipping orientations. Basaltic-ash-filled openings within this zone strike oblique to,

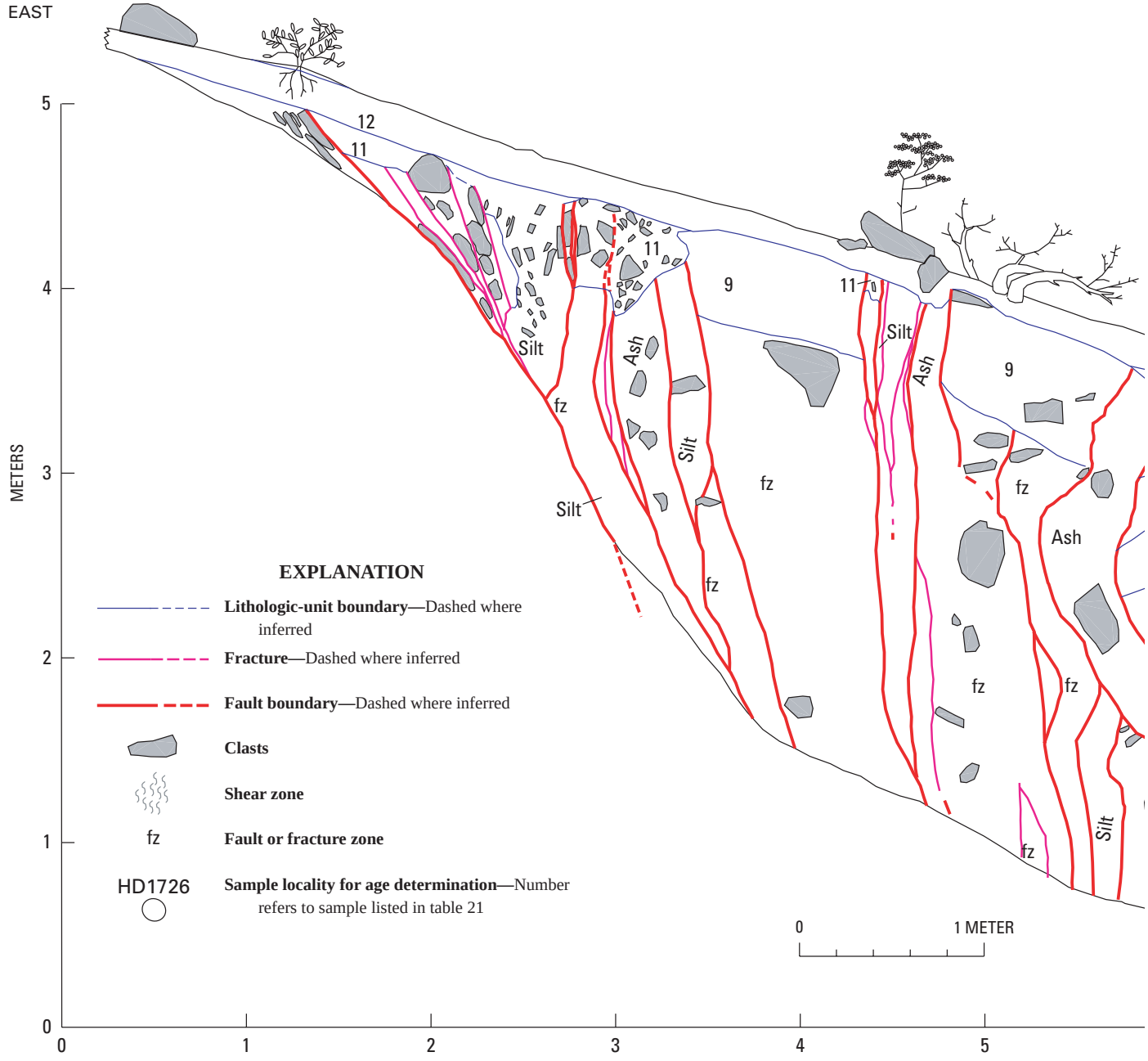

and dip into, the trench wall; these features are absent in the north wall of the trench.

Although the geologic relations exposed in trench SCF–T1 are not definitive enough for reliably determining offsets or numbers and dates of faulting events, several comparisons with the deformation in trench T8 are possible. The most recent faulting event evident in trench T8 is not observed in trench SCF–T1, other than possibly being represented by cemented fractures cutting the ash-filled fissures. The relatively large ash-related faulting event (Y, table 22) involved a fissure opening comparable to that at trench T8, indicating a similar offset. The estimated total displacement (approx 2 m) is reasonably similar to the estimated cumulative offset for trench T8. The presence of carbonate-cemented ($CaCO_3$ stage V morphology) gravel near the surface on the hanging wall of the Solitario Canyon Fault supports the interpretation that a hiatus in fault activity preceded the observed mid-Quaternary to late Quaternary events.

Trench SCF–T3

Trench SCF–T3 (figs. 2, 34) is located on an eroded remnant of hillslope colluvium, about 700 m north of trench SCF–T1 (fig. 2). The trench was located so as to possibly

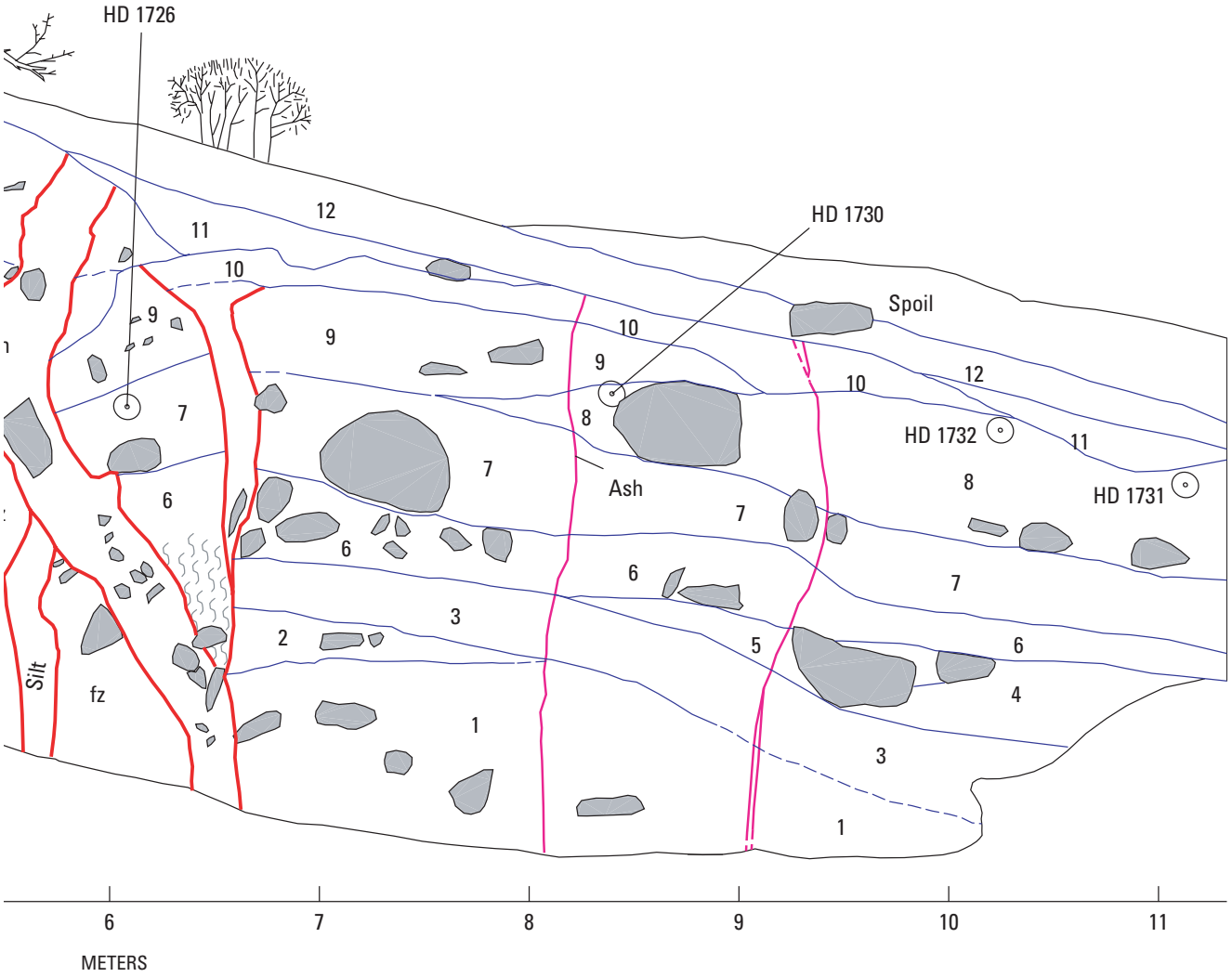

Figure 34. Log of south wall of trench SCF–T3 across the Solitario Canyon Fault in the Yucca Mountain area, southwestern Nevada (figs. 1, 2). See table 20 for correlation of map units.

provide a more complete record of faulting events than that observed in trenches T8 and SCF–T1.

Stratigraphy

Trench SCF–T3 (fig. 34) exposes hillslope and colluvial deposits downthrown against welded tuff of the Topopah Spring Tuff across the Solitario Canyon Fault. The colluvial deposits compose three distinct packages, each with a distinctive soil development. The two older units, which are moderately to extremely well cemented by silica and carbonate, are limited to the downthrown side of the fault. The upper soil horizons associated with the upper petrocalcic horizon have been stripped by erosion. The bedrock is present basically at the ground surface on the upthrown side of the fault. A thin (10–30 cm thick) deposit of Holocene colluvium and eolian silt overlies both the cemented colluvial deposits and the tuff.

The lowermost deposits (units 1, 2, fig. 34) in trench SCF–T3 are well cemented by silica and carbonate and appear to be truncated by a buried soil horizon (unit 3). The extensive silica and carbonate ($CaCO_3$ stage III–IV morphology) accumulation has largely obliterated the original sedimentary fabric of these three deposits, making both the defined stratigraphic contacts and buried soil horizons uncertain. On the basis of extensive silica and carbonate accumulation and stratigraphic position, units 1 and 2 are dated at early Pleistocene and are correlated with the oldest Quaternary deposits (unit Qa1, table 20) generally present in the Yucca Mountain area (figs. 1, 2).

Units 4 through 9 (fig. 34) also are entirely engulfed in carbonate, and most of the original sedimentary fabric is obliterated, indicating considerable antiquity. Silica-rich clast rinds in units 7 and 8 (samples HD 1726, HD 1730, HD 1731, HD 1732, fig. 34, all from large boulders) yielded a wide range of U-series ages, many older than 500 ka (table 21). On the basis of extensive silica and carbonate ($CaCO_3$ stage III–V morphology) accumulation, units 4 through 9 are dated at early to middle Pleistocene and are also correlated with the oldest Quaternary deposits (unit Qa1, table 20) generally present in the Yucca Mountain area (figs. 1, 2).

Unit 10 (fig. 34) is a thin, well-cemented ($CaCO_3$ stage IV morphology) colluvial deposit present on the downthrown side of the fault zone. The material may have been deposited in response to surface faulting. The original upper soil horizons associated with the accumulated carbonate have been stripped. Because this deposit appears to be localized and numerical-age control is absent, unit 10 cannot confidently be correlated with other units; however, the deposit is crosscut by the larger of two ash-filled fissures, a relation that, in combination with the amount of carbonate accumulation in the unit, indicates an age older than about 80 ka.

The uppermost deposits (units 11, 12, fig. 34) in trench SCF–T3 consist of silty gravel composed of eolian silt and colluvium. In the western part of the trench (west of sta. 9 m, fig. 34), unit 12 was disturbed during excavation. Soil development within these deposits consists of a fairly thin vesicular A (Av) horizon, minimal cambic (Bw) horizon, and $CaCO_3$ stage I–I+ morphology. Units 11 and 12 are dated at latest Pleistocene to early Holocene and are probably correlated with unit Qa5 (table 20).

Structure

Trench SCF–T3 (fig. 34) exposes a 3- to 5-m-wide fault zone bounded on the east by a bedrock fault plane dipping 62° W. (fig. 34). The fault zone, consisting largely of laminar or massive carbonate and carbonate-cemented gravel, includes several subvertical gravel- and ash-filled fissures and cemented fractures. The exposed relations indicate that the fault zone narrows at a shallow (<10 m) depth. The extensive carbonate accumulation has obscured much of the older fault fabric. Mid-Quaternary to late Quaternary faulting is evidenced by fissures filled with gravel, silt, and basaltic ash. Older carbonate-cemented gravel within the fault zone was likely emplaced in similar subvertical fissures.

The uppermost deposits (units 11, 12, fig. 34), consisting of mixed colluvium and eolian silt, do not appear to be faulted. Silt (unit 11) fills three openings: (1) a 30-cm-wide opening (sta. 2.5 m, fig. 34) that extends upward from the bedrock fault plane, (2) a uniform opening of a few millimeters along the bedrock/fault-zone contact (sta. 3 m), and (3) a narrow fracture within the carbonate-engulfed fault zone (sta. 4.3 m). Although these narrow openings may have resulted from minor fault-related extension, they do not appear to have been caused by measurable fault displacement. The 30-cm-wide opening is interpreted to be an erosional feature because, if it were fault related, an offset creating a much more noticeable scarp than is apparent in the exposure would be required, as well as slip along the bedrock fault plane, which also is not apparent.

Carbonate-filled fractures that cut and disturb an ash-filled fissure (stas. 3–3.5 m, fig. 34; see next paragraph) indicate that at least one fracturing event postdated the large ash-related event. Presumably, this fracturing event is equivalent to the most recent faulting event observed in trench T8 (fig. 2). No displacement associated with this event was measurable in trench SCF–T3.

Two fissures in trench SCF–T3 (fig. 34) contain abundant basaltic ash throughout their exposed vertical extents. Both fissures cut all but units 11 and 12 (fig. 34). The larger fissure (stas. 5.5–6.5 m, fig. 34) is filled mostly with gravel that has a basaltic-ash matrix. The smaller fissure (stas. 3–3.5 m, fig. 34) contains more ash than gravel clasts. Both fissures cut similar-age deposits, have similar ash contents, and contain similar secondary carbonate; accordingly, the two fissures are inferred to have formed during a single faulting event (Y, table 22). Although the offset associated with this event was not directly measurable, the combined fissure width (30–60 cm) indicates dip slip of 0.6 to 1.2 m. At the top of the petrocalcic horizon, both ash-filled fissures are erosionally truncated and buried by Holocene silt and colluvium, probably reflecting early Holocene stripping of the upper soil horizons down to the more resistant petrocalcic horizon.

An uncemented gravel- and silt-filled fissure (sta. approx 5.5 m, fig. 34) that is crosscut by the western ash-filled fissure contains minor basaltic ash in its upper part and may reflect an earlier ash-related faulting event, although reworking of ash from the younger crosscutting fissure is also possible. This earlier faulting event may be associated with the fault-related features (possible colluvial wedge [unit 10] and backtilted gravel) present at about station 6 m (fig. 34), which are much more cemented by carbonate than is the ash-filled fissure. This feature probably was formed during event W as observed in trench T8, but such an association would be difficult to substantiate. Except where cut by the two zones of late Quaternary fissuring, the uppermost well-cemented colluvial deposit (unit 9) extends across the fault zone, truncating older fault features and apparently representing a significant mid-Quaternary hiatus in seismicity. Faulting events predating unit 9 are evidenced by juxtaposition of older deposits against the fault zone, by a distinct fault contact within the fault zone (sta. 4.3 m, fig. 34), and by a carbonate-cemented fissure (sta. 5.3 m, fig. 34).

Although the juxtaposition of colluvial deposits against bedrock at the east end of trench SCF–T3 (fig. 34) precludes any direct measurement of fault displacements, displacements can be estimated on the basis of the position of deposits on the hanging wall. For example, the displacement of unit 9 can be estimated from the vertical separation between the base of units 11 and 12 (top of bedrock on the footwall) and the top of unit 9 on the hanging wall, which is about 60 to 70 cm (dip slip, 80–90 cm), assuming that a comparable thickness of unit 9 was eroded off the footwall after displacement occurred. Assuming that older units in the hanging wall also were deposited across the fault and rested on the bedrock surface of the footwall, displacements are estimated at about 1.6 m for units 6 and 7 and about 2.8 m for units 1 and 2.

Trench SCF–T4

Trench SCF–T4 (pl. 9) is the northernmost of the trenches spanning the Solitario Canyon Fault that is discussed in this chapter (fig. 2). The trench was excavated into an eroded remnant of hillslope colluvium to investigate the fault activity at a locality close to the west side of the proposed repository site for the storage of high-level radioactive waste storage at Yucca Mountain (fig. 1).

Stratigraphy

Trench SCF–T4 (pl. 9) exposes hillslope and fault colluvium downthrown against welded and nonwelded tuff of the Paintbrush Group (Day and others, 1998b). The nonwelded tuff, which fills a sliver between two principal fault strands, forms the footwall of the upper (eastern) fault strand. The older colluvial deposits (units 1–7) in the hanging wall are moderately to well cemented by silica and carbonate; the upper soil horizons associated with the petrocalcic horizons in these deposits have been erosionally stripped. The cemented colluvium and bedrock tuff are buried by deposits of less well indurated colluvium and eolian silt (units 8–10) of varying thickness.

The lowermost deposit (unit 1, pl. 9) exposed in trench SCF–T4 is well cemented by silica, indicating, in combination with its stratigraphic position, an early Pleistocene or older age (probably >1 Ma); the deposit may even be silicified bedrock.

Unit 1 is overlain by several hillslope colluvial deposits (units 2–6), the lower of which (units 2–4) are only moderately cemented ($CaCO_3$ stage II morphology), whereas the upper deposits (units 5–6) contain a well-developed petrocalcic horizon ($CaCO_3$ stage III–IV morphology). This contrast in cementation indicates that the upper units were deposited and subsequently plugged by soil development before much carbonate had accumulated in the lower units. Unit 4 pinches out downslope from the main Quaternary fault zone, indicating that the unit is a colluvial wedge related to surface faulting. On the basis of extensive silica and carbonate accumulation ($CaCO_3$ stage II–IV morphology), though somewhat less than that in the unit Qa1 deposits exposed in trenches T8, SCF–T1, and SCF–T3, units 2 through 6 are dated at early to middle Pleistocene (at least a few hundred thousand years to probably >500 ka) and are correlated with the oldest Quaternary deposits (unit Qa1, table 20) generally present in the Yucca Mountain area (figs. 1, 2).

Unit 7, which also thins downslope from the main fault zone (stas. 10–11 m, pl. 9), appears to be a small colluvial wedge deposited in response to faulting. The deposit is well cemented ($CaCO_3$ stage IV morphology), and the original upper soil horizons have been stripped. Unit 7 appears to be associated with the largest mid-Quaternary to late Quaternary faulting event (discussed below), which is dated at 80–60 ka. Although $CaCO_3$ stage IV morphology seems extreme for a deposit of this age, carbonate accumulation was likely accentuated by the position of the deposit at the base of a bedrock hillslope.

Bedrock is overlain by a colluvial deposit (unit 8, pl. 9) containing a weak argillic (Bt) soil horizon. The unit was deposited on an eroded, irregular surface, resulting in a varying thickness. On the basis of soil development and stratigraphic position, unit 8 is dated at late Pleistocene and is correlated with either unit Qa3 or Qa4 (table 20).

The uppermost deposits (units 9, 10) are composed of mixed colluvium and eolian silt. Soil development within these deposits is minimal, consisting of a fairly thin vesicular A (Av) horizon with $CaCO_3$ stage I morphology. On the basis of soil development, units 9 and 10 are tentatively dated at early Holocene through latest Pleistocene and are correlated with unit Qa5 (table 20).

Structure

Trench SCF–T4 (pl. 9; fig. 2) exposes two fault zones (stas. 5, 10.5 m, pl. 9), both of which are about 1 m wide and contain laminar and massive carbonate and brecciated and silicified tuff. The eastern fault zone separates welded tuff

(to the east) from nonwelded tuff (to the west), whereas the western fault zone separates nonwelded tuff from colluvial deposits on the hanging wall. The dips of these two fault zones (65° and 85° W.) indicate that they probably merge at shallow depth (10–15 m below the ground surface), and that the western fault zone likely splays subvertically from a west-dipping bedrock fault. Mid-Quaternary to late Quaternary activity is evidenced by at least three subvertical fissures separating the western fault zone from the hanging-wall deposits; one of these fissures is truncated by, and therefore predates, the upper petrocalcic horizon. No definitive evidence of Quaternary activity was observed along the eastern fault zone.

The largest fissure exposed in trench SCF–T4 (sta. 10.5 m, pl. 9) contains abundant basaltic ash and is cut by carbonate-filled fractures. The fractures may have formed contemporaneously with the most recent faulting event that is apparent at trench T8, but no radiometric ages are available to corroborate such a correlation. No offset was detected on these fractures in the trench. The basaltic-ash-filled fissure at station 10.5 m (pl. 9) widens upward from about 10 cm at the floor of the trench to about 20 cm at its uppermost extent. This fissure is overlain by a small colluvial wedge (unit 7) deposited against the fault zone on a backwasting scarp on the hanging wall. Similarities with the ash-filled fissures exposed at other trench sites along the Solitario Canyon Fault indicate that all of the fissures formed during the same faulting event.

The displacement associated with the ash-filled fissure in trench SCF–T4 (pl. 9) is not directly measurable, because no displaced units can be matched across the fault; however, the offset can be estimated from the maximum thickness of the unit 7 colluvial wedge (15–30 cm, depending on the amount of erosional backwasting into the fissure), the fissure width (10–20 cm), and the vertical separation (10–25 cm) of the base of units 8 through 10. The colluvial wedge provides a minimum estimate of the vertical offset; here, no erosional beveling of the footwall is evident, and so the wedge thickness may closely approximate the actual vertical offset. The upward widening of the ash-filled fissure and east-dipping fractures indicates deformation and tilting of the hanging wall, contributing uncertainty to estimates of offset based on fissure widths. Although each of these lines of evidence is relatively weak by itself, they all indicate dip slip of 20 to 40 cm (event Y, table 22).

A narrow (≤10 cm wide), well-cemented fissure (sta. approx 10.5 m, pl. 9) bounds the west side of the ash-filled fissure and cuts the upper petrocalcic horizon (units 5, 6). This fissure, which is truncated by erosional backwasting into the ash-filled fissure, is inferred to have formed during the same faulting event as that which created the second-largest fissures in trenches T8 and SCF–T3. Although the offset associated with this event is not measurable, the fissure width indicates an offset of about half that associated with the ash-filled fissure.

Fault relations observed in trench SCF–T4 (pl. 9), as well as the relatively small fault scarps along this segment of the Solitario Canyon Fault, indicate that the displacements here are much less than those displayed at the other trench sites. Estimated cumulative dip slip, based on the apparent downthrow of units 5 and 6, is 60 to 80 cm during mid-Quaternary to late Quaternary time (table 22). At least three episodes of earlier faulting are also indicated in the trench exposure, but data are insufficient for estimating displacements. A substantial structural discontinuity along the Solitario Canyon Fault exists between trenches SCF–T4 and T8, about where the Iron Ridge Fault splays off from the main fault trace (Day and others, 1998a). This discontinuity may have inhibited northward propagation of some ruptures and arrested some smaller events.

Trench SCF–T2

Trench SCF–T2 (pl. 10; fig. 2) was excavated across a scarp in an eroded remnant of hillslope colluvium at the base of the large west-facing escarpment formed by the Iron Ridge Fault, the main eastern splay of the Solitario Canyon Fault. The Iron Ridge Fault trends toward, and may extend far enough to intersect, the Stagecoach Road Fault to the south (Simonds and others, 1995). The trench was excavated to evaluate the paleoseismic history of the Iron Ridge Fault and thereby to assess the fault as a possible link between the Solitario Canyon and Stagecoach Road Faults.

Stratigraphy

Trench SCF–T2 exposes hillslope and fault-scarp colluvium downthrown against welded tuff of the Topopah Spring Tuff (pl. 10). The lowermost colluvial deposit (unit 1) is well cemented by silica and carbonate ($CaCO_3$ stage III–IV morphology). The deposit is exposed only near the bottom of the trench and is therefore difficult to examine in detail, but it appears to contain a buried soil horizon that was downthrown and remained relatively undeformed. Carbonate-filled fractures (2–3 cm wide) are truncated at the top of this deposit, indicating a substantial age difference with the overlying deposits. On the basis of extensive soil development and stratigraphic position, unit 1 is dated at probably early Pleistocene and is correlated with the oldest Quaternary deposits (unit Qa1, table 20) generally present in the Yucca Mountain area (figs. 1, 2).

Unit 1 (pl. 10) is overlain by colluvial deposits that thin markedly to the west, downslope from the fault; these deposits, especially the lower ones, are composed of at least some fault-scarp debris deposited in response to surface displacement along the Iron Ridge Fault. Unit 2 and the lower part of unit 3 have only moderate carbonate accumulation ($CaCO_3$ stage II morphology), whereas most of unit 3 and all of unit 4 contain a well-developed petrocalcic horizon ($CaCO_3$ stage III–IV morphology) that continues downslope into the overlying deposits. Units 2 through 4 are buried by hillslope colluvium (units 5, 6) that reflect a period of regrading and smoothing of the hillslope; units 4 and 5 are erosionally truncated. On the basis of soil development, units 2 through 6 are dated at middle Pleistocene or older (probably >500 ka) and are also

correlated with the oldest Quaternary deposits (unit Qa1, table 20) generally present in the Yucca Mountain area (figs. 1, 2).

Unit 7 (pl. 10), the uppermost deposit containing a strong petrocalcic horizon, also thins markedly downslope (pl. 9). The deposit may be composed of fault-scarp colluvium, but it is so eroded that its origin is obscure. Unit 7 is dated at middle Pleistocene or older and is also correlated with unit Qa1.

Units 8 and 9, which unconformably overlie units 4 through 7, are hillslope colluvial deposits that further regrade the slope and display noticeably less soil development than the underlying deposits. On the basis of carbonate accumulation ($CaCO_3$ stage II+ morphology), units 8 and 9 are dated at late Pleistocene and are tentatively correlated with unit Qa4 (table 20).

The uppermost deposits in trench SCF–T2 (units 10, 11, pl. 10) are composed of mixed colluvium and eolian silt. These deposits, especially unit 11, were disturbed during excavation in the western part of the trench. Soil development consists of a vesicular A (Av) horizon, a cambic (Bw) horizon, and $CaCO_3$ stage I morphology. Units 10 and 11 are dated at latest Pleistocene to early Holocene and are correlated with unit Qa5 (table 20).

Structure

Trench SCF–T2 (pl. 10; fig. 2) exposes a relatively narrow fault zone composed largely of laminar silica and carbonate deposits. Where it cuts unit 1, the fault zone is only partly exposed but appears to be about 60 cm wide; where it cuts units 2 through 4, it is about 30 cm wide. In addition to the main fault zone, a 2-m-wide fracture zone within the hanging wall is also exposed. Although stratigraphic relations are obscured by carbonate overprinting, the exposure provides at least general constraints on Quaternary activity along the Iron Ridge Fault.

A 2- to 3-cm-wide extensional opening (sta. 1.4 m, pl. 10) within the main fault zone extends with uniform width to at least 1-m depth (the limit of its exposure) and is filled with silt and fragmented carbonate. This feature could represent a minor faulting event (dip slip, possibly 5–10 cm) of probable Holocene age. Fractures in the uppermost deposits (units 10, 11) and a possible small scarp (approx 10 cm high) indicate that this faulting event postdates the youngest exposed deposits. Units 10 and 11, however, are composed largely of eolian silt, which is dynamic under wet/dry cycles; the observed fracturing could therefore be a secondary effect not directly related to faulting.

Direct evidence of offsets associated with mid-Quaternary to late Quaternary activity along the main Solitario Canyon Fault trace is absent. Only fractures and possible minor offsets, including the silt-filled opening discussed above, cut the petrocalcic horizon formed in units 3 and 4 (pl. 10). The apparent step in unit 9 (sta. approx 3.3 m, pl. 10) appears to be erosional because the fracture across it does not appear to displace lower, older features. The petrocalcic horizon in units 3 through 7 closely grades to the bedrock hillslope above the trench, and so large displacements subsequent to the formation of this soil horizon probably did not occur.

The most significant Quaternary fault activity evident in trench SCF–T2 (pl. 10) predates the petrocalcic horizon in units 3 through 7 and therefore is dated at middle Pleistocene or older. The colluvial-wedge deposits (units 2–4) and soil relations (petrocalcic horizon superimposed on both fault-scarp and hillslope colluvium) provide possible evidence that the observed fault displacement occurred as an episode of elevated activity, rather than as long-term, recurrent activity. The displacement involved can only be approximated; erosional truncation of cemented deposits on the downthrown side of the fault indicates a possible displacement of about 2 m. Preevent displacements of about 70 cm may also have occurred, on the basis of the apparent thicknesses of units 2 through 4, but the stratigraphic relations are too obscure for reliable estimates. Still-older activity is indicated by the wider fault zone and carbonate-filled fractures within unit 1, but the exposure is too limited for dating or estimating displacement.

Summary of Mid-Quaternary to Late Quaternary Activity on the Solitario Canyon Fault

The trenches examined during this study indicate a sequence of mid-Quaternary to late Quaternary surface-rupturing paleoearthquakes on the Solitario Canyon Fault that are manifested primarily as extensional fissures filled with gravel, silt, and basaltic ash. At least two, possibly as many as four, faulting events displace alluvial and colluvial gravel ranging in age from a few hundred thousand years to almost 1 Ma, indicating that the mid-Quaternary to late Quaternary activity was preceded by a fairly lengthy hiatus in seismicity.

The central trenches (T8, SCF–T3, SCF–T1) expose a largely singular fault trace, with an average strike of about N. 5° E. and a dip of 50°–60° W. Predominantly normal dip slip has displaced bedrock that is extensively exposed in the area (Tiva Canyon and Topopah Spring Tuffs of the Paintbrush Group) by an estimated maximum displacement of about 500 m (Day and others, 1998a). A subordinate component of left-lateral slip is indicated by bedrock striations in various places along the fault trace (rakes generally ranging from 50° to 70°; Simonds and others, 1995), but no evidence was observed as to whether these striations represent Quaternary displacements.

In the shallow exposures afforded by the trenches, Quaternary surface ruptures appear primarily as subvertical fissure openings that sole into a dipping bedrock fault plane. Secondary silica and carbonate accumulations along fractures and within fissure-fill material form a flaring-upward zone of laminar and massive carbonate and cemented gravel. The largest mid-Quaternary to late Quaternary fissuring events are clearly defined by gravel infilling within the

fault zone; earlier fissuring events are difficult to recognize because of carbonate overprinting. Additional minor fissuring is indicated by small displacements and (or) fracturing.

Total displacements associated with mid-Quaternary to late Quaternary activity on the Solitario Canyon Fault are not directly measurable because no offset stratigraphic markers can be reliably matched across the fault zone; only the uppermost, unfaulted deposits are present on both sides of the fault. However, offsets can be estimated from the downthrow of hanging-wall deposits, the vertical separation of erosional unconformities, and fissure widths (table 20). For example, offsets can be estimated from the fault dip and horizontal extension inferred from fissure widths, on the basis of the simple geometric model shown in figure 33. For the relatively large, ash-filled fissure exposed in trench T8 (fig. 31), which has mostly planar walls and a uniform width to where it narrows against the bedrock fault (indicating minimal hanging-wall deformation), this method yields a reasonably accurate dip-slip estimate of 1.1 to 1.3 m. Where fissures narrow and do not extend to the bedrock fault plane, however, uncertainties are relatively large.

Continuity of the fault scarp through trenches T8, SCF–T3, and SCF–T1 indicates that these trenches record similar faulting histories; the record of mid-Quaternary to late Quaternary surface ruptures within each trench appears to be reasonably consistent, at least for the largest faulting events. Minor surface breaks associated with moderate ($M \leq 6.5$) earthquakes are typically discontinuous (for example, dePolo, 1994); any smaller faulting events are thus unlikely to correlate between trenches. At trench SCF–T4 (pl. 9), on the northern section of the Solitario Canyon Fault, the two largest mid-Quaternary to late Quaternary surface ruptures appear to correlate with events on the central section of the fault, but only carbonate-filled fractures provide any possible evidence for smaller events. Preliminary observations in trench SCF–E1 (fig. 2), an excavated natural wash exposure across the southern section of the Solitario Canyon Fault, indicates that displacement is substantially less there than along the central section of the fault, confirming similar observations based on a relatively small scarp in mid-Quaternary deposits. The mid-Quaternary to late Quaternary activity along the Solitario Canyon Fault does not correlate with activity along the Iron Ridge Fault.

Sequence of Faulting Events

The following outline of the sequence of faulting events (youngest to oldest) on the Solitario Canyon Fault is based largely on the geologic relations observed along the south wall of trench T8 (fig. 31), where the most complete record of mid-Quaternary to late Quaternary surface ruptures is exposed and the largest offsets occurred. We emphasize that such observations and interpretations apply only to a limited section of this 18-km-long fault and are not necessarily characteristic of its entire extent. Individual faulting events are correlated between trenches as the available evidence permits.

Fracturing Events

Two fracturing events postdate the most recent well-defined faulting event (Z, table 22). The youngest fracturing event is indicated by silt-filled fractures exposed in trenches T8, SCF–T3, and SCF–T2, but no associated fault displacement is distinguishable at any of these sites. The absence of carbonate accumulation in these deposits indicates a Holocene age. A somewhat earlier fracturing event is evidenced by a silica- and carbonate-filled fracture in trench T8 that cuts all cemented deposits, including those that overlie and postdate event Z. Although similar fracturing was not observed at the other trench sites, conditions were unfavorable for preserving such evidence. The origin of the fractures is uncertain; they could have been caused by moderate earthquakes on the Solitario Canyon Fault, or they may be related to earthquakes on other nearby or regional faults. Alternatively, they could have a nontectonic origin (for example, bioturbation), although similar fractures exposed in washes throughout eastern Crater Flat are spatially associated with known Quaternary faults (Ramelli and others, 1989).

Event Z

The most recent, well-defined episode of fault displacement (event Z, table 22) is expressed in trench T8 (figs. 31, 32) by carbonate-filled fractures that cut the basaltic-ash-filled fissure (represented by event Y), by ash dragged along the fault, and by a narrow (10–15 cm wide) silt- and ash-filled fissure exposed in the north trench wall of the trench (fig. 32). On the basis of the geometry shown in figure 33, these features indicate an offset of 10 to 20 cm during this faulting event, conceivably reflecting afterslip associated with event Y, but interpreted to have occurred during a subsequent faulting event. The presence of ash may be interpreted to indicate that event Z was associated with eruptive activity at the nearby Lathrop Wells volcanic center, but considering the age of the ash associated with event Y, reworking of ash into this younger fissure is a more reasonable explanation.

In trenches SCF–T3, SCF–T1, and SCF–T4, possible evidence for event Z is in the form of carbonate-filled fractures that crosscut and (at trenches SCF–T3 and SCF–T4) appear to disturb the conspicuous ash-filled fissures, but no displacements are discernible. In trench SCF–T1, a small colluvial wedge deposited against the main fault zone (unit 17; sta. 10.5 m, pl. 8) and the loose silt- and gravel-filled zone within the main fault zone could relate to event Z, but soil development in the overlying, unfaulted deposits is probably older. Event Z is not apparent at trench SCF–T2, located on the Iron Ridge Fault. Various expressions of event Z among the trench sites indicate displacements ranging from 0 to 20 cm, probably averaging 10 cm.

An average U-series age of 15.5±4.3 ka on fracture-filling carbonate (sample HD 1071, table 21) associated with the dragged ash provides a possible minimum date for event Z. Although a maximum date is difficult to define, the event

probably postdates the secondary carbonate (sample HD 1070) within the event Y fissure (U-series age, 27–56 ka). Event Z is dated at 40–20 ka (preferred value, 30–20 ka).

Event Y

The four trenches across the Solitario Canyon Fault expose conspicuous fissures containing abundant basaltic ash. At each site, these ash-filled fissures represent the largest mid-Quaternary to late Quaternary surface ruptures and exhibit similar characteristics; they are therefore assumed to represent a single faulting event, penultimate event Y, which is expressed at trench T8 as a conspicuous 60- to 70-cm-wide fissure with planar walls. On the basis of a simple geometric model (fig. 33), that assumes rigid behavior of the hanging-wall block, the displacement associated with event Y is dip slip of 1.1 to 1.3 m (0.9–1.1 m of vertical displacement).

Event Y probably created the two conspicuous ash-filled fissures in trench SCF–T3 (fig. 34). Although the absence of offset stratigraphic markers makes any direct measurement of displacement difficult, the cumulative fissure width (30–60 cm) is interpreted to indicate a possible dip-slip displacement of 0.6 to 1.2 m (table 22). The uppermost value (1.2 m) may be an overestimate because the wider openings at the top of the fissures could be accentuated by tilting. Vertical separation (0.6–1.0 m) of the top of the petrocalcic horizon indicates cumulative mid-Quaternary to late Quaternary dip slip of 0.8 to 1.3 m.

Event Y is represented in trench SCF–T1 (pl. 8) by three ash-filled fissures in the hanging wall, two of which are subvertical, whereas the third is a minor, low-angle splay that dips into the south wall of the trench at an apparent angle much lower than its true dip. The cumulative width of the three ash-filled fissures is difficult to determine, especially considering the low-angle inclination of the third fissure, but is estimated at 25 to 50 cm, indicating dip slip of 40 to 80 cm. Owing to subsequent erosion, vertical separation of the former ground surface is not measurable.

Event Y is expressed in trench SCF–T4 (pl. 9) by a single ash-filled fissure whose width (10–20 cm) indicates a relatively small displacement (20–40 cm, table 22). Vertical separation of the assumed former ground surface and thickness of a colluvial wedge apparently associated with this faulting event yield similar estimated displacements.

At all the trench sites, ash-filled fissures are by far the most conspicuous surface ruptures cutting well-cemented alluvial and colluvial gravel ($CaCO_3$ stage III–V morphology). At trenches SCF–T1 and SCF–T3 (fig. 2), these gravel deposits are extremely well cemented ($CaCO_3$ stage V morphology), and a U-series age of 950±140 ka from trench SCF–T3 (sample HD 1726, table 21) indicates that the deposits may be as old as 1 Ma. Considerably less cementation of the gravel deposits was observed in trenches T8 and SCF–T4, and at least in trench T8 these deposits are probably no older than about 200 ka, on the basis of correlation with unit Qa3 (tables 2, 20).

A date of several tens of thousands of years before present for event Y (table 8) is indicated by a fairly well developed soil in the upper part of a fissure fill in trench T8 (figs. 31, 32) and in a cobbly-silt deposit capping the fissure. Thin silica and carbonate laminae are spaced throughout the upper 1 m of these deposits. U-series ages of 27–56 ka on secondary carbonate (sample HD 1070, table 21) and 114–124 ka on fracture-filling carbonate (sample HD 1072) provide minimum and maximum dates, respectively, for event Y. The closest approximation is considered to be the age of the basaltic ash, which is correlated with an eruption of the nearby Lathrop Wells volcanic center (fig. 1) at 77±6 ka (Heizler and others, 1999).

Event X

In trench T8, a relatively small faulting event is indicated by an apparent gravel-filled fissure sandwiched between events W and Y fissures (sta. 3.5 m, fig. 31). This well-cemented feature has a jumbled fabric, distinguishing it from the adjacent alluvial deposit (unit 9, fig. 31). A narrow gravel-filled fissure in trench SCF–T4 (pl. 9) may also reflect event X but is considered to be more likely related to event W, which is a larger and more pronounced feature at both trenches T8 and SCF–T3. Event X is problematic at trenches SCF–T3 and SCF–T1 but cannot be precluded at either site. Little information is available to constrain the offset associated with this possible faulting event; the width (approx 15 cm) of the apparent fissure in trench T8 approximates a dip-slip displacement of 20 to 30 cm. An average U-series age of 118±6 ka (sample HD 1072, table 21) on fracture-filling carbonate from trench T8 provides an apparent close minimum date for event X.

Event W

Event W is evidenced by fairly conspicuous fissures in trenches T8 (stas. 3.5–4 m, fig. 31) and SCF–T3 (sta. 5.5 m, fig. 34). The fissure in trench T8 extends as a narrowing-downward feature into older fault-zone carbonate in the western part of the fault zone. The fissure in trench SCF–T3, which is crosscut by the ash-bearing event Y fissure, contains silt, gravel, and minor basaltic ash; the presence of ash could reflect an episode of faulting and volcanism predating event Y, although the ash in the event W fissure could have been contaminated with event Y ash. The gravel-filled fissure bounding the west side of the ash-filled fissure in trench SCF–T4 probably also formed during event W. The date of event W is constrained by the estimated age (150–250 ka) of the deposits in trench T8 that were displaced by the faulting event, and by the average U-series age (118±6 ka) of the fissure fill apparently associated with event X.

Early Quaternary to Mid-Quaternary Hiatus in Seismicity

Well-cemented to extremely well cemented alluvium or colluvium is present at or very near the ground surface on the downthrown side of the Solitario Canyon Fault at all of the trench sites across it. The petrocalcic horizon within these

deposits is closely graded to the bedrock hillslope above the fault, indicating that before the mid-Quaternary to late Quaternary activity discussed above, little, if any, surface offset occurred over a period spanning several hundred thousand years. The U-series ages from trench SCF–T3 indicate that any significant earlier fault activity probably predates 900 ka.

Earlier Faulting

Despite the lengthy early Quaternary to mid-Quaternary hiatus in seismicity along the Solitario Canyon Fault, evidence does exist for earlier surface displacements. Precise ages and an event sequence for this earlier fault activity, however, are not definable from the available information. The fault activity indicated by the evidence described below should be considered a minimum for any activity that predates the sequence of mid-Quaternary to late Quaternary faulting events on the Solitario Canyon Fault.

Trenches T8 and SCF–T3 expose a well-developed fault zone that existed before mid-Quaternary to late Quaternary time, along which older gravel deposits (unit Qa1, tables 2, 20) are juxtaposed against bedrock. The main fault zone is an upward-thickening wedge separating the zone of vertical fissures from the bedrock fault plane. Evidence of individual events within the fault zone at these sites is largely obliterated by extensive silica and carbonate accumulation.

A gravel-filled fissure exposed in the south wall of trench T8 (sta. 2 m, fig. 31) indicates an earlier faulting event similar in magnitude to event W (table 8). The materials filling this older fissure are highly fractured and cut by 1- to 2-cm-thick silica veins but are not noticeably displaced. Similar, though less distinct, fractures were discerned within the fault zone in trench SCF–T3 (fig. 34). The degree of secondary silica and carbonate accumulation indicates a relatively early date for event W.

Earlier fault activity is best expressed in trench SCF–T1 (pl. 8), where the lowermost gravel deposits (units 1–4) are faulted and backtilted across a wider fault zone than that which cuts the overlying deposits (units 5–8). Trench SCF–T4 exposes evidence of at least three earlier faulting episodes, including a fissure capped by the upper petrocalcic horizon (possibly the same event as that recognized in trenches T8 and SCF–T3) and by an apparent colluvial wedge cut by that fissure.

The pre-late Quaternary fault activity on the Solitario Canyon Fault significantly predates eruptive activity at the nearby Lathrop Wells volcanic center (fig. 1); therefore, not all the Quaternary activity on the fault is explainable by the postulated association of faulting and volcanic activity for event Y.

Recurrence Intervals and Fault-Slip Rates

The occurrence of three or four faulting events over a time period of about 200 k.y. (presumed age of faulted deposits correlated with surficial unit Qa3 in trench T8) indicates an average recurrence interval of 50–70 k.y. during mid-Quaternary to late Quaternary time. A recurrence interval of about 35 k.y. is considered to be a minimum (two faulting events since the eruption of the Lathrop Wells volcanic center at 77±6 ka). A maximum recurrence interval of about 100 k.y. is indicated if only the two most definitive (and largest) faulting events (W, Y, table 8), are averaged over the 200-k.y. time period.

The average slip rate (dip slip) along the Solitario Canyon Fault during mid-Quaternary to late Quaternary time is estimated at 0.01 to 0.02 mm/yr, considering averages of 2.0 m of slip over 200 k.y. and 1.2 m of slip over 75 k.y. Averaging the fault slip over the past 900 k.y. (U-series age of faulted colluvium in trench SCF–T3) indicates a longer-term average slip rate of 0.002 to 0.003 mm/yr.

Possible Volcanically Related Fault Activity

The largest fissures at all four trench sites along the main Solitario Canyon Fault trace contain abundant basaltic ash. Historical-earthquake deformation shows that extensional openings begin to fill with detrital material during the first significant rainfall and invariably contain noticeable fill within weeks to months of fissuring. Angularity of the basaltic ash in the bottom of the fissure in trench T8 indicates minimal transport and, therefore, implies a local source, most likely the Lathrop Wells basaltic cone located 11 to 16 km to the south (fig. 1), dated at 77±6 ka (Heizler and others, 1999). The mixed silt, ash, and gravel in the upper fissure fill of trench T8 indicates that after the ash was largely depleted from the ground surface, the fissure filled more slowly with eolian material (silt and additional reworked ash) as debris washed in from upslope. Soil development and stratigraphic correlation support a late Pleistocene age for the fissure fill.

A cogenetic link between seismicity and volcanism was previously suggested by Swadley and others (1984), on the basis of the presence of ash in trench exposures across four different faults in the Yucca Mountain area, including trench T8 (fig. 2). The ash deposits exposed in older trenches were observed only in narrow (0.2–2 cm wide) vertical fractures, whereas the ash exposed in newer trenches across the Solitario Canyon Fault more definitively establishes a temporal association between seismicity and volcanism and indicates both more fault slip and a greater volume of ash than could be inferred from the older trenches.

Basaltic ash intermixed with silt is present in smaller fissures that both predate (trench SCF–T3, fig. 34) and postdate (north wall of trench T8, fig. 32) the conspicuous ash-filled fissures; these deposits may indicate additional faulting events of coincident surface rupture and volcanism, although reworking of ash from the large ash-filled fissures cannot be precluded. Apparent temporal clustering of faulting events in mid-Quaternary to late Quaternary time (see chap. 14), in combination with an apparent association of seismicity and

volcanism, is therefore considered as evidence that the pulse of mid-Quaternary to late Quaternary activity on the Solitario Canyon Fault is genetically linked with volcanic activity at the Lathrop Wells volcanic center (fig. 1).

Discussion

Structural and stratigraphic relations exposed in trenches across the Solitario Canyon Fault and elsewhere in the Yucca Mountain area (figs. 1, 2) are complicated by extensive carbonate overprinting and by relatively small surface offsets that are difficult to measure. Colluvial wedges (material shed from and deposited against fault scarps), which are commonly observed in trench exposures of normal faults, are generally absent in all the trenches. Three principal factors likely contribute to the paucity of colluvial wedges. First and foremost, surface displacements have occurred largely as extensional openings of steep fissures splaying from a dipping bedrock fault plane. Scarp erosion, backwasting, and deposition after such events must first fill the fissures; only after the fissures have been filled can colluvial wedges be formed. Second, surficial erosion after a faulting event is evident at all of the trench sites, as indicated by missing soil horizons and truncated fissures and stratigraphic contacts, and so colluvial wedges could be partly removed. In all the trenches, deposits of unit Qa5 (table 20) rest on these unconformities, indicating that appreciable erosion occurred during latest Pleistocene to early Holocene time. Third, small (≤0.5 m) vertical displacements are not conducive to formation of obvious colluvial wedges.

The information gained from the trenches across the Solitario Canyon Fault allows preliminary interpretations of surface rupture, but relatively large uncertainties preclude confident conclusions about fault offsets. The varying displacements do not support characteristic fault behavior (that is, recurrent faulting events with similar rupture distributions and offsets). Single-event displacements range from fracturing with no obvious displacement to possibly more than 1 m of slip associated with the largest fissuring event; most of the offsets are relatively small (no more than a few tens of centimeters). Similarly, limited geochronologic data indicate that faulting events have not occurred over regularly spaced time intervals. The apparent early Quaternary to mid-Quaternary hiatus in seismicity further indicates noncharacteristic behavior and contributes uncertainty to forecasting future fault activity. A conservative seismic-hazard assessment would be that we are still within a period of "elevated" activity and that the mid-Quaternary to late Quaternary record better reflects possible fault activity in the near future than does the entire Quaternary record.

Rather than behaving independently, some or all of the faults at Yucca Mountain may rupture together during individual seismic events or sequences (see chap. 14). Such distributive surface ruptures may be expected, on the basis of the high degree of fault interconnection and the presence of basaltic ash in fractures along multiple faults. Thus, the faults around Yucca Mountain can be considered to constitute one or more complex fault systems, rather than numerous independent faults. Uncertainties in age control and fault relations, however, likely will always limit how well seismic events can be correlated between faults. Also, it may be difficult to correlate small earthquakes on different faults, or even along individual fault traces. As evidenced by historical surface ruptures, small displacements commonly are highly discontinuous; such faulting events may cause significant offsets in some places but little or no offset in others. With regard to the Solitario Canyon Fault, one of its main splays, the Iron Ridge Fault, does not contain ash deposits or display evidence of displacement during the large penultimate event Y (table 8). Offset did occur, however, during earlier events that may coincide with earthquakes on other segments of the Solitario Canyon Fault.

Chapter 8

Quaternary Faulting on the Fatigue Wash Fault

By Jeffrey A. Coe, John Oswald, Giovanni Vadurro, and Scott C. Lundstrom

Contents

Abstract 111
Introduction and Setting 111
Methods 112
    Measurement of Scarp Profiles 112
    Logging of Trenches 112
Results 112
    Scarp Profiles 112
    Stratigraphy, Soils, and Age Constraints in Trenches CF1 and CF1A 112
    Structure Exposed in Trenches CF1 and CF1A 118
Paleoseismic Interpretations from Trench Data 119
    Event Z 119
    Event Y 119
    Event X 122
    Event W 122
    Event V 122
    Pre-Event V Deformation 122
Paleoseismic Interpretations from Scarp Data 122
Slip Rates and Recurrence Intervals 124
Faulting and Volcanism 124
Acknowledgments 124

Abstract

Studies of trenches excavated across the south-central section of the Fatigue Wash Fault in Crater Flat, and of scarp profiles near the trenches, provide evidence for five or more surface-rupturing paleoearthquakes on the fault since the middle Pleistocene. Trenches CF1 and CF1A expose a 3-m-thick sequence of alluvial gravel, colluvial wedges, eolian silt, and at least two well-developed silica- and carbonate-cemented soils. The main fault in trench CF1 ranges from 0.35 to 1.40 m in width and is characterized by two fissure fills and a carbonate-engulfed shear zone. The presence of basaltic ash in the youngest colluvial wedge and fissure fill indicates that one Quaternary faulting event correlates with an eruption of the nearby Lathrop Wells volcanic center at 77±6 ka.

Questionable fracturing of surficial deposits as young as 9±1 ka represents the most recent paleoseismic event (Z) on the Fatigue Wash Fault. A 20- to 40-cm offset on a surficial deposit with a minimum age of 17 ka may also have occurred during event Z. Penultimate event Y, which postdates the Lathrop Wells eruption, may be as young as 38±4 ka, whereas the next-older event (X) is dated by the eruption. Vertical displacement ranges from 18 to 35 cm for event Y and from 25 to 42 cm for event X. Event W predates the eruption but is dated at <102+42/−15 ka; displacement was 35 to 63 cm. One or more earlier faulting events that are also evident in trench exposures may be older than 400 ka.

Cumulative displacements measured on scarps formed in surficial deposits dated at older than 400 ka range from 1.3 to 2.8 m, indicating a long-term slip rate of 0.003 to 0.007 mm/yr on the Fatigue Wash Fault. Cumulative vertical displacement resulting from the four most recent faulting events (W–Z) in trench exposures is approximately 1.4 m but only 0.4 m after correction for local tilting of trench units. Net cumulative displacement, taking into account the tilting of surficial deposits and a strike-slip component of movement, is 0.6 m. That much offset within the past 102+42/−15 k.y. indicates an average slip rate of 0.004 to 0.007 mm/yr. Recurrence intervals range from 30 to 140 k.y. for the four latest faulting events.

Introduction and Setting

The Fatigue Wash Fault is a down-to-the-west, dip- to oblique-slip fault about 2.5 km west of the west edge of the proposed repository site for the storage of high-level radioactive wastes at Yucca Mountain (see chap. 3; fig. 2). To the northwest, the fault lies at the base of the prominent west flank of Jet Ridge before terminating near the prow of Yucca Mountain (Scott and Bonk, 1984; Simonds and others, 1995; Day and others, 1998b). The fault bifurcates about the midpoint of Jet Ridge to form a saddle in West Ridge. The splay that cuts West Ridge connects with the Windy Wash Fault on the west side of West Ridge. To the south, the Fatigue Wash Fault continues along the east edge of Crater Flat and appears to merge

with the Southern Windy Wash Fault just south of trenches CF2 and CF3 (fig. 2). Quaternary slip along the Fatigue Wash Fault has been documented in alluvial gravel deposits between its south and north intersections with the Windy Wash Fault (Simonds and others, 1995). Slickensides on bedrock fault planes range in rake from 14° to 70° (Scott and Bonk, 1984; Simonds and others, 1995). Slip indicators in Quaternary deposits were not observed.

In the early 1980s, trench CF1 (fig. 2) was excavated across a prominent west-facing scarp in surficial gravel along the central section of the Fatigue Wash Fault. The trench was oriented perpendicular to the fault on the sideslope of a modern channel, and Swadley and Hoover (1983) and Swadley and others (1984) provided a log of the principal stratigraphic and soil relations on the north wall. In 1992, trench CF1 was deepened about 1 m, and a shallow trench (CF1A, fig. 35) was excavated about 10 m to the south to expose the youngest units along the fault that had been disturbed or removed during the excavation of trench CF1. In 1995, scarp profiles were measured near both trenches and at localities to the north where the fault cuts lower to upper Pleistocene alluvium. This chapter summarizes the Quaternary paleoseismic history of the fault as interpreted from scarp profiles and detailed logs of exposures in trenches CF1 and CF1A, and supersedes a preliminary interpretation by Coe and others (1995).

Methods

Measurement of Scarp Profiles

A total of seven topographic profiles (SP1–SP7, table 24) were measured across the west-facing scarp of the Fatigue Wash Fault near trench CF1 (fig. 35): five (SP1–SP5) on the unit 1 surface (fig. 35), one (SP6) on the units 1–3 surface, and one (SP7) on the units 3–4 surface. Six of the profiles (SP1–SP6) were measured by using an electronic surveying instrument (total station), and one profile (SP7) was measured by hand, using a measuring tape and hand level. Measurements of scarp height, surface offset, and maximum scarp-slope angle were calculated from plots of these profiles according to the methodology and nomenclature (fig. 36) of Bucknam and Anderson (1979) and Machette (1989).

Logging of Trenches

Trenches were logged by field and close-range photogrammetric methods (see chap. 1 for details) in 1994. Lithologic units were described by using standard sedimentologic terminology, and soil-horizon descriptions follow the nomenclature of Birkeland (1984) and Machette (1985). Paleoearthquakes were identified on the basis of offset units across the fault, colluvial wedges or fault fissures, and the upward termination of fractures. U-series and thermoluminescence analyses were used to date lithologic units, soil horizons, and surface ruptures. Dating methods are described in chapter 2, and estimated ages of samples collected in the trenches are listed in table 23.

Results

Scarp Profiles

The seven scarp profiles (SP1–SP7) measured along the Fatigue Wash Fault are shown in figures 37*A* through 37*G*, respectively, and surface offsets and scarp heights are listed in table 24. All scarps are west facing and are interpreted to reflect dip- or oblique-slip movement. Some scarps are formed in surficial deposits of different ages (fig. 35), which we infer to provide a maximum age for a given scarp. Except for the two scarps along profile SP7, all scarps involve unit 1 alluvial deposits (fig. 35). Profiles SP3 through SP5 are entirely on unit 1, whereas profiles SP1 and SP2 start and end on unit 1 but cross a footslope colluvial deposit (unit cf, fig. 35). Profile SP6 crosses from unit 1 to units 1 through 3. On profile SP7 (fig. 37*G*), the Fatigue Wash Fault splays into two parallel traces, along each of which is a scarp (SP7a, SP7b) formed in units 3 and 4. Interpretations regarding the relations between scarp locations and surficial deposits, and implications with respect to the timing of faulting events, are discussed below in the section entitled “Paleoseismic Interpretations from Scarp Data.”

Stratigraphy, Soils, and Age Constraints in Trenches CF1 and CF1A

Trenches CF1 and CF1A (pl. 11) expose a sequence of alluvial gravel deposits (units 1, 2, 2a, 3, 4, 4a, table 25A), colluvial wedges (units 5, 6), eolian sand (unit 8), and hybrid/transitional deposits (units 2b, 4b, 7a, 7b). Alluvial gravel and eolian sand are present on both the upthrown and downthrown blocks of the fault, but colluvial wedges only on the downthrown block. Units 1 through 4 consist of moderately well sorted to well-sorted sandy gravel with sporadic cobbly lenses (units 2a, 4a). In general, these alluvial deposits are more poorly sorted on the upthrown than on the downthrown block. Processes controlling the deposition of units 2b and 4b are uncertain. Both units have sandy- to cobbly-gravel textures, are moderately well to well sorted, and thicken close to the fault. The texture indicates an alluvial origin, whereas the thickening indicates a colluvial origin. The preferred interpretation is that these units are composed of alluvial gravel that has been eroded locally to resemble wedges. Unit 5 consists of cobbly sand, interpreted to be a proximal-debris-facies colluvial wedge (Nelson, 1992). Unit 6 consists of silty sand containing basaltic ash; the unit is interpreted to be a colluvial wedge deposited predominantly by slopewash. The unit is closely associated with a fissure fill (2, pl. 11) in the fault zone that contains abundant basaltic ash. Unit 7a is U-shaped in cross section, is present only at the fault, and is poorly sorted;

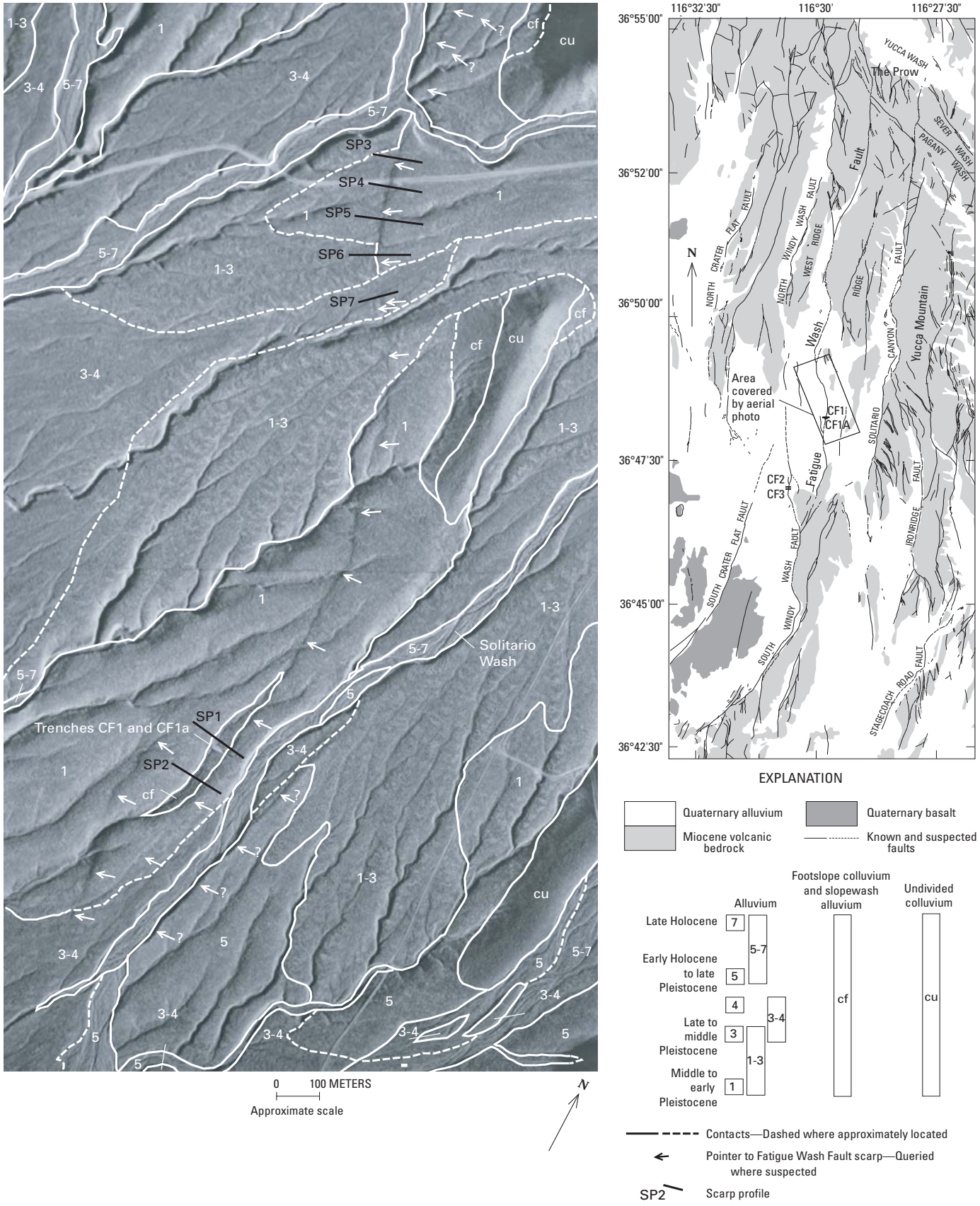

Figure 35. Distribution of surficial deposits in the vicinity of trenches CF1 and CF1A across the Fatigue Wash Fault in the Yucca Mountain area, southwestern Nevada (pl. 11; figs. 1, 2, 35), showing locations of topographic profiles SP1 through SP7 across west-facing scarp of fault.

Table 23. Numerical ages of deposits exposed in trenches CF1 and CF1A across the Fatigue Wash Fault in the Yucca Mountain area, southwestern Nevada.

[See plate 11 and figures 1, 2, and 35 for locations. Samples: TL–12 (error limit, ±2σ), thermoluminescence analysis by S.A. Mahan; HD (error limits, ±2σ), U-series analyses by J.B. Paces; TSV–386, TSV–387, U-series analyses by Szabo and O'Malley (1985); U5, U6, U-series analyses by Peterson and others (1995)]

Trench (pl. 11)	Sample	Unit and material sampled	Estimated age (ka)
CF1A	TL–12	8, buried Av soil horizon	9±1
CF1	HD 1608	1, clast rind	>401, >307
	HD 1610	5, clast rinds (inner, middle, outer)	65±4, 79±3, 325±21, 329±117, 331±10, 449±35, 447±46
	HD 1611	7, laminar K soil horizon	38±4, 172±7, 189±7
	HD 1612	7, laminar K soil horizon	102±2, 107±2, 111±1, 112±2, 116±2, 119±2, 125±1, 128±5, 169±3, 269±9
	HD 1729	5, laminar K soil horizon and clast rind	89±1, 93±1, 102±2, 115±2, 141±1
	TSV–386	Carbonate in fault-zone fill	27±3
	TSV–387	4, laminar carbonate	33±4
	U5	3, carbonate rind on clast	36±2
	U6	4, laminar horizon	60±1

Table 24. Data on topographic profiles across the west-facing scarp of the Fatigue Wash Fault near trench CF1 in the Yucca Mountain area, southwestern Nevada.

[See plate 11 and figures 1, 2, and 35 for locations and figure 36 for definitions of parameters]

Profile (fig. 37)	Surface offset (m)	Scarp height (m)	Scarp slope angle (°)
SP1	0.6	1.2	9.0
SP2	.4	1.5	9.8
SP3	.9	1.6	8.4
SP4	1.3	2.0	12.0
SP5	2.0	2.8	8.3
SP6	1.6	2.0	11.0
SP7a	.4	.8	5.2
SP7b	.2	.3	4.4

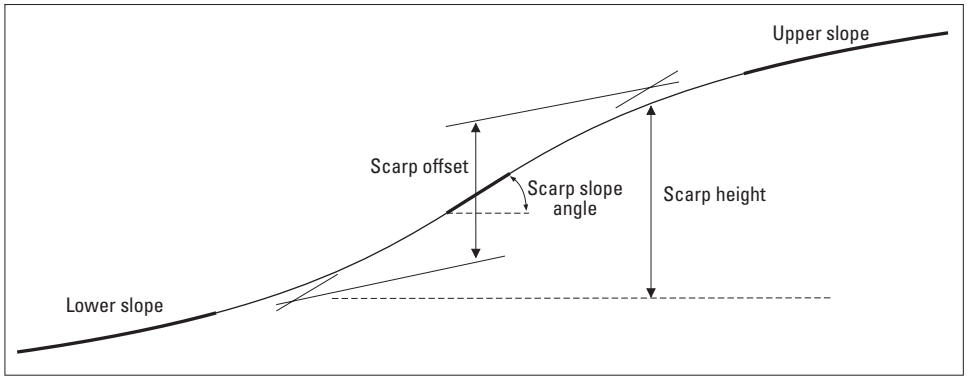

Figure 36. Schematic cross section illustrating parameters measured for topographic profiles (fig. 35; table 24). Adapted from Bucknam and Anderson (1979) and Anderson and others (1995).

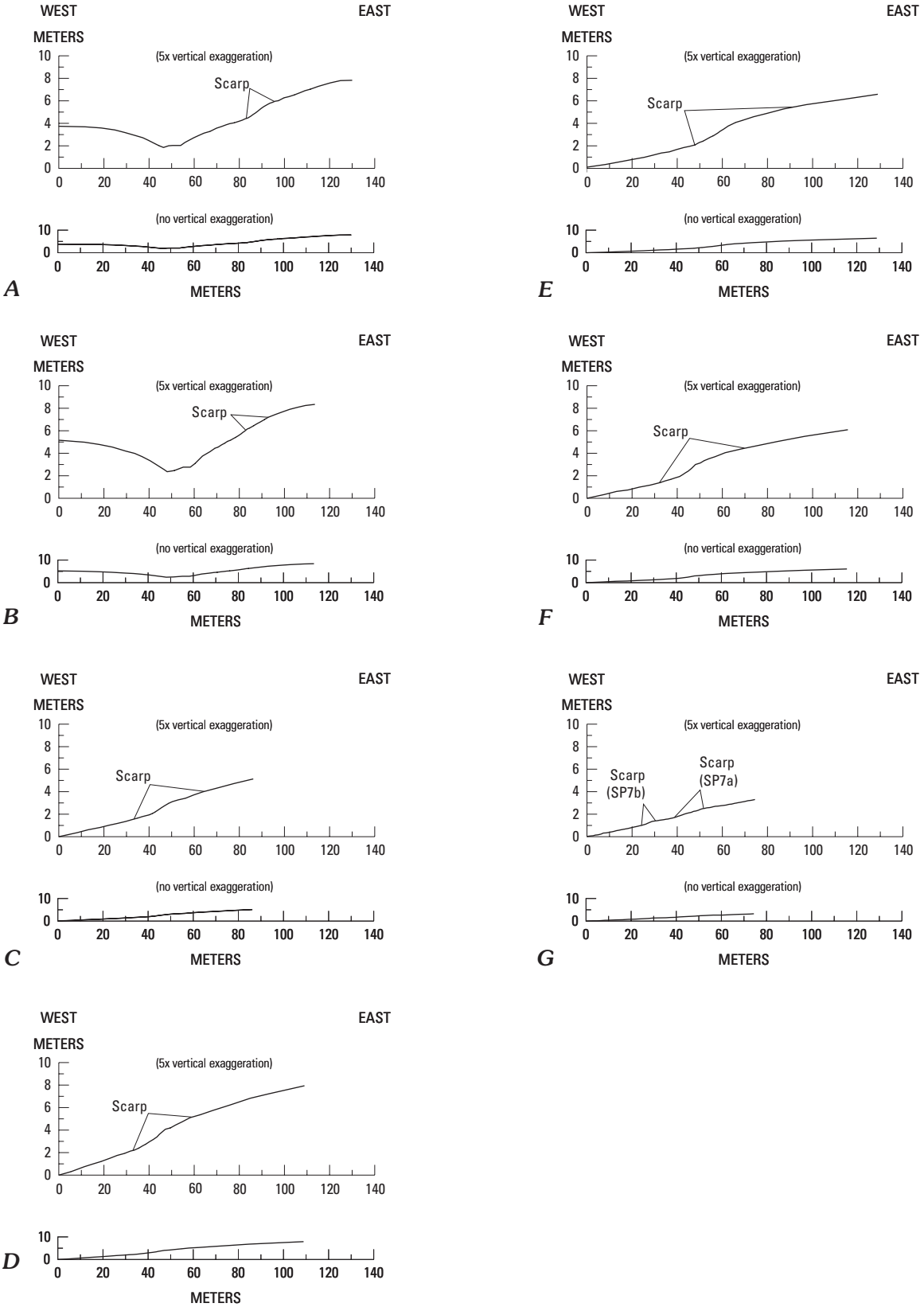

Figure 37. Topographic profiles SP1 through SP7 (*A*–*G*) across west-facing scarp of the Fatigue Wash Fault in the Yucca Mountain area, southwestern Nevada (pl. 11; figs. 1, 2, 35). Profile SP7 shows two discrete scarps interpreted to be two separate fault strands.

Table 25A. Summary of characteristics of lithologic units exposed in trench CF1 across the Fatigue Wash Fault in the Yucca Mountain area, southwestern Nevada.

[See plate 11 and figures 1, 2, and 35 for locations. Position: FW, footwall; HW, hanging wall. General lithology, listed in order from most to least abundant: bld, boulder; cbl, cobble; pbl, pebble; slt, silt; snd, sand. Matrix: c, coarse; f, fine; m, medium; masked, obliterated by pedogenic carbonate; pbl, pebble; slt, silt; snd, sand; vc, very coarse; vf, very fine. Cementation: CO_3, carbonate; ind, indurated; mod, moderate; non, uncemented; Si, silica; stg, strong; vstg, very strong; wk, weak. Deformation: EW_x, event wedge, with event designation; F, faulted; f, fractured; FF, fault fissure; U, unfaulted. n.a., not applicable]

Unit/ subunit	Position	General lithology	Clast size (cm)	Matrix	Cementation	Thickness (cm)	Shape	Deformation
1	FW	pbl cbl snd bld	<50	f-c snd	CO_3 mod	avg 100–>125	Tabular --------	F
2	FW	pbl cbl snd	<20	f-c pbl	CO_3 wk-mod	40–130	Lenticular tabular.	F
3	FW	pbl cbl snd w/minor bld	<40	pbl	CO_3 mod-stg	50–80	Tabular --------	F
4	FW	pbl cbl	<20	m snd	CO_3 stg	35	do ----------	F
4a	FW	pbl snd	<1	f-c snd	CO_3 mod	0–50	Lenticular	F
8	FW	snd pbl slt	<5	snd	CO_3 wk	20	Tabular --------	U
2	HW	pbl cbl snd	<40	f-m snd	CO_3 wk-mod	<160	do ----------	F
2a	HW	cbl pbl snd bld	.2–50	f-vc snd	CO_3 wk-mod	0–50	Lenticular -----	F
2b	HW	cbl pbl snd bld	.2–50	f-vc snd	CO_3 wk-mod	0–50	Wedge ---------	$EW_{w?}$, F
3	HW	pbl cbl snd	<25	snd w/minor slt	CO_3 w/Si mod-stg	60–70	Tabular --------	F
4	HW	pbl snd cbl w/minor bld	<50	f snd	CO_3 capped by Si vstg	0–100	Wedge ---------	F
4a	HW	cbl pbl snd	.2-50	f-vc snd	CO_3 mod-stg	0–30	Lenticular -----	F
4b	HW	pbl snd w/ minor cbl	<10	m snd	CO_3 mod	0–50	Wedge ---------	F
5	HW	snd cbl pbl w/minor bld slt	<30	slt-snd	CO_3 capped by Si stg	0–40	do ----------	EW_x,F
6	HW	snd pbl slt w/ minor cbl	.2–30	slt-snd	CO_3 stg	0–30	do	EW_x,F
7a	HW	snd slt pbl w/ minor cbl	<15	slt-snd	CO_3 wk	0–40	Irregular krotovina/ scour fill.	f
7b	HW	snd slt pbl w/ minor cbl	<15	slt-snd	CO_3 wk	0–30	Irregular wedge.	EW_Y, f?
8	HW	snd pbl slt	<20	slt-snd	CO_3 wk-mod	20–30	Tabular --------	f?
Shear zone	Fault zone	fines	<12	fines	CO_3 stg	max 25	Fissure ---------	FF, F
Fissure fill 1	Fault zone	pbl cbl snd	<15	snd	CO_3 stg	70–100	do ----------	FF, F
Fissure fill 2 (ash)	Fault zone	pbl snd cbl slt	<10	slt-snd	CO_3 wk	10–60	do ----------	FF, f

Table 25B. Descriptions of topographic profiles across the west-facing scarp of the Fatigue Wash Fault near trench CF1 in the Yucca Mountain area, southwestern Nevada.

[See plate 11 and figures 1, 2, and 35 for locations. See table 3 for soil-horizon terminology; prefixed numbers refer to differentiated soil horizons with increasing depth, and suffixed numbers to further differentiation of properties within an individual soil horizon. Colors from Munsell Soil Color Charts (Munsell Color Co., Inc., 1992). Texture: l, loam; s, sand; slt, silt. Structure—grade: 1, weak; 2, moderate; m, massive; sg, single grain—size: c, coarse; f, fine; m, medium—type: abk, angular blocky; pl, platy; sbk, subangular blocky. Consistence—dry: eh, extremely hard; h, hard; lo, loose; sh, slightly hard; so, soft; vh, very hard—wet: po, nonplastic; so, nonsticky. CO_3 stage morphology from Birkeland (1984). Effervescence in cold dilute HCl: e, some; em, moderate; eo, none; es, strong; ev, very strong; vse, very slight. Cementation—strength: ci, indurated; cs, strong; cw, weak—type: cont, continuous; disc, discontinuous. Lower horizon boundary—distinctness: a, abrupt; c, clear; g, gradual—topography: i, irregular; s, smooth; w, wavy. Roots—abundance: 1, few; 2, common—size: f, fine; m, medium; vf, very fine—location: disp, dispersed; frc, fractures; thruout, throughout. Pores—abundance: 3, many—size: f, fine; vf, very fine—shape: thruout, throughout; v, vesicular. Rhizoliths—abundance: 1, few—size: clast, clast faces; vf, very fine. n.a., not applicable; n.o., not observed. See table 24 for data on topographic profiles]

Soil horizon	Depth (cm)	Associated unit	Color		Gravel (vol pct)	Texture	Structure	Consistence		$CaCO_3$ stage	Effervescence (HCl)	Cementation	Lower horizon boundary	Roots	Pores	Rhizoliths	Fine fraction of total (<2 mm) (vol pct)	$CaCO_3$ in fine fraction (wt pct)
			Wet	Dry				Dry	Wet									
Profile SP1																		
Avk	0	8	10YR 5/4	10YR 7/3	10	slt l	2 vf-m sbk	so	so po	n.a.	es	n.o.	a s	1 f-m thruout	3 vf-f v thruout	n.o.	n.a.	6.1
Bk	14	8	10YR 5/4	10YR 7/3	40	slt l	1 vf-f sbk	sh	so ps	I–II	em	n.o.	a w	1 vf-f disp	n.o.	n.o.	.55	7.5
2Kqmb1	17	4a	10YR 8/3	10YR 8/1	40	n.a.	m-1 f pl	eh	n.a.	IV	es-ev	ci cont CO_3	c w	n.o.	n.o.	n.o.	.16	16.4
3Kqmb1	34	4	10YR 8/2	10YR 8/1	80	n.a.	m	eh	n.a.	III+	ev	ci cont CO_3	c i	n.o.	n.o.	n.o.	.09	23.8
4Bkb1	65	3	10YR 8/3	10YR 8/1	80	n.a.	sg-1 f-m abk	lo-vh	n.a.	I–III	eo-es	cw disc CO_3	c-g w	1 vf disp	n.o.	n.o.	.18	15.1
5Bkb1	130	2	10YR 7/2	10YR 8/1	90	n.a.	sg	lo-sh	n.a.	II+	es	?cw disc CO_3	c i	1 vf-f disp	n.o.	n.o.	.21	15.9
6Bkb2	167	1	10YR 7/3	10YR 7/2	90	sl	1 vf-c abk	h	so po	II–III	ev	cs disc CO_3	n.o.	1 vf-m disp	n.o.	n.o.	.51	23.9
Profile SP2																		
Av	0	8	10YR 4/3	10YR 6/3	5	slt l	1 vf-m sbk	so	so po	n.a.	eo-vse	n.o.	c s	2 vf-co thruout	3 vf-f v thruout	n.o.	0.71	3.4
Bk1	10	8	10YR 5/4	10YR 7/3	5–10	slt l	1-2 f-vc sbk	so-sh	so po	I–II	es	n.o.	c w	2 vf-co thruout	3 vf-f v thruout	n.o.	68	6.7
Bk2	26	7	10YR 5/5	10YR 7/3	25–30	slt l	2 f-m sbk	vh	so po	II	es	n.o.	a w	1-2 vf-m disp	n.o.	n.o.	.49	9.9
2Kqmb1	35	4	10YR 7/2–7/3	10YR 8/1	50–75	n.a.	m-1 f-c sbk	eh	n.a.	IV	es-ev	ci CO_3/SiO_2 cont	c-g w	1 vf frc	n.o.	n.o.	.18	40.6
3Bkqmb1	110	3	10YR 7/3 CO_3 5/7 Si	10YR 8/1 CO_3 6/4 Si	70–80	n.a.	1 vf-c sbk	sh-vh	so po	II–III	em-es eo for SiO_2	cw-cs disc CO_3/SiO_2	c-g w	1 vf-m disp	n.o.	1 vf clast	15	11.4
4Bkb1	150	2	10YR 5/3–4	10YR 7/3–2	80	s l	sg	lo	so po	I–III–	em-es	n.o.	c-g w	1 vf-f disp	n.o.	1 vf clast	.21	12.4
5Bkb1	210	2a	10YR 7/2–7/3	10YR 8/1	– –	sls	m1m abk	so po	h-vh	II	em-es	n.o.	cw	1 vf-f disp	n.o.	1 vf clast	.12	14.1
6Bkb1	260	2	10YR 5/3–4	10YR 7/3–2	80	s l	sg	lo	so po	I–III–	em-es	n.o.	n.o.	1 vf-f disp	n.o.	1 vf clast	.23	8.9

it is interpreted to be a channel or burrow fill. Unit 7b, which is present only on the hanging wall, contains platelets of silica and carbonate from the underlying soil in a younger matrix of silty sand; the unit is interpreted as a hybrid deposit formed by both pedogenic and eolian processes.

Unit 1 is present only in the hanging wall of the Fatigue Wash Fault. Units 2 through 4 have been correlated across the fault on the basis of similar gross lithologies and sedimentologic textures, but some correlations are problematic. Unit 2, for example, consists primarily of well-sorted pebbly gravel on the downthrown block of the fault but of more poorly sorted cobbly gravel on the upthrown block immediately adjacent to the fault. In support of this correlation, unit 2 laterally grades to well-sorted pebbly gravel away from the fault on the upthrown block and to cobbly gravel near the fault on the downthrown block. The correlation of unit 4 across the fault is equally problematic because the upper part of the unit on the south wall of trench CF1 (above unit 4a on the downthrown block) is absent on the upthrown block. We interpret the missing section to have been removed by erosion, as evidenced by the unconformity between unit 8 and units 4 and 4a on the upthrown block.

Two well-developed carbonate soils are exposed on the upthrown block of the Fatigue Wash Fault in trench CF1 (pl. 11). The upper parts of the younger of these two soils (soil profile 1, pl. 11, table 25B) have a $CaCO_3$ stage III–IV morphology, and the older soil (soil horizon 6Bkb2) has up to $CaCO_3$ stage III morphology. The upper parts of both soils were stripped by erosion before deposition of the immediately overlying units; the unconformity on top of unit 1 and soil horizon 6Bkb2 is especially conspicuous. A similar sequence of soils is also present on alluvial deposits on the downthrown block (soil profile 2, pl. 11).

On the basis of observed stratigraphic and structural relations and chronology (table 23), the following interpretations and conclusions relate to the estimated ages of the deposits and soils (in ascending order) exposed in trenches CF1 and CF1A:

1. U-series estimated ages of secondary silica immediately adjacent to clasts from soil horizon 6Bkb2 (soil profile 1, south wall, trench CF1, pl. 11) indicate that this soil horizon was developed on unit 1 before 400 ka (J.B. Paces, written commun., 2000).
2. The only age obtained for units 2 and 3 is 36±2 ka (sample 1–JWB–1–YM–35–U5; sample U5, table 23), a relatively young age that likely reflects the latest cycle of silica and carbonate infiltration into these deposits rather than being a valid representation of their depositional age, which, on the basis of the ages assigned to the overlying and underlying units (unit 1, min ~400 ka; unit 4, max ~150 ka), would appear to be much older.
3. The estimated age of unit 4 is 102+42/−15 ka, based on a statistical combination of the five ages listed for sample HD 1729 (table 23). The younger ages obtained on samples TSV–387 (33±4 ka) and 1–JWB–1–YM–35–U6 (60±1 ka; sample U6, table 23) are also considered to reflect one or more late cycles of silica and carbonate infiltration that postdate the depositional age of the unit.
4. In view of the ages assigned to unit 4 below and unit 6 above, the maximum and minimum ages for unit 5 are 102+42/−15 ka and 77±6 ka (age of fissure fill 2, pl. 11), respectively. U-series analyses of silica- and carbonate-rich rinds on a boulder from unit 5 (sample HD 1610, table 23) yielded seven ages, of which only the two youngest ages (65±4 ka, 79±3 ka) are close to the maximum age of unit 6, whereas the five older ages (ranging from 325±21 to 474±46 ka) may date rind layers (intermediate and inner layers) that coated the boulder when it was part of an older deposit.
5. No ages were obtained for unit 6, at least part of which appears to have been deposited nearly contemporaneously with the development of fissure fill 2, which contains ash erupted from the nearby Lathrop Wells volcanic center (fig. 1). The age of this ash (77±6 ka) establishes a maximum age for the unit, which consists of a colluvial wedge that also contains basaltic ash. Away from the fault zone, fissure fill 2 terminates at the base of unit 6, but associated fractures continue upsection from the fissure fill through unit 6 to the base of unit 7b. A minimum age for unit 6 cannot be established, but it may be >38±4 ka (see below).
6. Ages ranging from 38±4 to 269±9 ka were obtained on materials collected from unit 7 (that is, unit 7b; samples HD 1611, HD 1612, table 23). The older ages do not appear to provide a reliable estimated depositional age, inasmuch as the unit clearly postdates the eruption of the Lathrop Wells basaltic cone (fig. 1). Also, unit 7b contains plates of older carbonate-cemented soil reworked upward into an eolian matrix that may be dated at 38±4 ka, which is the youngest age obtained on sample HD 1611. A minimum age is represented by sample TL–12, dated at 9±1 ka (see below).
7. Sample TL–12, collected from the south wall of trench CF1A (pl. 11), indicates an age of 9±1 ka for unit 8.

In terms of the standard stratigraphic sequence of surficial deposits in the Yucca Mountain area, trench unit 1 probably correlates in time with unit Qa1 (tables 2, 20), units 2 and 3 with units Qa2 and Qa3, units 4 through 6 with unit Qa3, unit 7 with unit Qa4, and unit 8 with Qa5 (see chap. 2; fig. 3). A discrepancy exists between the age of unit 4 (102+42/−15 ka, equivalent to unit Qa3), exposed on the upthrown block of the fault (pl. 11), and that of unit Qa1 (early to middle Pleistocene), mapped on the upthrown block at the surface (fig. 35)—that is, our trench data indicate that in the immediate vicinity of the fault there is a surficial mantle equivalent in age to unit Qa3. We believe that this mantle exists, but because of its limited extent, it cannot be discriminated on the aerial photograph in figure 35.

Structure Exposed in Trenches CF1 and CF1A

The main fault zone in trench CF1 (fig. 35) ranges from about 35 to 140 cm in width and is characterized by two fissure fills and a shear zone engulfed with carbonate (pl. 11). The main fault zone strikes N. 10° E. and dips from

80° E. to 80° W. The carbonate shear zone is primarily in the upthrown block and is probably the progressive result of multiple faulting events. The oldest fissure fill (1, pl. 11) consists of cobbly sand containing preferentially aligned clasts indicative of filling processes. The fissure fill, which truncates units 2, 3, 4, and 4a on the downthrown block, appears to contain a small amount (<1 volume percent) of basaltic ash when viewed under a binocular microscope, but the ash is not readily visible in the trench exposure. This older fissure fill is truncated by a more conspicuous fissure fill (2, pl. 11) containing as much as 40 volume percent basaltic ash, with a Th content of 7.2 ppm, consistent with that of ash deposits originating from the Lathrop Wells basaltic cone (fig. 1; J.B. Paces, written commun., 1995). Fissure fill 2 terminates at the base of unit 6 (north and south walls of trench CF1, pl. 11), above which are zones of vertical extension fractures continuing upward to the base of unit 7b or 8 on the hanging wall, although the fracturing relations are difficult to interpret in detail because of dense accumulations of secondary carbonate.

Units 2, 3, 4, and 4a on the downthrown block are backrotated by the main fault zone about 5°–8° down to the east (trench CF1, pl. 11), and units 3 and 4 also are locally tilted toward the fault on the upthrown block; all the units appear to be rotated by the same amount. Away from the fault zone on both the upthrown and downthrown blocks, these units slope 3°–5° W., indicating that 8°–13° of backrotation has taken place on the downthrown block since the deposition of unit 4. No obvious fracture or fault that may have resulted from this backrotation is exposed on the downthrown block. One possible candidate is the fracture exposed closest to the west end of trench CF1. This fracture is at the position where the units begin to "roll over" (change dip direction) toward the fault, but it appears to be extensional; however, shear displacement may have occurred at depth.

Several sets of extension fractures, in addition to or including some of those discussed above, can be defined on the basis of their distinct stratigraphic levels of termination (pl. 11). Fractures in the first and oldest set terminate at the top of unit 1 on the upthrown block. Fractures in the second set, which includes only two poorly defined members, terminate between the base and middle of unit 4 on the downthrown block. Fractures in the third set terminate at the top of unit 4 (also the youngest carbonate soil horizon) on the downthrown block. Several fractures in this set "flower," or split into multiple splays, near the top of unit 4. Two faulting events are indicated by early shear and late extensional movement along one of the fractures in this set—that is, the third fracture from the west end of trench CF1 (on the south wall) underwent early shear movement that displaced unit 2a before the deposition of unit 3, and then had later extensional deformation that cut units 3 and 4. Fractures in the fourth set, which is poorly defined with only three members exposed in trench CF1A, terminate at the base of unit 6. The fifth and youngest set is represented by questionable fractures in units 7b and 8 (fig. 38).

Paleoseismic Interpretations from Trench Data

Trench data provide evidence which is interpreted to indicate that five or more surface-rupturing paleoearthquakes have occurred on the Fatigue Wash Fault since the middle Pleistocene. Vertical displacements resulting from individual faulting events (as measured at the fault and not corrected for tilting or rotation) range from 0 to 63 cm (table 26). The sequence of faulting events (Z to pre-V), as well as other possible events, is characterized below in order from youngest to oldest. We estimate vertical displacements and, where available, net cumulative displacement after restoration of locally tilted units. Because of the steep dip of the fault, the vertical displacements are nearly the same as dip-slip displacements. Net cumulative displacement is not estimated for individual faulting events, but the total net cumulative displacement is used to calculate slip rates.

Event Z

Questionable fracturing of units 7b and 8 (fig. 38) in trench CF1A (pl. 11), with a maximum date of <9±1 ka (sample TL–12, table 23), is interpreted to represent the latest paleoseismic event (Z) on the Fatigue Wash Fault. Such an event may correlate with the latest faulting event observed on the nearby Windy Wash Fault, which is dated at 3–2 ka (see chap. 9).

Event Y

The youngest faulting event (Y) observed in trenches CF1 and CF1A (pl. 11; fig. 35) is evidenced by the down-to-the-west displacement of unit 6. Additional evidence is provided by fractures that terminate at the base of unit 7b (for example, see log of south wall of trench CF1, pl. 11). Event Y thus postdates the deposition of unit 6 and predates the deposition of unit 7b. The relation of unit 6 to unit 7a, however, is problematic. Our interpretation is that a scarp was created and served as a zone of weakness, which was then utilized by a fluvial channel and (or) a burrowing animal, resulting in the deposition of unit 7a. Fractures in that unit also terminate at the base of unit 7b (fig. 38). Although a major influx of carbonate into the Fatigue Wash Fault zone has been dated at 27±3 ka (sample TSV–386, table 23; south wall of trench CF1, pl. 11), this carbonate rind is interpreted to represent an older deposit because of the fracture relations just described. Unit 7b, as well as the lower part of unit 8, may reflect post-event Y aggradation on the downthrown block; only the upper part of unit 8 is present on the upthrown block.

The estimated displacement of unit 6 (and underlying units) by event Y is based on the assumption that the top of unit 6 was once at the same elevation as the top of unit 4a on the upthrown block. The tops of units 4a and 6 (pl. 11) are also

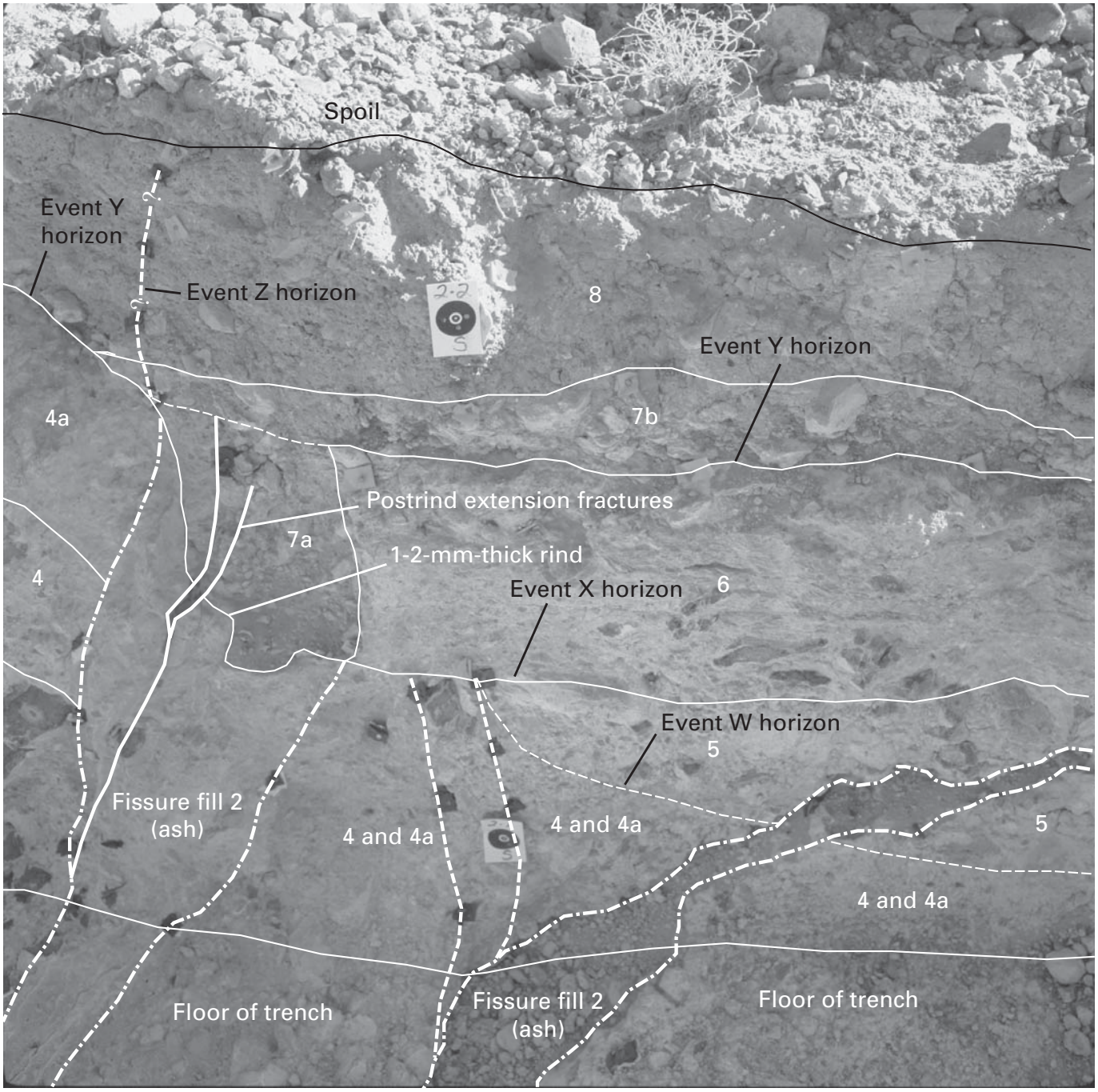

Figure 38. Stratigraphic units and faulting-event horizons exposed on south wall of trench CF1A across the Fatigue Wash Fault in the Yucca Mountain area, southwestern Nevada (pl. 11; figs. 1, 2, 35). Dark spots along some lines are markers that were emplaced to facilitate mapping.

Table 26. Estimated vertical displacements on the Fatigue Wash Fault in trenches CF1 and CF1A in the Yucca Mountain area, southwestern Nevada.

[See plate 11 and figures 1, 2, and 35 for locations. Event horizons are shown in figures 38 and 39. All values are west-side-down displacement unless otherwise noted; minimum (min), maximum (max), and preferred (pref) values are considered most reasonable because they take into account measurement error and uncertainties in locations of contacts. ?, stratigraphic constraints not available]

Event	Event horizon (figs. 38, 39	Dip (vertical) displacement (cm)												Best estimate of dip (vertical) displacement (cm)	Evidence	Comments
		South wall, trench CF1			North wall, trench CF1			South wall, trench CF1A			North wall, trench CF1A					
		min	max	pref	min	max	pref	min	max	pref	min	max	pref			
Z	Top of unit 7a (possibly as high as unit 8).	0	0	0	0	0	0	0	0	0	0	0	0	0	Questionable fractures that terminate in trench units 7b and 8.	No shear displacement observed along fractures in trenches. Event occurred after deposition of unit 7a.
Y	Top of unit 6.	11	28	18	13	28	21	11	30	24	7	52	35	25±10	Down-to-the-west displacement of massive carbonate soil (top of unit 4a on footwall to top of unit 6 on hanging wall); fractures that terminate at top of units 6 and 7a on the hanging wall.	Event occurred after deposition of unit 6, development of most of the massive carbonate soil (b1).
X	Base of unit 6.	32	?	32	42	?	42	33	?	33	25	?	25	42	Development of fissure fill 2, containing basaltic ash, and nearly contemporaneous deposition of unit 6.	Maximum thickness of unit 6 used for preferred displacement value.
W	Base of unit 5.	44	?	44	63	?	63	35	?	35	37	?	37	63	Deposition of unit 5, a colluvial wedge, and development of fissure fill 1; fractures that terminate at top of unit 4.	Maximum thickness of unit 5 used for preferred displacement value.
V	Base of unit 2b.	[1]19	?	35	0	?	63	?	?	?	?	?	?	54	Down-to-the-east displacement of unit 2a on fault just east of soil profile II on the south wall of trench CF1. Top of unit 2 at this site is not displaced. Change in sorting of unit 2 across main fault. Possible wedge deposit (unit 2b at main fault in trench CF1, pl. 11; fig. 39).	Event occurred during deposition of unit 2. Preferred separation calculated by using maximum height of unit 2b at the fault, minus any down-to-the-east separation of unit 2a just east of soil profile II. Maximum thickness of unit 2b minus down-to-the-east displacement used for preferred displacement value.
Pre-V deformation	Top of unit 1.	?	?	?	?	?	?	?	?	?	?	?	?	?	Multiple fractures that terminate at the top of unit 1 on the footwall.	Evidence for distinguishing individual events and associated displacements not observed.

[1]Down-to-the-east-displacement.

at the top of the youngest carbonate soil. A down-to-the-west step on top of this soil is clearly visible at the fault in all four trench-wall exposures. The preferred vertical distance (measured at four trench walls) of this step ranges from 18 to 35 cm (table 26). Our preferred vertical displacement for event Y at the trench sites is 25±10 cm. Event Y is dated between the age of fissure fill 2 (77±6 ka) and the age of unit 7b, which may be as old as 38±4 ka.

Event X

Evidence for event X consists of the development of fissure fill 2 (pl. 11; fig. 39), which contains abundant basaltic ash (max 40 volume percent), and the nearly contemporaneous deposition of parts of unit 6, which also contain basaltic ash, as a sedimentary wedge on the downthrown side of the fault. As stated earlier, segments of the fissure fill terminate at the base of unit 6, but poorly defined fractures continue upward through the unit. Displacement caused by event X is considered to be commensurate with the thickness of unit 6 as measured on the various trench walls. On the basis of these measurements, our best estimate of the vertical displacement caused by event X is 42 cm (table 26). The basaltic ash in fissure fill 2 has been dated at 77±6 ka (Heizler and others, 1999), which is considered to closely represent the date of event X.

Event W

Fissure fill 1 (pl. 11; fig. 39), deposition of a coarse-grained alluvial wedge (unit 5), and a well-defined set of extension fractures terminating at the base of unit 5 all provide evidence for the next-older surface-rupturing event (W) on the Fatigue Wash Fault. On the basis of measurements of the thickness of unit 5 in trenches CF1 and CF2 (fig. 35), the preferred vertical displacement is 63 cm (table 26). Given that unit 5 was deposited before fissure fill 2, the minimum date of event W is >77±6 ka, and the maximum date is <102+42/−15 ka, which is the age assigned to underlying unit 4.

The offset of trench units 2 through 4 (pl. 11; fig. 39), as observed in trenches CF1 and CF1A (fig. 35), reflects the combined effect of events W through Y. The total estimated displacement resulting from these faulting events is represented by the thicknesses of units 5 and 6, the down-to-the-west step at the top of unit 6, and the estimated thickness of deposits that were eroded off the top of units 4 and 4a before being buried by younger materials. This estimated thickness, however, is uncertain because the upper part of unit 4 is exposed only on the downthrown block. In view of this uncertainty, we believe that a reasonable approximation of the total displacement resulting from events W through Y is represented by the offset that is measurable by using the top of unit 3 on the walls of trench CF1 (pl. 11) as a datum. The vertical separation of this datum across the fault zone is about 1.4 m. This offset would indicate that about 10 cm of unit 4 was eroded off the upthrown block before the deposition of unit 5 (140 cm minus 130 cm for the combined thickness of units 5 and 6, and the down-to-the-west step at the top of unit 6; table 26).

Event V

Three lines of evidence are interpreted to indicate that a still-earlier faulting event (V) occurred during the deposition of unit 2 (pl. 11; fig. 39): (1) the wedge-shaped geometry of unit 2b on the north wall of the trench indicates a fault-derived unit (see Nelson, 1992); (2) the sorting of unit 2 changes drastically from the upthrown block, where it ranges in composition from well-sorted pebbly gravel to poorly sorted cobbly gravel, to the downthrown block, where it consists of well-sorted pebbly gravel interbedded with coarse lenses of channel gravel; and (3) one of the coarse lenses on the downthrown block is offset antithetically, down to the east, whereas the top of unit 2 directly above the lens shows no offset. On the basis of the maximum height of unit 2b minus the down-to-the-east displacement along the fracture near the west end of the trench, our best estimate for the vertical displacement from event V is 54 cm. The timing of this event is constrained between the minimum age of unit 1 (~400 ka) and the estimated age of unit 4 (102+42/−15 ka).

Pre-Event V Deformation

Multiple fractures that terminate at the top of unit 1 are evidence of a possible older event(s) exposed by trench CF1 (pl. 11; fig. 35). Because unit 1 is not exposed on the downthrown block, displacement caused by pre-event V deformation is indeterminable. Such an event(s) is dated at older than 400 ka.

Paleoseismic Interpretations from Scarp Data

As discussed above, the seven scarps that were studied along the trace of the Fatigue Wash Fault (fig. 35) were not all formed in the same surficial deposits. The latest faulting event recorded by any of the scarps is along profile SP7 (fig. 37*G*), where two small scarps (7a, 7b, table 24) on separate fault strands involve units 3 and 4 (fig. 35). The latest faulting event represented by these scarps thus postdates the deposition of this unit and so may be younger than at least the minimum age of unit 3 (34 ka; see chap. 2; fig. 3) and, possibly, even the minimum age of unit 4 (17 ka). Correlations of these surficial deposits with units exposed in trenches CF1 and CF1A (pl. 11; fig. 35) indicate a temporal equivalence with either unit 6 or unit 7b, or both. Although the evidence is equivocal, our preferred interpretation is that the 0.2-m offset on profile SP7b reflects event Z and the 0.4-m-offset on profile SP7a reflects both event Z and, possibly, event Y and (or) older faulting events.

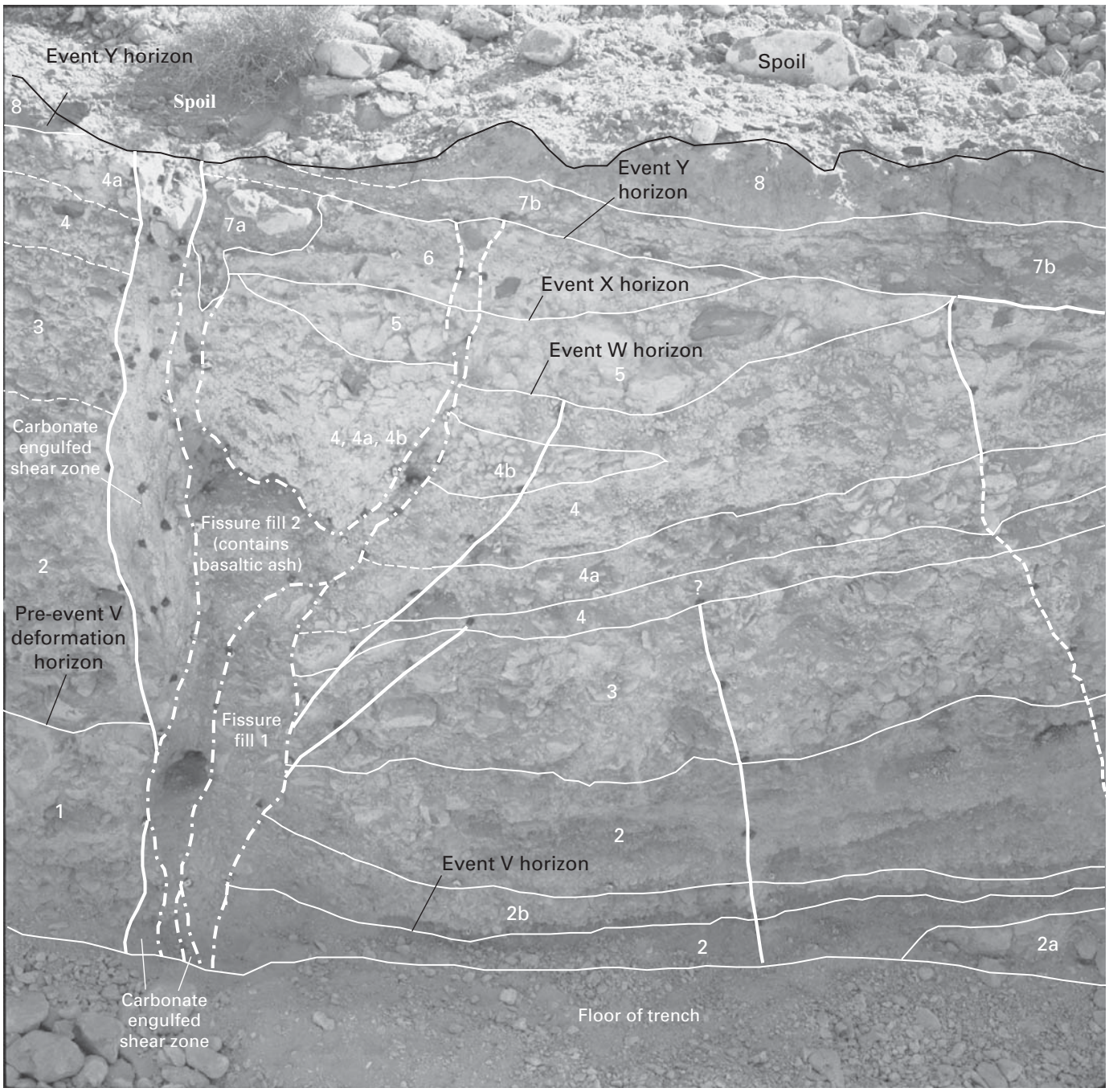

EXPLANATION

Fissure boundary

Fracture—Dashed where approximately located

Lithologic-unit boundary—Dashed where approximately located

2 **Lithologic unit**

Figure 39. Stratigraphic units and faulting-event horizons exposed on south wall of trench CF1 across the Fatigue Wash Fault in the Yucca Mountain area, southwestern Nevada (pl. 11; figs. 1, 2, 35). Dark spots along some lines and within fissure fill 2 are markers that were emplaced to facilitate mapping.

Evidence is also equivocal regarding the ages of offsets reflected by the scarps along profiles SP1 through SP6 (figs. 37*A*–37*F*), all of which involve surface unit 1 (profile SP6 involves units 1–3, fig. 35), which is dated at older than 400 ka. Thus, such offsets could have occurred during most or all of the faulting events recorded in trenches CF1 and CF1A, especially taking into account the larger displacements (0.9–2.0 m) recorded on profiles SP3 through SP6. The smaller offsets on profiles SP1 and SP2 as measured near the trenches on the same fault strand as profile SP7a, however, may reflect fewer faulting events.

Slip Rates and Recurrence Intervals

A slip rate for the Fatigue Wash Fault can be estimated from both fault-scarp and trench data. To determine the total net cumulative displacement of offset surfaces or stratigraphic horizons used in slip-rate calculations, both the dip- and left-oblique-slip motion of the fault must be taken into account. The dip of the main fault exposed in trench CF1 (pl. 11; fig. 35) ranges from 80° W. to 80° E. and is therefore considered to be vertical. Although no slickensides were observed in Quaternary deposits to indicate the rake of Quaternary fault movement, rakes of 14°–70° have been documented on bedrock fault planes along the northern section of the fault (Scott and Bonk, 1984; Simonds and others, 1995). We assumed a moderate rake of 45° along a vertical fault plane to determine net cumulative displacements of geomorphic surfaces and stratigraphic units for use in calculating slip rates, as discussed below. We emphasize, however, that a much broader range of slip rates would be calculated by using both the minimum and maximum rake angles (17° versus 70°).

Assuming that (1) the surface offsets measured on profiles SP3 through SP6 (figs. 37*C*–37*F*) reflect the cumulative displacement (0.9–2.0 m) of the unit 1 surface during the past 400 k.y. and (2) movement was oblique slip with a rake of 45°, the net total displacement on the Fatigue Wash Fault ranges from 1.3 to 2.8 m. Applying these values, the long-term slip rate is calculated to range from 0.003 to 0.007 mm/yr.

In trench CF1, (pl. 11; fig. 35), unit 1 is exposed only on the upthrown block, and unit 2 is discontinuous and poorly defined. Unit 3 is fairly well defined and is present on both sides of the fault, but its age is poorly established. Unit 4 is the oldest dated unit (102+42/−15 ka) and therefore is used to estimate a slip rate. The vertical offset of the base of unit 4 in trench CF1 (pl. 11) is about 1.4 m. If the backrotation of units 2 through 4 is removed, then the offset of the base of unit 4 is about 0.4 m. Based on the 0.4-m offset and a rake of 45°, the total net cumulative displacement of the base of unit 4 is about 0.6 m. The slip rate based on the net cumulative displacement (0.6 m) and the estimated maximum and minimum ages for unit 4 (102+42/−15 ka) ranges from 0.004 to 0.007 mm/yr for that time interval.

The elapsed periods (interseismic intervals) between the four latest faulting events on the Fatigue Wash Fault range from about 30 to 140 k.y.

Faulting and Volcanism

Event X is correlated with a volcanic eruption of basaltic ash that is interpreted to have originated from the Lathrop Wells basaltic cone and was deposited in fissure fill 2 (pl. 11). Additionally, basaltic ash probably related to event X on the Fatigue Wash Fault occurs in fissure fills exposed by trenches on several other faults in the Yucca Mountain area (for example, see chaps. 7, 9, 14). These relations strongly indicate a link between Quaternary volcanism and seismicity; therefore, a model linking volcanism and faulting activity should be considered as part of the tectonic history of the area.

Acknowledgments

We thank Chris Menges and Alan Ramelli for their constructive field reviews of the trench logs, as well as many helpful observations regarding the relative ages of surfaces cut by scarps north of the trenches. We gratefully acknowledge Jim Paces, Shannon Mahan, Ken Ludwig, and Beth Widmann for their geochronology work in the trenches. Helpful discussions with John Whitney, Emily Taylor, Bob Bucknam, Jim Paces, Ken Ludwig, and Chris deFontaine regarding trench and scarp data contributed greatly to this study. Chris deFontaine helped measure profile SP7 and prepared soil and lithologic descriptions. Dave Wehner provided an early set of stereophotographs of trench CF1, and Raytheon Services, Nev., provided surveying support in the trenches. Silvio Pezzopane, Chris Menges, Jim McCalpin, and Dick Keefer reviewed the manuscript.

Chapter 9

Quaternary Faulting on the Windy Wash Fault

By John W. Whitney, Frederic W. Simonds, Ralph R. Shroba, and Michele Murray

Contents

Abstract 125
Introduction 125
Trench Stratigraphy 126
Stratigraphic Units in Trenches CF2.5 and CF3 126
Stratigraphic Units in Trench CF2 128
Structures and Deformation in Trenches Across the Windy Wash Fault 130
Evidence and Interpretation of Past Surface Ruptures 130
Event Z 130
Event Y 131
Event X 131
Event W 131
Event V 132
Event U 132
Event T 132
Event S 132
Tectonic Interpretations 132
Recurrence Intervals 132
Slip Rates 133
Temporal-Spatial Variations 133
Comparison of Late Tertiary and Quaternary Slip Rates 134
Summary 134

Abstract

The Windy Wash Fault is traceable as fault scarps in surficial deposits in eastern Crater Flat and as faultline scarps on tilted fault blocks of Miocene tuff. Three trenches that were excavated in Quaternary alluvium and colluvium across the northern segment of the Southern Windy Wash Fault, expose evidence of as many as eight surface-rupturing paleoearthquakes during the mid-Quaternary to late Quaternary, between 400 and 3 ka (preferred dates); the average recurrence interval is 40–45 k.y. for the most recent four faulting events and 50–57 k.y. for all faulting events. The most recent surface-rupturing paleoearthquake, which occurred during the late Holocene, appears to have been the youngest faulting event in the vicinity of Yucca Mountain.

Total net displacement of exposed surficial deposits on the Windy Wash Fault is 3.7 m, and the average slip rate during the Quaternary is estimated at 0.011 mm/yr. On the basis of a displacement of about 101 m on a 3.7-Ma basalt flow along the fault, the slip rate since Pliocene time is estimated at 0.027 mm/yr. Taking into consideration possible interconnections with the adjacent Solitario Canyon and Fatigue Wash Faults, which also record Quaternary movement, an adjusted late Quaternary slip rate for the northern segment of the Southern Windy Wash Fault is comparable, indicating that deformation has been nearly constant for the past 3.7 Ma.

Introduction

The Windy Wash Fault in eastern Crater Flat, about 4 km west of the proposed repository site for the storage of high-level radioactive waste at Yucca Mountain (fig. 1), consists of three segments: the Northern Windy Wash Fault, a central fault segment, and the Southern Windy Wash Fault (figs. 2, 4). The combined features (see discussion in chap. 3) are traceable as fault scarps and faultline scarps in both bedrock and surficial deposits for distances ranging from less than 1 to as much as 3 km (O'Neill and others, 1991; Simonds and others, 1995). Along several segments, the fault forms the bedrock-alluvium contact (fig. 2; Day and others, 1998a). The 25-km-long fault is also distinguished as a clearly recognizable aeromagnetic anomaly.

Two trenches, CF2 and CF3 (fig. 2), were excavated in 1981 at sites about 60 m apart that cross a prominent scarp along the northern segment of the Southern Windy Wash Fault (fig. 2). After initial logging in 1981, Swadley and others (1984) reported evidence for two surface ruptures in these trenches and, on the basis of U-trend analyses of alluvial units in trench CF3 (Rosholt and others, 1985), suggested that the most recent event occurred sometime between about 260 and 40 ka, with a preferred date of middle Pleistocene for the most recent surface rupture.

Additional logging of trenches CF2 and CF3 was conducted in 1985, and evidence of multiple Quaternary surface-rupturing paleoearthquakes along the Windy Wash Fault, including a late Holocene event, was reported by Whitney and others (1986). A third, but shorter, trench (CF2.5, fig. 2) was excavated between trenches CF2 and CF3, and small test pits were also dug within the larger trenches at the fault planes.

Table 27. Numerical ages of deposits exposed in trenches CF2, CF2.5, and CF3 across the Windy Wash Fault in the Yucca Mountain area, southwestern Nevada.

[See plates 12–16 and figures 1 and 2 for locations. Samples: HD (error limits, ±2σ), U-series analyses by J.B. Paces; TL–3 through TL–5, thermoluminescence analyses from Whitney and others (1986); TL–59 (error limit, ±2σ), thermoluminescence analysis by S.A. Mahan; CF 6 (error limit uncertain), U-trend analysis by Rosholt and others (1985); U1–U4, U-series analyses by Peterson and others (1995)]

Trench	Sample	Unit and material sampled	Estimated age (ka)
CF2 (pls. 12, 13)	HD 1617	M, clast rind	333±62
	HD 1618	J, opaline silica laminae	105±2, 153±13
	HD 1619	M, clast rind	91±2, 96±2, 159±7, 264±12, 277±22, 278±13, 331±33
	HD 1620	M, clast rind	214±22, 270±135, 287±13
	HD 1621	M, clast rind	267±14, 311±56
Trench CF2.5 (pl. 14)	TL–3 through TL–5	B, buried Av soil horizon	3–6.5
Trench CF3 (pls. 15, 16)	TL-59	C, sand	11±2
	HD 1615, HD 1820	E, clast rinds	52±4, 62±4, 78±5, 86±5
	HD 1821	E, rhizolith, opaline silica stringers	12±0.2, 13±1, 47±1
	CF 6	D, buried B soil horizon	190±5
	U1 through U4	F, soil carbonate, carbonate on clast rinds	17±3, 38±3, 39±3, 82±9

In 1994, the trench logs were further revised, and additional samples were collected for U-series and thermoluminescence analyses, the results of which are listed in table 27.

Cosmogenic dating of the exposed bedrock scarp on the Northern Windy Wash Fault (figs. 2, 4) by Harrington and others (2000) was done to determine whether this scarp formed during the past 20 k.y. The 3.7-Ma basalt flow that is offset along the Southern Windy Wash Fault was studied to calculate the net cumulative fault slip since Pliocene time (Whitney and Berger, 2000).

Trench Stratigraphy

Trenches CF2 (pls. 12, 13), CF2.5 (pl. 14), and CF3 (pls. 15, 16) were excavated across scarps in alluvial deposits along the northern segment of the Southern Windy Wash Fault; they were photogrammetrically mapped in detail according to the procedures of Fairer and others (1989). Trenches CF2.5 and CF3 were excavated primarily in upper Quaternary alluvium, and trench CF2 through older, well-cemented gravel and cobbles juxtaposed with gravelly fine-grained colluvium that washed downslope across the fault after infrequent surface ruptures. An unnamed ephemeral stream that flowed west-southwestward across the Windy Wash Fault south of the fault scarp where trench CF2 is located deposited younger alluvium across the fault. Thus, an unusually long alluvial record and fault-displacement history is exposed in and between trenches CF2 and CF3. Subsequently, the stream was headwardly captured and diverted southward by another ephemeral stream that flowed along the base of the south ridge of Yucca Mountain (fig. 1) parallel to the Southern Windy Wash Fault.

Stratigraphic Units in Trenches CF2.5 and CF3

Units A through D (pls. 12–16) are present in all trenches and are labeled alphabetically, generally in the order of increasing age. Units E through H are present in the lower parts of trenches CF2.5 (pl. 14) and CF3 (pls. 15, 16) but are absent in trench CF2 (pls. 12 , 13). Correlations of units E through H with the units exposed in trench CF2 are discussed primarily in the unit descriptions for trench CF2.

Unit A consists of eolian sand that contains scattered pebbles and is capped by the modern desert pavement. In trenches, the unit is discontinuous and generally 12 to 20 cm thick. This surficial deposit has been reworked by overland flow and occurs as a fissure fill that was deposited after the most recent surface rupture. In trench CF2.5 (pl. 14), the fill is about 75 cm thick. Just south of trench CF2 (pls. 12, 13), where the fault plane in unit B was exposed by a bulldozer, loose sand of unit A was revealed in a delicately preserved 8- to 15-cm-wide fissure in unit B (fig. 40). At present, unit A continues to aggrade from eolian deposition and is reworked by surface wash from infrequent rainstorms. The deposit is dated at late Holocene because it overlies unit B, which is dated at middle to late Holocene.

Unit B is a thin silty sand deposit that is typical of the eolian silt which has been accumulating on most basin surfaces in the Mojave Desert during the Holocene, owing to an increase in aridity that took place in the region at the end of the Pleistocene (McFadden and others, 1987). In Crater Flat, the unit is either unconformably overlain by thin, loose sand of unit A or capped by desert pavement where unit A is absent. Unit B is generally 20 to 30 cm thick and is easily recognizable by its vesicular texture. It contains the greatest component of silt and clay (35–55 volume percent) of all map units and commonly includes scattered pebbles.

Unit B is the youngest unit offset by the most recent surface rupture. Where the fissure produced by this faulting event is wide, as in trench CF2.5 (pl. 14), large intact chunks of sand fell into the fissure and were buried by unit A. In trenches CF2 (pls. 12, 13) and CF3 (pls. 15, 16), however, the fissure is narrow and appears to have been healed by constant wetting and drying of the vesicular A soil horizon over time. In trenches CF2 and CF3, unit B is preserved on the hanging wall but is mostly or completely stripped off the footwall. Thermoluminescence analyses of the fine-grained-silt fraction of samples from trench CF2.5 (samples TL–3 through TL–5, pl. 14; table 27) range from 3 to 6.5 ka, indicating that eolian deposition on Crater Flat surfaces became a dominant process as the climate became more arid during the early to middle Holocene (Spaulding and Graumlich, 1986).

Unit C consists of loose, gravelly and silty sand; the characteristically poor sorting indicates that it was most likely deposited by one or more debris flows. The unit lies unconformably on eroded unit D. The long erosional hiatus at the contact between these two units is shown in a large pit that is exposed between stations 4 and 8 m, near the west end of the north wall of trench CF3 (pl. 15). Our preferred interpretation is that this feature was partly created by a large mass of former tree roots and (or) by a large maze of tunnels created by burrowing animals. At present, burrowing rodents commonly choose fault zones in which to burrow, and the spoil from their tunnels is commonly seen along fault scarps in Crater Flat. An alternative explanation is that the pit was originally a channel eroded into older deposits and then filled with unit C material. Unit C is generally thin (10–20 cm thick), except where it fills the pit in trench CF3 and where it is a major component of the fissure fill in trench CF2.5 (pl. 14). The unit is discontinuous in trench CF2 (pls. 12, 13).

Figure 40. Surface rupture from a late Holocene coseismic event exposed in vesicular A soil horizon that underlies modern desert pavement on scarp just south of trench CF2 across the Windy Wash Fault in the Yucca Mountain area, southwestern Nevada (figs. 1, 2). Fissure is 8 to 15 cm wide; hand trowel is 21 cm long.

Unit C has little soil development, with a weak Bk horizon, and underlies unit B of Holocene age. A thermoluminescence analysis sample (TL–59, table 27) yielded an age of 11±2 ka, indicating that unit C was deposited at the end of the latest cool, pluvial episode in the southern Great Basin. Dating in trench CF3 (pls. 15, 16) by Peterson and others (1995) indicates that unit C may be a little older, but still late Pleistocene. A radiocarbon analysis of desert varnish on the surface adjacent to trench CF3 dates the desert pavement at about 29 ka (Peterson and others, 1995). Similar ages (19–30 ka on five samples) were obtained for desert pavements believed to have formed over the "Late Black Cone" unit in Crater Flat (see table 2). Because unit C was the last alluvial/colluvial deposit that formed on the surface before the eolian deposition of units B and A, it is the most likely source of the gravel that forms the modern desert pavement. Thus, unit C may range in age from about 13 to 30 ka.

Unit D is distinctive because of its unique soil profile, which is characterized by a Bt horizon and an oxidized color. The unit consists primarily of a gravelly-silty sand, containing about 15 volume percent clasts in trench CF2 (pls. 12, 13) and 40 volume percent clasts in trench CF3 (pls. 15, 16). The average clay content is not as high as the soil development might suggest; laboratory analyses yielded a clay content of only 5 to 8 volume percent in three samples but 31 volume percent in a fourth sample. The thickness of the unit varies because surface erosion has stripped some of it off the hanging wall of the fault and all of it from the footwall, as well as from steep parts of the scarp at trench CF2 (pls. 12, 13). We suggest that the lower clay contents resulted from stripping away of the original upper Bt soil horizons. At the west end of trench CF2 (pls. 12, 13), unit D thickens noticeably where the surface slope flattens, owing to redeposition of sediment eroded from farther upslope. The position of the unit as the first buried soil, in combination with its distinctive color, ped development, and clay coatings, makes this unit a good candidate for correlation with the units exposed in other fault trenches in the Crater Flat area (figs. 1, 2).

Unit D is clearly offset by a surface rupture that predates the most recent faulting event along the Southern Windy Wash Fault (figs. 2, 4), because the unit is preserved on the hanging wall against the main fault plane in trench CF3 (pl. 15) but is mostly stripped away on the footwall. Additionally, unit D is offset more than the overlying units. A U-trend analysis by Swadley and others (1984) on the deposit yielded an estimated age of 190±50 ka (sample CF6, table 27), which indicates that deposition occurred near the end of the middle Pleistocene—a date that seems too old because it would indicate that no subsequent deposition occurred on this alluvial surface for more than 100 k.y. The presence of reworked basaltic ash, which is correlated with

the Lathrop Wells volcanic center to the south (fig. 1; F.V. Perry, written commun., 1996), in the matrix of unit D indicates that the Lathrop Wells basaltic cone had erupted before the unit was deposited. The main blanket of basaltic ash was erupted from the Lathrop Wells volcanic center at 77±6 ka (Heizler and others, 1999), providing a maximum age of about 80 ka for unit D.

Unit E consists of sandy-bouldery cobbles that were deposited by a stream only on the hanging wall and against the Southern Windy Wash Fault scarp (visible in trenches CF2.5 and CF3, pls. 14–16). Although the easternmost 4 to 5 m of the unit, against the fault plane, contains a large concentration of boulders, we refer to this deposit as an alluvial rather than a colluvial wedge, because the debris does not originate from, nor was it deposited across, a newly formed fault scarp. Before the underlying unit F was faulted, its surface was an active flood plain. After the coseismic surface rupture, the stream deposited a long, thin (max 50 cm thick) wedge of bouldery debris into the newly subsided segment of the flood plain. Rapid deposition is indicated by poor sorting of the clasts in unit E, in marked contrast to the good sorting of the underlying gravel in unit F. Not long after unit E was deposited, the ephemeral stream responsible for depositing units E and F and possibly older units, was diverted southward away from this site. The eolian sand of unit D was then deposited, followed by a long period of soil development.

Cobbles in the upper part of unit E are partly coated by rinds with $CaCO_3$ stage I morphology, and cobbles in the lower part of the unit have rinds with $CaCO_3$ stage II morphology. U-series analyses of two silica-rich stringers in the matrix, one carbonate rhizolith, and two silica-rich clast rinds from trench CF3 (pls. 15, 16) indicate that (1) silica deposition in the matrix occurred about 13–12 ka (sample HD 1821, table 27), (2) the rhizolith (a carbonate-filled root cast) is dated at about 47 ka, and (3) the clast rinds are dated at 78±5 ka to 86±5 ka (samples HD 1615, HD 1820), indicating that silica and carbonate deposition by soil processes continues over time in response to appropriate climatic conditions. Thus, the oldest ages most closely limit the minimum age of unit E and are stratigraphically correct because overlying unit D contains the 77±6-ka basaltic ash.

Unit F consists of well-sorted alluvial gravel with a sand matrix. The gravel clasts are imbricated, indicating streamflow from the east, are subangular to subrounded, and are commonly 2 to 4 cm in diameter. Larger clasts and a few thin discontinuous cobble lenses are also present. The good sorting and absence of debris-flow deposits indicate that the stream flowed for sustained periods of time during the year, and so the unit was probably deposited during pluvial climatic conditions. The gravel in unit F eroded into and was deposited across the underlying coarser cobble deposits of units G and H.

The base of unit F is offset more than its top, and the deposit is thicker on the hanging wall than on the footwall, indicating that coseismic surface ruptures occurred both during and after deposition of this unit. In trench CF3 (north wall, pl. 15), the angle of gravel imbrication increases at a depth of about 75 cm below the top of the unit on the hanging wall. This horizon was chosen as the position of the event horizon, although we recognize that the angle of imbrication may also have flattened, owing to changing alluvial conditions on the flood plain at that time. In trench CF2.5 (pl. 14), unit F is coarser in its lower part, and an internal disconformity indicates that deposition was interrupted and altered, possibly in response to a tectonic offset.

The time interval represented by unit F is unknown; however, the absence of any buried soils within it indicates a relatively constant rate of deposition. The good to very good sorting and absence of debris-flow deposits indicate that deposition may have taken place during a pluvial climate.

Four U-series analyses by Peterson and others (1995) on soil carbonate in unit F yielded ages ranging from 17±3 to 82±9 ka (samples U1–U4, table 27). As stated above, the variation in soil carbonate ages reflects times of climatically controlled secondary-carbonate deposition. The sample yielding the 17±3-ka age, for example, was deposited during the latest pluvial climate in the southern Great Basin. Thus, the oldest U-series age is the best minimum limiting age of the deposit. The maximum age of 82±9 ka agrees well with the U-series ages of 78±5 ka and 86±5 ka (samples HD 1615, HD 1820, table 27) for unit E, indicating that unit F was likely deposited during the late Pleistocene pluvial period of 105–90 ka.

Unit G is the lowest deposit exposed on the hanging wall of the Southern Windy Wash Fault (figs. 2, 4), adjacent to the main fault zone in trenches CF2.5 (pl. 14) and CF3 (north wall, pl. 15). The unit consists of a pebbly gravel with a sandy matrix; it contrasts with unit F by its strong cementation by secondary carbonate, and with unit H by its better sorting and its content of smaller clasts. The base of unit G is not exposed, and so its thickness is indeterminable. It appears to have been deposited only on the hanging wall against a paleoscarp after a surface-rupturing paleoearthquake (similar to unit E).

Unit H consists of a gravelly-sandy cobble deposit on the footwall that bears a strong physical resemblance to, and is correlated with, the coarse-grained gravel deposits on the footwall of trench CF2 (unit P, pls. 12, 13). Boulders as large as 30 cm in diameter are common. The deposit generally has a $CaCO_3$ stage III morphology; however, the upper part of the soil horizon on unit H was stripped away by erosion before unit F was deposited. Unit H was clearly offset during unit F time and later, but evidence of possible earlier faulting events is absent because so little of the unit is exposed at the base of trench CF3 (north wall, pl. 15). No age is available for unit H, except that it predates unit F.

Stratigraphic Units in Trench CF2

Trench CF2 (pls. 12, 13) was excavated across a 3-m-high scarp about 60 m north of trench CF3 (figs. 2, 4). Stratigraphic units A through D have textures and soil characteristics similar to those of the younger sequences exposed in trenches CF2.5 (pl. 14) and CF3 (pls. 15, 16), but are more discontinuous. The older units in trench CF2, however, differ markedly in texture from those in the other two trenches because they are primarily colluvial rather than alluvial, owing to the presence of the topographic high formed by the fault scarp. Because of the resulting lithologic differences, the lower units are designated E through

G (or H) in trenches CF2.5 and CF3, as described above, and I through P in trench CF2, as described below.

Units I through L in trench CF2 (pls. 12, 13) consist largely of gravelly sand composed of reworked eolian sand and colluvial gravel that were washed downslope over the Windy Wash Fault scarp. Some sand may also have been blown against the scarp. No sharp contacts exist between these hanging-wall colluvial deposits, and some depositional boundaries are obscured because of carbonate overprinting that has resulted from multiple episodes of soil development. In addition, several wedge-shaped deposits downslope appear to be gradational with adjacent units, whereas unit D tapers upslope and wedges out in the opposite direction because of surface erosion. Stonelines, carbonate stringers, and B soil horizons are primarily used to distinguish these fine-grained colluvial deposits, and some unit boundaries are identifiable.

In trench CF2 (pls. 12, 13), the colluvial deposits consist mainly of eolian sand and silt that accumulated against the Windy Wash Fault scarp on the hanging wall. These deposits bear little resemblance to the coarse cobbly-bouldery gravel on the footwall. The carbonate cementation on the surface of the footwall has a $CaCO_3$ stage II–III morphology, and surface erosion appears to have partly stripped away the original soil profile, including the K horizon. Because eolian deposition is common only during interpluvial climates, deposition on the hanging wall may not have occurred immediately after surface-rupturing paleoearthquakes; thus, the hiatus between faulting and hanging-wall deposition is difficult to determine in trench CF2.

Unit I consists of a colluvial wedge of primarily carbonate-cemented sand that contains some scattered gravel and cobbles. The unit appears to be a local subunit of unit J, proximal to the fault and distinguished by its wedge shape. Unit I underlies unit D in trench CF2 (pls. 12, 13) and is correlated stratigraphically with unit E in trenches CF2.5 (pl. 14) and CF3 (pls. 15, 16), which is also a wedge of sedimentary material against the fault, as described above. On the basis of this correlation, the minimum age of unit I is considered to be about 90 ka.

Unit J is primarily a slopewash deposit composed of gravelly silty sand. On the north wall of trench CF2 (pl. 12), a conspicuous sandy-cobbly gravel interbed terminates about halfway between the main fault zone and the west end of the trench. The deposit is cemented by carbonate with $CaCO_3$ stage II–III morphology that composes the K soil horizon in this unit. Thin stringers of discontinuous secondary carbonate are common. Unlike units I, K, and L, unit J does not thin downslope away from the fault zone, indicating that a long interval of hillslope erosion and redeposition took place after the coseismic surface ruptures that had created the space for units J, I, and D to be emplaced. After unit D was deposited on top of unit J, the landscape was stable long enough to form a reasonably mature soil profile characterized by a Bt horizon and a horizon with $CaCO_3$ stage II–III morphology.

Two U-series analyses of the silica matrix from two adjacent subhorizontal soil carbonate stringers in the lower part of the K horizon in unit J yielded ages of 105±2 and 153±13 ka (sample HD 1618, table 27) that are stratigraphically and sequentially consistent. If unit I correlates with unit E in trench CF3 (pls. 15, 16), then unit J correlates with the next-older unit (F) in trench CF3. Both units F and J are persistent in their respective trenches. The soil carbonate developed on unit E was dated at 78±5 to 86±5 ka (samples HD 1615, HD 1820, table 27), and we are confident that there was no depositional hiatus between units E and F. Thus, the age of unit J, as well as of unit F, ranges from 90 to about 180 ka.

Unit K consists of a wedge of colluvial silty sand that contains a few scattered clasts. On the north wall of trench CF2 (pl. 12), unit K disconformably overlies part of an older fissure fill in the main fault zone. This relation is also indicated on the south wall (pl. 13) but is not so clear cut. The absence of distinctive textural characteristics and abrupt contacts between units J, K, and L make these units difficult to differentiate.

Unit L is also a sandy colluvium that tapers downslope away from the main fault zone on the south wall of trench CF2 (pl. 13). This deposit appears to contain more scattered cobbles than unit K. On the north wall of the trench (pl. 12), unit L overlies a buried fault zone and a fissure fill that was created when unit M was deformed. Another wedge of colluvium is interpreted to be present against the main fissure; however, the stratigraphic correlation of this wedge is equivocal.

No direct dating was done on unit K or L; however, their ages can be interpolated between dated units J and M. Unit K is dated at older than 180 ka, younger than unit M. U-series analyses of silica from carbonate soils in unit M yielded ages ranging from about 91 to about 331 ka (sample HD 1619, table 27). Ages on the upper soils seem to cluster between 264 and 278 ka, indicating that both units K and L were deposited between about 300 and 180 ka (lower age limit of unit J). Because there are no well-developed B soil horizons on these two colluvial wedges, we suggest that both units may be closer in age to unit J than to unit M. Arbitrarily splitting the time interval between units K and L results in approximate ages of 180–220 ka for unit K and 220–260 ka for unit L.

Unit M dominates the lower walls in trench CF2 (pls. 12, 13) west of the main fault zone. Unlike the overlying fine-grained colluvial deposits, this unit consists primarily of alluvial gravelly sand with a $CaCO_3$ stage II+–III soil horizon developed on it. Its gravel content is about 80 volume percent at the west end of the trench and less than 15 volume percent near the fault; the gravel exhibits good sorting indicative of deposition by ephemeral streams rather than slopewash. Near the fault zone, the gravel interfingers with predominantly sandy material that appears to have been washed across a paleoscarp and deposited over a highly fractured, carbonate-cemented cobbly sand, which composes unit N. The sandy facies of unit M could be a coseismic wedge overlying the gravelly facies of unit M.

Unit M is the oldest stratigraphic unit dated in trench CF2 (pls. 12, 13). An experiment in U-series dating was conducted on opaline silica from secondary-carbonate rinds in the K soil horizon. Whole rinds were analyzed along with outer, intermediate, and inner rinds adjacent to clasts from the upper and lower parts of unit M. In all samples, the silica adjacent to the clast was older than the outer rind or the whole rind. Whole-rind analyses gave ages of 91±2 to 96±2 ka, whereas seven analyses of rinds adjacent to the clasts ranged from 277±22 to 333±62 ka (samples HD 1617, HD 1619, table 27). Three analyses

(samples HD 1617, HD 1619, HD 1621, table 27) yielded ages of more than 300 ka, indicating that the deposit is dated at older than 300 ka, possibly as old as 350 ka.

Unit N, which is exposed below unit M on the hanging wall adjacent to the main fault zone, consists of cobbly sand that contains as much as 35 volume percent clasts, all of welded tuff. The unit is clearly distinguishable from the overlying unit M because the sand matrix is well cemented by secondary carbonate and has a distinctive closely spaced fracturing, sometimes referred to as a raveled appearance. No direct dating of unit N was attempted; it is dated at older than 350–380 ka on the basis of the oldest U-series ages of 300–333 ka on silica-rich, carbonate clast rinds from the overlying unit M.

Unit P is a gravelly-sandy cobble deposit that occupies nearly all of the footwall of both walls in trench CF2 (pls. 12, 13). The unit is primarily clast supported and exhibits very good sorting and good rounding. The average clast size is 5 to 6 cm (median diameter), and boulders as large as 25 cm in diameter are common. Minor channels and crossbedding are also present. No buried soils or clear depositional breaks can be distinguished within the unit.

The surface of unit P was eroded over a substantial time interval. The footwall, extending back (eastward) from the fault at least 60 m, has a gentle convex surface across a west-dipping slope of about 19°. The internal stratification of unit P is horizontal, not warped, indicating that the surface slope is erosional. Surface erosion has partly stripped and in some places, largely removed the soil developed on unit P. The remaining soil is cemented by secondary carbonate with $CaCO_3$ stage II+ morphology and silica-rich rinds on clasts; in places, remnants of a K horizon with $CaCO_3$ stage III morphology are present.

In general, a coarse-grained gravel that has undergone continual surface erosion over time is difficult to date. Because unit P was not exposed on the hanging wall, we assume that it is below the floor of the trench and so predates any of the dated units on the hanging wall in trench CF2 (pls. 12, 13). The three oldest U-series ages for the hanging wall on clast rinds from unit M, are 311±56, 331±33, and 333±62 ka (samples HD 1621, HD 1619, and HD 1617, respectively, table 27). Unit N underlies unit M and has a well-developed soil on it. We estimate unit N to be older than 380 ka and suggest an age of at least 400 ka for the top of unit P, probably more than 450 ka. Correlation of unit P with the oldest units (G, H) exposed in trenches CF2.5 (pl. 14) and CF3 (pls. 15, 16) is uncertain.

Structures and Deformation in Trenches Across the Windy Wash Fault

In trench CF2 (pls. 12, 13), the main Windy Wash Fault zone is about 1.2 m wide on the north wall (pl. 12) and splits into two splays on the south wall, with a combined width comparable to that on the north wall (pl. 13). The fault planes strike N. 4°–20° W. and dip 77°–90° W. At least five fissure fills of different ages can be identified in the fault zone on the basis of crosscutting relations, depth of burial, carbonate cementation, and the presence of basaltic ash. The fissures are primarily filled with sand, silt, gravel, and carbonate-cemented clasts. Units K and L overlie two of the older fissure fills that are strongly sheared, and much carbonate has precipitated in the lower part of the fault zone because of easy infiltration.

West of the main fault zone in trench CF2 (pls. 12, 13) are two narrow (5–15 cm wide) secondary faults that display only small offsets. On the north wall (pl. 12), these two secondary faults define a small graben. Fractures are present primarily on the hanging wall within 10 m of the main fault; however, fractures are observed but with decreasing density to the end of the trench. Some fractures are buried by subsequent hanging-wall deposits and can be used to help define faulting-event horizons.

In trench CF3 (pls. 15, 16), the Windy Wash Fault is present as two splays, 4 to 6 m apart. A pit was excavated against the north wall (stas. 16–20 m, pl. 15) to expose the deeper fault fissure and the oldest offset deposits. At the base of the pit, the fault fissure is 65 cm wide and narrows to 15 to 30 cm in the unconsolidated, younger deposits. A strong contrast in fault width is evident by comparing the western fault strands on both walls in trench CF3. On the north wall (pl. 15), the fissure is narrow (<10 cm at sta. 14 m) and is associated with minor stratigraphic displacements; however, on the south wall the same strand is 20 to 40 cm wide (stas. 14–15 m) and is associated with one of the largest individual displacements (for example, top of unit E) recorded in the trench. Fewer fractures are preserved in trench CF3 than in trench CF2 (pls. 12, 13). No backtilting, folding, or warping was observed in any of the trenches. The main fissure in trench CF2.5 (pl. 14) is unlike that in any of the other trenches, in that it widens considerably within 1 m of the surface, resembling an inverted cone, or what is sometimes referred to as a flower structure on seismic profiles.

Evidence and Interpretation of Past Surface Ruptures

Event Z

The most recent faulting event (Z) on the Windy Wash Fault affected all units except the youngest unit (A) that overlies the vesicular silty Av soil horizon. This event is best represented in trench CF2.5 (pl. 14), where the Av soil horizon was broken up by extension across the fault zone and large fragments became incorporated into the loose sand and silt of unit A that was deposited on top of the older fissure fill. On the north wall of trench CF2.5, the Av soil horizon remained intact and was downdropped about 10 cm at the west edge of the fissure. In trench CF2 (pls. 12, 13), this faulting was recorded primarily by a 4- to 8-cm-wide fissure in the Av soil horizon that is filled with loose sand. The surface rupture caused by event Z was also exposed at the ground surface just south of trench CF2 by scraping off the desert pavement and loose sand of unit A from the buried vesicular A soil horizon of sandy silt (unit B). As shown in figure 40, the surface rupture there clearly created a small (8–15 cm wide) fissure, now filled with sand, through the middle and upper Holocene eolian

deposits. In trench CF3 (pls. 15, 16), event Z is recorded only on the western fault strand, where it is manifested primarily by cracking with but little fissure development. On the basis of the relations just described, event Z definitely ruptured the ground surface but is probably best described as a cracking or fracturing event with only minor (≤10 cm) local displacement.

Thermoluminescence analysis of Av soil horizons (Whitney and others, 1986) yielded ages ranging from about 3 ka (late Holocene) for the upper horizon to 6.5 ka for the lower horizon (samples TL–3 through TL–5, table 27). Because the upper part of the Av soil horizon is ruptured, event Z occurred during the past 3 k.y. We prefer a date of 3–2 ka because of the absence of a fresh scarp, the reforming of an Av soil horizon over some fault strands, and the undeformed appearance of the desert pavement above the fissure. Event Z on the Windy Wash Fault is the youngest documented surface rupture in the Yucca Mountain area (figs. 1, 2) and may correlate closely with Holocene faulting events on the nearby faults (see chap. 14).

Event Y

Event Y is represented at the top of unit D, the only unit with an oxidized Bt soil horizon. After the faulting event, the surface of this unit was modified by a relatively long period of erosion; the unit was stripped from some footwalls and is discontinuous on the hanging wall in trench CF2 (pls. 12, 13). Because of erosion, the base of unit D is the best reference horizon for measuring the fault offset caused by event Y. On the basis of exposures in the south wall of trench CF3 (stas. 14–15 m, pl. 16), which is the only place where this horizon is preserved on both the footwall and hanging wall directly adjacent to the fault zone, displacement ranges from 25 to 45 cm, depending on slope projections of the marker beds between the two fault blocks. Relations are not so clear in trench CF2.5 (pl. 14), although unit D is exposed on both the footwall and hanging wall, and even less so in trench CF2 (pls. 12, 13) where the unit is present only on the hanging wall. Considering all the measurements that were made or estimated in the three trenches, the average preferred displacement is 24 cm.

The maximum date of event Y is constrained by the presence of reworked basaltic ash, most likely originating from the eruption of the nearby Lathrop Wells volcanic center (fig. 1) at 77±6 ka (Heizler and others, 1999), in the matrix of unit D and by the U-series ages on clasts in unit E. The minimum date is constrained by the age of unit C, 13–30 ka. A long erosional period followed the formation of a Bt soil horizon on unit D, and the undulating surface of unit D is preserved on the hanging wall, indicating that much erosion of the unit had already occurred before event Y. Thus, we date event Y at about 75–30 ka (preferred value, ~40 ka).

Event X

Evidence for event X is related to the deposition of unit E, an alluvial deposit of coarse cobbles exposed on the hanging wall of the Windy Wash Fault in trenches CF2.5 (pl. 14) and CF3 (pls. 15, 16), and of unit I, a sandy colluvial wedge on the hanging wall in trench CF2 (pls. 12, 13). As discussed earlier, units E and I are considered to be correlative and were both deposited adjacent to a fault scarp.

The thickness of unit E reflects the approximate offset of unit F, as observed in trenches CF2.5 (pl. 14) and CF3 (pls. 15, 16), that was caused by event X. In trench CF3, slip occurred on two fault strands, with a total displacement ranging from 78 to 98 cm on the south wall (pl. 16) and from 71 to 96 cm on the north wall (pl. 15) (preferred value, 87 cm). In trench CF2.5, the displacement ranges from 33 to 54 cm on the one fault strand that is exposed. In trench CF2, the well-defined colluvial wedge (unit I) indicates an offset of 45 to 53 cm (preferred value, 50 cm).

The sandy matrix of unit E contains ash that is chemically similar to the basaltic ash from the Lathrop Wells volcanic center (fig. 1; F.V. Perry, written commun., 1996). The preferred age of the main Lathrop We t tlls ash sheet is 77±6 ka (Heizler and others, 1999). U-series analysis of silica from the inner carbonate rinds of clasts in unit E yielded ages of 78±5 and 86±5 ka (samples HD 1615, HD 1820, table 27). The ages of the rinds overlap with the age of the ash, indicating that event X was contemporaneous with, or occurred shortly after, deposition of the abundant basaltic ash and its reworking on the landscape.

Event W

Event W is the oldest faulting event for which reasonable age constraints can be assigned. The displacement from this event is best observed on the north wall of trench CF3 (pl. 15), where a pit was dug in the floor of the trench (between stas. 16 and 20 m) to expose the offset base of unit F, a fine-grained gravel characterized by very good sorting and imbrication. The base of unit F in trench CF3 is offset more than its upper surface, indicating that a coseismic surface rupture took place during the deposition of unit F. Event W is also evidenced by a fault that apparently offsets unit H in the footwall and terminates within unit F in trench CF2.5 (pl. 14). In trench CF2 (pls. 12, 13), unit J, which is correlated with unit F in trench CF3, was deposited on the hanging wall, probably in response to a surface rupture. Unlike the underlying colluvial wedges of units K and L, unit J persists and evens thickens downslope.

The displacement on the base of unit F ranges from 25 to 50 cm (preferred value, 35 cm) on one of the two fault strands. In trench CF2, displacement of unit J ranges from 18 to 25 cm on the north wall (pl. 12) and from 38 to 52 cm on the south wall (pl. 13). These offsets appear to be similar to those in trench CF3; the displacements may decrease slightly to the north.

Unit E and the underlying surface of unit F are dated at about 75–90 ka. The ages of clast rinds from near the base of unit J range from 105±2 to 153±13 ka (sample HD 1618, table 27). Assuming that the older age is closer to the maximum age of the base of the deposit, we date event W at 160–130 ka (preferred value, ~150 ka).

Event V

Event V is represented by a wedge of gravelly sand, mapped as unit K, on the hanging wall in trench CF2 (pls. 12, 13). Unit K clearly buries the west edge of the main fault zone (stas. 14.5–15.5 m, pl. 12). The unit is about 73 cm thick (range 70–83 cm) on the north wall and only 28 cm (range, 24–30 cm) thick on the south wall. The width of unit K on the south wall (pl. 13) is considered a minimum because the unit cannot be accurately traced back to the main fault zone, owing to the presence of an intervening zone of highly disturbed material. Also, the contact between units K and L is indistinct, primarily because no well-defined upper soil horizons were preserved on either unit; thus, the displacements represented by these wedges are only approximate, though well within the range of the described displacements. Event V is recorded in trenches CF2.5 (pl. 14) and CF3 (pls. 15, 16) by contrasting deposits (units G, H) across the main fault zone at the base of each trench. No thicknesses are available for either unit, and so no displacements are determinable in those trenches.

The date of event V is bracketed by the U-series ages of clast rinds in units J and M. The base of unit J is dated at about 160 ka, and younger soil ages on unit M cluster around 270 ka (sample HD 1619, table 27). No geologic or pedologic data are available to constrain the date of event V, and so we choose to arbitrarily place event V in the later half, and event U in the earlier half, of the interval between units J and M. On this basis, we date event V at about 220–180 ka, (preferred value, 200 ka).

Event U

In trench CF2 (pls. 12, 13), event U is represented by a small wedge of fine-grained deposits (unit L) that buried a fault fissure. On the north wall, two small wedges were mapped: the western wedge buried a fissure that subsequently remained dormant, and the eastern wedge is a poorly defined colluvial wedge against the main fault zone (pl. 12). On the south wall, unit L tapers downslope on the hanging wall over the distinctly gravelly unit M (pl. 13). The surface offset represented by unit L ranges from 15 to 24 cm on the south wall and from 30 to 60 cm on the north wall. If the eastern wedge on the north wall is not a deposit that resulted from event U, then the total offset on the north wall is only about 30 cm.

The date of event U is bracketed by U-series ages of clast rinds in units J and M. The base of unit J is dated at about 160 ka, and the ages of younger soils on unit M cluster around 270 ka. Deposition of unit L postdates the earlier of two surface-rupturing paleoearthquakes that occurred between these dates. We date event U at 260–220 ka (preferred value, ~240 ka).

Event T

Event T is represented by another surficial deposit, unit M, in trench CF2 (pls. 12, 13). Unlike the overlying younger units in this trench, however, most of unit M consist of alluvial cobbly-sandy gravel rather than colluvial sand that washed over the Windy Wash Fault scarp. The gravel content of the unit decreases near the fault, and unit M becomes a gravelly sand. The lateral textural contrast may indicate that the sandier part of the unit represents a colluvial sand that was deposited across the scarp shortly after event T and interfingered with the active-channel deposits.

The base of unit M is sharply defined because it unconformably overlies a highly fractured and sheared deposit of cobbly sand, unit N. The thickness of unit M ranges from 48 to 60 cm on the north wall (pl. 12) and from 55 to 65 cm on the south wall (pl. 13); the preferred surface displacement from event T is 50 to 60 cm.

Multiple ages were determined on clasts in unit M collected from the south wall (see samples HD 1617, HD 1620, HD 1621, table 27). U-series analyses of silica on the inner rinds of clasts yielded ages consistently older than those on whole rinds or on outer or intermediate rinds. Thus, the ages of the inner rinds best approximate the maximum age of the deposit. The three oldest ages are 311–333 ka, indicating that unit M is dated at about 280–380 ka, taking into account the 2σ error limits on these ages. Event T must have occurred during this time interval; we suggest a date of 370–300 ka (preferred value, 370–340 ka), constrained to precede the deposition of unit M.

Event S

The presence of unit N in trench CF2 (pls. 12, 13) provides the only evidence for event S. This cobbly-sand deposit bears no textural or sedimentologic similarities to the gravel and cobble deposits on the footwall, and so unit N is interpreted to have been deposited in response to a scarp-forming event before unit M was deposited. We date event S, on the basis of the age of the overlying unit M, at no later than 400–390 ka, probably earlier. The minimum displacement represented by unit N is approximately 0.5 m. Because unit N is strongly sheared and the overlying unit M is not, this shearing may represent another surface-rupturing paleoearthquake that occurred before event T, although the raveled appearance of unit N may, instead, be entirely related to event T.

Tectonic Interpretations

Recurrence Intervals

The paleoseismic record of the Windy Wash Fault is unusual in its detail in the Yucca Mountain area (figs. 1, 2) because several surface-rupturing paleoearthquakes are recorded by the various deposits exposed in the trenches. Five coseismic, scarp-forming events are recorded in trenches CF2.5 (pl. 14) and CF3 (pls. 15, 16) in alluvial and eolian deposits, and eight such events in trench CF2 (pls. 12, 13). Individual vertical offsets per event (preferred values) range from 4 to 88 cm and average about 36 cm.

Four events occurred after the deposition of unit J at the site of trench CF2 (pls. 12, 13) about 160 ka, indicating an

average recurrence interval of 40 k.y. for surface-rupturing paleoearthquakes since the end of the middle Pleistocene. In the same trench, seven events occurred since unit N was faulted and unit M was deposited against a paleoscarp on the Windy Wash Fault about 400–350 ka; the average recurrence interval between all faulting events is 50–57 k.y. We suggest that this recurrence interval may be somewhat longer than that observed in trench CF3, because the fine-grained texture of the deposits and the poor definition of the contacts between some hanging-wall units in trench CF2 make detection of small events (such as events Z and Y) difficult. If two or three of the mapped hanging-wall units in trench CF2 represent more than one faulting event, then the long-term average recurrence interval may be closer to 40 k.y., as observed in trench CF3. Therefore, the recurrence interval for this segment of the Windy Wash Fault is estimated at 40–57 k.y. (preferred average, 40–45 k.y.).

Slip Rates

A long-term average vertical-slip rate can be calculated on the Windy Wash Fault from the displacement of the oldest exposed unit (N) below the original surface of the footwall, which must be reconstructed to account for surface erosion over time. The total apparent vertical offset of unit N is 3.7 m on the north wall of trench CF2 (pl. 12), about 0.35 m greater than that measured on the south wall. This offset includes 1.2 m of displacement that is reconstructed (owing to erosion) on the footwall. Ages of soil horizons from unit M indicate that the unit was deposited by at least 350 ka, possibly 400 ka. The long-term average vertical-slip rate therefore ranges from 0.0092 to 0.0105 mm/yr.

To calculate the net fault-slip rate, the dip and left-oblique motion of the fault must be taken into consideration. Dips of the main fault zone are nearly vertical. No slickenlines were observed on fault planes to indicate the rake of latest motion on the fault, and so we assume a left-oblique motion of as much as 25° from dip slip, or a southwestward plunge of 65°, on the basis of the field data of Simonds and others (1995). This oblique slip geometrically translates into a multiplier of 1.1 for total slip. Thus, the long-term net-slip rate on the Windy Wash Fault is 0.01 to 0.0116 mm/yr (preferred value, 0.011 mm/yr). A slip rate independently calculated for the four latest faulting events in trench CF3 is the same as that calculated for the past 350–400 k.y. in trench CF2.

Temporal-Spatial Variations

Over the past 400 k.y., seven or eight coseismic surface ruptures have occurred on the Windy Wash Fault. The most recent event (Z) ruptured a late Holocene vesicular silty-sand deposit (Av soil horizon) that underlies the modern desert pavement (fig. 40) along the southern fault segment. This event does not appear to have ruptured the Northern Windy Wash Fault. Harrington and others (2000) used cosmogenic radiocarbon dating of the exposed bedrock scarp in northern Crater Flat to demonstrate that this scarp has been exposed for more than 20 k.y. The late Holocene faulting event may also have ruptured the Southern Crater Flat Fault, as observed in trench CFF–T1A (see chap. 10). Such a young event has not been observed on faults on the east side of Yucca Mountain (see chaps. 5, 14; fig. 59).

The colluvial wedge of sediment deposited on the hanging wall in response to event X (unit E in trench CF3 and unit I in trench CF2) contains sand-size shards of basaltic ash in the matrix. Basaltic ash is also present in one of the vertical, carbonate-cemented fissure fills in trench CF2 (pls. 12, 13). Chemical analysis of this ash (F.V. Perry, written commun., 1996) indicates that it, as well as basaltic ash in the main fault fissures of the Fatigue Wash and Solitario Canyon Faults (see chaps. 7, 8), most likely originated from the nearby Lathrop Wells volcanic center (fig. 1). The presence of basaltic ash in fault-related deposits in three adjacent fault zones indicates that slip was probably distributed on at least three faults in eastern Crater Flat during a paleoearthquake that occurred either during or shortly after the main ash-producing eruption

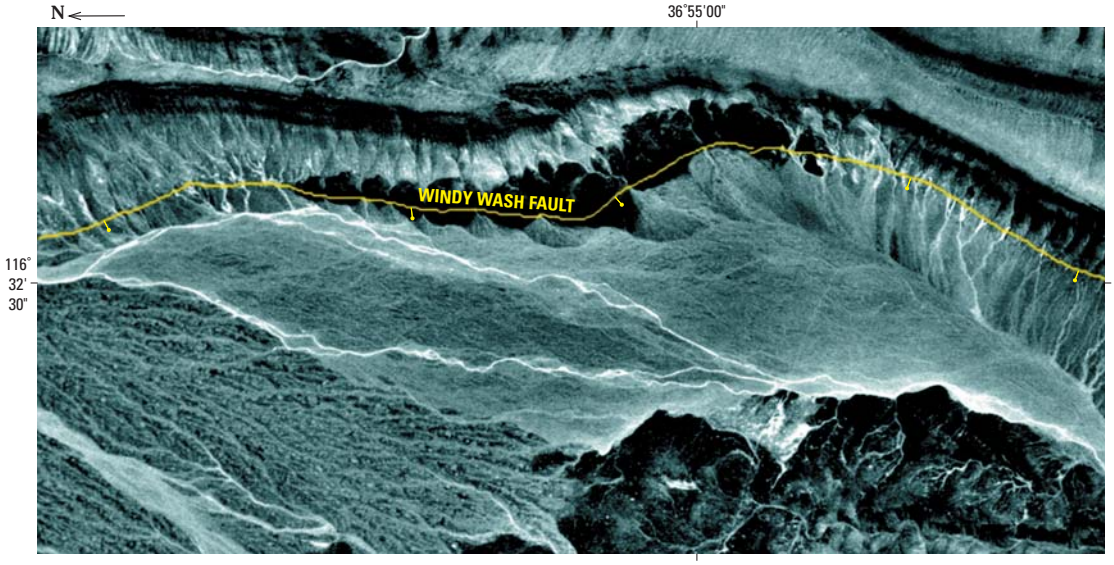

Figure 41. Southern Windy Wash area of Crater Flat in the Yucca Mountain area, southwestern Nevada (figs. 1, 2), showing Windy Wash Fault trace and offset 3.7-Ma basalt against south ridge of Yucca Mountain. Bar and ball on downthrown side of fault.

of the Lathrop Wells basaltic cone at 77±6 ka (Heizler and others, 1999; see chap. 14; fig. 59).

Unlike on the Stagecoach Road Fault and, possibly, the Solitario Canyon Fault (see chaps. 5, 7), no strong evidence of temporal clustering of seismicity was observed on the Windy Wash Fault. However, because surface ruptures with small displacements (<20 cm) are difficult to recognize in trenches across the Windy Wash Fault, we believe that one or two small paleoearthquakes may have occurred much closer in time to a larger faulting event than is indicated by the estimated average recurrence interval of 40–45 k.y. For example, the absence of strong soil development between colluvial-wedge units K and L may indicate that they were deposited nearly contemporaneously; however, surface erosion may have stripped away part of a deposit or its soil, such as in unit D. The relatively regular intervals between coseismic surface ruptures on the Windy Wash Fault are similar to the paleoseismic record on the Paintbrush Canyon Fault at Busted Butte (see chap. 5).

The slip rate and recurrence interval for the Southern Windy Wash Fault indicate that the fault is more active than the Fatigue Wash Fault (see chap. 8). The Fatique Wash Fault is a splay of the Windy Wash Fault, which defines the east edge of a small graben with a down-to-the-east segment of the Windy Wash Fault that begins about 200 m north of trench CF2. Clearly, the Southern Windy Wash Fault is more active than the central section and the Northern Windy Wash Fault. The long-term slip rate of the Windy Wash Fault is similar to those of the Bare Mountain, Solitario Canyon, and Paintbrush Canyon Faults.

Comparison of Late Tertiary and Quaternary Slip Rates

The Southern Windy Wash Fault cuts a 3.7–Ma basalt flow (fig. 41). An investigation by Whitney and Berger (2000), including shallow seismic-refraction surveys, was conducted to (1) determine the thickness of alluvium that overlies the offset basalt on the downthrown (west) block adjacent to the fault, (2) compare the offset of the Tertiary basalt with that of dated Quaternary deposits in the fault zone, and (3) determine the long-term slip rate on the Windy Wash Fault. The top of the exposed basalt flow on the footwall is 40.5 m above the adjacent land surface on the hanging wall, and the maximum depth of burial of the flow in the downthrown block is 56 m, as recorded by an 823-m-long seismic-refraction profile oriented perpendicular to the trend of the fault (Whitney and Berger, 2000). If 2 m of surface erosion, based on calculations of hillslope-erosion rates by Harrington and Whitney (1991) for the Yucca Mountain area (figs. 1, 2), is added, the total vertical offset of the basalt is about 98 m. Seismic profiling also recorded 18 m of apparent left-lateral slip. Factoring in that value at a ratio of 5:1 (vertical to lateral movement), the total net slip on the Windy Wash Fault is about 101 m, and the average slip rate for the past 3.7 m.y. is about 0.027 mm/yr.

The Quaternary slip rate on the Windy Wash Fault is about 0.011 mm/yr, as calculated from offset and dated carbonate soils. The long-term slip rate appears to be more than double the Quaternary slip rate, in which case tectonic activity would appear to have decreased since the Pliocene. However, if slip rates for Quaternary displacements on the Solitario Canyon Fault (0.01–0.02 mm/yr; see chap. 7) and the Fatigue Wash Fault (0.003–0.007 mm/yr; see chap. 8), which may be interconnected with the Southern Windy Wash Fault (see chap. 3), are added, the combined slip rate is comparable to the slip rate of 0.027 mm/yr since the Pliocene. If this interpretation is valid, then the Pliocene and late Quaternary fault-slip rates indicate that overall deformation has been nearly constant for the past 3.7 m.y.

Summary

The Windy Wash Fault is in the Crater Flat Basin, about 4 km west of the proposed repository site for the storage of high-level radioactive waste at Yucca Mountain. The fault is about 25 km long and can be divided into three segments: the Southern Windy Wash Fault, a central segment, and the Northern Windy Wash Fault. Three trenches (CF2, CF2.5, CF3) were excavated across the north end of the Southern Windy Wash Fault. Evidence for as many as eight coseismic surface ruptures was observed in trench CF2 and five ruptures in trenches CF2.5 and CF3. The timing of many of these faulting events was determined by dating soils in the faulted deposits by U-series analysis, volcanic ash correlation, or thermoluminescence analysis of fine silt. Individual displacements per event ranged from 4 to 87 cm (preferred values), mostly from 20 to 60 cm. The smallest offsets were detected for the two most recent surface ruptures, indicating that small surface ruptures may have occurred earlier but are now obscured because of long intervals of erosion and overprinting by strongly carbonate cemented soils.

Surface faulting occurred on the Windy Wash Fault about 3, 40, 75, 150, 200, 240, 340, and 400 ka (preferred values or midpoints of ranges of event timing). The recurrence interval for the last four faulting events is about 40–45 k.y. For the longer paleoseismic record in trench CF2, the average recurrence interval is 50–57 k.y. Assuming that two or three small-displacement events are obscured in middle Pleistocene deposits, we prefer a recurrence interval of 40 k.y. for the Windy Wash Fault. Total net displacement on the oldest hanging-wall deposit is 3.7 m, indicating a long-term average fault-slip rate of 0.01 to 0.0116 mm/yr.

An average slip rate of 0.027 mm/yr calculated for the Southern Windy Wash Fault over the past 3.7 m.y. was from a buried offset basalt flow, on the basis of seismic-refraction data. The Pliocene slip rate appears to exceed the Quaternary slip rate measured from trench studies. However, if the slip rates for the Fatigue Wash and Solitario Canyon Faults, which appear to be interconnected with the Southern Windy Wash Fault, are added, then the Pliocene and Quaternary slip rates are similar, indicating that overall deformation has been nearly constant over the past 3.7 m.y.

Chapter 10

Quaternary Faulting on the Southern Crater Flat Fault

By Emily M. Taylor

Contents

Abstract 135
Introduction 135
Stratigraphy 135
Paleoseismology 136
Trench CFF–T1A 142
Event Z 142
Event Y 142
Event X 142
Summary of Depositional and Faulting Events 143
Trench CFF–T1 143
Event Z 143
Event Y 143
Event X 144
Summary 144

Abstract

Two trenches, excavated across projections of the Southern Crater Flat Fault, expose middle Pleistocene to lower Holocene alluvium and fine-grained eolian deposits that record at least three surface-rupturing paleoearthquakes. On the basis of thermoluminescence analyses of fine-grained alluvial materials and U-series analyses of opaline silica sampled from the inner rinds of clasts, the most recent faulting event probably occurred 6–2 ka, the penultimate faulting event 40–10 ka, and an earlier faulting event 250–130 ka. Minimum recurrence intervals are about 5–90 k.y. The maximum total vertical-slip rate on the Southern Crater Flat Fault is estimated at 0.002 mm/yr.

Introduction

The Southern Crater Flat Fault is a down-to-the-west normal fault that is best exposed in a 2-km-long segment south of Stagecoach Road (fig. 2), where for some distance it is traceable as a well-defined scarp forming the bedrock (basalt)-alluvium contact (see chap. 3; Simonds and others, 1995). Quaternary faulting relations were studied in two trenches, CFF–T1 and CFF–T1A (figs. 2, 42), which were excavated in surficial deposits that intersect the fault trend at sites 0.5 to 1.0 km north of Stagecoach Road. Trench CFF–T1 is located on a subtle, rounded alluvium-disrupting scarp that forms a distinctive lineament on aerial photographs. Trench CFF–T1A, 100 m to the south, is located on a surface immediately adjacent to a drainage where the fault is exposed.

Stratigraphic correlations between trenches CFF–T1 (pl. 18) and CFF–T1A (pl. 17) are difficult, even though they are not far apart and the Quaternary deposits involved in the faulting are of similar age. One reason for the observed differences is that the aggradation sequence exposed in trench CFF–T1 was affected by a small drainage on the hanging wall. Another factor may be that not all segments of the Southern Crater Flat Fault were activated simultaneously during each of the three faulting events. For example, segments of the fault may have been triggered by movement on other nearby faults, such as the Windy Wash Fault that has parallel and (or) similar orientations (see chap. 3, fig. 4). The near-verticality and planarity of the fault in both exposures and the absence of bifurcating fractures toward the surface indicate a strike-slip component of movement, which can also result in stratigraphic variations along strike and add to the difficulties in correlating faulting events between the two trenches.

Stratigraphy

Trenches CFF–T1 (pl. 18) and CFF–T1A (pl. 17) expose Quaternary deposits of largely alluvial gravel, with minor amounts of fine-grained eolian sand. The development of distinctive soil horizons, commonly separated by erosional unconformities and capped by eolian deposits, has created stratigraphic markers that are extremely useful for paleoseis-

mic interpretations. Characteristics of the Quaternary lithologic units that were differentiated in each of the trenches are listed in tables 28 and 29.

Five samples of secondary opaline silica inner rinds on clasts and one sample of a younger soil were collected from trench CFF–T1A (pl. 17) for U-series and thermoluminescence analysis, respectively. Estimated rounded ages of various units, listed in table 30, are unit 2B, 9 ka (sample TL–61); unit 3K, 40–70 ka (sample HD 1959); unit 3Bk, 120–130 ka (sample HD 1958); and unit 4, 200–350 ka (avg ~250 ka; samples HD 1957, HD 1961). In terms of the standard Quaternary stratigraphic framework for the Yucca Mountain area (fig. 3), these ages indicate that unit 2 correlates most closely with unit Qa5, unit 3 with unit Qa3, and unit 4 with unit Qa2.

Paleoseismology

Trenches CFF–T1 (pl. 18) and CFF–T1A (pl. 17) expose the Southern Crater Flat Fault and provide evidence for at least three faulting events that may have caused surface ruptures during the Quaternary. These paleoearthquakes occurred in the past ~250 k.y., with a total measured offset of 24 to 65 cm, resulting in a maximum vertical slip rate of 0.002 mm/yr. The most recent faulting event offsets the Av soil horizon, which could be as young as 3 ka. Fault-plane striae on Quaternary deposits were not available to estimate net tectonic slip. The estimated slip for each faulting event is therefore for vertical slip only and is made by correcting for

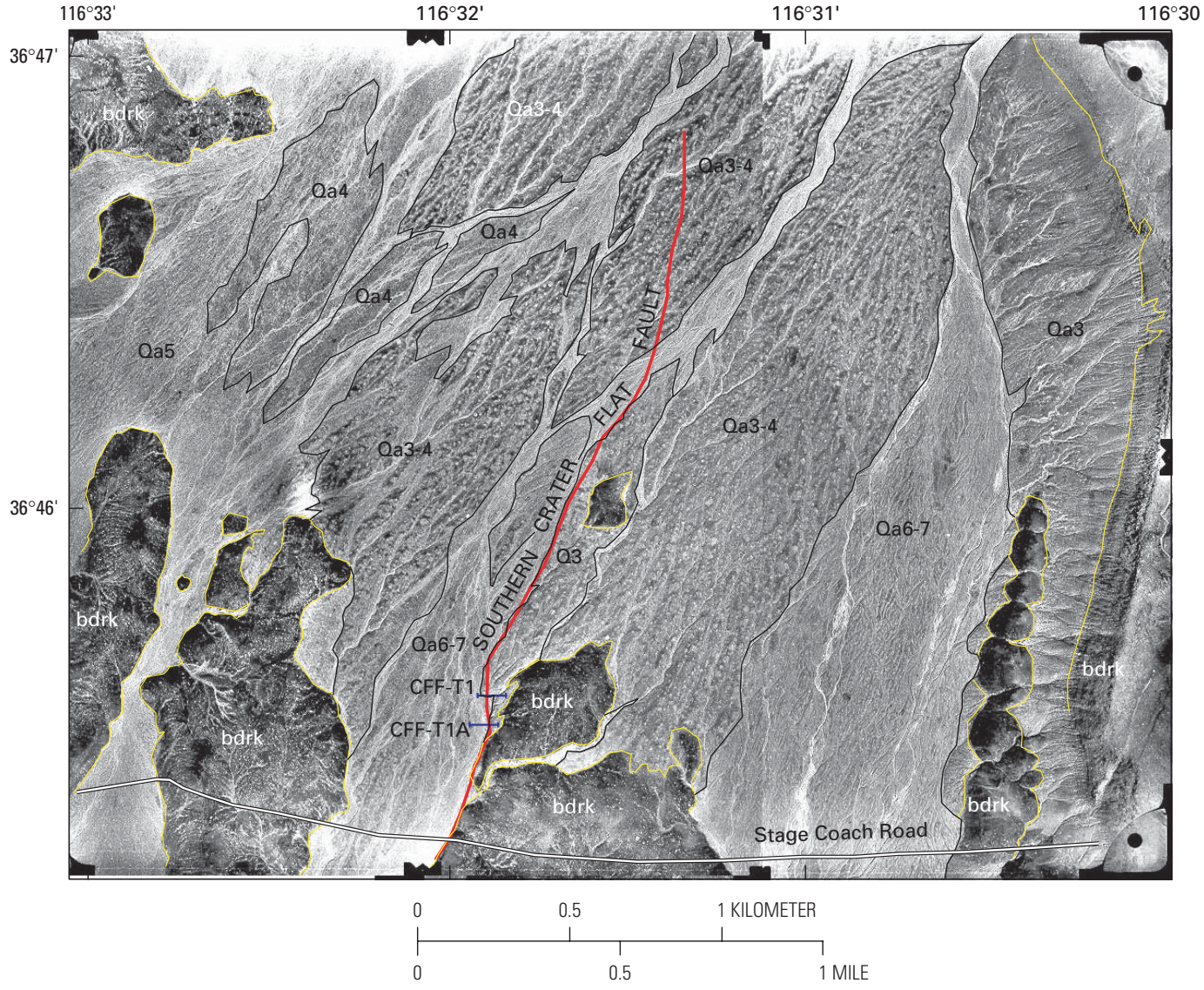

Figure 42. Southern Crater Flat Fault in the Yucca Mountain area, southwestern Nevada (figs. 1, 2), showing distribution of surficial deposits and locations of trenches CFF–T1 and CFF–T1A (pls. 17, 18; fig. 2). Red line, projection of the Southern Crater Flat Fault; yellow line, bedrock-alluvium contact. Map units refer to standard sequences of Quaternary surficial deposits at Yucca Mountain (table 2).

Table 28. Soil and stratigraphic units exposed on the north wall of trench CFF–T1A across the Southern Crater Flat Fault in the Yucca Mountain area, southwestern Nevada.

[See plate 18 and figures 1, 2, and 42 for locations. Colors from Munsell Soil Color Charts (Munsell Color Co., Inc., 1992). See table 14 for explanation of abbreviations. Do., ditto]

Field No., horizon, boundary	Unit	Dry color (<2-mm fraction)	Moist color (<2-mm fraction)	Texture	Structure (primary and secondary)	Consistence (dry, wet)	Clay films	Secondary carbonate (gravel and disseminated)	Gravel content (volume percent)	Parent material and lithology (sorting, angularity, bedding, imbrication, and support)	Miscellaneous (roots, pores, SiO_2, oxidation, concretions, salts)
Hanging-wall and footwall units											
1, Av, as	1	10YR 7.5/3	10YR 4/3	L-SiL	3 vco sbk, 2° 3 f-co sbk to sg	shss, ps	0	0, ev	5 (gr)	Well sorted, subangular, nonbedded, nonimbricated, matrix supported.	Continuous vesicles, 1° eolian.
2, Bk1, cs	1	10YR 8/3	10YR 5/4	L	2 m-co abk, 2° sg	lo-shss, ps	0	I, ev	40 (pb gr)	Moderately well sorted, subangular, nonbedded, nonimbricated, matrix supported.	– – –
3, 2Btwk, as (14 on footwall)	2	10YR 7/3	10YR 4/3	SL	1 m sbk	lo-shso, po	0	I–, ev	25 (cb pb gr)	Poorly sorted, subangular, nonbedded, nonimbricated, matrix supported.	– – –
Hanging-wall units											
21, 2Bwk2, as	2	7.5–10YR 7/3	10YR 4/3	SL	sg	lovss, ps	0	I–, filaments, e	70 (cb pb gr)	Moderately well sorted, subangular, nonbedded, nonimbricated, matrix supported.	– – –
4, 3K, gw (15 on footwall)	3	10YR 7/2.5	10YR 5/3	LS	3 vco abk, 2° sg	lo-ehso, po	0	II+, ev	80 (cb pb gr)	do ----------	– – –
5, 3Bk, as (16 and 17 on footwall)	3	10YR 8/2	10YR 5/4	LS	3 co sbk where cemented, 2° sg	lo-vhso, po	0	I, II+ in lenses ≤10 cm wide, ev	75 (cb pb gr)	Moderately well sorted, subangular, moderately well bedded, imbricated in lenses, clast supported except in cemented lenses.	– – –
5.5, 4Bkb1, as (18 on footwall)	4	10YR 7/2	10YR 5/3	LS	sg	lo-vhso,po	0	II+ in lenses	70 (cb pb gr)	Moderately well sorted, subangular, moderately well bedded, nonimbricated, clast supported.	– – –
6, 5Bkb1, bottom of trench (19 on footwall)	4	10YR 7.5/2	10YR 5/3	LS	sg, 3 f sbk where cemented	lo-vhso, po	0	II+, ev	70 (cb pb gr, few ≤8 cm)	Moderately well sorted, subrounded, nonbedded, nonimbricated, matrix supported.	– – –
Fault-zone units											
7, FZ1–1, as (1 and 2 on hanging wall and footwall)	FZ	10YR 6/2	10YR 4/3	L	3 m-co sbk	shvss, vsp	0	I–, ev	25 (pb gr)	Moderately well sorted, subangular to subrounded, nonbedded, nonimbricated, matrix supported.	Fault-related colluvial wedge, preserved Av soil horizon in places.

Table 28. Soil and stratigraphic units exposed on the north wall of trench CFF–T1A across the Southern Crater Flat Fault in the Yucca Mountain area, southwestern Nevada—Continued

Field No., horizon, boundary	Unit	Dry color (<2-mm fraction)	Moist color (<2-mm fraction)	Texture	Structure (primary and secondary)	Consistence (dry, wet)	Clay films	Secondary carbonate (gravel and disseminated)	Gravel content (volume percent)	Parent material and lithology (sorting, angularity, bedding, imbrication, and support)	Miscellaneous (roots, pores, SiO_2, oxidation, concretions, salts)
Fault-zone units											
8, FZ1–2, as, erosional unconformity	FZ	10YR 6.5/3	10YR 4/3	L-SiL	2 co sbk-abk	so-shvss, po	0	I, ev	30 (pb gr)	do ----------	Offset buried Av+Bk soil horizon preserved in places.
9, FZ2, aw, event horizon?, erosional unconformity		10YR 6/2	10YR 4/3	SL	3 m-co sbk	sovss, vsp	0	I, filaments, e	30 (pb gr with few cb)	do ----------	Gravel fill eroded into lower unit.
10, FZ3–1, cs, event horizon (4 and 5 on hanging wall; 15, 16, and 17 on footwall)	FZ	10YR 6.5/2	10YR 4/3	SL	sg	loso, po	0	II, ev	70 (pb gr)	Moderately well sorted, subangular, nonbedded, nonimbricated, matrix supported.	– – –
11, FZ3–2, aw erosional unconformity	FZ	10YR 6/2	10YR 4/4	LS	sg	loso, po	0	I, ev	70 (cb gr)	Poorly sorted, subrounded, moderately well bedded, nonimbricated, matrix supported.	– – –
12, FZ3–3, aw, event horizon (6 on hanging wall; 18 and 19 on footwall)	FZ	10YR 7/2	10YR 4.5/3	LS	3 f-m abk, 2° sg	ehso,po	0	II, ev	– –	Poorly sorted except in lenses, subangular to subrounded, moderately well to nonbedded, nonimbricated, matrix supported.	Stages 1and 2 silica. This unit is very localized and not exposed on the south wall.
13, FZ4, bottom of trench	FZ	10YR 7/2	10YR 5/3	LS	2 f-m sbk, 2° sg	ehso, po	0	I+, ev	80 (cb pb gr)	Poorly sorted, subrounded to subangular, moderately well bedded, nonimbricated, matrix supported.	Stage I silica.
20, fracture fill, bottom of trench	Fracture fill	10YR 7/2	10YR 5/3	SL	sg	loso, po	0	I (numerous rotated clasts), ev	50 (cb pb gr)	Nonsorted, subangular to subrounded nonbedded, nonimbricated, matrix supported.	– – –
Footwall units											
14, 2Btwk cw (3 on hanging wall)	2	7.5YR 7/2	7.5YR 4/4	SL	3 m-co sbk	sovss, vsp	0	0, ev	50 (pb gr)	Poorly sorted, subangular, nonbedded, nonimbricated, matrix supported.	Horizon is eroded by a channel in center of the footwall.
15, 3K cs (4 on hanging wall)	3	10YR 7/2	10YR 5/2	LS	3 co pl, 2° m	ehso, po	0	III, ev	90 (cb pb gr)	Moderately well sorted, subangular, moderately well bedded, nonimbricated, matrix supported.	– – –

Table 28. Soil and stratigraphic units exposed on the north wall of trench CFF–T1A across the Southern Crater Flat Fault in the Yucca Mountain area, southwestern Nevada—Continued

Field No., horizon, boundary	Unit	Dry color (<2-mm fraction)	Moist color (<2-mm fraction)	Texture	Structure (primary and secondary)	Consistence (dry, wet)	Clay films	Secondary carbonate (gravel and disseminated)	Gravel content (volume percent)	Parent material and lithology (sorting, angularity, bedding, imbrication, and support)	Miscellaneous (roots, pores, SiO_2, oxidation, concretions, salts)
Footwall units											
16, 3Bk1 cs (top of 5 on hanging wall)	3	10YR 7/2	10YR 4/3	LS	sg except in cemented lenses	lo-hso, po	0	I with lenses of III, e	85 (cb pb gr)	Poorly sorted, subrounded, moderately well bedded, nonimbricated, matrix supported.	– – –
17, 3Bk2 as (bottom of 5 on hanging wall)	3	10YR 6/2	10YR 4/3	LS	sg	loso, po	0	I, ev	80 (pb gr)	Moderately well sorted, subrounded, moderately well bedded, imbricated in places, clast supported.	– – –
18, 4Bk1b1 cs (6 on hanging wall)	4	10YR 8/2	7.5YR 5/4	SL	m	ehso, po	0	III to IV–, I on gravel, ev	80 (pb cb gr)	Poorly sorted, subangular to subrounded, nonbedded, nonimbricated, matrix supported.	– – –
19, 4Bk2b1 (bottom of 6 on hanging wall) (not sampled)	4	10YR 8/3	7.5YR 5.5/4	LS	3 f sbk, 2° m	ehso, po	0	I+, ev	70 (pb gr)	Moderately well sorted, angular, nonbedded, moderately imbricated, matrix supported.	Secondary carbonate infiltrated into basalt bedrock.
19, 4K+R, bottom of trench	4	10YR 7.5/3	10YR 5/4	LS	sg	loso, po	0	I, ev	70 (pb gr)	Moderately well sorted, subrounded, weakly bedded, locally well imbricated, matrix supported.	Secondary carbonate infiltrated into basalt bedrock. Stage I silica

Table 29. Soil and stratigraphic units exposed on the north wall of trench CFF–T1 across the Southern Crater Flat Fault in the Yucca Mountain area, southwestern Nevada.

[See plate 17 and figures 1, 2, and 42 for locations. Colors from Munsell Soil Color Charts (Munsell Color Co., Inc., 1992). See table 14 for explanation of abbreviations. Do., ditto]

Field No., horizon, boundary	Unit	Dry color (<2-mm fraction)	Moist color (<2-mm fraction)	Texture	Structure (primary and secondary)	Consistence (dry, wet)	Clay films	Secondary carbonate (gravel and disseminated)	Gravel content (volume percent)	Parent material and lithology (sorting, angularity, bedding, imbrication, and support)	Miscellaneous (roots, pores, SiO_2, oxidation, concretions, salts
Hanging-wall and footwall units											
1, Av, as	1	10YR 7/3	10YR 5/4	SL	3 co pl, 2° 1 f-co sbk	shvss, vsp	0	0, e	10 (pb gr)	Well sorted, subangular, nonbedded, nonimbricated, matrix supported.	– – –
2, Bk, cs	1	10YR 8/3	10YR 4/3	SL	1 m-co sbk, 2° sg	sovss, po	0	I–, ev	40 (pb gr)	do ----------	– – –
3, 2Btkwb1, cw	2	7.5YR 7/3	10YR 4/4	SL	3 f sbk, 2° sg	soso, po	0	0, ev	40 (pb gr)	do ----------	– – –
Hanging-wall units											
4, 3K, aw (erosional unconformity)	3	10YR 7/2	10YR 5/3	LS	sg, 3 pl in places	ehso, po	0	II+, ev	80 (cb pb gr, few bd)	Nonsorted, subangular to subrounded, nonbedded, nonimbricated, matrix supported.	– – –
5, 4K, ac	4	10YR 8/3	10YR 5/3	LS	3 vco pl to m	ehso, po	0	III–IV (less developed adjacent to fault zone), ev	80 (pb gr)	Moderately well sorted, subrounded, nonbedded, nonimbricated, matrix supported.	– – –
6, 4Bk, ac	4	10YR 7/2	10YR 5/4	LS	1 f sbk, 2° sg	loso, po	0	I–II (better developed in lenses), ev	80 (cb pb gr, few bd)	Poorly sorted, subangular, moderately well bedded, nonimbricated, matrix supported.	– – –
7, 5Bk1b1, cw	5	10YR 7/3	10YR 3/4	SL	3 f-m abk	hso, po	0	I– (increasing toward base), ev	60 (pb gr, few cb)	Moderately well sorted, subrounded, poorly bedded, nonimbricated, matrix supported.	Well-preserved argillic B soil horizon, in places, at top of unit.
8, k25B b1, as	5	10YR 7/2	10YR 6/3	SL	sg	loso, po	0	I+ (better developed near top), ev	80 (cb pb gr)	do ----------	– – –
9, 6Bk1b2, bottom of trench	6	10YR 7/2	10YR 6/3	LS	3 co-vco pl (in lenses), 2° 1 co-f sbk	h-ehso, po	0	I, ev	80 (pb gr)	Moderately well sorted, subangular, poorly bedded, nonimbricated, matrix supported.	– – –

Table 29. Soil and stratigraphic units exposed on the north wall of trench CFF–T1 across the Southern Crater Flat Fault in the Yucca Mountain area, southwestern Nevada—Continued

Field No., horizon, boundary	Unit	Dry color (<2-mm fraction)	Moist color (<2-mm fraction)	Texture	Structure (primary and secondary)	Consistence (dry, wet)	Clay films	Secondary carbonate (gravel and disseminated)	Gravel content (volume percent)	Parent material and lithology (sorting, angularity, bedding, imbrication, and support)	Miscellaneous (roots, pores, SiO_2, oxidation, concretions, salts
Fault-zone units											
14, FZ (N. 4°–6° E) 13–40 cm wide	FZ	10YR 6.5/3	10YR 4/4	LS	sg	loso, po	0	I, with frequent rotated clasts, ev	40–80 (pb gr, few bd)	Poorly sorted, subrounded, nonbedded, nonimbricated, matrix supported.	Many vertically oriented clasts lining fracture fill. No vertically oriented carbonate laminae.
Footwall units											
11, 3K, cw	3 (FW)	10YR 7/2.5	10YR 7.5/ 4.5	LS	3 vco pl in places, 2° sg	ehso, po	0	II, ev	80 (cb pb gr)	Moderately well sorted, subrounded, nonbedded, nonimbricated, matrix supported.	– – –
12, 3Bk1, as	3 (FW)	10YR 7/2	7.5YR 4/3	LS	sg	lo-ehso, po	0	II+ to III (in lenses), ev	80 (cb pb gr)	Moderately well sorted, subrounded to subangular, nonbedded, nonimbricated, matrix supported.	– – –
13, 4Ckn, bottom of trench	4 (FW)	10YR 8/3	10YR 4.5/3	LS	sg	loso, po	0	II+ to III	80 (cb pb gr)	Moderately well sorted, subangular, nonbedded, imbricated in places, clast supported.	Stage 1 silica. Clean channel gravel.

Table 30. Numerical ages of deposits exposed in trench CFF–T1A across the Southern Crater Flat Fault in the Yucca Mountain area, southwestern Nevada.

[See plate 18 and figures 1, 2, and 42 for locations. Samples: HD (error limits, ±2σ), U-series analyses by J.B. Paces; TL–61 (error limits, ±2σ), thermoluminescence analysis by S.A. Mahan]

Trench (pl. 17)	Sample	Unit and material sampled	Estimated age (ka)
CFF–T1A	TL–61	2, 2Bw soil horizon----------	9±1
	HD 1956	4, clast rind----------	263±16, 311±35, 352±26
	HD 1957	4, clast rind----------	210±12, 236±13, 247±12
	HD 1958	3, 3Bk soil horizon, clast rind---	120±5, 125±15, 128±6
	HD 1959	3, 3K soil horizon----------	40±2, 49±2, 60±9
	HD 1961	4, clast rind----------	260+∞/–110, 348±178

backtilting on the hanging wall and erosion on the footwall, where applicable. The estimated vertical slip for each faulting event is generally accurate to within ±10 cm.

Trench CFF–T1A (pl.17) provides a less ambiguous paleoseismic history than trench CFF–T1 (pl. 18). Age control exists on the deposits in trench CFF–T1A, and the units on the hanging wall and footwall are correlative. In the following discussions, trench CFF–T1A is therefore described first, and comparisons are then made with trench CFF–T1.

Trench CFF–T1A

In trench CFF–T1A (pl. 17), the Southern Crater Flat Fault is defined by two strands, 1.5 m apart, that bound an alluvium-filled graben in the intervening zone. Bedrock (basalt), exposed in the footwall, is in contact with downfaulted Quaternary deposits in the hanging wall to the west. The surficial units (1, 2, 3, and so on, pl. 17; table 28) are in an alternating sequence of alluvium and fine-grained eolian deposits. Individual units, generally separated by unconformities, are characterized by weakly cemented fine-grained materials at the top underlain by carbonate-cemented soil horizons that cap unconsolidated, matrix-supported gravel forming the base. Soils in the hanging wall appear to be less well developed than in the footwall. On the soils in the footwall, secondary carbonate accumulated in the uppermost 1 m of the deposits, which are relatively stable, with little aggradation and (or) erosion taking place. In contrast, aggradation of materials along a still-existing drainage channel that traverses the hanging wall resulted in the accumulation of thicker deposits on that (west) side of the fault (pl. 17) and the subsequent distribution of secondary carbonate through the upper 2 to 3 m of the deposit.

The two fault strands exposed in the trench cut to different depositional units or levels in the Quaternary sequence, and the observed stratigraphic relations provide a basis for estimating the number and relative timing of faulting events, as described below.

Event Z

The most recent faulting event recorded in the surficial deposits exposed in trench CFF–T1A (pl. 17) occurred on the strand that defines the eastern margin of the graben (pl. 17). This strand is the only splay that disrupts the surface soil in unit 1, including the Av soil horizon. Units FZ1–1 and FZ1–2 contain light-colored, weakly cemented Bk and Av soil-horizon materials that slumped adjacent to the fault and were subsequently buried by eolian deposits. Because the fault extends upward to near the ground surface and the overlying soils are poorly developed, the faulting event (Z) must have occurred relatively recently. Av soil horizons at the surface in the Yucca Mountain area (figs. 1, 2) generally range in age from 2 to 6 ka, and a thermoluminescence analysis of one sample (TL–61, table 30) collected in the fine-grained unit 2 (pl. 17), which was also offset, yielded a maximum estimated date for event Z of 9±1 ka. Therefore, surface rupture of the Av soil horizon occurred 9–2 ka (preferred value, 6–2 ka). About 18 to 20 cm of vertical offset that was measured at the top of unit 2 is assumed to represent the offset from event Z.

Event Y

Event Y occurred along the two splays of the Southern Crater Flat Fault that bound the graben (pl. 17). The western strand is marked by a truncated fissure fill that was enlarged during this faulting event and displaced all units except the modern soil (units 1, 2). The western splay did not fracture during event Z. Material appears to have been deposited into the graben before event Y, and was then rotated during the faulting event. This surface-rupturing paleoearthquake offset the moderately well developed K soil horizon ($CaCO_3$ stage II+–III morphology) developed on unit 3. The K soil horizon is preserved on the hanging wall (3K), the graben (FZ3–1), and the footwall (3K). Secondary carbonate in the 3K soil horizon (unit 3) was dated (U-series) as 40–70 ka (sample HD 1959, table 30). Unit 3 contains some black ash, which is tentatively correlated with the eruption of the nearby Lathrop Wells volcanic center (fig. 1) at 77±6 ka (Heizler and others, 1999). Ages of 120–130 ka (sample HD 1958, table 30) were also estimated from unit 3 at depth (3Bk soil horizon). Because the 3K soil horizon was formed before being displaced by event Y, this event is assumed to have occurred after 40 ka but before the paleochannel was deposited by approximately 9 ka (sample TL–61, table 30).

After event Y, a channel (unit 2) was eroded into the 3K soil horizon developed on unit 3 and removed evidence of the surface offset produced by the event. The Btwk soil horizon developed on unit 2 is preserved east of the margin of the paleochannel, where it was not eroded. These uncertainties make measurement of the offset difficult, but it is estimated at 5 to 15 cm (preferred value, 10 cm on the western fault splay), on the basis of projecting the contact between units 2 and 3 on the footwall westward across the fault zone and measuring the offset with the same contact on the hanging wall. This offset was then compared with the offset at the base of the 3K soil horizon across the fault zone.

Event X

Event X displaced units 4 and 5 and also occurred along the two graben-bounding fault splays. Fractures on the eastern splay are truncated at the top of a buried soil on unit 4. Material tilted eastward into the 1.5-m-wide graben between the exposed faults. Unit 4 is rotated and preserved in the base of the graben. Ages of secondary carbonate and opaline silica on inner rinds were estimated at 250 ka (average for unit 4; samples HD 1957, HD 1961, table 30) and 260–350 ka (unit 5; sample HD 1956, table 30), providing minimum ages for the deposits. Displacement occurred after the carbonate

was in place, thus the U-series analyses provide a maximum estimated date of 250 ka for event X. Because the fractures are truncated by unit 3, which has a minimum estimated age of 120–130 ka (sample HD 1958, table 30), the event is dated at no earlier than 250 – 130 ka. Subsequently, alluvium (unit 3) appears to have been rapidly deposited, thereby preserving the nearly vertical, well-cemented small fault scarp. The offset from this event is estimated at 17 to 32 cm (preferred value, 20 cm), resulting in an estimated total offset exposed in trench CFF–T1A (pl. 17) of 24 to 65 cm (preferred value, 48 cm) and a maximum vertical-slip rate of 0.002 mm/yr.

Summary of Depositional and Faulting Events

A series of schematic cross sections showing the sequential development of the structures exposed on the north wall of trench CFF–T1A (pl. 17) is shown in figure 43. The various stages, from oldest to youngest, are summarized as follows:

1. Alluvium (units 4, 5) accumulated on or adjacent to the bedrock scarp. Infiltrated silt capped and weakly cemented the alluvium, and a soil, characterized by a Bk horizon, developed on the surface. Event X displaced units 4 and 5, which were rotated into the graben.
2. Alluvium (unit 3) accumulated on the scarp and in the graben, and a soil (3K horizon) developed on the surface.
3. Event Y displaced the moderately well developed K soil horizon on top of unit 3. A fault fissure formed on the western fault strand, and unit 3 was rotated into the graben. The K soil horizon was preserved in the graben (unit FZ3–1).
4. A channel (unit 2) cut into the K soil horizon on top of unit 3 and eroded the surface offset recorded by event Y. Fine eolian sand and silt accumulated on the surface and infiltrated the underlying deposit. Incipient Bk and Bt soil horizons formed, capped by an Av soil horizon at the surface.
5. Event Z offset the modern soil. Av and Bk soil-horizon materials slumped against the fault and were buried by fine-grained eolian materials.

Trench CFF–T1

Quaternary deposits exposed in trench CFF–T1 (pl. 18), which are morphologically similar to those exposed in trench CFF–T1A, appear to record a comparable depositional history and are assumed to be contemporaneous. The buried soils are similarly characterized by weakly cemented fine-grained material above a zone cemented by secondary carbonate, and by a deeper zone of unconsolidated matrix-supported gravel. On the basis of the abundance of fine-grained materials and the morphology of the secondary carbonate, each soil is estimated to represent at least 10 k.y. of surface exposure. The buried soils are capped by erosional unconformities.

The fault is marked by a single fissure fill, as much as 40 cm wide, that narrows to a single fracture at the surface. No additional strands of the fault are present; however, discontinuous fractures were observed. The fault exposed in trench CFF–T1 (pl. 18) is oriented N. 4°–6° E., unlike the general trend of the fault strand exposed in trench CFF–T1A that is oriented N. 15°–28° E.

Event Z

Evidence for event Z includes a single fracture that penetrates the surface. Although the Av soil horizon (pl. 18) is not clearly offset, the Bk soil horizon, immediately below the Av soil horizon, is thickened in the fault zone and on the hanging wall, a relation that is interpreted to indicate a faulting event with an estimated offset of 5 to 10 cm. Such a small displacement at the surface may have healed rapidly, leaving no Av soil-horizon material apparently offset or buried. On the basis of a correlation of soil properties to those exposed in trench CFF–T1A (pl. 17), the surface rupture is dated at 9–2 ka (preferred value, 4–3 ka).

Event Y

Event Y displaced units 3 through 6 approximately 5 to 10 cm. Unit 3 is capped by a well-developed 3K soil horizon

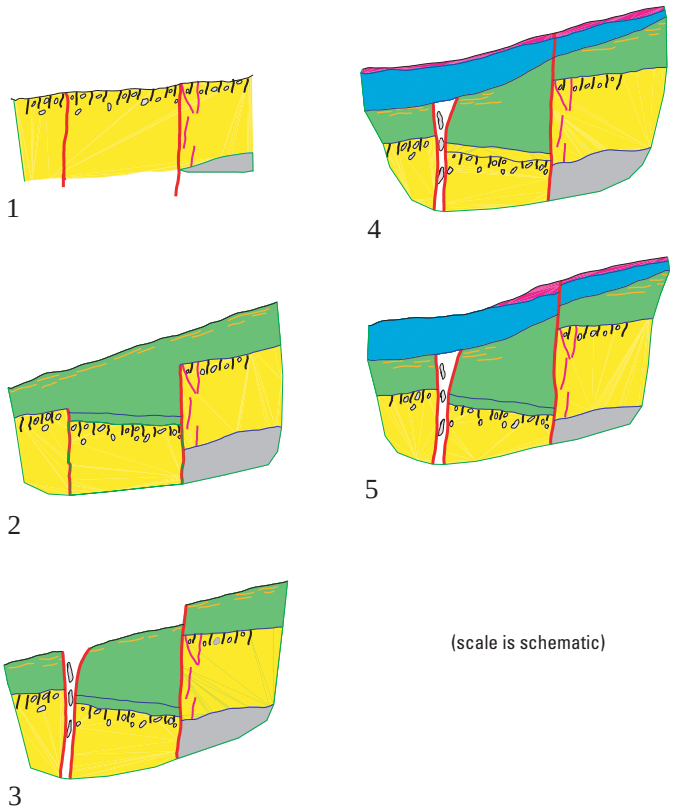

Figure 43. Schematic diagrams illustrating sequential development (stages 1–5) of structures on north wall of trench CFF–T1A (pl. 17; figs. 2, 42) across the Southern Crater Flat Fault in the Yucca Mountain area, southwestern Nevada (figs. 1, 2).

that formed before being displaced by this event. On the basis of correlating soil development with the dated units exposed in trench CFF–T1A (pl. 17), event Y is dated at later than 40 ka.

Event X

Event X displaced units 5 and 6 about 10 to 15 cm. Unit 5 has a minimum estimated age of 263±16 ka (sample HD 1956, table 30). A total offset of 20 to 40 cm, measured on the top of unit 5 in the deposits exposed in trench CFF–T1 (pl. 18), provides a maximum fault-slip rate of 0.002 mm/yr.

Summary

Geologic relations exposed in trenches CFF–T1A and CFF–T1 indicate that at least three surface-rupturing paleoearthquakes occurred on the Southern Crater Flat Fault during middle Pleistocene to early Holocene time. On the basis of thermoluminescence analyses of fine-grained alluvium and U-series analyses of secondary carbonate and opaline silica sampled from the inner rinds of clasts, event Z probably occurred 4–3 ka, event Y 40–10 ka, and event X 250–130 ka. Minimum recurrence intervals are about 5 to 90 k.y., and the maximum total vertical-slip rate is estimated at 0.002 mm/yr.

Chapter 11

Quaternary Faulting on the Northern Crater Flat Fault

By Jeffrey A. Coe

Contents

Abstract....145
Introduction and Setting....145
Methods....145
Stratigraphy, Soils, and Structure Exposed in Trench CFF–T2a....146
Paleoearthquakes....153
Quaternary Slip Rate and Average Recurrence Interval....154
Relation to the Southern Crater Flat Fault....154
Acknowledgments....154

Abstract

Quaternary activity on the Northern Crater Flat Fault was studied in a trench that exposes evidence of four or five surface-rupturing paleoearthquakes. The youngest faulting event is estimated to have occurred 6–4 ka, and the oldest about 500 ka. The total net cumulative displacement of the oldest deposits exposed in the trench (estimated age, >500 ka) is about 122 cm, which yields a slip rate of <0.0024 mm/yr. The average earthquake-recurrence interval is estimated at 165 k.y. for three interseismic intervals, or 124 k.y. for four interseismic intervals.

Introduction and Setting

The Northern Crater Flat Fault is a discontinuous, multistrand, normal to left-oblique-slip fault along the northeast edge of Crater Flat and the northwest flank of Yucca Mountain (figs. 1, 2). Characteristics of the fault are summarized in chapter 3 and were described by Simonds and others (1995).

In general, Quaternary deposits younger than middle Pleistocene are poorly preserved along the Northern Crater Flat Fault (see Faulds and others, 1994). The most extensive, relatively young deposits are on a large, middle to upper Pleistocene alluvial fan (units Qa3/Qa4, table 2). Therefore, to examine the paleoseismic history of the fault in the youngest deposits available, trench CFF–T2 (fig. 2) was excavated where the fault crosses this fan, as well as where it crosses a vegetation lineament that is on line with projections of scarps preserved in older deposits along the fault. An alternative trench (CFF–T2A) was located on a subtle scarp in lower to middle Pleistocene alluvial gravel about 1.5 km north of trench CFF–T2. The deposits in trench CFF–T2A are correlated with either unit Qa1 or unit Qa2 (see Faulds and others, 1994), more likely with unit Qa1, on the basis of the carbonate cementation exposed in the trench and the topographically rounded surface covered with abundant carbonate chips. Estimated ages for units Qa1 and Qa2 are 430–760 ka and 380+350/−110 ka, respectively (see chap. 2).

Both trenches were excavated in spring 1995. Trench CFF–T2 (fig. 2) did not intersect the fault; the vegetation lineament that led to siting of the trench may be a paleoearthquake-related feature, but one that produced no measurable offset of the alluvial fan in that locality. Fault offset was observed in trench CFF–T2A, however, and the Quaternary paleoseismic history of the Northern Crater Flat Fault, as determined from detailed logging and interpretation of the exposed geologic relations, is summarized in this chapter. Because trench CFF–T2A was excavated in lower to middle Pleistocene deposits, the paleoseismic record preserved in the walls of the trench may be incomplete with respect to possibly later faulting events.

Methods

Trench CFF–T2A (pl. 19) was logged by using field and close-range photogrammetric methods (see chap. 1). Stratigraphic units were described in accordance with standard sedimentologic terminology, and soil descriptions follow the nomenclature of Birkeland (1984) and Machette (1985). Paleoearthquakes were identified on the basis of offset units across the fault, colluvial wedges or fault fissures, and the upward termination of fractures (see chap. 1). U-series and thermoluminescence analyses were used to estimate the ages of stratigraphic units and soils and to date paleoearthquakes. Dating methods are described in chapter 2, and estimated ages of the materials collected in trench CFF–T2A are listed in table 31.

Table 31. Numerical ages of deposits exposed in trench CFF–T2A across the Northern Crater Flat Fault in the Yucca Mountain area, southwestern Nevada.

[See plate 19 and figures 1 and 2 for locations. Samples: TL–62 through TL–64 (error limits, ±2σ), thermoluminescence analyses by S.A. Mahan; HD 1964 and HD 1966 (error limits, ±2σ), U-series analyses by J.B. Paces]

Trench (pl. 19)	Sample	Unit and material sampled	Estimated age (ka)
CFF–T2A	TL–62	6, clast rind----------	5±1
	TL–63	4, silty sand----------	84±19
	TL–64	4, silty sand----------	495±434
	HD 1964	2, clast rind----------	>400
	HD 1966	5b, clast rind----------	32±2, 493±260

Stratigraphy, Soils, and Structure Exposed in Trench CFF–T2a

Trench CFF–T2A (pl. 19) exposes a sequence of alluvial sandy gravel (units 1–5) and eolian sand (unit 6); unit descriptions are listed in table 32. Units 1, 2, 4, 5, and 6 have characteristics typical of the alluvial gravel deposits around Yucca Mountain; they contain subangular to subrounded clasts of Tertiary volcanic rocks, are generally poorly to moderately well sorted, and range in texture from matrix to clast supported. Units 1, 4, 5, and 6 are present on both the downthrown and upthrown blocks of the fault, whereas units 2 and 3 are present on only the downthrown block. Unit 3 probably resulted from stripping of units 1 and (or) 2 on the upthrown (east) block. Disrupted pods of B soil horizon, which are common in unit 3, are believed to have originated on the upthrown block. Additionally, unit 3 has been extensively bioturbated from burrowing animals and from plant roots, as evidenced by abundant rhizoliths and an irregular base. Unit 2 has a well-developed carbonate soil that is absent on unit 3, and the top of the unit is irregular, indicating a period of erosion before the deposition of unit 3. Subunit 5a is a wedge-shaped deposit, with characteristics indicative of both alluvial and colluvial origins, that accumulated on the downthrown side of a small-displacement fault strand (pl. 19). Subunit 5d, consisting primarily of clasts from unit 5, is interpreted to have been deposited as an upper part of unit 5 that was later broken up to form a "rubble" zone resulting from movement on the directly underlying Northern Crater Flat Fault zone (pl. 19; fig. 44).

Age constraints on the exposed units in trench CFF–T2A include two thermoluminescence analyses of silty sand from unit 4 (samples TL–63, TL–64, pl. 19; table 31) and four U-series analyses of buried silica-carbonate soils that formed units 2 and 5. The two thermoluminescence analyses yielded radically different age estimates of 84±19 ka (sample TL–63) and 495±434 ka (sample TL–64). Although the age of sample TL–64 fits within the estimated ages for units Qa1 and Qa2, the extremely high dose rate for these two samples (8–10 grays/k.y.) indicates that neither estimated age is reliable (S.A. Mahan, oral commun., 2000).

Three moderately well developed silica/carbonate-cemented ($CaCO_3$ stage II–IV morphology) buried soils are exposed in the trench (see soil profiles on pl. 19 and soil descriptions in table 33). The youngest buried soil (b1) is formed on units 4 and 5 on the upthrown block and on units 3 through 5 on the downthrown block. This buried soil probably represents several cycles of erosion and soil formation, and the top forms a conspicuous stripped, irregular boundary with the overlying eolian unit 6 and a modern A soil horizon. U-series estimated ages of the opaline silica component of soil b1 range from 32±2 to 493±260 ka (sample HD 1966, pl. 19, table 31). The second-youngest buried soil (b2) is formed on unit 2 on the downthrown block. On the upthrown block, this soil is probably included as part of the carbonate soil designated b1 or b2. On the basis of a U-series analysis (sample HD 1964, pl. 19; table 31) the age of soil b2 on the downthrown block is estimated at older than 400 ka. The oldest buried soil (b3) is formed on unit 1 on both the upthrown and downthrown blocks.

The main fault zone exposed in trench CFF–T2A (pl. 19) has a flower-shaped geometry that ranges in width from about 0.8 m near the bottom of the trench to 3 m near the top (fig. 44). The central part of the fault zone consists of an intact triangular block of carbonate-cemented unit 5, with two main fissures on either side (fig. 44). The eastern fissure is nearly vertical and appears to extend from unit 5 upward into unit 6; the western fissure has dips ranging from about 10° near the top of the trench, through 40° midway down the trench wall, to vertical at the intersection with the eastern fissure about 1 m above the base of the trench. Fractures parallel both fissures. The central block and both fissures are believed to have formed by lateral shear and by downdropping of units on the west side of the fault. As the west side was downdropped by vertical and (or) lateral shear along the vertical part of the main fault trace, the central block became detached from the main downthrown block and tilted westward. The tilting (1) opened the near-vertical extensional fissure on the east side of the block, (2) opened the shallow fissure (by shear) on the west side, and (3) broke apart the upper part of the central block, thereby creating the rubble zone in subunit 5d. The scarp on the surface corresponds to the western fissure. Both fissures are filled by eolian/colluvial silty sand. A thermoluminescence analysis of a sample (TL–62, pl. 19; table 31) from fill in the western fissure yielded an estimated age of 5±1 ka.

Fractures extend to various stratigraphic levels, away from the main fault trace on both the upthrown and downthrown blocks (fig. 44). Individual fracture sets are difficult to distinguish, although two distinct sets are apparent: one set of shear fractures that terminate at the top of unit 4b on the upthrown block, and one set of primarily extensional fractures that terminate at the top of unit 5.

The downthrown block is backtilted and possibly slightly downwarped. Units 1 through 4 are backtilted and may be slightly convex upward, with the high point near soil profile III (pl. 19). Fractures near the west end of the trench may be related to backtilting or folding. The net cumulative vertical displacements described in the following sections were esti-

Table 32. Descriptions of stratigraphic units exposed on the south wall of trench CFF–T2A across the Northern Crater Flat Fault in the Yucca Mountain area, southwestern Nevada.

[See plate 19 and figures 1 and 2 for locations. Position: DB, downthrown block; UB, upthrown block. Descriptions of upthrown block are from observations made predominantly in the vicinity of soil profile I, and descriptions of downthrown in the vicinity of soil profile III. General lithology (in order from most to least abundant): pbl, pebble (2–60 mm); cbl, cobble (6–26 cm); bld, boulder (>26 cm); snd, sand (<2 mm); slt, silt. Matrix: c, coarse; f, fine; masked, obliterated by pedogenic carbonate; m, medium; pbl, pebble; slt, silt; snd, sand; vc, very coarse; vf, very fine. Cementation: CO3, carbonate; ind, indurated; mod, moderate; non, noncemented; Si, silica; stg, strong; vstg, very strong; wk, weak. Fabric includes degree of sorting and rounding of grains, bedding characteristics, degree of imbrication, type of internal support, and characteristics of lower contact. Deformation: EW, event wedge; F, faulted; FF, fissured. Do., ditto]

Unit or subunit	Position	General lithology	Clast size (cm) and abundance (vol pct)	Matrix	Cement	Thickness (cm)	Shape	Fabric	Miscellaneous features	Deformation
1	UB	pbl snd cbl slt	<22, 70–90	slt-c snd	CO_3, Si, stg	>95 (base not observed)	Tabular ---------	Poorly to moderately well sorted, subrounded, gravel beds continuous and extensive, moderate imbrication down to the east, matrix to clast supported, lower contact not exposed.	Matrix at top of unit contains eolian contribution.	F
4	UB	snd pbl cbl	<20, 30–80	f-c snd	CO_3, wk-mod	0–90 (avg 75)	Lenticular tabular.	Poorly to moderately well sorted, subangular to subround, local lenses of cobbles (unit 4a), poor imbrication down to the east, matrix supported, unconformable sharp lower contact.	– – –	F
4a	UB	pbl snd pbl	<29, 60–90	f-c snd	CO_3, wk-mod	0–35 (avg 20)	Lenticular ------	Moderately well sorted, subrounded, no bedding or imbrication, clast supported, gradational to sharp lower contact.	– – –	F
4b	UB	pbl cbl snd	<80, 70–90	f-c snd	CO_3, mod	0–30 (avg 25)	do ----------	Poorly to moderately well sorted, subangular, poor imbrication down to east, clast supported, sharp to gradational lower contact	– – –	F
4a/4b	UB	pbl snd cbl	<26, 50–70	f-c snd	CO_3, wk-mod	0–64 (avg 40)	do ----------	Poorly sorted, subrounded, jumbled appearance with pods of moderately well sorted gravel and some pebble alignment, matrix supported, unconformable sharp lower contact.	– – –	F
5	UB	pbl cbl snd bld	<53, 85–95	snd	CO_3 and Si, mod-stg	0–100 (avg 80)	Irregular; assumed to be originally tabular before erosion.	Moderately well to well sorted, subangular to subrounded, bedding that dips east, some crossbedding, moderate to strong imbrication down to the east, some upward grading, clast supported, sharp lower contact.	Top of unit has been stripped by erosion.	F
5a	UB	pbl snd cbl	<29, 85–95	f-c snd	CO_3, mod	0–18 (avg 14)	Lenticular/ wedge.	Poorly to moderately well sorting, subrounded to subangular, minor bedding, clast supported, gradational to sharp lower contact.	Probably alluvium and colluvium deposited on downthrown side of fault.	EW?, F

Table 32. Descriptions of stratigraphic units exposed on the south wall of trench CFF–T2A across the Northern Crater Flat Fault in the Yucca Mountain area, southwestern Nevada—Continued

Unit or subunit	Position	General lithology	Clast size (cm) and abundance (vol pct)	Matrix	Cement	Thickness (cm)	Shape	Fabric	Miscellaneous features	Deformation
5c	UB	pbl snd cbl	<20, 60–90	snd	CO_3, wk-stg	0–>180 (avg 120)	Irregular --------	Moderately well to well sorted, subrounded, distinct bedding, moderate to strong imbrication down to the east, clast supported, gradational to sharp lower contact.	Top of unit has been stripped by erosion.	F
6	UB	slt pbl cbl	<100, 5–10	slt-f snd	CO_3, wk	15–90 (avg 20)	Tabular with irregular base.	Well sorted, subrounded to rounded, no bedding or imbrication, laminar carbonate/silica clasts from soil on unit 5 are present in lower part of unit, matrix supported, lower contact is irregular and sharp.	– – –	F
1	DB	pbl snd slt cbl	<25, 70–90	f-c snd	CO_3, wk-well	>60 (base not exposed)	Top is irregular.	Poorly to well sorted, subangular to subrounded, bedded with poor to moderate imbrication, clast supported, lower contact not exposed.	Matrix at top 20 cm of unit contains eolian contribution.	F
2	DB	pbl snd cbl	<20, 70–95	f-c snd	CO_3, wk-stg	0–80 (avg 60)	Irregular; assumed to be originally tabular before erosion/bioturbation.	Poorly to moderately well sorted, subangular to subround, bedded with moderate imbrication down to east, clast supported, sharp lower contact.	Appears to have a sandy unit (1) at base.	F, probably deposited due to paleoearthquake that caused erosion on the UB
3	DB	slt pbl snd cbl	<15, 20–50	slt-c snd	CO_3, wk-mod	25–>110 (avg 50)	Tabular/irregular.	Poorly to well sorted for gravel and slt, respectively, subrounded, no bedding or imbrication, strongly bioturbated, contains carbonate-coated clasts from underlying unit, matrix supported, unconformable, irregular sharp lower contact.	Abundant pods of B soil horizon with 10YR 6/4-7/4 color.	Do.
4	DB	pbl cbl snd bld	<50, 60–80	f-c snd	CO_3, wk-mod	50–90 (avg 80)	Tabular ---------	Poorly to well sorted, subangular to subrounded, gravel bedding and sandy-cobble lenses common (see unit 4a), top of unit generally defined by sandy-cobble layer (unit 4b), strong imbrication down to the east, clast supported, sharp lower contact.	Few fragments of B soil horizon present.	F

Table 32. Descriptions of stratigraphic units exposed on the south wall of trench CFF–T2A across the Northern Crater Flat Fault in the Yucca Mountain area, southwestern Nevada—Continued

Unit or subunit	Position	General lithology	Clast size (cm) and abundance (vol pct)	Matrix	Cement	Thickness (cm)	Shape	Fabric	Miscellaneous features	Deformation
4a	DB	snd cbl pbl slt	<200, 70–80	slt-c snd	CO_3, mod	0–40 (avg 20)	Lenticular ------	Moderately well to well sorted, subangular to subrounded, no bedding or imbrication, clast supported, sharp lower contact.	Pods of B soil horizon present.	F
4b	DB	snd cbl pbl slt	<200, 70–80	slt-c snd	CO_3, mod	0–40 (avg 20)	do ----------	Moderately well to well sorted, subangular to subrounded, no bedding or imbrication, clast supported, sharp lower contact.	do ----------	F
5	DB	pbl cbl snd slt bld	<43, 70–90	slt-c snd	CO_3, stg	0–140 (avg 70)	Wedge, pinching to west; assumed to be tabular before erosion.	Poorly to moderately well sorted, subangular to subrounded, local bedding, moderate imbrication down to east, clast support, sharp lower contact.	Top of unit has been stripped by erosion.	F
5b	DB	cbl snd pbl bld	<40, 80–90	f-c snd	CO_3, mod stg	0–30 (avg 20)	Lenticular ------	Moderately well to well sorted, subround, no bedding or imbrication, clast support, gradational to sharp lower contact.	– – –	F
5d	DB	pbl cbl snd slt bld	<43, 70–90	slt-c snd	CO_3, stg	0–140 (avg 70)	Wedge, pinching to west; assumed to be tabular before erosion	Poorly to moderately well sorted, subangular to subrounded, local bedding, moderate imbrication down to east, clast supported, sharp lower contact.	Unit is the same as unit 5, except that it is a rubble zone created by faulting.	F
6	DB	slt pbl cbl snd	<20, 5–10	slt	CO_3, wk	15–40 (avg 20)	Tabular with irregular base.	Well sorted, angular to subangular, no bedding or imbrication, matrix supported, unconformable irregular lower contact.	Carbonate clasts from unit 5 have been pedogenically worked up into this unit; unit appears to redden downward, indicating weak B soil-horizon development.	F
Fissure fill	Fault zone	slt snd pbl cbl	<7, 5–10	slt-c snd	CO_3, wk	0–20 (avg 10)	Fissure with increasing width upward.	Moderately-well sorted, angular to subround, no bedding or imbrication, matrix supported, sharp boundaries.	– – –	FF

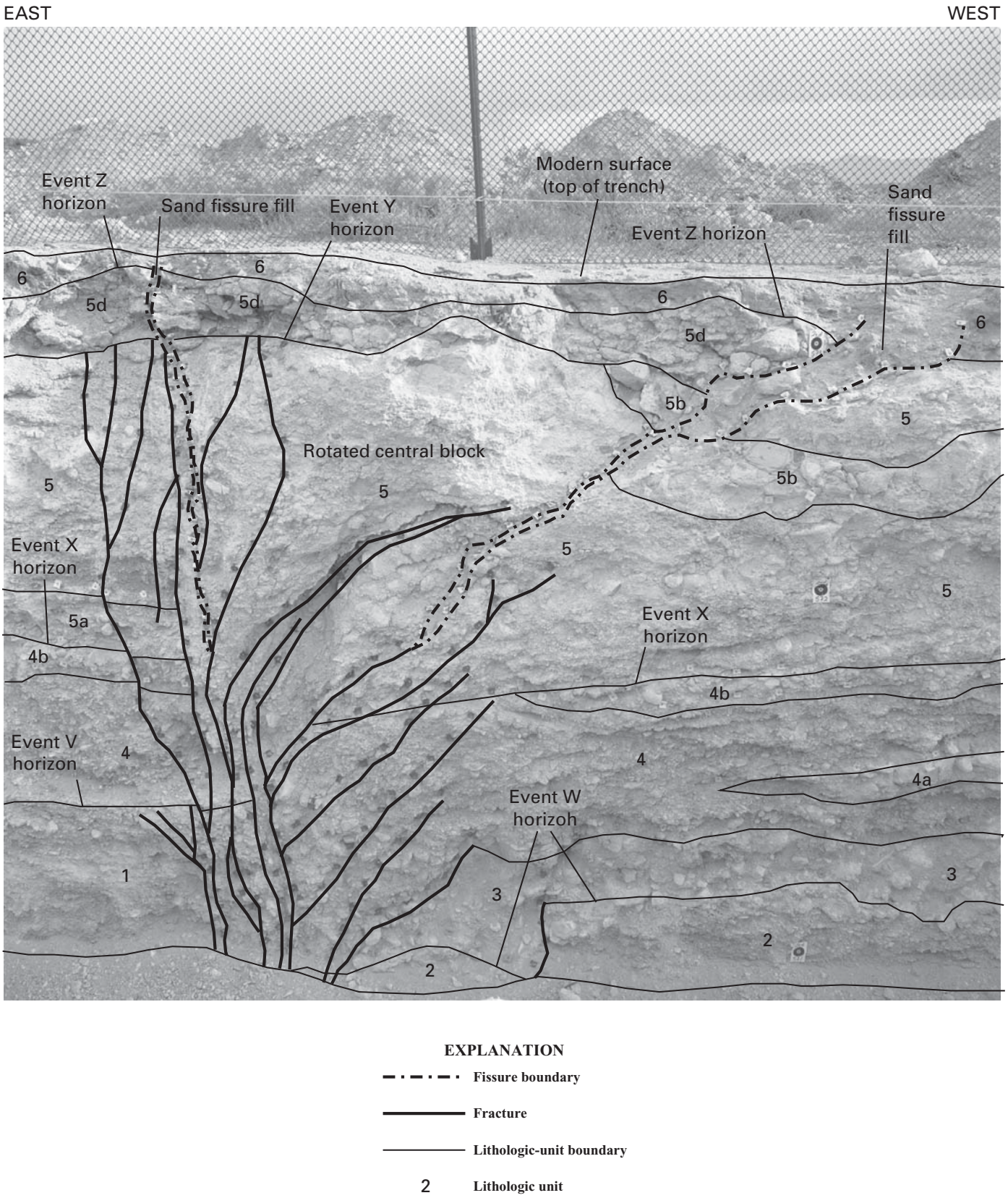

Figure 44. Part of south wall of trench CFF–T2A across the Northern Crater Flat Fault in the Yucca Mountain area, southwestern Nevada (pl. 19; figs. 1, 2), showing main fault zone, mapped surficial deposits, and event horizons marking Quaternary faulting events (V–Z). Dark spots along some lines are markers that were emplaced to facilitate mapping.

Table 33. Descriptions of soil profiles in trench CFF–T2A across the Northern Crater Flat Fault in the Yucca Mountain area, southwestern Nevada.

[See plate 19 and figures 1 and 2 for locations. See table 3 for soil-horizon terminology. Colors from Munsell Soil Color Charts (Munsell Color Co., Inc., 1992). Texture: lm, loam; slt, silt; snd, sand. Structure—grade: 1, weak; 2, moderate; 3, strong; m, massive; sg, single grain—size: c, coarse; f, fine; m, medium; v, very fine—type: abk, angular blocky; pl, platy; sbk, subangular blocky. Consistence—dry: eh, extremely hard; h, hard; lo, loose; sh, slightly hard; so, soft; vh, very hard—wet: po, nonplastic; ps, slightly plastic; so, nonsticky; ss, slightly sticky. CO_3 stage morphology from Birkeland (1984). Effervescence (in cold dilute HCl): e, some; em, moderate; eo, none; es, strong; ev, very strong; vse, very slight. Cementation: ci, indurated; cs, strong; cw, weak. Lower horizon boundary—distinctness: a, abrupt; c, clear; g, gradual—topography: i, irregular; s, smooth; w, wavy. Roots—abundance: 1, few, 2, common; 3, many—size: co, coarse; f, fine; m, medium; vf, very fine—location: frc, fractures; lam, laminae; ped, ped faces; thruout, throughout. Pores—abundance: 1, few; 2, common; 3, many—size: f, fine; m, medium; vf, very fine—shape: i, irregular or interstitial; v, vesicular—location: nod, carbonate nodules; ped, ped faces; thruout, throughout; upper, upper part of soil. Rhizoliths—abundance: 1, few; 2, common; 3, many—size: co, coarse; f, fine—location: thruout, throughout. n.o., not observed]

Horizon	Depth (cm)	Associated unit	Color		Gravel content (vol pct)	Texture	Structure	Consistence		CO_3 morphology stage	Effervescence	Cementation	Lower horizon boundary	Roots	Pores	Rhizoliths
			Wet	Dry				Dry	Wet							
Soil profile I																
Avk	0	6	10YR 6/4–5/4	10YR 7/3	5–15	sltlm	2vf-c sbk	sh	so-ss ps-p	n.o.	es-ev	n.o.	cw	2 vf-co thruout	3 vf-f thruout	n.o.
2Bkb1	12	5c	10YR 7/3	10YR 8/1	60–90	sndlm	2f-c abk, pl	vh	so-ss po	I–III	es-ev	cs	a-c w	2 vf-m thruout	n.o.	n.o.
3Bkb1	119	5	10YR 7/3	10YR 8/1	85–95	sndlm	1-2 f-m sbk m	vh	so po	II	es	cs	cw	1 vf-f thruout	n.o.	1 f-m thruout
4Bkb1 or 4Bkb2	141	4	10YR 7/3	10YR 8/1	50–70	sndlm	2 f-c sbk m	h-vh	so ss	II	es	cs	a s	1 vf thruout	2 vf-f v upper	2 m-co thruout
5Kqmb2 or 5Kqmb3	209	1	7.5YR 6/6	7.5YR 7/4	70–90	sndlm	2 m-c sbk, pl m	vh	so po	III–III+	es	ci	n.o.	n.o.	2 vf-f v upper	n.o.
Soil profile II																
Avk	0	6	10YR 6/4–5/4	10YR 7/3	10–20	sndlm	1-2f-m sbk	sh-h	so-po	n.o.	es-ev	n.o.	cw-i	2vf-m thruout	3vf-f v	n.o.
2Kqmb1	33	5	10YR 8/2	10YR 8/1	60–85	sndlm	m	vh-eh	so po	III–III+	es	cs-ci	a s	2 vf-f thruout	n.o.	n.o.
3Bkbl	130	4	10YR 7/3	10YR 8/1	30–80	sndlm	1-2 vf-c sbk m	sh	so po	II	es	cw-cs	a s	2f-m thruout	n.o.	2 f-m thruout
4Bkqmb2	222	1	10YR 7/3	10YR 8/1–8/3	70–90	sndlm	2-3f-c sbk, pl m	vh-eh	so po	III	es	cs-ci	n.o.	n.o.	3vf-f top 20 cm	n.o.
Soil profile III																
Avk	0	6	10YR 7/3	10YR 6/4	20–30	sndlm	1-2 vf-m sbk	sh-h	so po-ps	n.o.	es-ev	n.o.	a-c w	2 vf-co thruout	3 vf-f thruout	n.o.
2Kqmb1	30	5	10YR 8/2–7/2	10YR 8/1	5–10	sndlm	2 m-co sbk, pl m	vh-eh	so po	II–IV	es	cs-ci	c w	1 vf-f thruout	n.o.	1 vf-m thruout
3Bkb1	76	4	10YR 7/2	10YR 8/1	60–80	sndlm	m	h	so po	II	es	cs	c w	1 vf-f thruout	n.o.	1 f-m thruout
4Bkqb1	126	3	10 YR 5/4	10YR 6/4–7/4	20–50	sndlm	2 f-c sbk	so-CO_3 vh-SiO_2	so po	I	es-CO_3 eo-SiO_2	cs	a-c i	1 vf-f thruout	1-2 vf i SiO_2 pods	2 vf-co thruout
5Bkb2	180	2	10YR 7/2	10YR 8/1	70–95	sndlm	1-2 m sbk m	h-vh	so po	I–II	es	cw-ci	c s	1 vf-f thruout	n.o.	n.o.
6Bkb2	246	1	10YR 7/2	10YR 8/1	70–90	sndlm	1 f-c sbk m	h-vh	so po	II–III	es	cs	a s	n.o.	n.o.	1 m-co thruout

Figure 45. Part of south wall of trench CFF–T2A across the Northern Crater Flat Fault in the Yucca Mountain area, southwestern Nevada (pl. 19; figs. 1, 2), showing stratigraphic relations bearing on event X on upthrown block of fault. Dark spots along some lines are markers that were emplaced to facilitate mapping.

Table 34. Summary of faulting events on the Northern Crater Flat Fault in the Yucca Mountain area, southwestern Nevada.

[See plate 19 and figures 1 and 2 for locations. Displacements and ages are best estimates; reported displacements are generally accurate to within ±10 cm]

Event	Likelihood of occurrence based on available evidence	Event horizon	Evidence	Vertical displacement at the main fault (cm)	Net cumulative vertical displacement (cm)	Date (ka)
Z	Definite --------	Within unit 6 (fig. 44).	Units 5 and 5b offset; central block of unit 5 rotated, creating rubble zone (unit 5d) composed of clasts of unit 5 broken apart by rotation or lateral slip; sandy fissure fill terminates within unit 6; scarp at surface.	20, measured at the top of unit 5.	0–5; net cumulative vertical displacement for events Z, Y, and X is constrained by net cumulative vertical displacement at top of unit 4b/4, which is near 0.	6–4, based on 5±1-k.y. estimated thermoluminescence age for sandy fissure fill; <10, based on absence of carbonate cement in sand fissure fill.
Y	Moderate ------	Top of unit 5 (fig. 44).	Multiple fractures on upthrown and downthrown blocks that terminate at or near top of unit 5; fractures show no apparent shear displacement and differ from those related to event Z by having abundant carbonate coating.	0	0	>10, based on presence of carbonate coatings on fractures; <433, based on estimated minimum age of Quaternary unit Qa1 (table 2).
X	Definite --------	Top of unit 4b/4 (figs. 44, 45).	Fractures that terminate at base of unit 5; displacement of top of unit 4b/4; presence and geometry of unit 5a.	40; cumulative vertical displacement from events Z, Y, and X measured at the fault on top of unit 4b/4 is about 60 cm.	0–5	>400, based on U-series ages for soil from unit 5 (HD 1967, HD 1966); >433, based on estimated minimum age of Quaternary unit Qa1 (table 2).
W	High ----------	Top of unit 2 (fig. 44).	Differential displacement between top of unit 2 and base of unit 4; presence of unit 3 only on downthrown block, possibly owing to stripping of unit 2 off upthrown block.	50, half of estimated 100-cm displacement resulting from events W and V).	45	>>433, based on estimated minimum age of Quaternary unit Qa1.
V	Moderate ------	Top of unit 1 (fig. 44).	Differential displacement between top of unit 1 and base of unit 4; presence of unit 2 only on downthrown block, possibly owing to stripping of unit 1 on upthrown block after uplift from event.	50	45	>>433, based on estimated minimum age of Quaternary unit Qa1.

mated by removing the effects of backtilting and (or) downwarping adjacent to the fault zone and by projecting event horizons into the fault zone from undeformed sections on the downthrown and upthrown blocks.

Paleoearthquakes

Stratigraphic and structural evidence for at least four faulting events (Z–W, from youngest to oldest) and, possibly, as many as five faulting events (including an older event V) was observed in trench CFF–T2A (figs. 44, 45). Evidence, displacements, and ages for these faulting events are summarized in table 34.

Uncertainty exists as to whether events V and W were separate occurrences or represent only a single faulting event. The question concerns the relation between stratigraphic units 2 and 3, both of which are now preserved on only the downthrown block (fig. 44). With regard to unit 2 in particular, it cannot be determined whether (1) it was deposited only on the

downthrown block as a result of older event V, followed by the deposition of unit 3; or (2) it was initially deposited on both sides of the fault and subsequently eroded off the upthrown block during event W, resulting in the deposition of overlying unit 3 on the downthrown block. Because units 2 and 3 are separated by an unconformity, indicating a difference in age, the evidence favors an interpretation that two faulting events occurred before the deposition of unit 3.

Quaternary Slip Rate and Average Recurrence Interval

The cumulative vertical displacement of unit 1 on the Northern Crater Flat Fault is about 160 cm in trench CFF–T2A (pl. 19). The net cumulative vertical displacement, as calculated by correcting for backrotation of the downthrown block, is estimated at about 100 cm. To calculate the total net cumulative displacement, the dip and left-oblique slip of the fault must be taken into consideration. The main fault zone exposed in the trench is vertical to near-vertical. Although no slickensides were observed in Quaternary materials to indicate the rake of Quaternary movement, Simonds and others (1995) documented a rake of 55° S. on a bedrock fault plane near the trench site. Using this rake, in combination with a vertical fault and 100 cm of net cumulative vertical displacement, the total net cumulative displacement is estimated at 122 cm. Given the U-series estimated ages for the opaline component of the carbonate soils formed on units 2 through 5 (generally 400–493 ka, pl. 19; table 31), the age of unit 1 is conservatively dated at older than 500 ka. On the basis of an estimated 122 cm of total net cumulative displacement of this unit, a Quaternary fault slip rate of less than 0.0024 mm/yr is calculated.

The minimum age of 500 ka for unit 1, the indication that four or five faulting events (three or four interseismic intervals) occurred after the deposition of unit 1, and an estimated date of 5 ka for the most recent faulting event yield possible average paleoearthquake-recurrence intervals of 165 k.y. (three faulting events) and 124 k.y (four faulting events), assuming that the oldest event (W or V) occurred soon after the deposition of unit 1.

Relation to the Southern Crater Flat Fault

The relation between the Northern and Southern Crater Flat Faults (see chap. 10) is unclear. Results from mapping (Simonds and others, 1995) and paleoseismic investigations are inconclusive for determining whether these two faults are connected or are separate features. The timing of faulting events, however, is similar enough to allow for possible linkage of the two faults in the subsurface. The most recent event (Z) on each fault occurred within the past 10 k.y.: at 9–2 ka on the Southern Crater Flat Fault and at 6–4 ka on the Northern Crater Flat Fault. Events Y and X on the Southern Crater Flat Fault are estimated at <40 and >250 ka, respectively; events Y and X on the Northern Crater Flat Fault are estimated at 433–10 ka and >433 ka, respectively. Both faults have slip rates of about 0.002 mm/yr; however, this slip rate is based on a much shorter paleoseismic record for the Southern Crater Flat Fault than for the Northern Crater Flat Fault. The paleoseismic record for the Southern Crater Flat Fault covers only about the past 250 k.y., whereas the paleoseismic record on the Northern Crater Flat Fault covers about the past 500 k.y. The difference in record length, but the similarity in slip rates, indicates that the Northern Crater Flat Fault probably has a lower long-term slip rate than does the Southern Crater Flat Fault. This increase in slip rate from north to south in Crater Flat fits with the existing data from other faults (for example, Menges and others, 1994) and the most recent model for the formation of the Crater Flat Basin (Fridrich, 1999; Fridrich and others, 1999), indicating that the basin is opening in a fanlike pattern from north to south, with the pivot point located in the caldera complex north of Yucca Mountain (figs. 1, 2).

Acknowledgments

I gratefully acknowledge Chris de Fontaine and Michele Murray for their assistance in logging, describing, and interpreting trench CFF–2A. I also thank Jeff McCleary, Susan Olig, and John Whitney for their field reviews of the logging and paleoseismic interpretations.

Chapter 12

Quaternary Faulting on the Bare Mountain Fault

By Larry W. Anderson[1] and Ralph E. Klinger[1]

Contents

Abstract....155
Introduction....155
Quaternary Stratigraphy....157
Miocene to Pliocene(?) Gravel....157
Pliocene(?) to Lower Pleistocene Deposits....157
Lower to Middle Pleistocene Deposits....160
Middle Pliocene Deposits....160
Upper Pleistocene Deposits....160
Upper Pleistocene to Holocene Deposits....160
Upper Holocene to Modern Deposits....160
Characteristics of the Bare Mountain Fault....161
Tates Wash to Tarantula Canyon Wash....161
Tarantula Canyon Wash to Chuckwalla Canyon....161
Chuckwalla Canyon to South of Wildcat Peak....161
South of Wildcat Peak to Black Marble....161
South of Black Marble....162
Detailed Study Sites....163
Tarantula Canyon Trench Site....164
Topographic Profiles....164
Stratigraphy....166
Interpretation of Quaternary Fault Activity....166
Discussion....167
Wildcat Peak Trench Site....168
Stratigraphy....168
Interpretation of Quaternary Fault Activity....169
Discussion....169
Stirling Trench Site....170
Scarp Profiles....170
Stratigraphy....170
Interpretation of Quaternary Fault Activity....172
Discussion....172
Summary of Quaternary Faulting Events....173
Recurrence Interval and Slip Rate....174

[1]U.S. Bureau of Reclamation, Denver, Colo.

Abstract

Quaternary activity on the Bare Mountain Fault was investigated by detailed mapping of Pleistocene surficial deposits and detailed studies in trenches and test pits excavated at three sites along the fault trace. The combined data show that along most of this 20-km-long, east-dipping, down-to-the-east normal fault, the contact between bedrock (Paleozoic and Precambrian sedimentary rocks) and alluvium (primarily fan deposits) is sharp and relatively linear, in some sections faulted and in others depositional. Prominent scarps in Quaternary deposits, indicative of late Quaternary fault activity, are present at a few scattered localities.

One faulting event is recorded in the surficial deposits exposed in one trench, and at least two faulting events in the other two trenches. Available evidence indicates that the most recent event (at all three trench sites) occurred no later than about 16±1 ka, possibly much earlier. A penultimate faulting event recorded at two sites probably occurred several tens of thousands to several hundred thousand years earlier. Still-earlier faulting events may have disrupted Quaternary deposits at one trench site, but the evidence is equivocal. Average displacement per event is estimated at 1.0 to 1.5 m.

Trench data indicate that the recurrence interval for moderate to large surface-rupturing paleoearthquakes on the Bare Mountain Fault is long, probably at least tens of thousands of years. The most recent faulting event is interpreted to have affected most of the length of the fault simultaneously, rather than causing rupture only on some short segments. The late Quaternary slip rate is estimated at 0.01 mm/yr.

Introduction

The Bare Mountain Fault is a major east-dipping, down-to-the-east normal fault that forms the structural boundary between Bare Mountain, a prominent upland of exposed Paleozoic and Precambrian rocks, and Crater Flat, a basin to

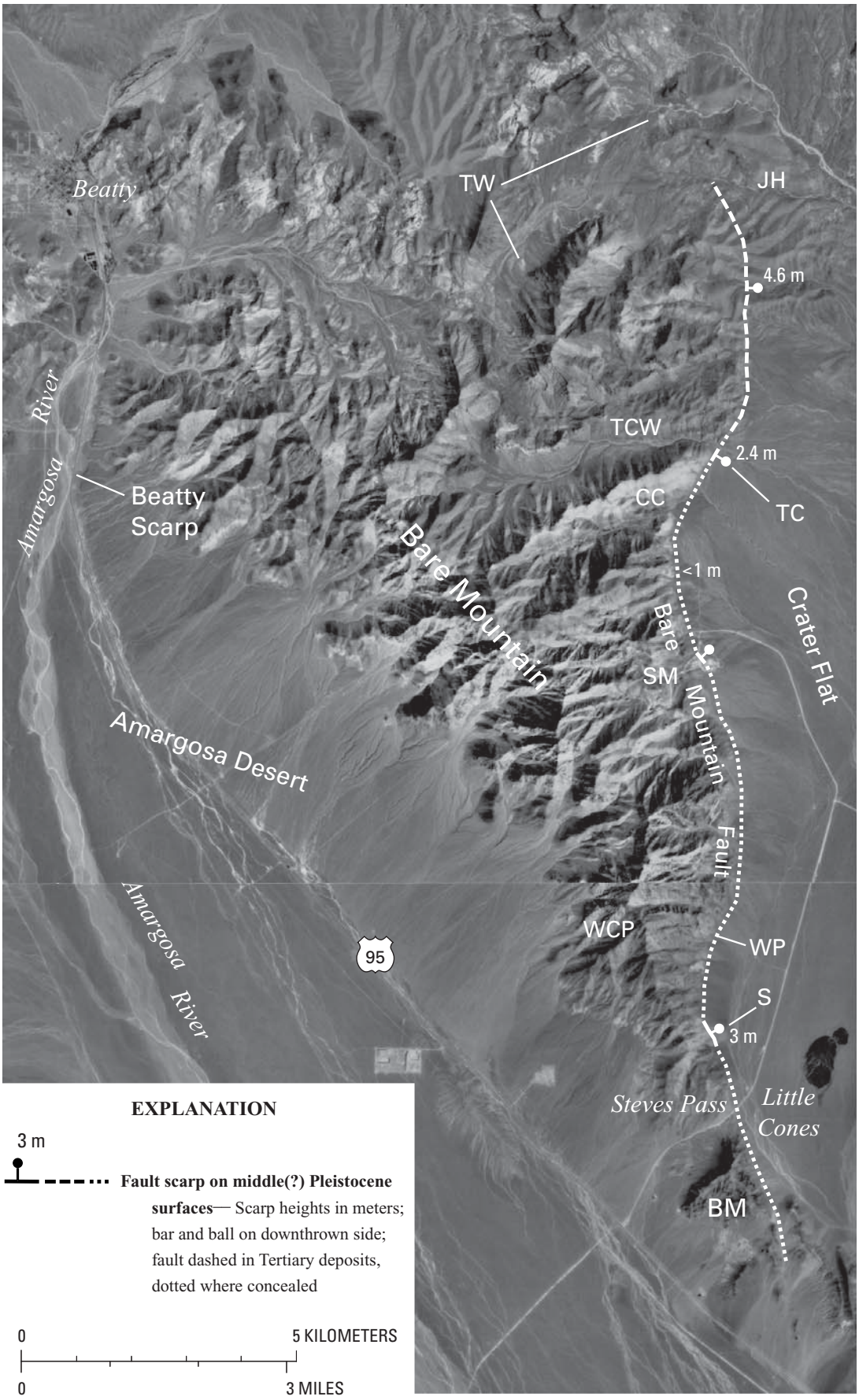

Figure 46. Bare Mountain Fault along east side of Bare Mountain, southwestern Nevada (figs. 1, 2). Trench sites: S, Stirling; TC, Tarantula Canyon; WP, Wildcat Peak. BM, Black Marble; CC, Chuckwalla Canyon; JH, Joshua Hollow; SM, Stirling Mine; TCW, Tarantula Canyon Wash; TW, Tates Wash; WCP, Wildcat Peak. Aerial-photographic mosaic from Project HAP–83, photographs 98–116 and 98–118, taken September 10, 1983.

the east that is filled by a thick sequence of Tertiary volcanic rocks and Quaternary alluvium (figs. 1, 46). Quaternary activity along the fault was first reported by Cornwall and Kleinhampl (1961), on the basis of (1) the sharp, relatively straight range front; (2) the small, relatively undissected alluvial fans along the east side of Bare Mountain; and (3) the linear alignment of Pleistocene volcanic cones in Crater Flat. A map by Swadley and Parrish (1988) showed that the range-front fault displaces lower Pleistocene deposits but is buried by younger, middle to upper Pleistocene deposits, whereas Reheis (1988) and Monson and others (1992) indicated that deposits as young as Holocene are faulted in several localities. Ferrill and others (1996) interpreted the slip rate on the Bare Mountain Fault to increase from north to south, partly because of an assumed change in the dip of the fault. During the present study, however, we determined on the basis of aerial-photographic interpretation and field mapping that (1) little evidence exists of latest Pleistocene or Holocene activity on the Bare Mountain Fault, (2) the dominant characteristic of most of the eastern range front of Bare Mountain is alluvium in depositional contact with bedrock, (3) actual displacements of Quaternary deposits are recognizable in only a few localities, and (4) the slip rate is low (~0.01 mm/yr) and does not increase (or change appreciably) from north to south.

The primary focus of this chapter is on the stratigraphic and structural relations of surficial deposits observed in natural exposures and trench excavations at three trench sites along the Bare Mountain Fault: Tarantula Canyon, Wildcat Peak, and Stirling (fig. 46).

Quaternary Stratigraphy

Surficial deposits, primarily alluvial fans of Quaternary age, were mapped earlier at a scale of 1:12,000 along the east flank of Bare Mountain by Anderson and Klinger (1996a). Colluvial and eolian deposits constitute much of the land surface in some areas, particularly near Black Marble (fig. 46), but they were not differentiated for this study. A common characteristic observed along the Bare Mountain range front is that older deposits have been eroded and are now covered with a thin (<1 m thick) veneer of younger material, as was also observed by Faulds and others (1994) and Peterson and others (1995) on the east side of Crater Flat near Yucca Mountain (fig. 1). Generally, we ignored this thin veneer in our mapping of surficial deposits during the present study.

We determined the relative ages of surficial deposits and associated geomorphic surfaces primarily by topographic position. We used the degree of desert-pavement development, the amount and degree of rock-varnish development on surface cobbles or boulders, the degree of preservation of original depositional topography (bar-and-swale topography), and, where observable, the degree of soil-profile development to distinguish and correlate the deposits. The criteria used for subdividing the surficial units along the east front of Bare Mountain are listed in table 35; these criteria are similar to those described by Hoover and others (1981), Swadley and others (1984), Taylor (1986), and Peterson and others (1995) for other surficial deposits at Yucca Mountain and in the adjacent areas. The geologic contacts are mostly similar to those of Swadley and Parrish (1988) and Monsen and others (1992), with only minor modifications; the few differences appear to result primarily from the larger scale of the mapping conducted for the present study.

Numerical ages of stratigraphic units were determined by Peterson and others (1995) at sites in Crater Flat. We examined surface characteristics and soil development at several of these sites to correlate the surficial deposits identified along Bare Mountain with dated deposits in nearby areas, as listed in table 36. The estimated ages of the Bare Mountain map units, based on regional stratigraphic correlations, are supported by the numerical ages of some of the deposits sampled in trenches along the range front during the present study. Neither felsic tephra erupted from regional sources (Izett and others, 1988) nor late Pleistocene basaltic ash erupted from local sources (for example, Heisler and others, 1999) that would aid in correlation and age assessments was identified along the Bare Mountain range front. Therefore, we consider the estimated ages and proposed correlations for the Bare Mountain surficial deposits to be only approximate. The estimated ages of various subdivisions of the Quaternary section are listed in table 4 (see chap. 2). Seven major surficial deposits, ranging in age from Miocene to Holocene, that were delineated along the east side of Bare Mountain are described below, in ascending order.

Miocene to Pliocene(?) Gravel

Stratified gravel deposits are present on a series of dissected hills and ridges at the northeast end of Bare Mountain, north of Tarantula Canyon and south of Joshua Hollow (fig. 46). Swadley and Parrish (1988) mapped these poorly consolidated deposits, and Monsen and others (1992) named them the Gravel of Sober-up Gulch. The deposits, at least 180 m thick, contain locally derived clasts of Proterozoic and Paleozoic sedimentary rocks, as well as clasts of Tertiary volcanic rocks. In the study area, the gravel beds are nearly flat-lying. Numerical ages of 7.7–8.7 Ma on tephra layers within the gravel deposits indicate a late Miocene age for the lower part of these deposits (Monsen and others, 1992).

Pliocene(?) to Lower Pleistocene Deposits

Pliocene(?) to lower Pleistocene deposits (unit Qta, table 35) have been identified only along the Bare Mountain range front, typically in small isolated remnants (for example, fig. 47). The deposits either are associated with the Bare Mountain Fault or are exposed locally in deep arroyos near the heads of alluvial fans. Unit Qta consists of gravel completely cemented with silica and carbonate. The original surfaces of the deposits are

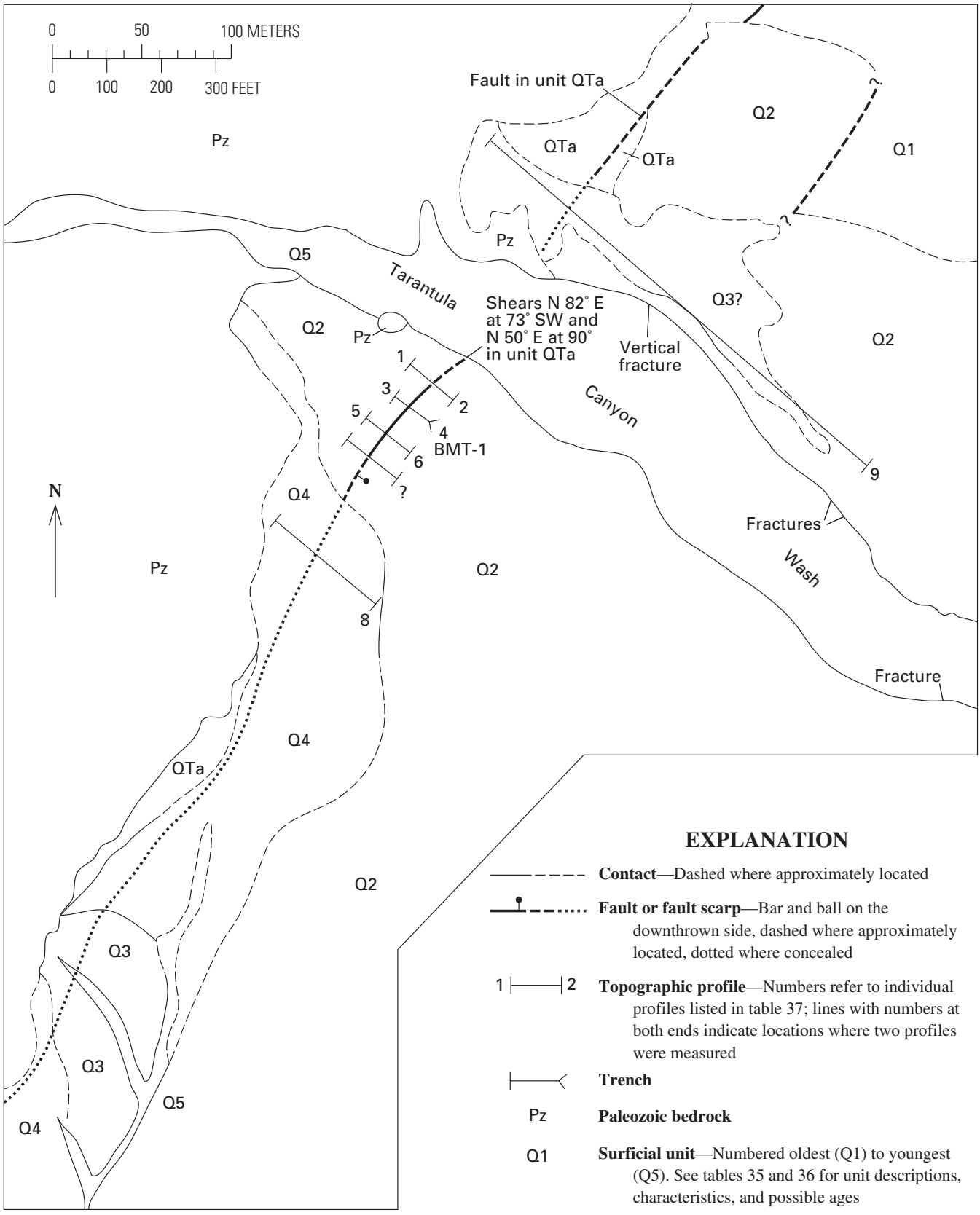

Figure 47. Geologic map of Tarantula Canyon trench site on the Bare Mountain Fault along east side of Bare Mountain, southwestern Nevada (pl. 20; figs. 1, 2). Base from enlarged low-Sun-angle aerial photograph taken in 1987 (State of Nevada, Yucca Mountain Low Sun Angle Project photograph 4–1a–10).

Table 35. Surface characteristics used to subdivide surficial deposits and geomorphic features along the Bare Mountain Fault, southwestern Nevada.

[See figures 1 and 2 for locations. Characteristics listed here may not depict the age of underlying deposits or reflect sedimentologic properties related to depositional history. Units are listed from youngest (top) to oldest (bottom). See table 3 for explanation of soil horizons]

Unit	Soil	Pavement	Desert varnish	Topography
Q5	May have weak Av/C profile; Av horizon <1 cm thick.	Generally absent; local incipient packing and horizontal orientation of clasts.	None ----------	High-relief bar and swale.
Q4	Thin Av horizon (several centimeters thick).	Poorly packed ----------	Weakly developed on quartzite clasts.	Bar and swale distinct but subdued; bars are coarser grained than adjacent swales.
Q3	Moderately well developed Av horizon (5–10 cm thick).	Moderately well to well packed on bars.	Moderately well developed on quartzite clasts.	Bar and swale subdued; transition between bars and swales diffuse.
Q2	Well-developed Av horizon (>10 cm thick).	Moderately well to well packed; carbonate rinds on clasts, fragments common in pavement.	Well developed on surface clasts.	Little or no evidence of bar and swale; surface is nearly smooth.
Q1	Av horizon may or may not be present, depending on topographic position.	Moderately well to well packed; pavement is being degraded; underlying petrocalcic horizon is locally exposed.	Moderately well to well developed on some surface clasts, absent on others.	Surface is dissected; small rills and drainages common.
QTa	Gravel completely cemented with carbonate or silica, or both; in places, surface veneered by younger unconsolidated deposits.	None ----------	None ----------	No original surfaces preserved.

Table 36. Correlation chart for Quaternary alluvial deposits in the vicinity of the Bare Mountain Fault, southwestern Nevada.

[See figures 1 and 2 for locations. Correlation is based on surface morphology and soil characteristics. Boundaries between the Holocene and Pleistocene and between the Pleistocene and Pliocene are dated at 10 and 1,650 ka, respectively]

Series	Bare Mountain			Crater Flat (Peterson and others, 1995)
	This study	Swadley and Parrish (1988)	Monsen and others (1992)	
Holocene	Q5	Q1a Q1b (<0.14 ka)	Qyf	Modern Crater Flat (>0.3–>1.3 ka)
	Q4	Q1c (<10 ka)		Little Cones (>6–>11 ka)
Pleistocene	Q3	Q2a	Qif	Late Black Cone (>17–>30 ka)
		Q2b (145–160 ka)		Early Black Cone (>159–>201 ka)
	Q2	Q2c (270–430 ka)		Yucca (>375 ka)
	Q1	?	QTof	Solitario (>433–659 but <730 ka)
Pliocene	QTa	Qta (1,100–2,000 ka)		

not preserved. The unit QTa deposits identified during the present study, which generally correspond to unit QTa of Swadley and Parrish (1988; see chap. 2; table 2), probably accumulated over a lengthy time interval. Although exposures are limited, no clasts of Tertiary volcanic rocks were observed in unit QTa deposits. Thus, the unit is apparently much younger than the Miocene to Pliocene(?) gravel described above.

Lower to Middle Pleistocene Deposits

Lower to middle Pleistocene deposits (unit Q1, table 35) are present at the surface primarily along the northern part of the Bare Mountain range front, north of the Sterling Mine (SM, fig. 46). The surfaces of these deposits are highly dissected, resulting in a ballena (rounded ridge and ravine) morphology, and are commonly littered with abundant carbonate rubble. Some quartzite clasts have a dark varnish. Av soil horizons may or may not be present. A test pit was excavated on a unit Q1(?) surface about 1.2 km south of Chuckwalla Canyon (CC, fig. 46). The soil profile is characterized by Av-Bk-Bw horizons to about 50-cm depth that overlie a strongly developed Bk horizon with $CaCO_3$ stage IV–V morphology (nomenclature of Birkeland, 1984). In most areas, however, the upper soil horizons have apparently been stripped, leaving the Bk horizon at or near the surface. On the basis of morphology and soil characteristics, unit Q1 is correlated with the Solitario or Yucca deposits of Peterson and others (1995), thus probably ranging in age from 375 to 730 ka (table 36).

Middle Pleistocene Deposits

Middle Pleistocene deposits (Q2, table 35) are common in the map area north of the Sterling Mine (SM, fig. 46). The large alluvial fan that emanates from Tarantula Canyon Wash (TCW, fig. 46) generally has the characteristics of a unit Q2 surface. Like most older deposits in the Bare Mountain area, the unit Q2 deposits probably span a long time interval and are dated at middle Pleistocene.

Surfaces on Q2 deposits are characterized by well-developed Av soil horizons (in some places >10 cm thick), moderately well packed to well-packed pavements, dark varnish on quartzite clasts, and a general absence of bar-and-swale topography. In many areas, however, especially adjacent to the range front, unit Q2 alluvial fans are typically buried by a thin veneer of younger unit Q4 deposits consisting of locally derived colluvial and eolian materials. Where this veneer is thin (<1 m thick), it does not seem to totally mask the better-developed surface characteristics of unit Q2 deposits. Soils characterized by A-Bw-Bk horizons that overlie strongly developed Bk horizons with $CaCO_3$ stage III–IV+ or silica morphology are also typical of these deposits in some localities. The surface characteristics and soil development indicate that unit Q2 approximately correlates with the Early Black Cone or Yucca deposits of Peterson and others (1995) and unit Q2c of Swadley and Parrish (1988) (table 36). Thus, unit Q2 is considered to range in age from 159 to 430 ka. Further constraints on the age of unit Q2 are discussed below in the subsection entitled "Stirling Trench Site."

Upper Pleistocene Deposits

Upper Pleistocene deposits (unit Q3, table 35) are the least common of the Quaternary units along the east side of Bare Mountain, represented by small fan remnants adjacent to the range front, with surface characteristics intermediate between those of units Q2 and Q4. In several areas, unit Q3 surfaces were initially identified on aerial photography by their height above adjacent unit Q4 surfaces. Subsequent field mapping revealed that the surface characteristics of unit Q3 also are more strongly developed than those of unit Q4. Unit Q3 surfaces have moderately well developed Av soil horizons (5–10 cm thick), moderately well packed to well-packed pavements, moderately developed varnish on quartzite clasts, and subdued bar-and-swale topography.

Soil on a possible unit Q3 remnant, exposed in a pit near Wildcat Peak (WP, fig. 46), is characterized by Avk-Bk horizons over a Bkb horizon with $CaCO_3$ stage II–III morphology. On the basis of its topographic position, surface morphology, and soil-profile characteristics, unit Q3 is probably correlated with unit Q2a of Swadley and Parrish (1988) and the Late Black Cone deposits of Peterson and others (1995) (table 36). Like other deposits along the eastern Bare Mountain range front, unit Q3 may range in age from about 17 to 100–200 ka.

Upper Pleistocene to Holocene Deposits

Upper Pleistocene to Holocene deposits (unit Q4, table 35) are some of the most abundant surficial deposits adjacent to Bare Mountain. They are characterized by thin (<5 cm thick) Av soil horizons, poorly developed desert pavement, weakly developed rock varnish on quartzite clasts, and distinct bar-and-swale topography. Unit Q4 soils typically have only Av-Avk-Bk horizons, with only $CaCO_3$ stage I–II morphology. The deposits are thin (1–3 m thick), typically forming a thin veneer over older deposits. As exposed in a test pit near Steves Pass (fig. 1), for example, they are 1.25 m thick, overlying a much older (unit Q2?) deposit with $CaCO_3$ stage III+–IV morphology. Unit Q4 has been differentiated only where it is thick enough (generally >1 m) to completely mask the underlying deposits.

Unit Q4 correlates with unit Q1c of Swadley and Parish (1988) and the Little Cones deposits of Peterson and others (1995). Thus, unit Q4 could range in age from only a few thousand years to 20 ka.

Upper Holocene to Modern Deposits

Upper Holocene to modern deposits (unit Q5, table 35) consist of coarse gravelly sand deposited in or adjacent to active washes. The deposits are characterized by their

unweathered appearance, pronounced bar-and-swale topography, general absence of soil development (generally weak Av over C horizons), and absence of vegetation, rock-varnish, and desert-pavement development. No soils were described on the unit Q5 deposits. Unit Q5 probably correlates with units Q1a and Q1b of Swadley and Parish (1988) and the late Crater Flat deposits of Peterson and others (1995) (table 36), indicating that they are only a few thousand years old at most.

Characteristics of the Bare Mountain Fault

Tates Wash to Tarantula Canyon Wash

The northernmost section of the Bare Mountain Fault is about 5 km long, extending from Joshua Hollow (JH, fig. 46) and Tates Wash (TW) on the north to Tarantula Canyon Wash (TCW) on the south. From Joshua Hollow southward for a distance of about 2 km, the fault is identifiable by tonal and vegetation lineaments primarily on Miocene and Pliocene(?) gravel and bedrock. The fault strikes N. 30° W. to nearly due north. Monsen and others (1992) showed alluvial-fan deposits of early Pleistocene and (or) Pliocene age to be faulted at Joshua Hollow Wash, but unequivocal evidence of faulting and a definitive scarp were not observed during the present study. At an unnamed wash about 2 km south of Joshua Hollow, the fault strikes nearly north-south, and a 4.6-m-high scarp is present on a small unit Q1 terrace. This scarp is the northernmost scarp that we identified along the fault zone. Between this unnamed wash and Tarantula Canyon, the fault consists of several strands that generally strike north. This section of the fault includes one scarp, 11 m high, on Miocene to Pliocene(?) gravel deposits.

At an unnamed wash 1.5 km north of Tarantula Canyon (TC, fig. 46), unit Q3 (table 35), overlies the Bare Mountain Fault without displacement. At a point about 0.5 km north of Tarantula Canyon, the fault strike changes to a more northeasterly trend. In this area, the fault is expressed as a fault contact between bedrock and unit QTa deposits and lower Quaternary deposits (units Q1, Q2). In several prospect pits, faults and shears in silica- and carbonate-cemented deposits (unit QTa) dip 45°–70° E. Small (less than 50 cm high) ridges of silica- and carbonate-cemented rock (unit QTa?), commonly with slickensides, are also present in several localities.

Tarantula Canyon Wash to Chuckwalla Canyon

The Bare Mountain Fault strikes about N. 50° E. from Tarantula Canyon Wash (TCW, fig. 46) on the north to Chuckwalla Canyon (CC) on the south. The most notable feature along this 2-km-long section of the fault is a fairly prominent, 1- to 2-m-high scarp on a middle Pleistocene alluvial fan (unit Q2, table 35) immediately south of Tarantula Canyon Wash that was identified by Swadley and Parrish (1988). The locality (Tarantula Canyon trench site, fig. 47) was selected for detailed study, as discussed below.

Reheis (1988) and Monsen and others (1992) showed that young alluvial-fan deposits are displaced along most sections of the Bare Mountain Fault between Tarantula Canyon Wash and Chuckwalla Canyon. However, no scarps on units Q3 and Q4 (table 35) alluvial-fan deposits were identified during the present study. Much of the fault is expressed as a fault contact between bedrock and unit QTa and as faults and shears that dip 30°–70° SE. in silica- and carbonate-cemented deposits (unit QTa) exposed in several prospect pits near Chuckwalla Canyon.

Chuckwalla Canyon to South of Wildcat Peak

The central section of the Bare Mountain Fault extends for approximately 10 km, from Chuckwalla Canyon (CC, fig. 46) on the north to just south of Wildcat Peak (WP). The fault strikes generally north and is marked for much of its length by an abrupt, fairly linear bedrock-alluvium contact. A scarp, which was identified by Swadley and Parish (1988), is present on unit Q1 (table 35) deposits near the Sterling Mine (SM, fig. 46). In a few places, evidence for Quaternary faulting involves exposures of unit Qta or Q1 deposits at or west of the range front. If the surface elevations of these deposits were extended eastward, they would project above the levels of surfaces on younger deposits (Swadley and Parrish, 1988), thus indicating fault offset. Evidence of Quaternary faulting is also indicated by sheared silica- and carbonate-cemented gravel (unit Qta?) exposed in several prospect pits (Reheis, 1988). Aerial photographs show a lineament on a unit Q3 alluvial fan 0.5 km north of the Sterling Mine. On the ground, the lineament appears to be an older scarp on a unit Q1 deposit that is nearly buried by a veneer of unit Q3 deposits. Relief across the feature is less than 1 m.

Immediately south of the Sterling Mine (SM, fig. 46), a silica- and carbonate-cemented shear is present in a unit Q2 (table 35) alluvial fan. Reheis (1988) identified similar shears in two trenches along the fault; exposures in one trench (BMT–2, fig. 48), immediately east of Wildcat Peak, led Reheis (1988) to conclude that the Bare Mountain Fault in this area had been the locus of late Pleistocene and, possibly, Holocene activity. Our mapping, however, indicates that unit Q3 alluvial fans apparently overlie the fault in several localities, indicating that the most recent fault activity in this area may be older than that reported by Reheis (1988). Primarily on the basis of the conclusions of Reheis (1988), the Wildcat Peak trench site (WP, fig. 46) was selected for additional study, as discussed below.

South of Wildcat Peak to Black Marble

The southern section of the Bare Mountain Fault extends for about 3 km, from just south of Wildcat Peak (WP, fig. 46) to the south end of Black Marble (BM). Near Wildcat Peak, the fault strikes due north, but at a point about 1 km southeast of

Wildcat Peak it changes in strike to approximately N. 30° W. At this point (Stirling trench site, fig. 49), a 1- to 3-m-high scarp trends north to northwest across a unit Q2 alluvial fan. This scarp, which was recognized by Monsen and others (1992), is the southernmost fault scarp identified during the present study. Owing to the presence of this scarp, the Stirling trench site was identified for detailed study, as discussed below. From the south end of the Stirling site to the south end of Black Marble, the Bare Mountain Fault is concealed by upper Pleistocene to Holocene alluvial fans (units Q3, Q4, table 35).

South of Black Marble

Bare Mountain loses its steep, linear, range-front morphology south of Black Marble (BM, fig. 46). The mountain also decreases in relief, basically terminating at the south end of Black Marble, but Paleozoic bedrock forms a series of low north-northwest-trending hills for a distance of about 3 km south of Black Marble. East-dipping Tertiary volcanic rocks (Miocene Timber Mountain Group) that are exposed farther to the southeast are topographically higher than the Paleozoic rocks; the

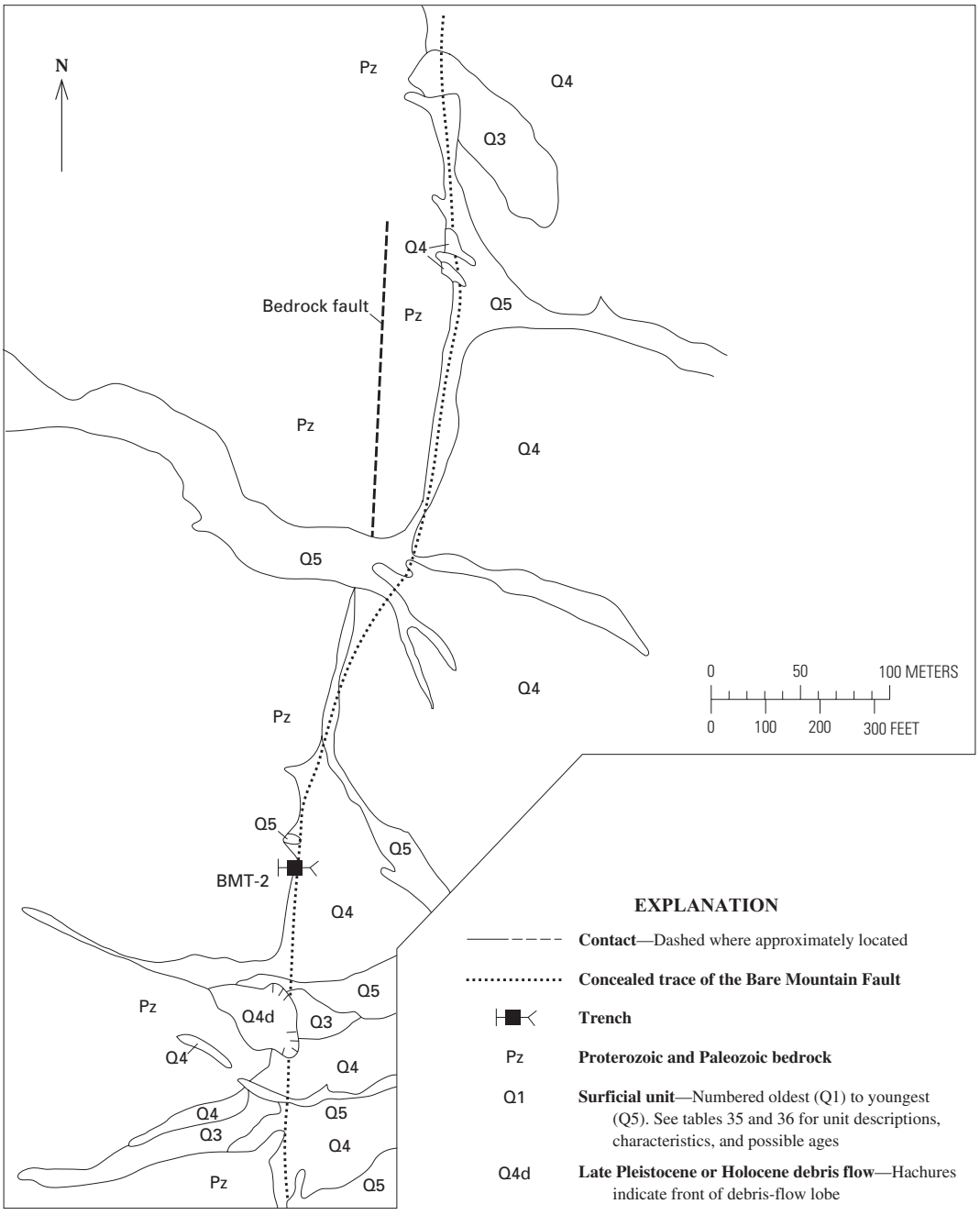

Figure 48. Geologic map of Wildcat Peak trench site on the Bare Mountain Fault along east side of Bare Mountain, southwestern Nevada (pl. 21; figs. 1, 2). Base from enlarged low-Sun-angle aerial photograph taken in 1987 (State of Nevada, Yucca Mountain Low Sun Angle Project photograph 4–1a–4).

volcanic rocks form the south margin of Crater Flat. No evidence of late Quaternary displacement was observed in this area.

Small outcrops of tilted and faulted Tertiary sedimentary rocks are present south of Black Marble (Swadley and Carr, 1987), indicating that post-Miocene faulting has occurred along the projection of the Bare Mountain Fault southeast of Black Marble. Geologic and geomorphic evidence obtained during the present study, however, indicates that little, if any, movement occurred on the Bare Mountain Fault in the area south of Black Marble during the late Quaternary.

Detailed Study Sites

Three trench sites—Tarantula Canyon, Wildcat Peak, and Stirling (figs. 47, 48, and 49, respectively)—were identified for detailed study of the Bare Mountain Fault. Two of the trench sites (Tarantula Canyon and Stirling) are located where distinct scarps are present on what appear to be middle Pleistocene (unit Q2, table 35) alluvial fans. Detailed study at these two sites consisted of geologic mapping, topographic

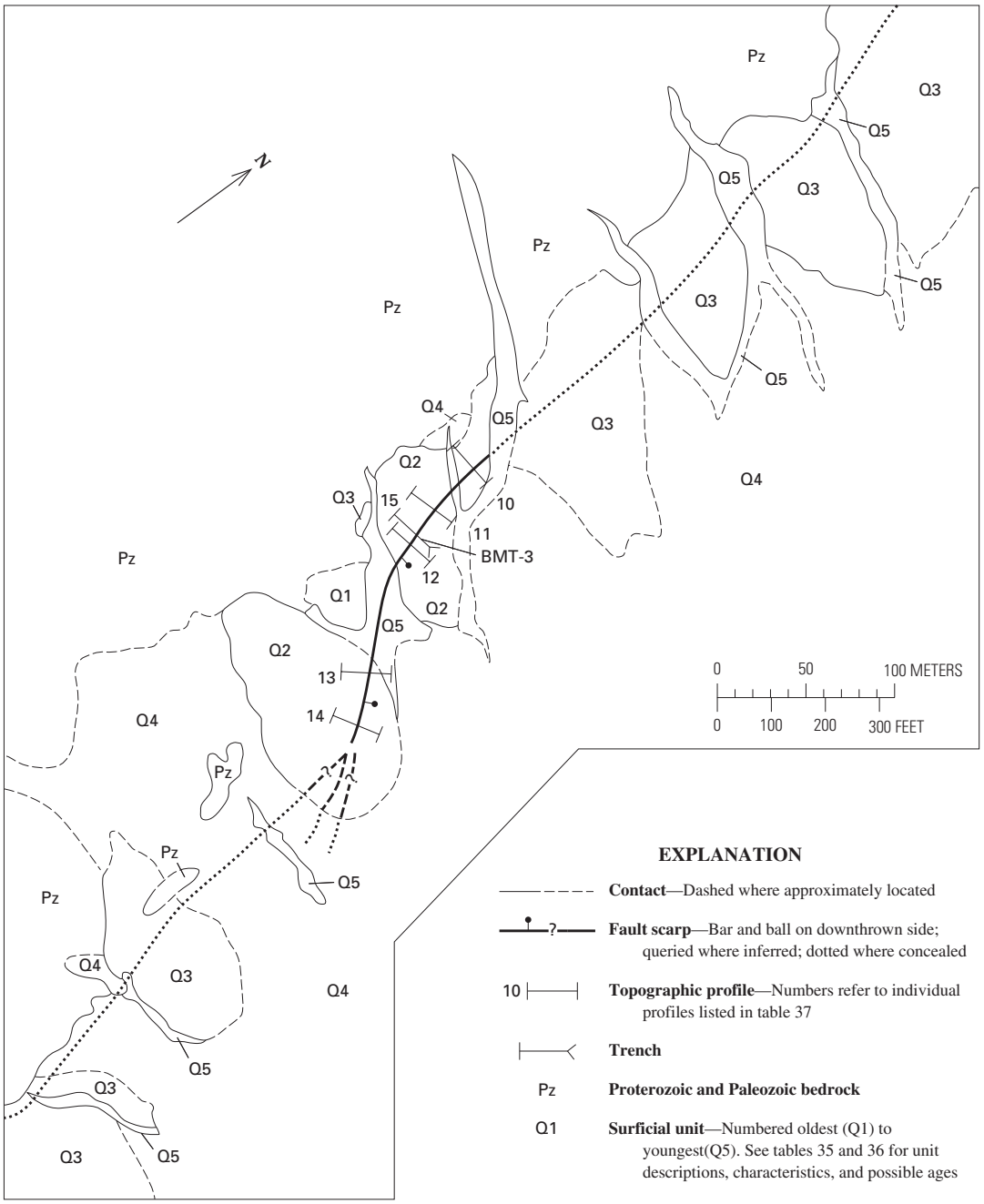

Figure 49. Geologic map of Stirling trench site on the Bare Mountain Fault along east side of Bare Mountain, southwestern Nevada (pl. 22; figs. 1, 2). Base from enlarged low-Sun-angle aerial photograph taken in 1987 (State of Nevada, Yucca Mountain Low Sun Angle Project photograph 4–1a–3).

profiling of the scarps, excavation of trenches across the scarps, mapping of the trench exposures, description of the soils and deposits exposed in the trenches, and collection of samples for numerical dating. The third trench site (Wildcat Peak) originally was a prospect or mineral-exploration pit; geologic relations exposed in the pit were initially described by Reheis (1988). Although a topographic scarp on alluvium is absent at this site, detailed mapping was conducted, and the former prospect pit was enlarged. The new excavation was also mapped in detail, soils were described, and samples were collected for numerical dating. In the following sections, we discuss the results of detailed study at these three trench sites.

Tarantula Canyon Trench Site

The Tarantula Canyon trench site (pl. 20), immediately east of the mouth of Tarantula Canyon (TC, figs. 46, 47) on the south side of the wash, is the only locality along the Bare Mountain range front where a fault scarp is present on a relatively flat alluvial fan.

The scarp, just south of the wash, is about 110 m long and as much as 2.4 m high. The surface on which the scarp is preserved was mapped as a unit Q2 alluvial fan (fig. 47; table 35), although its surface characteristics are not as well developed as on most unit Q2 surfaces in the study area. In the immediate vicinity of the scarp and adjacent to the range front, the unit Q2 alluvial fan is buried by a thin (<50 cm thick) veneer of younger alluvial, colluvial, and eolian deposits (not shown in fig. 47). This veneer, which is probably equivalent to unit Q4 deposits, is no older than early Holocene on the basis of the presence of artifacts dated at about 7 ka (G.M. Haynes, written commun., 1995).

North of Tarantula Canyon Wash (TCW, fig. 46), the Bare Mountain Fault is buried by younger unit Q2 or older unit Q3 deposits (mapped as unit Q3? in fig. 47) that appear to have originated as a debris flow from a small drainage north of Tarantula Canyon. The morphology and stratigraphic relations of these deposits indicate that they predate the incision of Tarantula Canyon Wash. The soil on this debris-flow deposit is well developed, with a B (Bt) horizon that has a sandy-clay texture, strong blocky structure, distinct clay films on ped faces and in pores, and a carbonate horizon with $CaCO_3$ stage II+ morphology. These characteristics support an age of at least late Pleistocene for the debris flow.

Farther north, the main fault trace is marked by scattered outcrops of silica- and carbonate-cemented gravel (unit QTa, table 35), in some places with linear fault-scarp-like ridges, 30 to 40 cm high. Faults and shears that strike N. 30°–40° E. and dip 47°–90° E. are exposed in two test pits north of Tarantula Canyon Wash (TCW, fig. 46). Scarps on younger Quaternary fans are absent to the north, primarily because no extensive late Pleistocene deposits are present in that area. Several silica- and carbonate-cemented fractures are observable in the walls of the wash downstream from the mouth of the canyon, and faint tonal, topographic, and vegetation lineaments are present on adjacent fan surfaces above the carbonate-cemented fractures. No displacements of distinct gravel beds were observed across any of these fractures; thus, a faulting (as opposed to fracturing) origin for these features is questionable.

About 200 m south of Tarantula Canyon Wash (TCW, fig. 46), the fault trace is marked by unit QTa outcrops. Although Monsen and others (1992) indicated that Holocene alluvial fans are faulted along this section of the fault, we observed no evidence of Holocene faulting. The fault is clearly buried by unit Q3 (late Pleistocene) and unit Q4 (latest Pleistocene to middle Holocene) deposits along this section (fig. 47).

Topographic Profiles

Nine topographic profiles were measured near the mouth of Tarantula Canyon (TC, figs. 46, 47). Topographic profiling has been widely used in the Western United States to approximate the ages of fault scarps (Wallace, 1977, 1980; Bucknam and Anderson, 1979; Nash, 1980, 1984; Machette and others, 1984; Hanks and Andrews, 1989). The technique is based on the assumption that a scarp developed in unconsolidated materials (regardless of origin) will degrade in a relatively predictable manner. Nash (1986) provided a good review of this technique.

On the south side of the Tarantula Canyon Wash (TCW, fig. 46), seven profiles (1–7, fig. 47) were measured across the scarp on the unit Q2 (table 35) surface. Farther south, one profile (8) was measured on a unit Q4 surface across a photolineament that trends southwest along the projected trend of the scarp on the unit Q2 surface. One 220-m-long profile (9) was measured on the north side of the wash, across the projection of the fault and scarp from the south side of the wash. Three profiles (1, 3, 5) were measured manually by using a tape, stadia rod, and hand level; the other six profiles (2, 4, 6–9) were measured by using an electronic surveying instrument (total station). An average of 7 measurements were made per profile to construct profiles 1, 3, and 5 (56–84 m long), and an average of 25 measurements per profile for profiles 2, 4, 6, and 7 (69–85 m long). The scarp heights, surface offsets, and maximum scarp-slope angles, which were measured from computer-generated plots of the profiles, are listed in table 37. The scarp heights of profiles measured on the unit Q2 surface (profiles 1–7) range from 1.1 to 2.4 m, surface offsets from 0.4 to 1.9 m, and maximum scarp-slope angles from 5.5° to 10°. The absence of compound scarps or obvious bevels in the profiles indicates that the Tarantula Canyon scarp resulted from a single faulting event. No scarp is discernible in the profiles measured across the photolineament south of Tarantula Canyon or across the projection of the fault scarp north of the wash in profiles 8 and 9, respectively, both of which were measured on surfaces younger than the unit Q2 alluvial fan containing the scarp.

In figure 50, maximum scarp angles are plotted against scarp heights for profiles across the scarp at Tarantula Canyon (TC, figs. 46, 47), along with plots for profiles measured across the Beatty scarp on the west side of Bare Mountain (Anderson and Klinger, 1996b). The age of the Beatty scarp is relatively well constrained by radiocarbon ages of about 9–13 ka (Swadley and others, 1988; Anderson and Klinger, 1996b). Superimposed on the scarp-profile data are a series of regressions calculated by Bucknam and Anderson (1979) for scarps of known age in the Great Basin Province. Data derived from the three profiles measured manually (1, 3, 5) cluster together and plot lower in figure 50 than those from the profiles measured electronically with the total station, even though profiles 1, 3, and 5 were measured along basically the same transects as profiles 2, 4, and 6, respectively. (Bucknam and Anderson's profiles were measured manually.) We conclude that the data collected manually, owing to the fewer number of points and the greater distance between measurements, yield profiles that are artificially smoothed and have lower scarp angles than do the profiles measured with surveying instruments. Regardless of slight differences in the data, the Tarantula Canyon scarp is clearly much older than the Beatty scarp because of the much lower maximum scarp-slope angles for the Tarantula Canyon scarp (fig. 50), which may be as old as 100 ka, on the basis of comparisons with the Beatty scarp.

Table 37. Data from topographic profiles on fault scarps along the Bare Mountain Fault, southwestern Nevada.

[All values were measured by hand and from computer-generated plots of profiles. Profiles 1–9 were measured at the Tarantula Canyon trench site (fig. 47), and profiles 10–15 at the Stirling trench site (fig. 49). Profiles 1, 3, and 5 were measured with hand level and stadia rod, profile 15 with hand level and 0.5-m-long rod, and all other profiles with electronic surveying instrument (total station). No scarp was observable in profiles 8 and 9. Profile 3 was measured along axis of trench BMT–1 (pl. 20) before excavation, and profile 4 immediately south of trench]

Profile	Scarp height (m)	Surface offset (m)	Maximum scarp-slope angle (°)	Surface-slope angle (°)
1	2.0	1.6	5.5	1.0
2	1.4	.9	7.0	2.0
3	2.2	1.5	6.0	1.5
4	2.4	1.9	10.0	1.5
5	1.9	1.5	6.0	1.0
6	1.8	1.1	8.5	2.0
7	1.1	.4	7.5	3.0
8	– –	– –	– –	– –
9	– –	– –	– –	– –
10	1.2	.8	14.0	5.0
11	2.5	1.1	18.0	9.5
12	2.3	1.1	17.5	8.5
13	1.3	.5	18.0	8.5
14	2.7	.9	15.0	8.5
15	3.3	.8	20.0	11.0

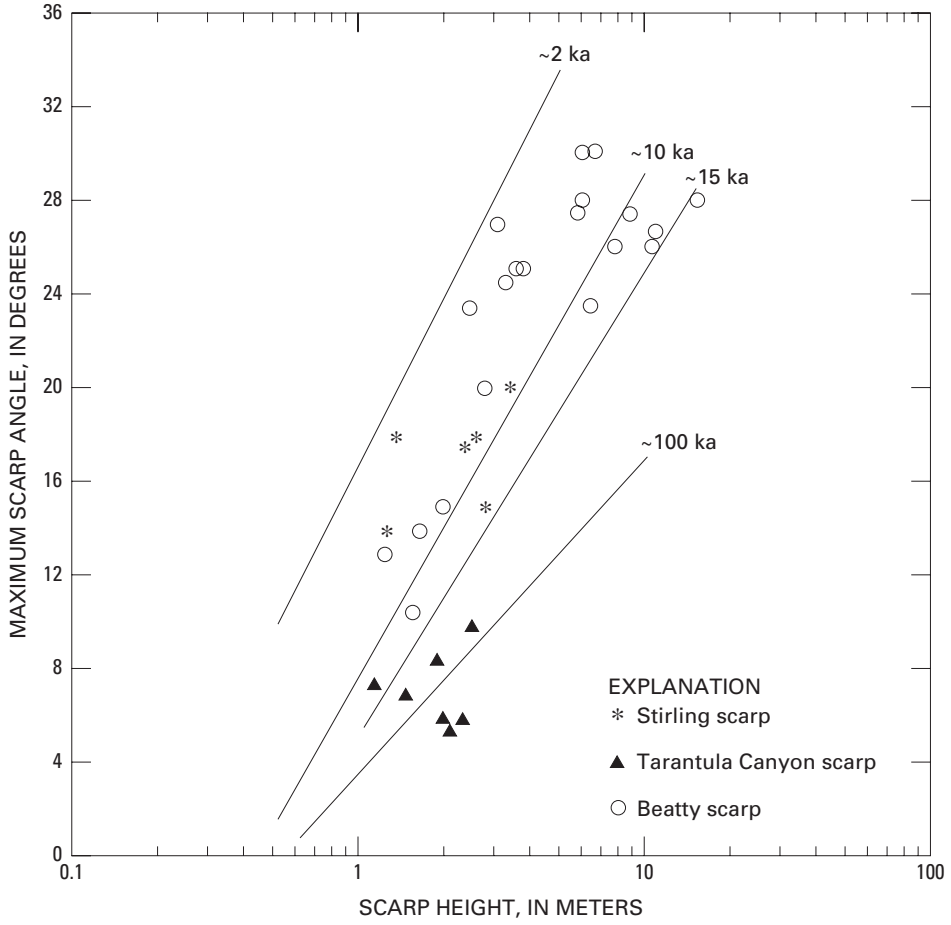

Figure 50. Scarp height versus maximum scarp-slope angle for topographic profiles of Stirling and Tarantula Canyon scarps along the Bare Mountain Fault on east side of Bare Mountain, southwestern Nevada (figs. 1, 2), in comparison with those of the Beatty scarp (Anderson and Klinger, 1996b) and regression lines for scarps of known age in the Basin and Range Province (modified from Bucknam and Anderson, 1979).

Stratigraphy

Trench BMT–1 (pl. 20; figs. 1, 47) is a 43-m-long excavation across the Bare Mountain Fault scarp at Tarantula Canyon (TC, figs. 46, 47). The oldest unit (I) recognized in the trench is known to be present only on the south wall (stas. 18–20 m, pl. 20); the upper part of this unit may also be present but was not identified with certainty in the floor of the trench (sta. 11 m). This indurated gravelly sand, which appears to be primarily of fluvial origin, is probably equivalent to unit QTa of Swadley and Parrish (1988), on the basis of its degree of induration and its relation to overlying deposits. Unit QTa is at the surface both north and south of the trench site (fig. 47). The contact between units I and II is sharp and distinct and appears to be an unconformity (pl. 20).

Unit II (pl. 20) is a moderately well stratified to well-stratified sandy gravel. A well-developed calcic horizon ($CaCO_3$ stage IV–IV+ morphology), 0.7 to 1.5 m thick, is present in the upper part of the unit. Unit III, consisting of gravelly-silty clay, is preserved only in the eastern part of the trench. The unit is interpreted to be an argillic (Bt) soil horizon associated with the calcic soil horizon formed in unit II. Whereas unit II is a fluvial gravel deposited by the main Tarantula Canyon stream, unit III consists of finer grained colluvium, fluvial, and eolian material that accumulated after abandonment and stabilization of the fan surface. Though differing from each other both genetically and texturally, the soil horizons developed on units II and III are believed to be part of the same soil because of their interrelations and the continuity of their boundaries. The relations between units II and III also indicate that their ages are similar.

Units II and III (pl. 20) are correlated with unit Q2 (table 35) on the basis of soil similarities. The strong development of the pedogenic carbonate ($CaCO_3$ stage IV–IV+ morphology), both in the upper part of unit II and in the test pit, indicates some antiquity for these deposits (Birkeland and others, 1991; Bull, 1991). These relations also indicate that unit Q2 probably correlates with unit Q2c of Swadley and others (1984) and Swadley and Parrish (1988) and with the Early Black Cone or Yucca unit of Peterson and others (1995) (table 32); thus, the minimum age of units II and III is estimated at 159 ka.

The uppermost and youngest unit (IV) in the trench consists of massive gravelly silt, considered to be correlative with unit Q4 (table 35) that forms only a thin veneer at the trench site and was not mapped at the surface (fig. 47). An archeological survey of the trench site before excavation recovered artifacts dated at least 7 ka from this unit (G.M. Haynes, written commun., 1995). A sample (TL–31, pl. 20; table 38) from unit IV collected for thermoluminescence analysis yielded an age of 6±1 ka, which is consistent with the estimated age of the artifacts and considered to be a minimum age for the unit (latest Pleistocene to early Holocene).

A weakly developed carbonate cement ($CaCO_3$ stage I+ morphology) in trench unit III (for example, stas. 17–18 m, pl. 20), is believed to be of late Pleistocene age. A sample (TL–32, pl. 20; table 38) from unit III yielded an age of 16±1 ka, which may represent the time when unit III was buried by unit IV. This age also provides a minimum date for the carbonate overprinting on unit III because carbonate probably began to accumulate shortly after the burial of unit III by unit IV. Such a date agrees with Peterson and others' (1995) age (>17–>30 ka) for the soil development on the Late Black Cone deposits (table 36). Thermoluminescence ages of buried soil horizons generally represent minimum dates for burial of the horizon (Forman and others, 1988). In the setting described above, however, the thermoluminescence age may reflect the latest infiltration and accumulation of carbonate with $CaCO_3$ stage I+ morphology, thus providing a minimum date for the latest faulting event.

Interpretation of Quaternary Fault Activity

A conspicuous fault, dipping 72° E. and coincident with the base of the surface scarp, is exposed on the south wall of trench BMT–1 (stas. 18–19 m, pl. 20; figs. 1, 47). The fault clearly displaces units I and II and part of unit III, apparently during a single faulting event. Although unit IV thickens east of the fault on the south wall of trench BMT–1, the unit appears to be unfaulted; its thickening appears to be due to typical downslope colluviation across the fault scarp.

Units II and III (pl. 20) form a single continuous soil profile; therefore, they were deposited long before the faulting event that displaced them, on the basis of the well-developed soil horizon preserved on the hanging wall near the fault. Unit III has been eroded from the footwall and is present only east of the fault, where the unit has been backtilted. We believe that the apparent thickening of unit III, where it overlies the fissure fill of unit II debris adjacent to the fault (sta. 18 m), resulted from the erosion of unit III deposits from the footwall and subsequent deposition after the faulting event. Thus, unit III, as mapped near the fault, probably includes some postfaulting, scarp-derived colluvium (reworked unit III). A separate colluvial-wedge unit could not be distinguished, possibly because of masking by subsequent pedogenesis. Backtilting and fissure filling similar to that observed in the south wall (stas. 17–19 m) are commonly observed in trench exposures across Quaternary normal faults and are features associated with historical surface-rupturing normal-faulting earthquakes in the Basin and Range Province (Nelson, 1992; McCalpin and others, 1994). The fissure fill that is composed solely of unit II material overlain by overthickened unit III deposits indicates only one faulting event since the deposition of units II and III. In addition, no buried soil horizons, stonelines, or texturally different fissure fills are present that would indicate multiple displacements of units II and III. Therefore, we interpret the above observations to indicate that the Tarantula Canyon trench site (fig. 47) has undergone only one faulting event since the deposition of those units.

Numerous fractures are present in the hanging wall in unit II (stas. 3–18 m, south wall, pl. 20). Though not recognizable in unit III, possibly either because they healed during subsequent pedogenesis or because they were never well

developed in the clayey material of that unit, the fractures are believed to have resulted from the faulting event that offset and backtilted both units II and III and created the scarp. Stratigraphic relations of the carbonate laminae filling some fractures in unit II also indicate that this unit may have been fractured not only during the 1.5-m-displacement faulting event but also during a later faulting event. If such faulting events occurred, no measurable displacement was observed. We conclude that if a paleoearthquake other than the 1.5-m-displacement faulting event occurred on the Bare Mountain Fault at Tarantula Canyon (TC, figs. 46, 47) and produced some of the fractures in unit II, its magnitude was below the threshold of surface rupture, which in the Basin and Range Province is believed to be about M_W=6.5 (dePolo, 1994).

Backtilting of unit II on the hanging wall is particularly pronounced between stations 16 and 18 m but is present in the trench eastward to at least station 5 m (south wall, pl. 20). To compensate for the backtilting, vertical separation resulting from the faulting event was measured by projecting the nearly flat surface of the calcic soil horizon from both ends of the trench into the fault. Total vertical separation of unit II across the fault is about 1.5 m down to the east (fault strikes N. 40° E. and dips 72° SE.). No indication of lateral or oblique slip was observed in the trench. Slickensides with near-vertical rakes on bedrock and on silica- and carbonate-cemented gravel along the fault north of Tarantula Canyon (TC, figs. 46, 47) indicate that past displacement on the fault in this area has been nearly pure dip slip.

Discussion

Unit IV is the only unfaulted deposit in trench BMT–1 (pl. 20; figs. 1, 47). Therefore, the age of this unit, which is estimated at latest Paleocene to early Holocene (6±1 ka; sample TL–31, table 38), provides a minimum date for the most recent faulting event at the Tarantula Canyon trench site. Four lines of evidence, from both the trench and the surrounding area, indicate that the date of the most recent faulting event may be much older than Holocene.

First, a distinct laminar carbonate layer, 0.5 to 1.5 cm thick, is present at the contact between units II and IV on the footwall block (stas. 18–23 m, south wall; stas. 20.5–23 m, north wall, pl. 20). This laminar carbonate layer appears to postdate the most recent faulting event because it drapes the 72°-dipping fault plane, coating cobbles and pebbles along the fault surface, and because it thins with depth, extending nearly to the bottom of the trench. The carbonate layer retains its laminar characteristics and is not brecciated, fractured, or striated, as would be expected if it had been faulted. In addition, pieces of this laminar carbonate are absent in the fissure-fill material. The laminar carbonate is not present on either trench wall where unit II has been backtilted downward. A similar carbonate layer on unit II is in the eastern part of the trench (sta. 8 m) and alternately truncates and infills fractures in unit II. Thus, the estimated time interval required to develop the 0.5- to 1.5-cm-thick laminar carbonate layer constrains the date of faulting better than the estimated age of unit IV alone. The thermoluminescence age of 16±1 ka (sample TL–32, pl. 20; table 38) on the carbonate may provide a minimum date for the most recent faulting event at Tarantula Canyon.

Table 38. Numerical ages of surficial deposits exposed in trenches BMT–1 and BMT–2 across the Bare Mountain Fault, southwestern Nevada.

[See plates 20 and 21 and figures 1, 2, 47, and 48 for locations. All samples, thermoluminescence analyses by S.A. Mahan; error limits, ±2σ]

Trench	Sample	Unit and material sampled	Estimated age (ka)
BMT–1 (pl. 20)	TL–31	IV, sediment surrounding artifact----	6±1
	TL–32	III, sand----------	16±1
BMT–2 (pl. 21)	TL–33	III, sandy-silty gravel----------	5.5–10

Second, pedogenic carbonate has overprinted unit III and is traceable across the fault zone (stas. 17–18 m, south wall, pl. 20) to the base of unit IV. The calcic soil horizon on unit III at the fault probably developed contemporaneously with the laminar carbonate layer at the top of unit II. The base of the calcic soil horizon approximately parallels the ground surface, indicating that this soil profile is unfaulted. Thus, the estimated time interval required to erode unit III, deposit unit IV, and develop $CaCO_3$ stage I+ morphology within both units III and IV also would constrain the date of faulting better than the estimated age of unit IV alone.

Third, the topographic profiles of the scarp support a date of several tens of thousands of years for the latest faulting event at Tarantula Canyon and the interpretation of only a single surface-rupturing paleoearthquake since the deposition of units II and III. As discussed above, the profile data indicate that the scarp at this site significantly predates the Beatty scarp (9–13 ka) and could be dated at near 100 ka. Also, no bevels or compound scarps are discernible in the scarp profiles. Furthermore, the surface offset (1.5 m) measured from the profile (3, table 37) at the trench site is consistent with the vertical separation (1.5 m) of unit II measured in the trench. These observations indicate only that one faulting event has occurred at the site and that it was relatively old.

Finally, the small debris-flow deposit (unit Q3?, fig. 47) mapped north of Tarantula Canyon Wash (TCW, fig. 46) postdates the latest faulting event. This deposit originated from a side drainage and buried unit Q2 alluvium. No fault scarp is present on the unit Q3? surface, as indicated by a topographic profile (9, fig. 47) that extends across the projection of the scarp. The debris-flow deposit that buries the fault has a well-developed argillic soil horizon with $CaCO_3$ stage II+ morphology; this deposit apparently accumulated before most of the downcutting along Tarantula Canyon Wash. Both of these pieces of evidence from the north side of Tarantula Canyon Wash support a date of at least several tens of thousands of years for the most recent surface rupture in the area.

Wildcat Peak Trench Site

The Wildcat Peak trench site (pl. 21; figs. 46, 48) is located at the Bare Mountain range front, east of a prominent peak of the same name. The site was selected for detailed study because, in a mining-exploration pit located at the fault zone, Reheis (1988) reported evidence indicative of late Pleistocene and, possibly, Holocene displacement. The pit does not cross, nor is it associated with, an obvious fault scarp on a Quaternary alluvial-fan surface.

Near the mining-exploration pit, which is identified in the present report as trench BMT–2 (figs. 1, 48), the range front is marked by an abrupt linear, N. 25° E.-trending contact between Paleozoic bedrock and Quaternary alluvial-fan deposits (primarily unit Q4, table 35). About 240 m northeast of the trench, the linear range front is on trend with a bedrock fault mapped by Monsen and others (1992); however, no features in Quaternary deposits interpreted to be fault scarps have been identified in this area.

Unit Q4 alluvial-fan deposits (latest Pleistocene to Holocene) are the most common along the range front at the Wildcat Peak trench site (pl. 21). Several small remnants of unit Q3 deposits also have been identified (fig. 48). At one locality, approximately 600 m north of trench BMT–2, a unit Q3 alluvial fan that crosses the range front is preserved. No scarp is present on the unit Q3 alluvial-fan surface, indicating that it postdates any surface rupture along the Bare Mountain Fault at this locality. At another locality about 100 m south of trench BMT–2, an arcuate, 50-m-long scarplike feature that is particularly prominent under low-sun-angle conditions was identified by Monsen and others (1992) as a fault displacing older alluvial-fan deposits. We interpret this scarplike feature, however, to be the frontal lobe of a small debris flow (unit Q4d, fig. 48) that postdates unit Q3 alluvium exposed farther east, on the basis of its more pronounced bar-and-swale morphology and a thinner Av soil horizon than are typical of the older unit.

Stratigraphy

Trench BMT–2 (pl. 21; figs. 1, 48) is located on an alluvial-fan complex of unit Q4 (table 35) age and between small active channels of unit Q5 age (fig. 48; active channels not shown). Four major alluvial and colluvial deposits, two possible fissure-fill units, and bedrock are exposed in the trench. Dolomite of Cambrian age forms the footwall; in the north wall it is highly resistant, though brecciated and fractured, and in the south wall it is hydrothermally altered (red versus unaltered grayish black), brecciated, and highly sheared. In the north wall, below the level of the former ground surface, the resistant bedrock is covered by a thick silica and carbonate coating. The silica and carbonate extend down to 3-m depth and form vertically orientated slabs, some with striations and grooves, between the alluvium and bedrock.

The four alluvial and colluvial deposits exposed in trench BMT–2 were derived from two different sources, as indicated by differences in the relative abundance of clasts from two of the Cambrian formations (Zabriskie Quartzite and Bonanza King Formation; see Monson and others, 1992) exposed nearby. Thus, correlation and differentiation of the units exposed in the two trench walls are difficult. Unit I, consisting of massive, sandy-bouldery gravel, is the lowermost and oldest unconsolidated deposit recognized in both walls of trench BMT–2. The unit consists of clast-supported gravel containing angular to subangular cobble- to boulder-size clasts, some as large as 75 cm in diameter. A unique characteristic is that, although the unit is immediately adjacent to dolomite of the Bonanza King Formation that forms the footwall, as much as 95 volume percent of the clasts in the unit are of Zabriskie Quartzite. A silica-carbonate soil horizon (Bk, $CaCO_3$ stage II+–III morphology; soil-profile description BMT–2S), from a few centimeters to nearly 50 cm thick, is present in the upper part of the unit (C, south wall, pl. 21). The silica-carbonate soil horizon associated with unit I overlies and either truncates or completely masks the shears and faults within unit I. On the north wall, a distinct stoneline consisting of clasts with thick silica and carbonate rinds and pendants is present at the top of unit I. Unit IC, a colluvial deposit that is present only on the north wall of trench BMT–2, is a sandy-cobbly gravel, as much as 30 cm thick. The unit also is characterized by thick silica and carbonate coatings and pendants on clasts and is differentiated from unit I by a distinct stoneline between the two units. Although the age of unit I is unknown, the moderate silica and carbonate cementation ($CaCO_3$ stage II+ morphology) indicates some antiquity, probably tens of thousands of years.

Unit II (pl. 21) consists of massive silty-sandy gravel, 20 to 70 cm thick, that has a distinctive erosional contact with the underlying unit I. Unit II is present only on the south wall of the trench and may be correlative with either unit IC or III on the north wall.

On the north wall, unit III (pl. 21) is a sandy-silty gravel, as much as 1 m thick. Approximately equal proportions of the clasts in this unit are of Bonanza King Formation and Zabriskie Quartzite. The unit has a moderately well developed carbonate soil horizon ($CaCO_3$ stage I+–II morphology), and individual clasts have carbonate coats and pendants. Unit III is differentiated from underlying units by its moderately well developed soil, its greater abundance of dolomite clasts, its finer texture, and the distinct stoneline at its base. The unit appears to be the equivalent of unit Q4 (table 35). Its soil-profile development indicates an age probably no older than latest Pleistocene, which is supported by a thermoluminescence age of 5.5–10 ka obtained for sample TL–33 (pl. 21, table 38).

Unit IV (pl. 21) consists of sandy-silty gravel, 15 to 40 cm thick. The unit in the south wall of the trench is composed of only 10 volume percent clasts of Bonanza King Formation, even though outcrops of this dolomite are immediately upslope. The unit has a weakly developed Av soil horizon in the upper few centimeters, as well as weak carbonate cementation ($CaCO_3$ stage I morphology). On the basis of soil-development characteristics, unit IV is dated at Holocene, possibly even late Holocene.

In addition to the above units, two possible fissure fills have been identified in trench BMT–2 (pl. 21; figs. 1, 48) on the basis of their loose texture and scattered clasts with nearly vertical long axes. In the north wall, between stations 3.5 and 6.5 m, fissure fill 1 lies within unit I. In the north wall (sta. 2.5 m), fissure fill 2 consists of a mass of loose material composed of clasts of laminar silica and carbonate, as well as quartzite. Fissure fill 2 lies between the bedrock surface and units I and III. In the south wall, fissure fill 1 is mapped between stations 7 and 8.5 m, and fissure fill 2 is immediately adjacent to the exposed bedrock. Clasts of laminar silica and carbonate are absent in fissure fill 2 in the south wall of the trench.

Interpretation of Quaternary Fault Activity

In trench BMT–2 (pl. 21; figs. 1, 48), the Bare Mountain Fault is expressed by fissure fills, altered and brecciated rock, and a bedrock fault surface that dips 62°–74° E. Because of the absence of readily correlatable units on opposite sides of the fault, the paleoseismic history of the Bare Mountain Fault at this site is difficult to decipher. The location of the trench, immediately adjacent to a bedrock outcrop, also results in very coarse grained deposits, in turn, making it difficult to identify fractures and faults and to differentiate stratigraphic units. However, evidence for at least two faulting events is apparent.

The first faulting event produced the fractures present in several places in unit I (pl. 21). This faulting event(s) also resulted in the formation of the large fissure fill (1, pl. 21) visible in both trench walls, identified by its loose texture and subvertical to vertical clast orientation. Clasts in the adjacent indurated unit I deposits are nearly horizontal. In the south wall of the trench, fissure fill 1 and individual shears or fractures east of station 8.5 m are clearly overprinted by the overlying Bk soil horizon (C, pl. 21); on the north wall, the fissure fill and associated fractures are overlain by unit IC. The amount of stratigraphic separation associated with this event(s) is not measurable in this trench.

A second faulting event appears to displace unit I and fissure fill 1 along the bedrock fault surface (stas. 8.5–9.5 m, south wall, pl. 21). Unit II partly infills the fault zone, but the unit II surface parallels the present ground surface and thus postdates the most recent faulting event. In addition, unit II is not fractured and shows no evidence of shearing. The distance from the top of unit I on the hanging wall to the top of bedrock on the footwall indicates that the displacement associated with this faulting event could be about 1 m; however, without correlative units on opposite sides of the fault, the exact displacement is not accurately measurable. As expressed in the north wall of the trench, the most recent faulting event apparently produced the loose zone (fissure fill 2) containing clasts of laminar silica and carbonate. Reheis (1988) suggested that the clasts in this loose zone could be faulted pieces of a laminar carbonate horizon, 1 to 2 cm thick, at the top of our unit I. However, the massiveness and laminarity of the silica and carbonate clasts in fissure fill 2 (typically 5–10 cm thick) indicate that the clasts are not from unit I. We interpret these clasts to be part of unit QTa (table 35) or a similar deposit. In the north wall, the unit we infer to be fissure fill 2 rests directly on the bedrock fault surface in the middle and lower parts of the trench, but what appears to be an upward extension of the fissure fill separates a small colluvial wedge (unit III?) next to the fault from the main part of unit III to the east. The implication of these relations, with regard to whether unit III is faulted, is discussed in the next subsection.

Unit IV is clearly unfaulted in trench BMT–2 (pl. 21; figs. 1, 48). Therefore, its age, probably no older than middle Holocene, provides a minimum date for the most recent faulting event at the Wildcat Peak trench site.

Discussion

Interpretation of the Quaternary activity on the Bare Mountain fault, as expressed in trench BMT–2 (pl. 21: figs. 1, 48), is difficult. Reheis (1988) concluded that evidence for two faulting events was present in the north wall of the trench. We agree with her conclusion but differ on interpretation of the dates for the two faulting events, partly because our interpretation relies substantially on geologic relations that either are observed on the surface in the area surrounding trench BMT–2 or are exposed in trenches BMT–1 (pl. 20) and BMT–3 (pl. 22), which were unavailable for Reheis' study.

The origin and date of deposition of at least the upper part of the loose zone of silica and carbonate rubble (fissure fill 2, pl. 21) between units III and III? on the north wall of the trench are uncertain. The deposit could be interpreted to indicate that units III and III? are faulted; however, evidence from the south wall of the trench and geologic relations observed north and south of the trench do not support such an interpretation. Similar to the interpretation from trench BMT–1 (pl. 20), the estimated age for the only exposed unit that is clearly unfaulted (unit IV, possibly late Holocene), provides a minimum date for the most recent surface rupture on the Bare Mountain Fault at the Wildcat Peak trench site (fig. 48). Two lines of evidence, however, indicate that the surface rupture there is probably no younger than latest Pleistocene.

First, in the south wall of trench BMT–2 (pl. 21), unit II overlies sheared fissure fill 2 at the bedrock-alluvium contact and appears to be unfaulted. Soil development on unit II displays $CaCO_3$ stage II morphology, indicating a pre-Holocene age.

Second, the surficial geology at the Wildcat Peak site (fig. 48) shows no evidence of scarps on upper Pleistocene deposits (unit Q3, table 35) north and south of the site. As discussed above, a unit Q3 alluvial fan (estimated to be late Pleistocene), 600 m north of trench BMT–2 (pl. 21; figs. 1, 48), is unfaulted, and unit Q4 alluvial fans (latest Pleistocene to Holocene) north and south of trench BMT–2 are unfaulted as well. If a Holocene faulting event occurred, all of these fans should show some evidence of faulting or fracturing in the form of vegetation lineaments, tonal contrasts, or topographic scarps.

Our initial conclusion regarding the faulting history at trench BMT–2 is that evidence exists for two faulting events during middle to late Pleistocene time. However, the most

recent faulting event probably was no later than late Pleistocene. Although the amount of displacement associated with faulting events at this study site is difficult to determine, the recurrence interval for faulting events appears to be long, on the basis of the soil horizon ($CaCO_3$ stage II+ morphology) developed on unit IC. This unit clearly postdates the penultimate faulting event but predates the most recent faulting event. The carbonate cementation in unit II on the south wall also indicates that a considerable time interval elapsed between the two faulting events at the trench site, an interpretation consistent with observations at the other trench sites (BMT–1, BMT–3).

Stirling Trench Site

The Stirling trench site (pl. 22; fig. 49), located near the south end of Bare Mountain about 1.5 km north of Steves Pass (fig. 46), was selected for detailed study because it is the only trench site toward the south end of the Bare Mountain Fault with a well-defined scarp on a middle Pleistocene alluvial-fan surface (unit Q2, table 35). The site is abreast of extensive outcrops of the Stirling Quartzite of Late Proterozoic age (Monson and others, 1992), which is the source for the monolithologic alluvial fans in the area. The range front at the Stirling trench site is relatively low, with only about 200 m of relief, indicating that the displacement of bedrock on the fault is less there than near Tarantula Canyon, where the topographic relief approaches 700 m.

The scarp in Quaternary deposits at the Stirling trench site is slightly arcuate, trends nearly north-south to about N. 40° W., and is approximately 250 m long (fig. 49) and 1 to 3 m high. The scarp is present on remnants that are interpreted to be part of a unit Q2 (table 35) alluvial fan (middle Pleistocene). The alluvial-fan deposits appear to be relatively thin, partly overlying bedrock of the Wood Canyon Formation (Monsen and others, 1992) of Early Cambrian and Late Proterozoic age. The unit Q2 alluvial-fan surface is fairly steep (average slope, 8°–11°), with a subdued bar-and-swale topography and a moderately well developed desert pavement. Boulders and cobbles on the alluvial-fan surface are of light-gray to white quartzite, derived from outcrops of the Stirling Quartzite upslope to the west (Monsen and others, 1992). Many of the quartzite clasts have moderately dark to dark rock varnish, and many clast bottoms are reddened. The middle Pleistocene age for the unit Q2 alluvial fan is based on collective surface characteristics (table 35) and the stratigraphic position of the alluvial fan relative to surrounding fans. No scarps have been identified on units Q3 and Q4 alluvial fans to the north and south of the scarp at the Stirling trench site.

Scarp Profiles

Six topographic profiles were measured at the Stirling trench site (pl. 22; fig. 49). Maximum scarp slopes range from 14° to 20°, and maximum scarp heights from 1.2 to 3.3 m (table 37). In figure 50, data for the Stirling scarp are plotted against data for the dated Beatty scarp (9–13 ka), the regressions of Bucknam and Anderson (1979), and the data for the Tarantula Canyon scarp. Scarp heights for the Stirling and Tarantula Canyon scarps are similar, but maximum slopes for the Stirling scarp are steeper than those for the Tarantula Canyon scarp and more comparable to those for the Beatty scarp. Although the Stirling scarp is younger (see fig. 50) and so has been subjected to a shorter period of degradation, we believe that the higher slope angles at that trench site result primarily from the steeper slope of the alluvial-fan surface there than at the Tarantula Canyon trench site (5°–11° versus 1°–3°).

Stratigraphy

Trench BMT–3 (pl. 22; figs. 1, 49), a 26-m-long excavation, exposes at least eight major lithologic units and (or) soil horizons. All the surficial deposits are of alluvial, colluvial, or eolian origin, and all the contained clasts are of Stirling Quartzite. Sheared and altered quartzite, believed to be in the Wood Canyon Formation, forms the oldest unit exposed in trench BMT–3; the unit is present only in the footwall. The upper 40 to 60 cm of the quartzite is strongly impregnated with carbonate.

Overlying the altered quartzite and known to be present only on the footwall is a carbonate-cemented sandy gravel (unit I, pl. 22). As exposed, the unit consists of a soil horizon with well-developed $CaCO_3$ stage IV morphology. Cementation is so strong that, when excavated, clasts of Stirling Quartzite break as readily as the carbonate cement. Unit I, which is typically 10 to 60 cm thick, appears to form a pediment gravel on the underlying Wood Canyon Formation. The strong carbonate cementation may have been enhanced by the shallow depth to bedrock below unit I, with the less permeable bedrock hindering infiltration to some extent. This soil development may also reflect some antiquity; however, because unit I remained near the ground surface on the footwall while deposits on the hanging wall were being buried, the carbonate soil horizon developed on unit I could be equivalent to one or more of the three carbonate soil horizons developed on units in the hanging wall.

Unit II, at the base of trench BMT–3 (pl. 22; figs. 1, 49) on the hanging wall, consists of poorly stratified sandy gravel, more than 50 cm thick. The unit, which has stage $CaCO_3$ I+–II morphology, is interpreted to be the Bk soil horizon associated with the A and Bt soil horizons preserved in the overlying unit V. Unit II? is a small wedge-shaped deposit, about 80 cm thick, consisting of carbonate-cemented, clast-supported, angular to subangular pebbles and cobbles in a sandy matrix on the footwall block. The deposit lies unconformably on both unit I and altered bedrock of the Wood Canyon Formation. Units II and II? are believed to be correlative on the basis of their stratigraphic position, apparent thicknesses, and similar sedimentologic characteristics. Although the carbonate development is more advanced in unit II? than in unit II, the difference is considered to be the result of one unit (II?) being at shallower depth on the footwall and the other unit (II) being more deeply buried on the hanging wall.

Unit III (pl. 20) consists of poorly stratified, sandy to clayey gravel, 40 to 60 cm thick, that is interpreted to be the A-Bt horizons of a buried soil (with unit II as the associated carbonate horizon). The unit is present only on the hanging-wall side of the fault and is distinguishable from overlying and underlying units by its generally smaller clast size and matrix-supported texture. The upper 25 cm is interpreted to be a buried A soil horizon because of its color, texture, and relation to the Bt soil horizon in the lower 20 to 50 cm. The unit has $CaCO_3$ stage II morphology, which may be partly inherited from overlying unit V. Units II and III on the hanging wall clearly are not correlative with units I and V on the footwall, on the basis of thickness and sedimentologic characteristics. Units II, II?, and III appear to form a single depositional package, partly because unit II? on the footwall clearly truncates unit I and because it underlies and is truncated by unit V.

Unit IV (pl. 22) consists of carbonate-cemented sandy gravel, typically 50 to 70 cm thick. Pebbles and cobbles are generally clast supported and exhibit subhorizontal fabric. The unit, which has $CaCO_3$ stage II+–III+ morphology, including incipient $CaCO_3$ stage IV morphology in its upper part (laminae several millimeters thick in places), is interpreted to be the calcic (Bk) soil horizon associated with overlying soil horizons in units V and VI. The strong carbonate cementation in unit IV appears to be similar to that in unit II?, indicating that both units represent the same period of soil formation, although they do not correlate depositionally or stratigraphically.

Unit V (pl. 22), on the footwall, consists of clayey gravel, generally 45 to 70 cm thick. The unit exhibits angular-blocky soil structure and clay films that are readily visible without magnification, with a strongly developed argillic (Bt) soil horizon that may partly be associated with the strong carbonate developed in unit I. However, although the contact between unit V and the underlying unit I is abrupt, it is also wavy and exhibits relief (10–35 cm; pl. 22). This contact indicates a hiatus marked by erosion of the top of unit I before deposition of unit V. The soil properties of unit V weaken toward the surface scarp and the associated fault zone, apparently owing to the unit's position on the steeper part of the slope. Thus, we have subdivided unit V into units V, Va, and Vb on the basis of soil development. Both units Va and Vb, though slightly weaker, retain argillic soil-horizon characteristics similar to those of the rest of unit V. On the basis of stratigraphic position, texture, and soil development, unit V on the footwall is correlated with unit V in the hanging wall.

Unit V (pl. 22), on the hanging wall, consists of angular clasts of Stirling Quartzite in a clayey, silty, and sandy matrix. The unit, which is 50 to 120 cm thick, displays strong prismatic structure; distinct clay films are visible without magnification. Unit V is interpreted to be the argillic (Bt) soil horizon associated with an overlying A soil horizon (unit VII) and an underlying carbonate soil horizon (unit IV). The upper part of unit V has $CaCO_3$ stage I+ to weak stage II morphology that appears to have been overprinted on the unit after deposition of unit VI. Unit V, along with units IV and VI, composes unit Q2 (fig. 49; table 35). Soil development on these units is consistent with the middle Pleistocene age estimated for unit Q2 (table 36).

Unit VI (pl. 22), a colluvial deposit composed of about 10 volume percent subangular pebbles and cobbles of Stirling Quartzite in a silty and sandy matrix, is continuous along the entire length of the trench but is generally much thicker on the hanging wall (30–50 cm thick) than on the footwall (10–20 cm thick; similar to unit IV in trench BMT–1, pl. 20). The unit, which is primarily the vesicular (Av) soil horizon associated with the alluvial-fan surface, includes a large eolian component. Unit VI, which also is partly composed of colluvium, loses much of its vesicularity as it crosses the scarp (stas. 10–16 m, south wall, pl. 22). The upper part of the unit displays a platy soil structure that imparts a laminar appearance.

Unit VII (pl. 22) consists of fine sand, 0 to 12 cm thick, that is probably eolian in origin. The unit forms a vesicular A (Av) horizon and is differentiated from unit VI on the basis of color, texture, and pedogenic structure. Unit VII was not differentiated on the south wall of the trench because of disturbance by excavating equipment. Its lower contact is marked by a weak stoneline that apparently represents the buried pavement of the underlying unit VI.

Two fissure fills, 1 and 2, in trench BMT–3 (stas. 11–14 m, pl. 22) are characterized by randomly oriented clasts and are uncemented to weakly cemented; fissure fill 2 is generally less strongly cemented than fissure fill 1.

At present, numerical ages have not been determined for any of the units in trench BMT–3 (pl. 22, figs. 1, 49); however, ages can be estimated on the basis of soil development, stratigraphic position, and correlations with dated units in other Bare Mountain trenches and elsewhere in the region. Unit VII is dated at Holocene (possibly late Holocene) because of its stratigraphic position and its absence of soil development. Units IV through VI appear to be a single depositional package on the basis of sedimentologic characteristics, stratigraphic relations, and soil development. Unit VI appears to be the Av soil horizon associated with units II? and V on the footwall and with units IV and V on the hanging wall. Unit V is a strongly developed Bt soil horizon, and units II? and IV are strongly developed Bk soil horizons. These three units are considered to represent unit Q2 (tables 35, 36), which likely correlates with the Early Black Cone alluvium of Peterson and others (1995). The minimum age of the Early Black Cone surface is estimated at 159–201 ka (table 36). Thus, the time interval represented by the depositional package and associated soils that compose units IV through VI is probably no younger than 159 ka.

Estimated ages for units I, II, II? and III are speculative; however, several properties indicate that they all are older than late Pleistocene. All four units are buried by unit Q2 (table 35). In addition, unit III has a well-developed argillic (Bt) soil horizon, and unit II is the associated carbonate soil horizon. Both units II and III are buried by units IV through VI and so have been below the soil-forming zone since at least 159 ka. Although the Bt soil horizon on unit III is not as well devel-

oped as on unit V, the time interval represented by the development of the Bt soil horizon in unit III probably extends at least several tens of thousands of years. Finally, unit I has a well-developed carbonate soil horizon. Unlike units II and III on the hanging wall, unit I has remained in the maximum carbonate-soil-forming zone, and so the strength of the carbonate soil horizon in unit I may represent much or all of the total time elapsed since deposition of the unit. These factors indicate that units I, II, and III are probably much older (200–500 ka) than unit Q2 (minimum estimated age, 159 ka) and its correlative units exposed in trench BMT–3.

Interpretation of Quaternary Fault Activity

Stratigraphic and structural relations exposed in trench BMT–3 (pl. 22; figs. 1, 49) indicate that at least two surface-rupturing paleoearthquakes have occurred on the Bare Mountain Fault at this site since the mid-Quaternary to late Quaternary. An obvious fault zone is exposed in the south wall of the trench (stas. 12–14 m), and the Wood Canyon Formation and Quaternary units II through V are all clearly faulted. The fault dips 79° E. Although unit VI thickens near the fault, it overlies the fault zone with no obvious displacement. However, because unit VI is interpreted to be the Av soil horizon associated with the underlying Bt and Bk soil horizons (units IV and V on the hanging wall and units II? and V on the footwall), the base of unit VI may have been offset by the most recent surface rupture. The absence of clear evidence for faulting and the thickening of unit VI across the scarp may reflect the time-transgressiveness of the unit, subsequent pedogenesis, and the relative mobility of the fine material on the alluvial-fan surface.

The sequence of events recorded by the strata exposed in trench BMT–3 (pl. 22; figs. 1, 49) is interpreted as follows: (1) erosion or pedimentation of the Wood Canyon Formation and subsequent deposition of unit I; (2) displacement of unit I by a possible faulting event(s), although no direct evidence was observed because deposits possibly correlative with unit I are not exposed on the hanging wall; (3) deposition of units II, II?, and III across the fault; (4) a period of landscape stability and development of the Bt soil horizon now preserved in unit III on the hanging wall (a correlative unit was apparently eroded off the footwall before unit V was deposited); (5) displacement of units II, II?, and III by faulting (referred to as event Y); (6) deposition of fissure fill 1 by erosion of units II, II?, and III; (7) deposition of units IV through VI across the fault; (8) a period of landscape stability and development of the Bt soil horizon on unit V and the Bk soil horizon on units II? and IV; (9) displacement of units IV through VI by faulting (referred to as event Z); (10) deposition of fissure fill 2 and thickening of unit VI in the hanging wall by erosion of material off the hanging wall; and (11) deposition of unit VII across the fault and development of the carbonate soil horizon ($CaCO_3$ stage I+–II morphology) on unit V on the hanging wall, on fissure fill 2 at the fault, and on unit V on the footwall.

The displacement associated with event Y is difficult to measure but was probably about 1.5 m. Unit III (pl. 22) appears to be backtilted toward the fault, resulting in an apparent vertical displacement of nearly 3 m if the top of that unit is projected toward the estimated position of the former ground surface. This interpretation assumes that a Bt soil horizon similar in thickness to the Bt soil horizon developed on unit III on the hanging wall was originally present above unit I on the footwall. However, if we assume that unit III had a slope similar to that of unit V and the present ground surface (approx 8°–11°), and if unit III is restored to that position, then the net slip resulting from event Y is about 1.5 m.

Measurements indicate a net slip for event Z of about 0.8 m and an apparent vertical displacement of about 0.7 m, both values determined by projecting the unit V (pl. 22) surface toward the fault zone from points about 7 m from the zone on both the hanging wall and the footwall, and by assuming a prefaulting surface slope of 11°. This slope was used because, at the trench, a scarp profile shows a relatively constant far-field slope of 11° for the unit Q2 alluvial-fan surface. These projections were also made to account for the backtilting of unit V and the apparent erosion of that unit on the footwall near the fault. Both the net slip and apparent vertical displacement agree with the surface offset of 0.8 m measured from the scarp profile (15, table 37).

Discussion

Clear evidence for at least two faulting events is preserved in trench BMT–3 (pl. 22; figs. 1, 49). The displacement associated with the latest event (Z) appears to have been about 0.8 m, but the date of this event is not well constrained. The only clearly unfaulted unit in trench BMT–3 is unit VII (Holocene). As described for trenches BMT–1 (pl. 20) and BMT–2 (pl. 21), however, the age and sedimentologic characteristics of the surficial deposits do not appear to provide an accurate estimate of the date of the most recent faulting event. A more realistic minimum date for this event can be estimated from the degree of carbonate accumulation ($CaCO_3$ stage I+–II morphology) that has subsequently overprinted unit V and fissure fill 2. On the basis of thermoluminescence analysis of a unit with similar carbonate morphology at the Tarantula Canyon trench site (pl. 20; fig. 47), we infer that the most recent event at the Stirling trench site (pl. 22; fig. 49) probably occurred before 16±1 ka (sample TL–32, table 38).

Additional geologic relations at the Stirling trench site (pl. 22; fig. 52) also support the interpretation that the most recent faulting event there is at least latest Pleistocene. No scarps are present on unit Q4 (latest Pleistocene to Holocene) and unit Q3 (late Pleistocene) alluvial fans immediately north and south of the trench site. Correlation of the unit Q3 alluvial fans to the Late Black Cone surface of Peterson and others (1995) indicates that the Q3 alluvial fans near the Stirling trench site are at least 17 ka, possibly older than 30 ka; the latest faulting event (Z) would therefore be still older. The characteristics of the fault scarp at the Stirling trench site,

which are similar to those of the fault scarp at the Tarantula Canyon trench site (pl. 20; fig. 47), also indicate that the most recent faulting event at the Stirling site is no younger than late Pleistocene and could be much older.

The number of earlier faulting events, their age, and their associated displacements can only be estimated. Bt soil-horizon development on units III and V (pl. 22) and carbonate-soil development on units I, II?, and IV provide evidence that a considerable time interval is represented by the strata exposed in trench BMT–3 (pl. 22, figs. 1, 49). Stratigraphic relations indicate that these units have been offset at least twice, and the soil development on units IV and V on the hanging wall and on units II? and V on the footwall support a conclusion that a considerable time interval (possibly as much as 100–200 k.y.) elapsed between the most recent faulting event (Z) and the penultimate faulting event (Y). Thus, event Y probably occurred several hundred thousand years ago. The degree of soil development on units II and III (soils preserved only on the hanging wall) also indicates a lengthy period of time (several tens of thousands to hundreds of thousands of years) between event Y and any earlier faulting event(s).

As discussed earlier, the net slip from penultimate event Y is estimated at 1.5 m. The displacement could conceivably be as much as 3 m (top of unit III to top of unit II? minus 0.8 m for the latest faulting event); however, by restoring the slope of unit IV to about 11°, which is the present slope of the unit Q2 (tables 35, 36) alluvial fan, we obtained the estimate of 1.5 m. This value is approximately double the estimated displacement from event Z (0.8 m), indicating either that the slips associated with faulting events at the Stirling trench site (pl. 22; fig. 49) have not been uniform or that the 1.5 m represents more than one faulting event. The first interpretation appears to be more likely because direct geologic evidence for additional faulting events is absent in the trench.

Summary of Quaternary Faulting Events

Evidence based on (1) geologic relations exposed in three trenches excavated across the Bare Mountain Fault trace along the east front of Bare Mountain; (2) the distribution, correlation, and estimated ages of Quaternary surficial deposits mapped in the vicinity of the trenches; and (3) the presence or absence of fault scarps in these deposits leads to the general conclusions that no faulting events have occurred during Holocene time and that the most recent faulting event was no later than late Pleistocene. The second conclusion is supported by observations that fault scarps indicative of Quaternary activity are present only on alluvial-fan deposits dated at middle Pleistocene (minimum estimated numerical age, 159 ka). A comparison of scarp profiles measured at the Tarantula Canyon trench site (pl. 20; fig. 47) along the Bare Mountain Fault with scarps of known ages elsewhere in the region also indicate a date possibly as early as, or earlier than, 100 ka. Younger, unfaulted alluvial-fan deposits are prevalent along the mountain front, thus also providing ample supporting evidence for the interpreted date of the most recent faulting event on the Bare Mountain Fault.

At least two Quaternary faulting events are recorded in two trenches (BMT–2, pl. 21; BMT–3, pl. 22), but only one in the third trench (BMT–1, pl. 20). The date of the most recent faulting event at all three trench sites appears to be about the same, on the basis of scarp-profile data, stratigraphic relations, fault characteristics, and soil development. Because these three sites span nearly the entire 20-km length of the Bare Mountain Fault, we conclude that this most recent faulting event ruptured nearly the entire fault rather than only local segments.

Dates of faulting events that predate the most recent event (Z) cannot be reliably estimated on the basis of data from either trench BMT–2 (pl. 21) or trench BMT–3 (pl. 22). Carbonate soil development in some of the deposits exposed in trench BMT–2 indicates that a considerable time interval elapsed between event Z and the penultimate event (Y), possibly several tens of thousands of years to several hundred thousand years. Similar lines of evidence in trench BMT–3 indicate that at least 100–200 k.y. elapsed between these two faulting events. One or more earlier faulting events may have occurred at the Stirling trench site, separated from event Y also by a long interval (several tens of thousands of years to several hundreds of thousands of years), but the evidence is inconclusive.

At the Tarantula Canyon trench site (pl. 20; fig. 47) near the north end of the Bare Mountain Fault (trench BMT–1), where we observed direct evidence for only one faulting event, the relatively flat alluvial-fan surface and the well-developed carbonate soil horizon present on unit V together provide an excellent datum for measuring single-event surface displacement or offset. After compensating for the backtilting of unit V on the hanging wall, the net tectonic displacement of this unit is 1.5 m, in good agreement with the surface offset measured from scarp profiles at the trench site. Net slip associated with the most recent faulting event (Z) at the Stirling trench site (trench BMT–3, pl. 22) is well constrained at about 0.8 m. Displacement from the penultimate faulting event (Y) is estimated at 1.5 m, but the evidence is equivocal, and this offset could represent more than one faulting event. In the context of fault displacements per event, however, we consider this 1.5-m offset to reflect event Y at the Stirling trench site. Accordingly, measured per-event displacements at the three trench sites on the Bare Mountain Fault are 0.8, 1.5, and 1.5 m, from which we infer that the typical or average displacement associated with a faulting event on the Bare Mountain Fault is probably 1.0 to 1.5 m.

Accurate measurements of displacement resulting from the most recent faulting event (Z) on the Bare Mountain Fault were made at trench BMT–1 (pl. 20; figs. 1, 47) near the north end of the fault and at trench BMT–3 (pl. 22; figs. 1, 49) near the south end. Because the measured displacements associated with historical surface-rupturing earthquakes show that displacement diminishes near the ends of faults, the displacements measured at these trench sites may not represent the maximum displacement that occurred everywhere along the

Bare Mountain Fault during this event. Although we have no specific information about the displacement near the center of the fault, our conclusion is that the per-event displacement probably averages about 1.0 to 1.5 m (see below). This value is higher than the 0.5-m displacement estimated by using the data of Wells and Coppersmith (1994) for a 20-km-long fault; however, considerable scatter exists in the limited data for displacement versus fault-rupture length on normal faults.

Recurrence Interval and Slip Rate

Even though numerical-age information is limited, the relative-age data, as noted earlier, indicate that the recurrence interval for moderate to large surface-rupturing paleoearthquakes on the Bare Mountain Fault is long, probably at least tens of thousands of years. In fact, the Bare Mountain Fault appears to be a low-activity fault similar to the Santa Rita and Horseshoe Faults in Arizona, in the southern part of the Basin and Range Province, where the recurrence interval for large earthquakes appears to range from tens of thousands of years to possibly several hundred thousand of years (Pearthree and Calvo, 1987; Piety and Anderson, 1991). Thus, the available evidence strongly indicates that the Bare Mountain Fault can best be characterized as a fault with moderate to large, but infrequent, earthquakes.

At the Tarantula Canyon trench site (pl. 20; fig. 47), a unit Q2 (tables 35, 36) alluvial fan (trench units II, V) with an estimated age of at least 159 ka is displaced 1.5 m along a 72°-dipping fault (pl. 20). On the basis of this relation, the resulting slip rate (net slip or dip slip) for the Bare Mountain Fault at this site is 0.01 mm/yr. Considering that unit Q2 is probably older than 159 ka, the actual slip rate is probably even less than 0.01 mm/yr.

At the Stirling trench site (pl. 21; fig. 48), a unit Q2 (tables 35, 36) alluvial fan is displaced only 0.8 m by the most recent faulting event along a 79°-dipping fault. However, trench BMT–3 (pl. 22; figs. 1, 49) also displays evidence for multiple events. Total calculated mid-Quaternary to late Quaternary displacement there is at least 2.3 m but could be as much as about 4 m (if backtilting is not removed). If we assume a minimum age of 200 ka for the older displaced surficial trench units (II, II?, and III) in trench BMT–3 and use the 4-m estimate for total displacement, the slip rate (net slip or dip slip) for the Bare Mountain Fault at the Stirling trench site would be as high as 0.02 mm/yr. Using a more conservative age estimate of 300–400 ka for the faulted units and a value of 2.3 m for the total displacement, the slip rate at the Stirling trench site is less than 0.01 mm/yr.

A unit Q1 deposit about 3 km north of Tarantula Canyon (TC, fig. 46) is displaced approximately 4 to 5 m. Assuming a minimum age of about 500 ka for this deposit (table 36), we estimate a vertical slip rate of about 0.01 mm/yr for the Bare Mountain Fault at this site. Although the age control on the deposit there is problematic (no trenches, test pits, or numerical ages), the similarity of the estimated slip rate to those estimated at the other two sites (Tarantula Canyon and Stirling) indicates that both the estimated age and the resulting slip rate are probably reasonable.

On the basis of data from the three trench sites, the average slip rate for the Bare Mountain Fault appears to be no higher than about 0.01 mm/yr (because the steep fault dips, vertical slip, dip slip, and net slip are all nearly identical). Thus, the slip rate does not vary appreciably from north to south. Given the apparent low rates of seismicity determined in this study, we believe that additional numerical ages on faulted deposits would probably not significantly change our estimates of either the slip rate or the recurrence interval for the Bare Mountain Fault.

Chapter 13

Paleoseismic Investigations on the Rock Valley Fault System

By Jeffrey A. Coe, James C. Yount, Dennis W. O'Leary, and Emily M. Taylor

Contents

Abstract....175
Introduction....175
Physiographic Setting....177
Characteristics of the Rock Valley Fault System....177
Trenching Activities....177
Previous Paleoseismic Work....177
Faults Trenched in 1995....180
Trench Stratigraphy, Structure, and Age Constraints....180
Northern Fault....180
Northern Strand of the Southern Fault....185
Southern Strand of the Southern Fault....190
Frenchman Flat Fault....190
Paleoseismic Interpretations....190
Chronology of Surface-Rupturing Paleoearthquakes....190
Event Z′....190
Event Y′....190
Event X′....190
Events W′ and V′....191
Slip Rates and Recurrence Intervals....194
Northern Fault....194
Medial Fault....194
Northern Strand of the Southern Fault....194
Southern Strand of the Southern Fault....194
Frenchman Flat Fault....194
Fault-System-Wide....194
Discussion....195
Acknowledgments....195

Abstract

Paleoseismic investigations in trenches excavated across five faults in the Rock Valley Fault system provide evidence for at least five surface-rupturing paleoearthquakes in the past several hundred thousand years. Four of the faults, designated the northern, medial, and southern (two strands) faults, are in the central section of the Rock Valley Fault system southeast of Skull Mountain; the fifth fault, designated the Frenchman Flat Fault, is in Frenchman Flat near the east end of the fault system. All five faults strike N. 65°–80° E. and are expressed as scarps or lineaments in Quaternary deposits. In general, displacements are predominantly strike slip (left lateral) with a dip-slip component.

Five faulting events affecting one or more faults in the Rock Valley Fault system are estimated to have occurred at approximately 160, 120, 40±24, 13±4, and 2–1 ka. The late Pleistocene slip rate for the fault system is about 0.1 mm/yr. Estimated displacements and slip rates for individual faults are, for the (1) northern fault: average net displacement per event (four events), 2.9 m; slip rate, 0.07±0.04 mm/yr; (2) medial fault: average net displacement per event (three events), 2.5 m; slip rate, 0.023±0.010 mm/yr; (3) northern strand of the southern fault: average net displacement per event (three events), 0.1 m; slip rate, more than 0.001±0.001 mm/yr; (4) southern strand of the southern fault: average net displacement per event (three events), 0.1 m; slip rate, 0.002±0.0005 mm/yr; and (5) Frenchman Flat Fault: net displacement (one event), more than 1 m; slip rate, indeterminable. The largest surface-rupturing paleoearthquake (penultimate faulting event) caused a total of about 4.2 m of net displacement along the Rock Valley Fault system in central Rock Valley.

Introduction

The Rock Valley Fault system occupies most of east-northeast-trending Rock Valley, about 25 km southeast of the proposed repository site for the storage of high-level radioactive wastes at Yucca Mountain (fig. 1). The fault system is composed of multiple east-northeast trending strike- and oblique-slip faults that form distinct scarps and lineaments in surficial deposits and demonstrate a considerable history of Quaternary movement. The fault system constitutes a significant tectonic boundary within the Walker Lane (O'Leary, 2000) between Miocene volcanic rocks of the southwestern Nevada volcanic field to the

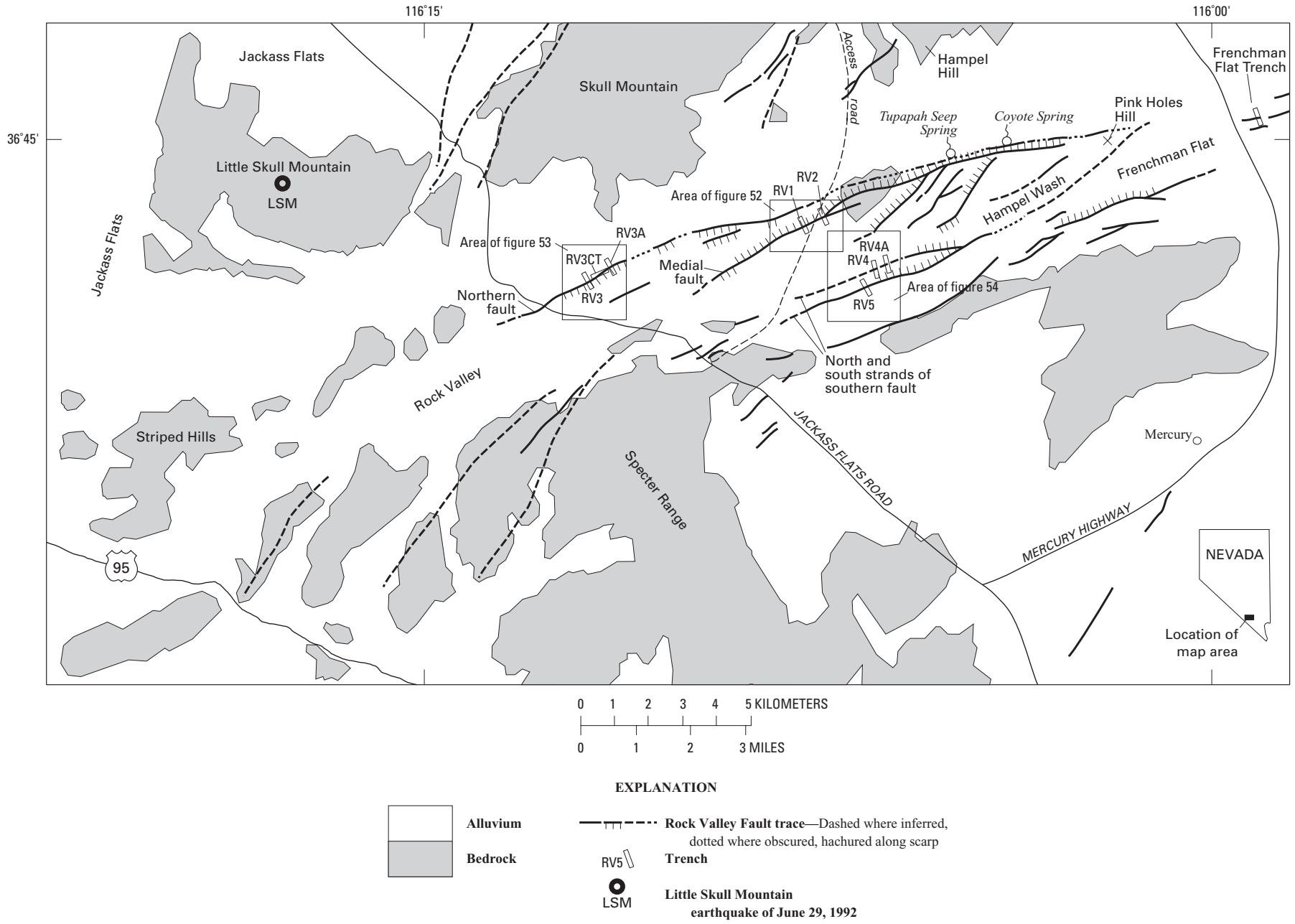

Figure 51. Geologic map of the Rock Valley area, southwestern Nevada, showing locations of trenches on the Rock Valley Fault system (figs. 1, 2).

north (Skull and Little Skull Mountains) and lower Paleozoic carbonate strata to the south (Specter Range, figs. 1, 51).

In addition to Quaternary tectonic activity, the Rock Valley Fault system has been the locus of recent, uncommonly shallow earthquakes, some of which are probably related to the aftershock sequence of the June 29, 1992, *M*=5.6 Little Skull Mountain, Nev., earthquake (Smith and Brune, 1993; Smith and others, 2000).

This chapter presents the Quaternary paleoseismic history of the Rock Valley Fault system as determined from detailed logging and interpretations of exposures in eight trenches excavated on faults along the north and south sides of the valley. Results from a previous paleoseismic investigation on a fault in central Rock Valley (Yount and others, 1987), as well as data from a trench in Frenchman Flat near the east end of the fault system, are also integrated into this summary of the paleoseismic history of the fault system.

Physiographic Setting

Rock Valley trends N. 70° E. from near U.S. Highway 95 eastward to Frenchman Flat (fig. 51), a distance of about 32 km. The valley, which gains its geographic definition from an alignment of adjacent uplands rather than by a conspicuous valley-floor depression, is primarily a tectonic rather than an erosional feature. The geomorphology of the valley floor is controlled by a network of faults (Rock Valley Fault system) that spans the length of the valley and occupies most of its width (~5 km). Frizzell and Zoback (1987) suggested that the current topographic expression of the valley probably developed after about 5 Ma. The erosion that has occurred and is presently occurring in Rock Valley is interpreted to be largely a consequence of tectonic activity—namely, differential movement (uplift or subsidence) between the east and west ends of the fault zone. A transverse drainage divide just east of the area 27 access road (fig. 51) separates the valley into an eastward-draining watershed (to Frenchman Flat by way of Hampel Wash) and a westward-draining watershed (to Amargosa Lake by way of Rock Valley Wash). The eastward-draining watershed is relatively deeply eroded; much Pleistocene alluvium has been stripped away, thus exposing the faults, the underlying Miocene rocks, and the pre-Pleistocene structural configuration of the valley floor. West of the drainage divide, the faults are expressed as lineaments or scarps in alluvium, but such features have not been observed west of long 116°15′ W. (fig. 51).

Characteristics of the Rock Valley Fault System

Three major fault sets compose the Rock Valley Fault system: (1) long, dominantly left lateral strike-slip faults that strike N. 65°–80° E.; (2) shorter normal, strike-slip or reverse relay faults, or both, that strike N. 25°–50° E.; and (3) minor normal and strike-slip faults that strike N. 10°–15° W. Three of the N. 65°–80° E.-striking faults are considered major in this study on the basis of their length, continuity, and expression in Pleistocene alluvial-fan surfaces. These faults, designated informally as the northern, medial, and southern faults (fig. 51), are composite structures that, from place to place along strike, consist of numerous subparallel planes that interlink or splay off toward the southwest. (See chap. 3 for various interpretations as to the total length of the fault system.)

The northern fault continues westward from Pink Holes Hill for a total inferred distance of about 18.5 km. The fault is not expressed in the Pleistocene surface east of the area 27 access road, where it is only about 250 m north of the medial fault, but is revealed in a few places by deep gully erosion. West of the area 27 access road, the northern fault is marked by scarps in fan remnants and curves to a more southerly strike that projects toward the south side of the Striped Hills (fig. 51).

The medial fault can be traced nearly continuously from Pink Holes Hill westward to the area 27 access road (fig. 51), a distance of about 9 km. The fault, mapped as the "Rock Valley Fault" by Frizzell and Zoback (1987), is approximately parallel to and 2.4 km north of the southern fault. The medial fault continues westward of area 27 for possibly another 7.5 km as a N. 55°–60° E.-trending scarp in Pleistocene alluvium. The fault was trenched by Yount and others (1987). Scarps mapped along the south side of Frenchman Flat (Poole, 1965) imply that the fault also extends approximately 12.5 km eastward from Pink Holes Hill.

The southern fault, which is mapped from near the Mercury Highway westward for a distance of about 14 km (fig. 51), is expressed as several well-exposed scarps, each as much as 2.5 km long. West of Hempell Wash, the fault is exposed in an alluvial fan as two 5- to 7-km-long, parallel splays (northern and southern strands of the southern fault, fig. 51). Farther west, the fault may be represented by lineaments and structures located north and west of the intersection of Jackass Flats Road and the area 27 access road. On the basis of the faults mapped by Barnes and others (1982), the southern fault is inferred to continue about 3 km eastward of the Mercury Highway for a total length of about 17 km.

Trenching Activities

Previous Paleoseismic Work

The Quaternary paleoseismic history of the medial fault in the Rock Valley Fault system was investigated in two trenches (RV1, RV2, figs. 51, 52) that were excavated in 1978 across a 0.5-m-high scarp. Detailed logs of these two trenches were presented by Yount and others (1987) and are not duplicated here; their results indicated at least two episodes of faulting on the fault (as discussed below) that resulted in a total vertical down-to-the-north displacement of 257 to 295 cm. The amount of strike-slip motion that may have been involved could not be determined because of the poorly developed

Figure 52. Surficial geologic map of area surrounding trenches RV1 and RV2 across medial fault of the Rock Valley Fault system in Rock Valley, southwestern Nevada (figs. 1, 2, 51). Map units modified from Hoover and others (1981). Compound units (1ab and so on) denote two lithologic units that cannot be delineated separately at 1:12,000 scale; fractional units (1c/2bc and so on) indicate that a veneer of younger deposits masks, but does not completely conceal, older deposits. Hachured areas, places where land surface has been modified by construction, filling, or excavation. From Yount and others (1987).

DESCRIPTION OF MAP UNITS

[Accompanies fig. 52]

1a **Active wash deposits**—Loose sand and gravel occupying well-defined channel floors. Unvegetated, lacking pavement. Channel form is unmodified. Correlated with unit Q1a of Hoover and others (1981)

1b **Deposits of young washes**—Similar to unit 1a. Generally lies 10 to 50 cm above floors of active washes. Sparsely vegetated. Original channel form is slightly modified. Generally mapped with unit 1a (as unit 1ab) because of scale. Correlated with unit Q1b of Hoover and others (1981)

1c **Young fan and wash deposits**—Sand and gravel composing small alluvial fans and elevated terraces in washes, 1 to 2 m above floors of active washes. Soils have very weak A/Cox profiles. Moderately vegetated. Channel forms are distinctly more subdued than those of unit 1a or 1b. Cobble-bearing debris-flow fronts are locally present on alluvial fans. Correlated with unit Q1c of Hoover and others (1981)

2b **Alluvial-fan and wash deposits**—With surface and lithologic characteristics similar to those of unit Q2 deposits, nested inside and below unit 2c deposits. Generally mapped with unit 2c (as unit 2bc) where slight differences in pavement and drainage development indicate likelihood of deposits of two different ages. Correlated with unit Q2b of Hoover and others (1981)

2c **Intermediate-age alluvial-fan and wash deposits**—Vesicular silt overlying interbedded coarse-grained gravelly sand and sandy gravel. Slight to moderate cementation of sand and gravel by pedogenic carbonate with $CaCO_3$ stage II morphology. Moderate to strong pavement development and moderate dissection, with extensive areas of original depositional surface remaining. Correlated with unit Q2c of Hoover and others (1981)

QTa **Old alluvial-fan deposits**—Indurated, poorly sorted, muddy to sandy cobble and boulder gravel. Moderate to strong cementation by pedogenic carbonate with $CaCO_3$ stages III and IV morphology. Pavement typically is moderately developed, owing to erosional degradation of land surface. Boulders are more common than on unit 2b or 2c surfaces. Carbonate-cemented material is commonly exposed at or near ground surface. Surface is dissected with rounded interfluves. Correlated with unit Qta of Hoover and others (1981)

Tpa **Rocks of Pavit Springs of Hinrichs (1968)**—Interbedded light-gray (10YR 7/2) to pale-brown (10YR 6/3), thin- to thick-bedded siltstone and sandstone and white (10YR 8/2) to light-brown (7.5YR 6/4) silicic tuff and tuff breccia. Siltstone and sandstone contain diatoms and thin ash partings. Fish and plant debris are locally present. Dominantly lacustrine basin-fill deposits, with minor interbeds of fluvial sandstone and conglomerate

bedding and coarse-grained texture of the exposed surficial deposits. No slickensides or other kinematic indicators were observed in the trenches; however, slickensides with a rake of 22° SW. that were observed on a bedrock exposure of the fault plane farther east in Hampel Wash (fig. 51) may indicate a lateral component of fault movement.

The trench in Frenchman Flat (fig. 51), which was excavated on a prominent northwest-facing scarp just east of the Mercury Highway north of Mercury, Nev. (fig. 51), was logged by the second author in 1985. The scarp appears to be on line with the medial or northern fault of the Rock Valley Fault system as projected eastward from central Rock Valley, but an interconnection between the scarp and these two faults is unknown. Stratigraphic and structural relations exposed in this trench are discussed in the next section.

Faults Trenched in 1995

Eight trenches were excavated along the northern and southern faults in the spring of 1995. Four of these trenches were on the northern fault (fig. 51), two perpendicular to the fault (trenches RV3, RV3A) and two parallel to the fault (trenches RV3CT, RV3CT2). Four trenches were excavated on the southern fault, two perpendicular to its northern splay (trenches RV4, RV4A) and two perpendicular to its southern splay (trenches RV5, RV5A). All of these trenches were logged except trenches RV3CT2 and RV5A, which did not intersect the fault.

Surficial geologic maps of the area surrounding the trenches on the northern and southern faults are shown in figures 53 and 54. The surficial deposits (units 1, 2, and so on) were differentiated primarily on the basis of distinct textural, morphologic, and topographic characteristics visible on aerial photographs. Numerical labels were used to indicate a general correlation to the standard stratigraphic sequence (for example, unit 1~unit Qa1, unit 2~unit Qa2, and so on) defined for the Yucca Mountain area (fig. 1; see chap. 2), but do not necessarily imply a precise age equivalency.

At trenches RV3 and RV3A (fig. 51), the northern fault cuts the units 3 and 5–7 geomorphic surfaces, respectively (fig. 53). Trench RV3 is located on a prominent, down-to-the-south scarp (see Swadley and Huckins, 1989). No evidence was observed for lateral displacement of surface features near the trenches. At trenches RV4 and RV5, the southern fault cuts the unit 3/4 geomorphic surface (fig. 54). Although no measurable scarp exists at trenches RV4 or RV5, conspicuous lineaments are visible on aerial photographs.

Trenches were logged by using field and close-range photogrammetric methods (see chap. 1 for details) between April 1995 and January 1996. Stratigraphic units were described by using standard sedimentologic terminology, and soil descriptions follow the nomenclature of Birkeland (1984) and Machette (1985). Offsets of lithologic units across faults, the presence of colluvial wedges or fault fissures, and upward terminations of fractures were interpreted as evidence of paleoearthquakes. U-series and thermoluminescence analyses were used to date lithologic units, soil horizons, and paleoearthquakes, as discussed in chapter 2; estimated numerical ages of samples collected in the trenches are listed in table 39.

Trench Stratigraphy, Structure, and Age Constraints

Logs of six trenches excavated in 1995 are shown on plates 23 through 25, and lithologic-unit and soil-horizon descriptions are listed in tables 40 and 41. The log of the trench at Frenchman Flat is shown on plate 26. Note that the numbering systems for units exposed in trenches are independent from those of the surficial map units shown in figures 53 and 54.

Northern Fault

Trenches on the northern fault expose a sequence of alluvial gravel, colluvium, and eolian sand (pl. 23; table 40). Units in trenches RV3 and RV3CT (fig. 51), which were excavated in middle Pleistocene gravel, are labeled independently from those in trench RV3A, which was excavated in Holocene gravel. In trenches RV3 and RV3CT, five major units are exposed. Units 1 and 3 consist of poorly sorted gravel that is interpreted to be debris-flow deposits. Unit 1 is exposed only in the upthrown block, whereas unit 3 is exposed in both the upthrown and downthrown blocks. Wedge-shaped subunits 3d and 3b, which are present at the fault in the downthrown block, are interpreted to be colluvial deposits. Unit 2, which consists of poorly sorted to well-sorted gravel that is present in both the downthrown and upthrown blocks, is interpreted to be an alluvial-fan flood deposit. Subunit 2a is a channel-fill deposit exposed in trench RV3CT. The thalweg of the buried channel at the base of unit 2a is used to estimate the cumulative fault slip, as described below. Unit 4, consisting of moderately well sorted to well-sorted sand that is present only in the downthrown block, thins away from the fault. A few reworked fragments of unit 4 are visible on the upthrown block, indicating that the unit may have been stripped from the upthrown block. Unit 4 is interpreted to be an eolian deposit that has undergone some alluvial and (or) colluvial reworking. Unit 5 consists of silty eolian sand that is present on both sides of the fault.

Exposed soils include an Avk horizon on unit 5, a Bkw to Btw horizon on unit 4, and two silica-carbonate soils, one formed on units 2 and 3 and one on unit 1 (table 41). The top of the youngest carbonate soil forms a conspicuous, stripped, irregular boundary with overlying unit 5 on the upthrown block but is continuous and diffuse with overlying units 4 and 5 on the downthrown block.

Age constraints on units 1 through 5 include one thermoluminescence age on a sample (TL–57, 12±5 ka, pl. 23; table 39) from unit 5 and three U-series ages on samples

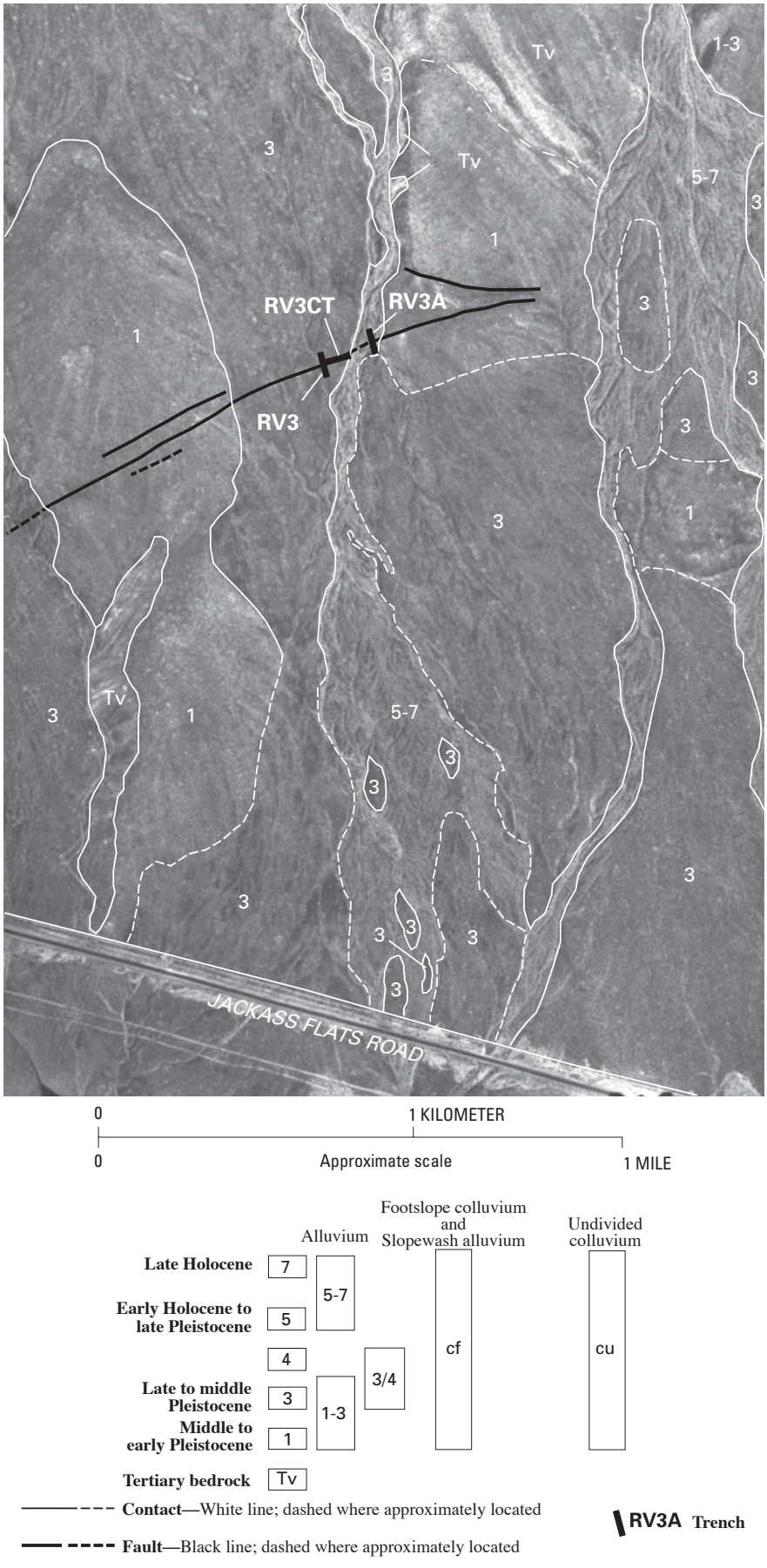

Figure 53. Surficial geologic map of area surrounding trenches RV3, RV3CT, and RV3A across northern fault of the Rock Valley Fault system in Rock Valley, southwestern Nevada (pl. 23; figs. 1, 2, 51).

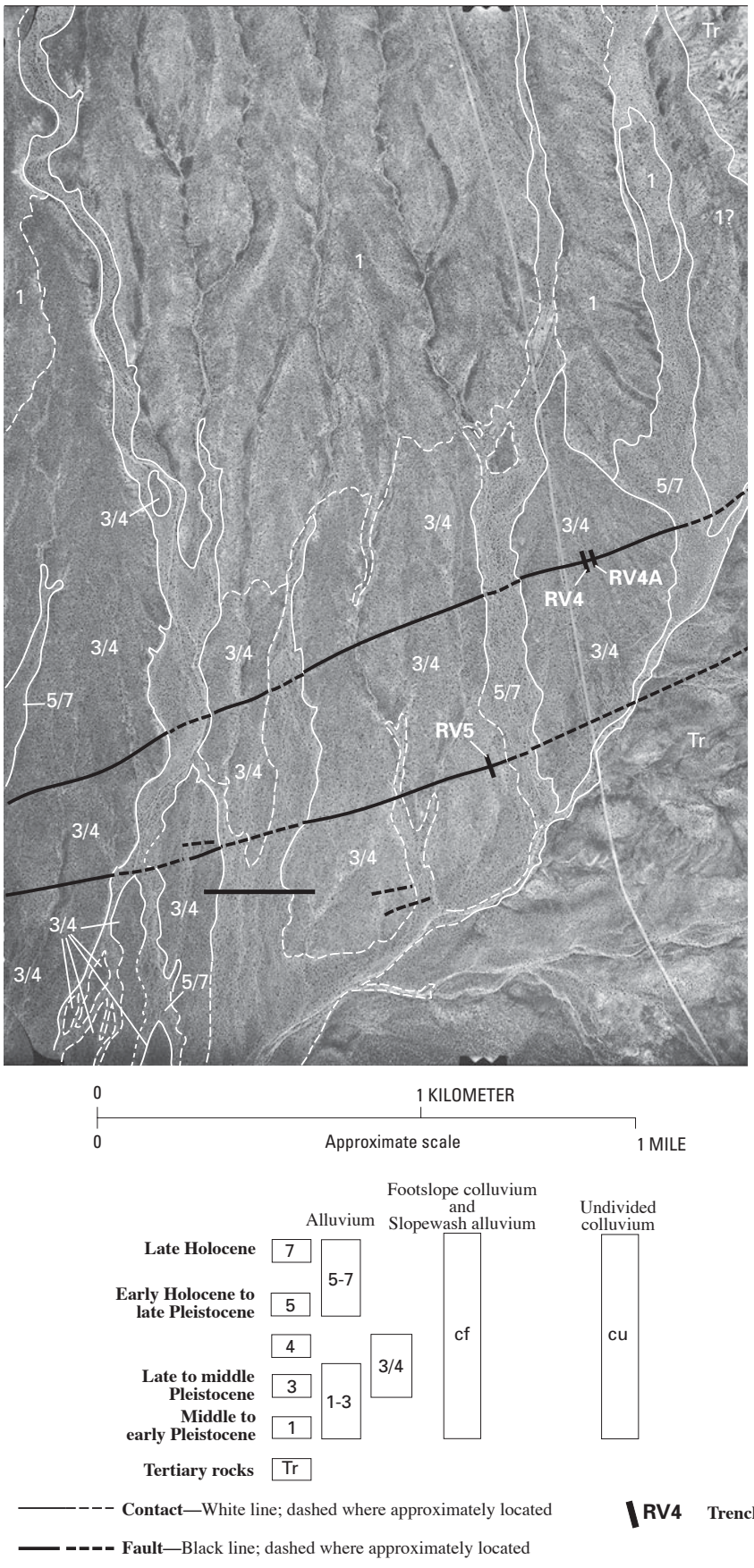

Figure 54. Surficial geologic map of area surrounding trenches RV4, RV4A, and RV5 across northern and southern splays of southern fault of the Rock Valley Fault system in Rock Valley, southwestern Nevada (pl. 24; figs. 1, 2, 51).

Table 39. Numerical ages of deposits exposed in trenches RV2, RV3, RV3A, RV4, and RV5 and in the trench in Frenchman Flat (FFT1) across the Rock Valley Fault system in the Yucca Mountain area, southwestern Nevada.

[See figures 1, 2, and 51 for locations. Samples: TL– (error limits, ±2σ), thermoluminescence analyses by S.A. Mahan; HD (error limits, ±2σ), U-series analyses by J.B. Paces. Do., ditto]

Trench	Sample	Unit and material sampled	Estimated age (ka)
RV 2[1]	TL–74	Base of 3Btkb2 soil horizon	47±4
	TL–75	Av soil horizon	7±1
RV 3	TL–57	5, buried Av soil horizon	12±5
(pl. 23)	HD 1812	3f, upper platy K soil horizon	74±13, 79±3
	HD 1955	3a, silica-rich clast rind	98±2, 102±3, 106±2
RV 3CT	HD 1954	1, silica-rich clast rind	367±55, 550±270
(pl. 23)			
RV 3A	TL–58	8, sandy lens	11±2
(pl. 23)			
RV 4	TL–53	5, buried Av soil horizon	2±0.5
(pl. 24)	TL–54	2e, sandy lens in alluvium	88±74, 92±62
	HD 1803	2e, rhizolith	26.5±0.2
	HD 1804	3, clast-rind K soil horizon	35±1, 50±1, 64±2
	HD 1805	3, opaline silica stringer in K soil horizon	16.4±0.3
RV 5	TL–55	Fissure fill	10±1
(pl. 25)	TL–56	Do	6±1
	HD 1807	Opaline silica laminae in fissure fill	10±2, 12±4, 46±9, 72±10
	HD 1809	1c, laminar K soil horizon	321±44
	HD 1810	Fissure fill, top of K soil horizon	9±3, 10±5
	HD 1811	1e, laminar K soil horizon	22.4±0.8, 50.0±2.6
FFT 1	TL–72	B, eolian fill	9±1
(pl. 26)	TL–73	B, Bk soil horizon	27±2

[1]Trench log not included in this report.

from the two silica-carbonate soils formed on units 1 through 3. One sample (HD 1812), from silica-carbonate rinds on clasts at the top of unit 3 on the downthrown block, yielded ages of 74±13 and 79±3 ka, indicating that the unit 3 deposits are older than 79 ka. A second sample (HD 1955), from near the base of unit 3 on the downthrown block, yielded an average age of 102±2 ka, indicating that the oldest part of unit 3 is older than 100 ka. A third sample (HD 1954), from unit 1 on the upthrown block near the base of trench RV3CT (fig. 51), yielded ages of 550±270 and 367±55 ka. These ages, in combination with ages from unit 3 and an estimated time interval represented by the erosion that occurred on the top of unit 1, indicate that unit 2 was probably deposited sometime between about 300 and 100 ka.

The fault exposed in trenches RV3 and RV3CT (fig. 51) is expressed primarily as a fissure filled with cobbly colluvium (fig. 55). The fissure narrows with depth and ranges in width from about 70 cm near the top of the B soil horizon to about 10 cm at the base of the trench. Units 1 through 4 are offset down to the south across the fissure. The fault strikes N. 66° E. and dips vertically at the trench site. Striae with a rake of 11° NE. (pl. 23) indicate that the downthrown (southern) block moved northeastward during at least one episode of Quaternary fault movement. The cumulative horizontal and vertical displacements that have occurred along the fault since middle to late Pleistocene time, which were estimated by using the thalweg of the channel at the base of unit 2a in trench RV3CT (pl. 23), are 14.2 and 1.2 m, respectively.

Trench RV3A (fig. 51) was excavated in lower to upper Holocene alluvium in an attempt to determine the timing of the most recent paleoearthquakes on the northern fault. The trench exposes a fault zone composed of two shear zones, the youngest of which is capped by a sequence of colluvial-wedge deposits (units 7a–7d, pl. 22; fig. 56). A thermoluminescence analysis of a sample (TL–58, table 39) from the lower part of overlying unit 8 yielded a date of 11±2 ka, which is interpreted to indicate that the unit was deposited approximately contemporaneously with unit 5 (12 ±5 ka) in trenches RV3 and RV3CT (fig. 51).

Table 40. Summary of the characteristics of lithologic units exposed in trenches across the Rock Valley Fault system in the Yucca Mountain area, southwestern Nevada.

[See figures 1, 2, and 51 for locations and table 41 for soil descriptions. Position: FW, footwall; HW, hanging wall. General lithology and matrix: bld, boulder; c, coarse; cbl, cobble; f, fine; gvl, gravel; m; medium; pbl, pebble; slt, silt; snd, sand. Deformation: EW, event wedge; F, faulted. Do., ditto]

Unit	Position	General lithology	Clast size (cm)	Matrix	Cementation	Thickness	Shape	Deformation	Interpretation
					Trench RV3, west wall				
5	HW	slt snd	<50	f snd	See soil description	See soil description	Tabular	F	Eolian material.
4	HW	bld cbl pbl snd	<40	snd	do	do	Wedge	F	Do.
3	HW	bld cbl snd pbl grv	15 (max 100)	snd	do	do	Lenticular	F	Debris-flow deposits.
2	HW	bld cbl snd pbl grv	10 (max 50)	c snd	do	do	Tabular	F	Alluvial gravel.
					Trench RV3A, east wall				
1	FW	snd bld cbl grv	0.2–40	m-c snd pbl	$CaCO_3$, stage III–IV	>50 (from floor)	Tabular	F	Alluvial gravel.
2	FW	cbl pbl snd gvl	.2–10	pbl	$CaCO_3$ stage II	60	do	F	Do.
3	FW	cbl bld snd	.2–40	m-c snd	$CaCO_3$ stage II–III	20–50	do	F	Debris-flow deposits.
3	HW	pbl cbl snd	.2–15	m-c snd	$CaCO_3$ stage II–III	>35	do	F	Do.
4	FW	pbl cbl bld snd gvl	1	pbl	$CaCO_3$ stage II–III	0–45	Lenticular	F	Alluvial gravel.
5	HW	pbl snd cbl gvl	.2–10	pbl	$CaCO_3$ stage I	0–50	Wedge	EW	Alluvial/colluvial wedge.
6	HW	pbl cbl snd to snd pbl cbl gvl	.2–30	m-c snd pbl	$CaCO_3$ stage I	20–70	Irregular	F	Alluvial gravel.
7	HW	snd cbl pbl gvl	.2–40	m-c snd pbl	$CaCO_3$ stage <I	0–40	Wedge	EW	Colluvial/eolian wedge.
8	HW	pbl cbl snd	.2–5	m-c snd	$CaCO_3$ stage <I	0–70	Lenticular	None	Alluvial sand and gravel.
9	HW	pbl snd cbl gvl	.2–30	pbl	$CaCO_3$ stage <I	0–50	Tabular	None	Do.
10	FW & HW	snd cbl bld pbl grv	.2–55	m-c snd	$CaCO_3$ stage I	0–70	do	None	Do.
11	FW & HW	pbl cbl snd	.2–40	m-c snd	$CaCO_3$ stage I	40	do	None	Do.
					Trench RV4, west wall				
1	FW–HW	snd cbl pbl gvl	<14	snd	See soil description	>30	Tabular	F	Alluvial sand and gravel.
2	FW–HW	cbl pbl snd	1–10	snd	do	See soil description	do	F	Do.
3	FW–HW	snd cbl pbl gvl	2–6	snd	do	do	do	F	Do.
4	FW–HW	cbl pbl snd	7–10	snd	do	do	do	F	Eolian material.
5	FW–HW	slt snd	7–10	snd	do	do	do	F	Do.
					Trench RV5, west wall				
1a	FW–HW	gvl snd	0.2–2	f-c snd	See soil description	>20	Tabular	F	Alluvial gravel.
1b	FW–HW	gvl snd	<1	f-c snd	do	0–10	do	F	Do.
1c	FW–HW	snd gvl	<2	f-c snd	do	30–50	do	F	Alluvial sand and gravel.
1d	FW–HW	snd cbl gvl	.2–15	f-c snd	do	0–35	Lenticular-tabular.	F	Alluvial deposits.
1e	FW–HW	gvl snd	.2–5	f-c snd	do	40–60	Tabular	F	Do.
2	FW–HW	pbl snd	.2–10	f-m snd	do	See soil description	do	F	Eolian material.
3	FW–HW	slt snd	.2–3	f-m snd	do	do	do	Fractured only	Do.

Northern Strand of the Southern Fault

Trenches RV4 and RV4A (fig. 51), which were excavated across the northern splay of the southern fault, expose a sequence of middle to upper Pleistocene alluvial sand and gravel and younger eolian sand (pl. 24; table 40). The two trenches expose the same five major units on both sides of the fault, labeled by using the same numbering scheme. Units 1 through 3 are interpreted to be alluvial-fan flood deposits, and units 4 and 5 are interpreted to be silty sand of eolian origin. Soils exposed in the trench include Avk and B horizons on unit 5, a buried Bw horizon on unit 4, and two buried silica-carbonate soils, one formed on units 3 and 2 and one on unit 1 (table 41).

Estimated ages for units 1 through 5 are based on one thermoluminescence analysis of a sample from unit 5, two U-series analyses of samples from the silica-carbonate soil formed on unit 3, and one thermoluminescence and one U-series analysis of samples from unit 2 (table 39). The thermoluminescence analysis, of a sample (TL–53, pl. 24; table 59) from unit 5, yielded an age of 2±0.5 ka; and the U-series analysis, of a sample (HD 1804) from the inner rind on a clast, yielded a maximum age of 64±2 ka. Another sample (HD 1805), from a silica-rich soil stringer, gave an age of 16.4±0.3 ka. Because sample HD 1804 was from the inner rind of a clast, we assume that its age is closer to the date of earliest soil formation on unit 3 than is that of sample HD 1805; therefore, we consider unit 3 to have been deposited before 62 ka. The two samples (TL–54, HD 1803) from unit 2 were from the silty-sand matrix and a silica-carbonate rhizolith, respectively. Sample TL–54 yielded ages of 88±74 and 92±62 ka, and sample HD 1803 an age of 90±74 ka. Despite the large error limits, we interpret these ages to indicate that unit 2 was deposited probably about 90 ka; the ages also imply that unit 3 was deposited about 90–62 ka.

The fault exposed in trenches RV4 and RV4A (fig. 51) is expressed as a zone of three to five fault strands that together range in width from about 1.7 m near the base of the trench to about 4.6 m near the top (pl. 24). Vertical-slip displacement along the fault appears to be slightly down to the north. All units are exposed on both sides of the fault zone (fig. 57). Although all units are cut by the fault strands, the cumulative vertical separation is less than 30 cm. The overall strike of the fault at the trench sites is N. 71° E., and various strands dip from about 45° to near vertical. The fault zone in both trenches has been disrupted by bioturbation, primarily from burrowing animals. In trench RV4A, the zone of disruption surrounding the fault is about 10 m wide. No striae were observed in either trench.

Southern Strand of the Southern Fault

Trench RV5 (fig. 51), which was excavated on the southern splay of the southern fault, exposes a sequence of alluvial sand and gravel, as well as eolian sand (pl. 25; table 40). Three major units are exposed: unit 1, which grades from sandy gravel to gravelly sand, is interpreted to be an alluvial-fan flood deposit; and units 2 and 3 consist of silty eolian sand. Exposed soils include an Av horizon on unit 3, a buried Bt horizon on unit 2, and a silica-carbonate soil ($CaCO_3$ stage II–IV morphology) on unit 1 (table 41).

Estimated ages for unit 1 are provided by two U-series analyses (pl. 25; table 39): (1) sample HD 1809, from a silica-rich rind on a clast in unit 1c, yielded ages of 324±275 ka and 321±44 ka; and (2) sample HD 1811, from a silica-rich platy horizon in unit 1e, yielded ages of 22.4±0.8 and 50.0±2.6 ka. Earlier studies of calcic-soil formation (for example, Machette, 1985) reported that such well-developed carbonate soils as that observed in trench RV5 (fig. 51) can take hundreds of thousands of years to develop. We interpret the 20–50-ka ages, therefore, to reflect a relatively late influx of silica and carbonate into the deposits, rather than an early influx closer in time to the age of the sediment. We consider the 320-ka age to be most representative of the oldest carbonate in the deposits, and so we date unit 1 at older than 320 ka.

In trench RV5 (fig. 51), the southern splay of the southern fault is expressed as a zone of four fault strands, most of which have shear fractures that are carbonate cemented and terminate at or near the top of unit 1e (figs. 53, 54). One shear zone appears to terminate at the base of unit 1e on the west wall but at the top of unit 1e on the east wall. Striae along one of the shears have a rake of 17° SW. Two of the fault strands have fissures filled with silty sand that are younger than the carbonate-cemented shear zones. The largest fissure, which ranges in width from about 5 cm near the base of the east wall to about 35 cm near the top (fig. 58), truncated and split a previously existing carbonate-cemented shear zone. Units 1 and 2 are cut and vertically offset, down to the north, by the fault strand with the widest fissure and carbonate-cemented shear zone. Cumulative vertical displacement measured at the top of unit 1 ranges from 12 to 22 cm. Unit 3 is cut by a fracture that extends upward from one of the fault strands exposed on the west wall (fig. 58). No shear offset is visible along this fracture, and so it may be pedogenic rather than tectonic.

A thermoluminescence analysis of a sample (TL–55, table 39; 10±1 ka) from unit 3, which is the fill in the widest fissure about 0.7 m below the ground surface, indicates that the fissure began filling about 10 ka and that unit 2 is older than 10 ka because blocks of unit 2 are mixed in with the unit 3 deposits (pl. 25). Another sample (TL–56), from a younger part of the fissure fill about 0.3 m below the ground surface, yielded an age of 6±1 ka. U-series ages on two samples (HD 1807, 72±10, 46±9, 12±4, 10±2 ka; HD 1810, 10±5, 9±3 ka) from silica-rich laminae along the edges of unit 1e that line the fissure indicate that the youngest silica-carbonate coating on the fissure is dated at about 9–11 ka, or about contemporaneous with the oldest fissure fill (unit 3). The older U-series ages on these samples may have resulted from obtaining the samples from coatings that existed in the carbonate-cemented shear zone before splitting by the fissure.

Table 41. Descriptions of soil profiles in trenches across the Rock Valley Fault system in the Yucca Mountain area, southwestern Nevada.

[See figures 1, 2, and 51 for locations. See table 3 for soil-horizon terminology. Colors from Munsell Soil Color Charts (Munsell Color Co., Inc., 1992). Texture: lm, loam; snd, sand. Structure—grade: 1, weak; 2, moderate; 3, strong; m, massive; sg, single grain—size: c, coarse; f, fine; m, medium; v, very fine—type: abk, angular blocky; pl, platy; sbk, subangular blocky. Consistence—dry: eh, extremely hard; h, hard; lo, loose; sh, slightly hard; so, soft; vh, very hard—wet: po, nonplastic; ps, slightly plastic; so, nonsticky; ss, slightly sticky. CO_3 stage morphology from Birkeland (1984). Effervescence (in cold dilute HCl): e, some; em, moderate; eo, none; es, strong; ev, very strong; vse, very slight. Cementation: ci, indurated; cs, strong; cw, weak. Lower horizon boundary—distinctness: a, abrupt; c, clear; g, gradual—topography: i, irregular; s, smooth; w, wavy. Roots—abundance: 1, few, 2, common—size: co, coarse; f, fine; m, medium; vf, very fine. Rhizoliths—abundance: 1, few. NA, not available; n.o., not observed]

Horizon	Depth (cm)	Associated unit	Color		Gravel content (wt pct)	Text	Structure	Consistence		CO_3 stage morphology	Effervescence	Cementation	Lower horizon boundary	Roots	Rhizoliths
			Wet	Dry				Dry	Wet						
Soil profile RV3–SPI															
Avk	0	5	10YR 4/4	10YR 6/3	3–5	sndlm	2 vco pl-sbk	sh	ss ps	n.a.	ev	n.o.	c s	1 vf-m thruout	n.o.
Bkw	16	5	10YR 3/4	10YR 6/3	5–10	sndlm	3 m-co sbk	sh-h	vss vps	I	ev	cs	a s	1-2 vf-m thruout	n.o.
2Btwk	48	4	7.5YR 3/4	7.5YR7/3	3–5	lmysnd	3 m-co pl	vh	so po	I	ev	cw	a w	1 f-m	n.o.
2Kqm	72	3	7.5YR 6/3	7.5YR8/1	10	lmysnd	3 vco-pl	eh	so po	IV	eh	ci	c i	1 vf	n.o.
2K	89	3	10YR 4/2	10YR7.5/1	50	lmysnd-snd	m-sg	lo	so po	II+–III	ev	cs	c s	1 vf	1
3Bk	175	2	10YR 3/1	10YR6/1	60	lmysnd-snd	sg	lo	so po	II	ev	n.o.	Bottom	n.o.	n.o.
Soil profile RV3–SPII															
Ak	0	5	10YR 4/3	10YR7/3	10	sndlm	1f-m sbk	so	ss-ps	I	ev	n.o.	a w	1vf-m	n.o.
2K	20	3	10YR 5/6	10YR7/2	50	snd	m	h	so po	III	ev	cs	a w	1 vf-f thruout	n.o.
B+K	121	2	10YR 4/2	10YR7.5/1	60–70	snd	sg	lo	so po	I–III	ev	n.o.	a s	1 vf-f	n.o.
3Kq	273	1	10YR 5/3.5	10YR7/2	70	lmsnd	m-sg	h	so po	III	ev	cs	Bottom	1 vf	n.o.
Soil profile RV4–SPI															
Avk	Top	– –	10YR 5/4	10YR 5/2	5	sndlm	2 vco-pl	sh	vssvps	– –	ev	n.o.	a w	1 vf thruout	n.o.
B	8	5	10YR 4/4	10YR 6/3	5–10	sndlm	2 m-co sbk	sh	vss vps	– –	eo	n.o.	a s	1 vf-co thruout	n.o.
2Bwbl	18	5	10YR 3	10YR 6/4	40–50	sndlm	3 co-abk	h	so po	– –	vse	n.o.	a s	1 m-co thruout	n.o.
2Kqmbl	34	4	10YR–7.5YR 6/4	10YR 8/0– 8/3	40–50	sndlm	3 vco-pl	eh	so po	IV	ev	cs-ci	a w	1 vf	n.o.
2Kbl	48	3	10YR 5/2	10YR 8/2	50	lmsnd	1–2 f-m sbk	lo so	so po	III	ev	cs	c w	1 m	1
2Bkbl	96	3	10YR	10YR	60	lmsnd	m-sg gr	lo	so po	I–II+	ev	cs	a s	1 f-m	1
3Bkbl	141	2	10YR 4/3	10YR 7/2	40–50	lmsnd	sg gr	lo	so po	I	ev	cs	a s	1 f snd lenses	1
4Bkb2	265	1	10YR 4/3	10YR 7/3	40–50	lmsnd	1 vf sbk	lo	so po	II–III–	ev	cs	Bottom	1 f	n.o.
Soil profile RV5–SPI															
Av	0	3	10YR 5/3	10YR 7/3	5	sndlm	3 vco pl	sh	vss vps	– –	sh	NA	a s	1 vf	n.o.
2Btbl	19	2	7.5YR 4/4	10YR 6/4	10	sndlm	2 m abk	sh-h	so po	– –	ev	NA	a w	1 f-m thruout	n.o.
3Kqmbl	37	1	10YR 7/2	10YR 8/2	30–40	lmsnd	3 vco pl	eh	so po	IV	ev	ci	c w	1 f	n.o.
3Kbl	64	1	10YR 7/2	10YR 8/2	20	lmsnd	m	eh	so po	III	ev	ci	c w	1 f	n.o.
3bk	102	1	10YR 4/3	10YR 7/2	40	lmsnd	m-sg	lo	so po	I–II	ev	cs	NA	None	1

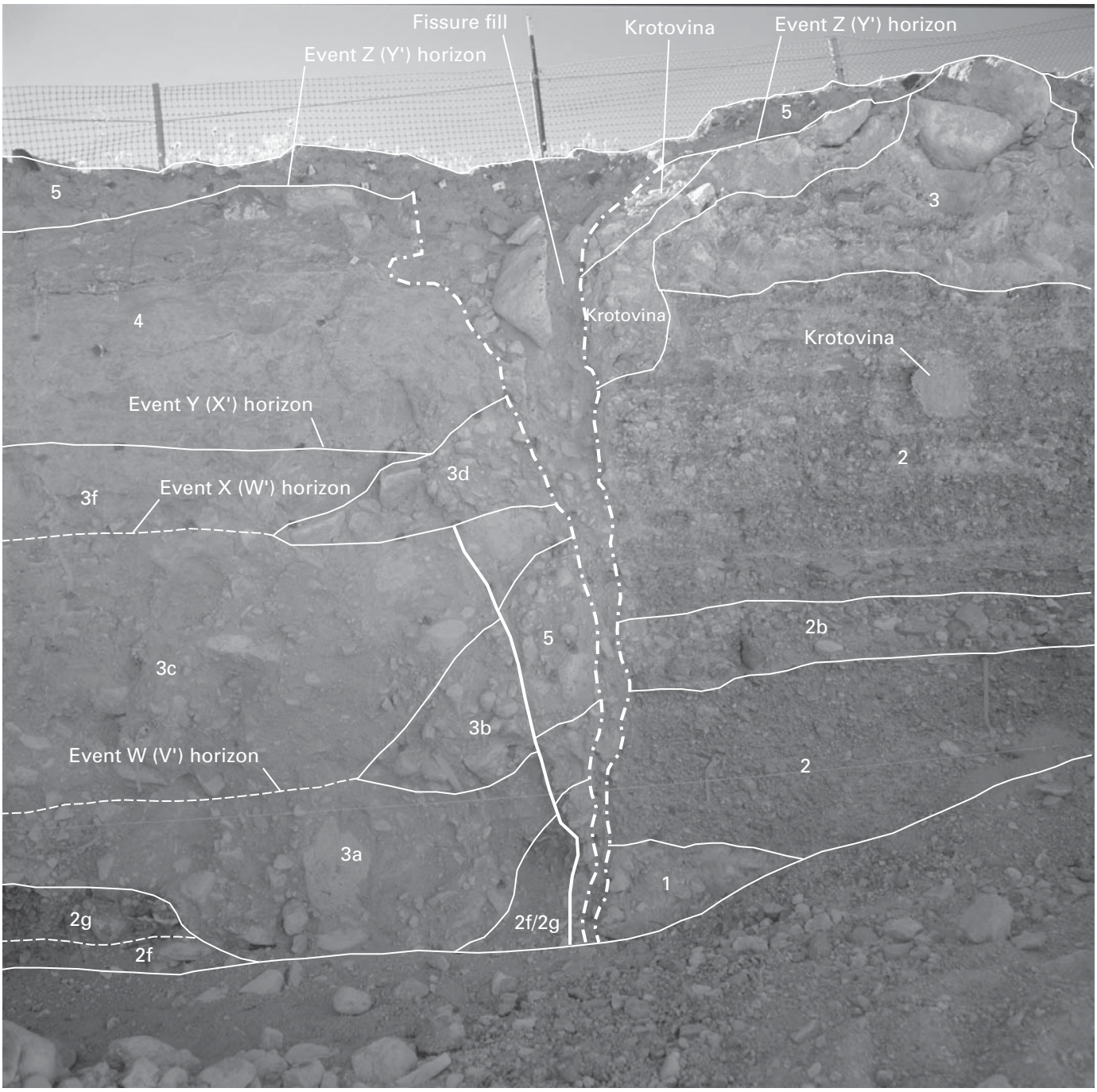

EXPLANATION

Fissure boundary

Fracture

Lithologic-unit boundary—Dashed where approximately located

2f **Lithologic unit**

Figure 55. Part of west wall of trench RV3 across northern fault of the Rock Valley Fault system in Rock Valley, southwestern Nevada (pl. 23; figs. 1, 2, 51). Faulting-event horizons are labeled according to both local- and fault-system-wide-event (in parentheses) schemes. No evidence for event Z′ was observed on northern fault strand. Trench wall is about 3 m high.

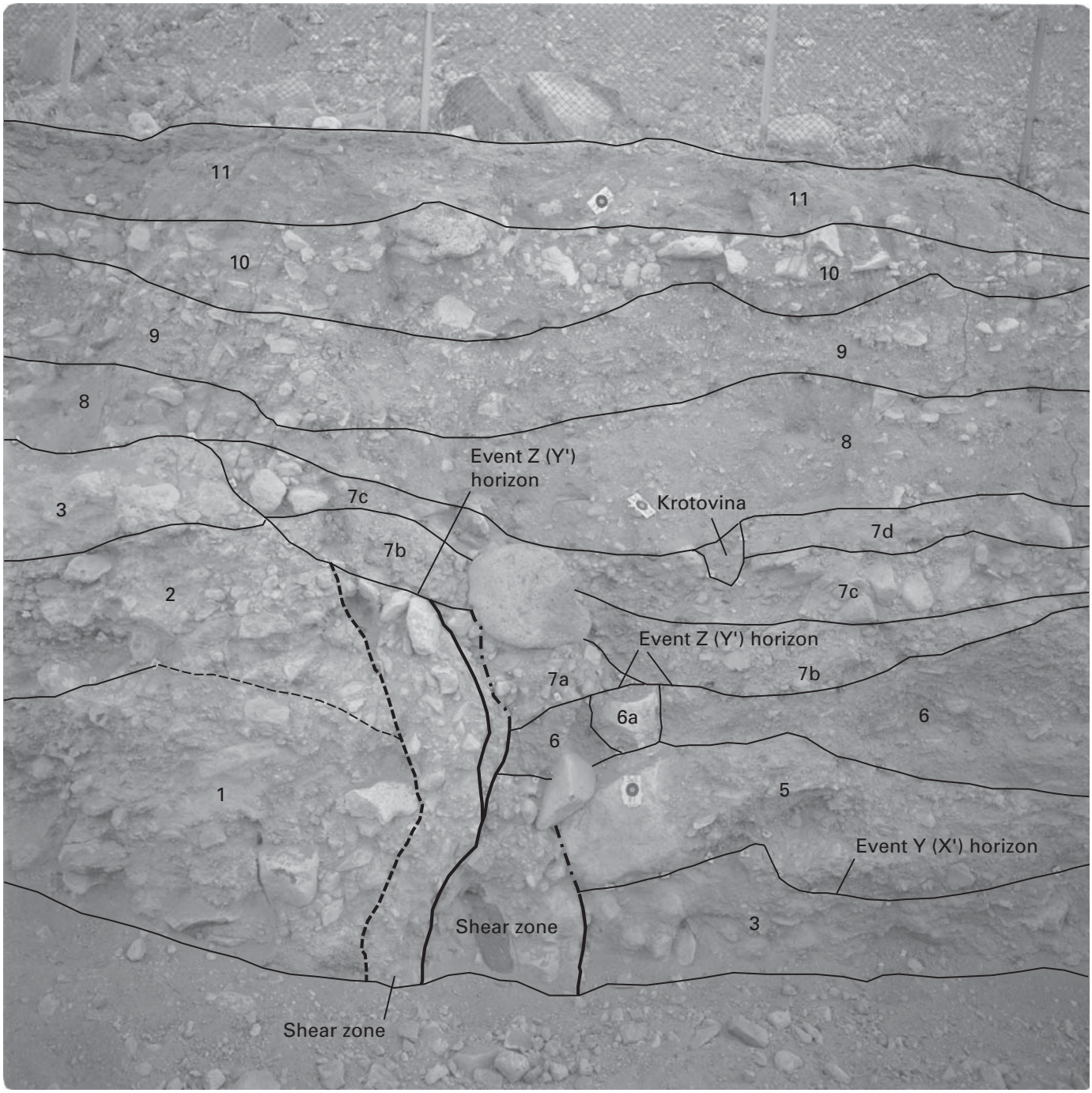

EXPLANATION

Free face

Fracture—Dashed where appoximately located

Lithologic-unit boundary—Dashed where approximately located

3 **Lithologic unit**

Figure 56. Part of east wall of trench RV3A across northern fault of the Rock Valley Fault system in Rock Valley, southwestern Nevada (pl. 23; figs. 1, 2, 51). Faulting-event horizons are labeled as in figure 58.

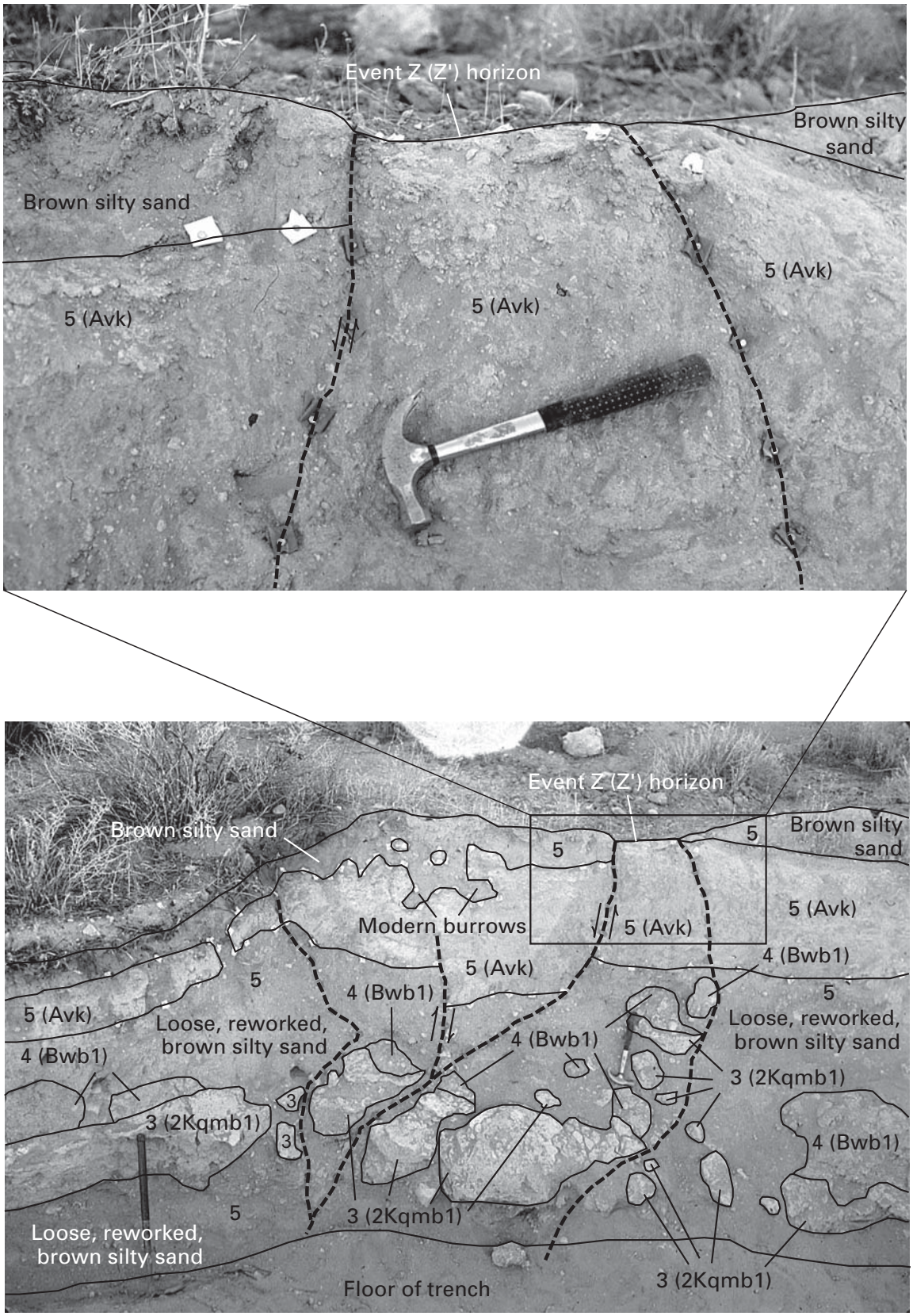

Figure 57. Central part of west wall of trench RV4A across northern strand of southern fault of the Rock Valley Fault system in Rock Valley, southwestern Nevada (pl. 24; figs. 1, 2, 51). Upper photograph shows detailed area outlined in lower photograph. Faulting-event horizons are labeled as in figure 58.

Frenchman Flat Fault

The trench in Frenchman Flat (fig. 51) exposes a sequence of sandy alluvial-fan gravel and eolian sand (pl. 26). Three major units were distinguished on the west wall of the trench: unit C, which consists of sandy gravel exposed on the lower part of the wall, is interpreted to be an alluvial-fan flood deposit; and units B and A, composed of silty sand, are interpreted to be primarily of eolian origin. Soils exposed in the trench include an Av horizon on unit A, a Bw horizon on unit B, and a moderately well cemented silica-carbonate horizon on unit C.

The Frenchman Flat Fault is expressed as a graben that downdrops units C and the Bw soil horizon of unit B; the overall sense of displacement is down to the north. The Bw soil horizon is visible in the graben but is covered by about 1 m of slopewash and eolian deposits mapped as a younger part of unit B with a less pronounced soil color. A thermoluminescence analysis of a sample (TL–73, table 39) from the Bw soil horizon exposed in the graben yielded an age for the part of unit B offset by the fault of about 27±2 ka. A thermoluminescence analysis of a sample (TL–72, table 39) from the sediment fill directly above the Bw soil horizon exposed in the graben yielded an age of 9±1 ka, indicating that the graben began filling at 10–8 ka.

Paleoseismic Interpretations

Chronology of Surface-Rupturing Paleoearthquakes

Evidence for paleoearthquakes, age constraints, and displacement data for each fault (or fault splay) are summarized in table 42. Paleoearthquakes are labeled in two ways: (1) a local-event-labeling scheme (events Z, Y, X, and so on, from youngest to oldest) that is unique to each fault or fault splay, and (2) an interpretative, fault-system-wide-event-labeling scheme using a prime (′). For example, five faulting events (Z–V) were identified in trenches on the northern fault, with event Z dated at about 13±4 ka. On a fault-system-wide basis, however, evidence was observed for one faulting event on the southern fault dated at about 2±0.5 ka, or about 10 k.y. later. Thus, event Z on the northern fault would have an interpretative label of Y′, identifying it as the penultimate faulting event in the paleoseismic record for the total Rock Valley Fault system. According to this interpretative scheme, event Y on the northern fault is labeled X′, event X is labeled W′, event W is labeled V′, and event V is labeled U′. In the following paragraphs, we discuss the temporal correlation of paleoearthquakes on a fault-system-wide basis. Evidence, age control, and our attempt at fault-system-wide-event correlation are considered to be most reliable for the most recent (Z′) and penultimate (Y′) faulting events. Where evidence for local events was documented at the same soil horizon (for example, B) on multiple faults, these events were grouped together as a single fault-system-wide event if age control was adequate for this purpose. Because this technique is generalizing, the fault-system-wide events described below are considered to be the minimum number within the entire Rock Valley Fault system.

Event Z′

Evidence for event Z′ was observed on the northern splay of the southern fault where the A soil horizon was vertically offset (table 42). Possible evidence for the event was observed on the medial fault and the southern splay of the southern fault where the A soil horizons were fractured but not vertically offset. A thermoluminescence analysis of a sample (TL–53, table 39) from the A soil horizon in trench RV4 (fig. 51) on the northern splay of the southern fault is interpreted to date event Z′ at later than 2±0.5 ka. In trenches on the medial fault and on the southern splay of the southern fault, the event is constrained to be younger than 7±1 ka (sample TL–75, trench RV2) and 6±1 ka (sample TL–56, trench RV5), respectively. Although the age constraints for each fault do not precisely correspond, we interpret the evidence to indicate that only one faulting event is represented because its stratigraphic position is the same in all the trenches—that is, at the top of the A soil horizon (see figs. 55, 57, 58). Total net displacement from event Z′ was probably less than 10 cm on both splays of the southern fault. If the event occurred on the medial fault, displacement was probably similar to that on the southern fault.

Event Y′

Evidence for event Y′ was observed in all the trenches (table 42). The event horizon was within or at the top of the B (Bk to Bt) soil horizon (pls. 24, 26; figs. 55, 58), except in trench RV3A, which was excavated in Holocene channel deposits (fig. 56). In general, thermoluminescence and U-series ages indicate that event Y′ probably occurred sometime between 72 and 7 ka. The timing is best constrained on the northern fault in trenches RV3 and RV3A (pl. 23), where the ages indicate that the event occurred about 13±4 ka. The length of the surface rupture associated with event Y′ was at least 23 km—the distance from the trench in Frenchman Flat trench to trench RV3 at the southwest end of the northern fault in central Rock Valley. Displacement along the northern fault was left lateral, down to the south; displacement along the southern and medial faults was left lateral, down to the north; and displacement along the Frenchman Flat Fault was down to the south, with an unknown strike-slip component. Total net displacements ranged from less than 10 cm on the northern splay of the southern fault to 267 cm on the northern fault.

Event X′

Evidence for event X′ was also observed in trenches on all faults (table 42). The event horizon is at or near the top

of the silica-carbonate soil horizon (pls. 24, 25; fig. 55). Its date is most tightly constrained in trench RV4 to 64–16 ka (samples HD 1804, HD 1805, table 39) on the northern splay of the southern fault, with a median value of 40±24 ka. Vertical displacement on the northern fault was down to the south, whereas along the medial and southern faults it was down to the north. Displacements for event X′ ranged from less than 10 cm on the northern splay of the southern fault to less than 362 cm on the northern fault.

Events W′ and V′

Evidence for events V′ and W′ was observed only in trench RV3 (fig. 57) on the northern fault (fig. 55; table 42). Both events are documented by colluvial wedges within unit 3. In a gross sense, U-series ages constrain the dates of both events at about 300–80 ka. However, because the best estimated age for the lower part of unit 2 (unit 2a) is 200 ±100 ka, we date the deposition of unit 3 at about 200–80

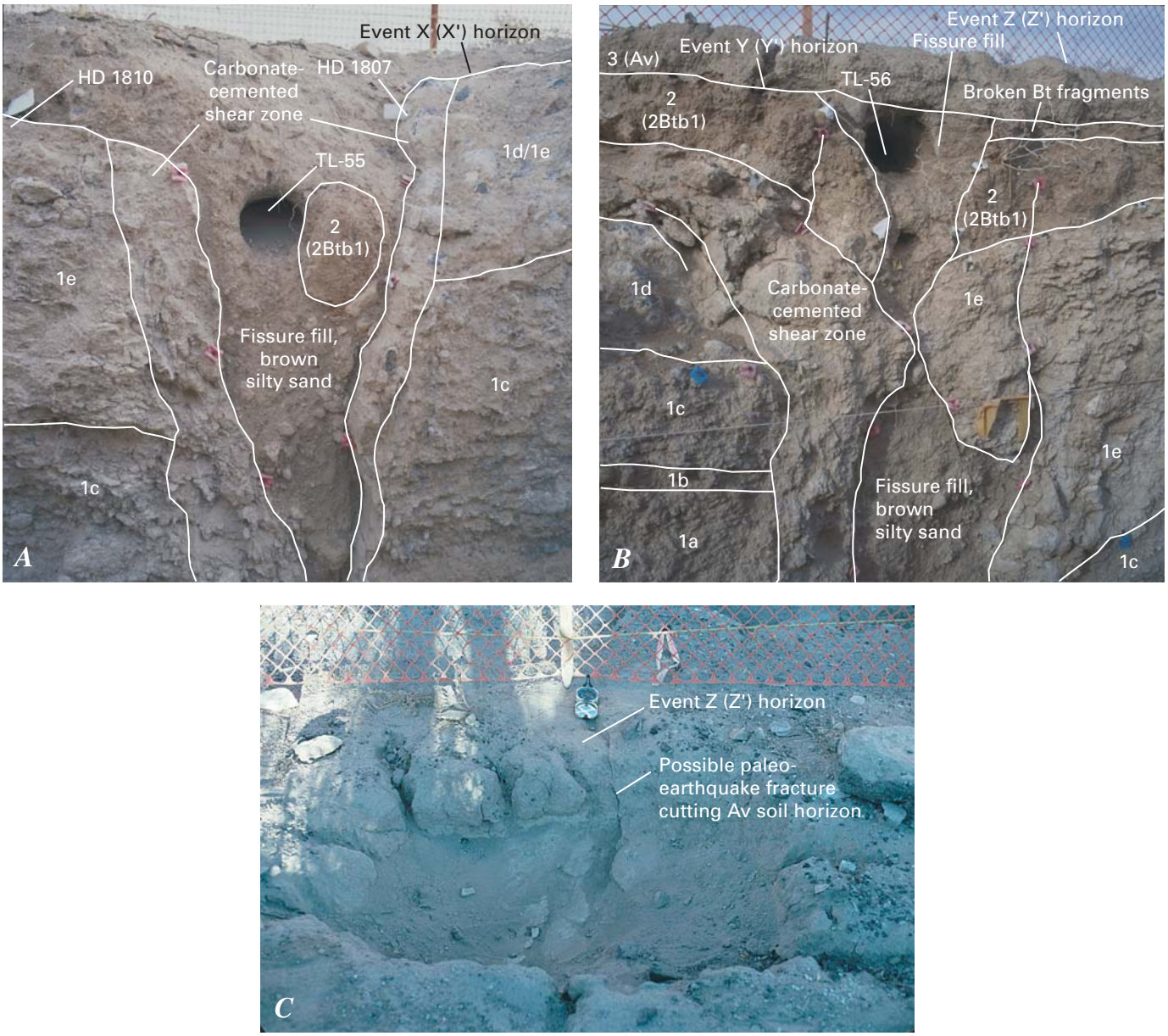

Figure 58. Parts of east and west walls of trench RV5 across southern strand of southern fault of the Rock Valley Fault system in Rock Valley, southwestern Nevada (pl. 25; figs. 1, 2, 51). *A*, Fault exposed in east wall. *B*, Fault exposed in west wall; Av soil horizon was stripped off during excavation. *C*, Possible paleoearthquake fracture extending to ground surface immediately west of west wall. Note compass for scale.

Table 42. Summary of faulting events on the Rock Valley Fault system in the Yucca Mountain area, southwestern Nevada.

[See figures 1, 2, and 51 for locations, and table 39 for estimated ages of samples. Fault displacements and event dates are best estimates. NA, not available]

Local event/ system-wide event	Likelihood of occurrence based on available evidence	Event horizon	Evidence	Vertical displacement	Net vertical displacement	Total net displacement	Estimated age
Northern fault of the Rock Valley Fault system—trenches RV3, RV3CT, and RV3A							
Z/Y'	Definite	Within Bkw soil horizon in trench RV3; at top of unit 6 in trench RV3A.	Fissure fill that terminates near base of A soil horizon in trenches RV3 and RV3CT; fractures that terminate at the base of unit 7b in trench RV3A; presence of a fining-upward sequence of colluvial-wedge deposits (units 7a–7d) in trench RV3A.	51 cm; (average of 63 cm measured as maximum height of unit 7 in trench RV3A, 84 cm measured at base of unit 5 in trench RV3CT, and 7 cm measured at base of unit 5 in trench RV3).	<51 cm, assuming minor back-rotation of downthrown block.	<267, cm calculated by using net vertical displacement and 11° rake. Cumulative net displacement for events Z–pre-W cannot exceed 14.3 m; therefore, 267 cm is considered a maximum.	13±4 ka; older than 11±2 ka (sample TL–58 from unit 8 in trench RV3A); probably younger than 12±5 ka (sample TL–57 from unit Bkw in trench RV3).
Y/X'	Moderate to high	Base of unit 4 in trenches RV3 and RV3CT and base of unit 5 in trench RV3A.	Wedge deposits. Unit 5 in trench RV3A and lower part of unit 4 in trench RV3.	69 cm; average of maximum thicknesses of 53 cm for unit 5 in trench RV3A, 109 cm for unit 4 in trench RV3, and 46 cm for unit 4 in trench RV3CT).	<69 cm, assuming minor back-rotation of downthrown block.	<362 cm, calculated by using estimated net vertical displacement and rake of 11°. Cumulative net displacement for events Z–pre-W cannot exceed 14.3 m; therefore, 362 cm is considered a maximum.	12–80 ka; older than 12±5 ka (sample TL–57); probably younger than approximately 80 ka (sample HD 1812).
X/W'	Moderate to high	Base of unit 3d in trenches RV3 and RV3CT.	Poorly defined wedge deposit (unit 3d) in trenches RV3 and RV3CT; subunits of unit 3 present on downthrown fault block, absent on upthrown block; displacement of unit 3b.	39 cm (maximum thickness of unit 3d in trench RV3).	<39 cm, assuming minor back-rotation of downthrown block.	<204 cm, calculated by using estimated average vertical tectonic displacement and rake of 11°. Cumulative net displacement for events Z–pre-W cannot exceed 14.3 m; therefore, 204 cm is considered a maximum.	About 120 ka; 80 to 300 ka, based solely on samples HD 1812 and HD 1954.
W/V'	Moderate to high	Base of unit 3b in trench RV3.	Poorly defined wedge deposit (unit 3b) in trench RV3.	63 cm (maximum thickness of unit 3b).	<63 cm, assuming minor back-rotation of downthrown block.	<330 cm, calculated by using estimated average vertical tectonic displacement and rake of 11°. Cumulative net displacement for events Z–pre-W cannot exceed 14.3 m; therefore, 330 cm is considered a maximum.	About 160 ka; 80 to 300 ka, based solely on samples HD 1812 and HD 1954.
Pre-W/ pre-V'	Low to moderate	Faulting events predating event V possibly occurred during deposition of unit 2a and before deposition of unit 3b in trench RV3, but little direct evidence exists on which to base reliable interpretations.	NA	NA	NA	NA	Older than 102–300 ka (samples HD 1955, HD 1954).
Medial fault of the Rock Valley Fault system—trenches RV1 and RV2 (Yount and others, 1987)							
Z/Z'	Poor to moderate	Top of Av soil horizon.	Possible fractures that cut Av soil horizon	If it occurred, probably 0–10 cm.	If it occurred, probably less than 10 cm.	If it occurred, probably less than 30 cm.	Younger than 7±1 ka (sample TL–75).
Y/Y'	Definite	Top of B soil horizon (unit C).	Multiple shear zones that terminate at top of B soil horizon. Vertical offset of B soil horizon.	<5–32 cm ----------	<32 cm, assuming minor back-rotation of downthrown block.	>32 cm, assuming oblique slip.	Older than 7±1 ka (sample TL–75); younger than 47±4 ka (sample TL–74).

Table 42. Summary of faulting events on the Rock Valley Fault system in the Yucca Mountain area, southwestern Nevada.—Continued

Local event/ system-wide event	Likelihood of occurrence based on available evidence	Event horizon	Evidence	Vertical displacement	Net vertical displacement	Total net displacement	Estimated age
Medial fault of the Rock Valley Fault system—trenches RV1 and RV2 (Yount and others, 1987)							
Pre-Y/Y'	Definite	Between the base of unit C and the top of unit E.	Differential offset of units C and E.	225–290 cm----------	<290 cm, assuming minor back-rotation of downthrown block.	>290 cm, assuming oblique slip.	Younger than 180 ka (Yount and others, 1987).
Northern strand of the Southern Rock Valley Fault system—trenches RV4 and RV4A							
Z/Z'	Definite	Top of Av soil horizon	Av soil horizon displaced; multiple fractures cutting Av soil horizon; wide disrupted zone in trench RV4A.	0–10 cm ----------	0–10 cm, measured at top of Av soil horizon.	Unknown, but probably at least 10 cm, assuming oblique slip.	Younger than 2.0±0.5 ka (sample TL–53).
Y/Y'	Moderate	Top of BW soil horizon (top of unit 4).	Silt fill in fault zone in trenches RV4 and RV4A is cut by fractures created by event Z; few poorly defined fractures appear to terminate within or at base of platy K soil horizon, which may be evidence for either this event or for next earlier event (X), or which may reflect both of these events.	0–10 cm ----------	0–10 cm	Unknown, but probably at least 10 cm, assuming oblique slip.	Older than 2±0.5 ka (sample TL–53); younger than 64±2 ka (sample HD 1804).
X/X'	Moderate	Top of unit 3	A few poorly defined fractures appear to terminate within or at base of platy K soil horizon, possibly reflecting either event Y or event X, or both; there is differential displacement of units 1–3 relative to unit 4.	0–10 cm ----------	0–10 cm	Unknown, but probably at least 10 cm, assuming oblique slip.	Older than 16.4±0.3 ka (sample HD 1805); younger than 64±2 ka (sample HD 1804).
Southern strand of the southern fault of the Rock Valley Fault system—trench RV5							
Z/Z'	Poor to moderate	Top of Av soil horizon.	Extension fractures cut Av soil horizon in trench RV 5 and in a shallow pit west of trench.	– –	– –	– –	Younger than 6±1 ka (sample TL–56).
Y/Y'	Definite	Top of Bt soil horizon (unit 2).	Silt-filled fissure containing pods of Bt soil-horizon material.	0–10 cm ----------	0–10 cm --------	0–34 cm, (computed using a 17° rake).	Older than 10±1 ka (sample TL–55); younger than 72±10 ka (sample HD 1807).
X/X'	High	Top of K soil horizon (unit 1).	Multiple fractures, which are differentiated from those of event Y by being engulfed by carbonate, terminate at or near top of K horizon; event probably occurred during carbonate soil formation.	2–22 cm ----------	2–22 cm --------	7–75 cm, (computed using a 17° rake).	Older than 10±5 ka (HD 1810); younger than 72±10 ka (sample HD 1807).
Trench in Frenchman Flat							
Z/Y'	Definite	Within B soil horizon (unit B).	Two shear zones that offset oldest part (Bw soil) of B soil horizon and form a graben.	As measured on west wall at base of unit B, 1.40 m down-to-the-north at the southern shear zone, 0.46 m down-to-the-south at the northern shear zone.	100±25 cm	>1.0±0.25 m, assuming oblique slip.	8–29 ka; older than 9±1 ka (sample TL–72); younger than 27±2 ka (sample TL–73).

ka. Therefore, for the purpose of determining recurrence intervals (see next section), we evenly distribute the faulting events within this time interval and estimate that event V′ occurred about 160 ka and event W′ about 120 ka. Total net displacement for event V′ was less than 330 cm down to the south, and slip for event W′ was less than 204 cm down to the south.

Slip Rates and Recurrence Intervals

Northern Fault

The total net cumulative displacement of unit 2a in trench RV3 (fig. 55) is about 14.3±2.8 m (pl. 23). Our best estimated age for unit 2a is 200±100 ka. Given these constraints and following the methods of McCalpin (1996, p. 457), we calculate the slip rate for the northern fault at 0.072±0.038 mm/yr.

At least four faulting events occurred between about 160 and 9 ka on the northern fault. Using the best estimated dates for these events (see preceding section), the best estimated recurrence intervals are about 27 k.y. (events Y′–X′), 80 k.y. (events X′–W′), and 40 k.y. (events W′–V′).

Medial Fault

The cumulative vertical offset of stratigraphic units reported by Yount and others (1987) on the medial fault in trench RV2 (fig. 51) is 2.57 to 2.95 m. Calculations using these values and a 22° rake from slickensides exposed in bedrock east of the trench indicate a net displacement ranging from 6.86 to 7.87 m. Yount and others (1987) reported U-trend ages of 180±40, 270±30, and 390±100 ka on three samples from one of the oldest displaced trench units that probably correlates with unit Qa2 and (or) unit Qa3 of the standard Yucca Mountain stratigraphic sequence (col. 1, table 2) and with unit Q2c of Swadley and others (1984) (col. 2, table 2). The U-trend ages, though considered to be generally unreliable (as discussed in chap. 2), fall in the middle to late Pleistocene, which is the time interval assigned to units Qa2–Qa3 and Q2c. The reported displacements and estimated age limits can therefore be expressed as 7.36±0.50 m and 315±140 ka, respectively, for calculating the slip rate according to the methods of McCalpin (1996), resulting in a slip rate of 0.023±0.010 mm/yr for the medial fault.

The best estimated dates for faulting events exposed in trenches on the medial fault are 13±4 ka for event Y′ and later than 180 ka for an earlier event(s), resulting in a single recurrence interval of about 170 k.y. Because the pre-event Y′ horizon is at the top of the K soil horizon, however, that event probably represents event X′, and so the recurrence interval between events Y′ and X′ on the medial fault is considered to be the same (27 k.y.) as that calculated for the other major faults in the Rock Valley Fault system.

Northern Strand of the Southern Fault

The cumulative vertical displacement of unit 2 in trench RV4 (fig. 51) is about 10±5 cm, but the net cumulative displacement could not be determined because no slip-direction indicators were observed in the trench. However, if we assume that the fault has oblique-slip movement—which is likely, considering the surface expression of the fault and the focal mechanisms of recent earthquakes in Rock Valley, as well as the 17° rake of slickensides observed in trench RV5 on the southern splay of the southern fault—then the minimum net cumulative displacement may be about 10±5 cm. The age of unit 2 was estimated at 88±74 ka by thermoluminescence analysis. Given these constraints and following the methods of McCalpin (1996), we calculate a minimum slip rate of 0.001±0.001 mm/yr.

Three faulting events have occurred on the northern splay of the southern fault in the past 40 k.y. Using the best estimated dates for these events, the recurrence intervals are about 9–10 k.y. (events Z′–Y′) and 27 k.y. (events Y′–X′).

Southern Strand of the Southern Fault

The cumulative vertical displacement of the top of unit 1 in trench RV5 is 12 to 22 cm down to the north (pl. 25). Using a displacement of 17±5 cm and a rake of 17° yields a cumulative net displacement of 58±17 cm. Unit 1 in trench RV5 is older than 320 ka. Given these constraints, the maximum slip rate for the southern splay of the southern fault is 0.002±0.0005 mm/yr.

Three faulting events have occurred on the southern splay of the southern fault in the past 40 k.y. Using the best estimated dates for these events, the recurrence intervals are about 9–10 k.y. (events Z′–Y′) and 27 k.y. (events Y′–X′).

Frenchman Flat Fault

The cumulative vertical displacement of the lower part of unit B (27±2 ka; sample TL–73, pl. 26; table 39) in the Frenchman Flat trench is about 1.0±0.25 m. No slickenlines were observed, and so the net cumulative displacement of unit B could not be determined; however, oblique-slip movement seems likely for the reasons already stated for other faults, and so 1.0±0.25 m should be considered the minimum net cumulative displacement. Because we observed evidence for only one surface-rupturing paleoearthquake (event Y′) in the trench, slip rates and recurrence intervals for the Frenchman Flat Fault could not be estimated.

Fault-System-Wide

The slip rate for the entire Rock Valley Fault system is estimated at 0.1 mm/yr by summing the estimated slip rates on the individual faults. The recurrence intervals for faulting events along one or more of these faults are about 9–10 k.y. (events Z′–Y′), 27 k.y. (events Y′–X′), 80 k.y. (events X′–W′), and 40 k.y. (events W′–V′).

Discussion

Low-angle striae and cumulative displacements of units in trenches indicate that Quaternary fault activity in central Rock Valley is predominantly transtensional—that is, the valley between the northern and southern faults, and particularly between the northern and medial faults, has been subsiding, and all the faults have a strong left-lateral-slip component. The striae range in rake from 11° to 22°, with a northeastward plunge on the down-to-the-south northern fault and a southwestward plunge on the down-to-the-north medial and southern faults. Fault-plane solutions from recent small earthquakes also indicate low-angle, left-lateral slip along near-vertical fault planes within the fault system.

The Quaternary slip rate of 0.1 mm/yr for the entire Rock Valley Fault system is close to the long-term (past 30 m.y.) slip rate of 0.089 mm/yr calculated by O'Leary (2000). This similarity indicates that slip along the fault system has remained relatively constant since middle Oligocene time.

At least two faulting events (X′, Y′) caused surface ruptures along two or more faults. Event X′ (40±24 ka) caused surface ruptures along the northern and southern faults, and, possibly, along the medial fault. Event Y′ (13±4 ka) caused surface displacement along all the faults in central Rock Valley, as well as along the Frenchman Flat Fault, indicating surface rupture over a distance of at least 23 km. The effect of event Y′ in western Rock Valley and Amargosa Valley is unknown. However, a recent study of scarps in Amargosa Valley along the possible southwestward extension of the Rock Valley Fault system indicates that the most recent faulting event was late Pleistocene (128–10 ka; Anderson and others, 1995). Therefore, event Y′ may have caused a surface rupture that extended from Frenchman Flat to Amargosa Valley (a distance of ~65 km).

Because of their close spacing (generally <2 km) and moderate to high degree of interconnectedness at the surface, individual faults within the Rock Valley Fault system probably would not extend as independent structures to seismogenic depths (typically ~15 km in the Great Basin). Therefore, we suspect that at least some (possibly most) of these faults merge at depth, and so an earthquake of a particular magnitude could cause surface ruptures along multiple faults in Rock Valley, as was especially evident during event Y′ in the past.

Acknowledgments

We thank Alan Ramelli, Jan Zigler, Michelle Murray, and Chris de Fontaine for their efforts in logging, describing, and interpreting the trenches. We also thank Jeff McCleary and Susan Olig for their field reviews of the logging and paleoseismic interpretations. We are grateful to Chris Menges for helping locate trenches RV3, RV4, and RV5 and for many helpful discussions and suggestions related to the calculation of moment magnitudes.

Chapter 14

Summary of the Temporal and Spatial Relations of Quaternary Faulting During the Past 100 k.y. at Yucca Mountain: Evidence for Distributive Surface Ruptures on Multiple Faults

By William R. Keefer and Christopher M. Menges

Contents

Abstract....197
Introduction....197
Temporal and Spatial Distribution of Quaternary Faulting Events....198
Conclusions....200

Abstract

We have used the estimated ages of displacements on eight Quaternary faults at Yucca Mountain to correlate the timing of surface ruptures on the various faults and to examine the evidence for distributive surface ruptures on multiple faults within the past 100 k.y. Trenching showed that fissures along three different faults on the west side of Yucca Mountain contain basaltic ash correlated with the eruption of the nearby Lathrop Wells volcanic center at 77±6 ka; thus, coeval surface ruptures on these faults were probably contemporaneous with that eruption. Though less certain, age data indicate additional cases where two or more faults may have been active simultaneously, including one faulting event with a narrowly defined date near 3 ka and three other faulting events at about 50, 30–20, and 13 ka, in all of which distributive surface ruptures may have occurred on multiple faults that are close to one another and, possibly, linked at depth.

Introduction

The purpose of this chapter is to evaluate paleoseismic data from all of the main trench sites at Yucca Mountain (fig. 2) for evidence of distributive surface ruptures on the major Quaternary faults. In particular, we address the following questions: (1) did distributive surface ruptures occur simultaneously on multiple faults, and (2) if so, what are the spatial relations of the affected faults? Our answers are based on a summary of the data on faulting events within only the past 100 k.y., as presented in the preceding chapters, because the age constraints on earlier faulting events are generally too broad or poorly defined for adequate temporal correlations. The Bare Mountain and Rock Valley Faults, which are outside the immediate area of Yucca Mountain, are not included in this summary.

The timing of an individual faulting event commonly is based on age determinations for the youngest deposit or soil horizon displaced by the event, relative to the maximum age of the oldest overlying deposit that postdates the event. Thus, resolution of the estimated date for the event itself critically depends on the time interval spanned by dated units that stratigraphically bracket the event horizon. This interval may vary widely; for example, in many places the youngest faulted and oldest unfaulted deposits or soils simply underlie and overlie an event horizon within the overall stratigraphic sequence exposed in a given trench. In other places, however, more precise age constraints on the event may be provided by a datable deposit or feature directly associated with the event itself (for example, fissure fills, scarp-derived colluvial wedges, and fracture or fault coatings terminated at the event horizon). Another source of uncertainty in time intervals is the reported analytical errors for each age determination itself.

The estimated dates for individual faulting events within the past 100 k.y. identified in the various trenches (fig. 2) excavated across each of the eight Quaternary faults at Yucca Mountain are plotted in figure 59 and listed in table 43. Many of these dates range widely (some as much as 50 k.y. or more) because of the inherent uncertainties in age assignments; thus, determining a date within narrow limits is generally

impossible for many paleoearthquakes. To reduce the uncertainty, many investigators selected either a preferred date or a more restricted interval within the estimated age range, on the basis of expert judgment that considered the stratigraphic position of an event horizon relative to dated units or assessments of the relative strengths and weaknesses of the available age control (table 43). Preferred estimated ages, where available, are plotted in figure 59 as heavier dots or lines within the estimated dates.

Temporal and Spatial Distribution of Quaternary Faulting Events

The available age data (table 43) indicate several possible distributive surface ruptures on two or more faults (fig. 59). The strongest case for coeval displacements on multiple faults is informally termed the "ash event." This event has been identified in trenches on three faults on the west side of

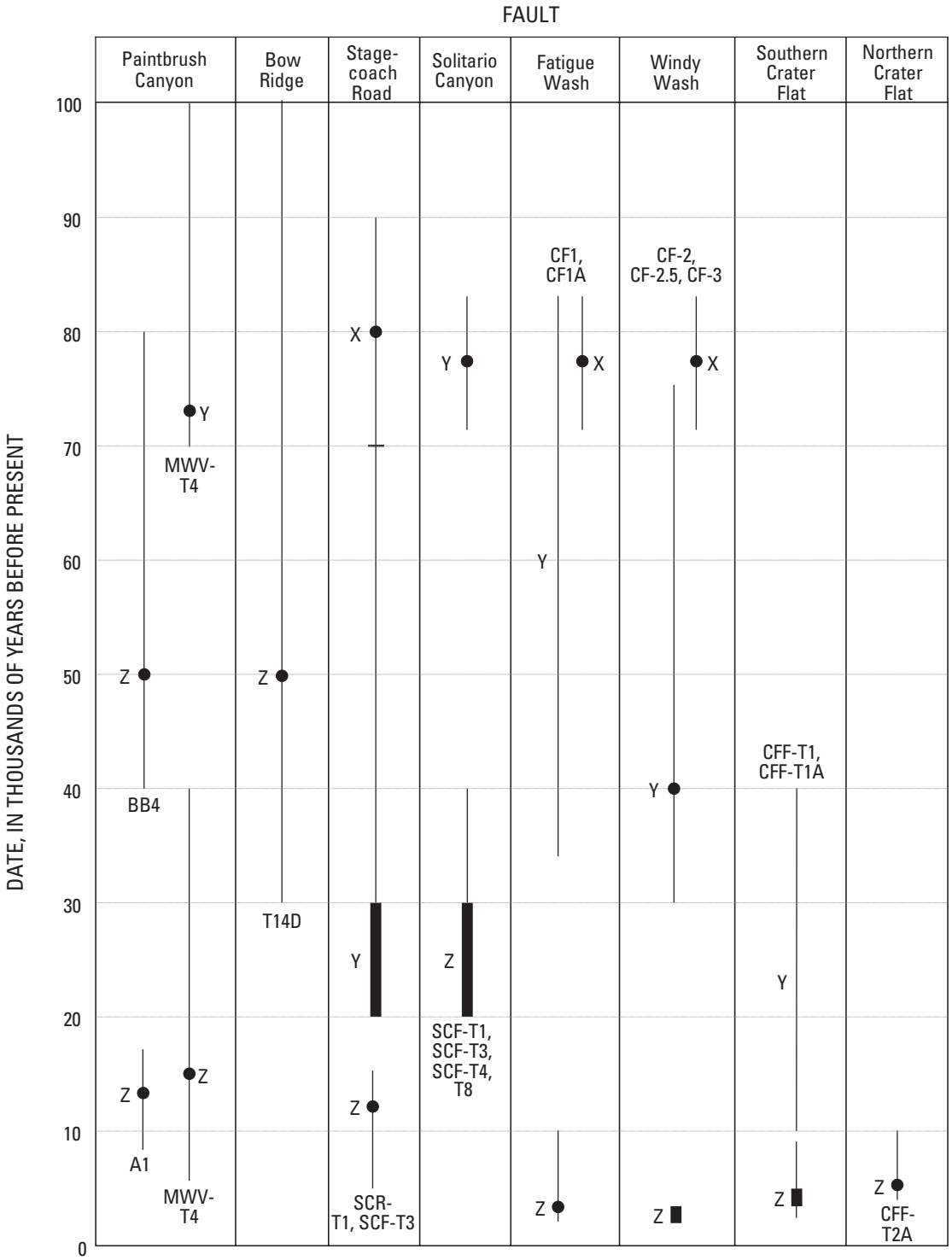

Figure 59. Ranges in estimated dates of Quaternary faulting events identified in trenches excavated in the Yucca Mountain area, southwestern Nevada (figs. 1, 2; table 43). Dots, preferred date (if one was selected); bold lines, preferred-date range. Letters X–Z refer to event-labeling scheme used in designated trench(es) (letter-number combinations).

Table 43. Estimated dates of faulting events during the past 100 k.y. in the Yucca Mountain area, southwestern Nevada

[See figures 1 and 2 for locations. Data from chapters 5 through 11. Faulting events are labeled according to scheme used in designated trench(es)]

Fault (fig. 2)	Trench (fig. 2)	Event	Date (ka)		
			Min	Pref	Max
Paintbrush Canyon------	A1	Z	9	13	17
	BB 4	Z	40	50	80
		Y	80	– –	150
	MWV–T4	Z	6	15	40
		Y	70	73	100
Bow Ridge----------	T14D	Z	30	50	130
Stagecoach Road--------	SCR–T1, SCR–T3	Z	5	12	15
		Y	20	30–20	70
		X	70	80	90
Solitario Canyon --------	SCF–T1, SCF–T3, SCF–T4, T8	Z	20	30–20	40
		Y	71	77	83
Fatigue Wash----------	CF1, CF1A	Z	2	3	10
		Y	34	– –	83
		X	71	77	83
Windy Wash----------	CF2, CF2.5, CF3	Z	2	3–2	3
		Y	30	40	75
		X	71	77	83
Southern Crater Flat ----	CFF–T1, CFF–T1A	Z	2	4–3	9
		Y	10	– –	40
Northern Crater Flat ----	CFF–T2A	Z	4	5	10

Yucca Mountain—event Y on the Solitario Canyon Fault, and event X on the Fatigue Wash and Windy Wash Faults (figs. 1, 2, 59)—on the basis of conspicuous fissures that contain geochemically correlated basaltic ash from an eruption of the nearby Lathrop Wells volcanic center (fig. 1) at 77±6 ka (Heizler and others, 1999). A reasonable interpretation is that the fissures formed simultaneously on these three faults during a single event temporally associated with that eruption (see chaps. 7–9). The affected faults lie within a 3- to 7-km-wide zone of interconnected and splayed faults aligned southward toward the Lathrop Wells basaltic cone (see chap. 3; figs. 1, 2).

The other five Quaternary faults at Yucca Mountain show no clear evidence of being affected by the ash event. Basaltic ash from the Lathrop Wells eruption is present in a fracture at the top of trench 14 on the Bow Ridge Fault. However, this fracture does not represent a specific faulting event, and similar ash is absent within the deposits recording the main rupture sequence exposed in trench T14D (fig. 2). The estimated date for event Y in trench MWV–T4 on the Paintbrush Canyon Fault is compatible with the date of the Lathrop Wells eruption; however, no basaltic ash was identified at that trench site. A basaltic ash was identified only in the lower part of trench A1 on the northern section of the Paintbrush Canyon Fault, but this ash differs geochemically from the Lathrop Wells ash and is correlated more closely with an older basaltic eruption at the Sleeping Butte cone, which lies 40 km to the northwest (see chap. 5). Although basaltic ash correlated with the Lathrop Wells eruption was identified in Quaternary deposits at the Busted Butte wall 4 locality on the Paintbrush Canyon Fault, in trenches SCR–T1 and SCR–T3 on the Stagecoach Road Fault, and in trenches CFF–T1 and SCF–T1A on the Southern Crater Flat Fault, in none of these sites was the presence of the ash identified with a dated faulting event. No basaltic ash was recognized within trench CFF–T2A on the Northern Crater Flat Fault. In summary, basaltic ash from the Lathrop Wells eruption either was not identified or was dispersed in deposits between event horizons on the Paintbrush Canyon, Stagecoach Road, and, probably, Bow Ridge, Southern Crater Flat, and Northern Crater Flat Faults.

A second probable distributive surface rupture, with an estimated date within a narrow time interval, is represented by event Z on the Fatigue Wash, Windy Wash, and Southern Crater Flat Faults (fig. 2). The preferred dates of this event on these three faults of 3, 3–2, and 4–3 ka, respectively (fig. 59; table 43), provide the only evidence for Holocene faulting activity observed at any of the trench sites in the Yucca Mountain area. The surface traces of the three faults lie close to one another, and they may be interconnected in a complex splay

pattern (fig. 4). During the Holocene faulting event (~3 ka), measurable displacements ranging from 10 to 20 cm occurred on the Windy Wash and Southern Crater Flat Faults; the event on the Fatigue Wash Fault is represented only by fracturing with no detected offset. In trenches on all three faults, however, the vesicular A (Av) soil horizon was affected. Concurrent movement may also have occurred on the nearby Northern Crater Flat Fault, but a closely constrained minimum date for event Z on that fault is 4 ka, as discussed in chapter 11.

Comparison of the dates of faulting events indicates three other possible distributive surface ruptures in the Yucca Mountain area during the past 100 k.y. However, correlations are less reliable than for the two faulting events just described, owing to the broader ranges in the estimated ages for the bracketing stratigraphic units (fig. 59).

1. Event Z on the Paintbrush Canyon Fault, as identified in trenches A1 and MWV–T4 (fig. 2), is dated as ranging from 17 to 9 ka and from 40 to 6 ka, respectively, (preferred values, 13 and 15 ka, fig. 59; table 43). These trench sites are 5 km apart on the northern segment of the fault (fig. 2); thus, simultaneous surface rupture is strongly possible. Event Z is dated at 15–5 ka (preferred value, 12 ka) from evidence observed in trenches SCR–T1 and SCR–T3 on the Stagecoach Road Fault. As indicated in chapter 3, a subsurface connection may exist between this fault and the southern segment of the Paintbrush Canyon fault a few kilometers southwest of Busted Butte; thus, structure and trench data support an interpretation of a simultaneous surface rupture at about 13 ka along the Stagecoach Road Fault and the northern section of the Paintbrush Canyon Fault. However, at the Busted Butte wall 4 site, the most recent faulting event (Z) identified on the Paintbrush Canyon Fault is dated at no later than 40 ka (fig. 59; table 43). Therefore, if simultaneous surface ruptures did occur at about 13 ka on the Paintbrush Canyon Fault north of Busted Butte and on the Stagecoach Road Fault south of Busted Butte, this faulting event was not reflected (or recognized) on the Paintbrush Canyon Fault in the intervening area.
2. Event Z on segments of the Solitario Canyon Fault system and event Y on the Stagecoach Road Fault occurred at preferred ages between 30 and 20 ka, indicating possible contemporaneous displacements. A surface-rupturing paleoearthquake may also have occurred on the Southern Crater Flat Fault during this same time interval; event Y on that fault is dated at 40 –10 ka, but no preferred date was assigned (table 43; see chap. 10).
3. The most recent event (Z) identified in trench T14D on the Bow Ridge Fault and at Busted Butte wall 4 on the southern section of the Paintbrush Canyon Fault (fig. 2) have both been assigned a preferred date of 50 ka (fig. 59), indicating possible simultaneous surface ruptures. The estimated dates are reasonably well constrained; minimum dates are derived from the ages of deposits or features that formed relatively soon after the event (that is, a colluvial wedge in trench T14D and an eolian mantle across a carbonate-filled fracture at Busted Butte wall 4). The Bow Ridge Fault is inferred to continue southward and southeastward in the subsurface to merge with the southern section of the Paintbrush Canyon Fault (see chap. 3), and so distributive surface ruptures could be expected. However, because such an event has not been recognized in trench MWV–T4 or A1 (fig. 59), both of which are farther north on the Paintbrush Canyon Fault (fig. 2), the relations, if interpreted correctly, would indicate that distributive surface ruptures occurred on the Bow Ridge Fault and on a segment of the Paintbrush Canyon Fault south of its inferred intersection with the Bow Ridge Fault.

Conclusions

Interpretations of temporal and spatial relations among the eight Quaternary faults at Yucca Mountain indicate, with varying degrees of confidence, that distributive surface ruptures may have occurred on various combinations of closely spaced and (or) possibly interconnected faults during paleoearthquakes within the past 100 k.y. The best examples of probable distributive surface ruptures on multiple faults are provided by (1) the presence of geochemically correlated basaltic ash dated at approximately 77 ka within the fissure fills of three faults on the west side of Yucca Mountain; and (2) a Holocene event, dated at about 3 ka, on three closely spaced faults on the west side of Yucca Mountain. Greater uncertainties exist in the dating of other distributive surface ruptures because the estimated ages of the bracketing stratigraphic units cannot be as narrowly defined as in these two examples. However, the accumulated data indicate possibly three additional faulting events at about 50, 30–20, and 13 ka, each involving two or three faults.

The occurrence of distributive surface ruptures has profound implications for seismic-hazard evaluations at Yucca Mountain. Distributive surface ruptures on multiple faults increase the estimated lengths and (or) surface displacements for a given faulting event, which in turn increases the maximum estimated magnitudes for the associated paleoearthquakes. Linking events on multiple faults into a single distributive surface rupture also bears directly on composite recurrence estimates for the Yucca Mountain fault system as a whole. All these input parameters are critical for seismic-source characterization of the proposed repository site for the storage of high-level radioactive wastes.

References Cited

Allen, C.R., 1986, Seismological and paleoseismological techniques of research in active tectonics, *in* Active tectonics: Washington, D.C., National Academy Press, p. 148–154.

Anderson, L.W., and Klinger, R.E., 1996a, Evaluation and characterization of Quaternary faulting—Bare Mountain fault, Nye County, Nevada: U.S. Bureau of Reclamation Seismotectonic Report 96–5, 78 p.

Anderson, L.W., and Klinger, R.E., 1996b, The Beatty scarp in Nye County, Nevada—an important Late Quaternary morphologic datum: Seismological Society of America Bulletin, v. 86, no. 5, p. 1650–1654.

Anderson, R.E., Crone, A.J., Machette, M.N., Bradley, L.A., and Diehl, S.F., 1995, Characterization of Quaternary and suspected Quaternary faults, Amargosa area, Nevada and California: U.S. Geological Survey Open-File Report 95–613, 41 p.

Barnes, Harley, Ekren, E.B., Rodgers, C.L., and Hedlund, D.C., 1982, Geologic and tectonic maps of the Mercury quadrangle, Nye and Clark Counties, Nevada: U.S. Geological Survey Miscellaneous Investigations Series Map I–1197, scale 1:24,000.

Birkeland, P.W., 1984, Soils and geomorphology: New York, Oxford University Press, 372 p.

Birkeland, P.W., Machette, M.N., and Haller, K.M., 1991, Soils as a tool for applied Quaternary geology: Utah Geological and Mineral Survey Miscellaneous Publication 91–3, 63 p.

Brocher, T.M., Hunter, W.C., and Langenheim, V.E., 1998, Implications of seismic reflection and potential field geophysical data on the structural framework of the Yucca Mountain–Crater Flat region, Nevada: Geological Society of America Bulletin, v. 100, no. 8, p. 947–971.

Bucknam, R.C., and Anderson, R.E., 1979, Estimation of fault-scarp ages from a scarp-height-slope-angle relationship: Geology, v. 7, no. 1, p. 11–14.

Buesch, D.C., Spengler, R.W., Moyer, T.C., and Geslin, J.K., 1996, Proposed stratigraphic nomenclature and macroscopic identification of lithostratigraphic units of the Paintbrush Group exposed at Yucca Mountain, Nevada: U.S. Geological Survey Open-File Report 94–469, 47 p.

Bull, W.B., 1991, Geomorphic responses to climate change: New York, Oxford University Press, 326 p.

Bull, W.B., and Ku, T.L., 1975, Age dating of the Late Cenozoic deposits in the vicinity of the Vidal nuclear generating station site: Southern California Edison Co., app. 2.5G, 41 p.

Carr, W.J., 1992, Structural model for western Midway Valley based on RF drillhole data and bedrock outcrops, *in* Gibson, J.D., Swan, F.H., Wesling, J.R., Bullard, T.F., Perman, R.C., Angell, M.M., and DiSilvestro, L.A., Summary and evaluation of existing geological and geophysical data near prospective surface facilities in Midway Valley, Yucca Mountain Project: Albuquerque, N.Mex., Sandia National Laboratories Report SAND 90–2491, 94 p.

Christiansen, R.L., and Lipman, P.W., 1965, Geologic map of the Topopah Spring NW quadrangle, Nye County, Nevada: U.S. Geological Survey Geologic Quadrangle Map GQ–444, scale 1:24,000.

Coe, J.A., Oswald, J.A., Vadurro, Giovanni, Paces, J.B., Ludwig, K.R., Widmann, Beth, Menges, C.M., Lundstrom, S.C., and deFontaine, C.S., 1995, Paleoseismic investigation of the Fatigue Wash fault, Crater Flat, Nye County, Nevada [abs.]: Eos (American Geophysical Union Transactions), v. 76, no. 46, p. 362.

Coe, J.A., Taylor, E.M., and Schilling, S.P., 1991, Close-range geophotogrammetric mapping of trench walls using multi-model stereo restitution software: American Society for Photogrammetry and Remote Sensing Annual Meeting, 1991, Technical Papers, v. 5, p. 30–43.

Coppersmith, K.J., 1991, Seismic source characterization for engineering seismic hazard analysis: International Conference on Seismic Zonation, 4th, Proceedings, v. 1, p. 3–60.

Cornwall, H.R., and Kleinhampl, F.J., 1961, Geology of the Bare Mountain quadrangle, Nevada: U.S. Geological Survey Geologic Quadrangle Map GQ–157, scale 1:62,500.

Crone, A.J., 1983, Amount of displacement and estimated age of a Holocene surface faulting event, eastern Great Basin, Millard County, Utah, *in* Crone, A.J., ed., Paleoseismicity along the Wasatch front and adjacent areas, central Utah: Utah Geological and Mineral Survey Special Studies 62, p. 49–55.

Crowe, B.M., Perry, F.V., Geissman, J.W., McFadden, L.D., Wells, S.G., Murrell, M.T., Poths, Jane, Valentine, G.A., Bowker, L.M., and Finnegan, K.P., 1995, Status of volcanism studies for Yucca Mountain site characterization project: Los Alamos, N.Mex., Los Alamos National Laboratory Report LA–12908–MS, 378 p.

Day, W.C., Dickerson, R.P., Potter, C.J., Sweetkind, D.S., San Juan, C.A., Drake, R.M., II, and Fridrich, C.J., 1998a, Bedrock geologic map of the Yucca Mountain area, Nye County, Nevada: U.S. Geological Survey Geologic Investigations Series Map I–2627, scale 1:24,000.

Day, W.C., Potter, C.J., Sweetkind, D.C., Dickerson, R.P., and San Juan, C.A., 1998b, Bedrock geologic map of the central block area, Yucca Mountain, Nye County, Nevada; U.S. Geological Survey Miscellaneous Investigations Series Map I–2601, scale 1:6,000.

dePolo, C.M., 1994, The maximum background earthquake for the Basin and Range province, western North America:

Seismological Society of America Bulletin, v. 84, no. 2, p. 466–472.

dePolo, C.M. and Slemmons, D.B., 1990, Estimation of earthquake size for seismic hazards, *in* Krinitzky, E.L., and Slemmons, D.B., eds., Neotectonics in earthquake evaluation: Geological Society of America Reviews in Engineering Geology, v. 8, p. 1–28.

Dickerson, R.P., and Drake, R.M., II, 1998, Geologic map of the Paintbrush Canyon area, Yucca Mountain, Nevada: U.S. Geological Survey Open-File Report 97–783, 25 p., scale 1:6,000.

Dohrenwend, J.C., Menges, C.M., Schell, B.A., and Moring, B.C., 1991, Reconnaissance photogeologic map of young faults in the Las Vegas 1°×2° quadrangle, Nevada, California, and Arizona: U.S. Geological Survey Miscellaneous Field Studies Map MF–2182, scale 1:250,000.

Fairer, G.M., Whitney, J.W., and Coe, J.A., 1989, A close-range photogrammetric technique for mapping neotectonic features in trenches: Association of Engineering Geologists Bulletin, v. 26, no. 4, p. 521–530.

Faulds, J.E., Bell, J.W., Feuerbach, D.L., and Ramelli, A.R., 1994, Geologic map of the Crater Flat area: Nevada: Nevada Bureau of Mines and Geology Map 101, 4 p., 2 sheets, scale 1:24,000.

Ferrill, D.A., Stamatakos, J.A., Jones, S.M., Rahe, Bret, McKague, H.L., Martin, R.H., and Morris, A.P., 1996, Quaternary slip history of the Bare Mountain fault (Nevada) from the morphology and distribution of alluvial fan deposits: Geology, v. 24, no. 6, p. 559–562.

Fitterman, D.V., 1982, Magnetometric resistivity survey near Fortymile Wash, Nevada Test Site, Nevada: U.S. Geological Survey Open-File Report 82–401, 27 p.

Forman, S.L., Jackson, M.E., and McCalpin, J.P., 1988, The potential of using thermoluminescence to date buried soils developed on colluvial and fluvial sediments from Utah and Colorado, U.S.A.; preliminary results: Quaternary Science Reviews, v. 7, no. 3–4, p. 287–293.

Frischknecht, F.C., and Raab, P.V., 1984, Time-domain electromagnetic soundings at the Nevada Test Site, Nevada: Geophysics, v. 49, no. 7, p. 981–992.

Frizzell, V.A., Jr., and Shulters, Jacqueline, 1990, Geologic map of the Nevada Test Site, southern Nevada: U.S. Geological Survey Miscellaneous Investigations Series Map I–2046, scale 1:100,000.

Frizzell, V.A., Jr., and Zoback, M.L., 1987, Stress orientation determined from fault slip data in the Hampel Wash area, Nevada, and its relation to the contemporary stress field: Tectonics, v. 6, no. 2, p. 89–98.

Gibson, J.D., Swan, F.H., Wesling, J.R., Bullard, T.F., Perman, R.C., Angell, M.M., and DiSilvestro, L.A., 1992, Summary and evaluation of existing geological and geophysical data near prospective surface facilities in Midway Valley, Yucca Mountain Project, Nye County, Nevada: Albuquerque, N.Mex., Sandia National Laboratories Report SAND 90–2491, 171 p.

Gile, L.H., Peterson, F.F., and Grossman, R.B., 1966, Morphological and genetic sequences of carbonate accumulation in desert soils: Soil Science, v. 101, no. 5, p. 347–360.

Hanks, T.C., and Andrews, D.J., 1989, Effect of far-field slope on morphologic dating of scarplike landforms: Journal of Geophysical Research, v. 94, no. B1, p. 565–573.

Harden, J.W., Slate, J.L., Lamothe, P.J., Chadwick, O.A., Pendall, E.G., and Gillespie, A.R., 1991a, Soil formation on the Trail Canyon alluvial fan, Fish Lake Valley, Nevada: U.S. Geological Survey Open-File Report 91–291, 22 p.

Harden, J.W., Taylor, E.M., Hill, C.L., Mark, R.K., McFadden, L.D., Reheis, M.C., Sowers, J.M., and Wells, S.G., 1991b, Rates of soil development from four soil chronosequences in the southern Great Basin: Quaternary Research, v. 35, no. 3, pt. 1, p. 383–399.

Harmsen, S.C., 1994, The Little Skull Mountain Nevada, earthquake of 29 June 1992; aftershock focal mechanisms and tectonic stress field implications: Seismological Society of America Bulletin, v. 84, no. 5, p. 1484–1505.

Harrington, C.D., Whitney, J.W., Jull, A.J.T., and Phillips, William., 2000, Cosmogenic dating and analysis of scarps along the Solitario Canyon and Windy Wash faults, Yucca Mountain, Nevada: U.S. Geological Survey Digital Data Series 58, 9 p.

Hatheway, A.W., and Leighton, F.B., 1979, Trenching as an exploratory method, *in* Hatheway, A.W., and McClure, C.R., Jr., eds., Geology in the siting of nuclear power plants: Geological Society of America Reviews of Engineering Geology, v. 4, p. 169–195.

Heizler, M.T., Perry, F.V., Crowe, B.M., Peters, Lisa, and Appelt, Robert, 1999, The age of the Lathrop Wells volcanic center; an $^{40}Ar/^{39}Ar$ dating investigation: Journal of Geophysical Research, v. 104, no. B1, p. 767–804.

Hinrichs, E.N., 1968, Geologic map of the Camp Desert Rock quadrangle, Nye County, Nevada: U.S. Geological Survey Geologic Quadrangle Map GQ–726, scale 1:24,000.

Hoover, D.L., 1989, Preliminary description of Quaternary and late Pliocene surficial deposits at Yucca Mountain and vicinity, Nye County, Nevada: U.S. Geological Survey Open-File Report 89–359, 45 p.

Hoover, D.L., and Morrison, J.N., 1980, Geology of the Syncline Ridge area related to nuclear waste disposal, Nevada Test Site, Nye County, Nevada: U.S. Geological Survey Open-File Report 80–942, 70 p.

Hoover, D.L., Swadley, WC, and Gordon, A.J., 1981, Correlation characteristics of surficial deposits with a description of surficial stratigraphy in the Nevada Test Site region: U.S. Geological Survey Open-File Report 81–512, 27 p.

Hopkins, D.M., 1975, Time-stratigraphic nomenclature for the Holocene epoch: Geoderma, v. 14, no. 1, p. 2.

Imbrie, John, Hays, J.D., Martinson, D.G., McIntyre, Andrew, Mix, A.C., Morley, J.J., Pisias, N.G., Prell, W.L., and Shackleton, N.J., 1984, The orbital theory of Pleistocene climate; support from a revised chronology of the Marine O record, *in* Berger, A.L., and others, eds., Milankovitch and climate; understanding the response to astronomical forcing: Dordrecht, Reidel, v. 1, p. 269–305.

Izett, G.A., Obradovich, J.D., and Mehnert, H.H., 1988, The Bishop Ash Bed (middle Pleistocene) and some older (Pliocene and Pleistocene) chemically and mineralogically similar ash beds in California, Nevada, and Utah: U.S. Geological Survey Bulletin 1675, 37 p.

Langenheim, V.E., and Ponce, D.A., 1994, Gravity and magnetic investigations of Yucca Wash, southwest Nevada, *in* High level radioactive waste management: American Nuclear Society Annual International Conference, 5th, Las Vegas, Nev., 1994, Proceedings, v. 4, p. 2272–2278.

Lipman, P.W., and McKay, E.J., 1965, Geologic map of the Topopah Spring SW quadrangle, Nye County, Nevada: U.S. Geological Survey Geologic Quadrangle Map GQ–439, scale 1:24,000.

Lundstrom, S.C., Wesling, J.R., Swan, F.H., Taylor, E.M., and Whitney, J.R., 1993, Quaternary allostratigraphy of surficial deposit map units at Yucca Mountain, Nevada—a progress report [abs.]: Geological Society of America Abstracts with Programs, v. 25, no. 5, p. A112.

Machette, M.N., 1985, Calcic soils of the southwestern United States, *in* Weide, D.L., ed., Soils and Quaternary geology of the southwestern United States: Geological Society of America Special Paper 203, p. 1–21.

Machette, M.N., 1989, Slope-morphometric dating, *in* Forman, S.L., ed., Dating methods applicable to Quaternary geologic studies in the western United States: Utah Geological and Mineral Survey Miscellaneous Publication 89–7, p. 30–42.

Machette, M.N., Personius, S.F., and Nelson, A.R., 1992, Paleoseismology of the Wasatch fault zone; a summary of recent investigations, interpretations, and conclusions: U.S. Geological Survey Professional Paper 1500–A, 71 p.

McCalpin, J.P., 1996, Paleoseismology: San Diego, Calif., Academic Press, 588 p.

McCalpin, J.P., Forman, S.L., and Lowe, Mike, 1994, Reevaluation of Holocene faulting at the Kaysville site, Weber segment of the Wasatch fault zone, Utah: Tectonics, v. 13, no. 1, p. 1–16.

McDonald, E.V., and McFadden, L.D., 1994, Quaternary stratigraphy of the Providence Mountains piedmont and preliminary age estimates and regional stratigraphic correlations of Quaternary deposits in the eastern Mojave Desert, California, *in* McGill, S.F., and Ross, T.M., eds., Geological investigations of an active margin: Geological Society of America, Cordilleran Section Fieldtrip Guidebook 8, p. 205–213.

McFadden, L.D., and Weldon, R.J., III, 1987, Rates and processes of soil development on Quaternary terraces in Cajon Pass, California: Geological Society of America Bulletin, v. 98, no. 3, p. 280–293.

McFadden, L.D., Wells, S.G., and Jercinovich, M.J., 1987, Influences of eolian and pedogenic processes on the origin and evolution of desert pavements: Geology, v. 15, no. 6, p. 504–508.

Menges, C.M., Oswald, J.A., Coe, J.A., Lundstrom, S.C., Paces, J.B., Mahau, S.A., Widmann, B.L., and Murray, Michele, 1998, Paleoseismic investigations of Stagecoach Road fault, southeastern Yucca Mountain, Nye County, Nevada: U.S. Geological Survey Open-File Report 96–417, 71 p.

Menges, C.M., Taylor, E.M., Vadurro, Giovanni, Oswald, J.A., Cress, Robert, Murray, Michele, Lundstrom, S.C., Paces, J.B., and Mahan, S.A., 1997, Logs and paleoseismic interpretations from trenches 14C and 14D on the Bow Ridge fault, northeastern Yucca Mountain, Nye County, Nevada: U.S. Geological Survey Miscellaneous Field Studies Map 2311.

Menges, C.M., Wesling, J.R., Whitney, J.W., Swan, F.H., Coe, J.A., Thomas, A.P., and Oswald, J.A., 1994, Preliminary results of paleoseismic investigations of Quaternary faults on eastern Yucca Mountain, Nye County, Nevada, *in* High level radioactive waste management: American Nuclear Society Annual International Conference, 5th, Las Vegas, Nev., 1994, Proceedings, v. 4, p. 2373–2390.

Monsen, S.A., Carr, M.D., Reheis, M.C., and Orkild, P.P., 1992, Geologic map of Bare Mountain, Nye County, Nevada: U.S. Geological Survey Miscellaneous Investigations Series Map I–2201, scale 1:24,000.

Morrison, R.B., 1991, Introduction, *in* Morrison, R.B., ed., Quaternary nonglacial geology—conterminous U.S., v. K–2 *of* The geology of North America: Boulder, Colo., Geological Society of America, p. 1–12.

Muller, D.C., and Kibler, J.E., 1984, Preliminary analysis of geophysical logs from drill hole UE–25p#1, Yucca Mountain, Nye County, Nevada: U.S. Geological Survey Open-File Report 84–649, 14 p.

Munsell Color Co., Inc., 1988, Munsell soil color charts: Baltimore.

Munsell Color Co., Inc., 1992, Munsell soil color charts (revised ed.): Baltimore.

Nash, D.B., 1980, Morphological dating of degraded normal fault scarps: Journal of Geology, v. 88, no. 3, p. 353–360.

Nash, D.B., 1984, Morphologic dating of fluvial terrace scarps and fault scarps near West Yellowstone, Montana: Geological Society of America Bulletin, v. 95, no. 12, p. 1413–1424.

Nash, D.B., 1986, Morphologic dating and modeling degradation of fault scarps, *in* Wallace, R.E., ed., Active tectonics: Washington, D.C., National Academy Press, p. 181–194.

Neal, J.T., 1985, Location recommendation for surface facilities for prospective Yucca Mountain nuclear waste repository: Albuquerque, N.Mex., Sandia National Laboratories Report SAND 84–2015, 54 p.

Neal, J.T., 1986, Preliminary validation of geology at site for repository surface facilities, Yucca Mountain, Nevada: Albuquerque, N.Mex., Sandia National Laboratories Report SAND 85–0815, 55 p.

Nelson, A.R., 1992, Lithofacies analysis of colluvial sediments—an aid in interpreting the recent history of Quaternary normal faults in the Basin and Range province, western United States: Journal of Sedimentary Petrology, v. 62, no. 4, p. 607–621.

North American Commission on Stratigraphic Nomenclature, 1983, North American stratigraphic code: American Association of Petroleum Geologists Bulletin, v. 67, no. 5, p. 841–875.

O'Leary, D.W., 2000, Tectonic significance of the Rock Valley Fault Zone, Nevada Test Site: U.S. Geological Survey Digital Data Series 58, 13 p.

O'Neill, M.J., Whitney, J.W., and Hudson, M.R., 1991, Photogeologic and kinematic analysis of lineaments at Yucca Mountain, Nevada—implications for strike-slip faulting and oroclinal bending: U.S. Geological Survey Open-File Report 91–623, 24 p.

Paces, J.B., Menges, C.M., Widmann, Beth, Wesling, J.R., Bush, C.A., Futa, Kiyoto, Millard, H.T., Maat, P.B., and Whitney, J.W., 1994, U-series disequilibrium and thermoluminescence ages of paleosols associated with Quaternary faults, east side of Yucca Mountain, *in* High level radioactive waste management: American Nuclear Society Annual International Conference, 5th, Las Vegas, Nev., 1994, Proceedings, v. 4, p. 2391–2401.

Pearthree, P.A., and Calvo, S.S., 1987, The Santa Rita fault zone—evidence for large magnitude earthquakes with very long recurrence intervals, Basin and Range Province of southeastern Arizona: Seismological Society of America Bulletin, v. 77, no. 1, p. 97–116.

Peterman, Z.E., and Futa, Kiyoto, 1996, Geochemistry of core samples of the Tiva Canyon Tuff from drill hole UE–25 NRG#3, Yucca Mountain, Nevada: U.S. Geological Survey Open-File Report 95–325, 19 p.

Peterson, F.F., Bell, J.W., Dorn, R.I., Ramelli, A.R., and Ku, T.L., 1995, Late Quaternary geomorphology and soils in Crater Flat, Yucca Mountain, southern Nevada: Geological Society of America Bulletin, v. 107, no. 4, p. 379–395.

Piety, L.A., 1994, Compilation of known and suspected Quaternary faults within 100 km of Yucca Mountain, Nevada and California: U.S. Geological Survey Open-File Report 94–112, 32 p., 2 sheets, scale 1:250,000.

Piety, L.A., and Anderson, L.W., 1991, The Horseshoe fault, evidence for prehistoric surface-rupturing earthquakes in central Arizona: Arizona Geology, v. 21, no. 3, p. 1, 4–8.

Ponce, D.A., 1993, Geophysical investigations of concealed faults near Yucca Mountain, southwest Nevada, *in* High level radioactive waste management: American Nuclear Society Annual International Conference, 4th, Las Vegas, Nev., 1993, Proceedings, v. 1, p. 168–174.

Ponce, D.A., and Langenheim, V.E., 1994, Preliminary gravity and magnetic models across Midway Valley and Yucca Wash, Yucca Mountain, Nevada: U.S. Geological Survey Open-File Report 94–572, 25 p.

Poole, F.G., 1965, Geologic map of the Frenchman Flat quadrangle, Nye County, Nevada: U.S. Geological Survey Quadrangle Map GQ–456, scale 1:24,000.

Potter, C.J., Dickerson, R.P., and Day, W.C., 1999, Nature and continuity of the Sundance fault, Yucca Mountain, Nevada: U.S. Geological Survey Open-File Report 98–266, 16 p., scale 1:2,400.

Ramelli, A.R., Sawyer, T.L., Bell, J.W., Peterson, F.F., Dorn, R.I., and dePolo, C.M., 1989, Preliminary analysis of fault and fracture patterns at Yucca Mountain, southern Nevada, *in* FOCUS '89—Nuclear Waste Isolation in the Unsaturated Zone: American Nuclear Society Annual Meeting, Las Vegas, Nev., 1989, Proceedings, p. 336–343.

Reheis, M.C., 1988, Preliminary study of Quaternary faulting on the east side of Bare Mountain, Nye County, Nevada, *in* Carr, M.D., and Yount, J.C., eds., Geologic and hydrologic investigations of a potential nuclear waste disposal site at Yucca Mountain, southern Nevada: U.S. Geological Survey Bulletin 1790, p. 103–111.

Reheis, M.C., Harden, J.W., McFadden, L.D., and Shroba, R.R., 1989, Development rates of late Quaternary soils, Silver Lake Playa, California: Soil Science Society of America Journal, v. 53, no. 4, p. 1127–1140.

Reheis, M.C., Sowers, J.M., Taylor, E.M., McFadden, L.D., and Harden, J.W., 1992, Morphology and genesis of carbonate soils on the Kyle Canyon fan, Nevada, U.S.A.: Geoderma, v. 52, no. 3–4, p. 303–342.

Reiter, Leon, 1990, Earthquake hazard analysis; issues and insights: New York, Columbia University Press, 254 p.

Rosholt, J.N., Bush, C.A., Carr, W.J., Hoover, D.L., Swadley, WC, and Dooley, J.R., Jr., 1985, Uranium-trend dating of Quaternary deposits in the Nevada Test Site area, Nevada and California: U.S. Geological Survey Open-File Report 85–540, 72 p.

Sarna-Wojcicki, A.M., Meyer, C.E., Wau, Elmira, and Soles, Stan, 1993, Age and correlation of tephra layers in Owens Lake drill core OL–92–1 and –2, *in* Smith, G.I., and Bischoff, J.L., eds., Core OL–92 from Owens Lake, southeast California: U.S. Geological Survey Open-File Report 93–683, 11 p.

Sawyer, D.A., Fleck, R.J., Lanphere, M.A., Warren, R.G., Broxton, D.E., and Hudson, M.R., 1994, Episodic caldera volcanism in the Miocene southwestern Nevada volcanic field; revised stratigraphic framework, $^{40}Ar/^{39}Ar$ geochronology, and implications for magmatism and extension: Geological Society of America Bulletin, v. 106, no. 10, p. 1304–1318.

Schwartz, D.P., 1988, Geologic characterization of seismic sources—moving into the 1990's, *in* von Thun, J.L., ed., Recent advances in ground-motion evaluation, v. 2 *of* Earthquake engineering and soil dynamics: American Society of Civil Engineers Geotechnical Special Publication 20, p. 1–42.

Scott, R.B., 1990, Tectonic setting of Yucca Mountain, southwest Nevada, *in* Wernicke, B.P., ed., Basin and Range extensional tectonics near the latitude of Las Vegas, Nevada: Geological Society of America Memoir 176, p. 251–282.

Scott, R.B., 1992, Preliminary geologic map of southern Yucca Mountain, Nye County, Nevada: U.S. Geological Survey Open-File Report 92–266, 28 p., scale 1:12,000.

Scott, R.B., Bath, G.D., Flanigan, V.J., Hoover, D.B., Rosenbaum, J.G., and Spengler, R.W., 1984, Geological and geophysical evidence of structures in northwest-trending washes, Yucca Mountain, southern Nevada, and their possible significance to a nuclear waste repository in the unsaturated zone: U.S. Geological Survey Open-File Report 84–567, 23 p.

Scott, R.B., and Bonk, Jerry, 1984, Preliminary geologic map of Yucca Mountain, Nye County, Nevada, with geologic sections: U.S. Geological Survey Open-File Report 84–494, 9 p., scale 1:12,000,

Senterfit, R.M., Hoover, D.B., and Chornack, M.P., 1982, Resistivity sounding investigation by the Schlumberger method in the Yucca Mountain and Jackass Flats area, Nevada Test Site, Nevada: U.S. Geological Survey Open-File Report 82–1043, 38 p.

Simonds, F.W., Whitney, J.W., Fox, K.F., Ramelli, A.R., Yount, J.C., Carr, M.D., Menges, C.M., Dickerson, R.P., and Scott, R.B., 1995, Map showing fault activity in the Yucca Mountain area, Nye County, Nevada: U.S. Geological Survey Miscellaneous Investigations Series Map I–2520, scale 1:24,000.

Slate, J.L., 1991, Quaternary stratigraphy, geomorphology, and geochronology of alluvial fans, Fish Lake Valley, Nevada and California, *in* Reheis, M.C., Sarna-Wojcicki, A.M., Meyer, C.E., McKee, E.H., Slate, J.L., Burbank, D.M., Sawyer, T.L., and Pendall, E.G., Late Cenozoic stratigraphy and tectonics of Fish Lake Valley, Nevada and California—road log and contributions to the field trip guidebook, 1991 Pacific Cell of Friends of the Pleistocene: U.S. Geological Survey Open-File Report 91–290, p. 94–113.

Smith, Christian, and Ross, H.P., 1982, Interpretation of resistivity and induced polarization profiles with severe topographic effects, Yucca Mountain area, Nevada Test Site, Nevada: U.S. Geological Survey Open-File Report 82–182, 82 p.

Smith, K.D., and Brune, J.N., 1993, A sequence of very shallow earthquakes in the Rock Valley fault zone, southern Nevada Test Site [abs.]: Eos (American Geophysical Union Transactions), v. 74, no. 43, supp., p. 417.

Smith, K.D., Shields, Gordon, and Brune, J.N., 2000, A sequence of very shallow earthquakes in the Rock Valley fault zone, southern Nevada Test Site: U.S. Geological Survey Digital Data Series 58, 11 p.

Spaulding, W.G., and Graumlich, L.J., 1986, The last pluvial climatic episodes in the deserts of southwestern North America: Nature, v. 320, no. 6067, p. 441–444.

Swadley, WC, 1983, Map showing surficial geology of Lathrop Wells quadrangle, Nye County, Nevada: U.S. Geological Survey Map I–1361, scale 1:48,000.

Swadley, WC, and Carr, W.J., 1987, Geologic map of the Quaternary and Tertiary deposits of the Big Dune quadrangle, Nye County, Nevada and Inyo County, California: U.S. Geological Survey Map I–1767, scale 1:48,000.

Swadley, WC, and Hoover, D.L., 1983, Geology of faults exposed in trenches in Crater Flat, Nye County, Nevada: U.S. Geological Survey Open-File Report 83–608, 15 p.

Swadley, WC, and Hoover, D.L., 1989a, Geologic map of the surficial deposits of the Jackass Flats quadrangle, Nye County, Nevada: U.S. Geological Survey Miscellaneous Investigations Series Map I–1994, scale 1:24,000.

Swadley, WC, and Hoover, D.L., 1989b, Geologic map of the surficial deposits of the Topopah Spring quadrangle, Nye County, Nevada: U.S. Geological Survey Miscellaneous Investigations Series Map I–2018, scale 1:24,000.

Swadley, WC, Hoover, D.L., and Rosholt, J.N., 1984, Preliminary report on late Cenozoic faulting and stratigraphy in the vicinity of Yucca Mountain, Nye County, Nevada: U.S. Geological Survey Open-File Report 84–788, 42 p.

Swadley, WC, and Huckins, H.E., 1989, Surficial geologic map of the Specter Range NW quadrangle, Nye County, Nevada: U.S. Geological Survey Miscellaneous Investigations Series Map I–1884, scale 1:24,000.

Swadley, WC, and Huckins, H.E., 1990, Geologic map of the surficial deposits of the Skull Mountain quadrangle, Nye County, Nevada: U.S. Geological Survey Miscellaneous Investigations Series Map I–1972, scale 1:24,000.

Swadley, WC, and Parrish, L.D., 1988, Surficial geologic map of the Bare Mountain quadrangle, Nye County, Nevada: U.S. Geological Survey Map I–1826, scale 1:48,000.

Swan, F.W., Schwartz, D.P., and Cluff, L.S., 1980, Recurrence of moderate to large magnitude earthquakes produced by surface faulting on the Wasatch fault zone, Utah: Seismological Society of America Bulletin, v. 70, no. 5, p. 1431–1462.

Swan, F.W., Wesling, J.R., Angell, M.M., Thomas, A.P., Whitney, J.W., and Gibson, J.D., 2001, Evaluation of the location and recency of faulting near prospective surface facilities in Midway Valley, Nye County, Nevada: U.S. Geological Survey Open-File Report 01–55, 66 p.

Swan, F.H., Wesling, J.R., and Thomas, A.P., 1993, Paleoseismic investigations of the Paintbrush Canyon fault in southern Midway Valley, Yucca Mountain, Nevada: preliminary results [abs.]: Geological Society of America Abstracts with Programs, v. 25, no. 5, p. A153.

Szabo, B.J., Carr, W.J., and Gottschall, W.C., 1981, Uranium-thorium dating of Quaternary accumulations in the Nevada Test Site region, southern Nevada: U.S. Geological Survey Open-File Report 81–119, 35 p.

Taylor, E.M., 1986, Impact of time and climate on Quaternary soils in the Yucca Mountain area of the Nevada Test Site: Boulder, University of Colorado, M.S. thesis, 217 p.

Taylor, E.M., and Huckins, H.E., 1995, Lithology, fault displacement, and origin of secondary calcium carbonate and opaline silica at trenches 14 and 14D on the Bow Ridge fault at Exile Hill, Nye County, Nevada: U.S. Geological Survey Open-File Report 93–477, 37 p.

U.S. Department of Energy, 1988, Site characterization plan: Office of Civilian Radioactive Waste Management Report DOE/RW–0199.

U.S. Geological Survey, 1984, A summary of geologic studies through January 1, 1983, of a potential high-level radioactive waste repository site at Yucca Mountain, southern Nye County, Nevada: Open-File Report 44–792, 103 p.

van den Bogaard, Paul, and Schirnick, Carsten, 1995, $^{40}Ar/^{39}Ar$ laser probe ages of Bishop Tuff quartz phenocrysts substantiate long-lived silicic magma chamber at Long Valley, United States: Geology, v. 23, no. 8, p. 759–762.

Wallace, R.E., 1977, Profiles and ages of young fault scarps, north-central Nevada: Geological Society of America Bulletin, v. 88, no. 9, p. 1267–1281.

Wallace, R.E., 1980, Degradation of the Hebgen Lake fault scarps of 1959: Geology, v. 8, no. 5, p. 225–229.

Wells, D.L., and Coppersmith, K.J., 1994, New empirical relationships among magnitude, rupture length, rupture width, rupture area, and surface displacement: Seismological Society of America Bulletin, v. 84, no. 4, p. 974–1002.

Wells, S.G., McFadden, L.D., and Harden, J., 1990, Preliminary results of age estimations and regional correlations of Quaternary alluvial fans within the Mojave Desert in southern California, *in* Reynolds, R.E., Wells, S.G., and Brady, R.H., compilers, At the end of the Mojave—Quaternary studies in the eastern Mojave Desert: Redlands, Calif., San Bernardino's County Museum Association, p. 45–54.

Wesling, J.R., Bullard, T.F., Swan, F.H., Perman, R.C., Angell, M.M., and Gibson, J.D., 1992, Preliminary mapping of surficial geology of Midway Valley, Yucca Mountain, Nye County, Nevada: Albuquerque, N.Mex., Sandia National Laboratories Report SAND 91–0607, 55 p., scale 1:6000.

Whitney, J.W., and Berger, D.L., 2000, A 3.7 million-year offset rate on the Windy Wash fault at the south end of Yucca Mountain, Nevada: U.S. Geological Survey Digital Data Series 58, 9 p.

Whitney, J.W., and Harrington, C.D., 1993, Relict colluvial boulder deposits as paleoclimate indicators in the Yucca Mountain region, southern Nevada: Geological Society of America Bulletin, v. 105, no. 8, p. 1008–1018.

Whitney, J.W., and Muhs, D.R., 1991, Quaternary movement on the Paintbrush Canyon-Stagecoach Road fault system, Yucca Mountain, Nevada [abs.]: Geological Society of America Abstracts with Program, v. 23, no. 5, p. 119.

Whitney, J.W., Shroba, R.R., Simonds, F.W., and Harding, S.T., 1986, Recurrent Quaternary movement on the Windy Wash fault, Nye County, Nevada [abs.]: Geological Society of America Abstracts with Programs, v. 18, no. 6, p. 787.

Whitney, J.W., Swadley, WC, and Shroba, R.R., 1985, Middle Quaternary sand ramps in the southern Great Basin, California and Nevada [abs.]: Geological Society of America Abstracts with Programs, v. 17, no. 7, p. 750.

Yount, J.C., Shroba, R.R., McMasters, C.R., Huckins, H.E., and Rodriguez, E.A., 1987, Trench logs from a strand of the Rock Valley fault system, Nevada Test Site, Nye County, Nevada: U.S. Geological Survey Miscellaneous Field Studies Map MF–1824.